INTEGRATIVE RESEARCH ON ORGANIC MATTER CYCLING ACROSS AQUATIC GRADIENTS,
2nd Edition

EDITED BY: Nicholas D. Ward, Thomas S. Bianchi, Patricia M. Medeiros, Michael Seidel, Richard G. Keil and Carol Robinson

PUBLISHED IN: Frontiers in Marine Science and Frontiers in Earth Science

frontiers Research Topics

frontiers

ISSN 1664-8714
ISBN 978-2-88966-154-1
DOI 10.3389/978-2-88966-154-1

About Frontiers

Frontiers is more than just an open-access publisher of scholarly articles: it is a pioneering approach to the world of academia, radically improving the way scholarly research is managed. The grand vision of Frontiers is a world where all people have an equal opportunity to seek, share and generate knowledge. Frontiers provides immediate and permanent online open access to all its publications, but this alone is not enough to realize our grand goals.

Frontiers Journal Series

The Frontiers Journal Series is a multi-tier and interdisciplinary set of open-access, online journals, promising a paradigm shift from the current review, selection and dissemination processes in academic publishing. All Frontiers journals are driven by researchers for researchers; therefore, they constitute a service to the scholarly community. At the same time, the Frontiers Journal Series operates on a revolutionary invention, the tiered publishing system, initially addressing specific communities of scholars, and gradually climbing up to broader public understanding, thus serving the interests of the lay society, too.

Dedication to Quality

Each Frontiers article is a landmark of the highest quality, thanks to genuinely collaborative interactions between authors and review editors, who include some of the world's best academicians. Research must be certified by peers before entering a stream of knowledge that may eventually reach the public - and shape society; therefore, Frontiers only applies the most rigorous and unbiased reviews.
Frontiers revolutionizes research publishing by freely delivering the most outstanding research, evaluated with no bias from both the academic and social point of view. By applying the most advanced information technologies, Frontiers is catapulting scholarly publishing into a new generation.

What are Frontiers Research Topics?

Frontiers Research Topics are very popular trademarks of the Frontiers Journals Series: they are collections of at least ten articles, all centered on a particular subject. With their unique mix of varied contributions from Original Research to Review Articles, Frontiers Research Topics unify the most influential researchers, the latest key findings and historical advances in a hot research area! Find out more on how to host your own Frontiers Research Topic or contribute to one as an author by contacting the Frontiers Editorial Office: researchtopics@frontiersin.org

INTEGRATIVE RESEARCH ON ORGANIC MATTER CYCLING ACROSS AQUATIC GRADIENTS,
2nd Edition

Topic Editors:
Nicholas D. Ward, Pacific Northwest National Laboratory, University of Washington, United States
Thomas S. Bianchi, University of Florida, United States
Patricia M. Medeiros, University of Georgia, United States
Michael Seidel, University of Oldenburg, Germany
Richard G. Keil, University of Washington, United States
Carol Robinson, University of East Anglia, United Kingdom

From mountains to the sea, fjords represent one of the earth's steepest aquatic gradients
Photo: Patricia Medeiros, Norway

The goal of this research topic was to motivate innovative research that blurs traditional disciplinary and geographical boundaries. As the scientific community continues to gain momentum and knowledge about how the natural world functions, it is increasingly important that we recognize the interconnected nature of earth systems and embrace the complexities of ecosystem transitions. We are pleased to present this body of work, which embodies the spirit of research spanning across the terrestrial-aquatic continuum, from mountains to the sea.

Publisher's note: In this 2nd edition, the following article has been updated: Sawakuchi HO, Neu V, Ward ND, Barros MdLC, Valerio AM, Gagne-Maynard W, Cunha AC, Less DFS, Diniz JEM, Brito DC, Krusche AV and Richey JE (2017) Carbon Dioxide Emissions along the Lower Amazon River. *Front. Mar. Sci.* 4:76. doi: 10.3389/fmars.2017.00076

Citation: Ward, N. D., Bianchi, T. S., Medeiros, P. M., Seidel, M., Keil, R. G., Robinson, C., eds. (2020). Integrative Research on Organic Matter Cycling Across Aquatic Gradients, 2nd Edition. Lausanne: Frontiers Media SA. doi: 10.3389/978-2-88966-154-1

Table of Contents

CHAPTER 4
ESTUARIES AND OCEANS

frontiers in Marine Science

EDITORIAL
published: 04 May 2017
doi: 10.3389/fmars.2017.00131

Editorial: Integrative Research on Organic Matter Cycling across Aquatic Gradients

Nicholas D. Ward *

Marine Sciences Laboratory, Pacific Northwest National Laboratory, Sequim, WA, USA

Keywords: carbon, cycling, aquatic, terrestrial, marine, continuum, gradients, organic

Editorial on the Research Topic

Integrative Research on Organic Matter Cycling across Aquatic Gradients

INTRODUCTION

The interface between freshwater and marine ecosystems provides a unique setting to examine the evolution of biogeochemical components derived from the landscape, inland waters, estuaries, and the ocean across distinct physiochemical gradients. A diverse body of work exploring this research topic is highlighted here with the goal of integrating our understanding of how organic matter (OM) is transported and transformed along the terrestrial-aquatic continuum and sparking interdisciplinary discussions on future research needs. The movement of water ultimately controls the transport and transformation of geochemical components as they move from land to sea (Ward et al.), and as such, contributions to this research topic will be described within the context of the hydrological cycle, starting with rainfall.

TERRESTRIAL FLOW PATHS

Rainfall passes through terrestrial vegetation and soil layers prior to entering rivers and streams, translocating and transforming carbon in the process. Neu et al. examined the concentration and flux of dissolved organic and inorganic carbon (DOC and DIC, respectively) in each flow path (i.e., rainfall, throughfall, stemflow, soil solution, groundwater, overland flow, and stream flow) in an Amazonian transitional forest. The highest DOC concentrations and fluxes were observed in throughfall and rainfall, particularly during the first storms after the dry season. DOC concentrations were order(s) of magnitude lower in the soils and streams compared to above-ground flowpaths while DIC levels were generally higher, illustrating that rapid transformations begin occurring to DOC before even entering a river network (Neu et al.).

Stubbins et al. evaluated the dissolved organic matter (DOM) composition of throughfall and stemflow in the Southeastern USA based on ultrahigh resolution mass spectrometry and optical properties. DOM composition was primarily related to surface characteristics of the terrestrial vegetation (i.e., tree type and the abundance of epiphytes) and also to the presence of atmosphere-derived particles, which presumably accumulate during dry periods and are mobilized during the first rainfall events of a water year as observed by Neu et al.

Hernes et al. similarly assessed source inputs of DOM from the landscape to rivers in a temperate watershed in northern California. Leached DOM was extensively transformed as it traveled through the subsurface as indicated by optical analyses and lignin phenol measurements. Hernes et al. further argued that interpretations of lignin biomarkers in water are obscured by complex source signatures and fractionation/transformation of DOM before reaching a main river channel. The take home point from these studies is that a considerable amount of "action" occurs before water and associated OM ever enters a river or stream.

OPEN ACCESS

Edited and reviewed by:
Eric 'Pieter Achterberg, GEOMAR Helmholtz Centre for Ocean Research Kiel (HZ), Germany

***Correspondence:**
Nicholas D. Ward
nicholas.ward@pnnl.gov

Specialty section:
This article was submitted to Marine Biogeochemistry, a section of the journal Frontiers in Marine Science

Received: *06 April 2017*
Accepted: *20 April 2017*
Published: *04 May 2017*

Citation:
Ward ND (2017) Editorial: Integrative Research on Organic Matter Cycling across Aquatic Gradients. Front. Mar. Sci. 4:131. doi: 10.3389/fmars.2017.00131

RIVERS AND STREAMS

The composition and abundance of OM in river systems is not only linked to the landscape, as described above, but also to processes occurring *in situ*. For example, Duan et al. evaluated downstream variability of DOC concentrations in the Mississippi River over a ∼20 year time period. DOC concentrations consistently decreased from the headlands to the river mouth, which was attributed to an imbalance between *in situ* processing and DOM inputs from floodplains and the landscape. The downstream decrease in DOC concentrations in the Mississippi River is in contrast to the behavior of other large river systems, which was attributed to the historic loss of wetlands in the Mississippi basin (Duan et al.).

The lower reach of the Amazon River is an example of a floodplain-rich system in contrast to the Mississippi River. Sawakuchi et al. assessed CO_2 emissions from the lower Amazon River to the atmosphere, which, along with revised estimates for the upper/central Amazon basin, increased the global inland water CO_2 emission estimate by 43%. This study highlighted two major gaps in current global CO_2 data coverage—tidally-influenced lower rivers and near-shore coastal oceans.

Although the Amazon River is well-known for high rates of CO_2 evasion, Gagne-Maynard et al. evaluated the importance of primary production in the Amazon River mainstem, which has typically been assumed to be irrelevant. However, based on an oxygen mass balance, primary production was estimated to occur at roughly 50% the rate of microbial respiration despite limited light attenuation. Further, constraining this interplay between photosynthesis and respiration is an important step in understanding the underlying mechanisms for both CO_2 outgassing and OM accumulation in large rivers. For example, Bertassoli et al. observed high potential for OM burial since the mid-Holocene in the Amazon's two major lowland clearwater tributaries, the Tapajós and Xingu rivers. Sediment cores showed sharp changes between oxic and anoxic periods attributed to hydrologic patterns, illustrating the potential sensitivity of OM burial to variable conditions caused by factors such as climate change and hydropower operations.

The studies described in Section Terrestrial Flow Paths focused largely on the importance of vegetation on determining the composition and abundance of OM that is ultimately mobilized into river networks. OM derived from biomass burning (i.e., pyrogenic OM) is another important source of OM to the aquatic environment but is less well-studied than vascular plant biomarkers. Myers-Pigg et al. assessed the transport and fate of both dissolved and particulate pyrogenic OM (levoglucosan, specifically) in two Arctic rivers in order to determine the role of sorption and selective partioning on pyrogenic OM decomposition and/or storage. Although certain types of pyrogenic carbon such as levoglucosan have been shown to be bioreactive over short time scales, associations with the particulate phase may result in burial, meaning the signatures of these biomarkers could have potential utility as wildfire indicators in the sediment record (Myers-Pigg et al.). The studies described above collectively illustrate the importance of hydrology on controlling the export, storage, and transformation of OM in inland waters.

ESTUARIES AND OCEANS

Various studies examined the transformation of DOM along estuarine and marine gradients. In a southeastern USA marsh-dominated estuary, microbes exhibited a preferential decomposition of marine-derived DOM, resulting in a post-incubation predominance of terrestrially-derived DOM, suggesting that this system is effective at exporting terrigenous DOM to the ocean (Medeiros et al.). Terrigenous DOM from sub-Arctic rivers was estimated to have a residence time of 5–7 years in the brackish Baltic Sea, with 50–67% being exported to the North Sea (Seidel et al.). Similarly, DOM in the temperate Delaware Bay estuary was observed to be relatively unaltered by photo and microbial oxidation on a molecular level along its salinity gradient likely due to high turbidity levels (Osterholz et al.). The relative stability of terrigenous DOM in these estuaries and shelf seas is perhaps indicative of the extensive decomposition that occurs in rivers prior to export or may also illustrate unfavorable environmental conditions for the decomposition of these molecules.

Short-term variability in fluorescent DOM (fDOM) concentrations were evaluated in high resolution throughout a year-long period in the subtropical Shark River estuary, which receives drainage inputs from the Everglades (Regier et al.). fDOM varied from 10 to 50% during tidal cycles, indicating rapid exchange with mangrove marshes and varied by more than 100% over multi-day periods due to both precipitation events and water management, illustrating the dynamic behavior of DOM sources, export, and transformation in estuaries. Storm events following long dry periods drastically altered the biogeochemistry of the subtropical Mission-Aransas estuary in Texas. The estuary became significantly less salty and warmer following storm events and large cyanobacteria blooms were observed concurrently with increased nutrient and carbon concentrations, demonstrating the potential role of storms on stimulating estuarine hypoxia (Reyna et al.).

Finally, the behavior of chromophoric DOM (CDOM), DOC, and chlorophyll was evaluated in the Southern Ocean from New Zealand to the western Ross Sea based on satellite remote sensing; all three parameters had the highest concentrations near New Zealand and consistently decreased toward the core of the Antarctic Circumpolar Current (ACC) at higher latitudes (D'Sa and Kim). Temperature and salinity gradients along this transect were primarily controlled by fronts associated with the ACC and the measured parameters were tightly coupled to these physical gradients illustrating the linkage between physical and biogeochemical processes.

The collection of work presented in this Research Topic illustrates the dynamic behavior of OM as it travels with water through the terrestrial biosphere, river networks, estuaries, and oceans. The fate of OM in the aquatic environment is closely tied to both its previous history and its present physical and biological surroundings. As such, it is essential to consider how OM has

already evolved prior to and after being exported from any given location along the continuum.

AUTHOR CONTRIBUTIONS

The author confirms being the sole contributor of this work and approved it for publication.

FUNDING

This work was supported by NSF DEB Grant #1256724, FAPESP Grant #08/58089-9, the Gordon and Betty Moore Foundation Marine Microbial Initiative, and the University of Florida Jon L. and Beverly A. Thompson Endowment.

ACKNOWLEDGMENTS

I would like to thank all of the authors who contributed to the Frontiers in Marine Science Research Topic: Integrative Research on Organic Matter Cycling Across Aquatic Gradients, the reviewers who kindly dedicated their time to the peer-review process, the Frontiers editorial team, and the editors of the Research Topic: Thomas Bianchi, Richard Keil, Patricia Medeiros, Michael Seidel, and Carol Robinson. I would also like to thank the Gordon and Betty Moore Foundation Marine Microbial Initiative for their generous donation to support open access publication fees for the Research Topic.

Conflict of Interest Statement: The author declares that the research was conducted in the absence of any commercial or financial relationships that could be construed as a potential conflict of interest.

frontiers in Marine Science

ORIGINAL RESEARCH
published: 28 June 2016
doi: 10.3389/fmars.2016.00114

Dissolved Organic and Inorganic Carbon Flow Paths in an Amazonian Transitional Forest

Vania Neu[1], Nicholas D. Ward[2]*, Alex V. Krusche[3] and Christopher Neill[4]*

[1] Instituto Socio Ambiental e dos Recursos Hidricos, Universidade Federal Rural da Amazônia, Belem, Brazil, [2] Department of Geological Sciences, University of Florida, Gainesville, FL, USA, [3] Centro de Energia Nuclear na Agricultura, Universidade de São Paulo, Piracicaba, Brazil, [4] The Ecosystems Center, Marine Biological Laboratory, Woods Hole, MA, USA

As a raindrop falls from the atmosphere, over vegetation and forest canopies, and enters soils and streams it experiences a dynamic exchange of carbon constituents with the surrounding environment. Understanding the magnitude and dynamics of carbon export in above and below ground flow paths is critical for constraining the influence of terrestrial and aquatic ecosystems on global carbon cycling. Here we examine the concentration and flux of dissolved organic and inorganic carbon (DOC and DIC) in rainfall, throughfall, stemflow, overland flow, soil solution, groundwater, and stream water in an Amazonian transitional forest located near the arc of deforestation. Rainfall was enriched in DOC by interactions with atmospheric particles derived from both biogenic and anthropogenic emissions, resulting in a flux of 82.3 kg C ha^{-1} yr^{-1}, which was the largest flux from each respective flow path. Forest throughfall, stemflow, and direct overland flow mobilized DOC from products of terrestrial primary production and decomposition. Net throughfall represented the second largest DOC flux (68.4 kg C ha^{-1} yr^{-1}), whereas stemflow and overland flow only had a flux of 1.5 and 3.9 kg C ha^{-1} yr^{-1}, respectively. Much of the DOC in above ground flow paths was removed from solution as the rain percolated through soil layers due to both biological decomposition and sorption/desorption to mineral surfaces, resulting in low concentrations in stream and groundwater (2.6 ± 2.4 mg L^{-1} and 1.45 ± 0.3 mg L^{-1}, respectively) relative to throughfall (43.9 ± 5.2 mg L^{-1}) and stemflow (30.6 ± 2.7 mg L^{-1}). The flux of DIC in each respective flow path was generally lower than for DOC, and likely driven by atmospheric gas exchange and inputs from respiration and decomposition. DOC concentrations in above ground flow paths were highest during the first rainfall after a dry period, whereas DIC concentrations generally increased throughout the rainy season as soil moisture increased.

Keywords: tropical forest, carbon, organic, inorganic, flow path, flux, rainfall, terrestrial

OPEN ACCESS

Edited by:
Selvaraj Kandasamy, Xiamen University, China

Reviewed by:
Wei-Dong Zhai, Shandong University, China
K. Suresh Kumar, University of Allahabad, India

****Correspondence:***
Vania Neu
vania.neu@ufra.edu.br;
Nicholas D. Ward
nickdward@gmail.com

Specialty section:
This article was submitted to Marine Biogeochemistry, a section of the journal Frontiers in Marine Science

Received: *14 April 2016*
Accepted: *16 June 2016*
Published: *28 June 2016*

Citation:
Neu V, Ward ND, Krusche AV and Neill C (2016) Dissolved Organic and Inorganic Carbon Flow Paths in an Amazonian Transitional Forest. Front. Mar. Sci. 3:114. doi: 10.3389/fmars.2016.00114

INTRODUCTION

Carbon derived from the terrestrial biosphere is mobilized by rainfall into soils, streams, and groundwater through numerous pathways. Before hitting a forest canopy or uncovered ground, a raindrop interacts with organic carbon (OC) rich particles in the atmosphere (Artaxo et al., 1988; Talbot et al., 1990). This interaction results in the enhancement of dissolved organic carbon (DOC) concentrations in precipitation (Andreae et al., 1990; Artaxo et al., 2005; Waterloo et al., 2006; Germer et al., 2007). Precipitation drives a flux of OC from the atmosphere to the landscape

via dry deposition, atmosphere washing, and incorporation of aerosols in rain drop condensation nuclei (Artaxo et al., 2005). Rainfall receives additional inputs of carbon as it travels through forest canopies (e.g., throughfall) and down trunks and stems (e.g., stem flow); litterfall also provides a significant source of fresh OC as rainfall percolates through subsurface soil layers into streams and groundwater (Qualls et al., 2002).

Much of the OC flux described above is removed from the water while traveling through soil layers as a result of both sorptive and biodegradative processes, leaving stream and groundwater with low DOC concentrations relative to above ground flow paths (Qualls and Haines, 1992; Schmidt et al., 2011). Remineralization rates of OC in soils are high and may be enhanced by global climate change (Feng et al., 2008). OC derived from terrestrial primary production and dissolved inorganic carbon (DIC) derived from root and soil respiration is mobilized from soil layers into streams and groundwater reservoirs. Rivers and streams are typically supersaturated with respect to CO_2 as a result of direct inputs of DIC and remineralization of terrestrially-derived OC (Raymond et al., 1997; Richey et al., 2002; Mayorga et al., 2005; Ward et al., 2013). Inland waters emit 2.1 Pg C yr^{-1}, globally, of which 70% comes from the tropics and 25% from the Amazon River, alone (Raymond et al., 2013).

Carbon fluxes to both the atmosphere and ocean are generally higher in tropical regions relative to temperate and high-latitude counterparts (Aufdenkampe et al., 2011). Covering a region of over 6 million km^2, the highly productive Amazon basin plays a significant role in the global carbon cycle. The Amazon rainforest is responsible for roughly 10% of global terrestrial primary production and the Amazon River represents roughly 20% of the world's freshwater flux (Field et al., 1998; Malhi et al., 2008). The extensive basin contains regions with relatively little human perturbation, and regions highly impacted by deforestation and burning. The Amazon rainforest naturally produces large amounts of OC-rich aerosols through biogenic emissions that are eventually entrained in rainfall (Talbot et al., 1990). The size and morphology of these particles is highly diverse with origins from plant sources such as pollen grains, fungi, algae, and plant fragments (Artaxo et al., 1988).

Deforestation and biomass burning, along with other anthropogenic emissions, can also add aerosols to the atmosphere. For example, aerosol concentrations in Amazonian regions situated in the arc of deforestation have increased during recent years as a result in enhanced anthropogenic activities (Artaxo et al., 2005). Aerosol concentrations were generally highest during the dry season in these regions due to large amounts of grass and forest burning in addition to dust derived from agricultural and exposed soil sites (Artaxo et al., 2005). The majority of the carbon from these aerosols is transported from the atmosphere to the land at the beginning of the wet season, with rainfall DOC concentrations decreasing with additional precipitation (Filoso et al., 1999; Johnson et al., 2006a; Germer et al., 2007).

Throughfall is an important component of forest carbon cycling. The primary carbon input pathway is canopy washing. In the Amazon rainforest, throughfall has been observed to represent roughly 75–90% of total rainfall (Lloyd and Marques, 1988; Filoso et al., 1999; Ferreira et al., 2005). Stemflow generally has even higher DOC concentrations than rainfall and throughflow, but the total flux is low since stemflow only represents 2–8% of total rainfall in the Amazon (Jordan, 1978; Lloyd and Marques, 1988). Overland flow occurs either when rainfall occurs more rapidly than soil infiltration (Horton, 1933) or when soils are completely saturated (Linsley et al., 1975). Overland flow generally has greater DOC concentrations than throughfall and is transported rapidly. However, as with stemflow, overland flow is generally low compared to other flow paths in preserved forests, resulting in a relatively small overland DOC flux (Johnson et al., 2006a; Waterloo et al., 2006). In surface soils and organic matter layers DOC concentrations are generally high as a result of initial enrichment of throughfall and leaching of decomposing organic matter; soil solution concentrations typically decrease with soil depth as a result of mineral sorption and OC remineralization (McClain et al., 1997; Liu and Sheu, 2003). The removal of OC in soils leaves stream and ground water with low DOC concentrations relative to the preceding flow paths (Qualls et al., 2002; Liu and Sheu, 2003; Waterloo et al., 2006; Johnson et al., 2006a).

The objective of the present study is to determine the concentration and flux of DOC and DIC in each respective flow path: rainfall, throughfall, stemflow, overlandflow, soil solution, groundwater, and streamwater in an Amazonian forest. Water samples were collected monthly between February 2007 and January 2008 using a series of collectors designed for each flow path. The forest studied here is transitional between tropical rainforest and savanna, and is situated in the arc of deforestation in Brazil (**Figure 1**). In recent decades this region has lost large amounts of forested area due to deforestation and land use change.

METHODS

Study Site

The study was conducted at Tanguro Ranch in the southern Amazonian state of Mato Grosso, Brazil. Tanguro Ranch (12° 53′ S, 52° 21′ W) lies southeast of the Xingu Indigenous Park in the municipalities of Canarana and Querência at an elevation of ∼350 m above sea level in the upper region of the Xingu drainage basin between the Tanguro and Darro Rivers (**Figure 1**). Topography of the region consists of wide plains and gentle slopes to the waterways in a landscape with little other pronounced relief. It lies on a portion of the Brazilian Shield underlain by Precambrian Gneisses of the Xingu Complex. Soils consist of Oxisols (Haplustox/Latossolo vermelho-amarelo distrófico) on the broad, flat uplands away from the rivers. These soils have a water table depth of 12−15 m and no impeding layers. Throughout the year the water table depth varies by 0.27 m in the lowland and 1.07 m in the plateau. Wetter, and occasionally inundated, soils (Gleissols) of similar origin are found along the river margins (Projeto Radambrasil, 1981).

The pre-agricultural vegetation of the Tanguro region is evergreen tropical forest (Walter, 1979; Ivanauskas et al., 2004) typical of the transition from Cerrado to the central Amazon rainforest. The vegetation of this transition zone has lower species

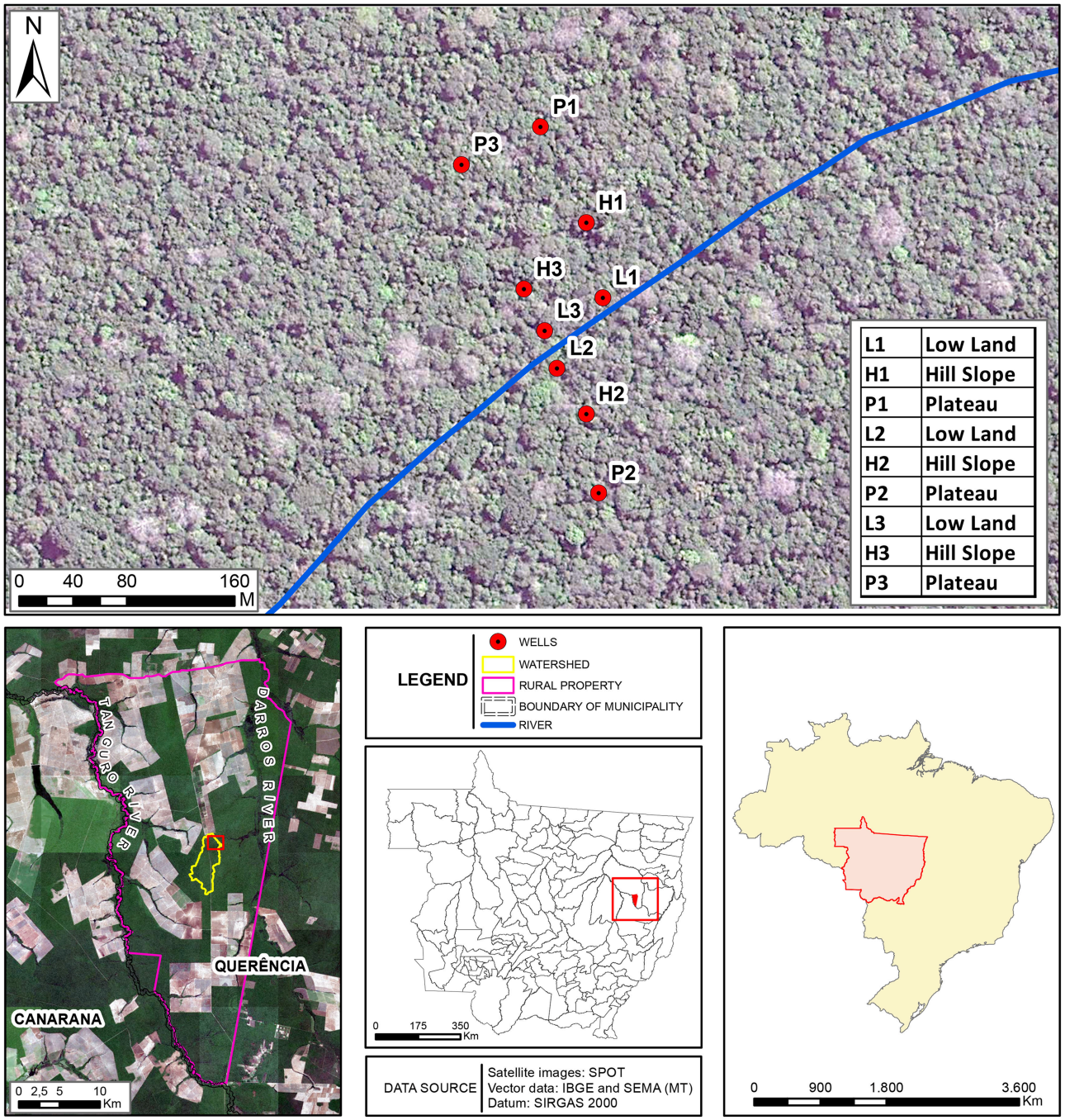

FIGURE 1 | Study site. Samples were collected in the Tanguro Ranch watershed in the Xingu drainage basin between the Tanguro and Darro Rivers.

diversity, smaller trees, and lower canopy heights compared to many previously studied Amazonian forests (Ivanauskas et al., 2004). The climate at Tanguro is humid tropical. Average annual precipitation from 1987 to 2007 was 1905 ± 271 mm and is strongly seasonal, with <5% of total annual precipitation falling between May and September (Vianello and Alves, 2002). June, July and August are the three driest months with typically less than 10 mm rain per month. Mean annual temperature is 25°C. During this study, hourly rainfall and rain intensity were recorded at a weather station 27 km south of the study boundaries. Daily rainfall was also measured in two collectors 2 and 5 km from the study site.

The completely forested watershed studied here covers an area of 13.20 km^2. The watershed is drained by a perennial first-order stream. Broad, flat plateaus typical of the region dominate the majority of the watershed's topography, which transitions into

a distinct shoulder hillslope zone and narrower/flatter lowland, near-stream zone. The watershed boundaries were delineated from Shuttle Mission Radar Topography data and validated with field measurements with a high-precision differential GPS (**Figure 1**). This watershed was divided into three parcels and nine sub-parcels. Each parcel lies along a topographic gradient, with three sub-parcels (lowland, hillside and plateau).

Sample Collection

Water samples were collected to assess the organic and inorganic carbon content of rainfall, throughfall, stemflow, overland flow, soil solution, groundwater, and streamwater between February 2007 and January 2008. Soil solution samples were collected with tension lysimeters on a monthly basis, however, soils were too dry to extract water from June to November. The lysimeter was rinsed with distilled water before use, and after installation the first collection was discarded. Tension lysimeters were installed at depths of 10, 50, 100, and 200 cm, in each sub-parcel (36 collectors total). Soil solution was collected from the lysimeters after setting the vacuum for 24 h at 0.6 bars. Samples were stored in acid-washed 250 mL glass bottles and sealed with silicone stoppers.

Overland flow samples were collected using 27 collectors installed along the nine sub-parcels (three collectors in each). The collectors consisted of a PVC pipe (200 cm wide with 15 cm diameter) that was closed in the two extremities with PVC caps. In one extremity the cap had a small opening connected to a reservoir (10 L capacity) to store the sample. The collectors have a transversal opening (3 × 190 cm), that allows the collection of water originating from overland flow. The collectors were inserted horizontally into the soil such that the opening of the collector was near the soil surface. Below the soil surface (3 cm), a small horizontal cut in the soil parallel to the collector was made in order to install a polystyrene plate (10 × 190 cm). This plate was fixed into the collector, and into the soil, making a connection between the soil and collector to permit the overland flow to enter the collector. The captivating area of each collector was delimited to 6 m^2 plots with wooden boards inserted into the soil. This was done to prevent the collection of water from areas uphill and lateral of each plot. The overland flow collectors were prepared for collection every 15 days by connecting the collector to the reservoir. Samples were collected from the reservoirs 1 day after each sampled rain event. The collectors were set to bypass the reservoir in between samplings, automatically discarding any water. During each sampling the volume of water collected in each collector was measured using a digital dynamometer (Insthutherm, Model DD-200).

Throughfall samples were collected biweekly with 27 collectors installed along the nine sub-parcels (three collectors in each). Collectors were dispersed randomly to avoid bias due to canopy density. The collector is a suspended channel made with a PVC pipe (150 cm wide with 15 cm diameter) that is closed on one end with PVC caps. The other end had a funnel connected to a reservoir (20 L capacity) to store the sample. The funnel was covered with plastic so as not to increase the capture area of water. The channel had a transversal opening (7 × 140 cm) in the direction of the tree's canopy. The captivating area of each collector was 980 cm^2. The collector was suspended 1 m above the soil surface. Rainfall was collected in the same type of collectors installed in triplicate in an open area.

Groundwater was collected every 15 days from nine wells in the watershed during the rainy season and monthly during the dry season. Screened groundwater wells made of 10 cm diameter PVC pipes were installed by hand at different depths depending on their position along the topographic gradient. Transversal cuts were made in the sides of the pipe 1.5 m from the bottom so that groundwater could flow in and out of the well. Lowland wells were between 1.69 and 2.14 m deep, hill slope wells were 4.84 to 6.25 m deep, and plateau wells were 7.07 to 9.65 m deep. Groundwater was collected with a manual collector, made with a PVC pipe (82 cm wide and 5 cm diameter) and a movable glass bottom. Roughly 3 L of water was removed prior to sample collection to insure that water that had most recently arrived at the well was collected.

Stemflow was collected along the catchment in three randomly located 10 × 10 m plots along the topographic gradient. In each plot collectors (48 total) were installed on trees with a diameter ≥5 cm. Polystyrene plates (2.5 cm wide) were fitted around the tree trunks in a downward spiral connected to a 20 L reservoir, starting 1.5 m above the forest floor, similar to the collectors described by Likens and Eaton (1970). To assess possible contamination from the collectors, plastic components of the collectors were immersed in deionized water for 3 days and the DOC was measured. There was no detectable organic contamination from the collectors.

Sample Analysis

The pH and conductivity of water samples was determined with Orion (model 250A) and Amber Science (model 2052) probes, respectively (Supplementary Tables 1–7). For DOC samples 30 mL of water was filtered through 0.7 μm pore size combusted GFF filters (Whatman) into combusted glass vials and preserved in the field with 75 mL of 6N HCl. DOC concentrations were measured on a Shimadzu total carbon analyzer (Model TOC-VCPH). For DIC samples 60 ml of water was filtered through 0.47 μm cellulose acetate membrane filters (Millipore) into acid-washed 60 mL HDPE bottles with no headspace to avoid degassing and preserved with thymol (100 mg/1000 ml of solution). DIC samples were analyzed for total organic carbon before acidification on a Shimadzu total carbon analyzer (Model TOC-VCPH). DIC samples were then acidified using 6N HCl and sparged to remove gas and reanalyzed for total organic carbon. DIC was calculated as the difference between non-acidified and acidified/sparged samples. This method may slightly underestimate DIC concentrations due to degassing during filtration. However, this method has been compared to DIC calculations from CO_2 values and the variation is typically minimal, whereas alkalinity titrations result in high amounts of error in DOC-rich acidic waters (Neu et al., 2011). Samples were stored in the dark at room temperature for roughly 1 week prior to analysis. Samples could not be kept cold since there was no electricity available at the field site.

Rainfall and Stream Discharge

Hourly rainfall and rain intensity was recorded at the Tanguro Ranch weather station 27 km south of the sampling location. Daily rainfall was also recorded in two collectors roughly 2 km from the watershed sampling point. Stream stage was recorded every 15 min from May to August 2007 with an ISCO 6200 automatic sampler equipped with a pressure transducer module. From August 2007 to August 2008 stream stage was recorded hourly with an Onset water level logger. A rating curve was developed by periodic measurements of stream discharge with a Global Water FP-101 current meter across a range of stream flows. Hourly stream flows for January to May 2007 were estimated from daily rainfall and rainfall-stream flow relationships from the same location derived from the 16-month stream flow record that began in May.

Flux Estimates

We estimated total annual DOC and DIC fluxes in throughfall based on our record of rainfall and intensity from Tanguro Ranch, measured DOC and DIC concentrations from the sampled rain events, extrapolated DOC and DIC concentrations for non-sampled events, and an estimate of canopy interception for a tropical forest. Precipitation during sampled events ($n = 10$) ranged from 0 to 115 mm and unsampled events ($n = 51$) ranged from 0 to 75 mm. We assumed that throughfall was on average 85% of precipitation (Lloyd and Marques, 1988; Filoso et al., 1999; Ferreira et al., 2005) to calculate total througfall volume duirng unsampled events. Average DOC and DIC concentrations from sampled events were used to estimate concentrations during unsampled events with similar amounts of precipitiation.

We estimated water volumes for stemflow during unsampled events from relationships of measured volumes (in mm) between throughfall and stemflow (**Figure 2A**):

$$SF = 6.35 \times 10^{-5} (TF)^2 + 0.0063 (TF) - 0.0252;\ r^2 = 0.86 \quad (1)$$

where SF is stemflow and TF is throughfall. Likewise, overland flow (OF) was calculated based on the following relationship between overland flow and throughlow (**Figure 2B**):

$$OF = 0.0116(TF) + 0.0383;\ r^2 = 0.84 \quad (2)$$

We then used these calculated volumes and mothly mean DOC concentrations in stemflow and overland flow from the nearest sampled event to calculate DOC fluxes for each unsampled event. We then summed DOC fluxes for all sampled and unsampled events to obtain an annual flux.

Statistical Analysis

The results were submitted to analysis of variance and subsequently Tukey median comparison test for the variables with statistically significant differences, using the GLM (General Linear Models) procedure, using SAS 9.1 software (Statistical Analysis System). The tests were considered significantly different for $p < 0.05$.

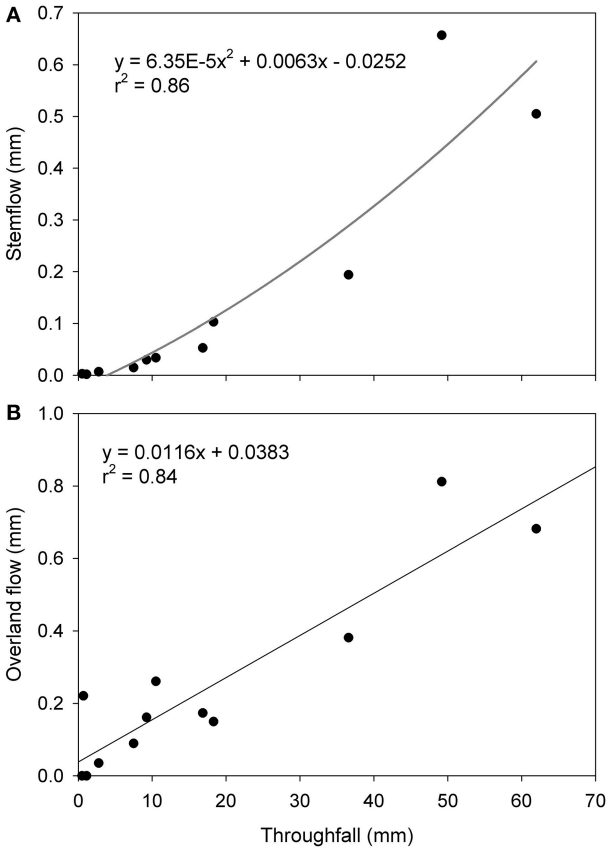

FIGURE 2 | Correlation between throughfall, stemflow, and overland flow. The correlation between throughfall and stemflow **(A)** and throughfall and overland flow **(B)** was used to calculate stemflow and overland flow for unsampled events.

RESULTS

Precipitation and Stream Discharge

Precipitation in 2007 totaled 1641 mm and was lower than the 1987–2007 mean of 1905 mm. The greatest difference between measured and historical mean precipitation occurred in March 2007 when precipitation totaled 34 mm in contrast to the long-term monthly average of 250 mm (**Figure 3**). Total precipitation from February 2007 to January 2008 was 1829 mm, of which roughly 476 mm occurred during times of sample collection. Precipitation and stream discharge were maximal from October to April. Annual average stream discharge was 17.9 ± 3.6 L s^{-1} (**Table 1**). Stream discharge throughout the year was primarily dominated by base flow (**Figure 3**).

Dissolved Organic Carbon

Concentrations of DOC showed the highest seasonal variation in above-ground flow paths (e.g., rainfall, throughfall, stemflow, and overland flow). The concentration of DOC in rainfall was highest at the beginning of the rainy season, reaching a maximum of 15.6 ± 0.3 mg C L^{-1} during the October 18, 2007 event, and declined throughout the rainy season, reaching a minimum of 3.3 ±

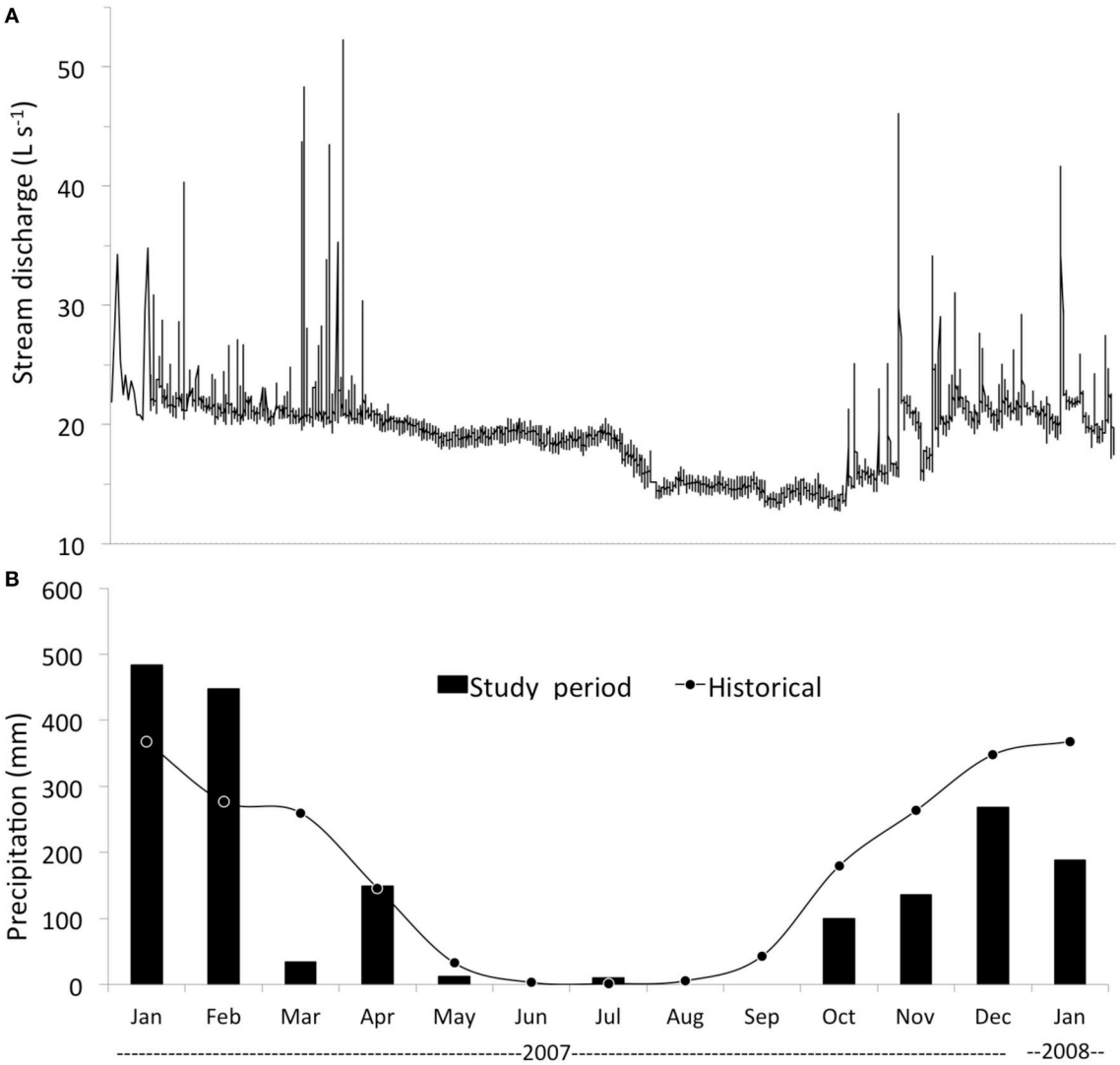

FIGURE 3 | Precipitation and discharge. Measurements of **(A)** Stream discharge and **(B)** historic average monthly precipitation (circles) and precipitation during the sampled rain events (bars) from January 2007 to January 2008.

0.2 mg C L^{-1} (**Figure 4**). The annual average DOC concentration in rainfall was 6.7 ± 3.7 mg C L^{-1} (**Table 1**). The concentration of DOC in throughfall was highest at the end of the dry season during the September 2007 rain event (126 ± 68 mg C L^{-1}), and declined throughout the rainy season. In April 2007, after a brief dry period the throughfall DOC concentrations increased from 35.7 ± 20.0 mg C L^{-1} during the March 2007 sampling to 77.5 ± 28.7 mg C L^{-1} (**Figure 4**). The annual average throughfall DOC concentration for lowland, hillside and plateau sub-parcels was 47.8 ± 6.5, 41.9 ± 4.6, and 42 ± 4.4 mg C L^{-1}, respectively, showing minimal variation between the different topographic regimes ($p = 0.66$).

Stemflow DOC concentrations varied both seasonally and as a function of tree diversity and the stem surface. In particular, stem rugosity and the presence or lack of epiphytes had a large influence on stemflow DOC in this study. The following species, characterized by a rugose bark and/or lichens on the stem, represent the majority of the trees sampled for stemflow and provided the greatest amount of DOC enrichment: *Amaioua guianensis* (bark with fissures and lichens), *Trattinickia burseraefolia* (bark with lichens), *Hirtelar bicornis, Trattinickia glaziovii, Xylopia amazonica, Miconia punctate, Pseudolmedia murure,* and *Miconia pyrifolia* (rugose bark and lichens on the stem). The following species, characterized by a smooth bark, were a minor fraction of the trees sampled and generally had low stemflow DOC concentrations: *Licania egleri, Protium guianense, Protium unifoliolatum, Vochysia vismifolia,* and *Envira cana*. As with rainfall DOC, stemflow DOC concentrations were highest at the beginning of the rainy season, reaching a maximum of 87.7 ± 53 mg C L^{-1} during the October 16, 2007 sampling, and steadily decreased throughout the rainy season (**Figure 4**). Annual average stemflow DOC concentrations in lowland, hillside and

TABLE 1 | Average concentrations and annual fluxes of DOC, DIC, and water across the topographic gradient.

Input/Flowpaths		DOC Concentration (mg C L^{-1})	DOC Flux Kg C ha^{-1} yr^{-1}	DIC Concentration (mg C L^{-1})	DIC Flux Kg C ha^{-1} yr^{-1}	[a]Water flux (mm yr^{-1})	Stream discharge (L s^{-1})
Rainfall		6.7 ± 3.7	82.4 ± 18.4	0.8 ± 0.7	38.8 ± 4.4	1403.1	–
[b]Throughfall	Lowland	47.8 ± 6.5	150.8 ± 75.6	2.5 ± 2.3	16.6 ± 8.2	1039.7	–
	Hillside	41.9 ± 4.6					
	Plateau	42.0 ± 4.4					
Stemflow	Lowland	31.7 ± 3.09	1.5 ± 0.8	1.5 ± 1.1	0.6 ± 0.1	14	–
	Hillside	32.5 ± 3.34					
	Plateau	27.6 ± 1.6					
Overlandflow	Lowland	57.2 ± 10.6	3.9 ± 1.6	1.3 ± 1.3	0.1 ± 0.1	7.3	–
	Hillside	39.6 ± 7.0					
	Plateau	40.9 ± 5.7					
[c]Soil Solution	Lowland	15.5 ± 0.9	–	7.7 ± 1.3	–	–	–
	Hillside	16.0 ± 1.4	–	7.1 ± 1.3	–	–	–
	Plateau	15.6 ± 1.36	–	6.7 ± 1.3	–	–	–
Groundwater	Lowland	2.0 ± 0.5	–	2.7 ± 0.3	–	–	–
	Hillside	1.4 ± 0.3	–	2.7 ± 0.3	–	–	–
	Plateau	1.0 ± 0.2	–	3.7 ± 0.4	–	–	–
Stream		2.9 ± 3.5	1.7 ± 0.2	2.0 ± 1.8	0.9 ± 0.2	–	17.9 ± 3.6

[a]*Water fluxes measured during the sampling period from February 15, 2007 to January 25, 2008.*
[b]*Values represent the gross throughfall DOC/DIC contribution (e.g., the sum of rainfall and net throughfall).*
[c]*Values represent the average of 10, 50, 100, and 200 cm lysimeter depths.*

plateau sub-parcels were 31.7 ± 3.09, 32.5 ± 3.3, and 27.6 ± 1.6 mg C L^{-1}, respectively. Whereas lowland and hillside parcels had similar stemflow DOC concentrations, concentrations in plateau parcels were generally lower ($p < 0.05$).

Overland flow did not occur in events with low precipitation (e.g., March and April 2007 samplings, with 5 and 6 mm of precipitation, respectively). Lowland parcels had the highest overland flow volume compared to the oxisoils of the hillside and plateau parcels. Compared to the other above-ground flow paths, overland flow had the highest DOC concentrations. As with other above-ground flow paths, overland flow DOC concentrations were highest at the beginning of the rainy season, reaching a maximum of 160 ± 110 mg C L^{-1} during the October 16, 2007 sampling. Annual average overland flow DOC concentrations in lowland, hillside and plateau sub-parcels were 57.2 ± 10.6, 39.6 ± 7.0, and 40.9 ± 5.7 mg C L^{-1}, respectively. Concentrations did not vary significantly along the elevation gradient ($p = 0.25$). Although overland flow had the greatest DOC concentrations, this flow path represented a small fraction of the total water flow.

In contrast to the high DOC concentrations observed above-ground, below-ground DOC concentrations were generally lower. Soil solution DOC concentrations were highest at 10 cm depth, with an average of 17.7 ± 2.0 mg C L^{-1} and decreased to 11.9 ± 1.0 mg L^{-1}, 16.4 ± 1.5 mg L^{-1}, and 14.9 ± 1.3 mg C L^{-1} at depths of 50, 100, and 200 cm depths, respectively. Differences with depth were statistically significant ($p < 0.05$), whereas there was little variation along the topographic gradient ($p = 0.33$). It was not possible to extract soil solution samples during the long dry season and at the beginning of the rainy season with the methodology used here, however, as with the above-ground flow paths, soil solution DOC concentrations appeared to peak and decrease throughout the rainy season (**Figure 4**). The highest observed soil solution DOC concentrations occurred during the December 2007 event, with a value of 24.6 ± 17 mg C L^{-1}. Litterfall typically accumulates and decomposes above ground during the dry season. Above ground flow paths transport DOC rich waters to the sub-surface, particularly during the first several periods of rainfall in a season.

Groundwater generally had the lowest concentration of DOC, and contrary to other flow paths, the highest values were observed during the dry season. The maximum groundwater DOC concentration was 4.9 ± 4.0 mg C L^{-1} during August 2007. Annual average concentrations of groundwater DOC in lowland, hillside, and plateau sub-parcels were 2.0 ± 0.5, 1.4 ± 0.3, and 1.0 ± 0.2 mg C L^{-1}, respectively, with little variation across the topographic gradient (**Table 1**; $p = 0.19$). However, the lowlands had the highest carbon stock in the soil profile (119 Mg C ha^{-1} at 140 cm depth) compared to hillside (119 Mg C ha^{-1}) and plateau (105 Mg C ha^{-1}) sub-parcels. Stream flow also had low DOC concentrations relative to the different flow paths, with an annual average concentration of 2.9 ± 3.5 mg C L^{-1} (**Table 1**). Stream DOC concentrations reached a maximum of 15.8 ± 0.2 mg L^{-1}

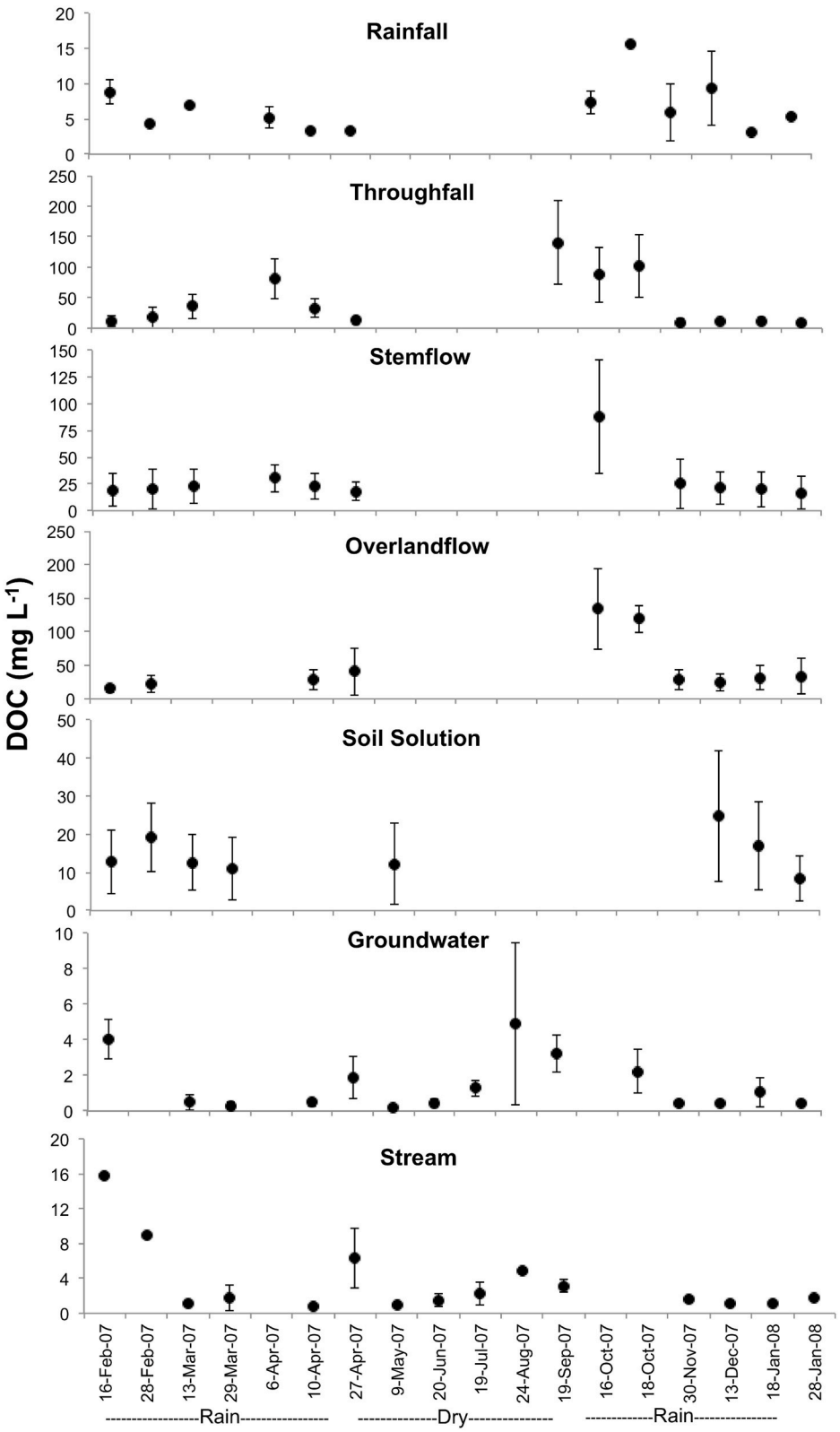

FIGURE 4 | Monthly DOC concentrations. Monthly measurements of the concentration of DOC in rainfall, throughfall, stemflow, overland flow, soil solution, groundwater, and stream water during rain events from February 2007 to January 2008.

during the February 16, 2007 sampling when discharge was high, and decreased throughout the rainy season.

Based on the above measurements, the annual DOC flux in the watershed was estimated to be 82.4 ± 18.4 kg C ha^{-1} yr^{-1} for rainfall (**Table 1**). The gross flux of DOC for throughfall was 142.6 ± 75.6 kg C ha^{-1} yr^{-1}, or 60.2 ± 77.8 kg C ha^{-1} yr^{-1} for net throughfall (i.e., the difference between gross throughfall and rainfall fluxes). DOC fluxes for stemflow, overland flow, and stream flow were 1.5 ± 0.8, 3.9 ± 1.6 and 1.7 ± 0.2 kg C ha^{-1} yr^{-1}, respectively (**Table 1**). It is important to note that the fluxes estimated for overland flow do not represent the actual flux to the stream, *per se*, since it is possible that the water collected with our methods could have potentially infiltrated less saturated soils further downslope before reaching the stream.

Dissolved Inorganic Carbon

Above-ground flow paths (e.g., rainfall, throughfall, stemflow, and overland flow) had relatively low DIC concentrations in contrast to the high DOC concentrations observed in these flow paths. The concentration of DIC in rainfall reached a maximum of 1.5 mg C L^{-1} during the February 28, 2007 sampling (**Figure 5**), with an annual average of 0.8 ± 0.7 mg C L^{-1} (**Table 1**). Throughfall DIC concentrations were generally highest near the end of the rainy season, with a maximum value of 4.5 ± 2.4 mg C L^{-1} during the April 6, 2007 sampling period. The annual average throughfall DIC concentration was 2.5 ± 2.3 mg C L^{-1}. Stemflow DIC concentrations increased at the beginning of the rainy period, reaching a maximum of 6.7 ± 3.2 mg C L^{-1} during the October 16, 2007 sampling period. The annual average DIC concentration in stemflow was 1.5 ± 1.1 mg C L^{-1}. Overland flow DIC concentrations reached a maximum of 2.4 ± 0.3 mg C L^{-1} during the February 6, 2007 sampling period, and had annual average of 1.3 ± 1.3 mg C L^{-1} (**Table 1**). The concentration of DIC in each of these above-ground flow paths did not significantly vary between lowland, hillside and plateau sub-parcels.

In contrast to observations of above-ground flow paths, below-ground flow paths had relatively high DIC concentrations that were above atmospheric CO_2 saturation levels. Soil solution DIC generally increased with soil depth, indicating CO_2 accumulation along the profile. Soil solution DIC did not vary significantly among the different sites ($p = 0.33$). The annual average soil solution DIC concentration was 3.2 ± 1.2 mg C L^{-1} at 10 cm depth, 2.9 ± 0.5 mg C L^{-1} at 50 cm depth, 6.3 ± 1.1 mg C L^{-1} at 100 cm depth, and 11.9 ± 1.6 mg C L^{-1} at 200 cm depth. Soil solution DIC concentrations were maximal during the February 16, 2007 sampling period with a value of 14.2 ± 13.9 mg C L^{-1}. In groundwater the annual average concentration of DIC in lowland, hillside and plateau sub-parcels was 2.7 ± 0.3, 2.7 ± 0.3, and 3.7 ± 0.4 mg C L^{-1}, respectively, differing along the topographic gradient, with the highest concentrations observed in plateau sub-parcels. Groundwater DIC concentrations reached a maximum of 8.7 ± 2.1 mg C L^{-1} during the March 13, 2007 sampling period (**Figure 5**). The annual average DIC concentration in stream flow was 1.6 ± 1.0 mg C L^{-1}, with a maximum of 6.5 mg L^{-1} observed during the March 13, 2007 sampling period.

The annual flux of DIC through above-ground flow paths was significantly lower than DOC fluxes ($p < 0.05$). Based on the above measurements, the annual DIC flux in the watershed was estimated to be 38.8 ± 4.4 kg C ha^{-1} yr^{-1} for rainfall. The DIC flux for gross throughfall was 16.6 ± 8.2 kg C ha^{-1} yr^{-1} resulting in a net throughfall flux of 22.2 ± 9.3 kg C ha^{-1} yr^{-1}. Stemflow, overland flow, and stream flow had DIC fluxes 0.6 ± 0.1, 0.1 ± 0.1, and 0.9 ± 0.2 kg C ha^{-1} yr^{-1}, respectively (**Table 1**).

DISCUSSION

Dissolved Organic Carbon

The concentration of DOC in rainfall was highest during the first large rainfall events after a long dry period and decreased throughout the wet season. This phenomenon is most likely a result of the accumulation of carbon-rich particulate material in the atmosphere during periods with minimal rainfall. This particulate material can be "washed" from the atmosphere during rainfall events (Greenfield, 1957) and a fraction of the particulate organic matter is solubilized into the dissolved phase in raindrops (Monteith et al., 2007). The atmospheric particulate material can be derived from a variety of natural and anthropogenic origins including aeolian transport, agricultural activities, and biomass burning (Ketseridis et al., 1976; Simoneit and Elias, 2000; Pio et al., 2001; Snyder et al., 2009). As with similar studies, our results indicate that the source of rainfall DOC that accumulates during dry periods is depleted during subsequent rainfall events, resulting in a decrease in rainfall DOC concentrations throughout the wet season (Filoso et al., 1999; Johnson et al., 2006a; Germer et al., 2007). Rainfall DOC fluxes in other regions studied in the Central Amazon were generally lower than our estimates. For example, rainfall fluxes in the Rio Negro region were roughly three times lower than the fluxes measured here (**Table 2**). Compared to the Xingu basin studied here, the Central Amazon generally experiences greater annual precipitation and is less impacted by deforestation and land use change (Andreae et al., 1990; Filoso et al., 1999; Waterloo et al., 2006). Rainfall DOC fluxes exceeding estimates made here were observed in other Amazonian regions that are highly influenced by biomass burning and land use alterations. For example a rainfall DOC flux of 106.5 kg ha^{-1} yr^{-1} was observed in Rondonia, Brazil, a site that is strongly affected by burning and land use alteration (**Table 2**; Artaxo et al., 2005; Germer et al., 2007).

As rainfall drains through the forest canopy, the throughfall becomes enhanced with DOC derived from leaf and plant surfaces, surficial decomposition processes, and animal excrement (Parker, 1983; Levia and Frost, 2003). Similar to rainfall, the enrichment of throughfall DOC was greatest during the first large rain events following a long dry period (**Figure 4**). Throughfall DOC concentrations dropped after subsequent rain events. Similar to the accumulation of carbon-rich particles in the atmosphere, organic carbon can accumulate on surfaces of the forest canopy during dry periods and be subsequently mobilized by throughfall during rain events. We not only observed enhanced throughfall DOC concentrations after a long dry season, but also after a month of dry weather from

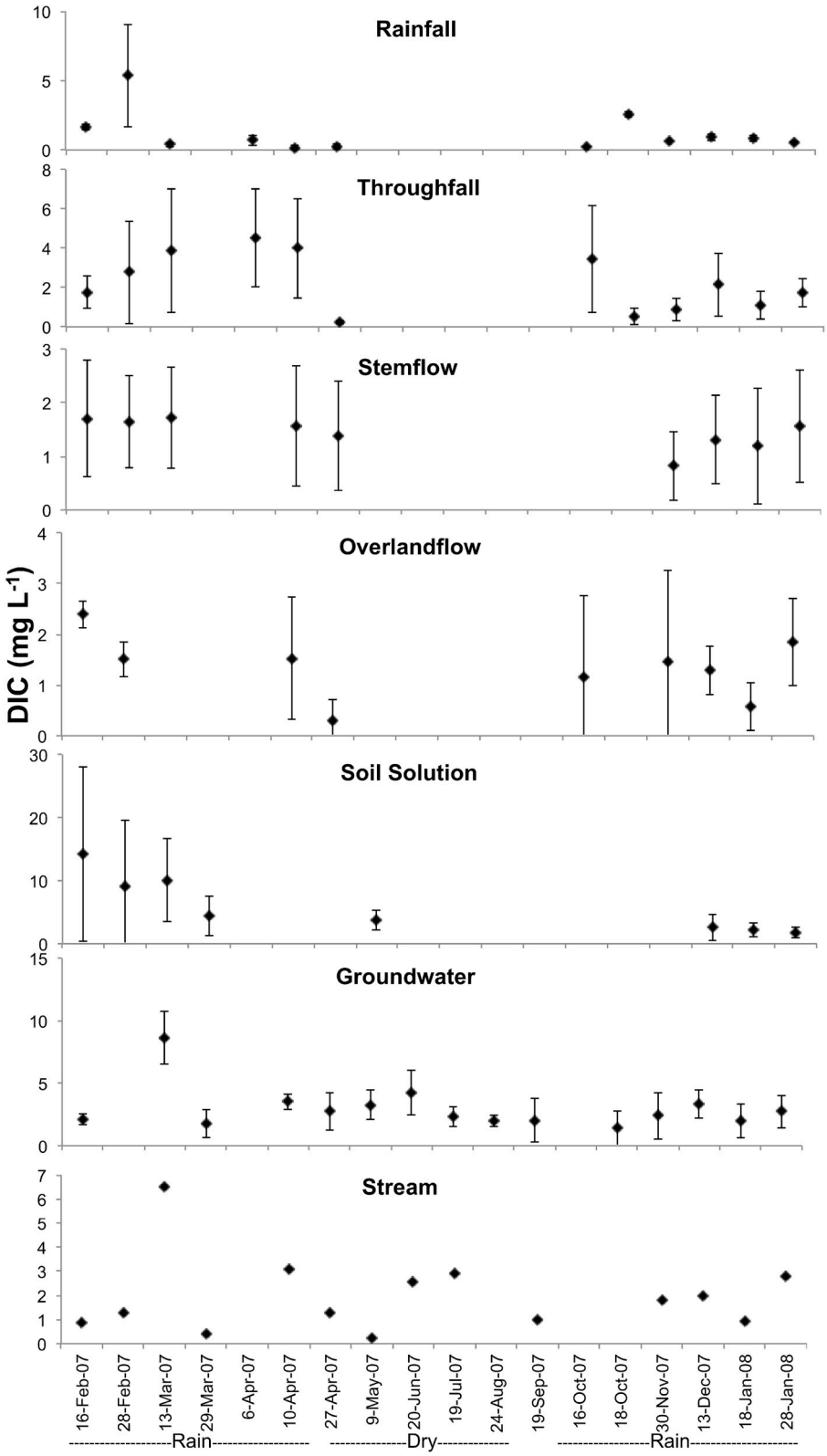

FIGURE 5 | Monthly DIC concentrations. Monthly measurements of the concentration of DIC in rainfall, throughfall, stemflow, overland flow, soil solution, groundwater, and stream water during rain events from February 2007 to January 2008.

TABLE 2 | Annual DOC fluxes for rainfall, throughfall, net throughfall, stemflow, and overland flow in the Amazon basin.

Study Location	Annual DOC flux (kg ha^{-1} yr^{-1})						References
	Rainfall	Throughfall	Net Throughfall	Stemflow	Overland Flow	Stream	
Canarana, MT	82.4	150.8	68.4	1.5	3.9	1.7	This study
Rondonia, RO	106.4	301.6	195.1	–	–	–	Germer et al., 2007
Juruena, MT	–	–	–	–	–	31.5	Johnson et al., 2006a
Paragominas, PA	123.4	149.0	–	–	–	4.1	Markewitz et al., 2004
Rio Negro, AM	27.5	190.0	–	–	–	–	Filoso et al., 1999

March to April 2007 (**Figures 2**, **3**). These results illustrate the importance of atmospheric deposition and forest metabolism on throughfall organic carbon content. Rainfall DOC, on the other hand, was elevated during the March 2007 sampling, and once again depleted by the April 2007 samplings, illustrating that the accumulation and solubilization of atmospheric particulates with rainfall may, in some cases, occur more quickly than the accumulation of OC in the forest canopy and mobilization by throughfall. This is likely because throughfall DOC originates from a range of sources including atmospheric particles and surficial processes and characteristics. A similar magnitude of DOC in throughfall (96.1 ± 68.0 mg C L^{-1}) was observed during the first rain after a long dry period in other Amazonian forests (Johnson et al., 2006a).

Stemflow and overland flow both had seasonal trends similar to throughfall (i.e., maximal DOC after the first rain event following a dry period). Stemflow generally represents a relatively minor flux of carbon. For example, here we measured an average DOC flux in stem flow of only 1.5 ± 1.1 kg C ha^{-1} yr^{-1}, roughly an order of magnitude less than the throughflow and rainfall fluxes (**Table 1**; **Figure 6**). Stemflow is primarily controlled by tree diameter, bark rugosity, epiphyte presence, and the forest ground flora biodiversity (Dalva and Moore, 1991; Liu and Sheu, 2003; Wang et al., 2004; Johnson and Lehmann, 2006). For example, forests with extensive palm undergrowth generally have increased stemflow due to enhanced water collection and dispersal by the large palm leaves (Lloyd and Marques, 1988; Germer et al., 2007). In this study, stemflow was largely influenced by bark rugosity and the presence of epiphytes, with much higher stemflow DOC concentrations observed in trees with rugose bark and lichen coverage than trees with a smooth bark. Surface complexities such as these can allow enhanced accumulation of organic matter both from production and decomposition processes.

Lowland and hillside sub-parcels generally contained greater coverage of stem epiphytes and higher stemflow DOC concentrations than plateau sites. The lowland and hillside parcels were in close proximity to the stream, resulting in enhanced air humidity and epiphyte production, whereas plateau sites were more exposed to wind and further from the stream. Although stemflow DOC concentrations were higher in lowland and hillside parcels, the DOC flux was greatest in plateau sites, which had a larger proportion of trees with a diameter at breast height >5 cm than lowland and hillside parcels (**Table 1**). The larger diameter trees provide a greater surface area for water to flow and organic carbon to solubilize (Dalva and Moore, 1991). Similar to our observations that stemflow represents a small DOC flux relative to total rainfall, other studies in the Amazon have shown that stemflow represents from roughly 2% (Lloyd and Marques, 1988) to 7–8% (Jordan, 1978) of the total rainfall. Although the stemflow DOC concentrations measured here and elsewhere were relatively high, the volume of water comprising stem flow was low, resulting in a relatively small DOC flux (Dalva and Moore, 1991; Hinton et al., 1998).

Overland flow was generally low throughout the study period. The forest soils were characterized by high clay content and aggregate stability, allowing a high degree of infiltration (Brandão, 2006). There was no overland flow present during rain events with less than 6 mm of precipitation. Overland flow was generally highest in the lowland sub-parcels since the riparian zone was primarily composed of saturated gleysols. These soils are generally slow draining and sloped toward the stream channel (Deckers et al., 1998). The highest concentrations and fluxes of DOC in overland flow were observed in the lowland sites (**Table 1**), most likely because, relative to plateau and hillside sites, higher levels of soil saturation allow a greater volume of water to be in contact with litter layers. The overland DOC flux from plateau and hillside sites, on the other hand, was low relative to other flow paths due to the soil type and relief characteristics. Overland flow represents a rapid pathway for carbon transport, and often contains the highest concentration of DOC relative to other flowpaths in regions with highly saturated soils, however the overland DOC flux is generally low because overland flow represents a relatively small fraction of total water flow (Johnson et al., 2006a; **Table 1**). As with other above ground flow paths, overland flow DOC concentrations were highest during the first rainfall following a long dry period (**Figure 4**).

A large amount of the DOC that enters soils as throughfall/stemflow is removed as it travels through soils into streams (Qualls et al., 2002; Liu and Sheu, 2003). For example, in the temperate Appalachian mountains, roughly 95% of the DOC in throughfall was lost in soils prior to entering streams; roughly 10–33% of this DOC loss was attributed to biodegradation, while the remaining DOC was hypothesized to be removed by mineral sorption (Qualls and Haines, 1992). In this study, soil surface layers generally had high DOC concentrations, which decreased with soil depth. Groundwater had much lower DOC concentrations than the preceding flow paths during the rainy season, similar to other observations in the

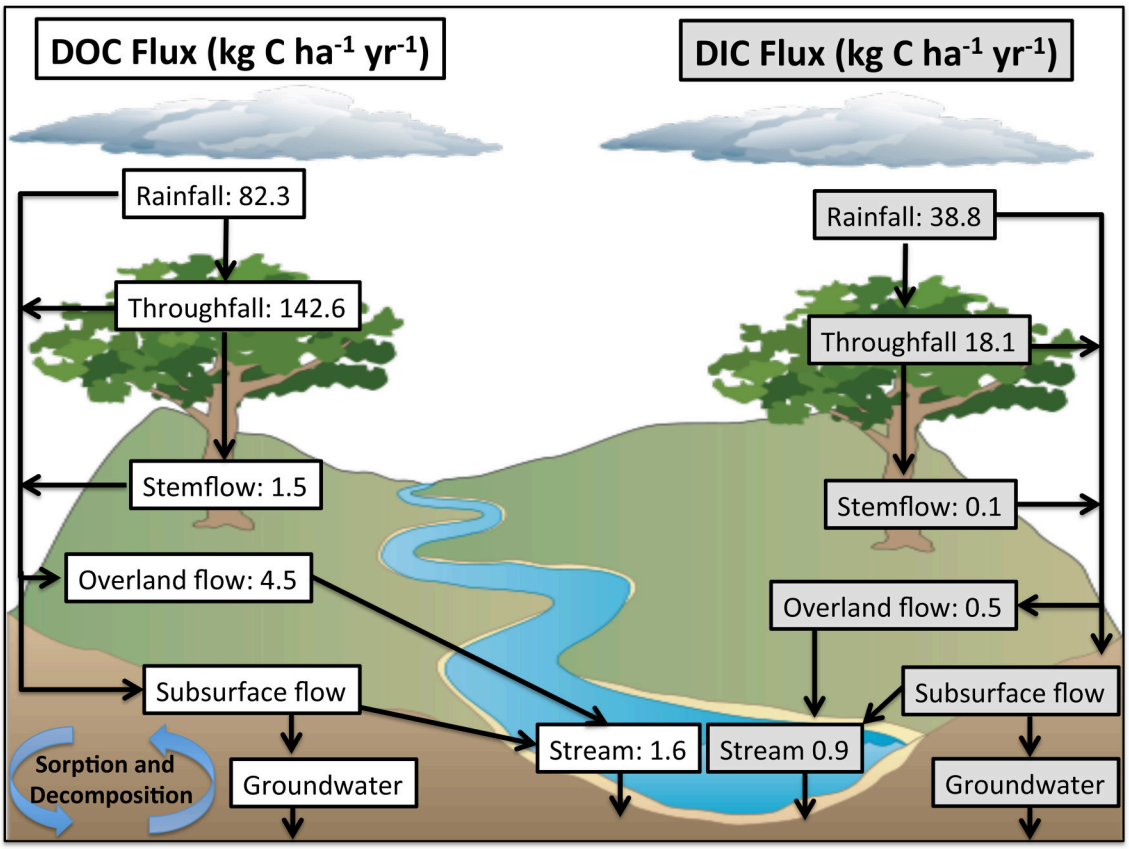

FIGURE 6 | Annual DOC and DIC fluxes. The average annual flux of DOC and DIC in rainfall, throughfall, stemflow, overland flow, and stream flow in the Tanguro Ranch watershed.

Amazon basin (Johnson et al., 2006a). Contrary to above-ground flow paths, groundwater DOC concentrations were highest during dry periods (**Figure 4**), indicating that groundwater DOC is primarily mobilized by baseflow and, perhaps, diluted by rapid rainfall. As rainfall percolates through subsoil layers, sorption of molecules onto iron and aluminum-rich mineral surfaces can remove a large fraction of the DOC. Sorption generally occurs rapidly relative to decomposition processes (McClain et al., 1997; Qualls et al., 2002; Liu and Sheu, 2003; Johnson et al., 2006a). Microbial degradation of OC in soils is another important pathway for DOC loss, and has potential to be enhanced by a warming climate (Feng et al., 2008). An emerging view is that the degree of OC decomposition in litterfall and soils is largely a component of environmental and biological conditions rather than intrinsic molecular properties (Schmidt et al., 2011).

Concentrations of DOC in the stream were a similar magnitude as in groundwater, on average, but increased during heavy rainfall after a dry period (e.g., February 2007). This is similar to other observations of DOC concentrations in temperate and tropical settings made during brief storm periods. For example, high frequency measurements have illustrated a strong correlation between stream discharge and DOC concentrations during rapid rain events (Boyer et al., 1997; Hinton et al., 1998; Buffam et al., 2001; Ward et al., 2012). These types of rapid loading events have been estimated to contribute to as much as 86% of annual OC export in temperate forested watersheds (Raymond and Saiers, 2010) and 71–85% of OC export in temperate agricultural watersheds (Dalzell et al., 2007). Similar to our observations of accumulation and mobilization of DOC in above ground flow paths, others have observed a seasonal accumulation of OC in surface soil and litter layers, which is mobilized at the beginning of the wet season (Buffam et al., 2001; Raymond and Saiers, 2010; Ward et al., 2012). In addition to enhanced concentrations, it has been observed in both temperate and high-latitude river systems that OC biodegradability can increases with peak discharge during rain events (Buffam et al., 2001; Fellman et al., 2009). Although we observed enhanced DOC concentrations during periods of increasing discharge, rapid loading events were not as important with regards to annual stream DOC fluxes as in the cases described above because stream flow was largely dominated by baseflow (**Figure 3**). In our study site, stream flow was low relative to the amount of precipitation, likely as a result of high evapotranspiration rates (not measured here). As a result, the estimated stream DOC flux of 1.6 kg C $ha^{-1}yr^{-1}$ was considerably lower than in other Amazonian

streams (**Table 2**). The flux of DOC in other Amazonian streams has been shown to be as high as 31.5 kg C $ha^{-1}yr^{-1}$ for white water streams and 190 kg C $ha^{-1}yr^{-1}$ for black water streams (Johnson et al., 2006a). Stream flow DOC fluxes are generally lower in subtropical forests, ranging from 4.1 kg C $ha^{-1}yr^{-1}$ (Qualls et al., 2002) to 25 kg C $ha^{-1}yr^{-1}$ (Liu and Sheu, 2003).

Dissolved Inorganic Carbon

Contrary to the relatively high levels of DOC in above ground compartments, the concentration of DIC was generally lowest in above-ground flow paths. Similar to other observations, above-ground DIC concentrations were generally near atmospheric CO_2 saturation (Johnson et al., 2006b). The highest DIC concentrations were observed in the soil solution and groundwater. DIC concentrations generally increased throughout the rainy season for each respective flow path (**Figure 5**). In contrast to DOC concentrations, above-ground DIC concentrations progressively increased throughout the wet season (**Figures 3**, **4**). The observed increase in soil solution DIC with precipitation is likely a result of enhanced biological decomposition and root respiration with increasing soil moisture. Soil solution DIC likely increased with soil depth since biological CO_2 production is rapid relative to atmospheric gas exchange (Bekele et al., 2007). Plateau parcels had higher DIC concentrations at 200 cm depth (3.7 ± 0.4 mg C L^{-1}) than hillside and lowland parcels (2.7 ± 0.3 mg C L^{-1}) likely due to a combination of relatively thicker soil layers that inhibit gas exchange and less soil moisture in plateau parcels.

Root respiration and remineralization of organic matter to CO_2 are the primary sources of DIC in soils and subsequent transport to groundwater reservoirs (Hope et al., 2004; Johnson et al., 2006b). Environmental conditions such as soil moisture/temperature, abiotic processes such as mineral sorption/desorption, and biological community composition/activity all influence rates of OC decomposition in soils (Schmidt et al., 2011). The fuels for OC remineralization range from simple substrates (e.g., carbohydrates) to molecularly complex compounds such as lignin macromolecules (Otto and Simpson, 2006; Feng et al., 2008; Kuzyakov, 2010; Thevenot et al., 2010). A similar range of organic carbon fuels are decomposed and remineralized to CO_2 in streams and river channels (Benner et al., 1986, 1995; Mayorga et al., 2005; Ward et al., 2013). Photo-oxidative processes represent an additional pathway for remineralization of OC to CO_2 in stream waters, and in some circumstances may enhance biological degradation rates (Hernes and Benner, 2003; Rodríguez-Zuniga et al., 2008; Spencer et al., 2009). Stream DIC concentrations were generally lower than in soil solution and groundwater because gas exchange occurs more rapidly in the aquatic environment (Hope et al., 2004; Johnson et al., 2006b).

CONCLUDING REMARKS

Understanding the magnitude and dynamics of carbon export in above and below ground flow paths is critical for constraining the influence of terrestrial and aquatic ecosystems on global carbon cycling. The evolution of carbon constituents along the continuum of terrestrial landscapes, inland waters, and ultimately the ocean is potentially largely dependent on initial interactions of raindrops with the surrounding environment. The results of this study illustrate the seasonality of carbon concentrations in above and below ground flow paths in tropical forests. Calculating a complete watershed carbon budget is logistically difficult, and, as such, flux estimates made here and elsewhere contain large uncertainties and methodological caveats that should be considered when making global comparisons. The flow paths examined here represent spatially-heterogeneous and rapid conduits, and as such, should be examined with increasingly high spatiotemporal resolution in order to fully unravel the complex underlying processes and inherent variability.

AUTHOR CONTRIBUTIONS

VN, AK, and CN conceived the experimental design and completed the field collections and sample processing. VN and NW interpreted the data and prepared the manuscript. All authors critically revised the manuscript and approved of the final submission.

FUNDING

This work was supported by FAPESP grant 03/13172-2, a FAPESP fellowship to VN and NSF Grant DEB 0640661 to CN.

ACKNOWLEDGMENTS

We thank Alexandra Montebelo and Gustavo Baldi for help with field sampling and laboratory analyses. We thank Dárlisson Nunes, Roberto Baena, Sandro, Ebes, Raimundo, and Artemizia Moitta of the Instituto de Pesquisa Ambiental na Amazonia (IPAM) for field help and IPAM and Daniel Nepstad for use of field facilities at Tanguro. Paul Lefebvre helped with watershed delineation, Shelby Hayhoe and Richard McHorney contributed stream discharge data. Access to Tanguro Rancho and rainfall data were provided by Grupo A. Maggi.

SUPPLEMENTARY MATERIAL

The Supplementary Material for this article can be found online at: http://journal.frontiersin.org/article/10.3389/fmars.2016.00114

REFERENCES

Andreae, M. O., Talbot, R. W., Berresheim, H., and Beecher, K. M. (1990). Precipitation chemistry in Central Amazonia. *J. Geophys. Res.* 95, 16987–16999. doi: 10.1029/JD095iD10p16987

Artaxo, P., Gatti, L. V., Leal, A. M. C., Longo, K. M., Freitas, S. R., Lara, L. L., et al. (2005). Química atmosférica na Amazônia: a floresta e as emissões de queimadas controlando a composição da atmosfera amazônica. *Acta Amazonica* 35, 185–196. doi: 10.1590/S0044-59672005000200008

Artaxo, P., Storms, H., Bruynseelsa, F., and Rieken, R. V. (1988). Composition and sources of aerosols from the Amazon Basin. *J. Geophys. Res.* 93, 1605–1615. doi: 10.1029/JD093iD02p01605

Aufdenkampe, A. K., Mayorga, E., Raymond, P. A., Melack, J. M., Doney, S. C., Alin, S. R., et al. (2011). Riverine coupling of biogeochemical cycles between, land, oceans, and atmosphere. *Front. Ecol. Environ.* 9, 53–60. doi: 10.1890/100014

Bekele, A., Kellman, L., and Beltrami, H. (2007). Soil profile CO_2 concentrations in forested and clear cut sites in Nova Scotia, Canada. *Forest Ecol. Manag.* 242, 587–597. doi: 10.1016/j.foreco.2007.01.088

Benner, R., Moran, M. A., and Hodson, R. E. (1986). Biogeochemical cycling of lignocellulosic carbon in marine and freshwater ecosystems: relative contributions of prokaryotes and eukaryotes. *Limnol. Oceanogr.* 31, 89–100. doi: 10.4319/lo.1986.31.1.0089

Benner, R., Opsahl, S., Chin-Leo, G., Richey, J. E., and Forsberg, B. (1995). Bacterial carbon metabolism in the Amazon River system. *Limnol. Oceanogr.* 40, 1262–1270. doi: 10.4319/lo.1995.40.7.1262

Boyer, E. W., Hornberger, G. M., Bencala, K. E., and McKnight, D. M. (1997). Response characteristics of DOC flushing in an alpine catchment. *Hydrol. Process* 11, 1635–1647.

Brandão, V. S. (2006). *Infiltração da água no solo*. Dissertation. Viçosa: Universidade Federal de Viçosa.

Buffam, I., Galloway, J. N., Blum, L. K., and McGlathery, K. J. (2001). A stormflow/baseflow comparison of dissolved organic matter concentrations and bioavailability in an Appalachian stream. *Biogeochemistry* 53, 269–306. doi: 10.1023/A:1010643432253

Dalva, M., and Moore, T. R. (1991). Sources and sinks of dissolved organic carbon in a forested swamp catchment. *Biogeochemistry* 15, 1–19. doi: 10.1007/bf00002806

Dalzell, B. J., Filley, T. R., and Harbor, J. M. (2007). The role of hydrology in annual organic carbon loads and terrestrial organic matter export from a midwestern agricultural watershed. *Geochim. Cosmochim. Acta* 71, 1448–1462. doi: 10.1016/j.gca.2006.12.009

Deckers, J. A., Nachtergaele, F., and Spaargaren, O. C. (1998). *World Reference Base for Soil Resources*. Leuven: Acco.

Hope, D., Palmer, S. M., Billett, M. F., and Dawson, J. J. C. (2004). Variations in dissolved CO_2 and CH_4 in a first-order stream and catchment: an investigation of soil-stream linkages. *Hydrol. Process* 18, 3255–3275. doi: 10.1002/hyp.5657

Fellman, J. B., Hood, E., Edwards, R. T., and D'Amore, D. V. (2009). Changes in the concentration, biodegradability, and fluorescent properties of dissolved organic matter during stormflows in coastal temperate watersheds. *J. Geophys. Res. Biogeosci.* 114, G1. doi: 10.1029/2008JG000790

Feng, X. J., Simpson, A. J., Wilson, K. P., Williams, D. D., and Simpson, M. J. (2008). Increased cuticular carbon sequestration and lignin oxidation in response to soil warming. *Nature Geosci.* 1, 836–839. doi: 10.1038/ngeo361

Ferreira, S. J. F., Luizão, F. J., and Dallarosa, R. L. G. (2005). Precipitação interna e interceptação da chuva em floresta de terra firme submetida à extração seletiva de madeira na Amazônia Central. *Acta Amazonica* 35, 55–62. doi: 10.1590/S0044-59672005000100009

Field, C., Behrenfeld, M., Randerson, J., and Falkowski, P. (1998). Primary production of the biosphere: integrating terrestrial and oceanic components. *Science* 281, 237–240. doi: 10.1126/science.281.5374.237

Filoso, S., Williams, M. R., and Melack, J. M. (1999). Composition and deposition of throughfall in a flooded forest archipelago. *Biogeochemistry* 45, 169–195. doi: 10.1007/BF01106780

Germer, S., Neill, C., Krusche, A. V., Gouveia Neto, S. C., and Elsenbeer, H. (2007). Seasonal and within-event dynamics of rainfall and throughfall chemistry in an open tropical rainforest in Rondônia, Brazil. *Biogeochemistry* 86, 155–174. doi: 10.1007/s10533-007-9152-9

Greenfield, S. M. (1957). Rain scavenging of radioactive particulate matter from the atmosphere. *J. Meteorol.* 14, 115–125. doi: 10.1175/1520-0469(1957)014<0115:RSORPM>2.0.CO;2

Hernes, P. J., and Benner, R. (2003). Photochemical and microbial degradation of dissolved lignin phenols: implications for the fate of terrigenous dissolved organic matter in marine environments. *J. Geophys. Res. Oceans.* 108, C9. doi: 10.1029/2002JC001421

Hinton, M. J., Schiff, S. L., and English, M. C. (1998). Sources and flowpaths of dissolved organic carbon during storms in two forested watersheds of the Precambrian Shield. *Biogeochemistry* 41, 175–197.

Horton, R. B. (1933). The role of infiltration in the hydrologic cycle. *Eos Trans. Am. Geophys. Union.* 14, 446–460. doi: 10.1029/TR014i001p00446

Ivanauskas, N. M., Monteiro, R., and Rodrigues, R. R. (2004). Estrutura de um trecho de floresta Amazônica na bacia do alto rio Xingu. *Acta Amazonica* 34, 275–299. doi: 10.1590/S0044-59672004000200015

Johnson, M. S., and Lehmann, J. (2006). Double-funneling of trees: stemflow and root-induced preferential flow. *Ecoscience* 13, 324–333. doi: 10.2980/i1195-6860-13-3-324.1

Johnson, M. S., Lehmann, J., Couto, E. G., Novães Filho, J. P., and Riha, S. J. (2006b). DOC and DIC in flowpaths of Amazonian headwater catchments with hydrologically contrasting soils. *Biogeochemistry* 81, 45–57. doi: 10.1007/s10533-006-9029-3

Johnson, M. S., Lehmann, J., Selva, E. C., Abdo, M., Riha, S., and Couto, E. G. (2006a). Organic carbon fluxes within and streamwater exports from headwater catchments in the southern Amazon. *Hydrol. Process* 20, 2599–2614. doi: 10.1002/hyp.6218

Jordan, C. F. (1978). Stem flow and nutrient transfer in a tropical rain Forest. *Oikos* 31, 257–263. doi: 10.2307/3543571

Ketseridis, G., Hahn, J., Jaenicke, R., and Junge, C. (1976). The organic constituents of atmospheric particulate matter. *Atmos. Environ.* 10, 603–610. doi: 10.1016/0004-6981(76)90045-7

Kuzyakov, Y. (2010). Priming effects: interactions between living and dead organic matter. *Soil Biol. Biochem.* 42, 1363–1371. doi: 10.1016/j.soilbio.2010.04.003

Levia, D. F., and Frost, E. E. (2003). A review and evaluation of stemflow literature in the hydrologic and biogeochemical cycles of forested and agricultural ecosystems. *J. Hydrol.* 274, 1–29. doi: 10.1016/S0022-1694(02)00399-2

Likens, G. E., and Eaton, J. S. (1970). A polyurethane stemflow collector for trees and shrubs. *Ecology* 51, 938–939. doi: 10.2307/1933996

Linsley, R. K. Jr., Kohler, M. A., and Paulhus, J. L. H. (1975). *Hydrology for Engineers*. New York, NY: McGraw-Hill Book Co.

Liu, C. P., and Sheu, B. H. (2003). Dissolved organic carbon in precipitation, throughfall, stemflow, soil solution, and stream water at the Guandaushi subtropical forest in Taiwan. *Forest Ecol. Manag.* 172, 315–325. doi: 10.1016/S0378-1127(01)00793-9

Lloyd, C. R., and Marques, A. D. (1988). Spatial variability of throughfall and stemflow measurements in Amazonian rainforest. *Agric. For. Meteorol.* 42, 63–73. doi: 10.1016/0168-1923(88)90067-6

Malhi, Y., Roberts, J. T., Betts, R. A., Killeen, T. J., Li, W., and Nobre, C. A. (2008). Climate change, deforestation, and the fate of the Amazon. *Science* 319, 169–172. doi: 10.1126/science.1146961

Markewitz, D., Eric Davidson, E., Moutinho, P., and Nepstad, D. (2004). Nutrient loss and redistribution after forest clearing on highly weathered soil in Amazonia. *Ecol. Appl.* 14, 177–199. doi: 10.1890/01-6016

Mayorga, E., Aufdenkampe, A. K., Masiello, C. A., Krusche, A. V., Hedges, J. I., Quay, P. D., et al. (2005). Young organic matter as a source of carbon dioxide outgassing from Amazonian rivers. *Nature* 436, 538–541. doi: 10.1038/nature03880

McClain, M., Richey, J. E., Brandes, J., and Pimentel, T. (1997). Dissolved organic matter and terrestrial-lotic linkages in the central Amazon basin of Brazil. *Global Biogeochem. Cycles* 11, 295–311. doi: 10.1029/97GB01056

Monteith, D. T., Stoddard, J. L., Evans, C. D., de Wit, H. A., Forsius, M., Høgåsen, T., et al. (2007). Dissolved organic carbon trends resulting from changes in atmospheric deposition chemistry. *Nature* 450, 537–540. doi: 10.1038/nature06316

Neu, V., Neill, C., and Krusche, A. V. (2011). Gaseous and fluvial carbon export from an Amazon forest watershed. *Biogeochemistry* 105, 133–147. doi: 10.1007/s10533-011-9581-3

Otto, A., and Simpson, M. J. (2006). Evaluation of CuO oxidation parameters for determining the source and stage of lignin degradation in soil. *Biogeochemistry* 80, 121–142. doi: 10.1007/s10533-006-9014-x

Parker, G. G. (1983). Throughfall and stemflow in the forest nutrient cycle. *Adv. Ecol. Res.* 13, 57–133. doi: 10.1016/S0065-2504(08)60108-7

Pio, C. A., Alves, C. A., and Duarte, A. C. (2001). Identification, abundance and origin of atmospheric organic particulate matter in a Portuguese rural area. *Atmos. Environ.* 35, 1365–1375. doi: 10.1016/S1352-2310(00)00391-5

Qualls, R. G., and Haines, B. L. (1992). Biodegradability of dissolved organic matter in forest throughfall, soil solution, and stream water. *Soil Sci. Am. J.* 56, 578–586. doi: 10.2136/sssaj1992.03615995005600020038x

Qualls, R. G., Haines, B. L., Swank, W. T., and Tyler, S. W. (2002). Retention of soluble organic nutrients by a forested ecosystem. *Biogeochemistry* 61, 135–171. doi: 10.1023/A:1020239112586

Radambrasil (1981). Folha SD. 22 Goiás: geologia, geomorfologia, pedologia, vegetação, uso potencial da terra. *Rio de Janeiro: DNPM* 636, 27–234.

Raymond, P. A., Caraco, N. F., and Cole, J. J. (1997). Carbon dioxide concentration and atmospheric flux in the Hudson River. *Estuaries* 20, 381–390. doi: 10.2307/1352351

Raymond, P. A., Hartmann, J., Lauerwald, R., Sobek, S., McDonald, C., Hoover, M., et al. (2013). Global carbon dioxide emissions from inland waters. *Nature* 503, 355–359. doi: 10.1038/nature12760

Raymond, P. A., and Saiers, J. E. (2010). Event controlled DOC export from forested watersheds. *Biogeochemistry* 100, 197–209. doi: 10.1007/s10533-010-9416-7

Richey, J. E., Melack, J. M., Aufdenkampe, A. K., Ballester, V. M., and Hess, L. L. (2002). Outgassing from Amazonian rivers and wetlands as a large tropical source of atmospheric CO_2. *Nature* 416, 617–620. doi: 10.1038/416617a

Rodríguez-Zuniga, U. F., Milori, D. M. B. P., Da Silva, W. T. L., Martin-Neto, L., Oliveira, L. C., and Rocha, J. C. (2008). Changes in optical properties caused by ultraviolet-irradiation of aquatic humic substances from the Amazon River Basin: seasonal variability evaluation. *Environ. Sci. Technol.* 42, 1948–1953. doi: 10.1021/es702156n

Schmidt, M. W., Torn, M. S., Abiven, S., Dittmar, T., Guggenberger, G., Janssens, I. A., et al. (2011). Persistence of soil organic matter as an ecosystem property. *Nature* 478, 49–56. doi: 10.1038/nature10386

Simoneit, B. R., and Elias, V. O. (2000). Organic tracers from biomass burning in atmospheric particulate matter over the ocean. *Mar. Chem.* 69, 301–312. doi: 10.1016/S0304-4203(00)00008-6

Snyder, D. C., Rutter, A. P., Collins, R., Worley, C., and Schauer, J. J. (2009). Insights into the origin of water soluble organic carbon in atmospheric fine particulate matter. *Aerosol Sci. Technol.* 43, 1099–1107. doi: 10.1080/02786820903188701

Spencer, R. G. M., Stubbins, A., Hernes, P. J., Baker, A., Mopper, K., Aufdenkampe, A. K., et al. (2009). Photochemical degradation of dissolved organic matter and dissolved lignin phenols from the Congo River. *J. Geophys. Res.* 114, G3. doi: 10.1029/2009JG000968

Talbot, R. W., Andreae, M. O., Berresheim, H., Artaxo, P., Garstang, M., Harriss, R. C., et al. (1990). Aerosol chemistry during the wet season in central Amazonia: the influence of long-range transport. *J. Geophys. Res.* 95, 955–969.

Thevenot, M., Dignac, M. F., and Rumpel, C. (2010). Fate of lignins in soils: a review. *Soil Biol. Biochem.* 42, 1200–1211. doi: 10.1016/j.soilbio.2010.03.017

Vianello, R. L., and Alves, A. R. (2002). *Meteorologia Básica e Aplicações*. (Viçosa: UFV), 449.

Walter, H. (1979). *Vegetation of the Earth and Ecological Systems of the Geo-biosphere*. New York, NY: Springer, 19–106.

Wang, M. C., Liu, C. P., and Sheu, B. H. (2004). Characterization of organic matter in rainfall, throughfall, stemflow, and streamwater from three subtropical forest ecosystems. *J. Hydrol.* 289, 275–285. doi: 10.1016/j.jhydrol.2003.11.026

Ward, N. D., Keil, R. G., Medeiros, P. M., Brito, D. C., Cunha, A. C., Dittmar, T., et al. (2013). Degradation of terrestrially derived macromolecules in the Amazon River. *Nat. Geosci.* 6, 530–533. doi: 10.1038/ngeo1817

Ward, N. D., Richey, J. E., and Keil, R. G. (2012). Temporal variation in river nutrient and dissolved lignin phenol concentrations and the impact of storm events on nutrient loading to Hood Canal, WA, USA. *Biogeochemistry* 111, 629–645. doi: 10.1007/s10533-012-9700-9

Waterloo, M. J., Oliveira, S. M., Drucker, D. P., Nobre, A. D., Cuartas, L. A., Hodnett, M. G., et al. (2006). Export of organic carbon in run-off from an amazonian rainforest blackwater catchment. *Hydrol. Process 20,* 2581–259. doi: 10.1002/hyp.6217

Conflict of Interest Statement: The authors declare that the research was conducted in the absence of any commercial or financial relationships that could be construed as a potential conflict of interest.

frontiers in Earth Science

ORIGINAL RESEARCH
published: 13 February 2017
doi: 10.3389/feart.2017.00009

The Genesis and Exodus of Vascular Plant DOM from an Oak Woodland Landscape

Peter J. Hernes[1], Robert G. M. Spencer[2], Rachael Y. Dyda[1], Anthony T. O'Geen[1] and Randy A. Dahlgren[1]*

[1] Department of Land, Air and Water Resources, University of California, Davis, Davis, CA, USA, [2] Department of Earth, Ocean and Atmospheric Science, Florida State University, Tallahassee, FL, USA

Evaluating the collective impact of small source inputs to larger rivers is a constant challenge in riverine biogeochemistry. In this study, we investigated the generation of dissolved organic matter (DOM) in a small oak woodland catchment in the foothills of northern California, the subsequent transformation in lignin biomarkers and chromophoric DOM (CDOM) parameters during transport through the landscape to an exporting stream, and finally the overall compositional impact on the larger receiving stream and river. Our study included a natural leaching experiment in which precipitation passing through oak, pine, and grass litter and duff samples was collected after each of a series of storms. Also included were soil trench samples to capture subsurface lateral flow, stream samples along with point-source reservoir inputs, and samples of canopy throughfall, stemflow, and gopher hole (bypass) flow. The litter/duff leaching study demonstrated changing DOM fractionation patterns throughout the season, as evidenced by changing lignin compositions in the leachates with each successive storm. This adds a necessary seasonal component to interpreting lignin compositions in streams, as the source signatures are constantly changing. Released DOM from leaching was modified extensively during transit through the subsurface to the stream, with preferential increases in aromaticity as evidenced by increases in carbon-normalized absorbance at 254 nm, yet preferential decreases in lignin phenols, as evidence by carbon-normalized lignin yields in the headwater stream that was less than half that of the litter/duff leachates. Our extensive number of lignin measurements for source materials reveals a much more complex perspective on using lignin as a source indicator, as many riverine values for syringyl:vanillyl and cinnamyl:vanillyl ratios that have previously been interpreted as degraded lignin signatures are also possible as unmodified source signatures. Finally, this study demonstrated that the impact of numerous small headwater streams can significantly overprint the DOM signatures of much larger rivers over relatively short distances spanning several to tens of kilometers. This finding in particular challenges the assumption that river studies can be adequately conducted by focusing only on the main tributaries.

Keywords: dissolved organic matter, lignin biomarkers, hydrologic flowpaths, overprinting, oak woodland, stream order, SUVA

OPEN ACCESS

Edited by:
Rick Keil,
University of Washington, USA

Reviewed by:
Mar Nieto-Cid,
Spanish National Research Council, Spain
Cedric G. Fichot,
Boston University, USA
Youhei Yamashita,
Hokkaido University, Japan

****Correspondence:***
Peter J. Hernes
pjhernes@ucdavis.edu

Specialty section:
This article was submitted to Marine Biogeochemistry, a section of the journal Frontiers in Earth Science

Received: *03 September 2016*
Accepted: *23 January 2017*
Published: *13 February 2017*

Citation:
Hernes PJ, Spencer RGM, Dyda RY, O'Geen AT and Dahlgren RA (2017) The Genesis and Exodus of Vascular Plant DOM from an Oak Woodland Landscape. Front. Earth Sci. 5:9. doi: 10.3389/feart.2017.00009

INTRODUCTION

The allure of pipe flow models for DOM in large rivers is unmistakable: large loads and rapid transit would seem to preclude the opportunity for any significant change. Over the past decade, this model has largely been debunked in terms of DOM processing and degradation, as we now know that considerable DOM transformation and remineralization occurs *in situ*, thereby enhancing the CO_2 outgassing signal from these rivers (Richey et al., 2002; Bouillon et al., 2012). However, the idea of pipe flow or unchanging large loads still persists in terms of tributary allochthonous sources to large rivers. It seems impossible, for example, to consider that streams with discharge <5% of the mainstem can significantly alter the mainstem DOM quality and quantity. Yet riverine chemistry represents an integrated signature of all upstream sources and processes within the catchment/basin, and even those small inputs must be incorporated into models of how riverine chemistry evolves.

Although rivers are grand integrators, it is clear that not all sources and processes are equally represented. Rather, some element of hydrologic connectivity must be incorporated into models of riverine chemistry, such that a soil or vegetation perched on top of a hill is much less connected than a soil or vegetation in the riparian zone. For example, the distinct lignin signature of conifer forests in the headwaters of the Sacramento River basin is overwhelmed by the lignin signature of wetlands and agricultural islands in the Sacramento/San Joaquin River Delta upon passage through the latter (Eckard et al., 2007). However, in terms of discharge, water movement, and land area, this is not a surprising finding as tidal pumping in the Delta essentially throws riverine discharge into reverse during the transition from low tide to high tide, and the land area of the Delta approaches 3000 km^2. In contrast, what happens to DOM dynamics in a non-tidally influenced system with stream inputs that are so small as to be considered insignificant sources?

Evaluating sources and processing of DOM in rivers requires a multitude of experimental, analytical, and sampling approaches, as well as attention to hydrologic flowpaths. Biomarkers such as lignin offer the specificity to trace DOM derived from angiosperm vs. gymnosperms, and woody vs. non-woody tissues (Hedges and Mann, 1979; Spencer et al., 2016). Optical parameters derived from UV-visible absorbance can trace the bulk properties of chromophoric DOM (CDOM) such as aromaticity, microbial vs. terrigenous sources, and high- vs. low-molecular weight properties (Traina et al., 1990; Helms et al., 2008; Spencer et al., 2013). Leaching experiments generate *a posteriori* sources of DOM that can be traced through the study region and evaluated for processing effects (Aufdenkampe et al., 2001; Hernes et al., 2007; Spencer et al., 2008). And of course, demarcating and sampling representative hydrologic flowpaths can be instrumental in determining how the bulk of DOM enters headwater streams, which in turn helps to understand which processes and depths within the soil column are most influential in transforming the initial leachate compositions (Sanderman et al., 2009; Swarowsky et al., 2012).

In this study, we took the approach of characterizing sources, transport, and processing of DOM within an oak woodland landscape from the nanoscale to tens of kilometers with the goal of quantifying the ways in which headwater catchment processes can influence the DOM chemistry of a large river. Because DOM export in the Mediterranean climate of the Sierra Nevada foothills is dominated by storm events, our leaching experiment and sampling strategy revolved around a time series approach during the rainy portion of the water year in January through April. Our suite of analyses included molecular lignin analyses as a biomarker for vascular plant sources and diagenetic change, optical parameters that capture the aromatic component of DOM, and bulk carbon analyses. We collected samples from a perched water monitoring system (trench) that was constructed to intercept hydrologic flowpaths at different depths within the soil profile, from samples of opportunity such as flow from gopher holes and stem/canopy flow, and from streams, reservoirs, and the Yuba River to which all DOM in our study region eventually flows. The central premise of our study was that the cumulative effects of small streams can have a quantitative and traceable impact on the DOM chemistry of a large river.

MATERIALS AND METHODS

Site Description

The litter/duff leaching experiment was conducted in the northern Sierra Nevada foothills at the University of California Sierra Foothill Research and Extension Center (SFREC), approximately 80 km north of Sacramento, CA (**Figure 1**). Additional water sampling occurred in and around SFREC (**Figure 1**), which experiences a Mediterranean climate with cool, moist winters and hot, dry summers. Elevation at the site ranges from 250 to 450 m. The mean annual air temperature is 15°C (January mean of 8.4°C, July mean of 25.9°C). Annual precipitation is 734 mm (307—1235 mm during the past 20 years) and falls exclusively as rainfall, primarily between November and March (Lewis et al., 2006). The dominant ecosystem at the site is oak woodland, which regionally constitutes a mixture of winter-deciduous blue oak (*Quercus douglasii* H.&A.; ∼45% coverage), an evergreen interior live oak (*Quercus wislizenii* A. DC.; ∼5% coverage), foothill pine (*Pinus sabiniana* Dougl.; ∼5% coverage), and mixed annual grasses (∼45% coverage, common species include soft chess [*Bromus hordeaceus*], ripgut brome [*Bromus diandrus*], red brome [*Bromus madritensis* spp. *rubens*], annual fescue [*Vulpia* sp.], wild oats [*Avena fatua* and *Avena barbata*], and medusahead [*Taeniantherum caput-medusae*]) (Chow et al., 2009; O'Geen et al., 2010).

Field Incubation and Measurements

Storm-associated leachates (eleven events) were collected during a 182-day field incubation (December 1, 2006 through May 31, 2007 comprising the entire rainy season) using fresh litterfall (equivalent to Oi horizon in soil taxonomy) and associated duff (i.e., litter decomposed at the soil surface over 2–4 years, or Oe/Oa horizons) for the four dominant vegetation components (Chow et al., 2009). Litter materials were collected during the first week of November, 2006 prior to any major rainfall events, and triplicate incubations were initiated in polyethylene trays (54 × 43 × 13 cm) using 200–300 g dry weight equivalent

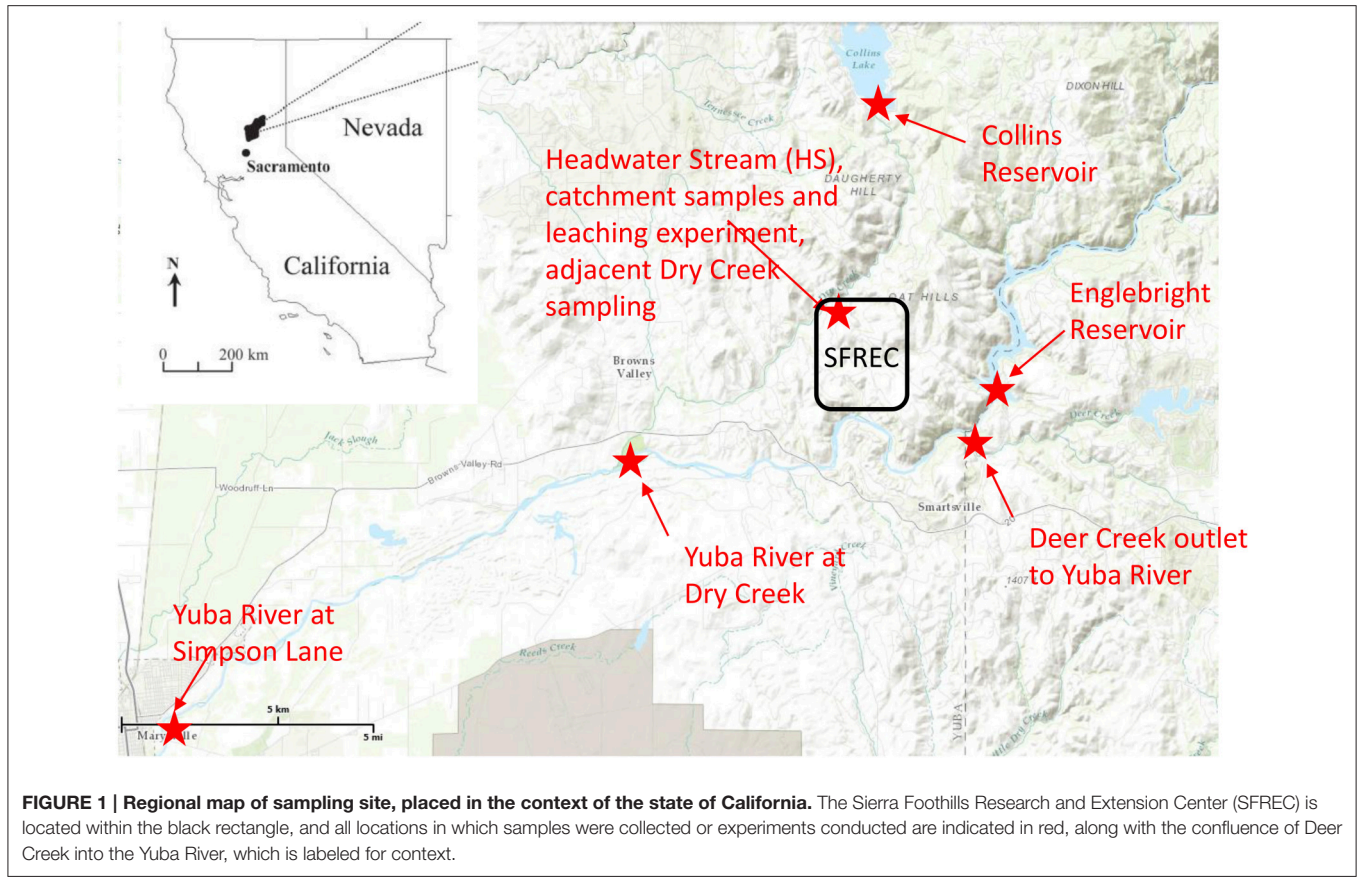

FIGURE 1 | Regional map of sampling site, placed in the context of the state of California. The Sierra Foothills Research and Extension Center (SFREC) is located within the black rectangle, and all locations in which samples were collected or experiments conducted are indicated in red, along with the confluence of Deer Creek into the Yuba River, which is labeled for context.

of most materials, but ~900 g for grass duff and ~500 g for foothill pine duff. Trays were covered with 0.1 cm mesh stainless steel screen to minimize particulate loss or inputs, then slightly tilted to allow rapid drainage. The trays were suspended one meter above the ground with polyethylene tubes connected to 50-L high density polyethylene (HDPE) carboys (**Supplementary Figure 1A**). Leachate volumes were measured from each tray the day following each rainfall event and one-liter subsamples (HDPE bottles) were collected for analyses after vigorous mixing. Carboys were emptied and rinsed after each collection. The mass of leachate DOC yielded from each tray for each rainstorm was calculated from the volume of leachate collected times the measured DOC concentration, and this was normalized by the original mass of material according to each tray (i.e., leached C per mass litter in units of mg g^{-1}). Remaining mass of material in each tray was measured at the end of the experiment. More details about the experiment and bulk measurements can be found in Chow et al. (2009). Although the experiment was conducted in triplicate, in most cases only a single lignin analysis was conducted due to time and expense. Those that were analyzed in duplicate or triplicate are reported in **Supplementary Table 1**.

While there are likely "bottle effects" in conducting a leaching/incubation experiment in this manner (e.g., differences in microbial activity, light conditions, and wetness compared to litters and duffs in contact with the natural soil), containing the materials in trays was necessary to maintain reasonable controls on the experiment. Although the experiment may not be a perfect proxy for natural leaching and degradation, the results are still informative as to overall dynamics.

Flowpath Continuum Sampling

In addition to the litter/duff leachates, a longitudinal continuum of samples was collected in order to evaluate the evolution of the primary DOM leachate signal along the hydrologic flowpath (**Figure 1**, **Supplementary Figure 2**). Sampling began in an ungrazed 36 ha catchment that contains an ephemeral stream, hereafter abbreviated as HS for "headwater stream," and is equipped with a perched water collection system (trench) to monitor and collect subsurface water flowing out of several distinct soil horizons, with collection trays inserted at the bottom of each of these horizons within the trench (**Supplementary Figure 1B**). Sampling depths included 0–10, 10–30, 30–60, and 60–100 cm, although we did not include any samples from the 60–100 cm depth in our analyses as flow was smaller and more sporadic in this layer than the other three. More details about the perched water sampling system can be gleaned from O'Geen et al. (2010). For this study, stream and trench samples were collected during two different rain events in mid-February 2007 and late January 2008, and the stream alone was sampled in late February 2007. Also included in the January 2008 rain event were stemflow and canopy throughfall for the

three tree species as well as gopher hole samples in which water was rapidly flowing out of the gopher holes during peak flow. The latter represent bypass flow as water flowing through gopher holes does not have the typical contact time with soils. The overall sampling within the HS catchment aimed at capturing prominent hydrologic flowpaths depicted in **Supplementary Figure 2**. The larger synoptic study linkages are depicted in **Figure 1**. Briefly, the Collins reservoir discharges into Dry Creek, for which HS is a representative tributary, and Dry Creek flows into the Yuba River. Englebright reservoir is on the Yuba River and its outflow was sampled along with downstream water from the Yuba River above the confluence with Dry Creek and again near Marysville, CA at Simpson Lane, ∼20 km downstream of the Dry Creek confluence. Both reservoirs, Dry Creek, and the Yuba River were sampled in conjunction with the late January 2008 storm event.

DOC and C-specific UV Absorbance ($SUVA_{254}$) Analyses

Leachates were pre-filtered through glass fiber filters (Whatman GF/F) and all leachates and water samples passed through a 0.2 μm polycarbonate membrane filters (Millipore), prior to DOC and UV-visible analyses. All samples were filtered within 24 h and analyzed within 72 h. DOC concentrations were measured on acidified samples (pH ∼ 2) using a Dohrmann UV-enhanced persulfate TOC analyzer (Phoenix 8000; MDL = 0.1 mg L^{-1}). UV absorbance at 254 nm was measured on a Helios Gamma UV/VIS Spectrophotometer (Thermo Fisher Scientific, Inc.). C-specific UV absorbance at 254 nm ($SUVA_{254}$) was determined by normalizing UV absorbance at 254 nm with DOC concentration and is reported in the units of liter per milligram carbon per meter (L mg C^{-1} m^{-1}).

Lignin Analyses

All dissolved lignin samples were filtered through a 0.2 μm membrane filter (Millipore polycarbonate) then frozen. Prior to cupric oxide (CuO) oxidation for lignin measurements, water was thawed (20 mL for leachates, 100–500 mL for water samples), acidified to pH 2 to minimize precipitation, then rotary evaporated to ∼3 mL. The concentrate was transferred to Monel reaction vessels (Prime Focus, Inc.) and dried under vacuum centrifugation. Weighed and ground litter and duff materials (10–80 mg) both pre- and post-experiment were transferred directly into the reaction vessels. Lignin analyses were carried out by CuO oxidation following a modified version as outlined by Hedges and Ertel (1982), Spencer et al. (2010a) and Hernes et al. (2013b). Following oxidation in 8% NaOH in the presence of excess CuO at 155°C for 3 h, samples were acidified and extracted three times with ethyl acetate, with the latter fraction evaporated under a gentle stream of ultrapure nitrogen. Samples were then stored frozen until analysis. Lignin phenols were trimethylsilyl derivatized using bis-trimethylsilyltrifluoromethylacetamide (BSTFA); separation of phenols was achieved using an Agilent 6890 gas chromatograph fitted with a DB5-MS capillary column (30 m, 0.25 mm inner diameter, J&W Scientific) and attached to an Agilent 5973 mass selective detector. Quantification was achieved using selected ion monitoring with cinnamic acid as an internal standard following the five-point calibration scheme of Hernes and Benner (2002). All samples were blank-corrected due to the presence of trace amounts of contamination in the NaOH reagent. At least one blank was run for every 10 sample oxidations performed. Blank concentrations of lignin phenols were low (40–55 ng) for the eight lignin phenols measured in this study (three vanillyl phenols: vanillin, acetovanillone, vanillic acid; three syringyl phenols: syringaldehyde, acetosyringone, syringic acid; and two cinnamyl phenols: p-coumaric acid, ferulic acid). Total blanks for these eight compounds never exceeded 5% of the sample yields (average 1.3%).

Lignin Mixing Model Calculations

Calculations of lignin overprinting were conducted using linear mixing models of lignin parameters. Depending on the question (i.e., is the goal to determine volumes of water mixed, or amounts of DOC mixed, or amounts of lignin mixed?), this is not strictly correct for ratios, which may not mix linearly over their entire range. In our case, we are primarily asking the question about how much lignin comes from each source, and with similar weighting (i.e., concentrations), linear mixing is a reasonable approximation. This exercise is not presented as a quantitatively precise calculation of mixing, but rather to demonstrate the potential for overprinting to exert significant controls on river DOC compositions. In light of this, the simplest approach that makes the point was chosen. Accurately modeling mixing of ratios necessitates an iterative approach that involves its own uncertainties related to assumptions about weighting, but ultimately leads to greater calculated proportions for the endmember with the most weight. In our case, we are interested in how much the HS stream as a representative endmember overprints larger creeks/rivers, and because lignin concentrations are higher in the composite HS sample than receiving waters, calculating mixed ratios more accurately (i.e., linear mixing of terms in the numerator separately from those in the denominator, and then calculating the ratio) would lead to higher calculated HS proportions than linear mixing of the entire ratio, hence our approach is conservative as to the question of overprinting.

Linear mixing models are typically used when a sample value is bracketed by two endmembers believed to be the primary sources for that sample. If the sample value is equidistant from either endmember value, then the sample is a 50% mixture of each endmember. Determining the percentage of either endmember is possible by calculating the relative offset between the sample value and an endmember and dividing this by the total difference between the two endmembers. For example, if Endmember A has a value of 0.9, Endmember B has a value of 1.0, and the sample value is 0.93, intuitively we know that there is a higher percentage of Endmember A represented in that sample than Endmember B because the sample value is closer to Endmember A. A linear mixing model calculates the percentage of Endmember A as follows: |Endmember B – Sample|*100%/|Endmember A – Endmember B|, or in this example, |1.0 – 9.3|*100%/|0.9 – 1.0| = 70% Endmember A. Calculated values >100% are possible if the endmembers do not bracket the sample, which is less helpful for attributing sources,

but can still provide context for the magnitude of compositional change that occurs.

RESULTS

Due to the large volume of data from this study, much of the data in figures consists of averages and does not capture the full range of values. However, many of these ranges are described below and the comprehensive dataset is available in **Table 1** and **Supplementary Tables 1**, **2**. Weighted averages presented for leachates in **Table 2** were computed only across a single tray/replicate, even when replicate samples were analyzed occasionally from other trays. Because there was variation in mass loss between replicate trays in any given storm, incorporating those replications in weighted averages would have been unnecessarily complicated with minimal added value.

Carbon loss from the leachate experiment has previously been reported by Chow et al. (2009). Briefly, total carbon lost, as determined by difference between pre- and post-litter/duff C mass, ranged from 8.8 to 34% (**Table 1**). The total lost as leached DOC (volume of leachate collected multiplied by DOC concentration) ranged from 1.4 to 12.8%, and after accounting for a small amount lost as particulate organic carbon in the leachates, the remainder by difference was attributed to remineralized organic carbon (OC) lost as carbon dioxide (CO_2), which ranged from 5.9 to 31.8% (**Table 1**; Chow et al., 2009).

Lignin concentrations in litter/duff leachates were highly variable, varying by nearly an order of magnitude from 0.15 to 12.1 mg L^{-1} (**Supplementary Table 1**). These values were one to three orders of magnitude larger than typical riverine values (Spencer et al., 2008; Hernes et al., 2013b; Mann et al., 2014). On average, lignin concentrations were 2- to 3-fold higher in the litter-derived leachates compared to duff-derived leachates. In general, there was some evidence of a "first flush" in the two December storm events, as lignin concentrations in all litter leachates were 2- to 4-fold higher in averaged December samples than the average over the remainder of the sampling period (**Supplementary Table 1**). Annual grass duff lignin was approximately 2-fold higher in December, while the other three duffs were similar across the sampling period.

Across the 15 month sampling period, HS DOC concentrations ranged from 2.2 to 17.2 mg L^{-1}, with all values >10 associated with a single storm on 1/4/2008 which was not part of the leaching experiment (**Supplementary Table 2**). During the snapshot synoptic sampling, DOC for the Collins reservoir sample was 2.9 mg L^{-1}, Englebright reservoir was 1.6 mg L^{-1}, Dry Creek was 4.8 mg L^{-1}, Yuba River near Dry Creek was 2.0 mg L^{-1}, and Yuba River at Simpson Lane was 2.4 mg L^{-1} (**Supplementary Table 1**). Calculations involving

TABLE 1 | Pairwise comparisons of lignin parameters for litter/duff materials pre- and post-experiment.

	S:V	C:V	(Ad:Al)v	(Ad:Al)s	Λ_8 (mg 100 mg OC^{-1})	Total lost C (%)	Lost as DOC (%)	Lost as CO_2(%)	Composition of respired lignin (by difference)			
									S:V	C:V	(Ad:Al)v	(Ad:Al)s
AGD-pre	1.08	0.37	0.41	0.57	0.72							
AGD-post	1.15	0.54	0.42	0.51	1.03	10.6	4.1	5.9	1.41	0.37	0.67	0.33
AGL-pre	1.21	0.59	0.29	0.44	6.05							
AGL-post	1.37	0.58	0.30	0.49	6.87	17.7	3.3	13.9	1.22	0.66	0.18	0.32
FPD-pre	0.02	0.03	0.33	0.32	4.20							
FPD-post	0.03	0.05	0.34	0.34	4.80	8.8	1.4	8.1	−0.01	−0.01	0.17	0.17
FPL-pre	0.01	0.10	0.31	0.63	4.63							
FPL-post	0.01	0.11	0.33	0.86	4.30	9.6	3.8	6.8	0.02	0.05	0.20	0.08
BOD-pre	0.87	0.12	0.36	0.32	2.14							
BOD-post	0.87	0.15	0.37	0.33	2.38	21.0	2.1	17.8	0.85	−0.15	0.14	0.06
BOL-pre	0.72	0.15	0.24	0.24	3.37							
BOL-post	0.86	0.15	0.28	0.29	3.99	27.1	12.8	15.3	−0.11	0.11	0.06	−1.16
LOD-pre	1.08	0.19	0.22	0.21	4.51							
LOD-post	1.12	0.13	0.28	0.28	4.64	34.0	2.4	31.8	0.96	0.35	0.10	0.06
LOL-pre	1.09	0.39	0.20	0.19	4.95							
LOL-post	1.14	0.30	0.27	0.26	5.39	28.1	5.9	22.9	0.86	0.79	−0.03	−0.11
Average Pre	1.01	0.24	0.30	0.33	3.82							
Average Post	1.09	0.25	0.32	0.36	4.17	19.6	4.5	15.3	0.87	0.27	0.19	-0.08

Negative values in the "Composition of respired lignin" columns indicate a calculated production of either the term in the numerator or the denominator. Average value for S:V and (Ad:Al)s in these columns does not include foothill pine due to minimal syringyl content.

AGD, annual grasses duff; AGL, annual grasses litter; FPD, foothill pine duff; FPL, foothill pine litter; BOD, blue oak duff; BOL, blue oak litter; LOD, live oak duff; LOL, live oak litter; S:V, sum of three syringyl phenols divided by sum of three vanillyl phenols; C:V, sum of two cinnamyl phenols divided by sum of three vanillyl phenols; (Ad:Al)v, vanillic acid divided by vanillin; (Ad:Al)s, syringic acid divided by syringaldehyde; Λ_8, sum of eight lignin phenols divided by organic carbon; OC, organic carbon; DOC, dissolved organic carbon.

TABLE 2 | Average lignin parameters and $SUVA_{254}$ values for oak woodland leachates, trench samples, and stream in comparison to snapshot parameters for down and upstream sources of water/DOM.

	S:V	C:V	(Ad:Al)v	(Ad:Al)s	Λ_8 (mg 100 mg OC^{-1})	$SUVA_{254}$ (L mg C^{-1} m^{-1})
AGD (9)	1.36	0.44	1.35	1.09	1.88	1.68
AGL (9)	1.16	0.33	1.05	1.25	5.68	1.87
FPD (8)	0.07	0.05	1.61	1.26	2.24	2.15
FPL (9)	0.04	0.08	0.56	1.09	2.56	0.95
BOD (9)	0.85	0.14	1.48	1.12	2.04	2.58
BOL (10)	1.02	0.13	0.41	0.53	1.72	2.27
LOD (9)	1.33	0.17	1.11	0.88	2.46	2.48
LOL (9)	0.97	0.29	0.41	0.48	2.27	1.59
Canopy/stemflow (6)						3.54
Gopher holes (6)						4.43
T 0-10 cm (6,4)	1.07	0.29	1.31	0.99	0.80	3.13
T 10-30 cm (7,4)	0.97	0.23	1.42	1.03	1.30	2.83
T 30-60 cm (6,0)	0.98	0.20	1.70	1.09	0.56	
HS (19, 45)	0.90	0.17	1.30	1.11	0.95	3.75
Dry Creek (1)	0.81	0.09	1.77	1.11	0.58	2.94
Collins (1)	0.63	0.07	1.92	1.21	0.58	3.12
Englebright (1)	0.49	0.07	2.00	1.15	0.36	4.38
Yuba River at Dry Creek (1)	0.69	0.14	1.55	1.13	0.59	3.08
Yuba River at Simpson Ln (2,1)	0.89	0.17	1.09	1.01	0.59	2.89

Leachate averages were weighted according to the mass of leached carbon during each storm event, hence are more likely to reflect the earlier storms. Number of samples averaged is in parentheses (two values indicate difference in number of lignin vs. $SUVA_{254}$), however replicate leachate samples are only counted as one. Canopy/stemflow lignin was not averaged due to distinct compositional differences between the pine and oak samples.

AGD, annual grasses duff; AGL, annual grasses litter; FPD, foothill pine duff; FPL, foothill pine litter; BOD, blue oak duff; BOL, blue oak litter; LOD, live oak duff; LOL, live oak litter; T, trench; HS, headwater stream in Sierra Foothills Research and Extension Center; S:V, sum of three syringyl phenols divided by sum of three vanillyl phenols; C:V, sum of two cinnamyl phenols divided by sum of three vanillyl phenols; (Ad:Al)v, vanillic acid divided by vanillin; (Ad:Al)s, syringic acid divided by syringaldehyde; Λ_8, sum of eight lignin phenols divided by organic carbon; $SUVA_{254}$, carbon-specific ultraviolet absorbance at 254 nm.

DOC utilized at least two decimal points and tabulated DOC is reported at two decimal points, however one decimal point is more representative of the accuracy and therefore the convention adopted for the text.

Lignin concentrations in the trench and HS samples were up to three orders of magnitude smaller than in the leachates (**Supplementary Table 1**: note units of mg L^{-1} for leachates vs. μg L^{-1} for everything else), ranging from 4.4 to 84.5 μg L^{-1}. HS lignin concentrations on average were significantly higher than trench samples (41.2 vs. 20.6 μg L^{-1}), suggesting that lignin in the streams does not solely come from subsurface sources. Lignin concentrations in the Collins reservoir was 16.7 μg L^{-1} and increased into Dry Creek at 27.6 μg L^{-1}, while the Englebright-to-Yuba River transition also resulted in increased lignin concentrations, from 5.6 μg L^{-1} in the former to 11.9 μg L^{-1} at the Dry Creek confluence to 13.9 μg L^{-1} at Simpson Lane (**Supplementary Table 1**).

In contrast to lignin concentrations, carbon-normalized yields of lignin were less variable between duff and litter leachates, with the exception of annual grasses, which averaged 5.68 mg 100 mg OC^{-1} in the litters compared to 2.16 mg 100 mg OC^{-1} in the duffs (**Table 2**). Average weighted carbon-normalized yields in the other six sample types ranged from 1.72 to 2.56 mg 100 mg OC^{-1}. These values are consistent with previous studies involving plant leachates (Hernes et al., 2007, 2013a; Pellerin et al., 2010). Carbon-normalized yields in the litters and duffs prior to leaching ranged from 0.72 mg 100 mg OC^{-1} in the annual grass duff to 6.05 mg 100 mg OC^{-1} in the annual grass litter, and averaged 3.82 mg 100 mg OC^{-1}, while post-leaching values were 1.03–6.87 mg 100 mg OC^{-1} with an average of 4.17 mg 100 mg OC^{-1}, indicating preferential leaching/degradation of non-lignin plant constituents (**Table 1**).

Carbon-normalized lignin yields in the trench and HS samples were consistently lower than that of the leachates, ranging from 0.12 mg 100 mg OC^{-1} (a trench sample) to 3.06 mg 100 mg OC^{-1} (a HS sample) with a combined average of 0.93 mg 100 mg OC^{-1}. Carbon-normalized yields in the Collins-to-Dry Creek system were essentially identical at 0.58 mg 100 mg OC^{-1}, while experiencing an increase from 0.35 mg 100 mg OC^{-1} to 0.59 mg 100 mg OC^{-1} in the Englebright-to-Yuba River system (**Table 2**).

Diagnostic lignin ratios include source indicators, S:V (indicator of angiosperms, or deciduous plants) and C:V (indicator of non-woody tissue), and diagenetic acid:aldehyde ratios for both vanillyl and syringyl phenols. The lowest dissolved S:V ratios were in the two reservoirs, at 0.63 for Collins (with Dry Creek at 0.81) and 0.49 for Englebright (with Yuba River at 0.69 and 0.89) (**Table 2**). HS and trench samples ranged from 0.51 to 1.17, while angiosperm (i.e., the oaks and grasses) leachates were somewhat higher at 0.75–1.62 (**Supplementary Table 1**). Angiosperm litters and duffs ranged from 0.72 to 1.21 prior

to leaching and 0.86 to 1.37 post-leaching. Trends in S:V were largely mirrored in C:V, with the lowest surface water dissolved values (0.07) in the two reservoirs (stemflow and canopy throughfall values were comparable or lower) and increasing into Dry Creek (0.09) and Yuba River (0.14 and 0.17). C:V in HS and trench samples ranged from 0.09 to 0.48, with an average of 0.21, while leachates ranged from 0.04 to 0.34 and on average was higher in the litter leachate than the duff leachate for all four plant types. Litter and duff C:V ranged from 0.03 to 0.59 prior to leaching and 0.05 to 0.58 post-leaching (**Table 1**).

Average dissolved vanillyl acid:aldehyde ratios, (Ad:Al)v, were lowest in the litter leachates (0.41–1.05), and generally higher in all other sample types (1.09–2.00) (**Table 2**). Litter and duff (Ad:Al)v ranged from 0.20 to 0.41 prior to leaching and 0.27 to 0.42 post-leaching (**Table 1**). Average dissolved syringic acid:aldehyde ratios, (Ad:Al)s, were less distinguishable between litters and duffs, ranging from 0.48 to 1.26, while all other samples varied from 0.99 to 1.21 (**Table 2**). Angiosperm litter and duff (Ad:Al)s ranged from 0.19 to 0.57 prior to leaching and 0.26 to 0.51 post-leaching (**Table 1**).

Absorbance of UV-visible light by CDOM can offer complementary information to lignin, as unsaturated compounds such as lignin polyphenols are largely responsible for absorbance patterns (Traina et al., 1990; Blough et al., 1993; Fooken and Liebezeit, 2000). In particular, carbon-specific UV absorbance (SUVA) exhibits strong correlations to aromaticity in DOM (Traina et al., 1990). In this study, $SUVA_{254}$ in any single leachate sample ranged from 0.45 L mg C^{-1} m^{-1} in the foothill pine litter leachate to 4.47 L mg C^{-1} m^{-1} in the blue oak litter leachate (**Supplementary Table 1**), corresponding to an approximation from past studies of <10% aromaticity to >30% aromaticity, respectively (Weishaar et al., 2003). Blue oak duff leachate on average had the highest $SUVA_{254}$ value at 2.58 L mg C^{-1} m^{-1} while foothill pine litter leachate was the lowest with an average $SUVA_{254}$ of 0.95 L mg C^{-1} m^{-1} (**Table 2**). The litter leachate $SUVA_{254}$ values (1.64 L mg C^{-1} m^{-1}) were on average ∼25% lower than the duff leachates (2.22 L mg C^{-1} m^{-1}). Across the continuum, $SUVA_{254}$ values were highest in the gopher hole water flows (4.43 L mg C^{-1} m^{-1} on average), lower in the stem flow and canopy throughfall samples (3.54 L mg C^{-1} m^{-1} on average) and HS samples (3.75 L mg C^{-1} m^{-1}), still lower in the 0–10 and 10–30 cm trench samples (3.13 and 2.83 L mg C^{-1} m^{-1}, respectively), and then exhibited a range of values in the reservoir, Yuba River, and Dry Creek samples (2.89–4.38 L mg C^{-1} m^{-1}) (**Table 2** and **Supplementary Tables 1**, **2**). For comparison, 21 site-averaged $SUVA_{254}$ values measured throughout the Sacramento River basin in 2002-3 ranged from 2.56 to 3.72 L mg C^{-1} m^{-1}, including an average value of 2.93 L mg C^{-1} m^{-1} at Yuba River at Simpson Lane (Chow et al., 2007).

DISCUSSION

Lignin Relativity As Demonstrated by Fractionation Effects in Leachates

Characterizing fractionation effects in lignin biomarkers has significantly improved interpretation of DOM and lignin parameters in various environments, explaining apparent degradation trends that previously were conundrums (Hernes et al., 2007, 2013a; Spencer et al., 2008, 2016). Lignin fractionation studies to date have primarily consisted of snapshot measurements, in which dissolved and particulate lignin is allowed to reach equilibrium, then a single measurement of each is compared to assess the magnitude of fractionation (Hernes et al., 2007, 2013a). Our system was much more dynamic, with repeated leaching with every rainstorm. We observed changing trends in fractionation across the season in 12 out of 24 plant material/diagnostic lignin parameter combinations ($p < 0.1$, **Figures 2**, **3**). Acid to aldehyde ratios, (Ad:Al)v, increased in five of the eight plant material leachates, S:V increased in live oak and foothill pine litter leachates and decreased in blue oak and annual grasses duff leachates, and C:V decreased in all the duff leachates except foothill pine duff. These seasonal changes add considerable complexity to interpretations of streamwater lignin measurements, but more broadly highlight the need for seasonal measurements of rivers and streams themselves—as well as source materials for DOM—as snapshots are simply inadequate for capturing all the dynamics of integrated river basin biogeochemistry.

Three different mechanisms separately or in combination could be responsible for the changing trends in leachates that we observed: (1) in the absence of significant degradation, the changing trends could simply represent a continuum of solubilities, with the early season ratios representing more soluble lignin and the late season ratios representing less soluble lignin, (2) in the absence of significant solubility differences in the initial litter/duff materials, the changing trends could be due to degradation of litter/duff lignin, which typically results in elevated (Ad:Al)v ratios and decreased S:V and C:V ratios, and (3) if neither solubility nor degradation of lignin is a significant factor, then degradation of cellulose or other organic matter that binds with lignin and inhibits leaching could be slowly releasing lignin of changing compositions. Although none of the mechanisms can be ruled out with certainty, there are some clues as to the overall reactivity of each material. For example, foothill pine litter, annual grasses duff, and foothill pine duff lost <10% of their initial mass due to mineralization of OC to CO_2, which would appear to favor a solubility control over a degradation control. On the other hand, live oak duff and live oak litter lost 23 and 32%, respectively, of OC to CO_2, which could favor a degradation control over solubility. Perhaps not surprisingly, four out of six lignin parameters for the two live oak materials were linearly correlated to OC loss, with the remaining two parameters showing more complex change (**Figures 2**, **3**). Blue oak litter lost 27% of its carbon over the course of the experiment, with roughly equal proportions to respiration and to DOC leaching (**Table 1**), and the linear relationship between (Ad:Al)v and leached carbon was the strongest of all correlations (**Figure 2**), perhaps a reflection of synergistic effects between leaching and respiration. At the molecular level, (Ad:Al)v in duff leachates are consistently higher than in litter leachates (**Figures 2**, **3**), which clearly indicates that degradation plays a role over the course of 2–4 years (i.e., the approximate age of the duffs), but it remains to be seen if degradation over a few months has the same impact.

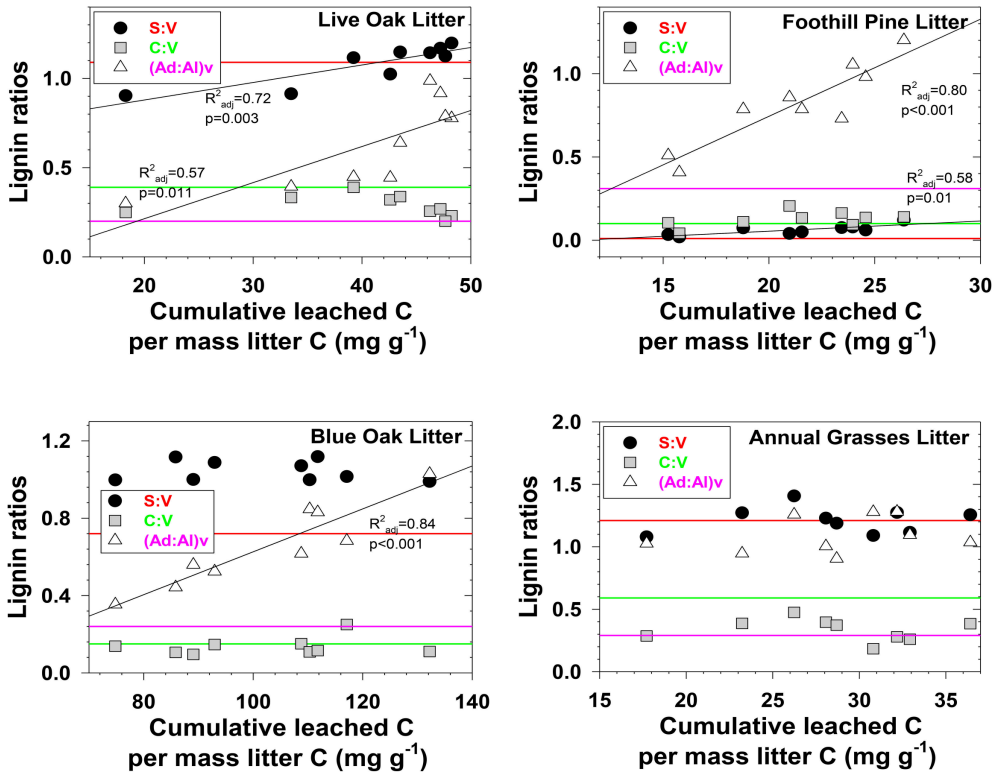

FIGURE 2 | Evolving lignin compositions in litter leachates with each successive storm, plotted against total cumulative leached carbon on a mass-normalized basis. Horizontal reference lines correspond to the starting lignin compositions of the original litters and are color matched to the lignin parameter in the legend.

Some uncertainty in interpreting fractionation effects on dissolved lignin can be mitigated by measuring particulate and dissolved lignin simultaneously, as it can be reasonably assumed that partitioning between DOM and POM in higher stream order systems is at equilibrium. For example, DOM- derived lignin measured in four rivers in Papau New Guinea demonstrated higher C:V, S:V, and (Ad:Al)v than in POM in 11 of 12 pairings by up to an order of magnitude (Burns et al., 2008), whereas in the Amazon River basin, ultrafiltered DOM C:V and S:V values were consistently lower than fine or coarse POM while (Ad:Al)v values were two to three times higher (Hedges et al., 2000). Our leachate study indicates that both plant sources and timing must be considered when interpreting the direction and magnitude of fractionated lignin measurements in riverine DOM and POM. However, we hypothesize that DOC:POC ratios will exert some level of control on whether the nature of partitioning in rivers is net sorption to or desorption from POM. Ultimately, interpreting DOM lignin data in absolute terms is simply not possible: lignin parameters are a relative accounting system and there must be points of comparison either internally across gradients or externally with particulate sources of dissolved lignin.

Leaching and Degradation

In all systems, mass balance must apply: the total amount of any individual lignin phenol in the initial parent materials must be accounted for in either the residual parent material, the cumulative leachate produced, the cumulate particulate material produced, remineralization to CO_2, and chemical transformation to other compounds, which could include other lignin phenols (i.e., conversion from aldehyde precursors to acid precursors). The latter two processes are challenging to determine experimentally/analytically and generally must be inferred. Carbon-normalized yields of lignin (Λ_8, mg lignin per 100 mg OC) increased in the residual material compared to the starting materials in seven out of the eight treatments (**Table 1**), indicating that lignin was more resistant to leaching and degradation than bulk carbon.

Composition of lignin remineralized to CO_2 can be approximated by difference using mass balance, in which carbon-normalized lignin yields can be used to calculate the mass of each lignin phenol in the pre-litter/duff materials, and then the mass from the post-litter/duff materials along with leached DOC lignin are subtracted to get respired lignin. Although our experimental design was not optimized for this analysis, the general trend indicates that remineralized lignin was slightly depleted in syringyl phenols, enriched in cinnamyl phenols, and depleted in vanillic and syringic acid relative to litter/duff materials (**Table 1**). However, the latter trend could also be explained by the conversion of aldehyde precursors to acid precursors (i.e., production of acid precursors in the

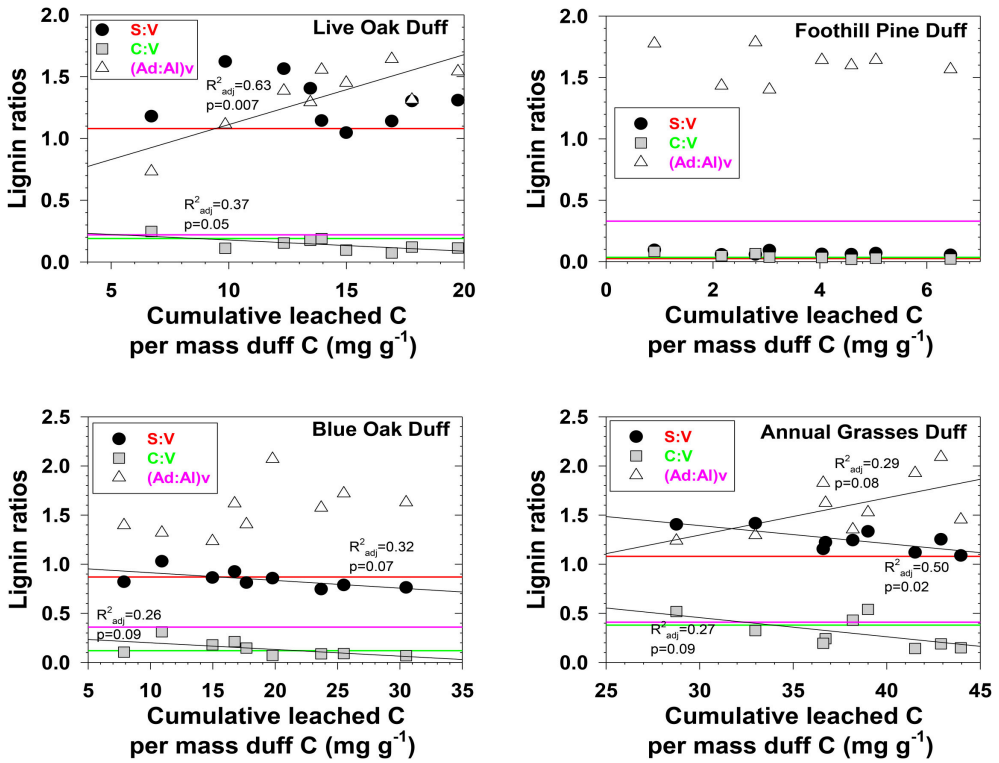

FIGURE 3 | Evolving lignin compositions in duff leachates with each successive storm, plotted against total cumulative leached carbon on a mass-normalized basis. Horizontal reference lines correspond to the starting lignin compositions of the original duffs and are color matched to the lignin parameter in the legend.

remaining litter/duff materials would lead to smaller amount-by-difference calculations), as is commonly thought to occur during degradation of lignin.

It is now well-documented that the process of leaching releases dissolved lignin with a different composition than the original plant material (Hernes et al., 2007, 2013a; Spencer et al., 2008). The magnitude of the fractionation can readily be seen in this study by comparing the time-series leachate data in **Figures 2**, **3** to the solid colored lines that represent the initial litter/duff material. However, a plot of S:V vs. C:V, which can be used to distinguish angiosperm (deciduous) tissues from gymnosperm (conifer) tissues and woody tissues from non-woody tissues (Hedges and Mann, 1979), puts this fractionation into interpretive context. For example, grass litter and duff leachates span C:V ratios from 0.1 to 0.6, with the lower value traditionally interpreted as degraded plant material while the higher value is considered fresh (**Figure 4**). (In general, litter C:V do appear higher than duff values (**Figure 4**), lending credence to the idea that C:V is responsive to degradation, however this does not appear the case for annual grasses, while systematic differences between litter and duff leachate S:V values are ambiguous.) In the bigger picture, all of the foothill pine, blue oak, and live oak C:V ratios, including fresh litters, are below the ranges originally considered (Hedges and Mann, 1979) as either gymnosperm or angiosperm non-woody tissues (**Figure 4**). Similar to the lower end of the grasses C:V values, all of these samples would traditionally be defined as degraded. Hence it is clear that the range of values for S:V and C:V in plant materials themselves are broader than once thought, let alone the values of leachates, which places even more importance on adequately characterizing source materials to rivers and streams before attempting to interpret dissolved lignin values.

DOM Export to Streams

In California oak woodlands, most DOM export from catchments is driven by storm events that rapidly mobilize DOM from the adjacent landscape which in turn flows to streams via several dynamic hydrologic flowpaths (Swarowsky et al., 2012). Scaling our litter/duff leachate yields (mass DOC released per mass of litter/duff) to a total annual amount of litter and duff on the landscape of HS (field observations of litter and duff horizon depths multiplied times density and area) indicates a net production of approximately 450 kg ha^{-1} DOC (Chow et al., 2009). In contrast, calculated stream yields from HS and other similar streams at the research site indicate a DOC export of approximately 0.03 kg ha^{-1} DOC. Rapid microbial remineralization of plant leachates has previously been demonstrated (Cleveland et al., 2004; Pellerin et al., 2010). Our study shows that DOM produced on the landscape is nearly quantitatively retained or remineralized, and DOM that does flow into adjacent streams has the potential to be highly modified by biotic and abiotic processes.

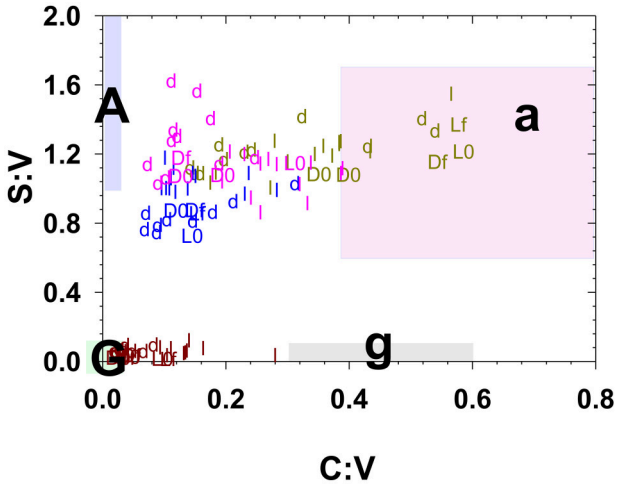

FIGURE 4 | Litter and duff leachates along with the starting and ending litter/duff materials plotted in S:V vs. C:V space. Small letters "l" and "d" represent leachate values, while capital "L" and "D" represent litter/duff materials with an appended "0" for initial and an appended "f" for final. Brown symbols are derived from foothill pine, light green from annual grasses, pink from live oak, and blue from blue oak. The shaded regions represent traditionally defined regions for angiosperm woods (A), angiosperm non-woody tissues (a), gymnosperm woods (G), and gymnosperm non-woody tissues (g) (Hedges and Mann, 1979).

Our study did not capture subsurface flow (i.e., trench samples) or stream dynamics for all storms across the leaching experiment, but were instead focused on two storm events in February 2007 and an additional sampling in January 2008 as part of an effort to capture a snapshot of DOM at multiple scales (stream orders) simultaneously. Hysteresis effects, in which DOC concentrations at a given discharge are significantly different between the rising and falling limbs of a storm, are well-known for streams and rivers (McGlynn and McDonnell, 2003), and similar variability extended to DOM composition as represented by lignin parameters (**Figure 5**). Short time-series sampling during the storm events revealed little in the way of consistent trends in how lignin parameters respond to DOM mobilization in HS (**Figure 5**), as S:V in any individual sampling event varied by up to 0.2, C:V by 0.1, (Ad:Al)v and (Ad:Al)s by 0.4, and Λ_8 by >2.0.

A portion of compositional variability is likely due to first-flush phenomena, which can be delayed by the necessity of wetting up in Mediterranean climates (O'Geen et al., 2010), however, changing contributions from different hydrologic flowpaths also must play a role (Swarowsky et al., 2012). The soil trench samples that isolate water transport through different soil horizons can be potentially helpful in parsing out these differences. Our most complete set of trench samples was collected in conjunction with the January 2008 storm, and it is clear that in terms of lignin compositions, the 10–30 cm depth was the most volatile, with large changes in every lignin parameter during the storm, while the 0–10 and 30–60 cm depths were more stable (**Figure 6**). The 10–30 cm depth during this storm event accounted for over half of the total flow measured in the trench (Swarowsky et al., 2012). Based on DOC (and to some extent lignin concentrations) in HS stream water that was higher than the trench samples, it is clear that there must be additional sources of DOM to the stream. Overland flow is generally not observed in this system due to rapid infiltration. However, during the January 2008 storm, water gushed out of gopher holes in the catchment, indicating a potential role for horizontal bypass flow, and the six samples collected during this study yielded DOC values of 3.9–8.7 mg L^{-1}, with a mean of 5.8 mg L^{-1}, which could partially account for the higher HS DOC values. Alternatively, if our leachate samples are proxies for bypass flow, then the potential contributions for bypass vs. subsurface DOC sources to HS can be evaluated compositionally with lignin property:property plots. In terms of S:V vs. C:V, HS most resembles the 30–60 cm depth trench sample and the blue oak duff leachate sample (**Figure 7A**), while (Ad:Al)v vs. (Ad:Al)s favors the 0–10 and 10–30 cm depths, along with the annual grass duff and blue oak duff leachates (**Figure 7B**). Of the two, S:V vs. C:V is more conducive to identifying sources (Hedges and Mann, 1979), and since blue oak comprises ∼45% of the vegetation in the catchment, it is not surprising that HS lignin would more closely resemble blue oak leachates. Yet the results of (Ad:Al)v vs. (Ad:Al)s actually seem to fit intuition, as the landscape is dominated by blue oak and annual grasses, and the 0–10 and 10–30 cm trench depths generate the most flow. This raises the possibility that in certain environments, acid:aldehyde ratios may have utility as a secondary source indicator, i.e., not useful for identifying the original plant materials, but becoming a "signature" of a water body. This has previously been postulated for water masses in marine environments where lignin diagenesis below the surface appears conservative on the timescale of centuries (Hernes and Benner, 2002). Given that annual grasses cover ∼45% of the landscape, it is a bit surprising that they are not more representative of HS in S:V vs. C:V space. However, percent coverage is not the critical factor, but rather, the total amount of litter/duff that accumulates from each vegetation type. Blue oak and foothill pine accumulate >20 times the amount in litter/duff materials per unit area compared to annual grasses (Chow et al., 2009), hence blue oak is the dominant vegetative source in this landscape and even foothill pine at ∼5% coverage has similar amounts of litter/duff materials compared to annual grasses.

In some systems, lignin compositions can be used quantitatively to determine relative contributions from different sources of vascular plant DOM (Eckard et al., 2007), however in this system the compositions of all the potential contributors are too similar for this type of analysis. Carbon-normalized yields of lignin are another quantitative tool that can be used to differentiate between vascular plant sources and non-vascular plant sources such as microbes or algae. Values of Λ_8 for HS averaged 0.95 mg lignin 100 mg OC^{-1}, which is significantly lower than weighted averages for all leachates (**Table 2**), including a Λ_8 value of 2.04 mg lignin 100 mg OC^{-1} for blue oak duff leachate, which appears to be the predominant source compositionally. This indicates that all leachate sources contain more than sufficient lignin to account for HS yields and that either lignin is preferentially lost relative to bulk carbon, or that HS DOM has been significantly augmented with algal/microbial

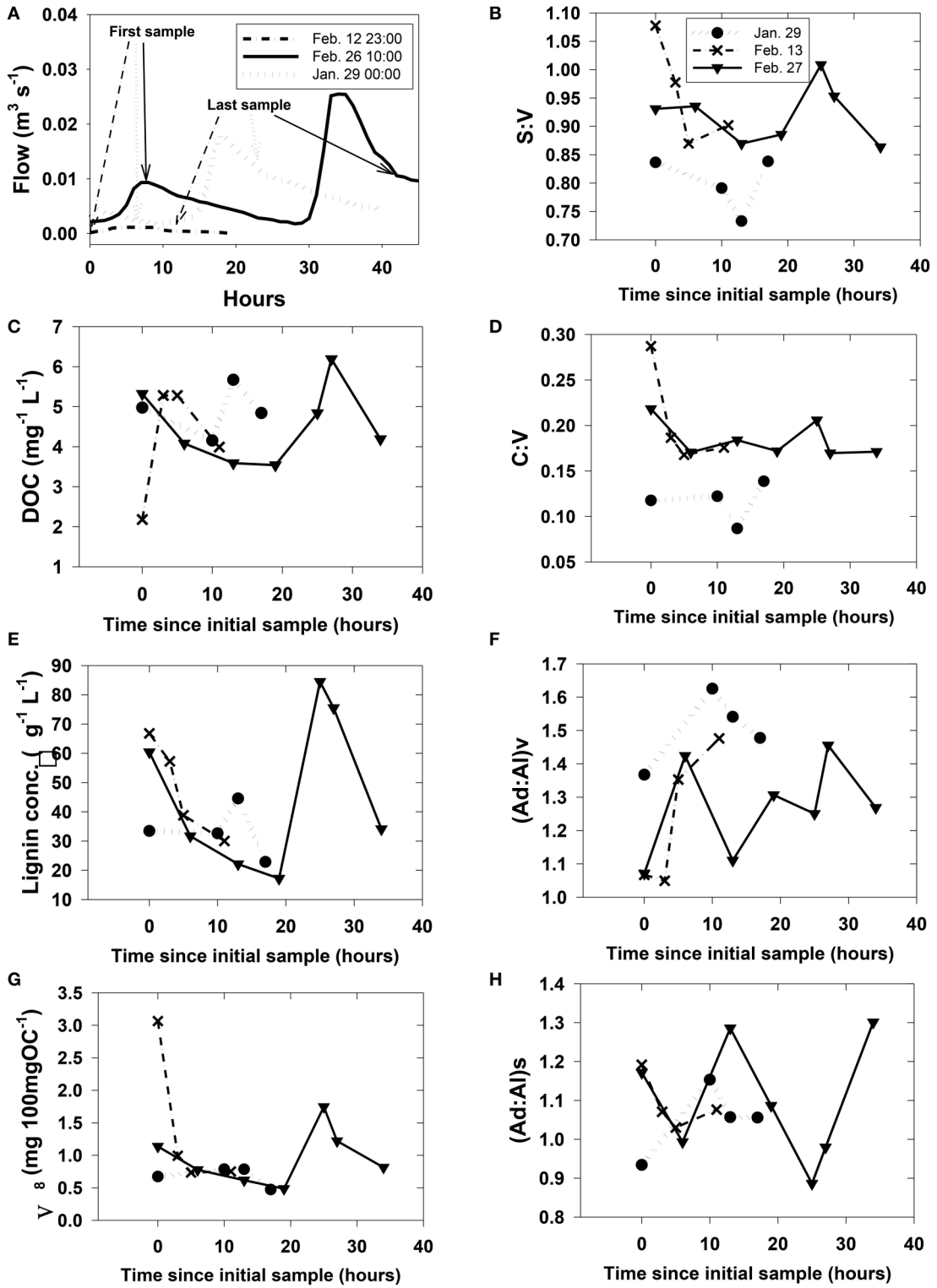

FIGURE 5 | Rapidly changing streamwater (HS) chemistry during three storms. Plot **(A)** shows discharge with greater context for each of the storms. Plots **(B)–(H)** were arbitrarily plotted with the first sample at time = 0 since the onset of storm runoff is difficult to pinpoint and sampling at each storm was initiated during a different phase of the runoff. However, the first and last sampling points for plots **(B)–(H)** are identified on their respective hydrographs in **(A)**.

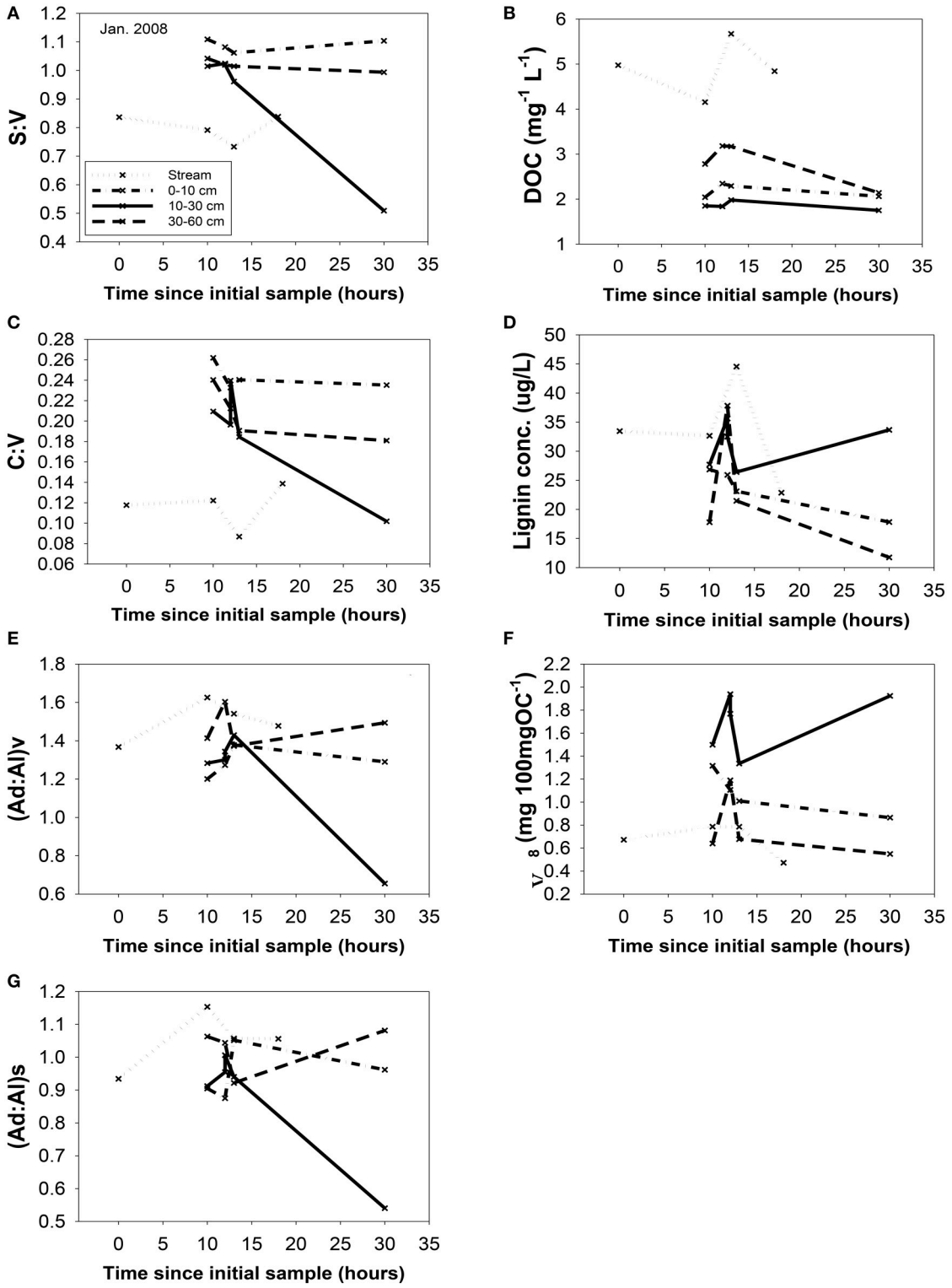

FIGURE 6 | Changing chemistry in the trench samples during the January, 2008 storm, with the streamwater (HS) chemistry as a reference point. All parameters are plotted vs. time: **(A)** S:V, **(B)** DOC, **(C)** C:V, **(D)** lignin concentration, **(E)** (Ad:Al)v, **(F)** carbon-normalized yields, Λ_8, and **(G)** (Ad:Al)s. Sampling time points are plotted relative to the first HS sample for that storm. All abbreviations were defined previously in the text.

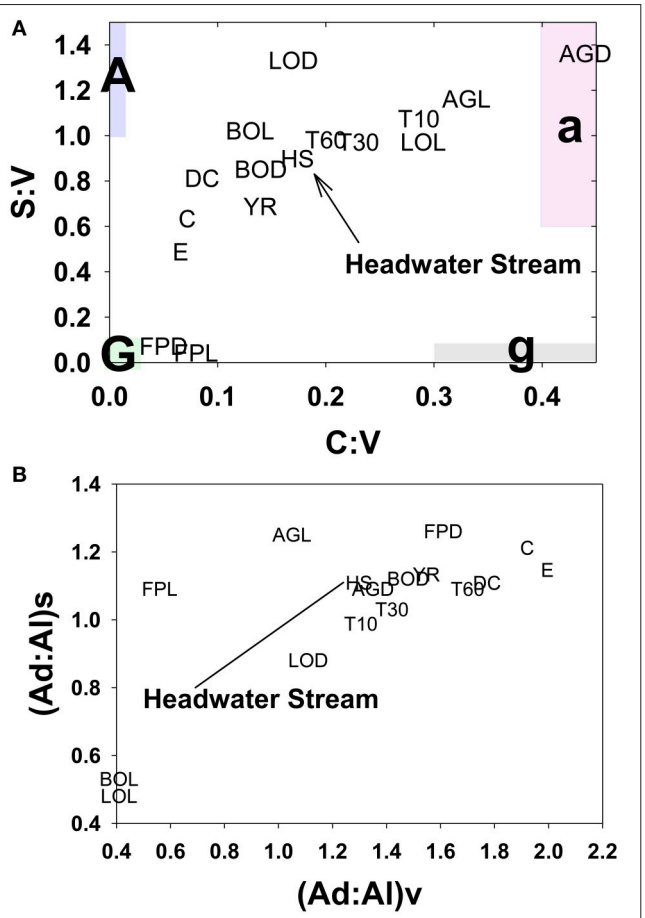

FIGURE 7 | HS lignin composition relative to multiple potential source compositions for (A) S:V vs. C:V and **(B)** (Ad:Al)v vs. (Ad:Al)s. Leachate and stream abbreviations are previously defined in the text, this plot also includes the following: E, Englebright; C, Collins; Y, Yuba; DC, Dry Creek; T10, 0–10 cm trench horizon; T30, 10–30 cm trench horizon; T60, 30–60 cm trench horizon.

sources. Again, the trench samples give an indication of where this modification may take place, as all trench Λ_8 values are significantly lower than the leachates, but the 0–10 and 30–60 cm depths are even lower than HS. Microbial communities are known contributors to the soil organic matter pool, so lower trench Λ_8 values could reflect dilution by non-vascular plant sources such as microbially-derived DOM. On the other hand, lignin phenols are also surface active and hence subject to sorption to soils (Kaiser et al., 1996; Hernes et al., 2007; Klotzbücher et al., 2016), which could preferentially remove lignin relative to bulk carbon. However, soils do not have infinite sites for lignin sorption, so over time the sorbed lignin would need to be degraded by microbes to free up those sites for the next storm event. Regardless of the mechanism for reducing Λ_8 values between leachates and passage through various soil horizons, the Λ_8 values of the three trench samples indicate that the 10–30 cm depth must constitute at least half the DOM in HS, if no other sources are considered, which is consistent with the fact that the 10–30 cm depth was the dominant hydrologic flowpath during the storm event (Swarowsky et al., 2012).

Optical properties do not have the specificity of biomarkers, but likely represent a larger proportion of the total DOM than any individual biomarker, and as such, can offer other clues as to the sources of DOM to streams. Carbon-normalized UV absorbance shows strong correlations to aromaticity (Traina et al., 1990), and in this study, HS $SUVA_{254}$ values averaged 3.75 L mg C^{-1} m^{-1}. In contrast, the weighted average $SUVA_{254}$ value for blue oak duff leachate was the highest of all the leachates at 2.58 L mg C^{-1} m^{-1}, yet still considerably lower than the stream values. Trench samples are closer in magnitude to HS streams, with lower $SUVA_{254}$ values (average 2.98 L mg C^{-1} m^{-1}) compared to streams indicating that DOC modification must occur in conjunction with other higher $SUVA_{254}$ sources, such as gopher holes ($SUVA_{254}$ values from 4.29 to 4.70 L mg C^{-1} m^{-1}) or stem-flow and canopy throughfall ($SUVA_{254}$ ranging from 3.04 to 3.83 L mg C^{-1} m^{-1}). Overall, the $SUVA_{254}$ values highlight a more complex picture of sources than perhaps lignin values alone. While blue oak is clearly an important contributor to stream DOM in this catchment, the optical properties of leachate DOM from blue oak duff still must undergo considerable modification before export to streams, including the preferential loss of non-aromatic carbon. This appears somewhat contradictory to the Λ_8 analysis in which leachates are also likely modified by preferential loss of lignin, which is an aromatic carbon component. However, lignin is just one of many different classes of aromatic compounds in organic matter, and the more straightforward conclusion is that $SUVA_{254}$ and lignin are tracing different components of DOM.

DOM Dynamics across a Continuum of Stream Orders

DOM chemistry at any given point in a river represents the sum of all sources and processes upstream. Those sources and processes are not weighted equally, as local landscape features tend to overprint more remote signatures (Eckard et al., 2007). In the regional system studied here, HS flows into Dry Creek, which in turn flows into the Yuba River. Dry Creek flows out of the Collins reservoir, so a stream like HS would act to overprint the Collins reservoir signature. Similarly, the Yuba River flows out of Englebright reservoir, and Dry Creek would act to overprint that signature. In reality, a complete picture of DOM dynamics would require continuous composition and concentration monitoring at all these sites over an extended time period, but our snapshot still provides insight into the evolution of DOM from catchments to higher order streams and rivers.

Among the many impacts of building dams, impounding river water in reservoirs can have a significant effect on both DOM quantity and quality (Oliver et al., 2016). Increased residence time allows for more input from algal sources and greater degradation of allochthonous DOM, the latter which is enhanced by sedimentation that increases optical transparency and allows photochemical degradation of aromatic-rich terrigenous DOM (Kraus et al., 2011). The dissolved lignin signatures of both the Collins and Englebright reservoirs appear consistent with these effects, as Λ_8 values are low (0.58 and 0.36 mg lignin 100 mg OC^{-1}, respectively), which can be achieved by both algal

production and lignin degradation, and the (Ad:Al)v values are the highest measured in our dataset (1.92 and 2.00). $SUVA_{254}$ values are more complicated to interpret: the $SUVA_{254}$ value in Collins of 3.12 L mg C^{-1} m^{-1} falls within the range that seems typical of rivers and streams in this region and is similar to values tracked in the San Luis Reservoir (2.94 L mg C^{-1} m^{-1} average) associated with the State Water Project (Kraus et al., 2011). In contrast, Englebright $SUVA_{254}$ of 4.38 L mg C^{-1} m^{-1} is considerably higher, but with low total DOC of 1.6 mg L^{-1}, it seems more likely that this high $SUVA_{254}$ results from conservative concentration of non-lignin aromatics, as opposed to production from new sources. In natural river systems, source inputs for river DOC are challenging to determine as a starting point, but the presence of these large and well-homogenized reservoirs serves as a strong backdrop for evolving DOM signatures downstream.

Dry Creek DOM clearly carries the signature of the Collins reservoir out of which it flows, as evidenced by identical Λ_8, as well as other lignin compositional parameters and $SUVA_{254}$ values that are all within 10–20% of Collins (**Table 2**). Although HS itself may not constitute a high enough discharge to overprint Dry Creek all by itself, it is representative of many small streams that discharge into Dry Creek along its transit from Collins reservoir to the Yuba River. In this context, the lignin compositional parameters of Dry Creek are all intermediate between Collins reservoir and HS, indicating a clear compositional shift to the Dry Creek signature imparted by HS and similar streams over the ∼7 km transit distance between Collins and the Dry Creek sampling point. A linear mixing model, |Dry Creek – Collins|*100%/|HS – Collins|, applied to each of the four lignin compositional parameters suggests that the proportion of Dry Creek DOM derived from HS and similar streams ranges from 13 to 101% (**Table 3**). Granted, this does not account for variations from stream to stream, nor does it account for *in situ* processing, but it provides a clear indication as to the potential collective impact of seemingly insignificant streams (in terms of discharge) on larger streams. Simply by DOC mass balance alone, the difference between Collins DOC at 2.9 mg L^{-1} and Dry Creek DOC at 4.7 mg L^{-1} indicates that small streams must account for ∼40% of the DOC in Dry Creek.

In comparison to the Collins to Dry Creek transformation, the Englebright to Yuba River at Dry Creek transformation appears greater over the ∼15 km reach between sampling points: Λ_8 values increase by >60% from 0.36 to 0.59 mg lignin 100 mg OC^{-1}, $SUVA_{254}$ values drop from 4.38 to 3.08 L mg C^{-1} m^{-1}, C:V values double, S:V values increase by ∼40%, and (Ad:Al)v values appear less degraded (**Table 2**). A ∼25% increase in DOC from 1.6 mg L^{-1} in Englebright compared to 2.0 mg L^{-1} in the Yuba River at Dry Creek reflects distinct inputs of carbon. Only one notable tributary, Deer Creek, enters the Yuba River in between Englebright reservoir and the Yuba River sampling point at Dry Creek, and discharge from Deer Creek was ∼8% that of the Yuba River at the time of sampling (**Figure 8**), although lag times between precipitation runoff and management decisions to release water from reservoirs adds nuance to interpretation. Hence the transformation in DOM in the Yuba River is not coming from a single point source, but must also be driven by the collective inputs from multiple smaller streams as well as DOM exchange with local landscape features and geomorphological features within the river channel itself. Given the relative magnitudes of the Yuba River compared to Dry Creek (<5% of the discharge of the Yuba River), it is somewhat surprising that Dry Creek is less impacted during transit than the Yuba River. However, this also reflects the challenges in making generalizations between processes in streams and rivers of significantly different orders (8th order for Yuba, 3rd or 4th order for Dry Creek).

Ultimately, there is great interest in gauging how well the DOM signature of a larger river like the Yuba River reflects the headwater sources. Clearly, the more diversity in landscapes within a river basin, the less likely river chemistry will mimic any single headwater source. In this case, there are distinct similarities in lignin chemistry and $SUVA_{254}$ between HS and the Yuba River despite the influence of reservoir effects on the Yuba River. Similar to the Dry Creek analysis, the Yuba River

TABLE 3 | Linear mixing models to demonstrate the magnitude of overprinting over 7–35 km reaches of Dry Creek and the Yuba River.

	S:V (%)	C:V (%)	(Ad:Al)v (%)	(Ad:Al)s (%)	Λ_8(%)
Collins to Dry Creek	67	13	24	101	1
Englebright to Yuba at Dry Creek	49	68	64	35	40
Englebright to Yuba at Simpson Lane	98	97	129	359	40

All changes in downstream values were in the direction of HS composition, however, some Yuba River at Simpson values were beyond even the HS compositions, and these are represented by percentages >100%. See Materials and Methods for more explanation of the linear mixing models.

HS, headwater stream in Sierra Foothills Research and Extension Center; S:V, sum of three syringyl phenols divided by sum of three vanillyl phenols; C:V, sum of two cinnamyl phenols divided by sum of three vanillyl phenols; (Ad:Al)v, vanillic acid divided by vanillin; (Ad:Al)s, syringic acid divided by syringaldehyde; Λ_8, sum of eight lignin phenols divided by organic carbon.

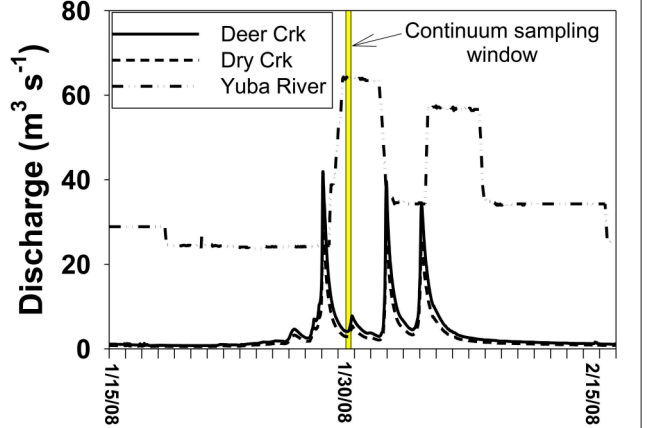

FIGURE 8 | Discharge context for the continuum sampling. Because Englebright is a managed reservoir, releases are not in synch with natural runoff and storm pulses from tributaries below the reservoir occur before the controlled release from the reservoir.

is bracketed well by Englebright vs. HS compositions, with linear mixing model calculations, |Yuba River – Englebright|*100%/|HS – Englebright|, indicating that 35–70% of the DOM at the Yuba River sampling point is derived from streams similar to HS (**Table 3**). This analysis can be extended even further with the Yuba River at Simpson Lane measurement ∼35 km downstream of Englebright. DOC has increased from 1.6 to 2.4 mg L^{-1}, and essentially, Yuba River at Simpson Lane lignin has completely converted to an HS-like signature, with three parameters at or near 100% and one greatly exceeding even the HS composite (**Table 3**). While parameterizing small source signatures as a single average is overly simplistic (among the many HS lignin measurements, there are individual samples that would sufficiently bracket Yuba River at Simpson with Englebright), this exercise overall speaks to the dominance of oak woodlands in the lower Yuba River basin.

Implications

This study captured DOM sources and processing at multiple scales, highlighting (1) the dynamic temporal changes in DOM source signatures even from the same source materials, (2) extensive modification and attenuation of DOM during transport through the landscape to the exporting stream, (3) more diversity in lignin source signatures than has previously been reported, and (4) the significant DOM overprinting capacity of small streams to much larger rivers. While these finding unquestionably address significant gaps in our knowledge of river basin biogeochemistry, they also highlight the greater challenges of river biogeochemistry research overall.

It is clear that novel and more comprehensive experimental designs must be brought into river research. A recent emphasis on time-series sampling in the past decade, for example, has led to significant modifications in measurements of river fluxes and seasonally evolving DOM and POM compositions (Hernes et al., 2008; Spencer et al., 2010b, 2016; Ellis et al., 2012). However, there is a great need for parsing out *in situ* sources and processing of riverine OM vs. external inputs, and one potential approach could be to pair studies of concrete-lined aquaducts with nearby rivers to try to constrain the relative role of external vs. internal. Lagrangian sampling of rivers could be useful for determining OM transformation hotspots (both new sources and processing) within a river channel, that could then lead to more intense investigations of sources and processing at those hotspots. Continual advancements in sensors that allow high temporal and spatial monitoring of colored DOM (CDOM) properties in rivers will undoubtedly help in capturing the complexity of river systems (Downing et al., 2012; Pellerin et al., 2012), but in spite of their potential, CDOM and fluorescent DOM (FDOM) by themselves have proven elusive in giving the chemical specificity that is needed to truly understand DOM dynamics. On the other hand, such sensors could also be used as targeting agents to point toward regions where chemical analyses can be put to the greatest use (Hernes et al., 2009).

River systems are incredibly complex both spatially and temporally, with flows that vary over several orders of magnitude, varying degrees of exchange in both directions with groundwater, varying landscapes through which they flow, changes in sediment loads that impact primary production and photochemical oxidation as well as sorption/desorption processes, and a myriad of point and non-point sources to deconvolute in order to interpret chemistry. In the collective attempts by the research community to narrow the scope of river studies to scales that are conceivably more accessible to interpretation, we lose the overall richness and complexity of the entire system. The overall connectedness of river chemistry to the landscape through which it flows re-emphasizes the incredible potential of rivers as canaries in the coal mine for capturing the effects of climate and land use change.

AUTHOR CONTRIBUTIONS

RAD and AO designed leaching experiment and field sampling scheme and conducted DOC analyses, hydrology measurements, and select UV-visible absorbance measurements. Lignin analyses were conducted by or under the supervision of RD and PH. RS conducted additional UV-visible measurements. The manuscript was written by PH, with the contribution of all authors.

FUNDING

This work was funded by the California State Water Resources Control Board (agreement no. 04-120-555-01), with additional contributions from National Science Foundation grant 1335622 (PH). Open access publication fees were supported in part by the Gordon and Betty Moore Foundation.

ACKNOWLEDGMENTS

The authors would like to thank Jiayou Deng, Alex Swarowsky, Tony Orozco, and Jeannie Evatt at the Department of Land, Air, and Water Resource for their field and lab support. Sarah Flores, Daniel Jara, and Jennifer Harfmann conducted lignin analyses on various subsets of the samples.

SUPPLEMENTARY MATERIAL

The Supplementary Material for this article can be found online at: http://journal.frontiersin.org/article/10.3389/feart.2017.00009/full#supplementary-material

Supplementary Figure 1 | Experimental setup for (A) litter and duff leaching during storms, and **(B)** subsurface lateral flow sampling via the trench.

Supplementary Figure 2 | Conceptual diagram of hydrologic flowpaths within the HS catchment at SFREC ultimately leading to export via HS. Percentages refer to the total lateral flow contributed by each soil layer during a typical storm event. The top three horizons correspond to the three perched water (trench) samples analyzed in this study. This figure is reproduced from O'Geen et al. (2010).

Supplementary Table 1 | All lignin data from the study, along with ancillary bulk data (when measured) and information, including leached volumes from the leachate study, DOC, $SUVA_{254}$, times, and dates.

Supplementary Table 2 | Additional DOC and $SUVA_{254}$ data from the study on samples that were not analyzed for lignin.

REFERENCES

Aufdenkampe, A. K., Hedges, J. I., Richey, J. E., Krusche, A. V., and Llerena, C. A. (2001). Sorptive fractionation of dissolved organic nitrogen and amino acids onto fine sediments within the Amazon Basin. *Limnol. Oceanogr.* 46, 1921–1935. doi: 10.4319/lo.2001.46.8.1921

Blough, N. V., Zafiriou, O. C., and Bonilla, J. (1993). Optical absorption spectra of waters from the Orinoco River outflow: terrestrial input of colored organic matter to the Caribbean. *J. Geophys. Res. Oceans* 98, 2271–2278. doi: 10.1029/92JC02763

Bouillon, S., Yambele, A., Spencer, R. G. M., Gillikin, D. P., Hernes, P. J., Six, J., et al. (2012). Organic matter sources, fluxes and greenhouse gas exchange in the Oubangui River (Congo River basin). *Biogeosciences* 9, 2045–2062. doi: 10.5194/bg-9-2045-2012

Burns, K. A., Hernes, P. J., Brinkman, D., Poulsen, A., and Benner, R. (2008). Dispersion and cycling of organic matter from the Sepik River outflow to the Papua New Guinea coast as determined from biomarkers. *Org. Geochem.* 39, 1747–1764. doi: 10.1016/j.orggeochem.2008.08.003

Chow, A. T., Dahlgren, R. A., and Harrison, J. A. (2007). Watershed sources of disinfection byproduct precursors in the Sacramento and San Joaquin rivers, California. *Environ. Sci. Technol.* 41, 7645–7652. doi: 10.1021/es070621t

Chow, A. T., Lee, S. T., O'Geen, A. T., Orozco, T., Beaudette, D., Wong, P. K., et al. (2009). Litter contributions to dissolved organic matter and disinfection byproduct precursors in California oak woodland watersheds. *J. Environ. Qual.* 38, 2334–2343. doi: 10.2134/jeq2008.0394

Cleveland, C. C., Neff, J. C., Townsend, A. R., and Hood, E. (2004). Composition, dynamics, and fate of leached dissolved organic matter in terrestrial ecosystems: results from a decomposition experiment. *Ecosystems* 7, 275–285. doi: 10.1007/s10021-003-0236-7

Downing, B. D., Pellerin, B. A., Bergamaschi, B. A., Saraceno, J. F., and Kraus, T. E. C. (2012). Seeing the light: the effects of particles, dissolved materials, and temperature on *in situ* measurements of DOM fluorescence in rivers and streams. *Limnol. Oceanogr. Methods* 10, 767–775. doi: 10.4319/lom.2012.10.767

Eckard, R. S., Hernes, P. J., Bergamaschi, B. A., Stepanauskas, R., and Kendall, C. (2007). Landscape scale controls on the vascular plant component of dissolved organic carbon across a freshwater delta. *Geochim. Cosmochim. Acta* 71, 5968–5984. doi: 10.1016/j.gca.2007.09.027

Ellis, E. E., Keil, R. G., Ingalls, A. E., Richey, J. E., and Alin, S. R. (2012). Seasonal variability in the sources of particulate organic matter of the Mekong River as discerned by elemental and lignin analyses. *J. Geophys. Res. Biogeosci.* 117, 15. doi: 10.1029/2011JG001816

Fooken, U., and Liebezeit, G. (2000). Distinction of marine and terrestrial origin of humic acids in North Sea surface sediments by absorption spectroscopy. *Mar. Geol.* 164, 173–181. doi: 10.1016/S0025-3227(99)00133-4

Hedges, J. I., and Ertel, J. R. (1982). Characterization of lignin by gas capillary chromatography of cupric oxide oxidation products. *Anal. Chem.* 54, 174–178. doi: 10.1021/ac00239a007

Hedges, J. I., and Mann, D. C. (1979). Characterization of plant tissues by their lignin oxidation products. *Geochim. Cosmochim. Acta* 43, 1803–1807. doi: 10.1016/0016-7037(79)90028-0

Hedges, J. I., Mayorga, E., Tsamakis, E., McClain, M. E., Aufdenkampe, A., Quay, P., et al. (2000). Organic matter in Bolivian tributaries of the Amazon River: a comparison to the lower mainstream. *Limnol. Oceanogr.* 45, 1449–1466. doi: 10.4319/lo.2000.45.7.1449

Helms, J. R., Stubbins, A., Ritchie, J. D., Minor, E. C., Kieber, D. J., and Mopper, K. (2008). Absorption spectral slopes and slope ratios as indicators of molecular weight, source, and photobleaching of chromophoric dissolved organic matter. *Limnol. Oceanogr.* 53, 955–969. doi: 10.4319/lo.2008.53.3.0955

Hernes, P. J., and Benner, R. (2002). Transport and diagenesis of dissolved and particulate terrigenous organic matter in the North Pacific Ocean. *Deep Sea Res. I* 49, 2119–2132. doi: 10.1016/S0967-0637(02)00128-0

Hernes, P. J., Bergamaschi, B. A., Eckard, R. S., and Spencer, R. G. M. (2009). Fluorescence-based proxies for lignin in freshwater dissolved organic matter. *J. Geophys. Res. Biogeosci.* 114, 10. doi: 10.1029/2009JG000938

Hernes, P. J., Kaiser, K., Dyda, R. Y., and Cerli, C. (2013a). Molecular trickery in soil organic matter: hidden lignin. *Environ. Sci. Technol.* 47, 9077–9085. doi: 10.1021/es401019n

Hernes, P. J., Robinson, A. C., and Aufdenkampe, A. K. (2007). Fractionation of lignin during leaching and sorption and implications for organic matter "freshness". *Geophys. Res. Lett.* 34, L17401. doi: 10.1029/2007GL031017

Hernes, P. J., Spencer, R. G. M., Dyda, R. Y., Pellerin, B. A., Bachand, P. A. M., and Bergamaschi, B. A. (2008). The role of hydrologic regimes on dissolved organic carbon composition in an agricultural watershed. *Geochim. Cosmochim. Acta* 72, 5266–5277. doi: 10.1016/j.gca.2008.07.031

Hernes, P. J., Spencer, R. G. M., Dyda, R. Y., Pellerin, B. A., Bachand, P. A. M., and Bergamaschi, B. A. (2013b). DOM composition in an agricultural watershed: assessing patterns and variability in the context of spatial scales. *Geochim. Cosmochim. Acta* 121, 599–610. doi: 10.1016/j.gca.2013.07.039

Kaiser, K., Guggenberger, G., and Zech, W. (1996). Sorption of DOM and DOM fractions to forest soils. *Geoderma* 74, 281–303. doi: 10.1016/S0016-7061(96)00071-7

Klotzbücher, T., Kalbitz, K., Cerli, C., Hernes, P. J., and Kaiser, K. (2016). Gone or just out of sight? The apparent disappearance of aromatic litter components in soils. *Soil* 2, 325–335. doi: 10.5194/soil-2-325-2016

Kraus, T. E. C., Bergamaschi, B. A., Hernes, P. J., Doctor, D., Kendall, C., Downing, B. D., et al. (2011). How reservoirs alter drinking water quality: organic matter sources, sinks, and transformations. *Lake Reserv. Manag.* 27, 205–219. doi: 10.1080/07438141.2011.597283

Lewis, D. J., Singer, M. J., Dahlgren, R. A., and Tate, K. W. (2006). Nitrate and sediment fluxes from a California rangeland watershed. *J. Environ. Qual.* 35, 2202–2211. doi: 10.2134/jeq2006.0042

Mann, P. J., Spencer, R. G. M., Dinga, B. J., Poulsen, J. R., Hernes, P. J., Fiske, G., et al. (2014). The biogeochemistry of carbon across a gradient of streams and rivers within the Congo Basin. *J. Geophys. Res. Biogeosci.* 119, 687–702. doi: 10.1002/2013JG002442

McGlynn, B. L., and McDonnell, J. J. (2003). Role of discrete landscape units in controlling catchment dissolved organic carbon dynamics. *Water Resour. Res.* 39, 18. doi: 10.1029/2002WR001525

O'Geen, A. T., Dahlgren, R. A., Swarowsky, A., Tate, K. W., Lewis, D. J., and Singer, M. J. (2010). Research connects soil hydrology and stream water chemistry in California oak woodlands. *Calif. Agric.* 64, 78–84. doi: 10.3733/ca.v064n02p78

Oliver, A. A., Spencer, R. G. M., Deas, M. L., and Dahlgren, R. A. (2016). Impact of seasonality and anthropogenic impoundments on dissolved organic matter dynamics in the Klamath River (Oregon/California, USA). *J. Geophys. Res. Biogeosci.* 121, 1946–1958. doi: 10.1002/2016JG003497

Pellerin, B. A., Hernes, P. J., Saraceno, J., Spencer, R. G., and Bergamaschi, B. A. (2010). Microbial degradation of plant leachate alters lignin phenols and trihalomethane precursors. *J. Environ. Qual.* 39, 946–954. doi: 10.2134/jeq2009.0487

Pellerin, B. A., Saraceno, J. F., Shanley, J. B., Sebestyen, S. D., Aiken, G. R., Wollheim, W. M., et al. (2012). Taking the pulse of snowmelt: *in situ* sensors reveal seasonal, event and diurnal patterns of nitrate and dissolved organic matter variability in an upland forest stream. *Biogeochemistry* 108, 183–198. doi: 10.1007/s10533-011-9589-8

Richey, J. E., Melack, J. M., Aufdenkampe, A. K., Ballester, V. M., and Hess, L. L. (2002). Outgassing from Amazonian rivers and wetlands as a large tropical source of atmospheric CO2. *Nature* 416, 617–620. doi: 10.1038/416617a

Sanderman, J., Lohse, K. A., Baldock, J. A., and Amundson, R. (2009). Linking soils and streams: sources and chemistry of dissolved organic matter in a small coastal watershed. *Water Resour. Res.* 45:W03418. doi: 10.1029/2008WR006977

Spencer, R. G. M., Aiken, G. R., Dornblaser, M. M., Butler, K. D., Holmes, R. M., Fiske, G., et al. (2013). Chromophoric dissolved organic matter export from U.S. rivers. *Geophys. Res. Lett.* 40, 1575–1579. doi: 10.1002/grl.50357

Spencer, R. G. M., Aiken, G. R., Dyda, R. Y., Butler, K. D., Bergamaschi, B. A., and Hernes, P. J. (2010a). Comparison of XAD with other dissolved lignin isolation techniques and a compilation of analytical improvements for the analysis of lignin in aquatic settings. *Org. Geochem.* 41, 445–453. doi: 10.1016/j.orggeochem.2010.02.004

Spencer, R. G. M., Aiken, G. R., Wickland, K. P., Striegl, R. G., and Hernes, P. J. (2008). Seasonal and spatial variability in dissolved organic matter quantity and composition from the Yukon River basin, Alaska. *Glob. Biogeochem. Cycle* 22, 13. doi: 10.1029/2008gb003231

Spencer, R. G. M., Hernes, P. J., Dinga, B., Wabakanghanzi, J. N., Drake, T. W., and Six, J. (2016). Origins, seasonality, and fluxes of organic matter in the Congo River. *Glob. Biogeochem. Cycle* 30, 1105–1121. doi: 10.1002/2016GB005427

Spencer, R. G. M., Hernes, P. J., Ruf, R., Baker, A., Dyda, R. Y., Stubbins, A., et al. (2010b). Temporal controls on dissolved organic matter and lignin biogeochemistry in a pristine tropical river, Democratic Republic of Congo. *J. Geophys. Res. Biogeosci.* 115:G03013. doi: 10.1029/2009JG001180

Swarowsky, A., Dahlgren, R. A., and O'Geen, A. T. (2012). Linking subsurface lateral flowpath activity with streamflow characteristics in a semiarid headwater catchment. *Soil Sci. Soc. Am. J.* 76, 532–547. doi: 10.2136/sssaj2011.0061

Traina, S. J., Novak, J., and Smeck, N. E. (1990). An ultraviolet absorbance method of estimating the percent aromatic carbon content of humic acids. *J. Environ. Qual.* 19, 151–153. doi: 10.2134/jeq1990.00472425001900010023x

Weishaar, J. L., Aiken, G. R., Bergamaschi, B. A., Fram, M. S., Fujii, R., and Mopper, K. (2003). Evaluation of specific ultraviolet absorbance as an indicator of the chemical composition and reactivity of dissolved organic carbon. *Environ. Sci. Technol.* 37, 4702–4708. doi: 10.1021/es030360x

Conflict of Interest Statement: The authors declare that the research was conducted in the absence of any commercial or financial relationships that could be construed as a potential conflict of interest.

frontiers in Earth Science

ORIGINAL RESEARCH
published: 28 March 2017
doi: 10.3389/feart.2017.00022

Molecular and Optical Properties of Tree-Derived Dissolved Organic Matter in Throughfall and Stemflow from Live Oaks and Eastern Red Cedar

Aron Stubbins[1], Leticia M. Silva[1], Thorsten Dittmar[2] and John T. Van Stan[3]*

[1] Department of Marine Sciences, Skidaway Institute of Oceanography, University of Georgia, Savannah, GA, USA, [2] Research Group for Marine Geochemistry, Institute for Chemistry and Biology of the Marine Environment, University of Oldenburg, Oldenburg, Germany, [3] Department of Geology and Geography, Georgia Southern University, Statesboro, GA, USA

OPEN ACCESS

Edited by:
Richard G. Keil,
University of Washington, USA

Reviewed by:
David Christopher Podgorski,
Florida State University, USA
Christian Schlosser,
GEOMAR Kiel, Germany

****Correspondence:***
Aron Stubbins
aron.stubbins@skio.uga.edu

Specialty section:
This article was submitted to Marine Biogeochemistry, a section of the journal Frontiers in Earth Science

Received: *28 November 2016*
Accepted: *20 February 2017*
Published: *28 March 2017*

Citation:
Stubbins A, Silva LM, Dittmar T and Van Stan JT (2017) Molecular and Optical Properties of Tree-Derived Dissolved Organic Matter in Throughfall and Stemflow from Live Oaks and Eastern Red Cedar. Front. Earth Sci. 5:22. doi: 10.3389/feart.2017.00022

Studies of dissolved organic matter (DOM) transport through terrestrial aquatic systems usually start at the stream. However, the interception of rainwater by vegetation marks the beginning of the terrestrial hydrological cycle making trees the headwaters of aquatic carbon cycling. Rainwater interacts with trees picking up tree-DOM, which is then exported from the tree in stemflow and throughfall. Stemflow denotes water flowing down the tree trunk, while throughfall is the water that drips through the leaves of the canopy. We report the concentrations, optical properties (light absorbance) and molecular signatures (ultrahigh resolution mass spectrometry) of tree-DOM in throughfall and stemflow from two tree species (live oak and eastern red cedar) with varying epiphyte cover on Skidaway Island, Savannah, Georgia, USA. Both stemflow and throughfall were enriched in DOM compared to rainwater, indicating trees were a significant source of DOM. The optical and molecular properties of tree-DOM were broadly consistent with those of DOM in other aquatic ecosystems. Stemflow was enriched in highly colored DOM compared to throughfall. Elemental formulas identified clustered the samples into three groups: oak stemflow, oak throughfall and cedar. The molecular properties of each cluster are consistent with an autochthonous aromatic-rich source associated with the trees, their epiphytes and the microhabitats they support. Elemental formulas enriched in oak stemflow were more diverse, enriched in aromatic formulas, and of higher molecular mass than for other tree-DOM classes, suggesting greater contributions from fresh and partially modified plant-derived organics. Oak throughfall was enriched in lower molecular weight, aliphatic and sugar formulas, suggesting greater contributions from foliar surfaces. While the optical properties and the majority of the elemental formulas within tree-DOM were consistent with vascular plant-derived organics, condensed aromatic formulas were also identified. As condensed aromatics are generally interpreted

as deriving from partially combusted organics, some of the tree-DOM may have derived from the atmospheric deposition of thermogenic and other windblown organics. These initial findings should prove useful as future studies seek to track tree-DOM across the aquatic gradient from canopy roof, through soils and into fluvial networks.

Keywords: Tree-DOM, dissolved organic matter (DOM), carbon, CDOM, deposition, dissolved organic carbon (DOC), stemflow, throughfall

INTRODUCTION

In forested catchments, trees represent the first interceptors of precipitation and the first potential source of dissolved organic matter (DOM) to the aquatic carbon cycle. The earliest trees appear in the fossil record approximately 385 million years ago (Stein et al., 2007), since when they have fundamentally altered terrestrial (Algeo et al., 2001; Gensel, 2001) and wetland ecosystems (Greb et al., 2006). Forests are estimated to have covered close to 50 million km^2 of the planet 5,000 years ago (FAO, 2016) equivalent to approximately 1/3rd of the earth's land surface. Just as forests transformed the global ecosystem, humans now have a similarly profound influence upon global ecology and biogeochemistry. Deforestation during the Anthropocene (Crutzen, 2002) has seen forest land cover reduced by approximately 50% to 31.7 million km^2 as of 2005 (Hansen et al., 2010) and was continuing at a rate of approximately 1.5 million km^2 $year^{-1}$ between 2000 and 2012 (Hansen et al., 2013).

Despite the vast and rapidly changing expanse of land covered and volume of precipitation intercepted by trees, only modest attention has been focused upon the DOM delivered by trees to downstream ecosystems (Kolka et al., 1999; Michalzik et al., 2001; Neff and Asner, 2001; Levia et al., 2011; Inamdar et al., 2012). Once intercepted, rainwater takes one of two hydrological flow paths to the forest floor: throughfall (water that drips from the canopy or falls directly through canopy gaps) and stemflow (water funneled by the canopy to the stem). Both stemflow (5–200 mg-C L^{-1}) (Moore, 2003; Tobón et al., 2004; Levia et al., 2011) and throughfall (1–100 mg-C L^{-1}) (Michalzik et al., 2001; Neff and Asner, 2001; Le Mellec et al., 2010; Inamdar et al., 2012) are enriched in DOM relative to rainwater (0.3–2 mg-C L^{-1}) (Willey et al., 2000).

The fate of exported tree-derived DOM (tree-DOM) will depend upon the chemistry of the tree-DOM, the nature of the receiving ecosystem and hydrological considerations. Significant losses and alteration of tree-DOM occurs as stemflow and throughfall enter soils due to sorption to mineral soils, which preferentially retain hydrophobic DOM fractions (Jardine et al., 1989; Kaiser and Zech, 1998, 2000). The spatially and temporally uneven delivery of biolabile tree-DOM to soil ecosystems during storms may fuel biogeochemical hot spots and hot moments (McClain et al., 2003; Vidon et al., 2010) and microbial utilization of biolabile organics in soils further modifies tree-DOM (Aitkenhead-Peterson et al., 2003). It has also been suggested that sunlight driven photoreactions (Mopper et al., 2015) may act as a sink for tree-DOM (Aitkenhead-Peterson et al., 2003). Photoreactions would be expected to preferentially remove aromatics, including black carbon (Stubbins et al., 2012b), while preserving and producing high H/C compounds such as aliphatics (Stubbins et al., 2010; Stubbins and Dittmar, 2015).

The degree to which tree-DOM is lost and altered by these processes before reaching a downstream aquatic ecosystem also depends upon the flow path traveled down the tree and from there to an inland water body (Inamdar et al., 2012). Direct input of stemflow or throughfall into a stream or lake will presumably result in negligible alteration prior to delivery. High levels of minimally modified tree-DOM may also reach inland waters during periods of heavy rainfall and resultant high flow when residence times within modifying ecosystems (e.g., soils) are reduced or bypassed completely in the case of overland flow. High flow pulses driven by heavy precipitation shunt reactive DOM downstream through river networks and are increasingly recognized as significant components of the fluvial carbon cycle (Raymond et al., 2016). These extreme, short lived pulses can account for the majority of annual river DOC loads being exported in just a few days per year (Raymond and Saiers, 2010). It remains unclear whether tree-DOM is delivered efficiently to fluvial systems during these pulse-shunt events.

To further understand the quality of tree-DOM, we collected stemflow and throughfall samples from broadleaved (oak) and needleleaved (cedar) trees with or without epiphytes during two storm events. The concentrations, optical properties and molecular signatures of the sampled tree-DOM are presented.

METHODS

Sample Site

Samples were collected on the Skidaway Institute of Oceanography (SkIO) campus, Georgia, USA (31.9885°N, 81.0212°W) (**Figure 1a**) during two rain events: Storm A on June 27th 2015 and Strom B on 28th June 2015 (**Table 1**). SkIO is in a subtropical climate zone (Köppen *Cfa*), with 30-year mean annual precipitation ranging from 750 to 1,200 mm that occurs as rainfall and mostly during the summer months (GA Office of the State Climatologist). Average daily temperatures in summer range between 30 and 35°C (Georgia Office of the State Climatologist, 2012). The elevation of SkIO ranges from 0 to 10 m above mean sea level. The sampling sites were flat (0–5% slopes) and underlain by Chipley fine sandy soils (https://websoilsurvey.sc.egov.usda.gov). Two species of tree were sampled: *Quercus virginiana* Mill. (southern live oak) referred to here as oak for brevity; and, *Juniperus virginiana* L. (eastern red cedar) referred to as cedar. The epiphytes *Tillandsia usneoides* L. (Spanish moss) and *Pleopeltis polypodioides* (resurrection fern) can be found to

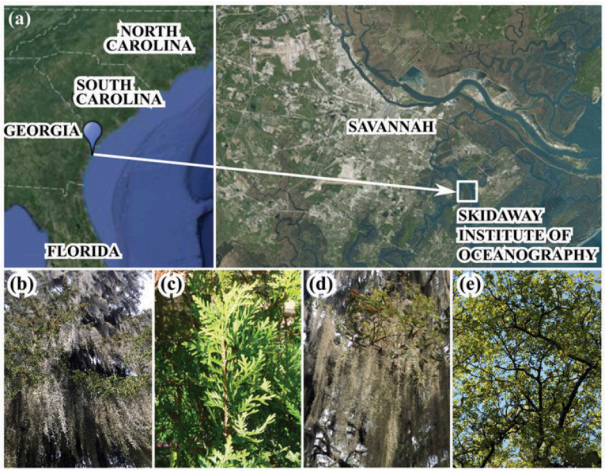

FIGURE 1 | (a) Map showing location of Skidaway Institute of Oceanography (Georgia, USA). Photographs of the trees sampled, including **(b)** epiphyte-covered cedar, **(c)** bare cedar, **(d,e)** mixed-epiphyte-covered oak.

cover these trees at high densities on SkIO (**Figures 1b–e**). A Spanish moss-covered cedar tree (cedar moss, **Figure 1b**) and an epiphyte-free cedar tree (bare cedar, **Figure 1c**) were chosen to assess whether the influence of epiphytes were apparent in the concentrations or quality of tree-DOM. Four oak trees were sampled, each with highly variable epiphyte coverage including, both resurrection ferns and Spanish moss (**Figures 1d,e**), which is typical of live oaks in the maritime southeastern US. Both stemflow and throughfall samples were collected for each tree type.

Sample Collection and Processing

All plastic and glassware were pre-cleaned by rinsing five times with ultrapure water (MilliQ), soaking in pH 2 ultrapure water (2 ppt 6N hydrochloric acid), re-rinsing five times with ultrapure water, and dried. Once dry, glassware was further baked at 450°C for 8 h. Twenty throughfall samplers (0.18 m^2, 0.5 m height, high density polyethylene (HDPE) bins) were deployed for each storm, three beneath each of four oaks (TF Oak 1–4), and four beneath the bare (TF Bare Cedar) and four beneath the epiphyte-covered cedars (TF Cedar Moss). An additional four throughfall samplers were placed upon open ground to sample rainwater (Rain). Stemflow samplers, which consisted of collars cut from polyethylene tubing wrapped about the trunk at 1.4 m height and connected to 10 L HDPE carboys, were installed on four oaks (SF Oak 1–4), the bare cedar (SF Bare Cedar) and the epiphyte-covered cedar (SF Cedar Moss). Throughfall and stemflow collectors were deployed approximately 1 h before rainfall commenced and collected within 1 h of rainfall ceasing. All sampling sites are within 10 min walk of Stubbins' laboratory at SkIO. Samples were rapidly returned to the laboratory and 0.2 μm filtered within 4 h of collection. Sample volumes were measured. Throughfall and rainwater volume fluxes (mm) were calculated by dividing the sample volumes by the surface area of the samplers (0.18 m^2).

Dissolved Organic Carbon Concentrations

After filtration, aliquots of sample were transferred to pre-combusted 40 mL glass vials, acidified to pH 2 (hydrochloric acid), and analyzed for non-purgable organic carbon using a Shimadzu TOC-VCPH analyzer fitted with a Shimadzu ASI-V autosampler. In addition to potassium hydrogen phthalate standards, aliquots of deep seawater reference material, Batch 10, Lot# 05-10, from the Consensus Reference Material Project (CRM) were analyzed to check the precision and accuracy of the DOC analyses. Analyses of the CRM deviated by <5% from the reported value for these standards (41–44 μM-DOC). Routine minimum detection limits in the investigator's laboratory using the above configuration are 2.8 ± 0.3 μM-C and standard errors are typically 1.7 ± 0.5% of the DOC concentration (Stubbins and Dittmar, 2012).

Colored Dissolved Organic Matter

Filtered sample (non-acidified) was placed in a 1 cm quartz absorbance cell situated in the light path of an Agilent 8453 ultraviolet-visible spectrophotometer and CDOM absorbance spectra were recorded from 190 to 800 nm. Ultrapure water provided a blank. Blank corrected absorbance spectra were corrected for offsets due to scattering and instrument drift by subtraction of the average absorbance between 700 and 800 nm (Stubbins et al., 2011). Data output from the spectrophotometer were in the form of dimensionless absorbance (i.e., optical density, OD) and were subsequently converted to the Napierian absorption coefficient, a (m^{-1}) (Hu et al., 2002). If sample absorbance (OD) exceeded 2 at 250 nm, samples were diluted 10-fold with ultrapure water and reanalyzed. Specific UV absorbance at 254 nm ($SUVA_{254}$; L mg-C^{-1} m^{-1}), an indicator of DOM aromaticity defined as the Decadic absorption coefficient at 254 nm (m^{-1}) normalized to DOC (mg-C L^{-1}) (Weishaar et al., 2003) was calculated along with spectral slope over the range 275–295 nm ($S_{275-295}$) (Helms et al., 2008). Spectral slope values are reported as positive values.

Fourier Transform Ion Cyclotron Resonance Mass Spectrometry

In the current study, whole water samples were analyzed without extraction or purification to provide the broadest analytical window prior to mass spectral analysis. Each stemflow sample (SF Oak 1–4; SF Cedar Moss; SF Bare Cedar) was analyzed. For throughfall samples, carbon-weighted composite samples were generated for each rainfall and throughfall sample by combining carbon-dependent volumes of sample (i.e., all four aliquots were combined for each of the rain samples and each cedar sampled for throughfall; three aliquots were combined for each of the four oak trees sampled for throughfall; the volume that each aliquot contributed to a composite sample was adjusted in order that the final composite sample contained an equal fraction of carbon from each aliquot). To generate consistent FT-ICR mass spectra all samples were analyzed under the same conditions, including DOC concentration. Therefore, all tree-DOM samples were diluted to the identical DOC concentration with ultrapure water (10 mg-C L^{-1}) and then further diluted 1:1 with methanol. However, as rainwater DOC (1–2 mg-C

TABLE 1 | Sample numbers, volumes, hydrological fluxes (calculated based upon the 0.18 m^2 surface area of rain and throughfall collectors), dissolved organic carbon concentrations (DOC), colored dissolved organic matter Napierian absorption coefficients at 300 nm (CDOM a_{300}), CDOM spectral slope values for the range 275–295 nm ($S_{275-295}$), and specific ultraviolet absorbance at 254 nm ($SUVA_{254}$) for rainwater and each of the stemflow (SF) and throughfall (TF) sample types collected during two storms.

Event	Sample name	*N*	Volume (mL)	Flux (mm)	DOC (mg-C L^{-1})	CDOM a_{300} (m^{-1})	$S_{275-295}$ (nm^{-1})	$SUVA_{254}$ (L mg-C^{-1} m^{-1})
Storm A 27/06/15	Rain	4	2778 ± 125	15 ± 1	2.3 ± 0.1	1.9 ± 0.9	0.0208 ± 0.0037	0.8 ± 0.2
	SF Oak	4	246 ± 140	N/A	46 ± 9	180 ± 83	0.0146 ± 0.0002	3.0 ± 0.9
	TF Oak	12	2172 ± 439	12 ± 2	15 ± 8	43 ± 22	0.0158 ± 0.0008	2.2 ± 0.3
	SF Cedar Moss	1	>10 L	N/A	52	321	0.0154	5.1
	TF Cedar Moss	4	1855 ± 355	10 ± 2	52 ± 9	153 ± 28	0.0165 ± 0.0001	2.4 ± 0.1
	SF Bare Cedar	1	>10 L	N/A	30	159	0.0145	4.1
	TF Bare Cedar	4	2996 ± 197	16.6 ± 1.1	13 ± 1	40 ± 4	0.016 ± 0.0002	2.5 ± 0.1
Storm B 28/06/15	Rain	4	3600 ± 91	20.0 ± 0.5	1.2 ± 0.1	0.7 ± 0.7	0.0457 ± 0.0237	0.8 ± 0.4
	SF Oak	4	1140 ± 674	N/A	78 ± 17	418 ± 99	0.0144 ± 0.0002	4.1 ± 0.1
	TF Oak	12	3488 ± 610	19.4 ± 3.4	10 ± 7	31 ± 19	0.0158 ± 0.0009	2.6 ± 0.4
	SF Cedar Moss	1	9583	N/A	71	378	0.0145	4.0
	TF Cedar Moss	4	2945 ± 200	16.4 ± 1.1	36 ± 9	113 ± 24	0.016 ± 0.0002	2.5 ± 0.2
	SF Bare Cedar	1	>10 L	N/A	25	129	0.0155	4.0
	TF Bare Cedar	4	3358 ± 294	18.7 ± 1.6	13 ± 2	48 ± 13	0.0157 ± 0.0006	2.9 ± 0.3

Values present are means ± one standard deviation.

L^{-1}; **Table 1**) was significantly lower than for tree-DOM and reducing all sample DOC concentrations to <1 mg-C L^{-1} would have impaired FT-ICR MS performance, rainwater samples were diluted 1:1 with methanol and run at their resulting DOC concentrations (Storm A: 1.1 mg-C L^{-1}; Storm B: 0.6 mg-C L^{-1}). As this impaired the quality of the rainwater FT-ICR MS data, this data is only used to contrast with the tree-DOM data in a cluster analysis and the molecular quality of rainwater DOM is not presented. In order to compare rainwater DOM to tree-DOM directly, the study design would have needed to include a DOM isolation and concentration step in order to allow all samples, rainwater included, to be analyzed by FT-ICR MS at the same concentrations. This option was not chosen as it would have reduced the analytical window for our focus of study: tree-DOM.

Once mixed 1:1 with methanol, samples were analyzed in negative mode electrospray ionization using a 15 Tesla FT-ICRMS (Bruker Solarix) at the University of Oldenburg, Germany. 500 broadband scans were accumulated for the mass spectra. After internal calibration, mass accuracies were within an error of <0.2 ppm. Elemental formulas were assigned to peaks with signal to noise ratios greater than five based on published rules (Koch et al., 2007; Stubbins et al., 2010; Singer et al., 2012). Peaks detected in the procedural blank (PPL extracted ultrapure water) were removed. Peak detection limits were standardized between samples by adjusting the dynamic range of each sample to that of the sample with the lowest dynamic range (dynamic range = average of the largest 20% of peaks assigned a formula divided by the signal to noise threshold intensity; standardized detection limit = average of largest 20% of peaks assigned a formula within a sample divided by the lowest dynamic range within the sample set; Spencer et al., 2014; Stubbins et al., 2014). Peaks below the standardized detection limit were removed. These peaks were removed in order to prevent false negatives within samples with low dynamic range.

For each elemental formula, we calculated the modified Aromaticity Index (AImod) (Koch and Dittmar, 2006, 2016), which indicates the likelihood of an elemental formula representing aromatic structures, from an AImod of zero, where formulas are aliphatic, through an intermediate range, where an elemental formula could indicate aromatic or non-aromatic isomers, to AImod values above 0.5, where an elemental formula is highly likely to represent aromatic isomers (Koch and Dittmar, 2006). These AImod values were calculated as:

$$\text{AImod} = (1 + \text{C} - 0.5\text{O} - \text{S} - 0.5(\text{N} + \text{P} + \text{H})) / (\text{C} - 0.5\text{O} - \text{S} - \text{N} - \text{P}) \quad (1)$$

AImod values 0.5–0.67 and >0.67 were assigned as aromatic and condensed aromatic structures, respectively (Koch and Dittmar, 2006). Compound classes were further defined as highly unsaturated (AImod < 0.5, H/C < 1.5, O/C < 0.9), unsaturated aliphatics ($1.5 \leq$ H/C < 2, O/C < 0.9, $N = 0$), saturated fatty acids (H/C ≥ 2, (O/C < 0.9), sugars (O/C ≥ 0.9) and peptides ($1.5 \leq$ H/C < 2, O/C < 0.9, $N < 0$). Since an individual formula could occur as multiple isomeric structures, these classifications only serve as a guide to the structures present within DOM. For instance, "peptides" have the elemental formulas of peptides, but their actual structure may differ.

Standardized peak intensities (z) within a sample were calculated following:

$$\text{z} = \frac{x - \mu}{\sigma} \quad (2)$$

where, x is the measured peak intensity, μ is mean peak intensity within the sample, and σ is the standard deviation in peak

intensity within the sample (Spencer et al., 2014). Cluster analysis of the standardized peak intensities of assigned formulas (Ward clustering in JMP®) was then performed (Spencer et al., 2014).

RESULTS

Dissolved Organic Matter Concentrations and Optical Properties

DOM concentrations, quantified as DOC, ranged from 1.1 to 2.4 mg-C L^{-1} in rainwater, 40 to 95 mg-C L^{-1} in oak stemflow, 2.2 to 28 mg-C L^{-1} in oak throughfall, 52 to 71 mg-C L^{-1} in epiphyte-covered cedar stemflow, 31 to 62 mg-C L^{-1} in epiphyte-covered cedar throughfall, 25 to 30 mg-C L^{-1} in bare cedar stemflow, and 12 to 16 mg-C L^{-1} in bare cedar throughfall across the two storms sampled.

Absorbance spectra decayed exponentially with increasing wavelength (**Figure 2**). Napierian absorption coefficients for CDOM at 300 nm ranged from 0.1 to 3.2 m^{-1} in rainwater, 101 to 526 m^{-1} in oak stemflow, 6 to 81 m^{-1} in oak throughfall, 321 to 378 m^{-1} in epiphyte-covered cedar stemflow, 95 to 148 m^{-1} in epiphyte-covered cedar throughfall, 129 to 159 m^{-1} in bare cedar stemflow, and 36 to 67 m^{-1} in bare cedar throughfall across the two storms sampled.

Spectral slope values for the range 275–295 nm for CDOM ranged from 0.0156 to 0.0673 nm^{-1} in rainwater, 0.0142 to 0.0147 nm^{-1} in oak stemflow, 0.0139 to 0.0169 nm^{-1} in oak throughfall, 0.0145 to 0.0154 nm^{-1} in epiphyte-covered cedar stemflow, 0.0157 to 0.0166 nm^{-1} in epiphyte-covered cedar throughfall, 0.0145 to 0.0155 nm^{-1} in bare cedar stemflow, and 0.0152 to 0.0165 nm^{-1} in bare cedar throughfall across the two storms sampled.

$SUVA_{254}$ values ranged from 0.5 to 1.3 L mg-C^{-1} m^{-1} in rainwater, 1.9 to 4.2 L mg-C^{-1} m^{-1} in oak stemflow, 1.6 to 2.8 L mg-C^{-1} m^{-1} in oak throughfall, 4.0 to 5.1 L mg-C^{-1} m^{-1} in epiphyte-covered cedar stemflow, 2.3 to 2.8 L mg-C^{-1} m^{-1} in epiphyte-covered cedar throughfall, 4.0 to 4.1 L mg-C^{-1} m^{-1} in bare cedar stemflow, and 2.4 to 3.3 L mg-C^{-1} m^{-1} in bare cedar throughfall across the two storms sampled.

The full dataset is presented in Table S1. Means and standard deviations for each data and sample type per storm are presented in **Table 1** and summarized in **Figure 3**. Patterns in DOC concentrations and DOM optical properties were similar between storms (**Figure 3**). Rainwater DOM had much lower values of DOC, CDOM, and SUVA, and much steeper spectral slope values than the tree-DOM samples. In general, the stemflow samples exhibited higher DOC, CDOM, and SUVA, and shallower spectral slopes, than their respective throughfall samples (**Figure 3**). The one exception being DOC for the epiphyte-covered cedar during storm A, when both stemflow and throughfall DOC concentrations were similar (**Figure 3A**).

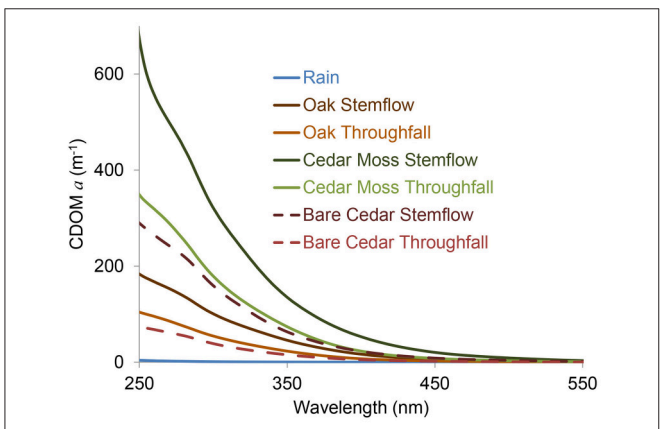

FIGURE 2 | Exemplary colored dissolved organic matter (CDOM) Napierian absorption coefficient (*a*) spectra for rainwater and each of the stemflow (SF) and throughfall (TF) sample types collected.

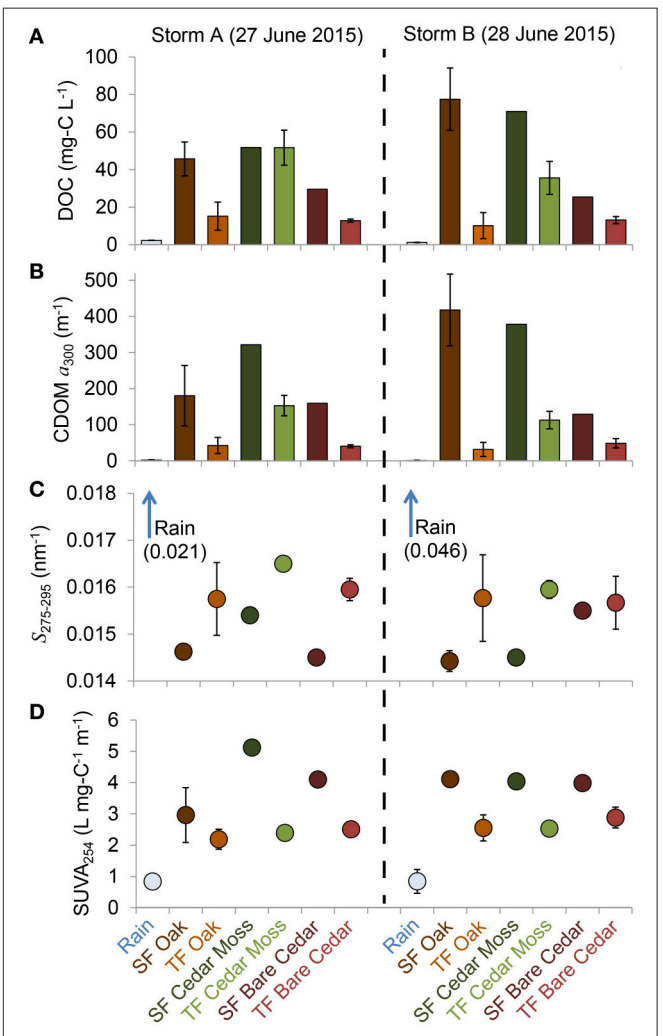

FIGURE 3 | Mean values for (A) dissolved organic carbon (DOC) concentration, **(B)** colored dissolved organic matter (CDOM) Napierian absorption coefficient at 300 nm (a_{300}), **(C)** spectral slope from 275 to 295 nm ($S_{275-295}$), and **(D)** specific ultraviolet absorbance at 254 nm ($SUVA_{254}$) for rainwater and each of the stemflow (SF) and throughfall (TF) sample types collected (see legend). Error bars represent 1 standard deviation and are not shown when they were narrower than the symbol.

Molecular Signatures of Tree-Derived Dissolved Organic Matter

Whole water samples mixed 1:1 with methanol yielded mass spectra (**Figure 4**) with sufficient resolution and signal to enable the assignment of 5,852 elemental formulas to tree-DOM. The raw mass spectra for oak and cedar stemflow displayed molecular signatures consistent with those of whole river water DOM run on the same instrument, under the same conditions, during the same month (Kolyma River data in **Figure 4**; Stubbins et al., 2017). Looking at one representative mass to charge (343 m/z; **Figure 4**), DOM in oak stemflow and cedar stemflow has similar molecular diversities (i.e., there are a similar number of peaks). However, the relative abundance of some peaks varies between samples, with some peaks being below detection in one sample and present in the other.

To further explore the diversity of tree-DOM and how it varied among the samples a cluster analysis of the standardized peak intensities of assigned formulas (Ward clustering in JMP®) was performed (Spencer et al., 2014). The distance graph for this cluster analysis revealed a sharp slope break at 4 clusters (**Figure 5**; lower panel). These four clusters were: rainwater, stemflow oak, throughfall oak, cedar, the latter including stemflow and throughfall from both the epiphyte-covered and bare cedar trees (**Figure 5**). Oak DOM, including both stemflow and throughfall, and cedar DOM are clearly separated (distance between clusters, $d = 17$). Oak stemflow and throughfall are also separated from one another (distance between clusters, $d = 12$). Although other clusters are formed, the distances between them are smaller ($d < 6$). For instance, the epiphyte-covered and bare cedar trees form distinct clusters, but with a cluster distance of <2 these samples have limited molecular differences. Based upon the cluster analysis, the molecular properties of three molecularly distinct types of tree-DOM are presented: oak throughfall, oak stemflow and cedar (**Table 2**). Data for the rainwater cluster are not presented.

The oak stemflow cluster comprised 4,765, oak throughfall 3,565, and cedar 3,643 formulas. All samples contained high proportions of CHO-only formulas (65–71%; **Table 2**). The oak stemflow was enriched in nitrogen compared to oak throughfall, and both were enriched in nitrogen compared to cedar DOM. Oak throughfall was enriched in sulfur and depleted in phosphorous compared to the other forms of tree-DOM, with cedar DOM being the most enriched in phosphorous.

The elemental formulas for each tree-DOM type were plotted in van Krevelen space (**Figures 6A–C**). Oak DOM spanned a broader range of van Krevelen space than cedar DOM. All types of tree-DOM contained high intensity elemental formulas in the region bounded by approximately H/C 1.1–1.6 and O/C 0.15 and 0.35. Oak DOM also had similarly high intensity elemental formulas in the approximate region H/C 0.5–1.0 by O/C 0.25–0.7.

All forms of tree-DOM covered a wide area of van Krevelen space and correspondingly included elemental formulas with a diverse range of possible structural properties (**Table 2**). All tree-DOM clusters had similar contributions from aromatic compounds (14–15%), but oak DOM was enriched in condensed aromatics (12–13%) compared to cedar DOM (10%). Highly unsaturated formulas were the most prominent molecular class in each type of tree-DOM and were enriched in cedar DOM (47%) compared to oak DOM (38–40%; **Table 2**). Combined aliphatics, including both unsaturated aliphatics and saturated fatty acids, constituted approximately 25% of peaks in all tree-DOM types. Sugar and peptide contributions were low across tree-DOM types, but were elevated in oak DOM compared to cedar DOM. Oak throughfall DOM had a lower average molecular mass (359 g mol^{-1}) compared to both oak stemflow and cedar DOM (382–383 g mol^{-1}). Average H/C and AImod

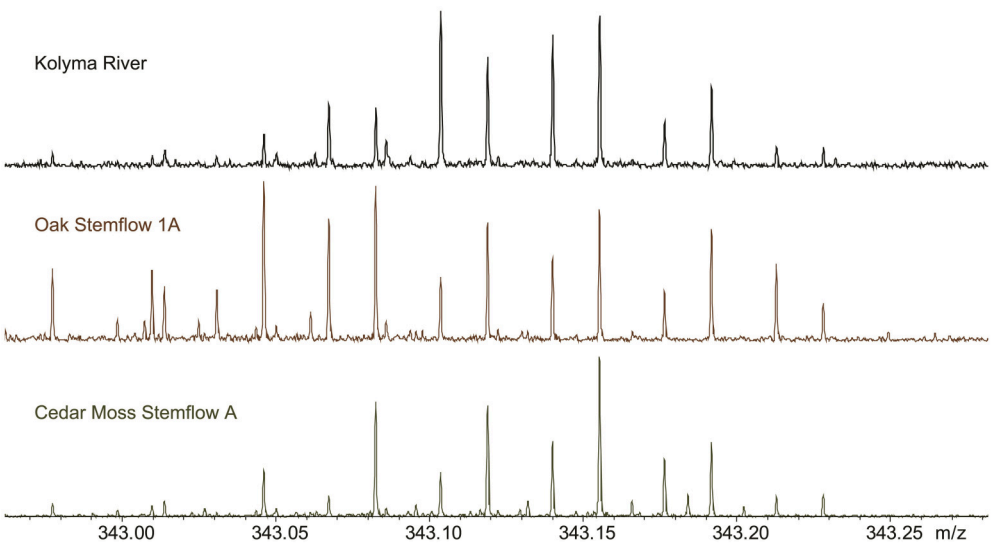

FIGURE 4 | Raw electrospray ionization Fourier transform ion cyclotron mass spectra in the 343 mass to charge (m/z) region for a representative river water sample (Kolyma River; Spencer et al., 2015), a live oak stemflow sample and a cedar stemflow sample.

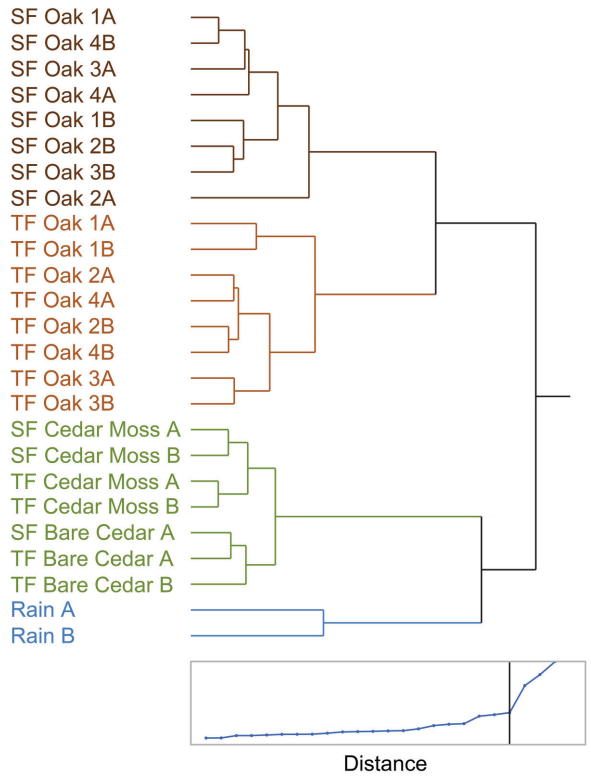

FIGURE 5 | Dendogram and distance scale from a hierarchical cluster analysis of the standardized elemental formula intensities indentified via electrospray ionization Fourier transform ion cyclotron mass spectrometry (Ward clustering in JMP®). SF, Stemflow; TF, Throughfall.

values for the clusters were similar. However, O/C decreased from oak stemflow > oak throughfall > cedar.

To reveal the quintessential molecular signatures of each tree-DOM type, the degree to which each elemental formula was enriched in a tree-DOM cluster relative to the mean for all tree-DOM types (i.e., mean intensity for a molecular formula in the whole dataset, excluding the two rain samples) was calculated as:

$$\text{Enrichment Factor} = \frac{\text{Mean Intensity in Clustered Samples}}{\text{Mean Intrensity in All Tree DOM Samples}} \quad (3)$$

An elemental formula was then classified as being enriched within a tree-DOM type if it exhibited an enrichment factor >1 and also had relatively low variations in intensity across the clustered samples (standard deviation <50% of mean intensity). The standard deviation term was included in the classification in order to exclude formulas which were not routinely enriched within the samples of a cluster. The results of this classification are presented in **Table 2** and in van Krevelen diagrams (**Figures 6D–F**). Dot size in the van Krevelen diagrams represents the mean intensity of an elemental formula in the mass spectrum, while dot color represents the degree of enrichment ranging from just above 1 (yellow) to 3 or higher (dark blue). Oak stemflow was enriched in a large number (**Table 2**) and wide variety of molecules (**Figure 6D**) compared to oak throughfall and cedar DOM (**Figures 6E,F**). However, many of the elemental formulas that were highly enriched in oak stemflow (enrichment factor >2; darker blues) were present at relatively low intensity (small size of the dots). Oak throughfall was also enriched in a wide variety of DOM types (**Figure 6E**), but had highest enrichment in the low H/C, low O/C region typical of condensed aromatics and within the region bounded by approximately H/C 1.1–1.6 and O/C 0.15 and 0.35 where the original van Krevelens (**Figures 6A–C**) revealed high abundance within all tree-DOM types. Finally, cedar DOM was enriched in elemental formulas with H/C values from approximately 1.0–1.5 and O/C 0.1–0.45 (**Figure 6F**).

Quintessential cedar DOM formulas (i.e., formulas that were consistently enriched in cedar DOM; **Table 2** right side) were enriched in CHO-only formulas (93%) compared to oak DOM (83–84%). The number of nitrogen containing quintessential formulas decreased in the order oak stemflow > oak throughfall > cedar, while sulfur containing quintessential formulas decreased in the order oak throughfall > cedar > oak stemflow, and phosphorous containing quintessential formulas decreased in the order cedar > oak stemflow > oak throughfall (**Table 2**). The average molecular mass, O/C, and AImod of quintessential oak stemflow formulas was higher than that for cedar and oak throughfall, while quintessential cedar formulas had the highest average H/C and lowest average O/C and AImod. Quintessential oak formulas were enriched in condensed aromatics (17–21%) and contained a small proportion of peptide (0.3%) and sugar (2.0–4.3%) formulas, while the quintessential cedar formulas included zero condensed aromatic, peptide or sugar formulas (**Table 2**). Quintessential oak stemflow formulas included approximately twice the percentage of aromatic formulas (23%) when compared to the other tree DOM types (12–13%). Quintessential cedar formulas were highly enriched in highly unsaturated formulas (71%), which represented approximately half of the quintessential oak stemflow formulas (53%), and about a third (30%) of quintessential oak throughfall formulas. Finally, quintessential oak throughfall formulas were enriched in unsaturated aliphatics (30%) compared to quintessential cedar (16%) and oak stemflow (5%).

Distribution plots further resolved variations in molecular mass, H/C, O/C, and AImod of the quintessential formulas that are enriched were the different tree-DOM types (**Figure 7**). Quintessential oak stemflow formulas covered a broad, relatively evenly distributed range in molecular mass, O/C, H/C and AImod, with the H/C distribution skewed toward lower values (center ~1.0; **Figure 7C**). Those formulas that were enriched in oak throughfall DOM exhibited pronounced peaks in abundance at low molecular mass (~260 g mol^{-1}; **Figure 7A**), low O/C (~0.24; **Figure 7B**), high H/C (~1.6; **Figure 7C**), and contained three spikes in AImod (0, ~0.2 and ~0.8; **Figure 7D**). Quintessential cedar formulas also exhibited marked peaks in molecular mass (~310 g mol^{-1}; **Figure 7A**), midranges in H/C (~1.0–1.2; **Figure 7C**) and AImod (~0.4; **Figure 7D**) and a peak in O/C that reached a maximum at ~0.36, but exhibited two smaller shoulders at 0.21 and 0.11 (**Figure 7B**).

TABLE 2 | Molecular signatures of tree-derived dissolved organic matter (DOM) within live oak stemflow, live oak throughfall and cedar (stemflow plus throughfall).

	Formulas within each cluster			Formulas enriched within each cluster		
	SF Oak	TF Oak	Cedar	SF Oak	TF Oak	Cedar
Total Formulas	4765	3565	3643	1887	859	322
CHO	3116 (65%)	2338 (66%)	2581 (71%)	1576 (84%)	714 (83%)	301 (93%)
With N	869 (18%)	552 (15%)	420 (12%)	254 (13%)	51 (5.9%)	0 (0%)
With S	574 (12%)	568 (16%)	403 (11%)	36 (1.9%)	92 (11%)	15 (4.7%)
With P	206 (4.3%)	107 (3%)	239 (6.6%)	21 (1.1%)	2 (0.2%)	6 (1.9%)
Condensed Aromatics	590 (12%)	471 (13%)	374 (10%)	330 (17%)	184 (21%)	0 (0%)
Aromatics	676 (14%)	549 (15%)	554 (15%)	431 (23%)	115 (13%)	39 (12%)
Highly Unsaturated	1922 (40%)	1340 (38%)	1706 (47%)	992 (53%)	258 (30%)	230 (71%)
Unsaturated Aliphatics	1134 (24%)	869 (24%)	809 (22%)	95 (5.0%)	261 (30%)	52 (16%)
Saturated Fatty Acids	43 (0.9%)	40 (1.1%)	38 (1%)	0 (0%)	1 (0.1%)	1 (0.3%)
Sugars	162 (3.4%)	135 (3.8%)	82 (2.3%)	37 (2.0%)	37 (4.3%)	0 (0%)
Peptides	244 (5.1%)	162 (4.5%)	80 (2.2%)	6 (0.3%)	3 (0.3%)	0 (0%)
Average Molecular Mass (g mol^{-1})	383	359	382	370	311	330
Average H/C	1.23	1.24	1.22	1.01	1.19	1.24
Average O/C	0.45	0.42	0.39	0.46	0.39	0.27
Average Almod	0.31	0.32	0.32	0.42	0.36	0.35

Percentages represent the relative contributions of each molecular class within each type of tree-DOM. Left side: values for all formulas within each type of tree-DOM. Right side: values for formulas that were enriched within each type of tree-DOM.

DISCUSSION

Concentrations and Optical Signatures of Tree-DOM

The high levels of DOC and CDOM in stemflow and throughfall relative to rainwater samples indicate that rainwater DOM was a very minor component of stemflow and throughfall DOM, with the majority of tree-DOM being entrained during interaction with the tree canopy and stem.

Mean DOC concentrations in throughfall (10–52 mg-C L^{-1}) and stemflow (25–78 mg-C L^{-1}) were both within the range of values reported by previous throughfall (1–100 mg-C L^{-1}) (Michalzik et al., 2001; Neff and Asner, 2001; Le Mellec et al., 2010; Inamdar et al., 2012) and stemflow (5–200 mg-C L^{-1}) (Moore, 2003; Tobón et al., 2004; Levia et al., 2011) studies. The observed range in tree-DOC concentrations is at the higher end or exceeds the mean DOC concentrations in major US rivers (1–12 mg-C L^{-1}; Spencer et al., 2012), but is consistent with the high DOC values observed in black water rivers draining swamps (e.g., St. Marys = 42 mg-C L^{-1}; Spencer et al., 2012). Given the small size of the current dataset (two storms, six trees), no estimates of DOC fluxes are made.

The optical properties of tree-DOM are broadly consistent with those for CDOM in other aquatic environments. Tree-DOM CDOM spectra exhibit an exponential increase in absorbance with decreasing wavelength (**Figure 2**). The range in mean spectral slope values ($S_{275\text{-}295}$) for stemflow (0.0144 nm^{-1}) and throughfall (0.0157–0.0165 nm^{-1}) are consistent with values for US rivers (0.012–0.023 nm^{-1}) (Spencer et al., 2012). Literature values for stemflow and throughfall spectral slope were not found for comparison. $SUVA_{254}$ values for stemflow (means 3.0–5.1 L mg-C^{-1} m^{-1}) from our oaks and cedars compare with ranges of 2.5–4.9 L mg-C^{-1} m^{-1} for American beech (*Fagus grandifolia*) and 3.7–6.2 L mg-C^{-1} m^{-1} for yellow poplar (*Liriodendron tulipfera*) (Levia et al., 2011). These values are all at the higher end or exceeding the range in mean $SUVA_{254}$ values reported for US rivers (1.3–4.6 L mg-C^{-1} m^{-1}) (Spencer et al., 2012) and are consistent with highly colored, aromatic-rich DOM (Weishaar et al., 2003). The mean $SUVA_{254}$ values for throughfall (2.2–2.9 L mg-C^{-1} m^{-1}) compare to previous literature values for throughfall of 1.8–4.7 L mg-C^{-1} m^{-1} (Inamdar et al., 2012) and also indicate a significant contribution of aromatics to throughfall DOM. All tree-DOM SUVA values were higher than for rainwater CDOM and all tree-DOM spectral slopes steeper than for rainwater DOM (**Figures 3C,D**), indicating tree-DOM to be more aromatic than the trace amounts of DOM in rainwater. Hydrological fluxes become enriched with aromatic compounds, including lignin degradation products, as contact time with bark increases (Guggenberger et al., 1994). Therefore, the enrichment of stemflow in highly aromatic, high $SUVA_{254}$ DOM compared to throughfall is likely due to the high hydrological connectivity of stemflow with tree bark and other sources of tree-derived organics. The aromatics in tree-DOM are likely dominated by autochthonous, tree-produced aromatics, such as lignin, and their degradation products (Guggenberger et al., 1994) that accumulate and are then washed off the tree surface during rain events. In addition, allochthonous organics delivered to the tree via atmospheric deposition (Guggenberger and Zech, 1994) could include aromatics derived from soils, combustion sources, or distal vegetation.

The quantity, but not the optical quality of tree-DOM exported during both storms varied with epiphyte cover. DOC

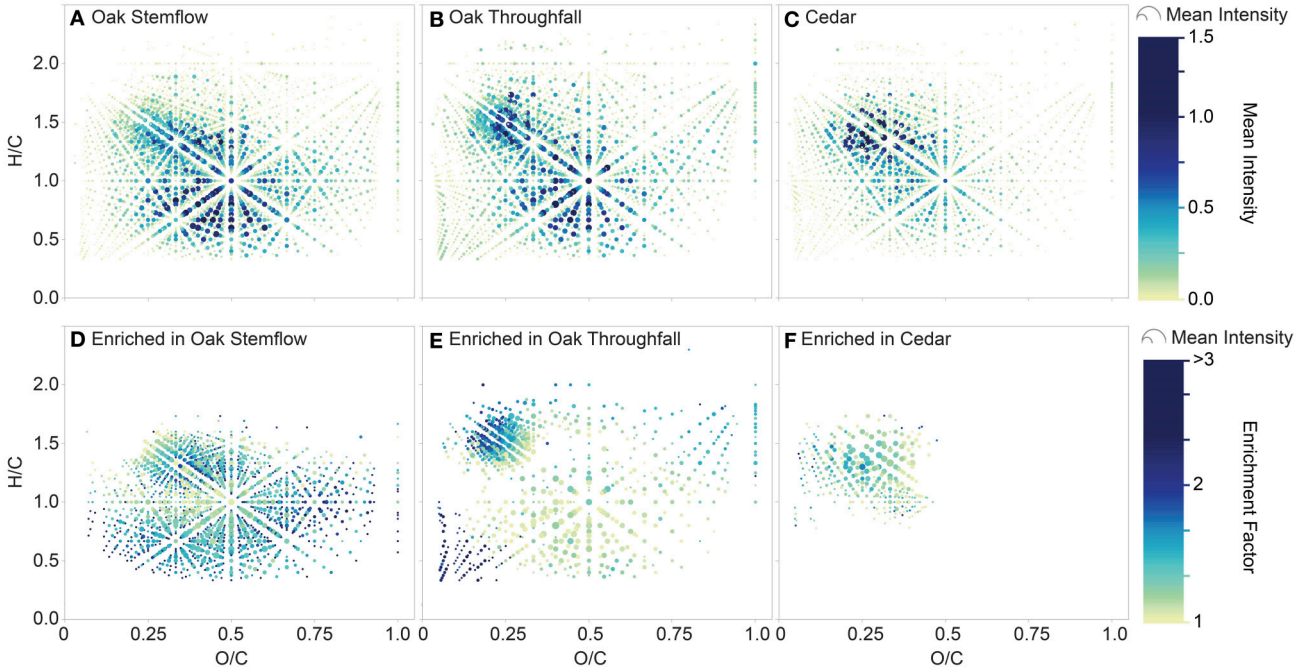

FIGURE 6 | van Krevelen diagrams displaying the molecular signatures of tree-derived dissolved organic matter (DOM). Upper panels: elemental formulas within **(A)** live oak stemflow, **(B)** live oak throughfall, and **(C)** cedar (stemflow plus throughfall). Symbols are colored and sized by the mean intensity of the elemental formulas within the samples constituting each type of tree-derived DOM. Lower panels: elemental formulas that were enriched within **(D)** live oak stemflow, **(E)** live oak throughfall and **(F)** cedar (stemflow plus throughfall) relative to the mean elemental formula intensities for all tree-derived DOM samples. Symbols are colored by the enrichment factor and sized by mean intensity of the elemental formulas within the samples constituting each type of tree-derived DOM.

concentration and CDOM were consistently lower in both stemflow and throughfall from the bare cedar than from the epiphyte covered cedar and the four oaks, which all had mixed epiphyte cover (**Table 1**; **Figures 1**, **3**). These results suggest that epiphytes were either a direct source of autochthonous, epiphyte organics or an intermediate accumulator of organics derived from the tree, fauna or atmospheric deposition. Research into the fluxes and quality of epiphyte DOM release is scarce. With respect to the dominant epiphytes encountered in our study, no data is available for resurrection ferns; while Spanish moss collected from nearby sites in coastal Georgia leached DOM with significantly lower $SUVA_{254}$ values (Van Stan et al., 2015) than for the current tree-DOM samples (**Table 1**). The Spanish moss samples leached in Van Stan et al. (2015) were cleaned of all canopy soil and any decaying or damaged moss. As such, these leachates contained organics derived directly from Spanish moss rather than from the more diverse canopy ecosystem and potential organic sources that the presence of Spanish moss in a tree cultivates. For the limited data collected in our study (two storms, six trees, one of which has no epiphyte cover), the presence of epiphytes increased DOC concentrations, but did not reduce the $SUVA_{254}$ values as would be expected if the additional DOC leached directly from healthy Spanish moss. Therefore, the DOM enrichment within stemflow and throughfall exported by epiphyte covered trees is likely due to the increase in hydrological contact time and flow path (Levia and Frost, 2003), the accumulation of organic matter from bark, litter and fauna facilitated by the presence of epiphytes in the canopy ecosystem (Hietz et al., 2002; Woods et al., 2012), and potentially, the increase in canopy surface area for atmospheric deposition (Rodrigo et al., 1999; Woods et al., 2012).

Molecular Signatures of Tree-DOM

The molecular signatures of whole water tree-DOM as revealed by negative mode electrospray ionization FT-ICR MS (**Figure 2**) share many features of whole water and extracted DOM from other aquatic environments (Mopper et al., 2007; Singer et al., 2012; Chen et al., 2014; Dittmar and Stubbins, 2014; Cawley et al., 2016). Shared features include a high diversity of elemental formulas distributed broadly in van Krevelen space (**Figures 6A–C**) and spanning a range of molecular classes (**Table 2**). The average molecular mass of tree-DOM (359–382 g mol^{-1}; **Table 2**) was greater than for Kolyma River whole water DOM run on the same mass spectrometer (336 g mol^{-1}) (Spencer et al., 2015), but lower than for Congo River whole water DOM run on a different mass spectrometer (424 g mol^{-1}) (Stubbins et al., 2010). Tree-DOM was also H-poor (H/C 1.22–1.24) and O-rich (O/C 0.39–0.45) compared to Kolyma River DOM (H/C 1.27; O/C 0.39) (Spencer et al., 2015). Average H/C and O/C were not reported for Congo River DOM (Stubbins et al., 2010). Other reports of elemental formulas for non-extracted river water DOM are scarce.

As for other whole water FT-ICR mass spectra for terrigenous DOM from freshwater environments (Stubbins et al., 2010,

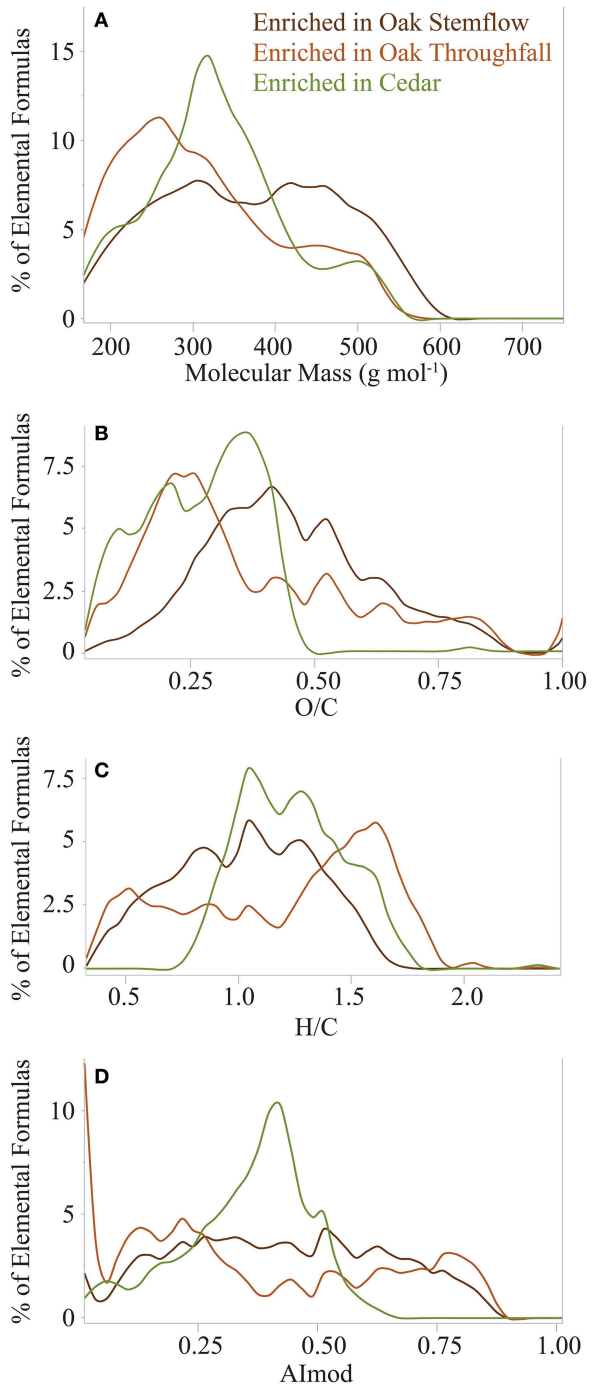

FIGURE 7 | Molecular mass (A), H/C **(B)**, O/C **(C)**, and modified aromaticity index (AImod; **D**) distributions of elemental formulas that were enriched within live oak stemflow, live oak throughfall and cedar (stemflow plus throughfall) relative to the mean elemental formula intensities for all tree-derived DOM samples.

2012a; Spencer et al., 2015), tree-DOM was dominated by CHO-only formulas and was rich in highly unsaturated molecules (**Table 2**). As they have a high degree of isomeric freedom, any single highly unsaturated elemental formula may represent a diverse array of structures of correspondingly diverse potential biogeochemical sources and functions (Stubbins et al., 2010). For instance, the possible isomers of any highly unsaturated formula include aromatic ring containing lignin degradation products derived from vascular land plants (Stubbins et al., 2010) and carboxylic-rich alicyclic molecules (Hertkorn et al., 2006) of indeterminate, potentially microbial origin. Due the high $SUVA_{254}$ values of tree-DOM and particularly stemflow DOM, it is likely that a significant proportion of the unsaturated formulas within tree-DOM represent vascular plant derived molecules that contain aromatic rings.

The modified aromaticity index classifies formulas as either aromatic or condensed aromatic (Koch and Dittmar, 2006, 2016). Tree-DOM was enriched in aromatic formulas (14–15%; **Table 2**) compared to Congo River whole water analyzed on a different FT-ICR mass spectrometer (9%) (Stubbins et al., 2010), but similar in aromatic content to Kolyma River whole water analyzed on the FT-ICR mass spectrometer used in the current study (13%) (Spencer et al., 2015) consistent with the view that river DOM is derived predominantly from the degradation products of vascular plants (Ertel et al., 1984) and the enrichment of similar compounds within tree-DOM.

Tree-DOM was also enriched in condensed aromatics (10–12%; **Table 2**) compared to both Congo (1%) (Stubbins et al., 2010) and Kolyma River (6%) (Spencer et al., 2015) samples. Condensed aromatics are known to form during the incomplete combustion of organics (Goldberg, 1985) and when observed in DOM are usually termed dissolved black carbon and ascribed a thermogenic source (Kim et al., 2004; Hockaday et al., 2006; Ziolkowski and Druffel, 2010). The ubiquity of dissolved black carbon in river waters (Dittmar et al., 2012; Jaffé et al., 2013; Stubbins et al., 2015; Wagner et al., 2015) is explained as resulting from the ubiquity of refractory, apparently thermogenic black carbon in soils (Forbes et al., 2006; Guggenberger et al., 2008; Schmidt et al., 2011). Other sources of black carbon to natural waters and landscapes include direct input from local combustion sources and atmospheric deposition from distant combustion sources. Atmospheric deposition has been posited as a source of organics to remote regions of the earth (Stubbins et al., 2012a; Spencer et al., 2014) and organics transported from global and regional sources of combustion (e.g., automobile, industrial, domestic, agricultural, wildfire, and biomass burning), as well as produced locally on the Skidaway Institute of Oceanography campus, could all produce black carbon for deposition to the trees sampled.

Aliphatic formulas (sum of unsaturated aliphatics and saturated fatty acids) were slightly enriched in tree-DOM (23–25%; **Table 2**) relative to Congo (19%) (Stubbins et al., 2010) and Kolyma River (22%) (Spencer et al., 2015) DOM. Tree-DOM was also enriched in sugar (2.3–3.8%) and peptide (2.2–5.1%) formulas compared to Kolyma River DOM (0.6% sugar; 2.2% peptide) (Spencer et al., 2015). Sugar and peptide formulas were not reported for the Congo River (Stubbins et al., 2010). All of these compound classes likely derive directly from foliar leachates, foliar washoff, and their breakdown products (Guggenberger and Zech, 1994; Michalzik et al., 2001; Kalbitz et al., 2007). However, similar molecular formulas

are also observed in atmospheric aerosols (Wozniak et al., 2008).

Quintessential Signatures of Oak Stemflow, Oak Throughfall and Cedar DOM

Tree-DOM molecular signatures were significantly different from rainwater DOM and clustered in three groups: oak stemflow, oak throughfall and cedar, the latter including stemflow and throughfall samples from both the epiphyte covered and bare cedars (**Figure 5**). Distinct differences between the molecular signatures of each class of tree-DOM were evident in van Krevelen plots (**Figures 6A–C**). In order to determine the elemental formulas that distinguished these three classes of tree-DOM from one another, the quintessential formulas associated with each type of tree-DOM were classified as those formulas that are consistently enriched across the samples within a cluster (Equation 3). Plotting the resultant data in van Krevelen space revealed that the above data treatment accentuated differences in the molecular signatures of oak stemflow, oak throughfall, and cedar DOM (**Figures 6D–F**). As noted in the results, dot size in the van Krevelen diagrams (**Figures 6D–F**) represents the mean intensity of an elemental formula in the mass spectrum, while dot color represents the degree of enrichment ranging from just above 1 (yellow) to 3 or higher (dark blue).

Quintessential oak stemflow formulas (**Figure 6D**) occupied much of the van Krevelen space typically populated by riverine DOM (e.g., Spencer et al., 2015 in which data for a Kolyma River whole water sample run on the same mass spectrometer is displayed). The van Krevelen is densely populated, as is also typical of riverine DOM samples. The enrichment of stemflow DOM in this diverse population of formulas indicates that the organics within oak stemflow are of more diverse origin or have undergone more extensive processing than the organics within oak throughfall and cedar DOM. The canopy structure and coarse bark of live oaks makes them excellent habitats for colonization by epiphytes, such as the Spanish moss and resurrection ferns observed on our sampled trees (**Figure 1d**), the accumulation of organic debris, and utilization by fauna. The development of these canopy microhabitats, replete with observable canopy soils within the trees on SkIO campus, may have led to the development of a rich molecular mix of organics for export. While of diverse stoichiometric composition, the quintessential oak stemflow elemental formulas were of higher average molecular mass and AImod (**Table 2**; **Figure 7A**), and enriched in aromatics, compared to quintessential oak throughfall and cedar formulas, suggestive of the greater interaction of stemflow with the oak bark, debris and canopy soils.

Quintessential oak throughfall formulas (**Figure 6E**) were not as evenly distributed in van Krevelen space as the quintessential formulas of oak stemflow suggesting formulas enriched in throughfall derive from more distinct sources and have undergone less processing. Compared to the quintessential formulas associated with oak stemflow and cedar, quintessential oak throughfall formulas were of low average molecular weight (311 g mol^{-1}) and were enriched in unsaturated aliphatics (30%) and sugars (4.3%; **Table 2**), suggesting significant inputs from the direct leaching or washing of foliar surfaces (Guggenberger and Zech, 1994; Michalzik et al., 2001; Kalbitz et al., 2007). Oak throughfall also contained elevated levels of condensed aromatics (21%; **Table 2**; **Figure 7B**) compared to the other tree-DOM classes, suggesting potential wash off of deposited combustion products from leaf surfaces.

By comparison to oak DOM, cedar DOM was enriched in CHO-only and highly unsaturated formulas (**Table 2**) of limited molecular diversity (**Figure 6F**; **Figure 7C**), suggesting cedar DOM is enriched in minimally processed non-descript tree-DOM.

CONCLUSIONS

The relatively high $SUVA_{254}$ values and abundance of aliphatics and aromatic formulas within tree-DOM are consistent with autochthonous (i.e., tree-derived) organics. However, the presence of condensed aromatics within tree-DOM also suggests that some of the DOM exported from trees derives from the atmospheric deposition of allochthonous organics. As electrospray ionization efficiency varies with analyte chemistry, the current dataset cannot be used to robustly quantify the contribution of condensed aromatics or other forms of deposited organics to tree-DOM export. Future work should therefore seek to quantify the contribution of condensed aromatics and other allochthonous forms of DOM to tree-DOM to assess how much of the tree-DOM flux is derived from autochthonous vs. allochthonous sources.

As the crowning headwaters of the terrestrial hydrological cycle, tree canopies are the point of first contact between precipitation and terrestrial ecosystems. The quality of tree-DOM as detailed by absorbance and FT-ICR MS is similar to the terrigenous DOM described in inland waters, but sufficiently distinct that optical and chemical signatures may be of use in tracking tree-DOM into receiving ecosystems including forest floor soils and inland waters. Further study is required to develop an understanding of the fate and ecological functions of tree-DOM within receiving ecosystems. Such knowledge will be essential in assessing how ongoing changes to forest cover distributions will impact both soil and aquatic ecosystems.

AUTHOR CONTRIBUTIONS

AS wrote the paper with input from other authors. AS and JV designed the study. LS collected the samples, analyzed samples and worked up the DOC and CDOM data sets. AS and TD analyzed the samples by FT-ICR MS and worked up the FT-ICR MS data.

SUPPLEMENTARY MATERIAL

The Supplementary Material for this article can be found online at: http://journal.frontiersin.org/article/10.3389/feart.2017.00022/full#supplementary-material

REFERENCES

Aitkenhead-Peterson, J., McDowell, W., Neff, J., Stuart, E., and Robert, L. (2003). "Sources, production, and regulation of allochthonous dissolved organic matter inputs to surface waters," in *Aquatic Ecosystems Interactivity of Dissolved Organic Matter*, eds S. E. G. Findlay and R. L. Sinsabaugh (New York, NY: Academic Press), 26–70. doi: 10.1016/b978-012256371-3/50003-2

Algeo, T. J., Scheckler, S. E., and Maynard, J. B. (2001). "Effects of the middle to late devonian spread of vascular land plants on weathering regimes, Marine Biotas, and Global Climate," in *Plants Invade the Land: Evolutionary and Environmental Approaches,* eds P. G. Gensel and D. Edwards (New York, NY: Columbia University Press), 213–236.

Cawley, K. M., Murray, A. E., Doran, P. T., Kenig, F., Stubbins, A., Chen, H., et al. (2016). Characterization of dissolved organic material in the interstitial brine of Lake Vida, Antarctica. *Geochim. Cosmochim. Acta* 183, 63–78. doi: 10.1016/j.gca.2016.03.023

Chen, H., Stubbins, A., Perdue, E. M., Green, N. W., Helms, J. R., Mopper, K., et al. (2014). Ultrahigh resolution mass spectrometric differentiation of dissolved organic matter isolated by coupled reverse osmosis-electrodialysis from various major oceanic water masses. *Mar. Chem.* 164, 48–59. doi: 10.1016/j.marchem.2014.06.002

Crutzen, P. J. (2002). Geology of mankind. *Nature* 415, 23–23. doi: 10.1038/415023a

Dittmar, T., De Rezende, C. E., Manecki, M., Niggemann, J., Coelho Ovalle, A. R., Stubbins, A., et al. (2012). Continuous flux of dissolved black carbon from a vanished tropical forest biome. *Nat. Geosci.* 5, 618–622. doi: 10.1038/ngeo1541

Dittmar, T., and Stubbins, A. (2014). "Dissolved Organic Matter in Aquatic Systems," in *Treatise on Geochemistry*, *2nd Edn.,* ed K. K. Turekian (Oxford: Elsevier), 125–156.

Ertel, J. R., Hedges, J. I., and Perdue, E. M. (1984). Lignin signature of aquatic humic substances. *Science* 223, 485–487. doi: 10.1126/science.223.4635.485

FAO (2016). "State of the World's Forests 2016," in *Forests and Agriculture: Land-Use Challenges and Opportunities* (Rome).

Forbes, M. S., Raison, R. J., and Skjemstad, J. O. (2006). Formation, transformation and transport of black carbon (charcoal) in terrestrial and aquatic ecosystems. *Sci. Total Environ.*370, 190–206. doi: 10.1016/j.scitotenv.2006.06.007

Gensel, P. G. (2001). "Introduction," in *Plants Invade the Land: Evolutionary and Environmental Approaches,* eds P. G. Gensel and D. Edwards (New York, NY: Columbia University Press), 1–2.

Georgia Office of the State Climatologist (2012). *Office of the State Climatologist*. Available online at: https://epd.georgia.gov/office-state-climatologist (Accessed September 13, 2013).

Goldberg, E. (1985). *Black Carbon in the Environment.* New York, NY: Wiley.

Greb, S. F., DiMichele, W. A., and Gastaldo, R. A. (2006). "Evolution and importance of wetlands in earth history," in *Wetlands Through Time*, eds W. A. DiMichele and S. Greb (Boulder, CO: Geological Society of America), 1–40.

Guggenberger, G., Rodionov, A., Shibistova, O., Grabe, M., Kasansky, O. A., Fuchs, H., et al. (2008). Storage and mobility of black carbon in permafrost soils of the forest tundra ecotone in Northern Siberia. *Glob. Chang. Biol.* 14, 1367–1381. doi: 10.1111/j.1365-2486.2008.01568.x

Guggenberger, G., and Zech, W. (1994). Composition and dynamics of dissolved carbohydrates and lignin-degradation products in two coniferous forests, NE Bavaria, Germany. *Soil Biol. Biochem.* 26, 19–27. doi: 10.1016/0038-0717(94)90191-0

Guggenberger, G., Zech, W., and Schulten, H.-R. (1994). Formation and mobilization pathways of dissolved organic matter: evidence from chemical structural studies of organic matter fractions in acid forest floor solutions. *Org. Geochem.* 21, 51–66. doi: 10.1016/0146-6380(94)90087-6

Hansen, M. C., Potapov, P. V., Moore, R., Hancher, M., Turubanova, S., Tyukavina, A., et al. (2013). High-resolution global maps of 21st-century forest cover change. *Science* 342, 850–853. doi: 10.1126/science.1244693

Hansen, M. C., Stehman, S. V., and Potapov, P. V. (2010). Quantification of global gross forest cover loss. *Proc. Natl. Acad. Sci. U.S.A.* 107, 8650–8655. doi: 10.1073/pnas.0912668107

Helms, J. R., Stubbins, A., Ritchie, J. D., Minor, E. C., Kieber, D. J., and Mopper, K. (2008). Absorption spectral slopes and slope ratios as indicators of molecular weight, source, and photobleaching of chromophoric dissolved organic matter. *Limnol. Oceanogr.* 53, 955–969. doi: 10.4319/lo.2008.53.3.0955

Hertkorn, N., Benner, R., Frommberger, M., Schmitt-Kopplin, P., Witt, M., Kaiser, K., et al. (2006). Characterization of a major refractory component of marine dissolved organic matter. *Geochim. Cosmochim. Acta* 70, 2990–3010. doi: 10.1016/j.gca.2006.03.021

Hietz, P., Wanek, W., Wania, R., and Nadkarni, N. M. (2002). Nitrogen-15 natural abundance in a montane cloud forest canopy as an indicator of nitrogen cycling and epiphyte nutrition. *Oecologia* 131, 350–355. doi: 10.1007/s00442-002-0896-6

Hockaday, W. C., Grannas, A. M., Kim, S., and Hatcher, P. G. (2006). Direct molecular evidence for the degradation and mobility of black carbon in soils from ultrahigh-resolution mass spectral analysis of dissolved organic matter from a fire-impacted forest soil. *Org. Geochem.* 37, 501–510. doi: 10.1016/j.orggeochem.2005.11.003

Hu, C., Muller-Karger, F. E., and Zepp, R. G. (2002). Absorbance, absorption coefficient, and apparent quantum yield: a comment on common ambiguity in the use of these optical concepts. *Limnol. Oceanogr.* 47, 1261–1267. doi: 10.4319/lo.2002.47.4.1261

Inamdar, S., Finger, N., Singh, S., Mitchell, M., Levia, D., Bais, H., et al. (2012). Dissolved organic matter (DOM) concentration and quality in a forested mid-Atlantic watershed, USA. *Biogeochemistry* 108, 55–76. doi: 10.1007/s10533-011-9572-4

Jaffé, R., Ding, Y., Niggemann, J., Vähätalo, A. V., Stubbins, A., Spencer, R. G. M., et al. (2013). Global charcoal mobilization from soils via dissolution and riverine transport to the oceans. *Science* 340, 345–347. doi: 10.1126/science.1231476

Jardine, P., McCarthy, J., and Weber, N. (1989). Mechanisms of dissolved organic carbon adsorption on soil. *Soil Sci. Soc. Am. J.* 53, 1378–1385. doi: 10.2136/sssaj1989.03615995005300050013x

Kaiser, K., and Zech, W. (1998). Soil dissolved organic matter sorption as influenced by organic and sesquioxide coatings and sorbed sulfate. *Soil Sci. Soc. Am. J.* 62, 129–136. doi: 10.2136/sssaj1998.03615995006200010017x

Kaiser, K., and Zech, W. (2000). Sorption of dissolved organic nitrogen by acid subsoil horizons and individual mineral phases. *Eur. J. Soil Sci.* 51, 403–411. doi: 10.1046/j.1365-2389.2000.00320.x

Kalbitz, K., Meyer, A., Yang, R., and Gerstberger, P. (2007). Response of dissolved organic matter in the forest floor to long-term manipulation of litter and throughfall inputs. *Biogeochemistry* 86, 301–318. doi: 10.1007/s10533-007-9161-8

Kim, S., Kaplan, L. A., Benner, R., and Hatcher, P. G. (2004). Hydrogen-deficient molecules in natural riverine water samples - Evidence for the existence of black carbon in DOM. *Mar. Chem.* 92, 225–234. doi: 10.1016/j.marchem.2004.06.042

Koch, B. P., and Dittmar, T. (2006). From mass to structure: an aromaticity index for high-resolution mass data of natural organic matter. *Rapid Commun. Mass Spectrometry* 20, 926–932. doi: 10.1002/rcm.2386

Koch, B. P., and Dittmar, T. (2016). From mass to structure: an aromaticity index for high-resolution mass data of natural organic matter. *Rapid Commun. Mass Spectrometry* 30, 250–250. doi: 10.1002/rcm.7433

Koch, B. P., Dittmar, T., Witt, M., and Kattner, G. (2007). Fundamentals of molecular formula assignment to ultrahigh resolution mass data of natural organic matter. *Anal. Chem.* 79, 1758–1763. doi: 10.1021/ac061949s

Kolka, R. K., Nater, E., Grigal, D., and Verry, E. (1999). Atmospheric inputs of mercury and organic carbon into a forested upland/bog watershed. *Water Air Soil Pollut.* 113, 273–294. doi: 10.1023/A:1005020326683

Le Mellec, A., Meesenburg, H., and Michalzik, B. (2010). The importance of canopy-derived dissolved and particulate organic matter (DOM and POM)–comparing throughfall solutionfrom broadleaved and coniferous forests. *Ann. For. Sci.* 67:411. doi: 10.1051/forest/2009130

Levia, D. F., and Frost, E. E. (2003). A review and evaluation of stemflow literature in the hydrologic and biogeochemical cycles of forested and agricultural ecosystems. *J. Hydrol.* 274, 1–29. doi: 10.1016/S0022-1694(02)00399-2

Levia, D. F., Van Stan, I., John, T., Inamdar, S. P., Jarvis, M. T., Mitchell, M. J., et al. (2011). Stemflow and dissolved organic carbon cycling: temporal variability in concentration, flux, and UV-Vis spectral metrics in a temperate broadleaved deciduous forest in the eastern United States. *Can. J. Forest Res.* 42, 207–216. doi: 10.1139/x11-173

McClain, M. E., Boyer, E. W., Dent, C. L., Gergel, S. E., Grimm, N. B., Groffman, P. M., et al. (2003). Biogeochemical hot spots and hot moments

at the interface of terrestrial and aquatic ecosystems. *Ecosystems* 6, 301–312. doi: 10.1007/s10021-003-0161-9

Michalzik, B., Kalbitz, K., Park, J.-H., Solinger, S., and Matzner, E. (2001). Fluxes and concentrations of dissolved organic carbon and nitrogen–a synthesis for temperate forests. *Biogeochemistry* 52, 173–205. doi: 10.1023/A:1006441620810

Moore, T. (2003). Dissolved organic carbon in a northern boreal landscape. *Glob. Biogeochem. Cycles* 17, 1109. doi: 10.1029/2003GB002050

Mopper, K., Kieber, D. J., and Stubbins, A. (2015). "Marine photochemistry: processes and impacts," in *Biogeochemistry of Marine Dissolved Organic Matter, 2nd Edn.*, eds D. A. Hansell and C. A. Carlson (New York, NY: Elsevier), 389–450.

Mopper, K., Stubbins, A., Ritchie, J. D., Bialk, H. M., and Hatcher, P. G. (2007). Advanced instrumental approaches for characterization of marine dissolved organic matter: extraction techniques, mass spectrometry, and nuclear magnetic resonance spectroscopy. *Chem. Rev.* 107, 419–442. doi: 10.1021/cr050359b

Neff, J. C., and Asner, G. P. (2001). Dissolved organic carbon in terrestrial ecosystems: synthesis and a model. *Ecosystems* 4, 29–48. doi: 10.1007/s100210000058

Raymond, P. A., and Saiers, J. E. (2010). Event controlled DOC export from forested watersheds. *Biogeochemistry* 100, 197–209. doi: 10.1007/s10533-010-9416-7

Raymond, P. A., Saiers, J. E., and Sobczak, W. V. (2016). Hydrological and biogeochemical controls on watershed dissolved organic matter transport: pulse-shunt concept. *Ecology* 97, 5–16. doi: 10.1890/14-1684.1

Rodrigo, A., Avila, A., and Gomez-Bolea, A. (1999). Trace metal contents in Parmelia caperata (L.) Ach. Compared to bulk deposition, throughfall and leaf-wash fluxes in two holm oak forests in Montseny (NE Spain). *Atmos. Environ.* 33, 359–367. doi: 10.1016/S1352-2310(98)00167-8

Schmidt, M. W. I., Torn, M. S., Abiven, S., Dittmar, T., Guggenberger, G., Janssens, I. A., et al. (2011). Persistence of soil organic matter as an ecosystem property. *Nature* 478, 49–56. doi: 10.1029/2008GB003327

Singer, G. A., Fasching, C., Wilhelm, L., Niggemann, J., Steier, P., Dittmar, T., et al. (2012). Biogeochemically diverse organic matter in Alpine glaciers and its downstream fate. *Nat. Geosci.* 5, 710–714. doi: 10.1038/ngeo1581

Spencer, R. G. M., Butler, K. D., and Aiken, G. R. (2012). Dissolved organic carbon and chromophoric dissolved organic matter properties of rivers in the USA. *J. Geophys. Res. Biogeosciences* 117, G03001. doi: 10.1029/2011jg001928

Spencer, R. G. M., Guo, W., Raymond, P. A., Dittmar, T., Hood, E., Fellman, J., et al. (2014). Source and biolability of ancient dissolved organic matter in glacier and lake ecosystems on the Tibetan Plateau. *Geochim. Cosmochim. Acta* 142, 64–74. doi: 10.1016/j.gca.2014.08.006

Spencer, R. G. M., Mann, P. J., Dittmar, T., Eglinton, T. I., McIntyre, C., Holmes, R. M., et al. (2015). Detecting the signature of permafrost thaw in Arctic rivers. *Geophys. Res. Lett.* 42, 2830–2835. doi: 10.1002/2015GL063498

Stein, W. E., Mannolini, F., Hernick, L. V., Landing, E., and Berry, C. M. (2007). Giant cladoxylopsid trees resolve the enigma of the Earth/'s earliest forest stumps at Gilboa. *Nature* 446, 904–907. doi: 10.1038/nature05705

Stubbins, A., and Dittmar, T. (2012). Low volume quantification of dissolved organic carbon and dissolved nitrogen. *Limnol. Oceanogr.* 10, 347–352. doi: 10.4319/lom.2012.10.347

Stubbins, A., and Dittmar, T. (2015). Illuminating the deep: molecular signatures of photochemical alteration of dissolved organic matter from North Atlantic Deep Water. *Mar. Chem.* 177, 318–324. doi: 10.1016/j.marchem.2015.06.020

Stubbins, A., Hood, E., Raymond, P. A., Aiken, G. R., Sleighter, R. L., Hernes, P. J., et al. (2012a). Anthropogenic aerosols as a source of ancient dissolved organic matter in glaciers. *Nat. Geosci.* 5, 198–201. doi: 10.1038/ngeo1403

Stubbins, A., Lapierre, J. F., Berggren, M., Prairie, Y. T., Dittmar, T., and del Giorgio, P. A. (2014). What's in an EEM? Molecular Signatures Associated with Dissolved Organic Fluorescence in Boreal Canada. *Environ. Sci. Technol.* 48, 10598–10606. doi: 10.1021/es502086e

Stubbins, A., Law, C. S., Uher, G., and Upstill-Goddard, R. C. (2011). Carbon monoxide apparent quantum yields and photoproduction in the Tyne estuary. *Biogeosciences* 8, 703–713. doi: 10.1029/2009GL041158

Stubbins, A., Mann, P. J., Powers, L., Bittar, T. B., Dittmar, T., McIntyre, C. P., et al. (2017). Low photolability of yedoma permafrost dissolved organic carbon. *J. Geophys. Res.* 122, 200–211. doi: 10.1002/2016JG003688

Stubbins, A., Niggemann, J., and Dittmar, T. (2012b). Photo-lability of deep ocean dissolved black carbon. *Biogeosciences* 9, 1661–1670. doi: 10.1029/2008GL036169

Stubbins, A., Spencer, R. G. M., Chen, H., Hatcher, P. G., Mopper, K., Hernes, P. J., et al. (2010). Illuminated darkness: molecular signatures of Congo River dissolved organic matter and its photochemical alteration as revealed by ultrahigh precision mass spectrometry. *Limnol. Oceanogr.* 55, 1467–1477. doi: 10.1890/0012-09658

Stubbins, A., Spencer, R., Mann, P. J., Holmes, R. M., McClelland, J., Niggemann, J., et al. (2015). Utilizing colored dissolved organic matter to derive dissolved black carbon export by Arctic Rivers. *Front. Earth Sci.* 3:63. doi: 10.3389/feart.2015.00063

Tobón, C., Sevink, J., and Verstraten, J. M. (2004). Solute fluxes in throughfall and stemflow in four forest ecosystems in northwest Amazonia. *Biogeochemistry* 70, 1–25. doi: 10.1023/B:BIOG.0000049334.10381.f8

Van Stan, J. T., Stubbins, A., Bittar, T., Reichard, J. S., Wright, K. A., and Jenkins, R. B. (2015). Tillandsia usneoides (L.) L.(Spanish moss) water storage and leachate characteristics from two maritime oak forest settings. *Ecohydrology* 8, 988–1004. doi: 10.1002/eco.1549

Vidon, P., Allan, C., Burns, D., Duval, T. P., Gurwick, N., Inamdar, S., et al. (2010). Hot spots and hot moments in riparian zones: potential for improved water quality management. *J. Am. Water Resour. Assoc.* 46, 278–298. doi: 10.1111/j.1752-1688.2010.00420.x

Wagner, S., Cawley, K. M., Rosario-Ortiz, F. L., and Jaffé, R. (2015). In-stream sources and links between particulate and dissolved black carbon following a wildfire. *Biogeochemistry* 124, 145–161. doi: 10.1007/s10533-015-0088-1

Weishaar, J. L., Aiken, G. R., Bergamaschi, B. A., Fram, M. S., Fujii, R., and Mopper, K. (2003). Evaluation of specific ultraviolet absorbance as an indicator of the chemical composition and reactivity of dissolved organic carbon. *Environ. Sci. Technol.* 37, 4702–4708. doi: 10.1021/es030360x

Willey, J. D., Kieber, R. J., Eyman, M. S., and Avery, G. B. (2000). Rainwater dissolved organic carbon: concentrations and global flux. *Glob. Biogeochem. Cycles* 14, 139–148. doi: 10.1029/1999gb900036

Woods, C. L., Hunt, S. L., Morris, D. M., and Gordon, A. M. (2012). Epiphytes influence the transformation of nitrogen in coniferous forest canopies. *Boreal Environ. Res.* 17, 411–425.

Wozniak, A., Bauer, J., Sleighter, R., Dickhut, R., and Hatcher, P. (2008). Technical Note: molecular characterization of aerosol-derived water soluble organic carbon using ultrahigh resolution electrospray ionization Fourier transform ion cyclotron resonance mass spectrometry. *Atmosp. Chem. Phys.* 8, 5099–5111. doi: 10.5194/acp-8-5099-2008

Ziolkowski, L. A., and Druffel, E. R. M. (2010). Aged black carbon identified in marine dissolved organic carbon. *Geophys. Res. Lett.* 37, L16601. doi: 10.1016/j.drs.2009.05.008

Conflict of Interest Statement: The authors declare that the research was conducted in the absence of any commercial or financial relationships that could be construed as a potential conflict of interest.

frontiers in Marine Science

ORIGINAL RESEARCH
published: 21 March 2017
doi: 10.3389/fmars.2017.00076

Carbon Dioxide Emissions along the Lower Amazon River

Henrique O. Sawakuchi[1,2], Vania Neu[3], Nicholas D. Ward[4,5], Maria de Lourdes C. Barros[1], Aline M. Valerio[6], William Gagne-Maynard[2], Alan C. Cunha[7], Diani F. S. Less[7], Joel E. M. Diniz[7], Daimio C. Brito[7], Alex V. Krusche[1] and Jeffrey E. Richey[2]*

[1] *Centro de Energia Nuclear na Agricultura, Universidade de São Paulo, Piracicaba, Brazil,* [2] *School of Oceanography, University of Washington, Seattle, WA, USA,* [3] *Instituto Sócio Ambiental e dos Recursos Hídricos, Universidade Federal Rural da Amazônia, Belém, Brazil,* [4] *Whitney Laboratory for Marine Bioscience, University of Florida, St. Augustine, FL, USA,* [5] *Marine Sciences Laboratory, Pacific Northwest National Laboratory, Sequim, WA, USA,* [6] *Departamento de Sensoriamento Remoto, Instituto Nacional de Pesquisas Espaciais, São José dos Campos, Brazil,* [7] *Departamento de Meio Ambiente e Desenvolvimento, Universidade Federal do Amapá, Macapá, Brazil*

A large fraction of the organic carbon derived from land that is transported through inland waters is decomposed along river systems and emitted to the atmosphere as carbon dioxide (CO_2). The Amazon River outgasses nearly as much CO_2 as the rainforest sequesters on an annual basis, representing ~25% of global CO_2 emissions from inland waters. However, current estimates of CO_2 outgassing from the Amazon basin are based on a conservative upscaling of measurements made in the central Amazon, meaning both basin and global scale budgets are likely underestimated. The lower Amazon River, from Óbidos to the river mouth, represents ~13% of the total drainage basin area, and is not included in current basin-scale estimates. Here, we assessed the concentration and evasion rate of CO_2 along the lower Amazon River corridor and its major tributaries, the Tapajós and Xingu Rivers. Evasive CO_2 fluxes were directly measured using floating chambers and gas transfer coefficients (k_{600}) were calculated for different hydrological seasons. Temporal variations in pCO_2 and CO_2 emissions were similar to previous observations throughout the Amazon (e.g., peak concentrations at high water) and CO_2 outgassing was lower in the clearwater tributaries compared to the mainstem. However, k_{600}-values were higher than previously reported upstream likely due to the generally windier conditions, turbulence caused by tidal forces, and an amplification of these factors in the wider channels with a longer fetch. We estimate that the lower Amazon River mainstem emits 20 Tg C year^{-1} within our study boundaries, or as much as 48 Tg C year^{-1} if the entire spatial extent to the geographical mouth is considered. Emissions from the Xingu and Tapajós lower tributaries contribute an additional 2.3 Tg C year^{-1}. Including these values with updated basin scale estimates and estimates of CO2 outgassing from small streams we estimate that the Amazon running waters outgasses as much as 0.95 Pg C year^{-1}, increasing the global emissions from inland waters by 15% for a total of 2.45 Pg C year^{-1}. These results highlight the lower reaches of large rivers as a missing gap in basin-scale and global carbon budgets. In the case of the Amazon River, the previously unstudied tidally-influenced reaches contribute to 5% of CO2 emissions from the entire basin.

Keywords: GHG emission, CO_2 emission, Lower Amazon, CO_2 outgassing, river, global CO_2 emission

OPEN ACCESS

Edited by:
Marta Álvarez, Instituto Español de Oceanografía, Spain

Reviewed by:
Hugh Daigle, University of Texas at Austin, USA
Katlin Louise Bowman, University of California, Santa Cruz, USA

****Correspondence:***
Henrique O. Sawakuchi
riqueoliveira@yahoo.com.br

Specialty section:
This article was submitted to Marine Biogeochemistry, a section of the journal Frontiers in Marine Science

Received: *03 October 2016*
Accepted: *02 March 2017*
Published: *21 March 2017*

Citation:
Sawakuchi HO, Neu V, Ward ND, Barros MdLC, Valerio AM, Gagne-Maynard W, Cunha AC, Less DFS, Diniz JEM, Brito DC, Krusche AV and Richey JE (2017) Carbon Dioxide Emissions along the Lower Amazon River. Front. Mar. Sci. 4:76. doi: 10.3389/fmars.2017.00076

INTRODUCTION

Rivers are no longer viewed as passive conduits from land to sea but, rather, play an active role in processing organic carbon derived from land and returning it to the atmosphere as carbon dioxide (CO_2) (Cole et al., 2007; Battin et al., 2009). The remaining organic and inorganic carbon that is exported to the coastal ocean is further processed, released to the atmosphere, or stored in marine waters and sediments (Medeiros et al., 2015; Ibanhez et al., 2016). Streams, rivers, and lakes have most recently been estimated to emit 2.1 Pg C year^{-1} to the atmosphere (Raymond et al., 2013), increasing from past estimates of 1.4 Pg C year^{-1} (Tranvik et al., 2009), and 0.8 Pg C year^{-1} (Cole et al., 2007). Although data coverage is more sparse, wetlands, which were not included in estimates by Raymond et al. (2013), emit another ∼2.1 Pg C year^{-1} (Aufdenkampe et al., 2011). These combined estimates, along with storage and export terms, imply that roughly 5.7 Pg C year^{-1} is transported through inland waters, with nearly 75% of this carbon being returned to the atmosphere (Le Quéré et al., 2015). Tropical regions have been identified as hotspots for aquatic CO_2 outgassing, representing ∼75% of global emissions, yet they are under-represented in global datasets, particularly with respect to direct measurements of fluxes and concentrations, which allows quantification of gas transfer velocity values that are used in regional and global models (Regnier et al., 2013; Wehrli, 2013).

The Amazon River is the largest river system in the world, responsible for 20% of the fresh water discharge to world's oceans and 25% of the emissions of CO_2 from inland waters to the atmosphere, globally (Richey et al., 2002; Raymond et al., 2013). The influence of the Amazon River on primary productivity in the Atlantic Ocean can be seen from space, driving a net uptake of CO_2 in the plume (Subramaniam et al., 2008). The source of dissolved CO_2 in large river systems shifts from headwaters to higher order rivers/streams. In small headwater streams the primary source is subsurface flow from riparian soils (Johnson et al., 2008). The relative contribution from soil respiration decreases compared to *in situ* production via microbial respiration as stream order increases (Butman and Raymond, 2011). The breakdown of young terrestrially-derived organic carbon (OC) by heterotrophic river microbes is thought to be the primary source of CO_2 in the Amazon River mainstem (Mayorga et al., 2005; Ward et al., 2013, 2016), although plant respiration and OC decomposition in floodplains also contribute to CO_2 supersaturation (Abril et al., 2014).

The majority of geochemical studies in the Amazon River have focused on the central Amazon, which represents about 30% of the 6 million km^2 drainage basin (Hedges et al., 1986, 2000; Moreira-Turcq et al., 2003). For example, the current basin-scale CO_2 budget for the Amazon River is based on aereal outgassing rates determined for this corridor, and outgassing rates were conservatively assumed to be 50% less in unstudied regions outside of the central corridor (Richey et al., 2002). The lower reaches of the Amazon River, between the historic gauging station, Óbidos, and ∼800 km downstream to the mouth, have not been included in current basin-scale budgets. This represents ∼13% of the basin's total surface area (in terms of land, not water surfaces) and is characterized by expansive floodplains and flooded forests, which likely provide large inputs of OC and CO_2 to the river. In fact, 75% of the particulate OC load is lost between Óbidos and the mouth largely due to degradation, while dissolved OC concentrations slightly increase due to constant inputs from the watershed and floodplains that balance OC degradation (Seidel et al., 2015; Ward et al., 2015). Tidal effects can be detected more than halfway upstream to Óbidos with flow completely reversing near the mouth. These forces increase water residence time and along with strong winds and wide channels (2–15 km) with a long fetch, create rough water surface conditions that likely promote CO_2 degassing. Including a quantitative evaluation of CO_2 emissions in this unique reach of the river is critical for constraining the basin scale carbon budget, which directly influences global estimates.

This study provides the first detailed evaluation of CO_2 concentrations and fluxes along the lower Amazon River and its major tributaries, the Xingu and Tapajós rivers. Direct measurements of CO_2 outgassing were made with floating domes for each hydrologic period (i.e., low, rising, high, and falling water) from 2014 to 2016 along with measurements of CO_2 concentrations and calculations of gas transfer velocities. Total CO_2 evasion was estimated for three discreet sections of the lower river: (1) the Amazon River main channel from Óbidos to the downstream study boundaries near Macapá, (2) the lower regions of the Tapajós and Xingu tributaries, and (3) the extended region from Macapá to the actual geographic river mouth. These estimates were used to calculate a range of updated basin scale CO_2 outgassing budgets based on previous estimates (Richey et al., 2002; Rasera et al., 2013), which were compared with global budgets.

METHODS

Study Area

A series of four expeditions were performed from 2014 to 2016 along the lower reach of the Amazon River, from Óbidos, the furthest downstream gauging station in the Amazon River mainstem, to the last two well-constrained channels near the river mouth at Macapá, ∼650 km downstream from Óbidos (**Figure 1**-Area 1). Tides drive a ∼3 m semi-diurnal variation in river depth, completely reversing river flow with no salinity intrusion. The river continues to widen and channelize between large islands an additional 150 km downstream of Macapá before being entirely disconnected from land and the riparian zone/floodplains (**Figure 1**-Area 2). The water entering the ocean can remain completely fresh at the surface as much as 60 km offshore from this point (**Figure 1**-Area 3; Molinas et al., 2014).

Between Óbidos and the ocean, an additional ∼20% discharge is added by lowland tributaries, primarily from the Tapajos and Xingu rivers, which are the largest clear water tributaries in the Amazon basin (Sioli, 1985; Mayorga and Aufdenkampe, 2002). The lower Amazon River, from Óbidos to the river mouth, is characterized by an intricate mixture of large channels, clear water tributaries, floodplain lakes and flooded forests, representing ∼13% of the total Amazon River drainage basin.

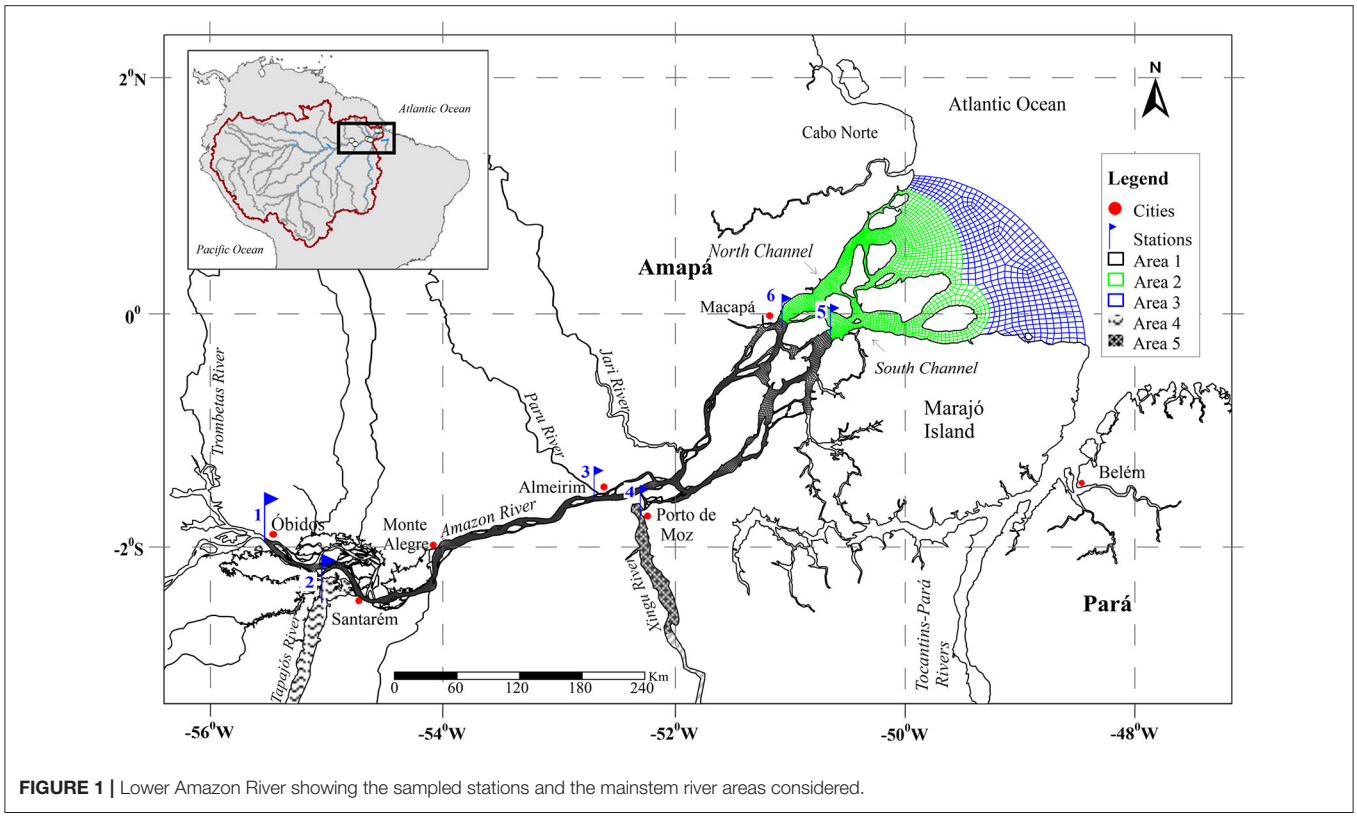

FIGURE 1 | Lower Amazon River showing the sampled stations and the mainstem river areas considered.

Measurements of pCO_2 and fluxes were carried out at different sites along the Amazon River main channel—Óbidos; Almeirim, which is halfway to the river mouth; and the north and south channels near Macapá—along with measurements near the outflow of the Tapajós and Xingu rivers (**Table 1**, **Figure 1**).

Partial Pressure of CO_2 and Flux Measurements

Measurements of the partial pressure of CO_2 (pCO_2), CO_2 fluxes (FCO_2), and calculations of gas transfer velocity (k) were made during each hydrological season (low, rising, high, and falling water). For Amazon River mainstem sites measurements were made at three sub-stations distributed equidistantly across the channel profile (e.g., center and left/right margin). Only a single station was sampled in the Tapajós and Xingu tributaries.

pCO_2 was determined using a plexiglas equilibration chamber filled with glass beads to enhance gas transfer interfaced to an Infrared Gas Analyzer (LICOR Instruments, LI-820) (Frankignoulle et al., 2001; Abril et al., 2014). Briefly, a submersible pump delivered approximately 1.5 L of water per minute flowing from the top to the bottom of the chamber, leaving approximately 0.4 L of internal air headspace. The equilibrated headspace was circulated from the top to the bottom of the chamber through a desiccating water trap, filled with Drierite for drying the air before enter in the gas analyzer using a small diaphragm pump (AS-200; Spectrex), at a flow rate of 150 mL min^{-1}. Values were recorded once pCO_2 readings remained stable.

Evasive CO_2 fluxes were directly measured from the river surface using a light weight floating chamber made of polypropylene and covered with reflective alumina tape to avoid internal heating (Galfalk et al., 2013). A floating collar made with a Styrofoam rod was attached around the chamber covering as little area as possible and positioned to leave the chamber edges submersed 2.5 cm into the water. The chamber was round with a volume and area of 7,500 ml and 0.071 m^2, respectively, and was interfaced to a second portable Infrared Gas Analyzer (LICOR Instruments, LI-820) using the same type of air pump and water trap as the equilibration chamber. Flux measurements started only after atmospheric air concentration readings by the analyzer were stable. The chamber was deployed for approximately 5 min and then lifted up to equilibrate with atmospheric air concentrations prior to the next measurement. On average three measurements were carried out for each location while drifting with the boat to avoid creating extra turbulence.

The flux of CO_2 across the air-water interface (FCO_2, mol m^{-2} s^{-1}) can be described by the following equation:

$$F_{CO_2} = \left(\frac{d\left(pCO_2\right)}{dt}\right)\left(\frac{V}{RT_KA}\right) \quad (1)$$

where $d(pCO_2)/dt$ is the slope of the CO_2 accumulation in the chamber (μatm h^{-1}), V is the chamber volume (m^3), T_K is air temperature (in degrees Kelvin, K), A is the surface area of the chamber at the water surface (m^2), and R is the gas constant (L atm K^{-1} mol^{-1}) (Frankignoulle, 1988). Measurements were

TABLE 1 | CO_2 fluxes to atmosphere (FCO_2), partial pressure of CO_2 in the water (pCO_2), gas transfer velocity (k_{600}) measurements according to site and season (mean ± SD) and measurements of mean depth (z), water velocity (w), discharge (Q) and wind speed (U_{10}).

ID	Site (River)	Sampling season	FCO_2	pCO_2	k_{600}	z	w	Q	U_{10}
			(μmol m^{-2} s^{-1})	(μatm)	(cm h^{-1})	(m)[a]	(cm s^{-1})	(m^3 s^{-1})	(m s^{-1})
1	Óbidos (Amazon)	Falling	16.06 ± 1.68	6148 ± 326	36.09 ± 13.78	54.2	183	257,277	6.6
		High	9.39 ± 2.04	6106 ± 441	17.74 ± 3.16	51.5	192	253,959	–
		Low	11.79 ± 4.04	2458 ± 6	54.32 ± 1.79	49.4	106	122,274	–
		Rising	5.89 ± 3.45	2572 ± 57	27.62 ± 16.59	32.8	106	122,172	4.5
2	Alter do Chão (Tapajós)	Falling	1.07	450	–	23.5	20	10,018	1.5
		High	1.75	1650	16.03			24,428	–
		Low	0.76	449	–	24	9	3,658	–
		Rising	2.4	896	–	10.7	27	10,480	5.4
3	Almeirim (Amazon)	Falling	13.59 ± 4.25	3857 ± 583	40.69 ± 14.71	28.1	182	282,688	3.5
		High	15.09	5406 ± 24	30.97	29.1	187	298,913	–
		Low	5.84 ± 1.97	1657 ± 168	52.11 ± 20.15	26.2	87	124,831	–
		Rising	2.49 ± 1.1	1714 ± 165	30.38 ± 15.5	16.8	102	137,117	3.2
4	Porto de Moz (Xingu)	Falling	2.39	508	174.22*			3,093	7.5
		High	7.85*	5001*	17.06			16,804	–
		Low	0.87	506	133.66*			1,674	–
		Rising	2.07	1117	42.92			14,288	4.1
5	Macapá South (Amazon)	Falling	3.9 ± 1.39	2471 ± 275	18.97 ± 7.1	24.6	50	146,473	4.8
		High	17.27 ± 0.26	4761 ± 3	42.27 ± 0.38	24	72	204,056	–
		Low	1.74	1490	16.03	17.5	31	132,998	–
		Rising	2.45 ± 0.99	1645 ± 197	28.65 ± 5.67	10.6	28	103,593	3.7
6	Macapá North (Amazon)	Falling	5.47 ± 3.05	3400 ± 565	20.51 ± 15.36	19.4	55	113,371	3.4
		High	16.79 ± 1.99	4489 ± 618	45.47 ± 13.08	18.5	64	140,692	–
		Low	3.71 ± 0.62	1272 ± 158	46.98 ± 0.04	22.7	48	61,539	–
		Rising	2.19 ± 0.87	1281 ± 22	15.8 ± 0.66	9.4	37	53,265	3.4

Outliers removed for statistical analysis.

discarded if the r^2-value from the slope of pCO_2 vs. time was lower than 0.90.

Gas Transfer Velocity (k) Estimation

Despite the difficulty of directly measuring piston velocity (k), it can be estimated by the relation between the diffuse flux and the difference among surface water and air-equilibrium concentrations given by the following equation (Wanninkhof et al., 2009):

$$F_{CO_2} = k \cdot (C_w - C_0) \quad (2)$$

where F is flux (mol m^{-2} d^{-1}), k the piston velocity (m d^{-1}), C_w is the concentration of CO_2 measured in the water (mol m^{-3}), and C_0 is the CO_2 concentration at the water surface in exchange with the atmosphere, where $C_{w,0}$ is given by the CO_2 partial pressure and solubility (i.e., $C_{w,0}$=$K_0 \times pCO_{2w,0}$). Thus, we have:

$$F_{CO_2} = k \cdot K_0 \left(pCO_{2w} - pCO_{20}\right) \quad (3)$$

where K_o (mol m^{-3} Pa^{-1}) is the aqueous-phase solubility of CO_2 as a function of temperature, pCO_{2w} and pCO_{20} are the partial pressures (Pa) of CO_2 in water and air inside the chamber, Then, substituting into Equation 1 and integrating partial pressure from time i to f, this equation can be rewritten as:

$$k = \frac{V}{A \cdot \alpha} ln \left(\frac{pCO_{2w} - pCO_{2i}}{pCO_{2w} - pCO_{2f}} \right) / \left(t_f - t_i\right) \quad (4)$$

where V is the chamber volume (cm^3), A is the chamber area (cm^2), α is the Ostwald solubility coefficient (dimensionless), t is time (h), and the subscripts i and f refer to initial and final times and partial pressures. The Ostwald solubility coefficient can be calculated from K_0 as a function of temperature as described by Wanninkhof et al. (2009), given by $K_0 = \alpha(RT_w)^{-1}$, where R (m^3 Pa K^{-1} mol^{-1}) is the ideal gas constant and T_w (K) is the water temperature.

After solving k, flux measurements, water and air concentration of CO_2 using the equation 2, and later normalized into k_{600}-values using the following equations (Jahne et al., 1987; Wanninkhof, 1992; Alin et al., 2011) derived from Equations 1–2:

$$k_{600} = k_T \left(\frac{600}{Sc_T} \right)^{-0.5} \quad (5)$$

where k_T is the measured k-value at *in situ* temperature (T), Sc_T is the Schmidt number calculated as a function of temperature (T):

$$Sc_T = 1911.1 - 118.11\ T + 3.4527\ T^2 - 0.041320\ T^3 \quad (6)$$

Hydrological and Climatological Characterization

Discharge, water velocity, and river depth were measured across the Amazon River channel sites during all cruises using a Sontek River Surveyor M9 Portable nine-beam 3.0/1.0/0.5 MHz acoustic Doppler Current Profiler (ADCP). Cross-channel ADCP transects were performed three to four times in the upstream sites with no tidal influence and 8–11 times through a complete tidal cycle (10–13 h) in sites with tidal influence in order to assess river velocity over the span of a tidal cycle and accurately calculate the total Amazon River discharge (Ward et al., 2015). Discharge measurements were not conducted in the Xingu River neither during high water season at Tapajós River. For the purpose of qualitative comparisons, we obtained data on average discharge, at the time of sampling or from long-term monthly or weekly averages from the nearest monitoring station(s) to fill these gaps. The hydrological stations searched were Óbidos at the Amazon River, Itiatuba at Tapajós River, and Altamira at the Xingu River. For sites in the Amazon, hydrological data came from the Brazilian national water agency web site (Agência Nacional de Águas, http://www.snirh.gov.br/hidroweb/).

Wind speed was measured during falling and rising water cruises with a weather station (Onset HOBO) installed on the boat or with a handheld weather station (Kestrel 5500). Wind speed was normalized to 10 m height (U_{10}) according to Alin et al. (2011) using the following equation:

$$\bar{u}_z = \left(\frac{u_*}{\kappa}\right) ln\left(\frac{z}{z_0}\right) \quad (7)$$

where $\bar{u}_z$ is the is mean wind speed (m s^{-1}) at the height z, u_* is friction velocity (m s^{-1}), κ is von Karman's constant (∼0.40), and z_0 is roughness length (10^{-5} m). Friction velocity was first calculated by rearranging equation (6) to solve for u_* and using the mean wind speed measured at 1.5 m as $\bar{u}_z$. Monthly historical wind data for comparison was obtained from the National Institute of Meteorology web site (Instituto Nacional de Meteorologia, http://www.inmet.gov.br).

Water temperature was measured with a Thermo-Orion 290APlus probe submerged in a continuously overflowing graduated cylinder.

Annual CO_2 Emissions from the Lower Amazon River

Data for the Tapajós and Xingu rivers were only acquired at one station near their river mouth. In both rivers the approximately last 100 km area is characterized as *Rias*, which have lake-like sedimentary dynamics (Archer, 2005). Thus, we only included this area of the tributaries for the outgassing budget for the lower Amazon River. We divided the main channel into two zones: (Area 1) our study boundaries from Óbidos to Macapá, which has a surface area of 7,118 km^2, and (Area 2) the region extending from Macapá to the geographical river mouth, which has an additional surface area of 11,261 km^2 (**Figure 1**). Although it has never been studied, we assume that Area 2 will have similar geochemical characteristics as the region near Macapá considering there are still inputs from land and the Amazon River water discharged to the ocean still remains completely fresh at the surface up to ∼100 km further offshore (**Figure 1**-Area 3; Molinas et al., 2014).

The CO_2 outgassing budget for Area 1 was determined by multiplying the average FCO_2 measured along the study boundaries by the surface area. For Area 2 we used the seasonal average FCO_2 measured across the North and South Macapá stations combined. FCO_2 results from each cruise were applied to a 3-month period for the particular hydrologic period and the sum of these values was used to represent annual estimates.

The surface area of the lower Amazon River main channel and lower regions of the Tapajós and Xingu rivers were estimated using the mesh generation tool of SisBaHiA (Base System for Environmental Hydrodynamic; www.sisbahia.coppe.ufrj.br). The finite element methods and mesh generation techniques used in SisBaHiA is detailed in Ern and Guermond (2004). Basically, the mesh is composed of biquadratic quadrilateral elements with specific area and the sums represent the total area of the studied surface.

Statistical Analyses

Statistical evaluations of the FCO_2 in the Lower Amazon River were done through non-parametric analysis due to the lack of normal distribution of the data (Shapiro–Wilk, $p < 0.05$, rejecting the null hypothesis of normality). Evaluation of the differences between broad hydrological settings such as tidally-influenced and tributaries vs. upstream mainstem locations were carried out by the Mann-Whitney test, and differences between sites were assessed by the Kruskal-Wallis test. The relationship among physical characteristics were done using Spearman correlation test. All analyses were performed with R (http://www.r-project.org).

RESULTS

FCO_2 Fluxes and pCO_2

The average pCO_2 and FCO_2 including all seasons and sites measured in the lower Amazon River and its tributaries was 2914 ± 1768 μatm and 6.31 ± 5.66 μmol m^{-2} s^{-1}, respectively. Tributaries had significantly lower pCO_2 and FCO_2 compared to the mainstem stations (Mann-Whitney, $p < 0.05$) with values of 1322 ± 1545 μatm and 2.4 ± 2.3 μmol m^{-2} s^{-1}, respectively, in the tributaries and 3218 ± 1656 μatm and 6.9 ± 5.8 μmol m^{-2} s^{-1}, respectively, in the mainstem (**Figure 2**). Both tributaries are considered clear water and are characterized by low suspended sediment loads and high primary productivity (Ward et al., 2015), which results in the fixation of dissolved CO_2 and reduction in pCO_2 and FCO_2. For this reason, the tributaries were considered separately from the mainstem for further comparisons.

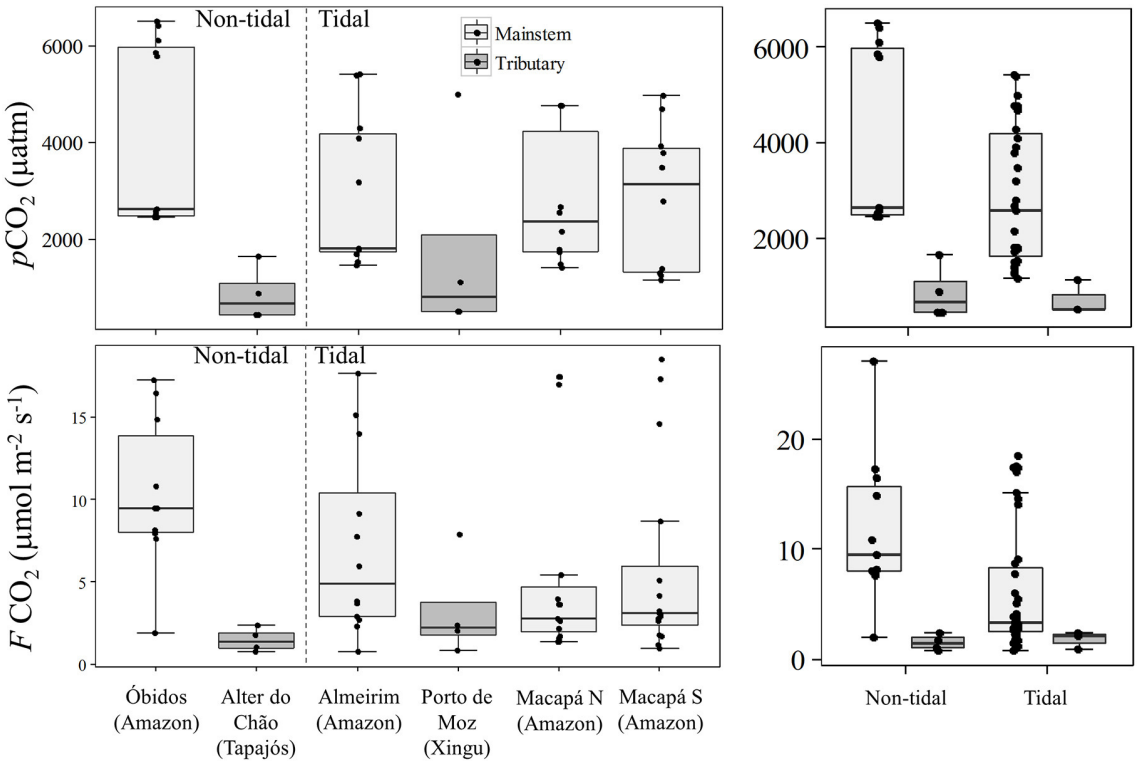

FIGURE 2 | Box plots showing the overall variability in pCO_2 and CO_2 flux to atmosphere in the Lower Amazon River mainstem and in two of the major Lower Amazon tributaries situated in the non-tidal or tidal river.

The outlier data points observed in the Xingu River (**Figure 2**) for both pCO_2 and FCO_2 occurred during the high water season (**Table 1**) likely because of the delivery of different source of water coming from a floodplain area that discharges just upstream of the sampling station during the high water season. For example, pCO_2 values as high as 10,000 ppm were observed at the confluence of the Xingu River and the Jaraçu River, which connects the Amazon and Xingu rivers through an extensive floodplain network (Ward et al., 2016). The intrusion of high suspended sediment water from a small channel was clearly observed during the high water sampling. Thus, the sampled water was a mixture of Xingu River water and Amazon River water fed through floodplains. Since this data point does not represent pure Xingu River water, the value was not considered in further comparisons.

There was no significant difference in pCO_2 and FCO_2 between the two tributaries (Mann-Whitney, $p > 0.05$), and pCO_2 was also not statistically different between the mainstem stations. Nevertheless, FCO_2 was significantly different between stations in the mainstem (Kruskal-Wallis, $p < 0.05$), with higher fluxes measured further upstream (**Figure 2**). Tidal and non-tidally influenced sites in the mainstem and tributaries were compared in order to evaluate the effects of tides play on pCO_2 and FCO_2. Tidally-influenced stations in the mainstem had slightly lower pCO_2 and FCO_2 than the non-tidal stations (Mann-Whitney, $p < 0.05$). No difference in pCO_2 or FCO_2 was observed between the Tapajos (non-tidal) and Xingu (tidal) rivers.

Seasonal variation was recognized for both pCO_2 and FCO_2 in the mainstem (Kruskal-Wallis, $p < 0.001$) with the highest values observed during the high water season and lowest values during the lower water season (**Figure 3**). pCO_2 was substantially higher in the Tapajós River during the high water season (**Table 1**). Although high pCO_2 and FCO_2 during high water in the Xingu River was attributed to floodplains fed by Amazon River source water, this was not the case in the Tapajós River (i.e., only pure Tapajós River water was present at the sampling station). However, the tributaries were only sampled at one location in the center of the channel, which limited our ability to make statistical inferences regarding seasonal differences.

Evaluation of k_{600}

The average k_{600} estimated for all stations was 33.60 ± 15.72 cm h^{-1}. There were no statistically significant differences between the mainstem and tributaries or non-tidal and tidal stations (**Figure 4**; Mann-Whitney, $p > 0.05$). The average k_{600} for the mainstem sites was 33.71 ± 15.63 cm h^{-1} compared to 32.58 ± 19.10 cm h^{-1} for the tributaries. Considering tidal vs. non-tidal stations, average k_{600}-values were 33.80 ± 16.97 cm h^{-1} and 33.53 ± 15.50 cm h^{-1}, respectively.

The primary control on k_{600} appeared to be seasonality considering the lack of spatial differences (**Figure 5**). We

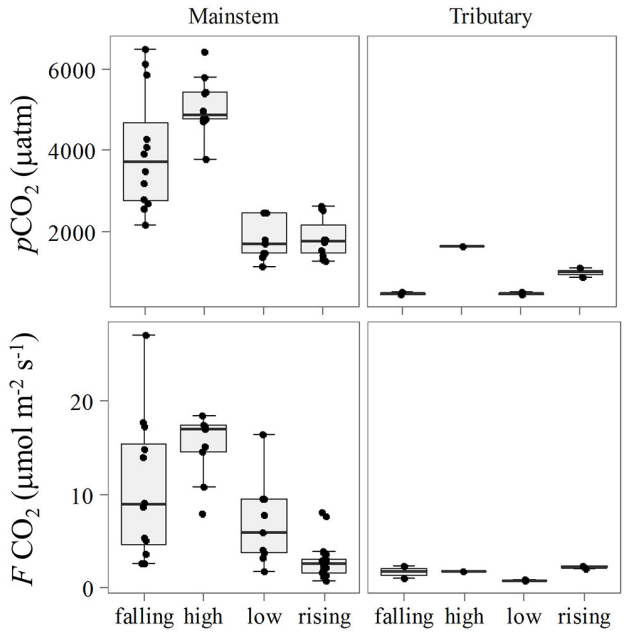

FIGURE 3 | Seasonal variation of pCO_2 and FCO_2 for the mainstem and tributaries.

observed higher values of k_{600} during the low water season in the mainstem (Kruskal-Wallis, $p < 0.05$), and during the rising water period in the tributaries (**Figure 3**). For the mainstem this pattern is in agreement with the historical monthly average of wind speed (**Figure 6**).

Environmental Characterization and Correlations with FCO_2, pCO_2, and k_{600}

The mean annual discharge (Q) at the mouth of the Amazon River to the ocean (i.e., the sum discharge measured near the mouth across the Macapá South and North channels, which integrate the discharge from all non-measured tributaries upstream) was 238,997 m^3 s^{-1}, ranging from 156,858 to 344,680 m^3 s^{-1} during low and high water periods, respectively (**Figure 7**). Water speed (w) for the mainstem sites ranged from 45 to 147 cm s^{-1}.

Wind speed (U_{10}) was measured in the river during the falling and rising water seasons and averaged 4.00 ± 1.95 m s^{-1}, ranging from 1.21 to 10.65 m s^{-1}. Mean values measured at each station in each season are shown on **Table 1**. To better assess the annual variability of wind speed in the lower Amazon River we evaluated the historical monthly average using data from 2000 to 2016 for stations located in cities along the lower Amazon River monitored by the Brazilian Institute of Meteorology (INMET). Higher wind speeds and higher seasonal variation were observed in the stations further downstream from Óbidos.

A Spearman correlation test was performed considering all stations to evaluate the relationship between pCO_2, FCO_2, and k_{600} with hydrological parameters and wind. A correlation matrix was generated for inter-comparisons of all these parameters among each other (**Table 2**). The strongest positive correlation was observed between pCO_2 and FCO_2 ($r = 0.8$, $p < 0.001$). However, pCO_2 was also positively correlated with all three measured hydrological parameters (**Table 2**). FCO_2 was correlated with depth (z) and k_{600}, while discharge (Q) was correlated with water speed, which in turn was correlated with depth. Unbinned wind speed did not present any direct correlation with any parameter considered in this study. However, average binned k_{600} for U_{10} bins of 0.5 m s^{-1} presented a stronger positive correlation (**Figure 8**; Spearman, $r = 0.7$, $p < 0.05$).

Upscaling CO_2 Emissions from the Lower Amazon River

The total flux of CO_2 from the main channel of the lower Amazon River was calculated for two zones (Figure 1) for each 3-month hydrologic period and annually (**Table 3**). The most conservative estimates (Area 1) only included the boundaries of this study, from Óbidos to Macapá, which had an average wetted surface area of 7,118 km^2. The flux of CO_2 from Area 1 was 20 Tg C year^{-1}. Area 2 extends from Macapá to the region of the mouth where the connection to land terminates, which had an additional surface area of 11,261 km^2. Area 2 had a total CO_2 flux of 28 Tg C year^{-1}, based on an extrapolation of average values measured across the north and south Macapá channels (**Table 3**). The sum of fluxes for these two zones, or the total emissions from Óbidos to the actual river mouth was 48 Tg C year^{-1}. The emissions from the lower Tapajós and Xingu rivers were 1.40 and 0.86 Tg C year^{-1}, respectively. Including these two tributaries to the budget would add more 2.26 Tg C year^{-1}.

DISCUSSION

In this study we measured pCO_2 and CO_2 fluxes from the water to atmosphere along with discharge, water current velocity and wind speed in the Lower Amazon River channel, from the last gauging station at Óbidos to the mouth. The two major clear water tributaries of the Amazon River had lower pCO_2 and FCO_2 values than the Amazon River mainstem, which is consistent with other studies (Alin et al., 2011; Rasera et al., 2013). This was expected based on the lower suspended sediment loads, which enables high rates of primary productivity as indicated by enhanced levels of Chlorophyll-*a* (Sioli, 1985; Mayorga and Aufdenkampe, 2002; Ward et al., 2015).

Previous pCO_2 measurements for sites within our study boundaries ranged from 1600 to 6037 µatm in the mainstem and from 70 to 1070 µatm in the tributaries, agreeing well with our observations (Alin et al., 2011; Borges et al., 2015). Direct FCO_2 measurements in the lower Amazon River mainstem and Tapajós River have only been reported by Alin et al. (2011) and ranged from 1.87 to 10.62 µmol m^{-2} s^{-1} in the mainstem and from 0.04

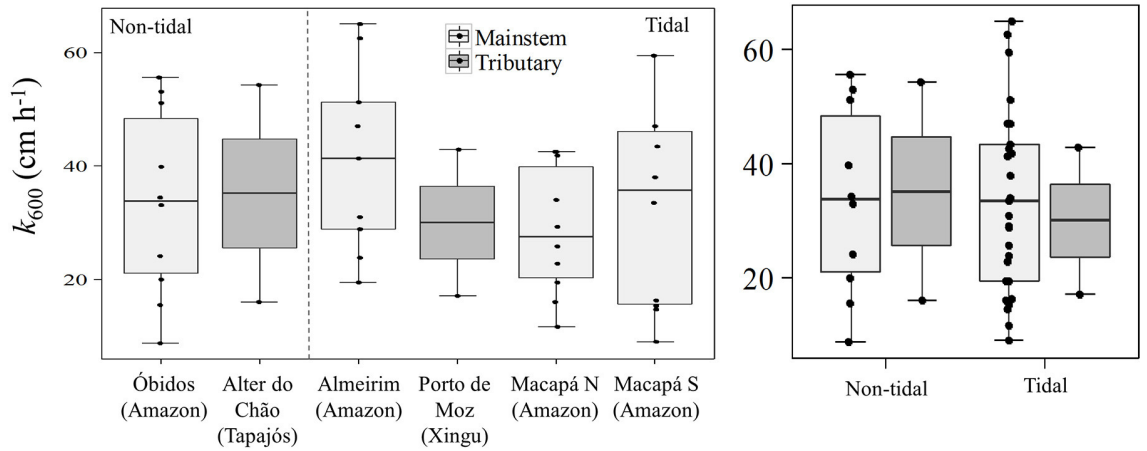

FIGURE 4 | Box plots showing the overall variability of k_{600} in the Lower Amazon River mainstem and in the tributaries situated in the non-tidal or tidal river.

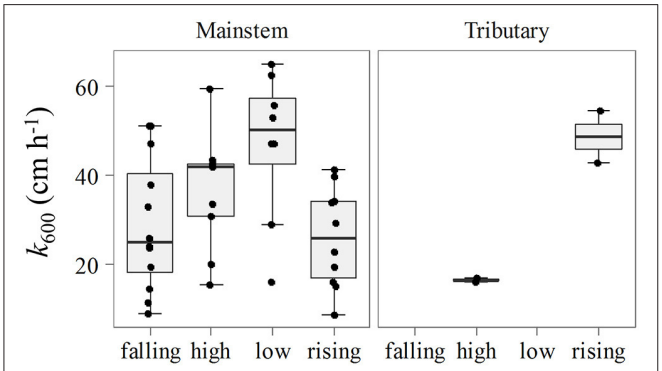

FIGURE 5 | Seasonal variation of k_{600} for the mainstem and tributaries.

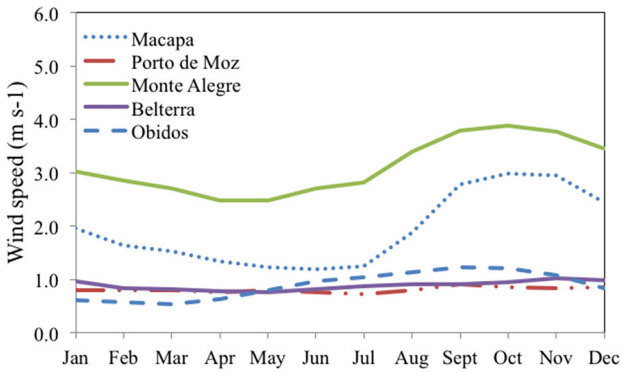

FIGURE 6 | Monthly averages from 2000 to 2016 of wind speed measured in stations located in the lower Amazon. Belterra station located near Tapajos River, Porto de Moz in Xingu River and Óbidos, Monte Alegre and Macapá in the Amazon River.

to 6.36 μmol m^{-2} s^{-1} in the Tapajós River, which is also similar to our measurements. The seasonal trend observed in pCO_2 in the lower Amazon River follows the hydrologic cycle as observed by Richey et al. (2002), with maximum CO_2 concentrations during high water and minimal concentrations during the lower water season. FCO_2 measurements followed the same trend since it was strongly correlated with pCO_2 (**Table 2**).

Despite the similar ranges of pCO_2 and FCO_2 our range of k_{600} was considerably higher than Alin et al. (2011). This can mostly be attributed to the higher wind speeds recorded in the river during our measurements compared with Alin et al. (2011). The furthest downstream station sampled by Alin et al. (2011) was near Santarém, which is roughly 500 km upstream of Macapá. We observed a downstream increase in wind speeds (**Figure 6**), which should lead to higher k_{600} values considering the typical correlation between wind speed and k_{600} in large rivers (Borges et al., 2004b; Alin et al., 2011; Rasera et al., 2013). Although we did not find any correlation between direct k_{600} calculations and the hydrological parameters or wind, the average binned k_{600} for U_{10} bins of 0.5 m s^{-1} presents a stronger positive correlation here and in the aforementioned studies (**Figure 8**). Channel width and the fetch length (i.e., the distance traveled by wind or waves across open water) also increases downstream, which amplifies the effects of wind, waves, and currents on surface water texture and turbulence. For example, the Amazon River is characterized by large sweeping curves and relatively narrow channels upstream of Santarém, which limits wave formation, whereas the main channel remains fairly straight for ∼250 km between Santarém and Almeirim, and remains straight again after a slight turn to the northwest for 2,250 km between Almeirim and Macapá.

The gas exchange coefficient and its variability within a system is among the most important factors controlling CO_2 emissions from different parts of a large basin (Raymond and Cole, 2001; Borges et al., 2004a,b; Alin et al., 2011; Striegl et al., 2012). In shallower streams and rivers where turbulence is high due to bottom friction, k_{600} can be expressed as a function of the water flow speed and depth, where shallower and faster streams tend to have higher k_{600}-values than slower streams (Raymond and Cole, 2001). In the Yukon basin, tributaries had higher k-values for CO_2 than the mainstem, and in the mainstem k increased

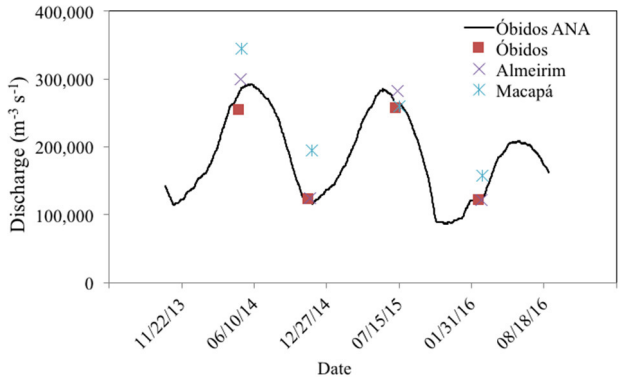

FIGURE 7 | Discharge measurements in the four cruises in the different hydrological phases compared with data from the Brazilian Water Agency (ANA) monitoring station at Óbidos.

TABLE 2 | Spearman correlation matrix showing the *r*-values in the top right side of the diagonal and adjusted *p*-values in the bottom left side in italic.

	pCO_2	FCO_2	k_{600}	Q	U_{10}	w	z
pCO_2	1	**0.800**	−0.087	**0.504**	0.160	**0.475**	**0.570**
FCO_2	***<0.0001***	1	**0.523**	0.273	0.368	0.367	**0.620**
k_{600}	*1.000*	***0.006***	1	0.052	0.234	0.052	0.073
Q	***0.014***	*0.502*	*1.000*	1	−0.007	**0.768**	0.169
U_{10}	*1.000*	*0.234*	*1.000*	*1.000*	1	−0.001	0.095
w	***0.028***	*0.083*	*1.000*	***<0.0001***	*1.000*	1	**0.5073**
z	***0.001***	***<.0001***	*1.000*	*1.000*	*1.000*	***0.002***	1

Bold numbers indicate significant correlations. Discharge (Q), wind speed (U_{10}), water velocity (w) and mean depth (z).

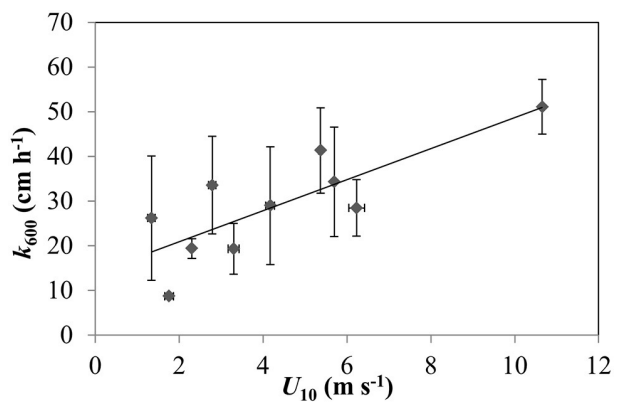

FIGURE 8 | Relationship between k_{600} binned averages with wind speed (U_{10}) bins of 0.5 m s^{-1} (Spearman, $r = 0.7$, $p < 0.05$).

downstream (Striegl et al., 2012). In the Amazon, a similar trend was observed where k_{600} was higher in rivers with narrower channels (<100 m wide) (Rasera et al., 2008; Alin et al., 2011).

In larger rivers and estuaries the main driving factors controlling k_{600} is wind and water currents, which in turn are attributed to a balance between several factors (e.g., discharge, tidal range and fetch) (Alin et al., 2011). In the Scheldt estuary water current is an important factor controlling k_{600} but its significance decreases with increasing wind speed (Borges et al., 2004b). In the Amazon and Mekong rivers, water currents are generally higher than in estuaries but with a more limited fetch and lower wind speeds (Alin et al., 2011). However, as previously mentioned, fetch dramatically increases along the lower Amazon River (**Figure 1**). The factors controlling k in large river basins is a mixture of all those described above. Wind are generally higher than those in headwater streams and current velocities are typically faster than in estuaries (Beaulieu et al., 2012). Additionally, the effect of wind on the water turbulence can be related to the water body orientation, shape, size, and direction of wind and water current. When wind and water currents are directionally opposed they can interact synergistically to produce unusually high k-values for any given wind speed (Zappa et al., 2007; Beaulieu et al., 2012). Prevailing winds in the lower Amazon are from the NE, which is the opposite direction of river outflow from Almeirim and Macapá (during an outgoing tide when net discharge is positive).

In large rivers and estuaries, the simple parametrization of k as a function of wind speed tends to be site specific due to local climatological, geomorphological, and hydrological characteristics, implying substantial errors in flux estimates using generic wind based functions from different systems (Borges et al., 2004a; Zappa et al., 2007). Rasera et al. (2013) used more detailed estimates of k_{600}, taking into account spatial variability including the difference between k_{600} for small (<100 m wide) and large (>100 m) rivers in the Amazon River, which nearly doubled estimates of basin-scale CO_2 emission from the Amazon basin estimated by Richey et al. (2002).

The lower Amazon River contains many of the features that would lead to very high gas transfer velocities and overall emissions. It is characterized by extremely wide channel(s) that flow in a convergent direction with the Intertropical Convergence Zone (ITCZ) creating a large fetch where the stronger winds can substantially increase turbulence, resulting in higher k_{600} as observed in this study. Not only are k-values high, but the lower river also has a very high amount of wetted surface area for CO_2 to escape from, particularly in wide channels near the mouth.

TABLE 3 | Seasonal CO_2 emissions in the Amazon River channel considering different areas.

Season	CO_2 emission (Tg C year^{-1})			
	Area 1	Area 2	Tributaries	Total
Area (km^2)	7,118	11,261	3,769	22,149
Falling	5.4	5.0	0.5	10.9
High	8.9	18.1	0.6	27.6
Low	3.9	2.9	0.3	7.1
Rising	1.9	2.5	0.8	5.1
Total	20.0	28.5	2.3	50.8

Estimates for tributaries only include the lower reaches measured in this study.

TABLE 4 | CO_2 emission estimates for rivers and streams in the Amazon.

	CO_2 emission (Pg C year^{-1})	References
Lower Amazon Area 1	0.020	This study
Lower Amazon Area 1 + Area 2 + tributaries	0.051	This study
Large rivers in Amazon upstream Óbidos	0.47	Richey et al., 2002
Large rivers in Amazon upstream Óbidos	0.80	Rasera et al., 2013
Amazon streams	0.10	Johnson et al., 2008

Here we considered two different areas for upscaling annual CO_2 emissions from the lower Amazon River. Our most conservative estimate, including the area from Óbidos to Macapá (Area 1), was 20 Tg C year^{-1}. Area 2, which extends to the geographic terminus of the river, is a relatively short distance compared to Area 1, but covers 58% more surface area than the Óbidos to Macapá reach (**Table 3**). Applying the average FCO_2 observed near Macapá, we estimate Area 2 to emit 28 Tg C year^{-1}, which combined with the upstream section totalize 48 Tg C year^{-1}. Emissions from the Xingu and Tapajós tributaries contribute an additional 2.3 Tg C year^{-1}, resulting in a total flux of 51 Tg C year^{-1} from the lower Amazon River basin. This estimate for the lower Amazon River, alone, is roughly 53% in magnitude compared to CO_2 emissions from all rivers in the conterminous United States (97 Tg C year^{-1}; Archer, 2005) and ∼12% of past estimates of basin-scale emissions from the Amazon (0.47 Pg C year^{-1}; Butman and Raymond, 2011) and ∼ 12% of past estimates of basin-scale emissions from the Amazon (0.47 Pg C year^{-1}; Richey et al., 2002).

Adding our estimations of the fluxes estimated for Area 1 and the sum of Area 1 and 2 to estimations by Butman and Raymond (2011) increases basin-scale CO_2 outgassing to 0.49 and 0.52 Pg C year^{-1}, respectively. A recent re-evaluation of basin-wide outgassing estimates upstream of Óbidos was done using a combination of direct flux measurements and more detailed k-values calculations along with observations by Alin et al. (2011) for tributaries and streams. It was estimated that basin scale CO_2 outgassing upstream from Óbidos was roughly 0.8 Pg C year^{-1} (Borges et al., 2004a). First order streams add an additional 0.1 Pg C year^{-1} to basin scale CO_2 fluxes in the Amazon basin (Battin et al., 2009). Adding our estimates for the lower river to these values results in basin-wide budgets of 0.92 Pg C year^{-1} and 0.95 Pg C year^{-1} for Area 1 and the sum of Area 1 and 2, respectively (**Table 4**). Replacing these new estimates for the Amazon in the global CO_2 budget by Borges et al. (2004b) increases the global budget by as much as 18% for a total of 2.48 Pg C year^{-1}.

In the case of this updated global budget, the Amazon River represents 38% of global CO_2 emissions. However, the contribution of other tropical rivers to the global budget are likely also underestimated considering that most tropical rivers are even less well-characterized than the Amazon, particularly in the lower reaches, where we've demonstrated that emissions can be high relative to the rest of the basin. Furthermore, we have not included the entirety of the Amazon in our newest budgets. For example, the Tapajós and Xingu rivers were not included due to their large spatial expanse and minimal data coverage. The lower portion of these tributaries, alone (**Figure 1**), emit roughly 2.3 Tg C year^{-1}, and these estimates do not encompass their entire surface area nor potentially elevated CO_2 concentrations closer to their headwaters.

Another factor that can lead to an underestimation of basin-wide budgets is not including Amazon River water that travels further offshore from Area 2 and along the coastline. For example, the Amazon River can remain unmixed with the ocean as far as 60 km offshore from Area 2 (Molinas et al., 2014). Abril et al. (2014) estimated that only 18% of the CO_2 from a point source would be degassed in a stretch of approximately 150 km downstream in the Amazon River taking into account a k-value of 15 cm h^{-1} and water current of 150 cm s^{-1}. Thus, it is reasonable to assume that the mouth of the Amazon is the last point source of CO_2 to the Amazon plume, sustaining significant emissions for a significant distance offshore. This region, along with near-shore coastal waters, is not included in any studies of CO_2 cycling in the Amazon River plume in the Atlantic Ocean due to a lack of sampling and terrestrial contamination of remote sensing products by adjacency effect near-shore (Cooley et al., 2007; Subramaniam et al., 2008). We estimate that Area 3 may emit up to an additional 31 Tg C year^{-1}, but note that this is a simple calculation based on measurements at Macapá. Further exploration of this offshore area is essential for constraining the total basin-wide CO_2 flux. Although it is too early to confidently incorporate this offshore freshwater region (Area 3) into basin-wide budgets, this rough estimation highlights that expansive regions of offshore freshwater plumes may be an important missing gap in aquatic carbon budgets.

CONCLUDING REMARKS

Numerous studies in the Amazon River have demonstrated its importance on global carbon budgets (Richey et al., 2002; Johnson et al., 2008; Rasera et al., 2013; Scofield et al., 2016). However, a missing gap in the continuum that connects the river network to the ocean has been neglected. Here we show that the lower reaches of the Amazon River are an active area in terms of freshwater CO_2 emissions from the Amazon, and perhaps the world, although, lower river reaches have yet to be adequately studied in other comparable tropical systems. A mixture of vast floodplains, tidally-flooded forests, and the surrounding watershed supplies the lower river with both CO_2 (Abril et al., 2014) and organic carbon, which is broken down extensively by heterotrophic bacteria (Ward et al., 2013, 2016). The downstream expansion of channel width and the alignment of a long fetch opposing the prevailing winds, which also increase toward the mouth, leads to high CO_2 emissions attributed to higher *k*-values in the lower river.

The enormous surface area of the lower Amazon River (18,379 km^2) is slightly less than half of the area of rivers and stream in the conterminous United States (Butman and Raymond, 2011), and similarly emits roughly half as much

CO_2 to the atmosphere. This area alone releases an amount of CO_2 in the same order of magnitude than the uptake by the Amazon River plume in the Atlantic Ocean (Kortzinger, 2003; Cooley et al., 2007; Subramaniam et al., 2008). We argue that the region where freshwater extends offshore should be included in basin-scale budgets considering that studies in the plume do not cover this area, however, there is no available data in this region to date. There is a pressing need to perform measurements of pCO_2 and FCO_2 along lower rivers and near-shore plume waters, which are currently large missing gaps in our coverage of regional and global scale carbon budgets.

AUTHOR CONTRIBUTIONS

JR, AK, HS, and NW responsible for the conception and design of the work. HS, VN, AV, WG, DL, and JD executed *in situ* measurements. HS, VN developed the data calculation and interpretation. MB conceived the areal estimations. JR, AK, HS, and NW organized overall project logistics. AC, DL, JD, and DB organized local logistics. All authors critically revised the manuscript and approved the final submission. All authors also agreed to be accountable for all aspects of the work related to the accuracy or integrity of any part of the work are appropriately investigated and resolved.

FUNDING

This study was supported by FAPESP Grants 12/51187-0, 2014/21564-2, and 2015/09187-1, NSF DEB Grant #1256724, and NSF IGERT grant DGE-125848.

ACKNOWLEDGMENTS

We thank Alexandra Montebello, for assistance in the laboratory at CENA. Gilvan Portela de Oliveira and Geison Carlos Xisto da Silva for logistical support in Macapá, Cica and the crew of the B/M Mirage for contributions made during the river cruises. Open access publication fees were supported by the Gordon and Betty Moore Foundation.

REFERENCES

Abril, G., Martinez, J. M., Artigas, L. F., Moreira-Turcq, P., Benedetti, M. F., Vidal, L., et al. (2014). Amazon River carbon dioxide outgassing fuelled by wetlands. *Nature* 505, 395–398. doi: 10.1038/nature12797

Alin, S. R., Rasera, M. F. F. L., Salimon, C. I., Richey, J. E., Holtgrieve, G. W., Krusche, A. V., et al. (2011). Physical controls on carbon dioxide transfer velocity and flux in low-gradient river systems and implications for regional carbon budgets. *J. Geophys. Res. Biogeosci.* 116:G01009. doi: 10.1029/2010jg001398

Archer, A. W. (2005). "Review of amazonian depositional systems," in *Fluvial Sedimentology VII*, eds M. S. Blum and S. Leclair (Oxford: Blackwell Publishing Ltd.), 17–39.

Aufdenkampe, A. K., Mayorga, E., Raymond, P. A., Melack, J. M., Doney, S. C., Alin, S. R., et al. (2011). Riverine coupling of biogeochemical cycles between land, oceans, and atmosphere. *Front. Ecol. Environ.* 9, 53–60. doi: 10.1890/100014

Battin, T. J., Luyssaert, S., Kaplan, L. A., Aufdenkampe, A. K., Richter, A., and Tranvik, L. J. (2009). The boundless carbon cycle. *Nat. Geosci.* 2, 598–600. doi: 10.1038/ngeo618

Beaulieu, J. J., Shuster, W. D., and Rebholz, J. A. (2012). Controls on gas transfer velocities in a large river. *J. Geophys. Res. Biogeosci.* 117:G02007. doi: 10.1029/2011jg001794

Borges, A. V., Abril, G., Darchambeau, F., Teodoru, C. R., Deborde, J., Vidal, L. O., et al. (2015). Divergent biophysical controls of aquatic CO_2 and CH_4 in the World's two largest rivers. *Sci. Rep.* 5:15614. doi: 10.1038/srep 15614

Borges, A. V., Delille, B., Schiettecatte, L. S., Gazeau, F., Abril, G., and Frankignoulle, M. (2004a). Gas transfer velocities of CO_2 in three European estuaries (Randers Fjord, Scheldt, and Thames). *Limnol. Oceanogr.* 49, 1630–1641. doi: 10.4319/lo.2004.49.5.1630

Borges, A. V., Vanderborght, J. P., Schiettecatte, L. S., Gazeau, F., Ferron-Smith, S., Delille, B., et al. (2004b). Variability of the gas transfer velocity of CO_2 in a macrotidal estuary (the Scheldt). *Estuaries* 27, 593–603. doi: 10.1007/bf02907647

Butman, D., and Raymond, P. A. (2011). Significant efflux of carbon dioxide from streams and rivers in the United States. *Nat. Geosci.* 4, 839–842. doi: 10.1038/ngeo1294

Cole, J. J., Prairie, Y. T., Caraco, N. F., McDowell, W. H., Tranvik, L. J., Striegl, R. G., et al. (2007). Plumbing the global carbon cycle: integrating inland waters into the terrestrial carbon budget. *Ecosystems* 10, 171–184. doi: 10.1007/s10021-006-9013-8

Cooley, S. R., Coles, V. J., Subramaniam, A., and Yager, P. L. (2007). Seasonal variations in the Amazon plume-related atmospheric carbon sink. *Glob. Biogeochem. Cycles* 21:GB3014. doi: 10.1029/2006gb002831

Ern, A., and Guermond, J.-L. (2004). *Theory and Practice of Finite Elements*. New York, NY: Springer-Verlag.

Frankignoulle, M. (1988). Field-measurements of air sea CO_2 exchange. *Limnol. Oceanogr.* 33, 313–322.

Frankignoulle, M., Borges, A., and Biondo, R. (2001). A new design of equilibrator to monitor carbon dioxide in highly dynamic and turbid environments. *Water Res.* 35, 1344–1347. doi: 10.1016/s0043-1354(00)00369-9

Galfalk, M., Bastviken, D., Fredriksson, S., and Arneborg, L. (2013). Determination of the piston velocity for water-air interfaces using flux chambers, acoustic Doppler velocimetry, and IR imaging of the water surface. *J. Geophys. Res. Biogeosci.* 118, 770–782. doi: 10.1002/jgrg.20064

Hedges, J. I., Clark, W. A., Quay, P. D., Richey, J. E., Devol, A. H., and Santos, U. D. (1986). Compositions and fluxes of particulate organic material in the Amazon River. *Limnol. Oceanogr.* 31, 717–738.

Hedges, J. I., Mayorga, E., Tsamakis, E., McClain, M. E., Aufdenkampe, A., Quay, P., et al. (2000). Organic matter in Bolivian tributaries of the Amazon River: a comparison to the lower mainstream. *Limnol. Oceanogr.* 45, 1449–1466. doi: 10.4319/lo.2000.45.7.1449

Ibanhez, J. S. P., Araujo, M., and Lefevre, N. (2016). The overlooked tropical oceanic CO_2 sink. *Geophys. Res. Lett.* 43, 3804–3812. doi: 10.1002/2016gl068020

Jahne, B., Munnich, K. O., Bosinger, R., Dutzi, A., Huber, W., and Libner, P. (1987). On the parameters influencing air-water gas exchange. *J. Geophys. Res. Oceans* 92, 1937–1949. doi: 10.1029/JC092iC02p01937

Johnson, M. S., Lehmann, J., Riha, S. J., Krusche, A. V., Richey, J. E., Ometto, J., et al. (2008). CO_2 efflux from Amazonian headwater streams represents a significant fate for deep soil respiration. *Geophys. Res. Lett.* 35:L17401. doi: 10.1029/2008gl034619

Kortzinger, A. (2003). A significant CO_2 sink in the tropical Atlantic Ocean associated with the Amazon River plume. *Geophys. Res. Lett.* 30:2287. doi: 10.1029/2003gl018841

Le Quéré, C., Moriarty, R., Andrew, R. M., Peters, G. P., Ciais, P., Friedlingstein, P., et al. (2015). Global carbon budget 2014. *Earth Syst. Sci. Data* 7, 47–85. doi: 10.5194/essd-7-47-2015

Mayorga, E., and Aufdenkampe, A. K. (2002). "Processing of bioactive elements in the amazon river system," in *The Ecohydrology of South American Rivers and Wetlands*, ed M. E. McClain (Wallingford: IAHS Press), 1–24.

Mayorga, E., Aufdenkampe, A. K., Masiello, C. A., Krusche, A. V., Hedges, J. I., Quay, P. D., et al. (2005). Young organic matter as a source of

carbon dioxide outgassing from Amazonian rivers. *Nature* 436, 538–541. doi: 10.1038/nature03880

Medeiros, P. M., Seidel, M., Ward, N. D., Carpenter, E. J., Gomes, H. R., Niggemann, J., et al. (2015). Fate of the Amazon River dissolved organic matter in the tropical Atlantic Ocean. *Glob. Biogeochem. Cycles* 29, 677–690. doi: 10.1002/2015gb005115

Molinas, E., Vinzon, S. B., Vilela, C. D. X., and Gallo, M. N. (2014). Structure and position of the bottom salinity front in the Amazon Estuary. *Ocean Dynamics* 64, 1583–1599. doi: 10.1007/s10236-014-0763-0

Moreira-Turcq, P., Seyler, P., Guyot, J. L., and Etcheber, H. (2003). Exportation of organic carbon from the Amazon River and its main tributaries. *Hydrol. Processes* 17, 1329–1344. doi: 10.1002/hyp.1287

Rasera, M. F. F. L., Ballester, M. V. R., Krusche, A. V., Salimon, C., Montebelo, L. A., Alin, S. R., et al. (2008). Estimating the surface area of small rivers in the southwestern Amazon and their role in CO_2 outgassing. *Earth Interactions* 12, 1–16. doi: 10.1175/2008ei257.1

Rasera, M. F. F. L., Krusche, A. V., Richey, J. E., Ballester, M. V. R., and Victória, R. L. (2013). Spatial and temporal variability of pCO_2 and CO_2 efflux in seven Amazonian Rivers. *Biogeochemistry* 116, 241–259. doi: 10.1007/s10533-013-9854-0

Raymond, P. A., and Cole, J. J. (2001). Gas exchange in rivers and estuaries: choosing a gas transfer velocity. *Estuaries* 24, 312–317. doi: 10.2307/1352954

Raymond, P. A., Hartmann, J., Lauerwald, R., Sobek, S., McDonald, C., Hoover, M., et al. (2013). Global carbon dioxide emissions from inland waters. *Nature* 503, 355–359. doi: 10.1038/nature12760

Regnier, P., Friedlingstein, P., Ciais, P., Mackenzie, F. T., Gruber, N., Janssens, I. A., et al. (2013). Anthropogenic perturbation of the carbon fluxes from land to ocean. *Nat. Geosci.* 6, 597–607. doi: 10.1038/ngeo1830

Richey, J. E., Melack, J. M., Aufdenkampe, A. K., Ballester, V. M., and Hess, L. L. (2002). Outgassing from Amazonian rivers and wetlands as a large tropical source of atmospheric CO_2. *Nature* 416, 617–620. doi: 10.1038/416617a

Scofield, V., Melack, J. M., Barbosa, P. M., Amaral, J. H. F., Forsberg, B. R., and Farjalla, V. F. (2016). Carbon dioxide outgassing from Amazonian aquatic ecosystems in the Negro River basin. *Biogeochemistry* 129, 77–91. doi: 10.1007/s10533-016-0220-x

Seidel, M., Yager, P. L., Ward, N. D., Carpenter, E. J., Gomes, H. R., Krusche, A. V., et al. (2015). Molecular-level changes of dissolved organic matter along the Amazon River-to-ocean continuum. *Mar. Chem.* 177, 218–231. doi: 10.1016/j.marchem.2015.06.019

Sioli, H. (1985). *Amazônia: Fundamentos de Ecologia da Maior Região de Florestas Tropicais*. Petrópolis: Editora Vozes.

Striegl, R. G., Dornblaser, M. M., McDonald, C. P., Rover, J. R., and Stets, E. G. (2012). Carbon dioxide and methane emissions from the Yukon River system. *Glob. Biogeochem. Cycles* 26, GB0E05. doi: 10.1029/2012gb004306

Subramaniam, A., Yager, P. L., Carpenter, E. J., Mahaffey, C., Bjorkman, K., Cooley, S., et al. (2008). Amazon River enhances diazotrophy and carbon sequestration in the tropical North Atlantic Ocean. *Proc. Natl. Acad. Sci. U.S.A.* 105, 10460–10465. doi: 10.1073/pnas.0710279105

Tranvik, L. J., Downing, J. A., Cotner, J. B., Loiselle, S. A., Striegl, R. G., Ballatore, T. J., et al. (2009). Lakes and reservoirs as regulators of carbon cycling and climate. *Limnol. Oceanogr.* 54, 2298–2314. doi: 10.4319/lo.2009.54.6_part_2.2298

Wanninkhof, R. (1992). Relationship betwenn wind-speed and gas-exchange over the ocean. *J. Geophys. Res. Oceans* 97, 7373–7382. doi: 10.1029/92jc00188

Wanninkhof, R., Asher, W. E., Ho, D. T., Sweeney, C., and McGillis, W. R. (2009). Advances in quantifying air-sea gas exchange and environmental forcing. *Ann. Rev. Mar. Sci.* 1, 213–244. doi: 10.1146/annurev.marine.010908.163742

Ward, N. D., Bianchi, T. S., Sawakuchi, H. O., Gagne-Maynard, W., Cunha, A. C., Brito, D. C., et al. (2016). The reactivity of plant-derived organic matter and the potential importance of priming effects along the lower Amazon River. *J. Geophys. Res. Biogeosci.* 121, 1522–1539. doi: 10.1002/2016jg003342

Ward, N. D., Keil, R. G., Medeiros, P. M., Brito, D. C., Cunha, A. C., Dittmar, T., et al. (2013). Degradation of terrestrially derived macromolecules in the Amazon River. *Nat. Geosci.* 6, 530–533. doi: 10.1038/ngeo1817

Ward, N. D., Krusche, A. V., Sawakuchi, H. O., Brito, D. C., Cunha, A. C., Moura, J. M. S., et al. (2015). The compositional evolution of dissolved and particulate organic matter along the lower Amazon River—Óbidos to the ocean. *Mar. Chem.* 177, 244–256. doi: 10.1016/j.marchem.2015.06.013

Wehrli, B. (2013). Biogeochemistry: Conduits of the carbon cycle. *Nature* 503, 346–347. doi: 10.1038/503346a

Zappa, C. J., McGillis, W. R., Raymond, P. A., Edson, J. B., Hintsa, E. J., Zemmelink, H. J., et al. (2007). Environmental turbulent mixing controls on air-water gas exchange in marine and aquatic systems. *Geophys. Res. Lett.* 34:L10601. doi: 10.1029/2006gl028790

Conflict of Interest: The authors declare that the research was conducted in the absence of any commercial or financial relationships that could be construed as a potential conflict of interest.

frontiers in Marine Science

ORIGINAL RESEARCH
published: 07 February 2017
doi: 10.3389/fmars.2017.00026

Evaluation of Primary Production in the Lower Amazon River Based on a Dissolved Oxygen Stable Isotopic Mass Balance

William C. Gagne-Maynard[1], Nicholas D. Ward[1,2,3], Richard G. Keil[1], Henrique O. Sawakuchi[1,4], Alan C. Da Cunha[5], Vania Neu[6], Daimio C. Brito[5], Diani F. Da Silva Less[5], Joel E. M. Diniz[5], Aline De Matos Valerio[7], Milton Kampel[7], Alex V. Krusche[4] and Jeffrey E. Richey[1]*

[1] School of Oceanography, University of Washington, Seattle, WA, USA, [2] Marine Sciences Laboratory, Pacific Northwest National Laboratory, Sequim, WA, USA, [3] Whitney Laboratory for Marine Bioscience, University of Florida, St. Augustine, FL, USA, [4] Centro de Energia Nuclear na Agricultura, Universidade de São Paulo, Piracicaba, Brazil, [5] Departamento de Meio Ambiente e Desenvolvimento, Universidade Federal do Amapá, Macapá, Brazil, [6] Instituto Sócio Ambiental e dos Recursos Hídricos, Universidade Federal Rural da Amazonia, Belem, Brazil, [7] Departamento de Sensoriamento Remoto, Instituto Nacional de Pesquisas Espaciais, São José dos Campos, Brazil

OPEN ACCESS

Edited by:
Hongbin Liu, The Hong Kong University of Science and Technology, Hong Kong

Reviewed by:
Benoit Thibodeau, University of Hong Kong, Hong Kong
Bingzhang Chen, Japan Agency for Marine-Earth Science and Technology, Japan

***Correspondence:**
Nicholas D. Ward
nicholas.ward@pnnl.gov

Specialty section:
This article was submitted to Marine Biogeochemistry, a section of the journal Frontiers in Marine Science

Received: *02 November 2016*
Accepted: *24 January 2017*
Published: *07 February 2017*

Citation:
Gagne-Maynard WC, Ward ND, Keil RG, Sawakuchi HO, Da Cunha AC, Neu V, Brito DC, Da Silva Less DF, Diniz JEM, De Matos Valerio A, Kampel M, Krusche AV and Richey JE (2017) Evaluation of Primary Production in the Lower Amazon River Based on a Dissolved Oxygen Stable Isotopic Mass Balance. Front. Mar. Sci. 4:26. doi: 10.3389/fmars.2017.00026

The Amazon River outgasses nearly an equivalent amount of CO_2 as the rainforest sequesters on an annual basis due to microbial decomposition of terrigenous and aquatic organic matter. Most research performed in the Amazon has been focused on unraveling the mechanisms driving CO_2 production since the recognition of a persistent state of CO_2 supersaturation. However, although the river system is clearly net heterotrophic, the interplay between primary production and respiration is an essential aspect to understanding the overall metabolism of the ecosystem and potential transfer of energy up trophic levels. For example, an efficient ecosystem is capable of both decomposing high amounts of organic matter at lower trophic levels, driving CO_2 emissions, and accumulating energy/biomass in higher trophic levels, stimulating fisheries production. Early studies found minimal evidence for primary production in the Amazon River mainstem and it has since been assumed that photosynthesis is strongly limited by low light penetration attributed to the high sediment load. Here, we test this assumption by measuring the stable isotopic composition of O_2 ($\delta^{18}O$-O_2) and O_2 saturation levels in the lower Amazon River from Óbidos to the river mouth and its major tributaries, the Xingu and Tapajós rivers, during high and low water periods. An oxygen mass balance model was developed to estimate the input of photosynthetic oxygen in the discrete reach from Óbidos to Almeirim, midway to the river mouth. Based on the oxygen mass balance we estimate that primary production occurred at a rate of 0.39 ± 0.24 g O m^3 d^{-1} at high water and 1.02 ± 0.55 g O m^3 d^{-1} at low water. This translates to $41 \pm 24\%$ of the rate of O_2 drawdown via respiration during high water and $67 \pm 33\%$ during low water. These primary production rates are 2–7 times higher than past estimates for the Amazon

River mainstem. It is possible that at high water much of this productivity signal is the result of legacy advection from floodplains, whereas limited floodplain connectivity during low water implies that most of this signal is the result of *in situ* primary production in the Amazon River mainstem.

Keywords: photosynthesis, tropical rivers, respiration, oxygen, mass balance

INTRODUCTION

A considerable body of work over the last several decades has demonstrated that the world's inland waters are generally supersaturated with carbon dioxide (CO_2), resulting in a large flux of CO_2 from rivers and lakes to the atmosphere (Cole et al., 2007; Battin et al., 2009). This state of supersaturation is driven by the balance between CO_2 outputs such as primary production, degassing, and export and CO_2 inputs from soils/sediments, the riparian zone, physical and biological decomposition of organic matter (OM) derived from both the terrestrial biosphere (Mayorga et al., 2005; Ward et al., 2013) and aquatic production (Kritzberg et al., 2004; del Giorgio and Pace, 2008), and aquatic plant respiration in floodplains (Abril et al., 2014). Rivers outgas an order of magnitude more CO_2 than lakes on a global scale (Raymond et al., 2013). This is commonly attributed to higher rates of primary production relative to respiration in still waters compared to flowing rivers (Tranvik et al., 2009).

Although it is clear that rivers provide a positive flux of CO_2 to the atmosphere in most cases, quantifying the relative amount of carbon/energy that is produced vs. consumed in an ecosystem is central to understanding its overall productivity and the potential movement of energy up trophic levels (Odum, 1971). For example, rapid rates of carbon remineralization do not preclude productive fisheries. Lower and higher trophic levels depend on both autochthonous and terrestrial carbon/energy sources to thrive, and the balance in food sources to freshwater ecosystems is tightly linked to hydrology (Hoffman et al., 2008). Likewise, recent evidence has shown that the presence of fresh algal biomass and exudates can stimulate the breakdown of less reactive OM such as terrestrially-derived molecules, implying that systems receiving large inputs of both allochthonous and autochthonous OM are likely highly efficient at recycling carbon (Guenet et al., 2014; Bianchi et al., 2015; Ward et al., 2016).

In large turbid river systems such as the Amazon River it has long been assumed that primary production is minimal relative to heterotrophic respiration due to high sediment loads and low light penetration relative to river depth (Fisher, 1979; Devol et al., 1987; Richey et al., 1990; Hedges et al., 2000). In fact, early measurements of primary production based on ^{14}C uptake indicated rates of primary production that are about an order of magnitude lower than respiration in the Amazon River mainstem, while clearwater tributaries in the basin's lowlands exhibited significantly higher rates of primary production (Wissmar et al., 1981; Benner et al., 1995). However, several studies have more recently found evidence for a higher relative contribution of primary production (and subsequent breakdown of algal OM) to ecosystem metabolism in the Amazon River based on the stable isotopic signature of dissolved oxygen ($\delta^{18}O\text{-}O_2$) and the presence of algal biomarkers in the mainstem (Quay et al., 1995; Mortillaro et al., 2011; Ellis et al., 2012). Similar observations of high rates of primary production and algal abundance have also been made in the mainstem of the Congo River, a similar large tropical system (Descy et al., 2017).

These emerging results suggest that there is a large gap between the conventional understanding of production in turbid tropical rivers, and what is actually occurring in the environment. Gross primary production and respiration rates are critical components in understanding the production, transformation and export of OM and other biogeochemically important nutrients in aquatic ecosystems. The balance between these two is a key measure of the net metabolic state of the ecosystem. As rivers worldwide are saturated with respect to atmospheric CO_2 and outgas this CO_2 at a massive scale, understanding the exact dynamics of photosynthesis and respiration remain key to understanding the role of river systems in global biogeochemical cycles and have further implications on ecosystem productivity as previously described (Cole and Caraco, 2001; Butman and Raymond, 2011).

The Amazon River is the largest source of freshwater to the world's oceans and outgases 0.5 Pg C $year^{-1}$, which is roughly 25% of recent global estimates (Richey et al., 2002; Raymond et al., 2013). The Amazon River ecosystem also supports the world's most diverse fishery with over 2500 unique species and is among the primary sources of protein for the region (Junk et al., 2007). The massive contribution of the Amazon basin to global biogeochemical cycling and regional economics makes it an ideal setting for evaluating large-scale processes. The lower Amazon River, from Óbidos to the river mouth, is an understudied component of the Amazon basin, but is a region where the interplay between primary production and heterotrophic respiration likely rapidly evolves due to a gradient in environmental conditions (Ward et al., 2016). Most historic measurements of the Amazon River have only been made as far downstream as Óbidos, roughly 800 km from the mouth of the river (Hedges and Clark, 1986; Quay et al., 1992; Moreira-Turcq et al., 2013). The lower Amazon watershed represents ∼13% of the total drainage basin and is composed of a mixture of wide channels, flooded forests, clear water tributaries and floodplain lakes (Ward et al., 2015). The lower reach of the river is also subject to tidal effects, increasing the residence time of the water and increasing connectivity between flooded forests and the mainstem.

Previous studies have used $\delta^{18}O\text{-}O_2$ values to estimate gas exchange (Jamieson et al., 2012) and estimate net metabolism (i.e., the ratio of respiration to photosynthesis) in steady-state systems (Quay et al., 1995; Bocaniov et al., 2012) as well as non-steady-state systems (Tobias et al., 2007; Holtgrieve et al.,

2010). Past estimates of primary production in the Amazon River are based on a steady-state assumption (i.e., no diel variability in $\delta^{18}O\text{-}O_2$) (Quay et al., 1995; Ellis et al., 2012); however, if primary production is actually occurring at appreciable rates in the mainstem of the river this steady-state assumption should not hold true.

This study seeks to examine the occurrence and magnitude of primary production within the lower Amazon River relative to respiration, from the historic downstream gaging station, Óbidos, to the river mouth. Measurements of the concentration and stable isotopic composition of dissolved oxygen made along the lower river and throughout a diel cycle were used to construct an oxygen mass balance for a discreet reach of the system in an effort to determine the relative contribution of primary production and respiration to ecosystem metabolism.

MATERIALS AND METHODS

Measurements of the concentration and stable isotopic composition of dissolved oxygen were made along the lower Amazon River and coupled with measurements of microbial respiration rates (Ward et al., unpublished) and gas transfer velocities (Sawakuchi et al., unpublished) made during the same study period to construct an oxygen mass balance for the lower river. The stable isotopic composition of water ($\delta^{18}O\text{-}H_2O$) was also measured for calculations associated with $\delta^{18}O\text{-}O_2$.

Study Area

Two expeditions were performed along the lower Amazon River during high water (May 2014) and low water (November 2015). The upstream boundary was Óbidos, the historic downstream gaging station, which is roughly 800 km from the river mouth (**Figure 1**). The downstream boundary was the northern and southern channels near the city of Macapá (NMCP and SMCP, respectively), which is ∼650 km downstream of Óbidos. Sampling was also performed in the Amazon River mainstem midway to the mouth near the city of Almeirim and near the mouth of the two primary clearwater tributaries downstream of Óbidos, the Xingu and Tapajós rivers. The Tapajós and Xingu rivers add ∼10% to the total discharge of the Amazon River

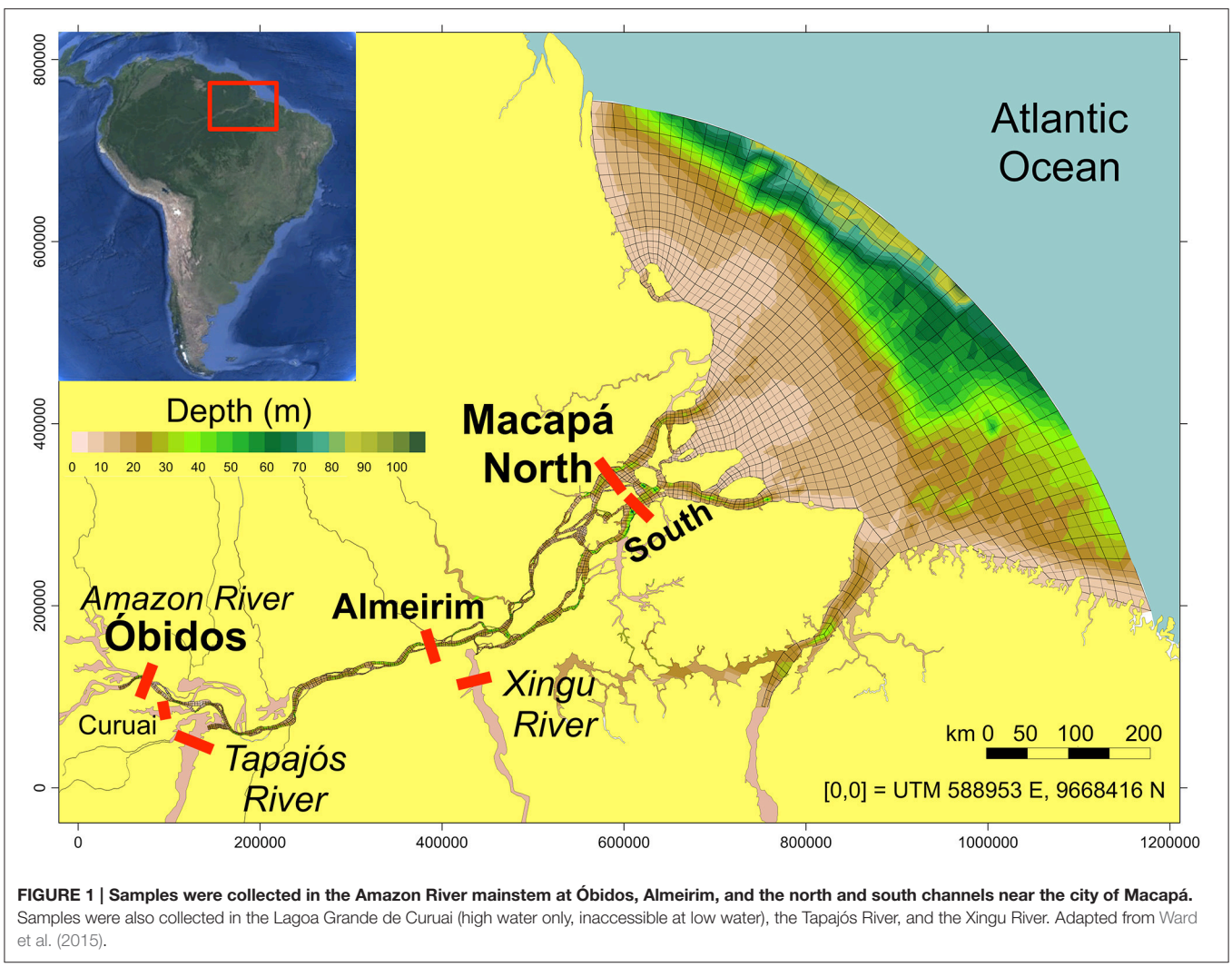

FIGURE 1 | Samples were collected in the Amazon River mainstem at Óbidos, Almeirim, and the north and south channels near the city of Macapá. Samples were also collected in the Lagoa Grande de Curuai (high water only, inaccessible at low water), the Tapajós River, and the Xingu River. Adapted from Ward et al. (2015).

(Sioli, 1985; Molleri et al., 2010). The lower Amazon River is characterized by a mixture of large channels, clear water tributaries, floodplain lakes and flooded forests, representing ∼13% of the total Amazon River drainage basin (Ward et al., 2015). River discharge throughout the study period was reported by Ward et al. (2016) and is also shown in **Table 1**.

Sample Collection

Water was collected at three equidistant cross-channel sites at each of the five stations on the mainstem (**Figure 1**) using a Shurflo submersible pump with a 297 μm mesh screen at 50% river depth and from the surface (Ward et al., 2016). Sampling was only performed at one central station in the Tapajós and Xingu rivers at surface and 50% depth. Only one cross channel station was sampled in these tributaries due to their large channel width and relatively low depth, which results in little variability in chemical parameters across the channel. A graduated cylinder was continuously overflowed without bubbles using the submersible pump. Dissolved O_2 concentrations were measured using a YSI ProOdo optical probe submerged in the overflowing cylinder and temperature was similarly measured using a Thermo Orion 4-star meter. Continuous measurements of dissolved O_2 concentrations and temperature were also made while the ship was underway using a YSI Exo 2 sonde placed in an overflowing bucket with water pumped from the ship's intake.

Samples were collected for analysis of the stable isotopic composition of water ($\delta^{18}O$-H_2O) in 15–50 mL centrifuge tubes and do not require preservation before analysis. Samples were collected for analysis of the stable isotopic composition of dissolved O_2 in 12 mL exetainers (Barth et al., 2004). Four replicate samples were collected at 50% depth and the surface at all cross channel sites. To assess diel variability in O_2 saturation and $\delta^{18}O$-O_2, surface water samples were collected on a 3 hr interval for 15 h (evening to morning) at the center of the channel near Óbidos during late high water/early falling water (July, 2015).

Prior to sample collection, exetainers were rinsed with MilliQ water and combusted at 500°C. Fifty microliters of saturated mercuric chloride was added to each exetainer as a preservative. The exetainers were then dried and flushed with helium gas and capped in a pure helium glove box to remove any trace of atmospheric O_2. Samples were collected by immersing the exetainers in the overflowing graduated cylinder. The vials were opened, filled completely, and then capped without removing them from the cylinder to prevent bubbles. To ensure the halt of all biological activity, an additional 50 μL of saturated mercuric

TABLE 1 | River discharge, O_2 saturation, the stable isotopic composition of dissolved O_2, and the stable isotopic composition of H_2O in the lower Amazon River.

Station/Date	Depth (m)	Discharge (m^3 s^{-1})	[Dissolved O^2] (% saturation)	δ^{18} O-O_2 (‰ VSMOW)	δ^{18} O-H_2O (‰ VSMOW)
ÓBIDOS					
1-May-14	55	253,879	46.4 ± 4.8	24.4 ± 0.6	−5.7 ± 0.1
6-Nov-14	51	122,274	79.2 ± 1.9	24.0 ± 0.4	−3.8 ± 0.2
Average	53	167,241	62.8 ± 23.2	24.2 ± 0.3	−4.7 ± 1.3
ALMEIRIM					
4-May-14	29	298,913	53.0 ± 1.2	25.0 ± 0.3	−5.4 ± 0.4
10-Nov-14	26	124,831	88.9 ± 1.8	24.8 ± 1.5	−3.9 ± 0.3
Average	28	207,004	71.0 ± 25.4	24.9 ± 0.2	−4.7 ± 1.1
NORTH MACAPÁ					
6-May-14	19	140,624	58.1 ± 1.0	26.5 ± 1.0	−5.3 ± 0.4
15-Nov-14	19	61,539	93.2 ± 1.7	23.1 ± 0.7	−3.0 ± 0.9
Average	19	92,200	75.6 ± 24.8	24.8 ± 2.4	−4.1 ± 1.6
SOUTH MACAPÁ					
9-May-14	24	204,056	59.9 ± 3.1	24.0 ± 0.8	−5.2 ± 0.3
14-Nov-14	24	132,998	92.8 ± 3.5	23.6 ± 1.0	−3.5 ± 0.3
Average	24	146,780	76.3 ± 23.3	23.8 ± 0.3	−4.4 ± 1.2
CURUAI					
2-May-14	N.D.	N.D.	94 ± 2	23.3 ± 0.14	−5.3 ± 0.3
7-Nov-16	N.D.	N.D.	N.D.	N.D.	N.D.
TAPAJÓS RIVER					
2-May-14	N.D.	3,658	87.4 ± 7.8	23.9 ± 0.9	−5.0 ± 0.1
7-Nov-16	24	10,018	94.8 ± 6.4	23.4 ± 0.3	−3.8 ± 0.4
Average	24	8,052	91.1 ± 5.2	23.7 ± 0.4	−4.4 ± 0.8
XINGU RIVER					
5-May-14	15	17,583	86.0 ± 0.6	21.9 ± 0.5	−3.6 ± 0.1
12-Nov-16	15	1,650	97.3 ± 0.6	21.0 ± 0.9	−2.1 ± 0.3
Average	15	9,180	91.6 ± 8.0	21.5 ± 0.6	−2.8 ± 1.0

chloride solution was injected through the septa. Septa were then coated with a thin layer of vacuum grease. Samples were analyzed within 2 months at the University of Washington Oceanography Stable Isotope Lab.

Analysis of $\delta^{18}O$-O_2 and $\delta^{18}O$-H_2O

For $\delta^{18}O$-O_2 samples pure helium was pumped into the exetainer until half of the water was displaced 1 day prior to analysis. The vials were injected with 50 μL of 50% H_3PO_4 to convert all carbonate species to CO_2. Isotopic ratios of headspace gases were determined by simultaneously measuring masses 32, 34, and 40 (i.e., ^{16}O-^{16}O, ^{18}O-^{16}O, and ^{40}Ar) on a Finnegan Delta XL mass spectrometer (Thermo Electron). Dissolved oxygen concentrations were calculated based on the O_2:Ar ratio (masses 32 and 40) and the estimated dissolved Ar concentration as a function of water temperature (Weiss, 1970). These values were compared to measurements taken with the YSI ProOdo and YSI Exo 2 sonde described above and were roughly equivalent (i.e., within ~5%). The stable isotopic composition of water (^{18}O-H_2O) was measured on 15 mL whole water samples using a Picarro L2130-I Analyzer.

Mass Balance Calculations

A dissolved oxygen mass balance was calculated for the Amazon River mainstem reach between Óbidos and midway to the mouth near the city of Almeirim (**Figure 2**). Two mass balance models were developed with the same set of inputs/outputs—one model uses only bulk parameters and the other includes the stable isotopic composition of O_2 and associated fractionation factors.

Inputs of O_2 included the measured/calculated flux of O_2 through Óbidos, measured/calculated O_2 fluxes from the Tapajós River (**Figure 1**), calculated O_2 gas exchange with the atmosphere (concentrations in the river were consistently below atmospheric saturation), estimated floodplain inputs, and primary production, which was the unknown parameter that was solved for. O_2 outputs included microbial respiration rates measured by Ward et al. (unpublished) and the measured/calculated flux of O_2 through Almeirim. In brief, respiration rates were measured in the dark in rotating incubation chambers interfaced to an YSI Exo 2 sonde equipped with an optical dissolved O_2 probe. Respiration rates were calculated based on the linear drawdown of O_2 during a roughly 24 hr period in duplicate 2.85 L chambers. Respiration rates include uncertainty associated with differences between replicates and averaged sites (±1 SD) and an additional 3% uncertainty due to the lack of inclusion of benthic respiration rates (more details on this in both the results and discussion sections).

This particular section of the river was chosen because the river maintains one well-constrained channel, for the most part, and river flow is not reversed by tides in this reach (although discharge is dampened semi-diurnally at Almeirim). This mass balance was not performed from Almeirim to Macapá because the river becomes extensively channelized and semi-diurnal tidal variation greatly complicates estimations of floodplain connectivity. The uncertainty associated with each mass balance parameter was propagated to our final calculation of primary production.

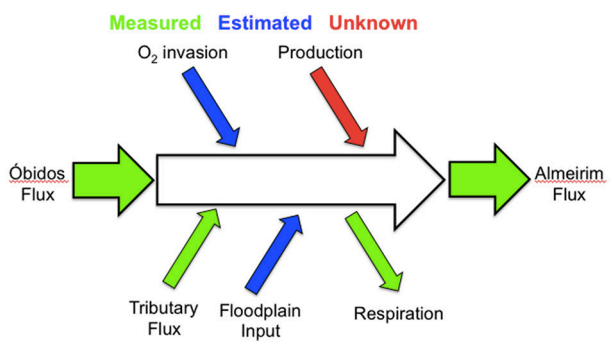

FIGURE 2 | Schematic for the mass balance of O_2 and ^{18}O-O_2 between Óbidos and Almeirim based on measured parameters (green), estimated parameters (blue), and unknown parameters (red).

Calculation of O_2 Gas Exchange

The molecular diffusivity of O_2 across the air-water interface is described by the gas transfer velocity parameter (k). Gas transfer velocities can be calculated for other gases (and temperatures) based on the ratio of Schmidt numbers (Sc) (Jähne et al., 1987):

$$k_{Sc1} / k_{Sc2} = \sqrt{(Sc_1 / Sc_2)}$$

where k_{Sc1} and k_{Sc2} are the gas transfer velocities of a reference gas with a unknown and known value, respectively, and Sc_1 and Sc_2 are the respective Schmidt numbers for each gas. To determine the gas transfer velocity of O_2, we converted calculated k_{CH4} values that were determined simultaneously (Sawakuchi, unpublished). We calculated Sc for O_2 and CH_4 at 28°C (measured mean temperature of the water) following Wanninkhof (1992) and used these values and the calculated k_{CH4} to determine k_{O2}.

The flux of a gas across the air-water interface was calculated as follows:

$$F = k(C_w - C_{eq})$$

where F is flux (mol m^{-2} d^{-1}), k is the gas transfer velocity (m d^{-1}), C_w is the concentration of gas measured in the water (mol m^{-3}) and C_{eq} is the concentration of a water sample at equilibrium with the atmosphere at *in situ* temperature. Water temperatures ranged from 27.5 to 28.5°C over the course of our study. As such, we used a constant value of 28°C for all necessary equations. The equilibrium concentration of oxygen at 28°C was calculated using Henry's Law. Fluxes were calculated using varied k values calculated as described above, the calculated equilibration concentration and the average concentration of dissolved O_2 for this reach of the river during high and low water periods. Uncertainty the gas transfer was calculated as the combination of analytical error and the standard deviation between observations at Óbidos and Almeirim (± 1 SD).

River Discharge

The water mass balance for this reach can be described by the following equation:

$$Q_{OBD} + Q_{TAP} + Q_{flood} = Q_{ALM}$$

where Q_{OBD} is the discharge through Óbidos ($m^3\ s^{-1}$), Q_{TAP} is discharge from the Tapajós River tributary, Q_{flood} is discharge from floodplains, and Q_{ALM} is discharge through Almeirim. Discharge was measured across the Amazon River main channel at Óbidos and Almeirim and across the mouth of the Tapajós River using a Sontek River Surveyor M9 Portable nine-beam 3.0 MHz/1.0 MHz/0.5 MHz acoustic Doppler Current Profiler (Ward et al., 2015). Discharge from floodplains was estimated by subtracting the measured discharge at Óbidos and the Tapajós River from the measured discharge at Almeirim. It should be noted that this does not necessarily represent the total amount of water that passed through floodplain complexes, but, rather, additional discharge added along this reach of the river from water stored in floodplains.

O_2 Mass Balance

In order to calculate the non-measured/estimated oxygen inputs (i.e., primary production), two mass balance equations were used based on bulk O_2 measurements (Equation 4) and both bulk and stable isotopic O_2 measurements (Equation 5):

$$O_{2ALM} = \frac{\left[Q_{OBD}\ O_{2,OBD} + Q_{TAP}O_{2,TAP} + Q_{flood}O_{2,flood} + AF - VR + VP\right]}{Q_{ALM}}$$

where A is the area of the river, F is the flux of O_2 from the atmosphere to the river, V is the volume of the river, R is the average measured respiration rate, and P is the average rate of primary production, which was solved for. $O_{2,ALM}$, $O_{2,OBD}$, $O_{2,TAP}$, and, $O_{2,flood}$, are the measured concentrations of dissolved O_2 at Almeirim, Óbidos, the Tapajós River, and the Lagoa Grande de Curuai floodplain lake, respectively. Uncertainty for the flux terms to/from Óbidos, the Tapajós River, and Almeirim are based on the analytical error of the O_2 probe, variability in O_2 concentrations with depth and across the channel, and discharge measurements (±1 SD).

Using equation 4 alone can give an estimate of inputs of O_2 via primary production between Óbidos and Almeirim, but this can be improved by adding a mass balance for the stable isotopic composition of O_2 as follows:

$$\begin{aligned} {}^{18:16}O_{2,ALM} = [&Q_{OBD}O_{2,OBD}{}^{18:16}O_{2,OBD} \\ &+ Q_{TAP}O_{2,TAP}{}^{18:16}O_{2,TAP} \\ &+ Q_{flood}O_{2,flood}{}^{18:16}O_{2,flood} \\ &+ AF^{18:16}O_g\alpha_g - V \times R^{18:16}O_2 \times \alpha_R \\ &+ VP^{18:16}O_w\alpha_P] \ / \ [Q_{OBD}O_{2,OBD} \\ &+ Q_{TAP}O_{2,TAP} + Q_{flood}O_{2,flood} + AF - VR + VP] \end{aligned}$$

where $^{18:16}O_2$ is the ratio of ^{18}O to ^{16}O calculated from $\delta^{18}O$-O_2 values for each respective term relative to the Vienna Standard Mean Ocean Water (VSMOW) standard, $^{18:16}O_g$ and $^{18:16}O_w$ are the stable isotopic compositions of atmospheric oxygen and river water, respectively. α_R, α_P, and α_g are the fractionation factors of respiration, photosynthesis, and gas exchange respectively. A value of 0.982 was used for α_R, a value of 0.997 was used for α_g, and a value of 1.000 was used for α_P considering O_2 produced via primary production reflects the stable isotopic composition of the water (Quay et al., 1995). The above equations were solved for P, or the rate of primary production within this reach. Uncertainty from each model parameter (±1 SD) was propagated through to the final result. All calculations were performed based on the average temperature of 28°C.

RESULTS

Dissolved O_2 Saturation

Dissolved oxygen was under-saturated relative to the atmosphere at all sampling locations at both high and low water with an annual average value of 79.3 ± 18.1% across the study boundaries. The highest and least variable O_2 saturation levels were found in the Tapajós and Xingu clearwater rivers, with seasonal average values of 86.7 ± 1.0 and 96.0 ± 1.8% at high and low water, respectively (**Table 1**). The lowest O_2 saturation levels were observed during high water in the Amazon River mainstem, specifically at Óbidos. Across all mainstem sites including the mouth, average O_2 saturation was 54.3 ± 6.0% at high water compared to 88.5 ± 6.5% at low water (**Table 1**).

O_2 saturation in the mainstem exhibited a downstream increase from Óbidos to the river mouth with an annual average value of 62.8 ± 23.2% at Óbidos, 71.0 ± 25.4% at Almeirim, and 76.0 ± 19.6%. The downstream increase was most evident during low water, with values increasing from 79.2 ± 1.9% at Óbidos to 93.0 ± 0.3% across the mouth. During the high water period O_2 saturation increased from 46.4 ± 4.8% at Óbidos to 59.0 ± 1.3% across the mouth (**Table 1**).

The partial pressure of CO_2 was previously measured along the same study boundaries (Sawakuchi et al., under review; Ward et al., 2016). There was a negative correlation between the molar concentration of dissolved O_2 and CO_2 across the study boundaries (**Figure 3**). Spatial variability of O_2 and CO_2 in the entire study region, including both the Amazon River mainstem and tributary sites, was higher during the high water period. For example, CO_2 concentrations ranged from 86.9 to 200.7 μmol L^{-1} and 36.7 to 61.5 μmol L^{-1} during high and low water, respectively (**Figure 3**). O_2 concentrations varied from 90.0 to 150.8 μmol L^{-1} and 160.3 to 197.2 μmol L^{-1} at high and low water, respectively, across our study boundaries. The slope of the relationship between O_2 and CO_2 concentrations was 2.2 times higher during low water.

Dissolved O_2 Stable Isotopic Composition

The oxygen stable isotopic composition of water (i.e., $\delta^{18}O$-H_2O) is influenced by isotopic fractionation during each phase of the hydrologic cycle. Annually-averaged $\delta^{18}O$-H_2O was −4.3 ± 1.1‰ across the entire study boundary. $\delta^{18}O$-H_2O was the most negative in the Amazon River mainstem at high water

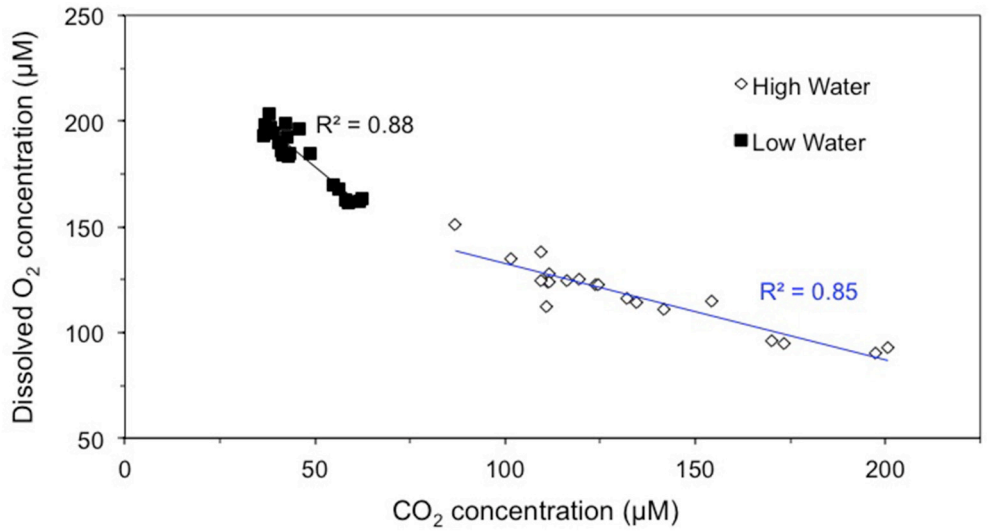

FIGURE 3 | The molar concentration of CO_2 vs. O_2 at high and low water.

with an average value of −5.4 ± 2.1‰ compared to −3.6 ± 0.4‰ at low water (**Table 1**). $\delta^{18}O$-H_2O was more positive in the clearwater tributaries (average = −3.6 ± 1.2‰) compared to the Amazon River mainstem (average = −4.5 ± 1.0‰). There was also a downstream increase in $\delta^{18}O$-H_2O from Óbidos to the river mouth. For example, at high water an average $\delta^{18}O$-H_2O value of −5.7 ± 0.1‰ was observed at Óbidos compared to −5.2 ± 0.1‰ across the river mouth. The difference between the mainstem and tributaries is likely due to differences in the isotopic composition of rainfall, since much of the water flowing through the mainstem is derived from far upstream.

The annual average stable isotopic composition of dissolved oxygen (i.e., $\delta^{18}O$-O_2) was 23.8 ± 1.4‰ across the entire study boundary. The highest $\delta^{18}O$-O_2 values were observed in the Amazon River mainstem at high water with an average value of 25.0 ± 1.1‰ compared to 23.9 ± 0.7‰ at low water. The clearwater tributaries had consistently lower and less seasonally variable $\delta^{18}O$-O_2 values, varying from 22.9 ± 1.5‰ at high water to 22.2 ± 1.7‰ at low water (**Table 1**). The Xingu River had the lowest $\delta^{18}O$-O_2 values across all sites (annual average = 21.5 ± 0.6‰). $\delta^{18}O$-O_2 and oxygen saturation levels were negatively correlated during both sampling seasons (**Figure 4**). Higher $\delta^{18}O$-O_2 values were found at sites with lower oxygen saturation levels and vice versa. The regression slope between $\delta^{18}O$-O_2 values and oxygen saturation, while following the same trend, was steeper for samples collected at low water compared to water.

It is typically assumed that $d^{18}O$-O_2 should remain at steady state in the Amazon River mainstem considering the low levels of light penetration and limited primary production (Quay et al., 1995; Ellis et al., 2012). To test this assumption we measured O_2 saturation and $d^{18}O$-O_2 throughout a day/night cycle in the center of the channel at Óbidos. While the overall

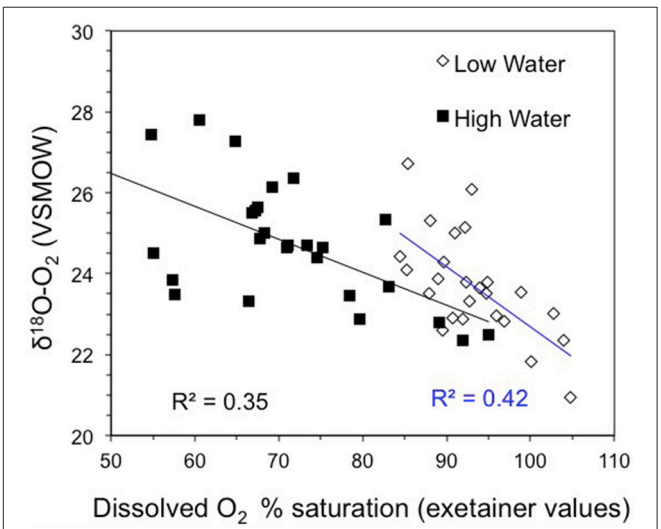

FIGURE 4 | $\delta^{18}O$-O_2 vs O_2 saturation from exetainer measurements at high and low water.

oxygen saturation levels did not vary significantly relative to the signal noise over a 15 hr period, our results indicate that $d^{18}O$-O_2 does follow a diel cycle even in the Amazon River mainstem (**Figure 5**). The minimum $d^{18}O$-O_2 was observed at 19:00, roughly 1 h after sunset (24.7 ± 0.6‰) and the maximum value was observed at 06:00 just prior to sunset (26.4 ± 0.3‰), followed by a decrease to 25.3 ± 0.7‰ at 08:00 (**Figure 5**). The difference in $d^{18}O$-O_2 values observed between midnight and 06:00 and the rest of the diel cycle were statistically significant based on an unpaired *t*-test within a 95% confidence interval ($p = 0.02$). It should be noted that a complete 24 h cycle was not able to be captured due to logistical constraints of the field campaign.

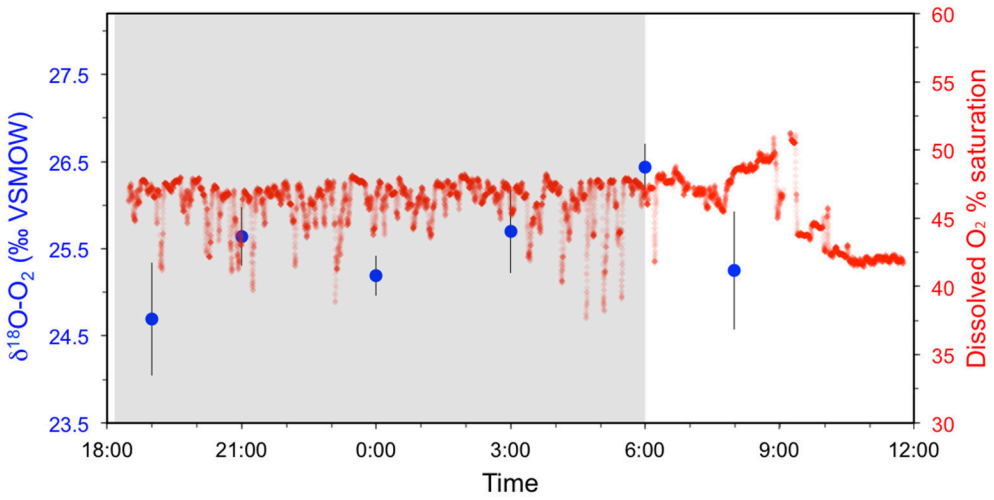

FIGURE 5 | Diel O_2 saturation (red) and $\delta^{18}O$-O_2 (blue) measurements made in the center of the channel at Obidos. The shaded portion of the chart represents hours between sunset and sunrise.

Oxygen Mass Balance Model

In the past, $\delta^{18}O$-O_2 values have been used to calculate the ratio of photosynthesis to respiration (P:R) under a steady state assumption for the Amazon River (Quay et al., 1995; Ellis et al., 2012). However, considering diel variability of $d^{18}O$-O_2 was observed, a steady state assumption is not accurate. Thus, in order to determine the rates of photosynthetic oxygen input into the mainstem of the lower Amazon River, we used a mass balance model that takes into account the various sources and sinks of O_2 within the system (**Figure 2**). Because the stable isotopic composition of dissolved O_2 is also known, we were able to calculate two separate O_2 budgets to model the system based on the following: (1) bulk O_2 concentrations only (i.e., Equation 4) and (2) the concentration and stable isotopic composition of O_2 (i.e., Equation 5). Including $d^{18}O$-O_2 observations and literature-derived fractionation factors for each process expressed in Equation 5 resulted in a slight increase in each model parameter compared to the bulk O_2 mass balance, however, the resulting calculated P:R ratios were essentially equivalent (**Table 2**). For this reason, we report the average value for each parameter from these two different models below.

Although O_2 concentrations were considerably lower in the Amazon River mainstem during high water (**Table 1**), the flux of O_2 through Óbidos and Almeirim were greater due to higher river discharge rates. The average flux of O_2 through Óbidos at high water, determined using both models, was 901 ± 87 kg O s^{-1} compared to 739 ± 80 kg O s^{-1} at low water (**Table 2**). The flux of O_2 through Almeirim was consistently greater than at Óbidos, with values of 1228 ± 112 kg O s^{-1} at high water and 853 ± 83 kg O s^{-1}. This difference was greatest during high water with a 36% increase in O_2 flux from Óbidos to Almeirim compared to a 15% increase during the low water period.

Aside from primary production, gas exchange was the dominant source of O_2 to this reach of the river, resulting in an inward flux of 722 ± 169 kg O s^{-1} at high water and 565 ± 130 kg O s^{-1} at low water. The Tapajós River provided an additional 81 ± 10 kg O s^{-1} to the Amazon River mainstem during high water and 25 ± 3 kg O s^{-1} during low water, which represents about 20–25% of the difference in fluxes between Óbidos and Almeirim during both seasons. We estimate that the flux of O_2 from adjacent floodplains to the mainstem was roughly 247 ± 75 kg O s^{-1} during high water (**Table 2**). At low water, we considered floodplain discharge to be zero considering that river discharge at Almeirim was lower than the sum discharge from Óbidos and the Tapajós River, indicative of water entering and being stored in the floodplains. Further, the Lagoa Grande de Curuai was inaccessible during this sampling period, illustrating the limited floodplain connectivity to the mainstem during this time.

TABLE 2 | Dissolved O_2 fluxes through Óbidos, Almeirim, floodplains, and the Tapajós River and from respiration, gas exchange, and primary production using mass balance models derived from (1) bulk O_2 concentrations and (2) O_2 stable isotopic compositions.

Staion/Process	High Water O_2 fluxes (kg O s^{-1})		Low Water O_2 fluxes (Nov. 2014)	
	Bulk O_2 Model	^{18}O–O_2 Model	Bulk O_2 Model	^{18}O-O_2 Model
Óbidos (In)	890 ± 85	911 ± 87	731 ± 82	748 ± 80
Tapajós River (In)	80 ± 8	81 ± 10	24 ± 3	25 ± 3
Floodplains (In)	244 ± 73	250 ± 75	0	0
Almeirim (Out)	1,213 ± 112	1,244 ± 112	842 ± 81	863 ± 83
Gas Exchange (In)	714 ± 166	729 ± 169	558 ± 127	571 ± 130
Respiration (Out)	1,210 ± 173	1,217 ± 174	1,438 ± 364	1,455 ± 368
Production (In)	496 ± 287	489 ± 291	968 ± 403	974 ± 407
P:R ratio	0.41 ± 0.24	0.40 ± 0.25	0.67 ± 0.33	0.67 ± 0.33

Positive values indicate inputs and negative values indicate outputs.

Aside from the flux through Almeirim, respiration was the primary O_2 output. The average water column respiration rate measured across the Amazon River mainstem sampling sites was 0.95 ± 0.10 g O m^3 d^{-1} at high water and 1.52 ± 0.35 g O m^3 d^{-1} at low water (Ward et al., unpublished). Benthic respiration rates were not measured, however, literature data is available from sites further upstream. Average benthic respiration rates of 1.46 g O m^2 d^{-1} have been reported for the central Amazon River (Devol et al., 1987). Considering that the average river depth is ∼40 m between Óbidos and Almeirim (**Table 1**), benthic respiration rates represent only 3% of depth-integrated water column respiration rates. Since benthic respiration was not measured in our study region, we have included this 3% error to the uncertainty in our total respiration estimate rather than adding a separate model parameter similar to calculations made by Devol et al. (1987). Water column respiration rates were multiplied by the volume of water between Óbidos and Almeirim (1.09×10^{11} m^3 at high water and 8.17×10^{10} m^3 at low water), resulting in a consumption of 1228 ± 112 kg O s^{-1} at high water and 1447 ± 368 kg O s^{-1} at low water (**Table 2**).

With all O_2 inputs and outputs other than primary production either measured or estimated we then solved for primary production as the difference between the mass balance outputs and inputs. Primary production was estimated to add 492 ± 291 kg O s^{-1} to the Amazon River mainstem between Óbidos and Almeirim at high water and 971 ± 407 kg O s^{-1}. This corresponds to a P:R ratio of 0.41 ± 0.24 at high water, 0.67 ± 0.33 at low water, and 0.54 ± 0.41 annually-averaged. When multiplied by the measured respiration rates, this corresponds to a primary production rate of 0.39 ± 0.24 g O m^3 d^{-1} at high water, 1.02 ± 0.55 g O m^3 d^{-1} at low water, and 0.70 ± 0.58 g O m^3 d^{-1} annually-averaged.

DISCUSSION

Dissolved Oxygen Balance

The stable isotopic composition of dissolved O_2 (i.e., $\delta^{18}O$-O_2) is primarily regulated by three processes: air-water gas exchange, respiration, and photosynthesis. In a system purely affected by gas-exchange, the $\delta^{18}O$-O_2 would be 24.2‰ (relative to VSMOW) due to the dissolution of atmospheric O_2 (23.5‰) and the equilibrium fractionation of 0.7‰ that occurs during gas dissolution (Kroopnick, 1975; Benson and Krause, 1984). Photosynthesis produces O_2 with a $\delta^{18}O$ of the surrounding water because there is little fractionation observed during photosynthesis (Guy et al., 1993). Respiration selectively fractionates oxygen by consuming O_2 that is more depleted than the average, which enriches the remaining pool of O_2. Thus, photosynthesis is expected to deplete the $\delta^{18}O$-O_2 of a system while respiration will enrich the $\delta^{18}O$-O_2.

Bulk O_2 levels were consistently undersaturated relative to the atmosphere across the entire study boundary. Likewise, $\delta^{18}O$-O_2 values were consistently more enriched in the Amazon River mainstem relative to values expected due to gas transfer with the atmosphere alone (i.e., 24.2‰; **Table 1**), indicating a predominance of respiration relative to photosynthesis. These factors both reflect the net heterotrophic state previously observed in both the Amazon River (Mayorga et al., 2005) and river systems worldwide (Cole et al., 2007), which results in a net flux of CO_2 to the atmosphere (Richey et al., 2002; Alin et al., 2011; Raymond et al., 2013).

However, these bulk and stable isotopic O_2 observations do not preclude the input of photosynthetically-produced oxygen into the mainstem. In fact, our observations of diel variability in $\delta^{18}O$-O_2 values at Óbidos clearly indicate a shift in the balance between primary production and respiration in the mainstem throughout a day/night cycle. Our observations were consistent with daytime production depleting $\delta^{18}O$-O_2 and nighttime respiration enriching the signal, implying that O_2 does not remain at a steady-state as previously assumed (Quay et al., 1995; Wassenaar, 2012).

The more depleted $\delta^{18}O$-O_2 values observed in the Amazon River mainstem during low water indicate a relatively higher amount of primary production relative to respiration during low water. This makes sense considering that suspended sediment concentrations are generally higher during high water in the Amazon River mainstem, limiting primary production (Hedges and Clark, 1986; Moreira-Turcq et al., 2003, 2013).

Respiration rates also vary seasonally, influencing the ratio of production to respiration. The highest respiration rates observed here and in the literature occur during the low water period (Benner et al., 1995; Ellis et al., 2012; Ward et al., 2013), which implies that photosynthesis rates would need to be proportionally higher to achieve a shift in P:R ratios during the low water period. In fact, our mass balance model predicted this difference. We estimate that primary production was 2.0 times higher in the Óbidos to Almeirim reach during low water based on our mass balance models (**Table 2**). Average measured respiration rates were 1.6 times greater in the mainstem during low water, but when integrated across the entire volume of water in the Óbidos to Almeirim reach, the total respiration flux was only 1.2 times greater at low water compared to high water. These differences result in the observed shift in the ratio of P:R from 0.41 ± 0.24 at high water to 0.67 ± 0.33 at low water.

O_2 levels were closer to atmospheric saturation in the Tapajós and Xingu rivers (**Table 1**), and $\delta^{18}O$-O_2 values were below 24.2‰ (**Table 2**), indicating a predominance of primary production relative to respiration in the less turbid clearwater tributaries. Sediment levels are significantly lower in these tributaries compared to the Amazon River mainstem, and high rates of primary production are reflected in elevated chlorophyll *a* concentrations relative to the Amazon River (Moreira-Turcq et al., 2013; Ward et al., 2015, 2016). Interestingly, respiration rates have been observed to be higher in clearwater tributaries than in the Amazon River mainstem throughout the Amazon basin (Benner et al., 1995; Ellis et al., 2012), yet these tributaries are overall less net heterotrophic. The elevated respiration rates observed in clearwater tributaries have been attributed to both the breakdown of algal organic matter (Benner et al., 1995; Ellis et al., 2012) and the enhanced breakdown of terrestrially-derived organic matter due to priming effects, i.e., the enhanced breakdown of a recalcitrant substrate due to the

presence of a labile substrate (Bianchi et al., 2015; Ward et al., 2016).

Previous studies have used $\delta^{18}O\text{-}O_2$ values to estimate gas exchange(Jamieson et al., 2012) and estimate net metabolism (e.g., the P:R ratio) in steady-state systems(Quay et al., 1995; Bocaniov et al., 2012) as well as non-steady-state systems (Tobias et al., 2007; Holtgrieve et al., 2010; Hotchkiss and Hall, 2014). For the Amazon River mainstem it has been estimated that the ratio of P:R is roughly 0.25 based on $\delta^{18}O\text{-}O_2$ values and a steady state assumption (Quay et al., 1995), which is 2.2 times lower than our annual average P:R estimate. Primary production rates have also been estimated based on $^{14}C\text{-}NaHCO_3$ uptake experiments; the average rate of primary production was estimated to be 0.10 ± 0.06 g O m^3 d^{-1} in the Amazon River mainstem and 1.45 ± 0.75 g O m^3 d^{-1} in the Tapajós and Xingu rivers (Wissmar et al., 1981). This is roughly 6.7 times lower than our mass balance estimates and 2.9 lower than estimates based on multiplying our measured rates of respiration by P:R ratios determined by Quay et al. (1995). We argue that this difference is due to the fact that bottle experiments cannot adequately capture the complex ecosystem dynamics occurring along the entire river reach, whereas a mass balance integrates these signals. Our mass balance results are in agreement with observations of a significant abundance of phytoplankton biomarkers in the mainstem of the Amazon (Mortillaro et al., 2011). Likewise, primary production has recently been found to be important in the main channel of the Congo River (Descy et al., 2017).

Limitations and Future Considerations

One factor that remains difficult to constrain is whether this input of isotopically depleted O_2 is conclusively from *in situ* production in the mainstem itself or is the legacy of advection from lateral floodplain lakes. These floodplain lakes have high rates of productivity and there is evidence of their legacy biomass in the Amazon mainstem (de Moraes Novo et al., 2006; Abril et al., 2014). This input of floodplain-derived oxygen is reflected in the ratio of CO_2 to O_2 measured at high and low water (**Figure 3**). At high water, the ratio is higher, likely due to the input of root respiration-derived CO_2 from the floodplains. At high water, these flooded macrophytes draw down oxygen from the atmosphere to their roots, thereby producing CO_2 without the concomitant drawdown of O_2 from the water column. Thus, it is possible that the isotopically depleted O_2 signals observed at high water is actually the legacy of floodplain production and not mainstem production. However, at low water, there is little evidence of macrophyte root respiration as the river loses connectivity with the floodplains. Thus, it is likely the production signal observed at low water is primarily from *in situ* production within the mainstem rather than floodplains.

Another factor that we did not consider is the importance of benthic respiration from the riverbed. However, past estimates suggest that benthic respiration in the OM-poor sandy sediments only accounts for ∼3% of our measured water column respiration rates (Devol et al., 1987). Thus we did not include a benthic respiration term in our mass balance, but rather added 3% error to our total respiration term. In some estuarine settings benthic respiration has been shown to be the dominant factor controlling dissolved oxygen concentrations and stable isotopic compositions (Lehmann et al., 2009), however this does not appear to be the case in the fast-flowing, deep river setting where reactive organic matter is highly abundant in the water column but relatively depleted in sediments (Richey et al., 1990; Hedges et al., 2000; Moreira-Turcq et al., 2013).

We did not attempt this same mass balance calculation for the river reach between Almeirim and Macapá due to the complex nature of this region. The river evolves into a series of sub-channels in the lower reaches limiting the applicability of a simplistic model, whereas the reach between Óbidos and Almeirim represents a single, well-constrained channel for the most part. Further, semi-diurnal flow reversals due to tides make it even more difficult to quantify connectivity and import/export from floodplain networks near the river mouth. Future efforts will be applied to unraveling the complex tidally-influenced reach of the river. It should also be noted the floodplain discharge used in this mass balance does not represent the total amount of water that passed through floodplain systems, but, rather, excess water entering the river from floodplains between Óbidos and Almeirim. It is difficult to accurately constrain the amount of water that passes through the Lagoa Grande de Curuai, for example, but this will be the focus of future hydrodynamic modeling efforts to further constrain our mass balance estimates.

CONCLUSIONS

Early investigations of biogeochemical cycling in the Amazon River found minimal rates of primary production in the turbid mainstem relative to the productive clearwater tributaries (Fisher, 1979; Wissmar et al., 1981). Here, we have shown that there is evidence for primary production within the Amazon River mainstem based on an O_2 mass balance, which exceeds past estimates based on a steady-state stable isotopic model by 2.0 times (Quay et al., 1995) and is 6.7 times higher than estimates from radiocarbon uptake experiments (Wissmar et al., 1981). The Amazon River is a major source of CO_2 to the atmosphere, but understanding the interplay between photosynthesis and respiration is critical for understanding the fundamental mechanisms driving these fluxes and the overall productivity of the ecosystem. Likewise, *in situ* primary production has been shown to be an important factor in elevating both bulk respiration rates (Ellis et al., 2012) and the breakdown of terrestrially-derived organic matter (Ward et al., 2016). Although this result does not undermine the idea of the Amazon River as a net heterotrophic system, it does indicate that more work remains to understand the dynamic interplay between production and respiration in large turbid river systems.

AUTHOR CONTRIBUTIONS

WG performed the collection and analysis of δ18O-O_2 samples and developed the O_2 mass balance.

VN, NW, DD, and JD. performed measurements of dissolved O_2 concentrations. VN and HS. performed estimations of gas transfer velocities used in the mass balance. NW and WG. performed measurements of respiration used in the O_2 mass balance. JR, AD, and DB performed measurements of river discharge. The field sampling scheme was developed and led by JR, AK, RK, NW, and HS. Field and sampling logistics were undertaken by all authors. All authors contributed to the preparation of the manuscript and approved its final submission.

FUNDING

This study was supported by FAPESP Grant # 08/58089-9 and NSF DEB Grant # 1256724. WGM was funded by an NSF IGERT grant DGE-1258485.

ACKNOWLEDGMENTS

We thank the crew of the B/M Mirage for contributions made during the river cruises, Dr. Gordon Holtgrieve for his advice on oxygen isotopes and the Quay Lab at UW for assistance in isotopic analysis.

REFERENCES

Abril, G., Martinez, J. M., Artigas, L. F., Moreira-Turcq, P., Benedetti, M.F., Vidal, L., et al. (2014). Amazon River carbon dioxide outgassing fuelled by wetlands. *Nature* 505, 395–398. doi: 10.1038/nature12797

Alin, S. R., Rasera, M. D. F. F. L., Salimon, C. I., Richey, J. E., Holtgrieve, G. W., Krusche, A. V., et al. (2011). Physical controls on carbon dioxide transfer velocity and flux in low-gradient river systems and implications for regional carbon budgets. *J. Geophys. Res. Biogeosciences* 116:G01009. doi: 10.1029/2010jg001398

Barth, J. A. C., Tait, A., and Bolshaw, M. (2004). Automated analyses of $^{18}O/^{16}O$ ratios in dissolved oxygen from 12-mL water samples. *Limnol. Oceanogr. Methods* 2, 35–41. doi: 10.4319/lom.2004.2.35

Battin, T. J., Luyssaert, S., Kaplan, L. A., Aufdenkampe, A. K., Richter, A., and Tranvik, L. J. (2009). The boundless carbon cycle. *Nat. Geosci.* 2, 598–600. doi: 10.1038/ngeo618

Benner, R., Opsahl, S., Chin-Leo, G., Richey, J. E., and Forsberg, B. R. (1995). Bacterial carbon metabolism in the Amazon River system. *Limnol. Oceanogr.* 40, 1262–1270. doi: 10.4319/lo.1995.40.7.1262

Benson, B. B., and Krause, D. (1984). The concentration and isotopic fractionation of oxygen dissolved in freshwater and seawater in equilibrium with the atmosphere. *Limnol. Oceanogr.* 29, 620–632. doi: 10.4319/lo.1984.29.3.0620

Bianchi, T. S., Thornton, D. C. O., Yvon-lewis, S. A., King, G. M., Eglinton, T. I., Shields, M. R., et al. (2015). Positive priming of terrestrially derived dissolved organic matter in a freshwater microcosm system. *Geophys. Res. Lett.* 42, 5460–5467. doi: 10.1002/2015GL064765

Bocaniov, S. A., Schiff, S. L., and Smith, R. E. H. (2012). Plankton metabolism and physical forcing in a productive embayment of a large oligotrophic lake: insights from stable oxygen isotopes. *Freshw. Biol.* 57, 481–496. doi: 10.1111/j.1365-2427.2011.02715.x

Butman, D., and Raymond, P., A. (2011). Significant efflux of carbon dioxide from streams and rivers in the United States. *Nat. Geosci.* 4, 839–842. doi: 10.1038/ngeo1294

Cole, J. J., and Caraco, N. F. (2001). Carbon in catchments: connecting terrestrial carbon losses with aquatic metabolism. *Mar. Freshw. Res.* 52, 101–110. doi: 10.1071/MF00084

Cole, J. J., Prairie, Y. T., Caraco, N. F., McDowell, W. H., Tranvik, L. J., Striegl, R. G., et al. (2007). Plumbing the Global carbon cycle: integrating Inland waters into the terrestrial carbon budget. *Ecosystems* 10, 172–185. doi: 10.1007/s10021-006-9013-8

del Giorgio, P. A., and Pace, M. L. (2008). Relative independence of organic carbon transport and processing in a large temperate river: the Hudson River as both pipe and reactor. *Limnol. Oceanogr.* 53, 185–197. doi: 10.4319/lo.2008.53.1.0185

de Moraes Novo, E. M. L., de Farias Barbosa, C. C., de Freitas, R. M., Shimabukuro, Y. E., Melack, J. M., Filho, W. P., et al. (2006). Seasonal changes in chlorophyll distributions in Amazon floodplain lakes derived from MODIS images. *Limnol.* 7, 153–161. doi: 10.1007/s10201-006-0179-8

Descy, J. P., Darchambeau, F., Lambert, T., Stoyneva-Gaertner, M. P., Bouillon, S. and Borges, A. V. (2017). Phytoplankton dynamics in the Congo River. *Freshw. Biol.* 62, 87–101. doi: 10.1111/fwb.12851

Devol, A. H., Quay, P. D., and Richey, J. E. (1987). The role of gas exchange in the inorganic carbon, oxygen, and 222Rn budgets of the Amazon River. *Limnol. Oceanogr.* 32, 235–248. doi: 10.4319/lo.1987.32.1.0235

Ellis, E. E., Richey, J. E., Aufdenkampe, A. K., Krusche, A. V., Quay, P. D., Salimon, C., et al. (2012). Factors controlling water-column respiration in rivers of the central and southwestern Amazon Basin. *Limnol. Oceanogr.* 57, 527–540. doi: 10.4319/lo.2012.57.2.0527

Fisher, T. R. (1979). Plankton and primary production in aquatic systems of the Central Amazon basin. *Comp. Biochem. Physiol. Part A. Physiol.* 62, 31–38. doi: 10.1016/0300-9629(79)90739-4

Guenet, B., Danger, M., Harrault, L., Allard, B., Jauset-Alcala, M., Bardoux, G., et al. (2014). Fast mineralization of land-born C in inland waters: first experimental evidences of aquatic priming effect. *Hydrobiologia* 721, 35–44. doi: 10.1007/s10750-013-1635-1

Guy, R. D., Fogel, M. L., and Berry, J., A. (1993). Photosynthetic fractionation of the stable isotopes of oxygen and carbon. *Plant Physiol.* 101, 37–47. doi: 10.1104/pp.101.1.37

Hedges, J. I., and Clark, W. A. (1986). Compositions and fluxes of particlate organic material in the Amazon River. *Limnol. Oceanogr.* 31, 717–738. doi: 10.4319/lo.1986.31.4.0717

Hedges, J. I., Mayorga, E., Tsamakis, E., McClain, M. E., Aufdenkampe, A., Quay, P., et al. (2000). Organic matter in Bolivian tributaries of the Amazon River: a comparison to the lower mainstream. *Limnol. Oceanogr.* 45, 1449–1466. doi: 10.4319/lo.2000.45.7.1449

Hoffman, J. C., Bronk, D. A., and Olney, J. E. (2008). Organic matter sources supporting lower food web production in the tidal freshwater portion of the York River estuary, Virginia. *Estuar. Coast.* 31, 898–911. doi: 10.1007/s12237-008-9073-4

Holtgrieve, G. W., Schindler, D. E., Branch, T. A., and Teresa, Z. A. (2010). Simultaneous quantification of aquatic ecosystem metabolism and reaeration using a Bayesian statistical model of oxygen dynamics. *Limnol. Oceanogr.* 55, 1047–1063. doi: 10.4319/lo.2010.55.3.1047

Hotchkiss, E. R., and Hall R. O. Jr. (2014). High rates of daytime respiration in three streams: Use of $\delta^{18}O_{O2}$ and O_2 to model diel ecosystem metabolism. *Limnol. Oceanogr.* 59, 798–810. doi: 10.4319/lo.2014.59.3.0798

Jähne, B. J., Münnich, K. O. M., Bösinger, R., Dutzi, A., Huber, W., and Libner, P. (1987). On the parameters influencing air-water gas exchange. *J. Geophys. Res.* 92, 1937–1949. doi: 10.1029/JC092iC02p01937

Jamieson, T. S., Schiff, S. L., and Taylor, W. D. (2012). Using stable isotopes of dissolved oxygen for the determination of gas exchange in the Grand River, Ontario, Canada. *Water Res.* 47, 781–790. doi: 10.1016/j.watres.2012.11.001

Junk, W. J., Soares, M. G. M., and Bayley, P. B. (2007). Freshwater fishes of the Amazon River basin: their biodiversity, fisheries, and habitats. *Aquat. Ecosyst. Health Manag.* 10, 153–173. doi: 10.1080/14634980701351023

Kritzberg, E. S., Cole, J. J., Pace, M. L., Grane, W., and Bade, D. L. (2004). Autochthonous versus allochthonous carbon sources of bacteria: results from whole-lake ^{13}C addition experiments. *Limnol. Oceanogr.* 49, 588–596. doi: 10.4319/lo.2004.49.2.0588

Kroopnick, P. M. (1975). Respiration, photosynthesis, and oxygen isotope fractionation in oceanic surface water. *Limnol. Ocean.* 20, 981–988. doi: 10.4319/lo.1975.20.6.0988

Lehmann, M. F., Barnett, B., Gélinas, Y., Gilbert, D., Maranger, R. J., Mucci, A., et al. (2009). Aerobic respiration and hypoxia in the Lower St. Lawrence Estuary: stable isotope ratios of dissolved oxygen constrain oxygen sink partitioning. *Limnol. Oceanogr.* 54, 2157–2169. doi: 10.4319/lo.2009.54.6.2157

Mayorga, E., Aufdenkampe, A. K., Masiello, C., A., Krusche, A. V., Hedges, J. I., Quay, P. D., et al. (2005). Young organic matter as a source of carbon dioxide outgassing from Amazonian rivers. *Nature* 436, 538–541. doi: 10.1038/nature03880

Molleri, G. S., Novo, E. M. D. M., and Kampel, M. (2010). Space-time variability of the Amazon River plume based on satellite ocean color. *Cont. Shelf Res.* 30, 342–352. doi: 10.1016/j.csr.2009.11.015

Moreira-Turcq, P., Bonnet, M. P., Amorim, M., Bernardes, M., Lagane, C., Maurice, L., et al. (2013). Seasonal variability in concentration, composition, age, and fluxes of particulate organic carbon exchanged between the floodplain and Amazon River. *Glob. Biogeochem. Cycles* 27, 119–130. doi: 10.1002/gbc.20022

Moreira-Turcq, P., Seyler, P., Guyot, J. L., and Etcheber, H. (2003). Exportation of organic carbon from the Amazon River and its main tributaries. *Hydrol. Process.* 17, 1329–1344. doi: 10.1002/hyp.1287

Mortillaro, J. M., Abril, G., Moreira-Turcq, P., Sobrinho, R. L., Perez, M., and Meziane, T. (2011). Fatty acid and stable isotope (^{13}C, ^{15}N) signatures of particulate organic matter in the lower Amazon River: seasonal contrasts and connectivity between floodplain lakes and the mainstem. *Org. Geochem.* 42, 1159–1168. doi: 10.1016/j.orggeochem.2011.08.011

Odum, E. P. (1971). *Fundamentals of Ecology*. Philadelphia,PA: W.B. Saunders.

Quay, P. D., Wilbur, D., Richey, J. E., Devol, A. H., Benner, R. and Forsberg, B. R. (1995). The ^{18}O: ^{16}O of dissolved oxygen in rivers and lakes in the Amazon Basin: determining the ratio of respiration to photosynthesis rates in freshwaters. *Limnol. Oceanogr.* 40, 718–729.

Quay, P. D., Wilbur, D. O., Richey, J. E., Hedges, J. I., Devol, A. H., and Victoria, R. (1992). Carbon cycling in the Amazon River: implications from the 13C compositions of particles and solutes. *Limnol. Oceanogr.* 37, 857–871. doi: 10.4319/lo.1992.37.4.0857

Raymond, P. A., Hartmann, J., Lauerwald, R., Sobek, S., McDonald, C., Hoover, M., et al. (2013). Global carbon dioxide emissions from inland waters. *Nature* 503, 355–359. doi: 10.1038/nature12760

Richey, J. E., Hedges, J. I., Devol, A. H., Quay, P. D., Victoria, R., Martinelli, L., et al. (1990). Biogeochemistry of carbon in the Amazon River. *Limnol. Oceanogr.* 35, 352–371. doi: 10.4319/lo.1990.35.2.0352

Richey, J. E., Melack, J. M., Aufdenkampe, A. K., Ballester, V. M., and Hess, L. L. (2002). Outgassing from Amazonian rivers and wetlands as a large tropical source of atmospheric CO_2. 6416, 6413–6416. doi: 10.1038/416617a

Sioli, H. (1985). *Amazônia: Fundamentos de Ecologia da Maior Região de Florestas Tropicais*. Petrópolis: Editora Vozes.

Tobias, C. R., Böhlke, J. K., and Harvey, J. W. (2007). The oxygen-18 isotope approach for measuring aquatic metabolism in high productivity waters. *Limnol. Oceanogr.* 52, 1439–1453. doi: 10.4319/lo.2007.52.4.1439

Tranvik, L. J., Downing, J. A., Cotner, J. B., Loiselle, S. A., Striegl, R. G., Ballatore, T. J., et al. (2009). Lakes and reservoirs as regulators of carbon cycling and climate. *Limnol. Oceanogr.* 54, 2298–2314. doi: 10.4319/lo.2009.54.6_part_2.2298

Wanninkhof, R. (1992). Relationship Between Wind Speed and Gas Exchange. *J. Geophys. Res.* 97, 7373–7382. doi: 10.1029/92JC00188

Ward, N. D., Bianchi, T. S., Sawakuchi, H. O., Gagne-maynard, W., Cunha, A. C., Brito, D. C., et al. (2016). The reactivity of plant-derived organic matter and the potential importance of priming effects along the lower Amazon River. *J. Geophys. Res. Biogeosci.* 121, 1522–1539. doi: 10.1002/2016jg003342

Ward, N. D., Keil, R. G., Medeiros, P. M., Brito, D. C., Cunha, A. C., Dittmar, T., et al. (2013). Degradation of terrestrially derived macromolecules in the Amazon River. *Nat. Geosci.* 6, 530–533. doi: 10.1038/ngeo1817

Ward, N. D., Krusche, A. V., Sawakuchi, H. O., Brito, D. C., Cunha, A. C., Moura, J. M. S., et al. (2015). The compositional evolution of dissolved and particulate organic matter along the lower Amazon River-Óbidos to the ocean. *Mar. Chem.* 177, 244–256. doi: 10.1016/j.marchem.2015.06.013

Wassenaar, L. I. (2012). Dissolved oxygen status of Lake Winnipeg : spatio-temporal and isotopic ($\delta^{18}O - O_2$) patterns. *J. Great Lakes Res.* 38, 123–134. doi: 10.1016/j.jglr.2010.12.011

Weiss, R. F. (1970). The solubility of nitrogen, oxygen and argon in water and seawater. *Deep Sea Res. Oceanogr. Abstr.* 17, 721–735. doi: 10.1016/0011-7471(70)90037-9

Wissmar, R. C., Richey, J. E., Stallard, R. F., and Edmond, J. M. (1981). Plankton metabolism and carbon processes in the Amazon River, its tributaries, and flooplan waters, Peru-Brazil, May-June 1977. *Ecology* 62, 1622–1633. doi: 10.2307/1941517

Conflict of Interest Statement: The authors declare that the research was conducted in the absence of any commercial or financial relationships that could be construed as a potential conflict of interest.

frontiers in Marine Science

ORIGINAL RESEARCH
published: 22 February 2017
doi: 10.3389/fmars.2017.00044

The Fate of Carbon in Sediments of the Xingu and Tapajós Clearwater Rivers, Eastern Amazon

Dailson J. Bertassoli Jr.[1], André O. Sawakuchi[1], Henrique O. Sawakuchi[2], Fabiano N. Pupim[1], Gelvam A. Hartmann[3], Michael M. McGlue[4], Cristiano M. Chiessi[5], Matthias Zabel[6], Enno Schefuß[6], Tatiana S. Pereira[7], Rudney A. Santos[1], Samantha B. Faustino[8], Paulo E. Oliveira[1] and Denise C. Bicudo[8]*

[1] *Institute of Geosciences, University of São Paulo, São Paulo, Brazil,* [2] *Environmental Analysis and Geoprocessing Laboratory, Center for Nuclear Energy in Agriculture, University of São Paulo, Piracicaba, Brazil,* [3] *Instituto de Geociências, Universidade Estadual de Campinas, Campinas, Brazil,* [4] *Department of Earth and Environmental Sciences, University of Kentucky, Lexington, KY, USA,* [5] *School of Arts, Sciences and Humanities, University of São Paulo, São Paulo, Brazil,* [6] *MARUM-Center for Marine Environmental Sciences, University of Bremen, Bremen, Germany,* [7] *Federal University of Pará, Campus de Altamira, Altamira, Brazil,* [8] *Department of Ecology, Instituto de Botânica, São Paulo, Brazil*

OPEN ACCESS

Edited by:
Carol Robinson, University of East Anglia, UK

Reviewed by:
Michael Gonsior, University of Maryland Center For Environmental Sciences, USA
Armstrong-Altrin John S., National Autonomous University of Mexico, Mexico

****Correspondence:***
Dailson J. Bertassoli Jr.
dailson.bertassoli@gmail.com

Specialty section:
This article was submitted to Marine Biogeochemistry, a section of the journal Frontiers in Marine Science

Received: *07 November 2016*
Accepted: *07 February 2017*
Published: *22 February 2017*

Citation:
Bertassoli DJ Jr., Sawakuchi AO, Sawakuchi HO, Pupim FN, Hartmann GA, McGlue MM, Chiessi CM, Zabel M, Schefuß E, Pereira TS, Santos RA, Faustino SB and Oliveira PE and Bicudo DC (2017) The Fate of Carbon in Sediments of the Xingu and Tapajós Clearwater Rivers, Eastern Amazon. Front. Mar. Sci. 4:44. doi: 10.3389/fmars.2017.00044

The Xingu and Tapajós rivers in the eastern Amazon are the largest clearwater systems of the Amazon basin. Both rivers have "fluvial rias" (i.e., lake-like channels) in their downstream reaches as they are naturally impounded by the Amazon mainstem. Fluvial rias are widespread in the Amazon landscape and most of the sedimentary load from the major clearwater and blackwater rivers is deposited in these channels. So far, little is known about the role of Amazon rias as a trap and reactor for organic sediments. In this study, we used organic and inorganic geochemistry, magnetic susceptibility, diatom, and pollen analyses in sediments (suspended, riverbed, and downcore) of the Xingu and Tapajós rias to investigate the effects of hydrologic variations on the carbon budget in these clearwater rivers over the Holocene. Ages of sediment deposition (~100 to 5,500 years) were constrained by optically stimulated luminescence and radiocarbon. Major elements geochemistry and concentration of total organic carbon (TOC) indicate that seasonal hydrologic variations exert a strong influence on riverine productivity and on the input and preservation of organic matter in sediments. Stable carbon isotope data ($\delta^{13}C$ from −31.04 to −27.49‰) and pollen analysis indicate that most of the carbon buried in rias is derived from forests. In the Xingu River, diatom analysis in bottom sediments revealed 65 infrageneric taxa that are mostly well-adapted to slack oligotrophic and acidic waters. TOC values in sediment cores are similar to values measured in riverbed sediments and indicate suitable conditions for organic matter preservation in sediments of the Xingu and Tapajós rias at least since the mid-Holocene, with carbon burial rates varying from about 84 g m^{-2} yr^{-1} to 169 g m^{-2} yr^{-1}. However, redox-sensitive elements in sediment core indicate alternation between anoxic/dysoxic and oxic conditions in the water-sediment interface that may be linked to abrupt changes in precipitation. The variation between anoxic/dysoxic and oxic conditions in the water-sediment interface controls organic matter mineralization and methanogenesis. Thus, such changes promoted by hydrological variations significantly affect the capacity of Amazon rias to act either as sources or sinks of carbon.

Keywords: Amazon, Carbon Cycle, Xingu River, Tapajós River, greenhouse gases

INTRODUCTION

Recent research has undermined the view of rivers as passive conveyors of organic matter, and demonstrates their role in the transport, modulation, and deposition of carbon (Cole et al., 2007; Tranvik et al., 2009; Aufdenkampe et al., 2011; Ward et al., 2015). Inland waters emit at least 0.8 Pg of carbon per year (Cole et al., 2007; Tranvik et al., 2009). Approximately one fourth of it comes from rivers (Cole et al., 2007). The Amazonian rivers represent about 15% of the terrestrial gross primary production and 25% of the global rivers emissions of CO_2 (Field, 1998; Richey et al., 2002). Most studies that have considered organic matter remineralization and carbon storage in the region focused on the Amazon mainstem and its floodplains (Richey et al., 2002; Bouchez et al., 2010, 2012; Abril et al., 2014; Ward et al., 2015). However, the lack of geochemical data to constrain the role of major clearwater tributaries of the Amazon River as a source or sink of organic sediments limited the understanding of the carbon cycling dynamics across the terrestrial and aquatic environments of the Amazon basin.

The Xingu and Tapajós rivers represent the largest Amazon clearwater rivers, with mean annual discharges of 9,700 and 13,500 m^3s^{-1} (Latrubesse et al., 2005), respectively. They drain crystalline and sedimentary rocks of the Central Brazil shield and are characterized by relatively low concentrations of suspended sediments, slightly alkaline waters (Sioli, 1984), and high fluxes of methane to the atmosphere (Sawakuchi et al., 2014). Both rivers are naturally impounded by the Amazon mainstem, which give rise to broad downstream lake-like channels known as "fluvial rias" (Gourou, 1949; Archer, 2005). The Xingu and Tapajós rivers have strong seasonal variations, with mean monthly water discharges varying from approximately 1,000 to 20,000 m^{-3} s^{-1} in the Xingu River and 4,000 to 30,000 $m^{-3}s^{-1}$ in the Tapajós River (ANA, 2016). The peak discharges of these clearwater rivers occurs from February to May. The Amazon River, however, has a mean monthly water discharge that varies from approximately 105,000 m^{-3} s^{-1} to 235,000 m^{-3} s^{-1}, with peak discharge from April to July (ANA, 2016). The lag between the peak discharge of the Amazon River and its clearwater tributaries is responsible for strong backwater effects in the Xingu and Tapajós rivers (Meade et al., 1991). The sudden drop in water flow velocity and channel widening related to the hydraulic blockage and backwater effect by the Amazon mainstem prevent most of the Xingu and Tapajós suspended and bedload sediments from entering the Amazon River. These conditions turn rias into massive sinks for organic and inorganic sediments and natural reactors for carbon derived from the headwaters. Fluvial rias in the downstream section of the Xingu and Tapajós rivers reach up to 15 km width and around 150 km length. Hundreds of rias and paleo-rias occupy the Amazonian landscape and connect all clearwater and blackwater tributaries to the Amazon River, playing an important role for the transport and deposition of fine-grained sediments in the Amazon fluvial system. Thus, the accumulation of fine-grained sediments in rias has a strong effect on carbon processing and transport to the Amazon River and the Atlantic Ocean. To date, studies addressing Amazonian fluvial rias focus mainly on climatic and sediment deposition changes, without consensus about their genesis (Sioli, 1984; Keim et al., 1999; Vital and Stattegger, 2000; Bertani et al., 2014). The extant Amazon rias appear to have been formed after the Last Glacial Maximum (LGM, 23–19 ka) (Archer, 2005; Irion et al., 2011). The prevailing hypothesis suggests that the incised valleys formed during the low sea level phase of the LGM were flooded and accumulated sediments during the Holocene transgression (Archer, 2005; Irion et al., 2006, 2011). Sediment cores retrieved from the Tapajós Ria contain fine-grained sediments with 2.2–3.5% of total organic carbon and sedimentation rates reaching up to 6.5 mm yr^{-1} (Irion et al., 2006). This reinforces the potential of rias as location of sediment deposition and carbon processing in the Amazon fluvial system.

Rias show sedimentary dynamics similar to that of lakes and reservoirs, which bury more than 200 Tg of organic carbon annually (Dean and Gorham, 1998). Despite the widespread distribution in the Amazon and dominance of organic-rich sediments (Irion et al., 2011), rias are poorly studied with respect to their role as sink or source of carbon in the Amazon basin. According to Sawakuchi et al. (2014), methane fluxes in Amazon rivers account for 22–28% of the global river emissions of methane and the Amazon rias are hotspots of methane production. Rias also serve as analogs for carbon processing in artificial reservoirs like the recently build reservoirs of the Belo Monte hydropower plant in the Xingu River and future reservoirs planned for the Tapajós River (Winemiller et al., 2016). Clearwater Amazon rivers are the main target in the energy expansion plans of the Brazilian government (EPE/MME, 2007), which regards hydropower as inexpensive and clean energy, however, without consideration of impacts of river impoundment on Amazon ecosystems (Fearnside, 2014; Winemiller et al., 2016) and emission of greenhouse gases (Barros et al., 2011; de Faria et al., 2015). To assess the combined effect of carbon fluxes in Amazon rivers, it is imperative to fully understand carbon burial and emission rates in all main Amazon sedimentary environments. In this paper, we focus on carbon dynamics in the rias of the Xingu and Tapajós rivers. Geochemical, magnetic susceptibility, pollen, and diatom analyses combined with luminescence and radiocarbon dating are used to constrain the sources and fate of carbon in sediments of the Xingu and Tapajós rivers on millennial timescales. We integrated our data and results from previous literature to evaluate the origin and content of organic matter and to understand major controls affecting carbon burial in the Xingu and Tapajós rias.

MATERIALS AND METHODS

Sediment Sampling

Sediment cores and samples of riverbed and suspended sediments collected from Xingu, Tapajós and Amazon rivers are presented in **Figure 1** and in Supplementary Material (Table S1). Suspended sediment samples were taken both during the dry and wet seasons from Xingu, Tapajós, and Amazon rivers in order to fully encompass variations in sediment composition related to hydrological changes. Suspended and riverbed sediment samples from the Amazon mainstem were

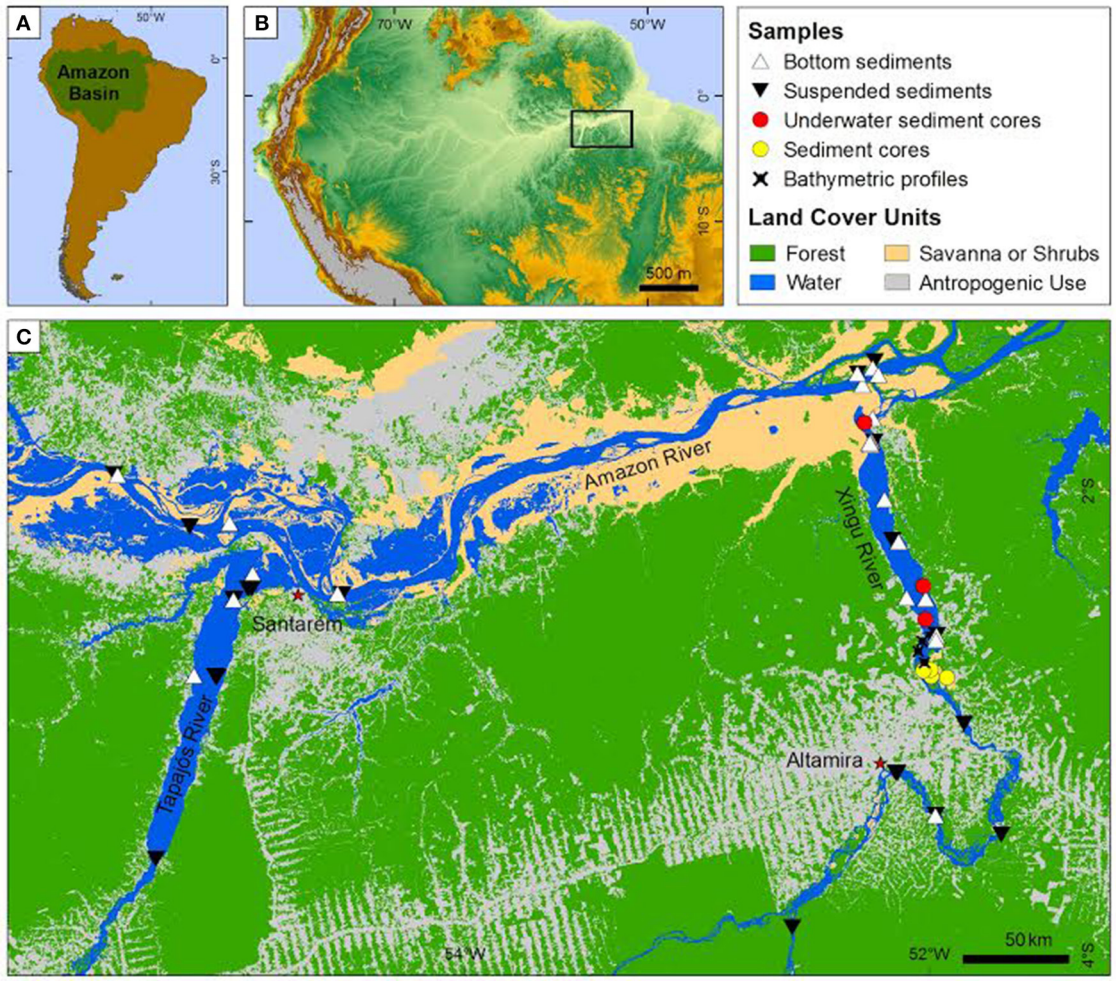

FIGURE 1 | Study area, location of sediment samples (suspended, riverbed and cores) and bathymetric profiles. In this work, underwater sediment cores were named "XC" and sediment cores from islands were named "EMB." Land-use map from Almeida et al. (2016).

collected upstream and downstream the Tapajós and Xingu rivers mouths (**Figure 1**) in order to evaluate the effect of input of sediments from the Xingu and Tapajós rivers on the Amazon River. Suspended sediment samples were collected through water pumped at approximately 60% of the water depth in the channel thalweg. For each sample, four liters of water were filtrated using cellulose acetate membranes (pore size of 0.45 μm). Riverbed sediments were collected using a Van Veen grab sampler. A total of 23 suspended sediment samples and 28 riverbed sediment samples were used in this study.

Sediment cores of the Xingu Ria were collected from deeper portions of the lake-like channel covered by muddy sediments (named "XC") and from islands in the upstream section of the Xingu Ria (named "EMB"). The locations were selected based on water depth profiles and riverbed sediment sampling (further details in Sawakuchi et al., 2015). Underwater sediment cores from the Xingu Ria channel were retrieved by divers using PVC tubes of up to 6 m in length and percussion method (Sawakuchi et al., 2015). Three underwater sediment cores, characterized by dark gray to brown muds with thicknesses of 300 cm (XC02), 370 cm (XC03), and 470 cm (XC05), respectively, were retrieved from the Xingu Ria. Unconsolidated sediments from islands of the Xingu Ria head were collected using a piston-corer attached to a manual auger. Four sediment cores composed of fine to medium sands and muddy organic sediments were obtained from the islands: EMB13-07 (555 cm), EMB13-13 (430 cm), EMB13-17 (250 cm), and EMB13-21 (345 cm). Samples for luminescence dating were collected using opaque plastic tubes.

Bathymetric profiles were recorded along the upstream part of the Xingu Ria using sonar and GPS equipment. Samples collected with the Van Veen grab sampler were used to characterize riverbed sediments along bathymetric profiles. Water depth profiles and texture of riverbed sediments of the Xingu Ria are shown in **Figure 2**.

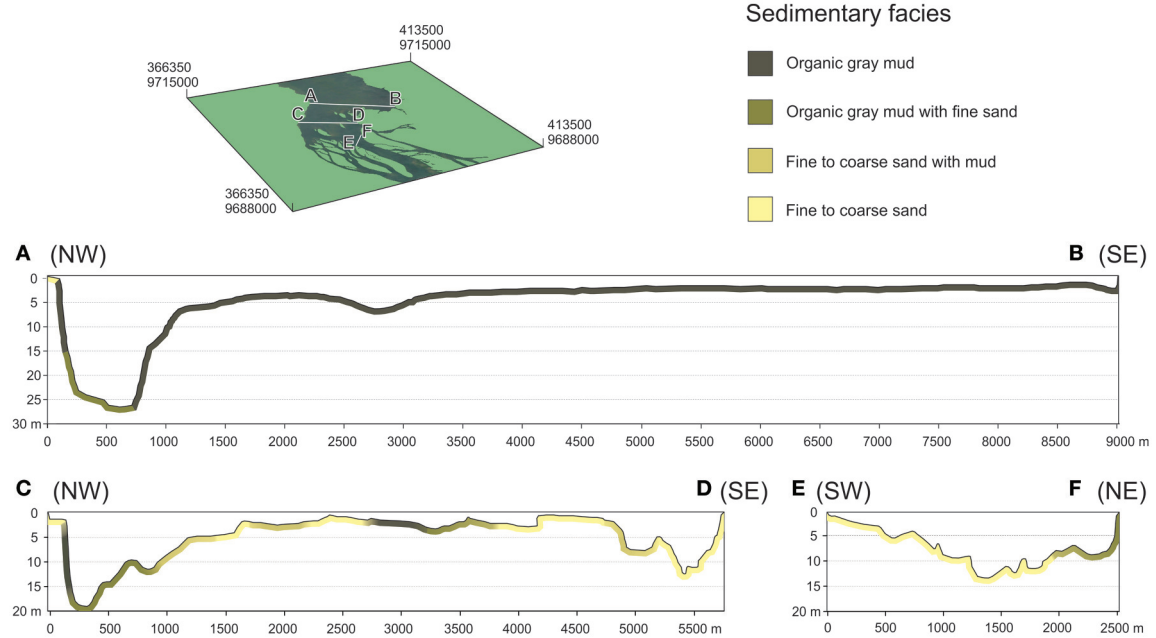

FIGURE 2 | Bathymetry and riverbed sediment texture in the upstream sector of the Xingu Ria.

Organic and Inorganic Geochemistry of Sediments

Total organic carbon (TOC) content and its stable carbon isotope ratios ($\delta^{13}C_{org}$) were measured in 28 riverbed sediments samples at MARUM, University of Bremen. Sediments from the core XC05 were sampled at 2 cm intervals for total carbon coulometric and x-ray fluorescence (XRF) analysis at the University of Kentucky.

Major elements (P, Ca, Fe, Mn, Al, Ti, K) concentrations were determined with an Agilent 720 inductively coupled plasma—optical emission spectrometer (ICP-OES) for 23 samples of suspended sediments and with a Bruker Tracer IV SD energy dispersive x-ray fluorescence (XRF) spectrometer for 13 riverbed sediments samples and 234 samples of the sediment core XC05. ICP-OES analysis of suspended sediments and XRF analysis of riverbed sediments were performed at MARUM, University of Bremen. For ICP-OES analysis, digestion of suspended material was performed with a MLS 1200 MEGA microwave system. For this purpose, 7 ml HNO_3 (65%), 0.5 ml HF (40%), 0.5 ml HCl (30%), and 0.5 ml MilliQ were added to about 50 mg sample material (filter plus suspended material) previously placed into Teflon liners. All acids were of supra-pure quality. For XRF analysis, sediments were prepared by freeze drying, grinding by hand with an agate mortar and pestle, and sieving to ∼125 μm prior to packing into inert sample boats sealed with an ultra-thin mylar window. Individual XRF scans for each sample were made through the mylar window over 90 s, in order to maximize signal-to-noise. Major elements (atomic numbers 11 through 30) were collected under a ∼9 torr vacuum, by setting the XRF filter to 15 keV and 35 μA. Trace elements (atomic numbers 20 through 51), were collected at 40 keV and 15 μA without a vacuum. Calibration of unknowns utilized Bruker proprietary software (S1CALPROCESS with TR2.cfz and MA1.cfz) and a reference catalog of mudrock chemistry described in Rowe et al. (2012). Internal consistency of the XRF was verified by routine scanning of the SARM41 shale standard (Ring, 1989). The chief focus of our analysis was the major rock-forming (Al, Ca, K, Ti, P) and redox-sensitive (Mn, Fe) elements. Inorganic chemistry data provide insights on mineralogy as well as depositional environments and hydrodynamic processes, especially when paired with organic carbon data (Sageman et al., 2003; Algeo and Rowe, 2012; Scott and Lyons, 2012).

Total organic carbon (TOC) was determined using a LECO CS 200 CS-Analyzing System and an UIC Coulometrics Inc. Carbonate Coulometer (Engleman et al., 1985). The LECO method determines total carbon content through combustion of a powdered sample (Jarvie, 1991). Values of TOC were obtained by subtracting total inorganic carbon determined by the coulometer from total carbon. This method is routinely employed in paleoenvironmental analysis due to its accuracy and small sample size requirements (Jackson and Roof, 1992; Schulte et al., 2000; e.g., Böning et al., 2005). The precision of the analysis, based on analysis of internal standards and replicates, was typically better than ± 0.15%. The $\delta^{13}C_{org}$ signature of decarbonated samples was analyzed on a Finnigan MAT Delta plus coupled to a CE elemental analyzer. $\delta^{13}C_{org}$ is reported using the delta notation relative to the Vienna Pee Dee Belemnite (VPDB). The uncertainty was less than ± 0.1‰.

Results were analyzed using R software (R Core Team, 2015). Major changes in hydrology and paleoenvironmental conditions were determined using constrained hierarchical cluster analysis

of geochemistry and magnetic susceptibility data by the method of incremental sum of squares (CONISS, Grimm, 1987).

Magnetic Susceptibility

Magnetic susceptibility measurements were performed at the Paleomagnetic Laboratory (USPMag) of the Institute of Astronomy, Geophysics and Atmospheric Sciences of the University of São Paulo (IAG/USP). Magnetic susceptibility is used here as a complimentary method to identify significant variations in paleoenvironmental conditions or sediment composition in core XC05. A total of 194 paleomagnetic specimens were collected from the sediment core using cubic plastic boxes (8 cm^3) placed side-by-side throughout the core. Low-field magnetic susceptibility of individual specimen was measured using a Kappabridge MFK1-FA system (AGICO Ltd). Two different frequencies (976 and 15616 Hz) were used in a 200 Am^{-1} field at room temperature (Dearing et al., 1996). All data were mass normalized due to the irregular sample mass inside cubic boxes.

Pollen and Diatom Analyses

Riverbed samples were subsampled for pollen analyses (Table S1). Samples were processed for extraction of pollen grains using the protocol established by Colinvaux et al. (1999). The analyses were performed in the Institute of Geosciences of the University of São Paulo (IGc/USP) under a microscope with magnification of 600x. A minimum of 300 terrestrial pollen grains were counted per sample. Aquatic taxa and spores are not included in the sum of pollen assemblage. The pollen grains and spores were identified using the pollen reference collection of the University of São Paulo and other published reference materials (Erdtman, 1952; Roubik and Moreno, 1991; Colinvaux et al., 1999). The raw pollen count data were entered into the Tilia software (Grimm, 2011), in order to calculate the taxa percentages and concentrations.

Riverbed and sediment core XC05 were subsampled for diatom analyses. Diatom analysis followed standard procedures discussed by Battarbee et al. (2001). Slides were mounted with Naphrax® as medium. Optical observations and counts were conducted at a magnification of 1000x with a Zeiss Axioskop 2 plus microscope. At least 400 valves were counted per slide. Taxonomy and nomenclature followed published literature sources (e.g., Round et al., 1990; Krammer, 2000; Rumrich et al., 2000; Metzeltin and Lange-Bertalot, 2007) and the on-line catalog of valid names (California Academy of Sciences, 2011).

CH_4 and CO_2 in Sediment Pore Waters

Sediment core XC05 was sub-sampled in field on the same day of collection for the assessment of dissolved methane and carbon dioxide concentrations in pore waters. Aliquots of 5 ml of wet sediment were collected with an open-ended 5 ml polypropylene syringe after carefully drilling holes at 10 cm intervals. Immediately after collection, the aliquots were injected into a 120 ml vial containing 10 ml of NaOH (5%), capped with butyl rubber stoppers and sealed with aluminum crimps. Control standards of ambient air were collected during sampling for corrections. In the Center for Nuclear Energy in Agriculture of the University of São Paulo (CENA/USP), samples were shaken for headspace equilibration and 60 ml of gas sample was retrieved from vials headspace using a 60 ml syringe and analyzed by Cavity Ring Down Spectroscopy using a Picarro G2201-i device. Samples were slowly injected following the pump flow, taking care not to change the internal pressure, which can be monitored by the analyzer. The 60 ml analyzes took approximately 3 min to pass through the analyzer giving a steady measurement for roughly 40 s that was checked with three standard gas mixtures for concentration and carbon isotope composition of CH_4. Reproducibility between replicates presented a variation of the standard deviation >0.5% for concentration and >0.9% for $\delta^{13}C_{CH4}$. Readings of concentration (ppm) and $\delta^{13}C_{CH4}$ (‰) by the analyzer were slightly different than the standard reference values. Thus, sample results were corrected according to a standard calibration curve.

Optically Stimulated Luminescence and Radiocarbon Datings

Optically stimulated luminescence (OSL) dating was carried out in fine silt or sand quartz aliquots from cores XC02, XC03, and XC05 in the Luminescence and Gamma Spectrometry Laboratory of the IGc/USP. Quartz aliquots for luminescence measurements were prepared under subdued red light. Wet sieving and settling procedures were used to isolate the 4–11 or 180–250 μm grain sizes. The target grain size fractions were submitted to oxygen peroxide (H_2O_2) and hydrochloric (HCl 10%) treatments to remove organic matter and carbonates, respectively. Heavy liquid separation of quartz sand grains was performed using lithium metatungstate solution at densities of 2.75 and 2.62 g cm^{-3} to remove heavy minerals and feldspar grains, respectively. Concentrates of quartz sand grains were etched with hydrofluoric acid (HF 38%) for 40 min in order to remove the outer rind of quartz grains damaged by alpha particles and remnant feldspar grains. Luminescence measurements were performed in two automated Risø OSL/TL reader model DA-20 equipped with blue (470 nm) and infrared (870 nm) LEDs for light stimulation, Hoya U-340 filter for light detection in the ultraviolet band and built-in beta radiation sources ($^{90}Sr/^{90}Y$) delivering dose rates of 0.088 and 0.135 Gy s^{-1} (for aluminum discs). Equivalent doses were determined through the single-aliquot regenerative dose protocol (Murray and Wintle, 2000). For fine silt, a mean a-value of 0.04 was considered for calculation of alpha dose rate in quartz. Tests with infrared stimulation indicated absence of feldspar in the fine silt concentrates. A dose recovery test was performed to set up the luminescence measurements protocol to the studied samples batch. Samples equivalent doses were calculated through the Central Age Model (Galbraith et al., 1999). The concentrations of K, ^{238}U and ^{232}Th for dose rate calculations were determined using high resolution gamma spectrometry with a high purity germanium detector (relative efficiency of 55% and energy resolution of 2.1 KeV) encased in an ultralow background shield. Samples were packed in sealed plastic containers and stored for at least 28 days for radon equilibration before gamma spectrometry. Radiation dose rates were calculated using conversion factors outlined by Guérin et al. (2011). Radiation dose rates were corrected for water

saturation (water weight/dry sample weight). Cosmic dose rates were calculated through samples latitude, longitude, elevation and burial depth, according to Prescott and Hutton (1994).

Accelerator mass spectrometry (AMS) radiocarbon (^{14}C) dating was performed on leaves and charcoal fragments retrieved from the sediment cores. Samples were treated in the Radiocarbon Laboratory of the Illinois State Geological Survey and submitted to the Keck Carbon Cycle AMS Laboratory of the University of California-Irvine for AMS ^{14}C analysis. The ^{14}C dates were calibrated using the program Calib 7.0 and the calibration curve IntCal 13 (Stuiver and Reimer, 1993; Reimer et al., 2013).

RESULTS

Geochemistry of Suspended and Riverbed Sediments

Geochemical results are summarized in **Tables 1, 2** (discretized dataset in Table S1). Strong variations in suspended sediment composition were identified between wet and dry seasons in the Xingu, Tapajós, and Amazon rivers (**Table 1**, **Figure 3**). Seasonal changes in suspended sediments of the Xingu and Tapajós rivers include the increase in the relative amount of P in sediments of the dry season, which is directly related to primary productivity (Engstrom and Wright, 1984; Dean and Gorham, 1998). The P/Ti ratio is an effective proxy to evaluate the sedimentation of phosphorous regardless of terrigenous input and it avoids dilution effects caused by changes in sedimentation rate (Latimer and Filippelli, 2002; Filippelli et al., 2003). Average P/Ti ratios in the Xingu River vary from 0.66 in the wet season to 4.20 in the dry season. Seasonal changes in P concentration have lower amplitudes in the Tapajós River, with the P/Ti ratio shifting from 0.75 to 0.94 from the wet to the dry seasons, respectively. The Fe/K ratio is a useful indicator of mineralogical stability, since the most stable rock-forming minerals have lower Fe/K ratios (K-feldspar, muscovite, and quartz) and unstable minerals tend to be richer in iron content (Herron, 1988; Armstrong-Altrin and Machain-Castillo, 2016). Fe/K ratios increase during the wet season both in the Xingu and Tapajós rivers, with relatively little variation in the Amazon River (**Table 3**). In the Xingu River, Ca concentrations increase from 0.09 to 0.35 mg l^{-1} and P concentration from 0.03 to 0.71 mg l^{-1} between the wet and dry season. Fe concentrations shift from 1.11 to 2.56 mg l^{-1} from the wet to the dry season. The inverse pattern is observed in the Amazon River, with Ca, P, and Fe concentrations decreasing in the dry season (**Table 1**, **Figure 3**). In the Tapajós River, these shifts between wet and dry seasons have lower amplitude, with Ca concentration varying from 0.07 to 0.13 mg l^{-1}, P varying from 0.03 to 0.05 mg l^{-1} and Fe varying from 0.99 to 0.76 mg l^{-1}.

TABLE 2 | Summary of major elements concentrations, TOC and $\delta 13C_{org}$ of bulk organic matter in bottom sediments of the Xingu, Tapajós, and Amazon rivers.

River	Xingu	Tapajós	Amazon
n	5	2	7
Mg (mg/kg)	1547 ± 737	5803	6009 ± 180
Al (mg/kg)	75685 ± 7649	54944 ± 20699	70821 ± 2270
K (mg/kg)	7342 ± 1577	8772 ± 7754	15204 ± 418
Ca (mg/kg)	3195 ± 608	3592 ± 1904	5987 ± 222
Ti (mg/kg)	3119 ± 425	3111 ± 1642	4366 ± 67
Mn (mg/kg)	330 ± 99	226 ± 183	438 ± 51
Fe (mg/kg)	26999 ± 7462	16367 ± 13823	25948 ± 1702
Si (mg/kg)	196160 ± 13454	228105 ± 1280	221458 ± 4768
TOC (%)	2.25 ± 0.582	0.2	0.59 ± 0.068
$\delta 13C_{org}$ (%)	−28.645 ± 0.288	-	−28.02 ± 0.201

Data of individual samples are presented in Table S1 of the Supplementary Material.

Pollen and Diatoms in Riverbed and Core Sediments

In total, 45 pollen taxa were identified in riverbed sediments of the Xingu Ria (Figures S1–S4). The vegetation represented by pollen retrieved from riverbed sediments has great diversity and high percentages of forest elements. Arboreal taxa encountered in the samples include *Acalypha*, *Alchornea*, Annacardiaceae, Apocynaceae, Arecaceae, *Attalea*, *Bignoniaceae*, *Cecropia*, *Combretum*, *Dalbergia*, *Didymopanax*, *Euterpe*, *Fabacea*, *Genipa*, *Machaerium*, *Mauritia*, *Mauritiella*, *Matayba*, *Melastomataceae*, *Mimosa*, Myrtaceae, Palmae, *Psidium*, *Psychotria*, *Sapium*, *Spondias*, *Sterculiaceae*, *Stigmaphyllon*, *Talisia,* and *Zygia*. Terrestrial herbaceous elements are represented by *Alternanthera*, Asteraceae, *Bambusa*, *Begonia*, *Caesaria*, Lamiaceae, *Phyllanthus*, *Pilea*, Poaceae, Polygonaceae

TABLE 1 | Variation of major elements concentrations in suspended sediments of the Xingu, Tapajós, and Amazon rivers during the wet and dry seasons.

River	Season	*n*	Mg (mg/l)	Al (mg/l)	K (mg/l)	Ca (mg/l)	Ti (mg/l)	Mn (mg/l)	Fe (mg/l)	P (mg/l)
Xingu	dry	6	0.30 ± 0.102	6.31 ± 1.205	0.80 ± 0.272	0.35 ± 0.068	0.22 ± 0.057	0.19 ± 0.022	2.56 ± 0.572	0.71 ± 0.051
	wet	5	0.07 ± 0.009	1.72 ± 0.283	0.06 ± 0.014	0.09 ± 0.015	0.05 ± 0.011	0.05 ± 0.006	1.11 ± 0.110	0.03 ± 0.003
Tapajós	dry	4	0.09 ± 0.023	2.37 ± 0.650	0.08 ± 0.023	0.13 ± 0.027	0.06 ± 0.015	0.12 ± 0.23	0.76 ± 0.150	0.05 ± 0.004
	wet	3	0.05 ± 0.006	1.68 ± 0.350	0.03 ± 0.019	0.07 ± 0.027	0.04 ± 0.007	0.03 ± 0.006	0.99 ± 0.251	0.03 ± 0.008
Amazon	dry	2	0.46 ± 0.055	5.47 ± 0.737	0.81 ± 0.140	0.38 ± 0.035	0.21 ± 0.032	0.04 ± 0.005	2.50 ± 0.266	0.05 ± 0.002
	wet	3	2.24 ± 0.269	23.43 ± 2.122	5.01 ± 0.613	1.63 ± 0.195	1.19 ± 0.164	0.18 ± 0.027	14.40 ± 1.051	0.27 ± 0.017

Data of individual samples are presented in Table S1 of the Supplementary Material.

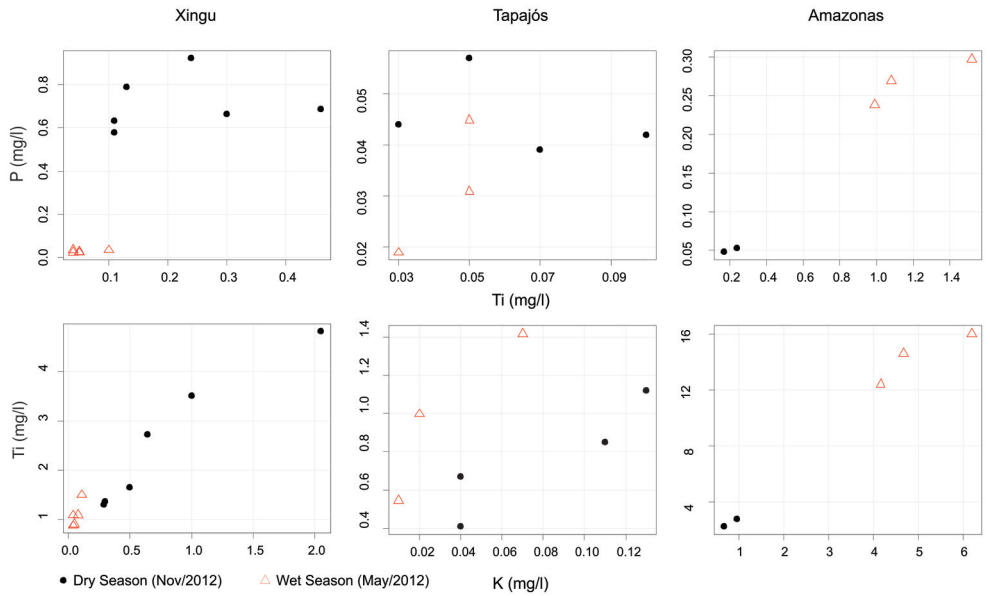

FIGURE 3 | Scatterplots comparing P, Ti and K concentrations in suspended sediments collected in the Xingu, Tapajós and Amazon rivers during the wet and dry seasons.

TABLE 3 | Variation of elemental ratios in suspended sediments of the Xingu, Tapajós, and Amazon rivers during the wet and dry seasons.

River	Season	*n*	Fe/K	P/K	Ti/Ca	Mn/K	P/Mg	Fe/Ca	P/Ti	Fe/Mn	Ti/Al	Al/Ca
Xingu	dry	6	3.74	1.35	0.61	0.35	3.45	7.24	4.20	13.36	0.034	18.37
	wet	5	19.15	0.58	0.59	0.93	0.45	12.54	0.66	24.67	0.031	19.01
Tapajós	dry	4	10.84	0.80	0.50	2.29	0.63	6.26	0.94	7.55	0.026	19.32
	wet	3	41.76	1.36	0.76	1.36	0.62	16.86	0.75	32.11	0.025	29.75
Amazonas	dry	2	3.12	0.06	0.54	0.04	0.11	6.65	0.25	71.67	0.038	14.52
	wet	3	2.91	0.05	0.73	0.03	0.12	8.93	0.23	83.52	0.051	14.47

and *Symmeria*. *Sagitaria*, Cyperaceae, Alismataceae represent taxa of aquatic herbs. Spores identified in the analysis include Polypodiaceae, *trilete* and Monolete. The palynologic data indicate that riverbed sediments of the Xingu Ria record the input of sediments from areas where the predominant vegetation type is forest (Figure S5).

Regarding the diatoms, a total of 65 infrageneric taxa were identified in riverbed sediments of the Xingu Ria. *Eunotia* and *Gomphonema* were the most represented genera regarding species number (24.6% of total species), followed by genus *Aulacoseira* (9.2%) (Figure S6). *Eunotia* species are mostly acidophilic, oligotrophic, and typified by a dominant periphytic habitat (Round et al., 1990; van Dam et al., 1994; Moro and Fürstenberger, 1997; Hamilton and Siver, 2010). Due to the secretion of mucilage by the apical pore fields, *Gomphonema* is a common genus in periphytic algal communities, being well represented in richness and density (Tremarin et al., 2009). *Aulacoseira* is a common planktonic genus inhabiting lacustrine and running freshwaters, developing in various trophic conditions (Denys et al., 2003; Zalat and Vildary, 2007). Ecological information at species level is required to use this genus as indicator of water quality (Bicudo et al., 2016).

Diatoms presented well-preserved frustules throughout the core. Assemblages from the core XC05 base showed little variation among genera, and besides the planktonic genus *Aulacoseira*, comprised benthic and periphytic genera that require surfaces for developing (e.g., *Eunotia, Pinnularia and Surirella*), suggesting a water column under acidic and oligotrophic conditions with high light penetration. Genera *Surirella*, *Diploneis*, *Aulacoseira*, *Placoneis*, *Gomphonema*, *Encyonema,* and *Eunotia* were observed throughout the core, suggesting a relatively uniform slack water environment.

Chronology, Magnetic and Geochemistry Data of Sediment Cores

Sediments of the three studied underwater cores (XC02, XC03, and XC05) are composed of dark gray to brown organic-rich muddy sediments. As highlighted in **Figure 2**, these sediments are similar to the modern surface sediments that accumulate in

TABLE 4 | Radionuclides concentrations, radiation dose rates, equivalent doses and luminescence ages of sediment samples retrieved from cores XC02, XC03, and XC05.

Sample	Depth (cm)	U (ppm)	Th (ppm)	K (%)	Cosmic dose rate (Gy/ka)	Total dose rate (Gy/ka)	Equivalent dose (Gy)	Age (years)
XC02-10	10	5.35 ± 2.66E-1	1.50 ± 8.87 E-1	0.67 ± 0.06	0.19 ± 0.01	1.72 ± 0.29	4.3 ± 0.3	2503 ± 462
XC02-293	293	4.54 ± 2.12E-1	15.58 ± 8.30E-1	0.67 ± 0.05	0.13 ± 0.01	1.7 ± 0.28	5.6 ± 0.1	3295 ± 542
XC03-10	10	3.70 ± 1.87E-1	7.66 ± 5.10E-1	1.13 ± 0.06	0.19 ± 0.02	2.55 ± 0.41	0.3 ± 0.2	118 ± 81
XC03-363	363	3.19 ± 1.67E-1	6.48 ± 4.55E-1	1.14 ± 0.06	0.12 ± 0.01	2.48 ± 0.41	3.1 ± 0.1	1251 ± 211
XC05-45	45	4.53 ± 1.69E-1	19.95 ± 7.64E-1	0.7 ± 0.04	0.08 ± 0.01	2.05 ± 0.08	6.2 ± 0.3	3025 ± 185
XC05-140	140	4.73 ± 1.77E-1	20.94 ± 8.01E-1	0.741 ± 0.04	0.07 ± 0.01	2.21 ± 0.09	7.1 ± 0.1	3219 ± 133
XC05-239	239	4.36 ± 1.69E-1	21.86 ± 8.35E-1	0.74 ± 0.045	0.07 ± 0.01	2.17 ± 0.08	7.3 ± 0.1	3360 ± 138
XC05-340	340	4.34 ± 1.66E-1	20.72 ± 7.98E-1	0.71 ± 0.04	0.06 ± 0.01	1.99 ± 0.07	7.4 ± 0.1	3718 ± 147
XC05-440	440	4.16 ± 1.62E-1	2.21 ± 8.3E-1	0.791 ± 0.04	0.06 ± 0.01	2.06 ± 0.08	8.4 ± 0.1	4086 ± 159

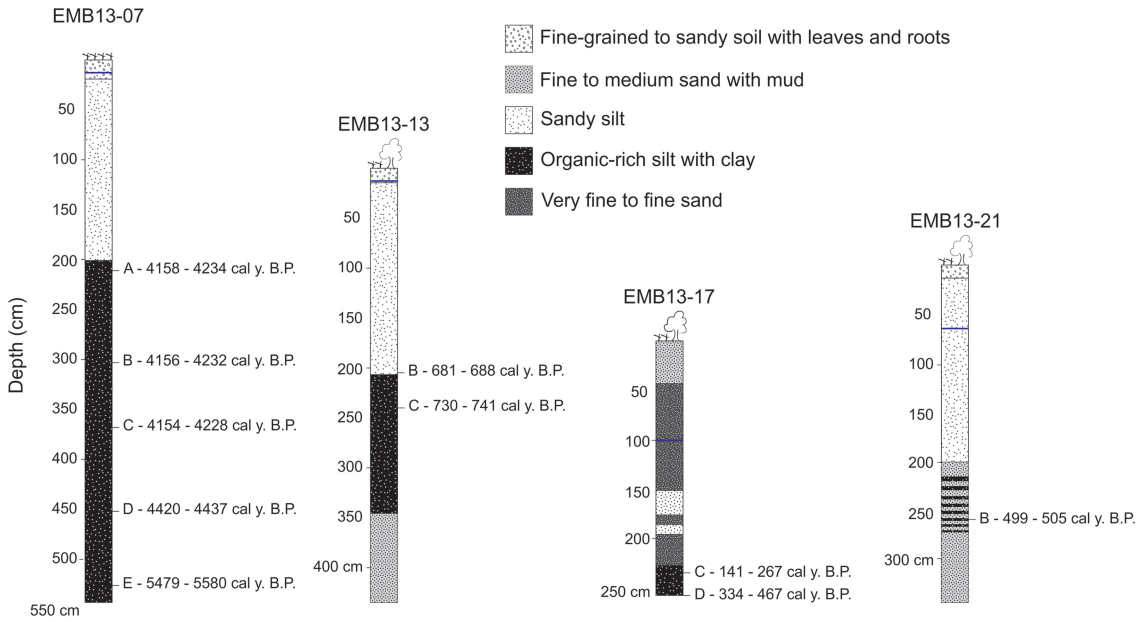

FIGURE 4 | Radiocarbon ages in sediment depth profiles of stabilized bar of the Xingu Ria head. Ria sediments are represented by organic-rich muds buried by organic-poor floodplain sediments.

most of the rias. Samples from the top and bottom of sediment cores XC02 (10–293 cm), XC03 (10–363 cm) and XC05 (45–440 cm) were collected for OSL dating. The luminescence ages of cores XC02, XC03, and XC05 ranged from 118 ± 81 to 4,086 ± 159 years (**Table 4**), suggesting that the Xingu Ria is a slack water environment acting as trap of fine-grained sediments at least since the middle Holocene. XC02 sediments showed ages from 2,503 ± 462 to 3,295 ± 542 years. XC03 and XC05 sediments cover periods from 118 ± 81 to 1,251 ± 211 years, and from 3,025 ± 185 to 4,086 ± 159 years, respectively. Sediment depth profiles described in the islands of the head of the Xingu Ria (EMB13-07, EMB13-13 and EMB13-17) show dark gray organic-rich sediments interlayered with sands and light gray floodplain sediments (**Figure 4**). Radiocarbon ages obtained in the dark gray muds, which likely represent buried ria sediments, varied from 141–267 to 5,479–5,580 cal years BP (**Table 5**, **Figure 4**).

Luminescence and radiocarbon ages allowed the calculation of sedimentation rates for the organic-rich sediments of the Xingu Ria. In the Xingu Ria, sedimentation rates calculated through luminescence ages of core XC05 varied between 0.27 cm yr^{-1} and 0.70 cm yr^{-1} (average of 0.37 cm yr^{-1}). The rate of deposition of core XC05 increases from about 0.28 cm yr^{-1} during the period of ∼4,100 to ∼3,300 years ago to an average of 0.60 cm yr^{-1} during the period of ∼3,300 to ∼3,000 years ago. Cores XC02 and XC03 presented average sedimentation rates of 0.36 cm yr^{-1} and 0.31 cm yr^{-1}, respectively. Sedimentation rates for organic-rich sediments underneath floodplain sediments of the Xingu Ria head were 0.24 cm yr^{-1}, 0.78 cm yr^{-1}, 0.05 cm yr^{-1} in profiles EMB13-07, EMB13-13 and EMB13-17, respectively (**Figure 4**).

TABLE 5 | Radiocarbon ages of sediment cores EMB13-07, EMB13-13, EMB13-17, and EMB13-21.

Sample	Analyzed material	Depth (cm)	^{14}C Age (years BP)	Calibrated ^{14}C age (cal years BP)
EMB13-07 A	leaf	210	3185 ± 15	4158–4234
EMB13-07 B	leaf	303	3180 ± 15	4156–4232
EMB13-07 C	leaf	373	3805 ± 20	4154–4228
EMB13-07 D	leaf	458	3975 ± 15	4420–4437
EMB13-07 E	leaf	532	4765 ± 25	5479–5580
EMB13-13 B	charcoal	210	765 ± 15	681–688
EMB13-13 C	leaf	248	835 ± 15	730–741
EMB13-17 C	leaf	230	145 ± 15	141–267
EMB13-17 D	charcoal	240	360 ± 20	334–467
EMB13-21 B	charcoal	260	425 ± 15	499–505

In the Tapajós Ria, sedimentation rates were calculated through radiocarbon ages presented in Irion et al. (2006). Rates of sediment deposition in the Tapajós Ria vary from 0.24 cm yr^{-1} to 0.65 cm yr^{-1} (average of 0.37 cm yr^{-1}).

Magnetic susceptibility measurements were performed on the XC05 core. Low-field magnetic susceptibility varies from 3.4×10^{-8} to 1.9×10^{-7} m^{3}kg^{-1} (**Figure 5**). Strong magnetic susceptibility variations (peaks) may indicate variations in sedimentation rate or increased magnetic mineral concentrations. The dendogram of geochemical data demonstrates abrupt shifts in the compositional similarity of sediments deposited at 3,690–3,650, 3,345–3,335, and 3,235–3,240 years ago. These shifts fit well with peaks in magnetic susceptibility and P, Fe, Mn, and TIC concentration as well as with the decrease in TOC and lithophilic elements (**Figure 5**).

Ti concentration reveals significant positive correlations with Al ($r = 0.81$, $n = 198$) and K ($r = 0.75$, $n = 198$). These elements were used as proxies for the relative contribution of terrigenous sediment input from the Xingu River to the downstream Xingu Ria lake (Engstrom and Wright, 1984; Boës et al., 2011). Results show significant inverse correlation among P concentration and lithophilic elements represented by Ti ($r = -0.31$, $n = 198$), Al ($r = -0.32$, $n = 198$) and K ($r = -0.46$, $n = 198$). P concentration also shows significant positive correlations with Fe ($r = 0.57$, 198), TIC ($r = 0.51$, $n = 198$) and Mn ($r = 0.51$, $n = 198$).

Total organic carbon (TOC) concentration varies between 1.77 and 3.35% (average of 2.45%) in sediment core XC05. The measured concentrations are similar to values in samples from bottom sediments of the Xingu Ria (Häggi et al., 2016). Values of $\delta^{13}C_{org}$ range from −31.04 to −27.49‰, and indicate that organic matter from bottom sediments of the Xingu Ria is mainly derived from arboreal C3 vegetation (Table S1). This is supported by palynological data, with pollen assemblages dominated by forest taxa (Figure S1).

CH_4 concentrations in pore waters reach values up to 25% (volume) in XC05 sediment core (**Figure 5**). The values of $\delta^{13}C_{CH4}$ in pore waters of XC05 core range from −71 to −57‰ PDB. Higher (more positive) values of $\delta^{13}C_{CH4}$ often agree with peaks in magnetic susceptibility, Fe concentration and P/Ti (**Figure 5**). This suggests that CH_4 oxidation in pore waters might increase during drier periods.

DISCUSSION

Despite the relatively low suspended load in clearwater rivers, the composition of suspended sediments in the Xingu and Tapajós rivers are organic-rich in comparison with white water rivers, showing a marked variation between the dry and wet seasons. Major variations in sediment composition occur due to seasonal changes of hydrology, driving the input of organic and inorganic compounds and regulating primary productivity. The seasonal changes in river discharge controls the relative concentrations of lithophilic elements (Ti, Al, K) compared to elements influenced by redox conditions in the water column and riverbed (P, Fe, Mn). While the uncertainty of organic carbon sources and its stability through time limits its use as proxy for lake productivity or paleo-redox conditions, phosphorous concentration is a useful indicator of paleo-productivity (Engstrom and Wright, 1984; Dean and Gorham, 1998; Boyle, 2001). In order to compensate for fluctuations in allochthonous (terrigenous) inputs of sediments to the ria lake, the P to Ti ratio was chosen as productivity indicator (Latimer and Filippelli, 2002; Filippelli et al., 2003). Average P/Ti values vary from 4.20 to 0.66 in suspended sediments of the Xingu River during the dry and wet seasons, respectively. The higher values during the dry season are linked to higher primary productivity favored by low water turbidity.

There are significant positive correlations between Fe and Ca ($p = 0.71$, $n = 198$), Fe and P ($p = 0.57$, $n = 198$) and Fe and TIC ($p = 0.97$, $n = 198$) concentrations in core XC05, which point to biogeochemical controls on Fe and TIC deposition in sediments. The high concentration of Fe relative to K in suspended sediments transported during the dry season suggests that assimilation of Fe in sediments is favored by the increase in organic productivity and oxygenated bottom waters (**Table 3**). Major decreases in TOC concentrations are correlated to peaks of P/Ti, TIC, Fe and Mn, suggesting lower preservation of organic matter during drier periods (**Figure 5**). The lack of correlation between TOC and TIC in core XC05 indicates that the shallow bathymetry during drier low-water periods likely decreased calcite solubility, enhanced evaporation and led to the elevated concentration of the carbonate ions (Kelts and Talbot, 1990). Mn and Fe in sediments are remobilized under reducing conditions and precipitated in the presence of oxygenated waters (Davison, 1993). Lower values of Fe/Mn ratios, proposed by Mackereth (1966) as a redox proxy, are correlated with peaks of P/Ti, suggesting abrupt shifts in redox conditions during sediment deposition in the Xingu Ria. Peaks of P/Ti indicate dominant wetter conditions punctuated by dry events at 3,690–3,650, 3,345–3,335, and 3,235–3,240 years ago (**Figure 5**). Nutrient-rich and oxygenated waters favor the accumulation of P, Fe and Mn in sediments deposited under drier and low-water level periods. In contrast, TOC is negatively correlated with P, Fe and Mn concentrations due to the lower organic matter preservation under oxic conditions prevailing during drier periods. During the

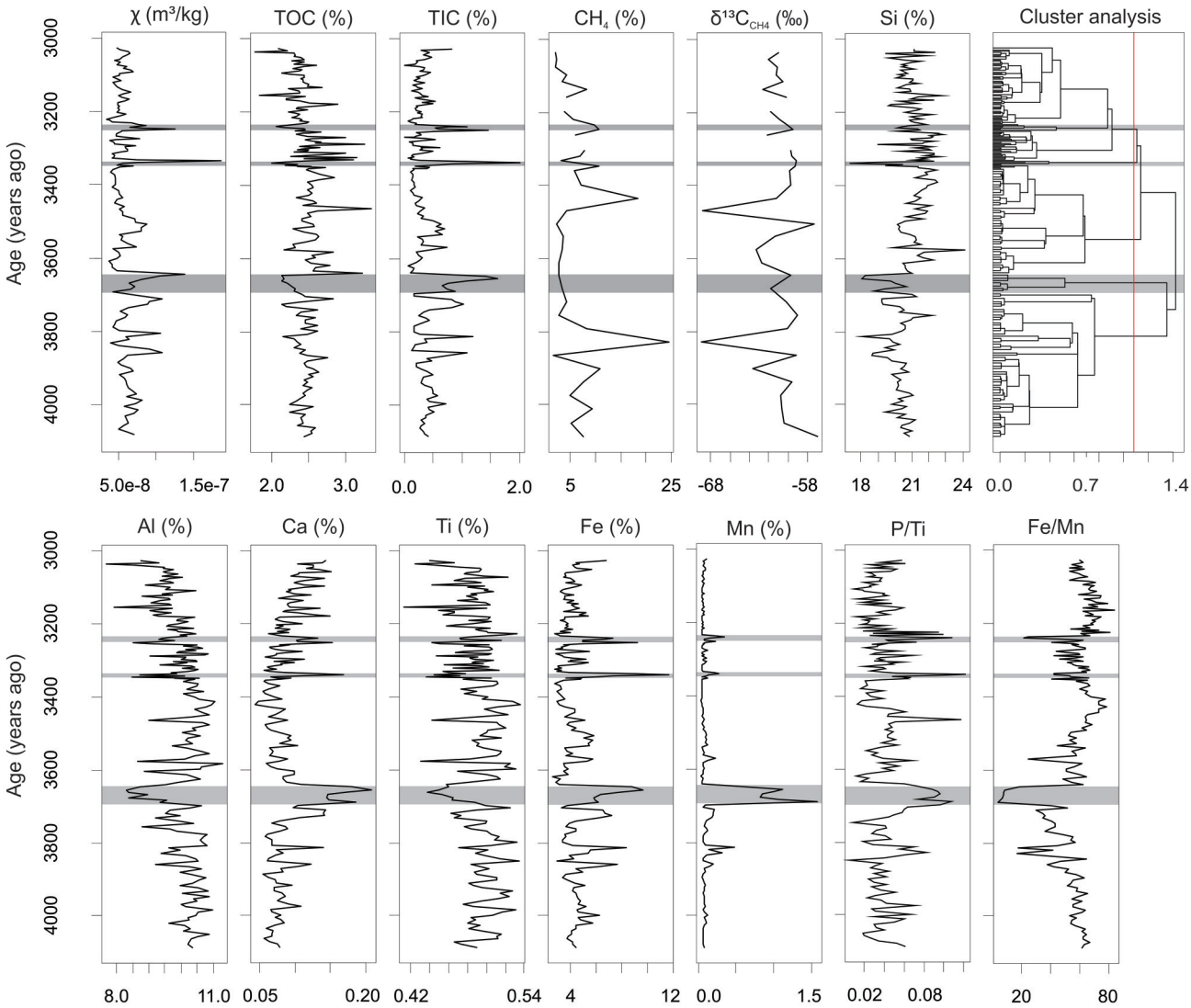

FIGURE 5 | Variation of magnetic susceptibility (χ), CH_4 concentration, $\delta^{13}C_{CH4}$ and major elements geochemistry in sediment core XC05. Grey areas reveal abrupt shifts in compositional similarity of sediments highlighted by hierarchical cluster analysis.

low water season, the shallower water column would be better mixed and the oxic water in contact with the bottom sediment would lead to a faster degradation of the deposited organic matter. Thus, considering the redox and productivity proxies already described, the variation in TOC concentration through time is mainly derived from changes in the water-sediment interface from anoxic/dysoxic (higher TOC) to oxic (lower TOC) conditions that may be related to hydrologic changes in the area drained by the Xingu River.

Fine-grained sediments accumulated in Amazon rias have relatively high concentration of organic carbon (average TOC of 2.45%) compared to fine-grained sediments deposited in floodplains under influence of white water rivers such as the Amazon River (0.4–1.4%; Moreira-Turcq et al., 2004; Aniceto et al., 2014; Moreira et al., 2014). Thus, rias formed in large clearwater rivers such as the Xingu and Tapajós rivers act as hotspots for carbon storage within rivers in the Amazon Basin. These areas are present at least since the middle Holocene, considering the ages obtained for the sediment cores from the Xingu (>4,000 years, this study) and Tapajós rivers (>9,600 years, Irion et al., 2006). Stable carbon isotope data ($\delta^{13}C_{org}$ from −31.04 to −27.49‰) indicate a dominant contribution of C3 plants and possibly phytoplankton for the organic particles accumulated in the ria bottom. Palynological data document a large contribution of C3 arboreal plants as major sources of carbon in sediments of the Xingu and Tapajós rias. The labile organic matter derived from phytoplankton may be rapidly consumed and turned into CO_2 in the oxic surface sediment layer, while the more recalcitrant terrestrial organic matter accumulates. Also, once buried in the anoxic sediment, the

autochthonous and labile organic matter may be used to fuel the CH_4 production within sediments. This mechanism is in accord with the high CH_4 concentrations in pore waters and released to the atmosphere obtained by this work and by Sawakuchi et al. (2014). Despite the large carbon storage, the Xingu and Tapajós rias show the highest fluxes of CH_4 to the atmosphere among the major Amazon tributaries (Sawakuchi et al., 2014), suggesting that sedimentary conditions suitable for organic matter preservation favor anoxic conditions in the sediments, where CH_4 can be produced and released to the atmosphere. This is supported by the high concentrations (up to 24%) of CH_4 in sediment pore waters of the Xingu Ria, with $\delta^{13}C_{CH4}$ varying from −70.4 to −56.9‰, suggesting low CH_4 oxidation rates. These results indicate that rias in clearwater Amazon rivers are significant organic carbon sinks and sources of CH_4 to the atmosphere. They should be considered as distinct environments in the Amazon in order to refine modern carbon balance assessments.

The pollen assemblages show a high diversity of arboreal taxa, pointing to the *terra firme* and *igapó* forests as main sources of organic matter within sediments of the Xingu River catchment. Despite the increasing deforestation in the Xingu catchment during the last several decades (Barona et al., 2010), organic carbon stored in riverbed sediments is mainly derived from forest. This could be related to a delay in transfer of the deforestation signal to river sediments, or a dominant input of organic matter from the *igapó* flooding forest tract along the river channel. The diatom assemblages in riverbed sediments and the sediment core point to a slack water environment in the Xingu Ria since the middle Holocene. Considering that the organic matter pool in sediments of the Xingu and Tapajós rias is mainly terrigenous and derived from forested areas, the input of carbon to the ria sediments is favored during high precipitation episodes while carbon preservation is controlled by duration and frequency of dry periods. Low sedimentation rates combined with well oxygenated waters due to higher primary productivity in the water column favor organic matter degradation in riverbed sediments during dry periods. Despite high rates of organic matter degradation during low-water periods, the higher primary productivity favors the uptake of CO_2 and carbon recycling in the water column and riverbed. During high-water phases, the flux of CO_2 to the atmosphere increases due to lower primary productivity, while higher sedimentation rates favor organic matter preservation and carbon uptake in sediments. High primary production is the main indicator of CO_2 undersaturation observed in large clearwater rivers in the Amazon during the low-water phase (Rasera et al., 2013).

The sediment cores retrieved in the Xingu Ria have ages varying from 3,025 ± 185 to 4,086 ± 159 years (XC05), from 118 ± 81 to 1,251 ± 211 years (XC03) and from 2,503 ± 462 to 3,295 ± 542 years (XC02). The cores were collected in the deepest part of the river profile and core tops with ages between 3,025 ± 185 (XC05) and 2,503 ± 462 (XC02) years indicate erosional processes and sediment reworking within the ria. The lack of recent deposits indicates that erosion due to channel migration may remobilize sediments in certain portions of the ria. The average sedimentation rate obtained in this study for the Xingu Ria is 0.35 cm yr^{-1} since the middle Holocene (∼4,000 years). On millennial timescales, sediment deposition rates at different locations are relatively stable. A similar average sedimentation rate of 0.37 cm yr^{-1} was also observed for the Tapajós Ria over the last ∼11,000 years Irion et al. (2006). Sedimentation rates from 0.35 to 0.37 cm yr^{-1} are relatively high compared to sedimentation rates observed in low latitude lakes, which are typically around 0.05 to 0.25 cm yr^{-1} (Cross et al., 2000; Chu et al., 2002; Hodell et al., 2005; Caballero et al., 2006; Conroy et al., 2008; McGlue et al., 2011). Our data show that sedimentation rates varied through time in core XC05. The temporal and spatial variations in sedimentation rates would result from hydrologic changes and sediment reworking within the Ria. The migration of underwater channels and wave action would be the major autogenic processes responsible for sediment remobilization and spatial changes in sedimentation rates. Temporal variations would also be related to precipitation changes affecting sediment supply and accommodation space within the ria. Additional data are required to calculate sedimentation rates with higher temporal resolution and allow a comparison with paleoprecipitation records. This is necessary to constrain the major controls on sedimentation rates and the role of precipitation changes for carbon burial. The TOC concentration in core XC05 varies from 1.77 to 3.35% (average of 2.45%), similar to TOC values measured in bottom sediments collected in the Xingu Ria (average of 2.36%) (Häggi et al., 2016). Irion et al. (2006) showed TOC values with low variation in the Tapajós Ria, varying from 2.2 to 2.9% in sediments younger than 7,500 years. The high sedimentation rates would reduce the effectiveness of degradation processes, implying that the Xingu and Tapajós rias are potentially massive carbon sinks on a millennial timescale.

We estimated rates of organic carbon burial in the Xingu and Tapajós rias based on a dry bulk density of 1.3 g cm^{-3} for the bottom ria sediments, average sedimentation rates of 0.35 cm yr^{-1} and 0.37 cm yr^{-1} (Irion et al., 2006) for the Xingu and Tapajós rias, respectively, and the minimum and maximum TOC concentrations obtained in this work and by Irion et al. (2006). In the Xingu Ria, carbon burial ranges from 84 g m^{-2} yr^{-1} to 159 g m^{-2} yr^{-1} (average of 116 g m^{-2} yr^{-1}) and from 106 to 169 g m^{-2} yr^{-1} (average of 121 g m^{-2} y^{-1}) in the Tapajós Ria. Assuming that 75% (conservative estimate) of the ria surface is covered by fine-grained organic-rich sediments (**Figure 2**), the Xingu Ria buries from 0.08 Tg C yr^{-1} to 0.16 Tg C yr^{-1} (average of 0.11 Tg C yr^{-1}) and the Tapajós Ria buries from 0.19 Tg C yr^{-1} to 0.30 Tg C yr^{-1} (average of 0.21 Tg C yr^{-1}). Conceding that the Xingu and Tapajós Rias were totally flooded at least since the middle Holocene (∼5,000 years), around 560 Tg C and 1050 Tg C of carbon are stored in sediments of the Xingu and Tapajós rias, respectively.

A rough attempt to estimate the carbon budget of the Xingu Ria is possible considering the average accumulation rate of carbon in sediments of the Xingu Ria of 0.11 Tg C yr^{-1} (this study) and the carbon evasion estimates of 8 Tg C yr^{-1} as CO_2 (Sawakuchi et al., this volume) and 0.053 Tg C yr^{-1} as CH_4 (Sawakuchi et al., 2014) fluxes to the atmosphere.

These estimates indicate that despite the significant carbon pool and storage, the Xingu Ria is a net source of carbon to the atmosphere. Furthermore, the Xingu Ria can serve as an analog for sediment accumulation and carbon processing in the reservoirs of the Belo Monte hydropower plant. The multidecadal carbon sedimentation pattern estimated for the Xingu Ria allows projections about sediment accumulation and carbon processing in the Belo Monte reservoirs.

CONCLUSIONS

The lowermost sectors of the Tapajós and Xingu rivers have lake-like (fluvial ria) sedimentary dynamics due to the impoundment by the Amazon mainstream during the Holocene. This lake-like physiography hinders the transfer of sediments to the Amazon River and induces the accumulation of fine-grained organic-rich sediments derived from upstream areas. Thus, the downstream reaches of these major clearwater rivers are sinks for particulate organic matter chiefly derived from arboreal forest (*terra firme* and *igapó*). Wetter periods favor the supply and preservation of forest-derived organic matter in sediments while drier periods increase the organic productivity in the water column and favor degradation of organic matter in riverbed sediments. Microbial consumption of organic matter in the oxic surface layers of the sediment contributes to the anoxic conditions that prevail within sediments, with methanogenesis being an important path for biodegradation of particulate organic matter. During dry and low-water level periods, the flux of CH_4 to the atmosphere increases while the CO_2 flux decreases due to the higher organic productivity within the water column. Thus, seasonal variations play an important role for carbon dynamics in clearwater rivers. Despite the significant carbon storage that occurs in the Xingu and Tapajós rias at least since the middle Holocene, our carbon balance estimates indicate that Amazon rias would act as source of carbon to the atmosphere. A future drier climate as projected for eastern Amazonia would reduce the carbon sink potential of clearwater rivers and increase the methane flux to the atmosphere.

AUTHOR CONTRIBUTIONS

DJB, AS, and HS were responsible for design of the study and preparation of the manuscript. AS, HS, GH, DJB, and FP organized overall project logistics. DJB and HS executed the sampling and analysis of CH_4 in sediment core and performed calculations of carbon balance. FP and AS executed luminescence dating. GH performed magnetic susceptibility analysis. MM, FP, and DJB performed sampling and geochemical analysis of the sediment core. CC, MZ, and ES executed geochemical analysis of suspended and riverbed sediments. TP collaborated with sediment and greenhouse gas sampling and supported local logistics. RS and PO executed palynology analysis. SF and DCB performed diatom analysis. All authors contributed to data interpretation and critically revised the manuscript for final submission.

FUNDING

This study was funded by FAPESP grants #2011/06609-1, #2014/23334-4, #2016/02656-1 and CAPES grant #AUXPE 2043/2014.

ACKNOWLEDGMENTS

We thank Luciana Nogueira and Thays Desiree Mineli for the support with luminescence dating procedures. Bailee Hodelka, Joseph Lucas, and Jason Backus assisted with XRF and coulometry measurements. We also thank the reviewers for constructive criticisms and valuable comments. Open access publication fees were supported by the Gordon and Betty Moore Foundation Marine Microbial Initiative.

SUPPLEMENTARY MATERIAL

The Supplementary Material for this article can be found online at: http://journal.frontiersin.org/article/10.3389/fmars.2017.00044/full#supplementary-material

REFERENCES

Abril, G., Martinez, J.-M., Artigas, L. F., Moreira-Turcq, P., Benedetti, M. F., Vidal, L., et al. (2014). Amazon River carbon dioxide outgassing fuelled by wetlands. *Nature* 505, 395–398. doi: 10.1038/nature12797

Algeo, T. J., and Rowe, H. (2012). Paleoceanographic applications of trace-metal concentration data. *Chem. Geol.* 324–325, 6–18. doi: 10.1016/j.chemgeo.2011.09.002

Almeida, C. A., de, Coutinho, A. C., Esquerdo, J. C. D. M., Adami, M., Venturieri, A., Diniz, C. G., et al. (2016). High spatial resolution land use and land cover mapping of the Brazilian Legal Amazon in 2008 using Landsat-5/TM and MODIS data. *Acta Amaz.* 46, 291–302. doi: 10.1590/1809-4392201505504

ANA (2016). *Hidroweb: Sistema de Informações Hidrológicas.* Available online at: http://www.snirh.gov.br/hidroweb/ (Accessed October 1, 2016).

Aniceto, K., Moreira-Turcq, P., Cordeiro, R. C., Fraizy, P., Quintana, I., and Turcq, B. (2014). Holocene paleohydrology of Quistococha Lake (Peru) in the upper Amazon Basin: influence on carbon accumulation. *Palaeogeogr. Palaeoclimatol. Palaeoecol.* 415, 165–174. doi: 10.1016/j.palaeo.2014.08.018

Archer, A. W. (2005). Review of amazonian depositional systems. *Fluv. Sedimentol.* VII, 17–39. doi: 10.1002/9781444304350.ch2

Armstrong-Altrin, J. S., and Machain-Castillo, M. L. (2016). Mineralogy, geochemistry, and radiocarbon ages of deep sea sediments from the Gulf of Mexico, Mexico. *J. South Am. Earth Sci.* 71, 182–200. doi: 10.1016/j.jsames.2016.07.010

Aufdenkampe, A. K., Mayorga, E., Raymond, P. A., Melack, J. M., Doney, S. C., Alin, S. R., et al. (2011). Riverine coupling of biogeochemical cycles between land, oceans, and atmosphere. *Front. Ecol. Environ.* 9, 53–60. doi: 10.1890/100014

Barona, E., Ramankutty, N., Hyman, G., and Coomes, O. T. (2010). The role of pasture and soybean in deforestation of the Brazilian Amazon. *Environ. Res. Lett.* 5:24002. doi: 10.1088/1748-9326/5/2/024002

Barros, N., Cole, J. J., Tranvik, L. J., Prairie, Y. T., Bastviken, D., Huszar, V. L. M., et al. (2011). Carbon emission from hydroelectric reservoirs linked to reservoir age and latitude. *Nat. Geosci.* 4, 593–596. doi: 10.1038/ngeo1211

Battarbee, R. W., Jones, V. J., Flower, R. J., Cameron, N. G., Bennion, H., Carvalho, L., et al. (2001). "Diatoms," in *Tracking Environmental Change Using Lake Sediments: Terrestrial, Algal, and Siliceous Indicators*, eds J. P. Smol, H. J. B. Birks, W. M. Last, R. S. Bradley, and K. Alverson (Dordrecht: Springer Netherlands), 155–202.

Bertani, T. C., Rossetti, D. F., Hayakawa, E. H., and Cohen, M. C. L. (2014). Understanding Amazonian fluvial rias based on a late pleistocene-holocene analog. *Earth Surf. Process. Landforms*. 40, 285–292. doi: 10.1002/esp.3629

Bicudo, D. C., Tremarin, P. I., Almeida, P. D., Almeida-Zorzal, S., Wengrat, S., Faustino, S. B., et al. (2016). Taxonomy and ecology of Aulacoseira species (Bacillariophyta) from tropical reservoirs in Brazil. *Diatom Research*. 31, 199–215. doi: 10.1080/0269249X.2016.1227376

Boës, X., Rydberg, J., Martinez-Cortizas, A., Bindler, R., and Renberg, I. (2011). Evaluation of conservative lithogenic elements (Ti, Zr, Al, and Rb) to study anthropogenic element enrichments in lake sediments. *J. Paleolimnol.* 46, 75–87. doi: 10.1007/s10933-011-9515-z

Böning, P., Cuypers, S., Grunwald, M., Schnetger, B., and Brumsack, H. J. (2005). Geochemical characteristics of Chilean upwelling sediments at ∼36°S. *Mar. Geol.* 220, 1–21. doi: 10.1016/j.margeo.2005.07.005

Bouchez, J., Beyssac, O., Galy, V., Gaillardet, J., France-Lanord, C., Maurice, L., et al. (2010). Oxidation of petrogenic organic carbon in the Amazon floodplain as a source of atmospheric CO_2. *Geology* 38, 255–258. doi: 10.1130/G30608.1

Bouchez, J., Gaillardet, J., Lupker, M., Louvat, P., France-Lanord, C., Maurice, L., et al. (2012). Floodplains of large rivers: weathering reactors or simple silos? *Chem. Geol.* 332–333, 166–184. doi: 10.1016/j.chemgeo.2012.09.032

Boyle, J. F. (2001). "Inorganic Geochemical Methods in Palaeolimnology," in *Tracking Environmental Change Using Lake Sediments: Physical and Geochemical Methods*, eds W. M. Last and J. P. Smol (Dordrecht: Springer Netherlands), 83–141.

Caballero, M., Vázquez, G., Lozano-García, S., Rodríguez, A., Sosa-Nájera, S., Ruiz-Fernández, A. C., et al. (2006). Present limnological conditions and recent (ca. 340 yr) palaeolimnology of a tropical lake in the Sierra de Los Tuxtlas, eastern Mexico. *J. Paleolimnol.* 35, 83–97. doi: 10.1007/s10933-005-7427-5

California Academy of Sciences (2011). *Catalogue of Diatom Names. Compil. by Elisabeth Fourtanier J. Patrick Kociolek*. Available online at: http://research.calacademy.org/research/diatoms/names/index.asp (Accessed October 1, 2016).

Chu, G., Liu, J., Sun, Q., Lu, H., Gu, Z., Wang, W., et al. (2002). The "Mediaeval Warm Period" drought recorded in Lake Huguangyan, tropical South China. *Holocene* 12, 511–516. doi: 10.1191/0959683602hl566ft

Cole, J. J., Prairie, Y. T., Caraco, N. F., McDowell, W. H., Tranvik, L. J., Striegl, R. G., et al. (2007). Plumbing the global carbon cycle: integrating inland waters into the terrestrial carbon budget. *Ecosystems* 10, 172–185. doi: 10.1007/s10021-006-9013-8

Colinvaux, P. A., De Oliveira, P. E., and Patiño, J. E. M. (1999). *Amazon: Pollen Manual and Atlas*. Dordrecht: Harwood Academic Publishers.

Conroy, J. L., Overpeck, J. T., Cole, J. E., Shanahan, T. M., and Steinitz-Kannan, M. (2008). Holocene changes in eastern tropical Pacific climate inferred from a Galápagos lake sediment record. *Quat. Sci. Rev.* 27, 1166–1180. doi: 10.1016/j.quascirev.2008.02.015

Cross, S. L., Baker, P. A., Seltzer, G. O., Fritz, S. C., and Dunbar, R. B. (2000). A new estimate of the Holocene lowstand level of Lake Titicaca, central Andes, and implications for tropical palaeohydrology. *Holocene* 10, 21–32. doi: 10.1191/095968300671452546

Davison, W. (1993). Iron and Manganese in lakes. *Earth Sci. Rev.* 34, 119–163. doi: 10.1016/0012-8252(93)90029-7

Dean, W. E., and Gorham, E. (1998). Magnitude and significance of carbon burial in lakes, reservoirs, and peatlands. *Geology* 26, 535–538. doi: 10.1130/0091-7613(1998)026<0535:MASOCB>2.3.CO;2

Dearing, J. A., Dann, R. J. L., Hay, K., Lees, J. A., Loveland, P. J., and Maher, B. A. (1996). Frequency-dependent susceptibility measurements of environmental materials. *Geophys J. Int.* 12, 228–240. doi: 10.1111/j.1365-246X.1996.tb06366.x

de Faria, F. A. M., Jaramillo, P., Sawakuchi, H. O., Richey, J. E., and Barros, N. (2015). Estimating greenhouse gas emissions from future Amazonian hydroelectric reservoirs. *Environ. Res. Lett.* 10:124019. doi: 10.1088/1748-9326/10/12/124019

Denys, L., Muylaert, K., Krammer, K., Joosten, T., Reid, M., and Rioual, P. (2003). Aulacoseira subborealis stat. nov. (Bacillariophyceae): a common but neglected plankton diatom. *Nov. Hedwigia* 77, 407–427. doi: 10.1127/0029-5035/2003/0077-0407

Engleman, E. E., Jackson, L. L., and Norton, D. R. (1985). Determination of carbonate carbon in geological materials by coulometric titration. *Chem. Geol.* 53, 125–128. doi: 10.1016/0009-2541(85)90025-7

Engstrom, D. R., and Wright, H. E. (1984). "Chemical stratigraphy of lake sediments as a record of environmental change," in *Lake Sediments and Environmental History,* eds E. Y. Haworth and J. W. G. Lund (Leicester: University of Leicester Press), 11–67.

EPE/MME (2007). *Plano Nacional de Energia 2030.* Rio de Janeiro: Empresa de Pesquisa Energética, Ministério de Minas e Energia, 1–408.

Erdtman, G. (1952). Pollen Morphology and Plant Taxonomy. *Geol. Föreningen i Stock. Förhandlingar* 74, 526–527. doi: 10.1080/11035895209453507

Fearnside, P. M. (2014). Impacts of Brazil's Madeira River Dams: unlearned lessons for hydroelectric development in Amazonia. *Environ. Sci. Policy* 38, 164–172. doi: 10.1016/j.envsci.2013.11.004

Field, C. B. (1998). Primary production of the biosphere: integrating terrestrial and oceanic components. *Science* 281, 237–240. doi: 10.1126/science.281.5374.237

Filippelli, G. M., Sierro, F. J., Flores, J. A., Vázquez, A., Utrilla, R., Pérez-Folgado, M., et al. (2003). A sediment-nutrient-oxygen feedback responsible for productivity variations in Late Miocene sapropel sequences of the western Mediterranean. *Palaeogeogr. Palaeoclimatol. Palaeoecol.* 190, 335–348. doi: 10.1016/S0031-0182(02)00613-2

Galbraith, R. F., Roberts, R. G., Laslett, G. M., Yoshida, H., Olley, J. M., Galbraith, R. F., et al. (1999). Optical dating of single and multiple grains of quartz from Jinmium rock shelter, Northern Australia: Part I, Experimetal design and statistical models. *Archaeometry* 41, 339–364. doi: 10.1111/j.1475-4754.1999.tb00987.x

Gourou, P. (1949). Observações geográficas na Amazônia. *Rev. Brasil. Geogr.* 11, 355–408.

Grimm, E. (1987). CONISS: a FORTRAN 77 program for stratigraphically constrained cluster analysis by the method of incremental sum of squares. *Comput. Geosci.* 13, 13–35.

Grimm, E. C. (2011). *TILIA software version 1.7.16*. Springfield: Illinois State Museum, Research and Collection Center.

Guérin, G., Mercier, N., and Adamiec, G. (2011). Dose-rate conversion factors: update. *Ancient TL* 29, 5–8.

Häggi, C., Sawakuchi, A. O., Chiessi, C. M., Mulitza, S., Mollenhauer, G., Sawakuchi, H. O., et al. (2016). Origin, transport and deposition of leaf-wax biomarkers in the Amazon Basin and the adjacent Atlantic. *Geochim. Cosmochim. Acta* 192, 149–165. doi: 10.1016/j.gca.2016.07.002

Hamilton, P. B., and Siver, P. A. (2010). A Morphological Investigation of Eunotia fennica (*Bacillariophyceae*) from a freshwater acidic pond in newfoundland, Canada. *Proc. Acad. Nat. Sci. Philadelphia* 160, 89–98. doi: 10.1635/053.160.0110

Herron, M. M. (1988). Geochemical classification of terrigenous sands and shales from core or log data. *J. Sediment. Res.* 58, 820–829.

Hodell, D. A., Brenner, M., and Curtis, J. H. (2005). Terminal Classic drought in the northern Maya lowlands inferred from multiple sediment cores in Lake Chichancanab (Mexico). *Quat. Sci. Rev.* 24, 1413–1427. doi: 10.1016/j.quascirev.2004.10.013

Irion, G., Bush, M. B., Nunes de Mello, J. A., Stüben, D., Neumann, T., Müller, G., et al. (2006). A multiproxy palaeoecological record of Holocene lake sediments from the Rio Tapajós, eastern Amazonia. *Palaeogeogr. Palaeoclimatol. Palaeoecol.* 240, 523–535. doi: 10.1016/j.palaeo.2006.03.005

Irion, G., de Mello, J. A. S. N., Morais, J., Piedade, M. T. F., Junk, W. J., and Garming, L. (2011). "Development of the Amazon Valley During the Middle to Late Quaternary: Sedimentological and Climatological Observations," in *Amazonian Floodplain Forests: Ecophysiology, Biodiversity and Sustainable Management*, eds J. W. Junk, F. M. T. Piedade, F. Wittmann, J. Schöngart, and P. Parolin (Dordrecht: Springer), 27–42.

Jackson, L. L., and Roof, S. R. (1992). Determination of the forms of carbon in geologic materials. *Geostand. Newsl.* 16, 317–323. doi: 10.1111/j.1751-908X.1992.tb00495.x

Jarvie, D. M. (1991). "Total organic carbon (TOC) analysis," in *Treatise of Petroleum Geology: Handbook of Petroleum Geology, Source and Migration Processes and Evaluation Techniques*, ed R. K Merrill (Tulsa, OK, American Association of Petroleum Geologists), 113–118.

Keim, G., Irion, G., Behling, H., Junk, W. J., and Nunes de Mello, J. (1999). "The sediment deposits of lago calado, a ria lake in central amazonia (Brazil), as indicator for postglacial water level rise of the Amazon river," *Extended Abstract*

(8 pages) in the Abstract-Volume (CD-Rom) of the International Symposium on "Hydrological and Geochemical Processes in Large Scale River Basins" (Manaus), 1–5.

Kelts, K., and Talbot, M. (1990). "Lacustrine carbonates as geochemical archives of environmental change and biotic/abiotic interactions," in Large Lakes: Ecological Structure and Function, eds M. M. Tilzer and C. Serruya (Berlin:Springer), 288–315.

Krammer, K. (2000). "The genus Pinnularia," in *Diatoms of the European Inland Waters and Comparable Habitats*, Vol. 1., ed H. Lange-Bertalot (A.R.G. Gantner Verlag), 1–703.

Latimer, J. C., and Filippelli, G. M. (2002). Eocene to Miocene terrigenous inputs and export production: geochemical evidence from ODP Leg 177, Site 1090. *Palaeogeogr. Palaeoclimatol. Palaeoecol.* 182, 151–164. doi: 10.1016/S0031-0182(01)00493-X

Latrubesse, E. M., Stevaux, J. C., and Sinha, R. (2005). Tropical rivers. *Geomorphology* 70, 187–206. doi: 10.1016/j.geomorph.2005.02.005

Mackereth, F. J. H. (1966). Some chemical observations on post-glacial lake sediments. *Philos. Trans. R. Soc. B Biol. Sci.* 250, 165–213. doi: 10.1098/rstb.1966.0001

McGlue, M. M., Silva, A., Corradini, F. A., Zani, H., Trees, M. A., Ellis, G. S., et al. (2011). Limnogeology in Brazil's "forgotten wilderness": a synthesis from the large floodplain lakes of the Pantanal. *J. Paleolimnol.* 46, 273–289. doi: 10.1007/s10933-011-9538-5

Meade, R. H., Rayol, J. M., Conceição, S. C., and Natividade, J. R. G. (1991). Backwater effects in the Amazon River Basin of Brazil. *Env. Geo. Water Sci.* 18, 105–114. doi: 10.1007/BF01704664

Metzeltin, D., and Lange-Bertalot, H. (2007). "Tropical Diatoms of South America II. Special remarks on biogeographic disjunction," in Iconographia Diatomologica, Annotated diatom micrographs, Vol. 18, ed H. Lange-Bertalot (Stuttgart: Koeltz Scientific Books), 1–877.

Moreira, L. S., Moreira-Turcq, P., Kim, J. H., Turcq, B., Cordeiro, R. C., Caquineau, S., et al. (2014). A mineralogical and organic geochemical overview of the effects of Holocene changes in Amazon River flow on three floodplain lakes. *Palaeogeogr. Palaeoclimatol. Palaeoecol.* 415, 152–164. doi: 10.1016/j.palaeo.2014.03.017

Moreira-Turcq, P., Jouanneau, J. M., Turcq, B., Seyler, P., Weber, O., and Guyot, J. L. (2004). Carbon sedimentation at Lago Grande de Curuai, a floodplain lake in the low Amazon region: insights into sedimentation rates. *Palaeogeogr. Palaeoclimatol. Palaeoecol.* 214, 27–40. doi: 10.1016/j.palaeo.2004.06.013

Moro, R. S., and Fürstenberger, C. B. (1997). *Catálogo dos Principais Parâmetros Ecológicos de Diatomáceas Não-Marinhas*. Ponta Grossa: UEPG, 1–282.

Murray, A. S., and Wintle, A. G. (2000). Luminescence dating of quartz using an improved single-aliquot regenerative-dose protocol. *Radiat. Meas.* 32, 57–73. doi: 10.1016/S1350-4487(99)00253-X

Prescott, J. R., and Hutton, J. T. (1994). Cosmic ray contributions to dose rates for luminescence and ESR dating: large depths and long-term time variations. *Radiat. Meas.* 23, 497–500. doi: 10.1016/1350-4487(94)90086-8

Rasera, M. F. F. L., Krusche, A. V., Richey, J. E., Ballester, M. V. R., and Victória, R. L. (2013). Spatial and temporal variability of pCO_2 and CO_2 efflux in seven Amazonian Rivers. *Biogeochemistry* 116, 241–259. doi: 10.1007/s10533-013-9854-0

R Core Team (2015). *R: A Language and Environment for Statistical Computing*. Available online at: http://www.r-project.org/.

Reimer, P. J., Bard, E., Bayliss, A., Beck, J. W., Blackwell, P. G., Bronk Ramsey, C., et al. (2013). IntCal13 and Marine13 Radiocarbon Age Calibration Curves 0–50,000 Years cal BP. *Radiocarbon* 55, 1869–1887. doi: 10.2458/azu_js_rc.55.16947

Richey, J. E., Melack, J. M., Aufdenkampe, A. K., Ballester, V. M., and Hess, L. L. (2002). Outgassing from Amazonian rivers and wetlands as a large tropical source of atmospheric CO_2. 6416, 6413–6416. doi: 10.1038/416617a

Ring, E. (1989). *The Preperation and Certification of Fourteen South African Silicate Rocks for Use as a Reference Materials*. MIntek Report M393.

Roubik, D. W., and Moreno, E. (1991). Pollen and spores of Barro Colorado Island [Panama]. *Monogr. Syst. Bot. Missouri Bot. Gard.* 36, 1–268.

Round, F. E., Crawford, R. M., and Mann, D. G. (1990). *Diatoms: Biology and Morphology of the Genera*. Cambridge: Cambridge University Press, 1–747.

Rowe, H., Hughes, N., and Robinson, K. (2012). The quantification and application of handheld energy-dispersive x-ray fluorescence (ED-XRF) in mudrock chemostratigraphy and geochemistry. *Chem. Geol.* 324, 122–131. doi: 10.1016/j.chemgeo.2011.12.023

Rumrich, U., Lange-Bertalot, H., and Rumrich, M. (2000). *Diatoms of the Andes (from Venezuela to Patagonia/Tierra del Fuego)*. Koenigstein: Koeltz Scientific Books, 1–649.

Sageman, B. B., Murphy, A. E., Werne, J. P., Ver Straeten, C. A., Hollander, D. J., and Lyons, T. W. (2003). A tale of shales: the relative roles of production, decomposition, and dilution in the accumulation of organic-rich strata, Middle–Upper Devonian, Appalachian basin. *Chem. Geol.* 195, 229–273. doi: 10.1016/S0009-2541(02)00397-2

Sawakuchi, A. O., Hartmann, G. A., Sawakuchi, H. O., Pupim, F. N., Bertassoli, D. J., Parra, M., et al. (2015). The Volta Grande do Xingu: reconstruction of past environments and forecasting of future scenarios of a unique Amazonian fluvial landscape. *Sci. Drill.* 3, 1–12. doi: 10.5194/sd-20-21-2015

Sawakuchi, H. O., Bastviken, D., Sawakuchi, A. O., Krusche, A. V., Ballester, M. V. R., and Richey, J. E. (2014). Methane emissions from Amazonian Rivers and their contribution to the global methane budget. *Glob. Chang. Biol.* 20, 2829–2840. doi: 10.1111/gcb.12646

Schulte, S., Mangelsdorf, K., and Rullkötter, J. (2000). Organic matter preservation on the Pakistan continental margin as revealed by biomarker geochemistry. *Org. Geochem.* 31, 1005–1022. doi: 10.1016/S0146-6380(00)00108-X

Scott, C., and Lyons, T. W. (2012). Contrasting molybdenum cycling and isotopic properties in euxinic versus non-euxinic sediments and sedimentary rocks: refining the paleoproxies. *Chem. Geol.* 324, 19–27. doi: 10.1016/j.chemgeo.2012.05.012

Sioli, H. (1984). "The Amazon and its main affluents: Hydrography, morphology of the river courses, and river types," in *The Amazon: Limnology and Landscape Ecology of a Mighty Tropical River and its Basin*, ed H. Sioli (Dordrecht: Springer), 127–165.

Stuiver, M., and Reimer, P. J. (1993). Extended ^{14}C Data base and revised CALIB 3.0 ^{14}C age calibration program. *Radiocarbon* 35, 215–230. doi: 10.1017/S0033822200013904

Tranvik, L. J., Downing, J. A., Cotner, J. B., Loiselle, S. A., Striegl, R. G., Ballatore, T. J., et al. (2009). Lakes and reservoirs as regulators of carbon cycling and climate. *Limnol. Oceanogr.* 54, 2298–2314. doi: 10.4319/lo.2009.54.6_part_2.2298

Tremarin, P. I. , Bertolli, L. M., de Faria, D. M., Costin, J. C., and Ludwig, T. A. V. (2009). Gomphonema Ehrenberg e Gomphosphenia Lange-Bertalot (Bacillariophyceae) do Rio Maurício, Paraná, Brasil. *Biota Neotropica* 9, 111–130. doi: 10.1590/S1676-06032009000400013

van Dam, H., Mertens, A., and Sinkeldam, J. (1994). A coded checklist and ecological indicator values of freshwater diatoms from the Netherlands. *Net. J. Aquat. Ecol.* 28, 117–133, doi: 10.1007/bf02334251

Vital, H., and Stattegger, K. (2000). Lowermost Amazon River: evidence of late quaternary sea-level fluctuations in a complex hydrodynamic system. *Quat. Int.* 72, 53–60. doi: 10.1016/S1040-6182(00)00020-3

Ward, N. D., Krusche, A. V., Sawakuchi, H. O., Brito, D. C., Cunha, A. C., Moura, J. M. S., et al. (2015). The compositional evolution of dissolved and particulate organic matter along the lower Amazon River-Óbidos to the ocean. *Mar. Chem.* 177, 244–256. doi: 10.1016/j.marchem.2015.06.013

Winemiller, K. O., McIntyre, P. B., Castello, L., Fluet-Chouinard, E., Giarrizzo, T., Nam, S., et al. (2016). Balancing hydropower and biodiversity in the Amazon, Congo, and Mekong. *Science* 351, 128–129. doi: 10.1126/science.aac7082

Zalat, A., and Vildary, S. S. (2007). Environmental change in Northern Egyptian Delta lakes during the late Holocene, based on diatom analysis. *J. Paleolimnol.* 37, 273–299. doi: 10.1007/s10933-006-9029-2

Conflict of Interest Statement: The authors declare that the research was conducted in the absence of any commercial or financial relationships that could be construed as a potential conflict of interest.

frontiers in Marine Science

ORIGINAL RESEARCH
published: 15 February 2017
doi: 10.3389/fmars.2017.00038

Flux of Dissolved and Particulate Low-Temperature Pyrogenic Carbon from Two High-Latitude Rivers across the Spring Freshet Hydrograph

Allison N. Myers-Pigg[1†], Patrick Louchouarn[1,2] and Roman Teisserenc[3]*

[1] Department of Oceanography, Texas A&M University, College Station, TX, USA, [2] Department of Marine Sciences, Texas A&M University at Galveston, Galveston, TX, USA, [3] EcoLab, Université de Toulouse, CNRS, Institute National Polytechnique de Toulouse, Université Paul Sabatier Toulouse, France

OPEN ACCESS

Edited by:
Nicholas David Ward,
University of Florida, USA

Reviewed by:
Rudolf Jaffe,
Florida International University, USA
Alysha Coppola,
University of Zurich, Switzerland

***Correspondence:**
Allison Myers-Pigg
anmp@tamu.edu

†Present Address:
Allison N. Myers-Pigg,
Memorial University of Newfoundland,
Department of Earth Sciences,
St. John's, NL, Canada

Specialty section:
This article was submitted to Marine Biogeochemistry, a section of the journal Frontiers in Marine Science

Received: 07 October 2016
Accepted: 31 January 2017
Published: 15 February 2017

Citation:
Myers-Pigg AN, Louchouarn P and Teisserenc R (2017) Flux of Dissolved and Particulate Low-Temperature Pyrogenic Carbon from Two High-Latitude Rivers across the Spring Freshet Hydrograph. Front. Mar. Sci. 4:38. doi: 10.3389/fmars.2017.00038

A number of recent studies have documented that pyrogenic carbon (PyC) is an integral and significant proportion of DOM in worldwide rivers. This material originates from all fractions of the PyC continuum, from highly condensed PyC to more functionalized components that retain some structural identity of fuel molecules. Understanding the transfer of PyC to river systems is paramount for Arctic regions, given the projected increase in frequency and intensity of forest fires within these ecosystems. However, the environmental distribution and concentration of soluble and particulate PyC, parameters that govern the overall fate of PyC in aquatic systems, has so far been unstudied. Here, we analyze the concentration and phase distribution of the anhydrosugar biomarker levoglucosan, as a proxy for low-temperature PyC, in two high-latitude river systems: a small sub-Arctic Canadian river, the Great Whale River in northern Québec, and the largest Arctic River, the Yenisei River in north-central Siberia. Low-temperature PyC, as estimated by levoglucosan concentrations, is exported predominantly in the dissolved phase. Peak export of low-temperature PyC occurs during the spring freshet period in both rivers. Seasonal variability of dissolved and particulate PyC export in each river elucidated that the export of PyC in the particulate and dissolved phases were temporally decoupled throughout the peak discharge events. While the present work confirms that levoglucosan is exported in particulate phase at a high enough level to enter sedimentary deposits and record historical wildfire signatures, as the phase distribution varies between rivers and during different flow regimes, spatial and temporal differences may affect the usage of levoglucosan as a PyC proxy in depositional settings.

Keywords: pyrogenic carbon, levoglucosan, freshet, Arctic Rivers, dissolved pyrogenic carbon, particulate pyrogenic carbon

INTRODUCTION

Vegetation fires affect carbon cycling in all major earth systems. These fires release 1.6–2.8 petagrams of carbon (Pg C) to the atmosphere worldwide (Santín et al., 2016), mostly as gaseous CO_2. However, inefficient combustion conditions in the environment regularly leave a proportion of the fire-affected carbon pool as carbonaceous residues, called pyrogenic carbon (PyC), which varies in molecular structure and environmental reactivity. The fate of pyrogenic carbon (PyC) in the environment, and the subsequent impact PyC has on carbon cycling, are a result of both its transport and degradation potential. As PyC is comprised of a continuum of materials, of which their formation and resulting chemical structures are temperature dependent (Masiello, 2004), the nature of PyC varies dramatically along the PyC continuum. The PyC continuum is marked by sequential changes in the proportion of chemical markers of combustion by-products, and increased aromatic condensation level (decreasing the ratio of Hydrogen to Carbon; H/C ratios) along temperature gradients (0–1,000°C; Kuo et al., 2008a,b, 2011a; Keiluweit et al., 2010; **Figure 1**). At low-temperatures (150–300°C), macropolymer dehydration and fragmentation leads to the release of free monomers and oligomers rich in −OH and −COOH functionalities (Kuo et al., 2008a,b, 2011a; Keiluweit et al., 2010; Harvey et al., 2012; Norwood et al., 2013). At these temperatures, the formation of anhydrosugars (levoglucosan and its isomers, mannosan, and galactosan) is prevalent (Kuo et al., 2008a; **Figure 1**). At intermediate temperatures (350–500°C), the rapid disappearance of recognizable plant lignocellulosic macromolecules, and the rapid drop in levoglucosan yields around 300–400°C (Kuo et al., 2008a, 2011a), occur synchronously with a steep increase in the proportion of amorphous aromatic structures (Keiluweit et al., 2010; Schneider et al., 2011; Harvey et al., 2012) as noted by the rapid decrease in H/C ratios and the rise in benzene polycarboxylic acids (BPCA), selective molecular markers of aromatic clusters (Ziolkowski and Druffel, 2010; Schneider et al., 2011; **Figure 1**). At the highest range of the temperature continuum (>500°C), PyC is characterized by increasing graphene-like structures in highly condensed

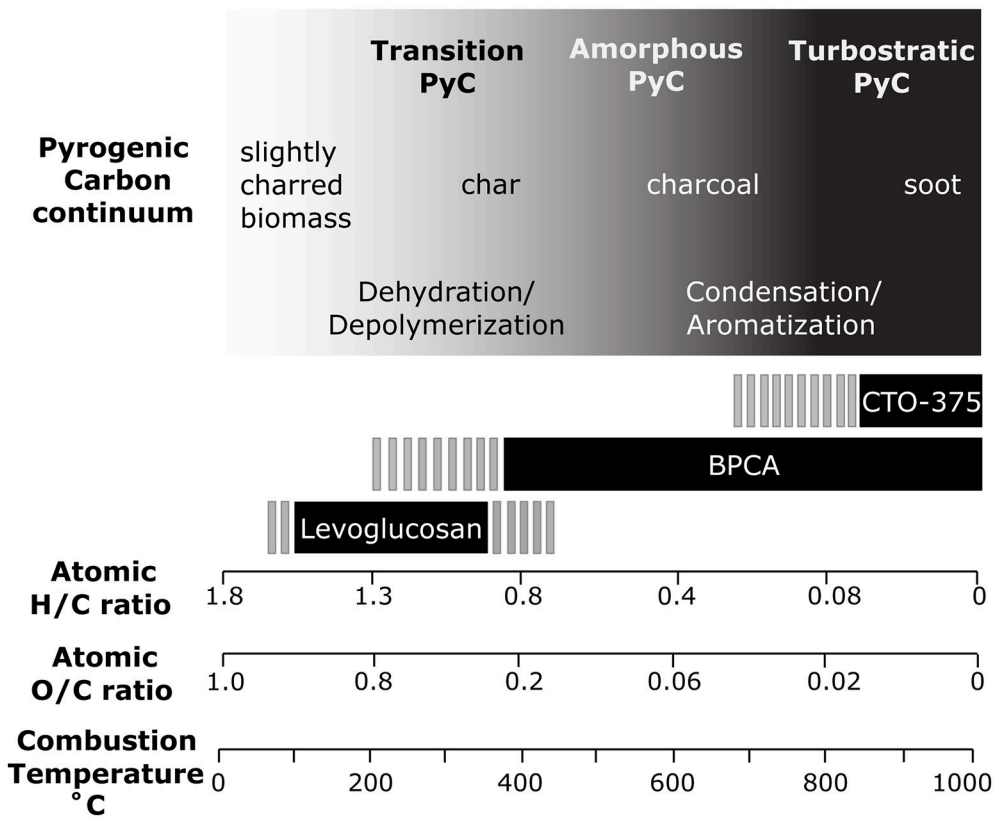

FIGURE 1 | Updated pyrogenic carbon continuum inspired by Masiello (2004), including modifications inspired by Kuo et al. (2008a) and Hammes et al. (2007). This figure includes changes in the proportion of chemical markers of combustion by-products and the increased aromatic condensation level observed in biomass chars along a heat treatment temperature (HTT) gradient (0–1,000°C; Keiluweit et al., 2010; Harvey et al., 2012). Decreasing H/C ratios and O/C ratios along the HTT are synthesized from Kuo et al. (2008a), Keiluweit et al. (2010), and Schneider et al. (2011). Note that these vary dependent on feedstock and the scales on this figure are non-linear. Biomarker ranges derived from a variety of sources: benzene polycarboxylic acids (BPCA) from Schneider et al. (2010) and Schneider et al. (2011), levoglucosan range from Kuo et al. (2008a) and upper limit uncertainty from Lakshmanan et al. (1970), Chemo-thermal oxidation (CTO-375) range from Kuo et al. (2008a).

turbostratic aromatics, marked by the increase in condensation levels of molecular markers such as BPCAs (Keiluweit et al., 2010; Schneider et al., 2011). This PyC-derived turbostratic carbon is relatively unordered (Nguyen et al., 2010) and is therefore structurally different than graphite found in natural environments, which is derived from high temperature and pressure conditions (such as within metamorphic rock) and is likely more ordered and highly crystalline (Brandes et al., 2008). High-temperature PyC can also be formed from the condensation of gas-phase intermediates (i.e., soot carbon; Schmidt and Noack, 2000; Hammes et al., 2007). As the lability of organic matter decreases along the PyC continuum (Ascough et al., 2011), the reactivity potential of PyC in the environment decreases with higher combustion temperatures (Masiello, 2004).

Wildfires are an important source of PyC to Arctic environments (Preston and Schmidt, 2006; Hansen et al., 2013; Santín et al., 2015). However, both the overall export and mechanisms for export of PyC within these systems is still an area of active research. Soil regimes in these systems vary widely; for example, the Yenisei River watershed is underlain by every type of permafrost regime, causing the soil active layer depth to vary dramatically within high latitude watersheds (Kawahigashi et al., 2004). It has been suggested that subsoil transport is a primary mechanism for PyC export from terrestrial to aquatic systems (Güereña et al., 2015), which may be regulated by soil-PyC associations. Czimczik and Masiello (2007) suggest that the ability of soil minerals to sorb PyC may be a main controller of PyC storage within soils, similar to bulk soil organic matter (SOM). When PyC is incorporated into soils, it may be associated with soil minerals (Hockaday et al., 2007; Knicker, 2011). PyC-mineral interactions observed on the surface of charcoals may also influence associations of PyC with minerals in the dissolved phase within soils (Hockaday et al., 2007), as soil mineral-DOM interactions affect the quantity of DOM exported from soil layers (Kaiser and Guggenberger, 2000; Kawahigashi et al., 2006). The distribution of PyC in Arctic soil profiles indicates vertical movement of PyC between soil layers (Guggenberger et al., 2008), pointing toward transport of Py-DOC within soil profiles. In many high-latitude systems, the highest PyC content within soils is associated with soil mineral layers (Rodionov et al., 2006; Guggenberger et al., 2008). In permafrost regions, DOM export is controlled by active layer thickness and extent of seasonally thawed mineral layers above permafrost regimes (Kawahigashi et al., 2004). These relationships within soils may affect both the phase and timing of PyC export to aquatic systems. Additionally, these processes may govern the turnover time of soil PyC, which is generally <100 years in boreal ecosystems (Hammes et al., 2008). This is much less than the millennial time-scales traditionally thought for PyC turnover in soils, and accounts for all loss processes (decomposition, leaching, erosion). Therefore, the translocation of PyC from soils into riverine systems is likely an important process for PyC cycling.

Export of high-temperature dissolved PyC (dissolved PyC will be henceforth referred to as Py-DOC; high temperature Py-DOC is also known as dissolved black carbon, or DBC) to aquatic systems does not appear to be controlled by fire history (Ding et al., 2013; Wagner et al., 2015), implying that high-temperature PyC needs to be functionalized before export, i.e., the solubility of high-temperature PyC is likely a function of charcoal age and exposure to "weathering" processes (Abiven et al., 2011). This idea is supported by the continual mobilization and export of high-temperature Py-DOC in deforested ecosystems long after slash-and-burn agriculture has stopped (Dittmar et al., 2012). However, as low-temperature Py-DOC also appears to be non-correlated to recent fire history (Myers-Pigg et al., 2015), the processes controlling the export of low- and high-temperature Py-DOC may be coupled. The relationship between Py-DOC from throughout the continuum and bulk DOC in Arctic river systems (Jaffe et al., 2013; Myers-Pigg et al., 2015; Stubbins et al., 2015) indicates that the mechanisms governing their export are similar. Therefore, it is likely that PyC export is controlled by similar processes as bulk organic matter. However, the temporal variability in PyC mobilization, as well as the variability of PyC export from the entire PyC continuum needs to be further explored before final conclusions on overall PyC export characteristics can be drawn. The export from terrestrial to aquatic systems is important to quantify in order to understand the impacts of PyC on carbon cycling (Masiello and Louchouarn, 2013).

Recent studies have documented the transfer of PyC to river systems in the dissolved and particulate phases, originating from all portions of the PyC continuum, from highly resistant PyC to more soluble, labile components (Dittmar et al., 2012; Jaffe et al., 2013; Myers-Pigg et al., 2015; Wagner et al., 2015; Wang et al., 2016). Understanding the transfer of PyC to aquatic systems is especially pertinent for Arctic regions, given the projected increase in frequency and intensity of boreal forest fires (Kasischke et al., 1995; Running, 2006; Soja et al., 2007) and a larger proportion of PyC created in these environments (Santín et al., 2015). The phase in which these materials are mobilized throughout the environment has implications on its availability for *in-situ* degradation/transformation, and ability for PyC to be stored in long-term carbon pools (Czimczik and Masiello, 2007; Santín et al., 2016). For example, PyC in the dissolved phase (Py-DOC) can be quickly remineralized (Stubbins et al., 2012; Ward et al., 2014; Myers-Pigg et al., 2015), while PyC in the particulate phase (Py-POC) may be buried in intermediate carbon pools along transport paths (such as river sediments) or on continental margins (Hunsinger et al., 2008; Cotrufo et al., 2016). Given the high potential for biological degradation of levoglucosan and other low-temperature PyC on environmentally relevant time scales (Norwood et al., 2013), one might expect that low-temperature PyC produced in the environment is quickly degraded *in-situ* during transport from terrestrial systems. However, a few studies have shown that biomarkers of low-temperature biomass combustion by-products (levoglucosan and isomers) can be found in sedimentary and soil records 100's–1,000's of years old and help trace fire events induced by climate cyclicity and/or anthropogenic activities (Elias et al., 2001; Hunsinger et al., 2008; Kuo et al., 2011b; Kirchgeorg et al., 2014; Gao et al., 2016). Chemical functionality of low-temperature PyC should favor mobilization and transport in the aqueous phase and therefore, preservation of low-temperature PyC and deposition into sedimentary records may be a function of source

and/or associations of low-temperature PyC with minerals or high-temperature PyC components.

Here, we present the first study to our knowledge that analyzes the phase distribution of low-temperature PyC, using levoglucosan as a biomarker proxy, in two high-latitude systems: a small sub-Arctic Canadian River, the Great Whale River, in northern Québec, and the largest Arctic River, the Yenisei River, in north-central Siberia throughout various flow regimes, to discover the evolution and relative importance of phase distribution on the export of low-temperature PyC in these high-latitude systems.

MATERIALS AND METHODS

For each river, we collected particulate and dissolved organic matter across the spring freshet period. Approximately 100 L of river water was pre-filtered for gross particulates (64 μm) in the field and transported to a field laboratory station in either in the village of Whapmagoostui-Kuujjuarapik for the Great Whale River (2012), or Igarka for the Yenisei River (2014), and immediately filtered using tangential flow filtration (TFF, 0.45 μm filter size) to separate the particulate and dissolved/colloidal phases. The particulate portion, 64–0.45 μm, was concentrated to around 1 litter and immediately frozen. The dissolved portion, <0.45 μm, was isolated using a portable reverse osmosis system (Serkiz and Perdue, 1990), and the concentrate was also frozen. Samples were then transported to the Laboratoire d'Écologie Fonctionnelle et Environnement (EcoLab) laboratory in Toulouse, France, for further treatment. The samples were all freeze-dried at EcoLab, France, and chemical analyses were performed at Texas A&M University at Galveston, USA.

Percent OC (% OC) was determined on vapor-phase acidified (to remove carbonates) freeze-dried subsamples on a Costech Elemental Analyzer. Freeze-dried subsamples were then analyzed for fire-derived biomarkers, monomeric lignin phenols (syringyl, cinnamyl, and vanillyl phenols) and anhydrosugars (levoglucosan, mannosan, galactosan), following methods outlined in Louchouarn et al. (2009), Shakya et al. (2011), and Myers-Pigg et al. (2015). Briefly, biomarkers were extracted from freeze-dried materials, pre-spiked with deuterated (*d*-7) levoglucosan (NIST SRM 2267), using 9:1 dichloromethane:methanol on an accelerated solvent extractor (ASE 200; Dionex) at 1500 PSI and 100°C. Sample were then concentrated in a RapidVap (LabConco) under Argon gas at 50°C, dried to completion in a CentriVap centrifugal concentrator (LabConco) at 50°C, and re-suspended in pyridine. Extracts were then derivatized for 15 min using O-bis (trimethylsilyl) trifluoroacetamide containing 1% trimethylchlorosilane (9:1 BSTFA:TMCS) at 75°C, and analyzed on a Varian triple quadrupole 480-300 GC-MS system using a fused silica column (J&W DB-5MS, 30 m × 0.25 mm i.d., 0.25 μm film thickness; Agilent Technologies). Each sample was injected splitless using helium as a carrier gas. Monomeric lignin phenol and anhydrosugar analyses were performed independently under single ion monitoring (SIM) mode, and using specific ions for compound determination. Sample detection limits, recoveries, and precision were determined through concurrently running blanks, standard reference materials (SRM 1649b), and replicates. All quality control parameters were within the ranges presented in Louchouarn et al. (2009).

Ratios of monomeric lignin phenols (syringyl/vanillyl: S/V) and anhydrosugars (levoglucosan to its isomer mannosan: L/M) were calculated to determine sources of PyC in the dissolved and particulate phases (**Table 1;** Kuo et al., 2008a; Myers-Pigg et al., 2015).

Low-temperature Py-DOC concentrations (**Table 1**) were calculated according to the methodology outlined in Myers-Pigg et al. (2015), using measured levoglucosan concentrations and a conversion factor based on the ratio of levoglucosan to low-temperature Py-DOC potentially present at the sampling site. Briefly, transit times were calculated between sample locations and average fire locations in each watershed to account for degradation during transit. The experimentally-derived ratio of levoglucosan to Py-DOC (Norwood et al., 2013), corresponding to each calculated transit time, was used to convert measured levoglucosan concentrations into an estimate of low-temperature Py-DOC in the rivers (Myers-Pigg et al., 2015). Fire locations were assumed to be concentrated at ∼52–53°N for the Yenisei River (Myers-Pigg et al., 2015; Ponomarev et al., 2016); the range of fire locations from 1980 to 2014 using fire data from the Canadian Forest Service (2016) were used for the Great Whale River (Figure S1). Error of fire location for each sampling point was propagated for the Py-DOC and Py-POC calculations (**Figure 3**).

To estimate the concentrations of low-temperature Py-POC in each river, mass-weighted distribution coefficients (K_ds; **Table 2**) were calculated by the following equation:

$$K_d = \frac{[l \text{ in POM mg kg}^{-1}]}{[l \text{ in DOM mg L}^{-1}]} \quad (1)$$

where the concentrations of levoglucosan (l) is measured in the isolated particulate and dissolved matter from each river (**Figure 2**; **Table 2**). Low-temperature Py-POC concentrations were then calculated using K_d values for levoglucosan calculated in Equation 1, substituting Py-DOC concentrations for l in

TABLE 1 | Average levoglucosan concentrations, low-temperature PyC concentrations, suspended particulate matter (SPM), and source signature ratios from free lignin phenols and anhydrosugars (syringyl/vanillyl: S/V and levoglucosan/mannosan: L/M) for the Yenisei River and Great Whale River.

	Yenisei River	Great Whale River
Dissolved Levoglucosan μg L^{-1}	0.057 ± 0.032	0.054 ± 0.053
Particulate Levoglucosan μg gdw^{-1}	0.27 ± 0.14	0.94 ± 0.34
Particulate Levoglucosan μg L^{-1}	0.002 ± 0.002	0.008 ± 0.011
Low-Temperature Py-DOC mg L^{-1}	0.02 ± 0.004	0.002 ± 0.0009
Low-Temperature Py-POC mg L^{-1}	0.001 ± 0.0002	0.001 ± 0.0004
SPM mg L^{-1}	11 ± 6.4	19 ± 32
S/V (Both Phases)	0.44 ± 0.21	0.29 ± 0.19
L/M (Both Phases)	4.2 ± 1.2	3.2 ± 3.7

TABLE 2 | LogK_d values for various PyC biomarkers in different systems.

	Watershed Size 10^6 km^2	Biomarker used	Average LogK_d L kg^{-1}
Poudre River (Wagner et al., 2015)	0.005	BPCA	4.0 ± 0.6
Great Whale River (This study)	0.043	Levoglucosan	4.4 ± 0.2
Smaller Rivers in Northwest Territories and Nunavut (Yunker et al., 2002)	0.083 ± 0.045	PAHs	4.5 ± 0.2
Mackenzie River/Delta (Yunker et al., 1994, 2002)	1.78	PAHs	4.8 ± 0.8
Yenisei River (This study)	2.54	Levoglucosan	3.7 ± 0.3
	Ocean Size 10^6 km^2		
Beaufort Sea (Yunker et al., 1994, 2002)	0.18	PAHs	6.3 ± 0.4
Pacific Ocean (Ziolkowski and Druffel, 2010; Coppola et al., 2014)	165.2	BPCA	5.8

*Systems are ordered by watershed/basin size. Note the similarities of LogK_d values of high and low-T PyC biomarkers in rivers, suggesting the export of the entire PyC continuum is linked. Data for partition coefficients is from Yunker et al. (1994, 2002); Ziolkowski and Druffel (2010); Coppola et al. (2014); Wagner et al. (2015) and this study (**Table 1**), and calculated using Equation (1).*

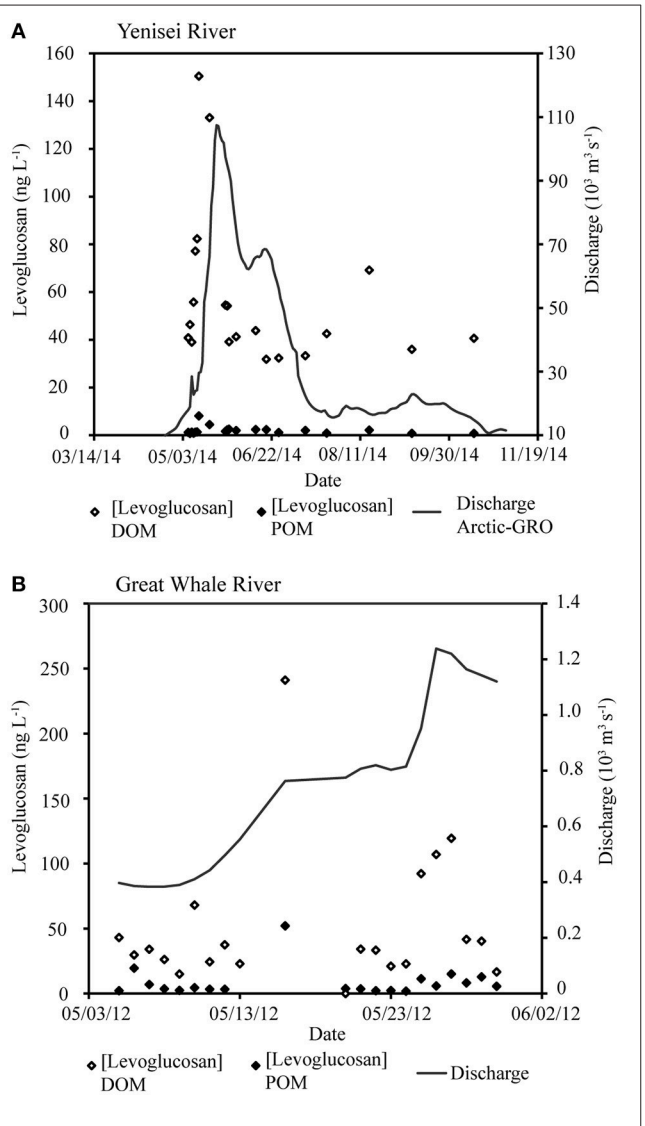

FIGURE 2 | (A) Levoglucosan concentrations throughout the freshet hydrograph in the Yenisei River in 2014, **(B)** the Great Whale River in 2012.

DOM in Equation 1 and solving for the concentration of Py-POC in mg kg^{-1}. These concentrations were then scaled to mg L^{-1} using total suspended solids (TSS; suspended particulate material, SPM) measured in mg L^{-1} (**Table 1**).

Fluxes of Py-DOC and Py-POC were calculated by scaling Py-DOC and Py-POC concentrations to discharge in each river (**Figure 3**). The percentage of flux in Py-DOC vs. in Py-POC was calculated by dividing the Py-POC flux calculated at a specific time point by the sum of Py-DOC and Py-POC fluxes at the same time point, multiplied by 100%(**Table 3**).

Low-temperature PyC phase distribution in these systems were also compared to high-temperature PyC phase distribution in other systems (**Table 2**), using concentrations of low- and high-temperature PyC biomarkers to calculate distribution coefficients as in Equation 1. These distribution coefficients are a reflection of the environmental distribution of PyC and, therefore, reflect all factors influencing this phase distribution, including source, association with minerals, and particle physical properties (such as surface area, porosity, number of reactive sites, etc.).

RESULTS

Arctic River

Levoglucosan concentrations in the dissolved and particulate phase increase with increasing discharge (**Figure 2**). Particulate organic carbon (POC) in the Yenisei River was 0.08 ± 0.02 kg OC kg^{-1} throughout the sampling period. Monomeric lignin phenol ratios (syringyl/vanillyl: S/V) are 0.44 ± 0.21 in the Yenisei River (**Table 1**), and the ratios of levoglucosan to its isomer mannosan (L/M) are 4.2 ± 1.2 (**Table 1**).

The timing of peak export of low-temperature Py-DOC and Py-POC were decoupled in the Yenisei River throughout the freshet period (**Figure 3**). Low-temperature Py-DOC peaks during the rising limb of the hydrograph, while low-temperature Py-POC peaks during the recession limb for the Yenisei River (**Figure 3**). LogK_d values, the measure of environmental phase distribution, for levoglucosan were nearly one order of magnitude lower during peak flow in the Yenisei River

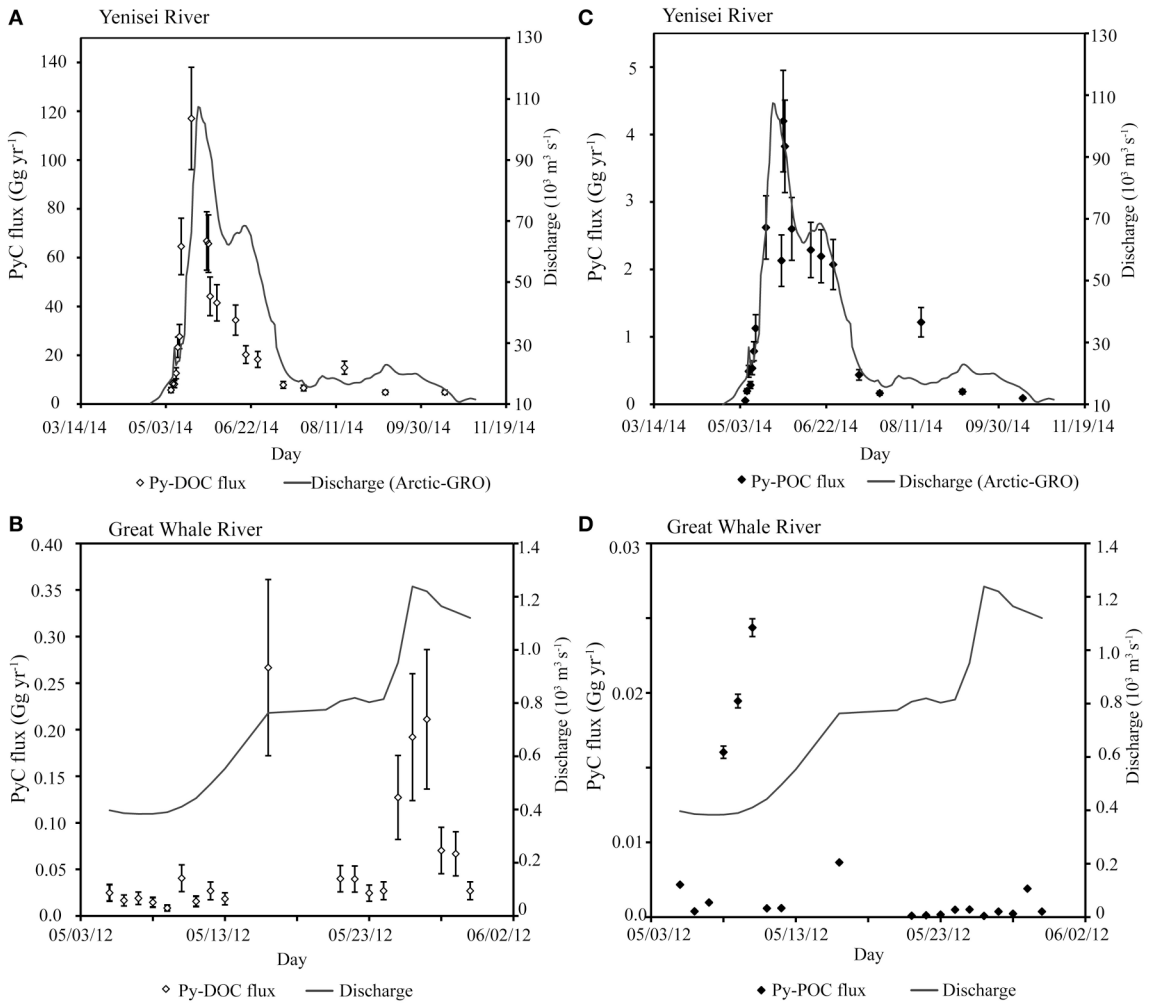

FIGURE 3 | PyC fluxes with discharge. (A) Py-DOC fluxes with discharge Yenisei River in 2014 **(B)** Py-DOC fluxes with discharge Great Whale River in 2012 **(C)** Py-POC fluxes with discharge Yenisei River in 2014 **(D)** Py-POC fluxes with discharge Great Whale River in 2012.

TABLE 3 | Average yearly flux estimates for Py-DOC and Py-POC, and average % PyC in the particulate phase for the Great Whale River and the Yenisei River.

River	Low-Temperature Py-DOC flux Gg yr^{-1}	Low-Temperature Py-POC flux Gg yr^{-1}	% PyC in particulate phase
Yenisei River	29.9 ± 5.27	1.4 ± 0.25	4.5 ± 2.8
Great Whale River	0.06 ± 0.02	0.003 ± 0.001	8.9 ± 17

(Figure S2) than during base flow, indicating a higher proportion of total PyC in the dissolved phase during high flow regimes. $LogK_d$ values of levoglucosan are within the same range as estimated $logK_d$ values for higher temperature PyC markers (BPCA) in rivers (**Table 2** and references therein).

Sub-Arctic River

POC in the Great Whale River was 0.17 ± 0.08 kg OC kg^{-1} throughout the sampling period. Monomeric lignin phenol ratios S/V are 0.29 ± 0.19 and L/M ratios are 3.2 ± 3.7 (**Table 1**). In the Great Whale River, the flux of levoglucosan and low-temperature Py-DOC increased with increasing discharge, while the flux of low-temperature Py-POC decreased with increasing discharge (**Figures 2**, **3**). $LogK_d$ values decreased with increasing discharge (Figure S2).

DISCUSSION

Characterization of Organic Matter and Pyrogenic Carbon

Free monomeric lignin phenol ratios in both phases (syringyl/vanillyl: S/V), coupled with levoglucosan and its isomer, mannosan (L/M), are within the range of values reported for gymnosperm source inputs in charcoals, aerosols, and soils, suggesting that low-temperature PyC in the Yenisei River and the Great Whale River in both phases are influenced predominantly by gymnosperm fire fuels (**Table 1**, source ratios from Kuo et al., 2011a). These ratios are consistent with previously reported

source reconstructions for Py-DOC in Arctic Rivers (Myers-Pigg et al., 2015).

Absolute concentrations of levoglucosan in the dissolved phase are on the lower end of the range previously reported in river DOM. For the Yenisei River, concentrations in this study are 0.06 ± 0.04 μg L^{-1} vs. 0.8 ± 0.5 μg L^{-1} from 2004 to 2006 (Myers-Pigg et al., 2015). Differences in the observed concentrations may be dependent on interannual variability in the mechanisms that govern export of PyC, such as hydrological flow regimes. However, further research must be done to ascertain the varying importance of the mechanisms that control PyC export to and through aquatic systems. Concentrations of levoglucosan in the particulate phase of the studied rivers are also low (**Figure 2**; **Table 2**, 0.73 ± 1.1 μg gdw^{-1}) compared to concentrations of levoglucosan in surface sediments from a river plume (1.3–6.9 μg gdw^{-1}) of a small, mountainous stream (Hunsinger et al., 2008). It should be noted that erosion, resuspension, and deposition of PyC along transport is particularly high in mountainous systems (Cotrufo et al., 2016). This may affect the total amount of PyC transported in the particulate phase to estuarine systems compared to the relatively larger river systems in this study, which also have relatively smaller proportions of total carbon exported in the particulate phase.

Differences in Phase Distribution throughout the Hydrograph

In watersheds that contain permafrost coverage (such as the watersheds in this study), the permafrost can act as a boundary layer, causing rapid translocation of water to river systems during spring thaw events, which influences SOM transport to rivers. The depth of the soil active layer, in which organic matter has the ability to exchange with the surface terrestrial ecosystem, though generally quite shallow in these regions, tends to vary based on location within a basin. In a subwatershed of the Yenisei River, storage of PyC is largest in areas with permafrost and shallow active layers, whereas mineral soils with thick active layer or lacking permafrost stored less PyC, suggesting increased mobility of PyC from the latter (Guggenberger et al., 2008). The same study showed that most of the export of PyC occurs during the period of snowmelt with dominance of surface flow pointing to a strong relationship between PyC concentrations and hydrological regime. This may help to explain the observed lack of relationship between fire frequency and riverine export of dissolved black carbon (DBC as determined by BPCAs; Ding et al., 2013, 2014), and the strong reported relationships between DBC and hydrological cycling (Jaffe et al., 2013), particularly in Arctic systems (Stubbins et al., 2015).

Here, low-temperature Py-DOC peaks during the rising limb of the hydrograph in the Yenisei River (**Figure 3A**). This early peak of low-temperature Py-DOC is not mirrored in bulk DOC concentrations, which increase linearly with discharge ($R^2 = 0.82$, $p < 0.001$; graph not shown). This apparently "early" release of Py-DOC has not been previously observed, as Py-DOC from both high and low-temperature portions of the continuum have been previously correlated to discharge and DOC in these and other systems (Jaffe et al., 2013; Myers-Pigg et al., 2015; Stubbins et al., 2015). However, here we present the first dataset with targeted high resolution sampling during spring peak flow. Hence, the decoupling of Py-DOC and DOC during the rising limb may be a phenomenon not previously captured. During the rest of the hydrograph (low flow, peak flow, and the falling limb) low-temperature Py-DOC is correlated to bulk DOC ($R^2 = 0.63$, $p < 0.001$), as has been previously observed. Therefore, further high-resolution sampling is needed to understand Py-DOC dynamics during the early part of the spring freshet period in other years to determine if the periodic decoupling of Py-DOC and DOC is systematic or only an isolated case. This decoupling of low-temperature Py-DOC and DOC in the rising limb of the hydrograph may be linked to the mobilization of a different source of Py-DOC during this period than during other flow regimes.

Although very little research has been done on the transport of particulate PyC from river systems, it has been suggested that transport in this phase may be of importance in recently fire-affected ecosystems (Wagner et al., 2015), where increased surface run off (Moody et al., 2013), soil erosion (Shakesby and Doerr, 2006), and increases in TSS (Ryan et al., 2011) have been observed. In the study regions, particulate carbon export is often a small proportion of the total carbon export; POC export accounts for ∼15% of the total OC flux from the pan-Arctic per year (Holmes et al., 2012; McClelland et al., 2016). Around 23% of the total POC export occurs during the spring freshet period in both the Great Whale River and Yenisei River (Hudon et al., 1996; McClelland et al., 2016), making high-resolution sampling important to capture temporal variability in the Py-POC flux. As previous work estimates that Py-POC export in Arctic Rivers is between 3 and 9% of total POC fluxes (Elmquist et al., 2008), transport of Py-POC may be an important portion of the total POC in Arctic Rivers. Here, we find that low-temperature Py-POC comprises 4.5 ± 2.8% of the low-temperature PyC flux from the Yenisei River (**Figure 3**; **Table 3**). These relatively lower levels of export of low-temperature Py-POC in our systems has implications for the usage of levoglucosan to track fire activity in depositional records, as low-temperature PyC determined from levoglucosan is exported predominantly in the dissolved phase. In the Yenisei River, low-temperature Py-POC export peaks during the falling limb of the freshet hydrograph (**Figure 3C**), which may reflect varying sources of PyC between phases or variations in export mechanisms between the two phases. For example, the composition and bioavailability of OM exported from soils in high-latitude systems is a function of active layer depth and mineral soil association (Kawahigashi et al., 2006). Terrestrial organic carbon (as determined by n-alkanoic acids) in the particulate phase has been found to associate with two distinct pools of soil carbon released during the spring freshet period; a young pool dominated by humics and an old pool with a mineral soil component (Vonk et al., 2010). This observed difference in mobilization of terrestrial OC may also influence the mobilization of PyC in high-latitude systems, which in turn, affects availability for transformations during transport, as a large portion of labile materials, if associated with a mineral layer, may be protected from biodegradation during transport (Hedges

et al., 1997; Kaiser and Guggenberger, 2000; Vonk et al., 2010). During the freshet period, low-temperature PyC is proportionally exported more in the dissolved phase than during low-flow (**Figure 3**; Figure S2). This may be due to hydrophilic DOM, such as low-temperature PyC (chemical functionality in **Figure 1**), bypassing association with soils within the active layer, and directly entering the aquatic system (Kawahigashi et al., 2006) during high-flow regimes. Because high-flow regimes release the largest proportion of yearly DOM and POM during a relatively short time period (Amon et al., 2012; Holmes et al., 2012; McClelland et al., 2016), these flow regimes are similarly expected to contribute substantially to the overall flux of PyC from high-latitude rivers. Additionally, since PyC is predominantly released in the dissolved phase, this may allow highly functionalized and hydrophilic portions of PyC to be more accessible to *in-situ* microbial degradation and lead to increased riverine respiration rates during this period (Masiello and Louchouarn, 2013).

In the Great Whale River, physical protection of PyC may regulate its release from soils. Only around 10% of the total DOC is released in this river system during the ice break-up period (Hudon et al., 1996), as opposed to almost half of the DOC released from the major Arctic Rivers during the spring freshet period (Holmes et al., 2012). This observation suggests that the timing and release of organic matter from small southern boreal watersheds are driven by different controls than those operating in the major Arctic Rivers. The flux of organic matter may be normalized in these latter systems by the size of the watersheds, whereas soil heterogeneities in smaller southern boreal watersheds may show a strong influence of soil processes. For example, in southern boreal forests, accumulation of large, long-lived stocks of PyC have been observed in mineral horizons with little to no soil profile development (Miesel et al., 2015). The opposite has been reported in boreal forests containing mineral soils underlying thick active layers (Guggenberger et al., 2008). The Great Whale River watershed is itself highly heterogeneous and contains a variety of soil types including discontinuous permafrost (Bhiry et al., 2011). However, and in conjunction with high fire return intervals, the export of PyC from this watershed may be more regulated by soil processes than hydrological flow regimes, as highlighted by the lack of a clear relationship of PyC export with hydrography (**Table 3**; **Figure 3**).

Implications for the Entire Pyrogenic Carbon Continuum

The similarity between phase distribution calculated for high-temperature PyC components (BPCA and PAHs) and low-temperature PyC (levoglucosan) suggest that low- and high-temperature PyC may be exported similarly from river systems (**Table 2**). However, as physical weathering has been shown to be an important loss process for both high- and low-temperature charcoals, although on very different time scales (Naisse et al., 2015), understanding the ages of these exported carbon pools is necessary before final conclusions on their similarities can be determined. Additionally, given the fact that bulk DOC and POC in Arctic River systems have vastly different ages (e.g., Goñi et al., 2005; Amon et al., 2012), we must understand the sources and ages of dissolved and particulate PyC in order to fully understand how export of Py-DOC and Py-POC might be linked both temporally and throughout the PyC continuum. For example, high-temperature PyC (as determined by the CTO-375 method; PyC range covered by the method in **Figure 1**) has been found to contain two distinct sources between the particulate and dissolved phases in river systems (Wang et al., 2016), and much of this high-temperature PyC can be derived from fossil fuels (up to 33% of the DBC and around 50% of the PBC). In contrast, the sources of low-temperature PyC (derived from biomass burning) using biomarker source ratios appear to be similar in our studied rivers (S/V and L/M; suggesting gymnosperm sources in both phases). Therefore, it may become important to characterize potential variability of PyC generation during biomass burning and its effects on PyC mobilization. Isotopic approaches may help identify some of this variability (e.g., isotopic fractionation of levoglucosan occurs during atmospheric processes; Sang et al., 2016).

The apparent order of magnitude increase in the ratio of Py-DOC to Py-POC for high-temperature PyC from rivers to oceans (**Table 2**; calculated from Ziolkowski and Druffel, 2010; Coppola et al., 2014; Wagner et al., 2015) suggests that Py-POC plays an increasingly important role in PyC cycling through transport from riverine to oceanic systems. This may be due to the potential degradation of dissolved PyC during transit (Stubbins et al., 2012; Masiello and Louchouarn, 2013; Ward et al., 2014; Myers-Pigg et al., 2015) and/or the importance sorption of Py-DOC to Py-POC in marine systems (Coppola et al., 2014). Sorption processes and transfer to sediments are considered as one of the major loss processes for Py-DOC in the world's ocean (Coppola et al., 2014). Py-DOC exported from Arctic Rivers could sorb to sinking particulates once it enters the Arctic Ocean. This has implications on how much Py-DOC may survive transport and end up in regions of North Atlantic Deep Water formation (Stubbins et al., 2015), vs. what is sorbed to sinking particles and buried on the vast Arctic continental shelves. Measures of Py-POC in Arctic Ocean sediments and sinking particles (using CTO-375 method) suggest that Py-POC quickly sinks and is stored within coastal margins (Fang et al., 2016). To understand loss terms and PyC cycling, the relative proportion of all component of the PyC continuum in the dissolved and particulate phases during transfer to and within ocean systems must be further explored.

Flux Estimates from Rivers for Arctic Pyrogenic Carbon

The percentage of the total PyC flux from these rivers in the particulate phase varies dramatically throughout the hydrograph. During low-flow stages ($<2 \times 10^4$ m^3 s^{-1}), low-temperature Py-POC was 3.1 $\pm$ 2.3% of the total PyC flux in the Yenisei River, while during high flow low-temperature Py-POC was 5.1 $\pm$ 2.8% of this flux. This is much less than a calculated distribution of Py-POC in worldwide flux estimates (~16% of total PyC flux from rivers; Santín et al., 2016). This is also lower than previous estimates of Py-POC fluxes from the pan-Arctic (~8% of total PyC flux) using pan-Arctic Py-POC

flux estimates calculated using BC/POC ratios from Elmquist et al. (2008) and pan-Arctic POC fluxes from McClelland et al. (2016) and pan-Arctic Py-DOC fluxes from Stubbins et al. (2015). However, as our estimates measure *in-situ* phase distribution based on biomarker composition within rivers, they can represent a conservative estimate of the amount of Py-POC exported from the studied Arctic Rivers. Additionally, previous Py-POC flux estimates from Arctic Rivers rely on measurements of the most refractory PyC (using the CTO-375 method; see **Figure 1** for range of detection within the PyC continuum) in estuarine sediments to estimate *in-situ* Py-POC fluxes (see Elmquist et al. (2008) for further explanation of previous Py-POC flux calculations). As refractory PyC analytical methods (such as CTO-375 method) may overestimate PyC contribution in environmental samples (Hammes et al., 2007), higher temperature PyC can be derived from both fossil fuel combustion and biomass burning, and the most refractory portion of the PyC continuum measured by these techniques may be more particle associated than other forms of PyC, the previously reported flux estimates may overestimate the actual distribution of PyC transported from Arctic Rivers. In environments where POC export is a proportionally important part of the TOC flux, the relative influence of Py-POC on the total export of PyC from the region may be of higher significance. For example, in the Great Whale River, total POC export accounts 18.9% of the total OC export (Hudon et al., 1996), slightly higher than the average Arctic River system (∼15%; Holmes et al., 2012; McClelland et al., 2016). In this river system, Py-POC was 8.9 ± 17.5% of the total PyC flux (**Figure 3**; **Table 3**). The export of low-temperature PyC varied with the hydrograph (**Figure 3**), implying that the export of PyC in the particulate phase varies throughout the year. This is important to consider when looking at PyC in deposited sedimentary records and estimating the impact of fire on past climate, as the records of these signatures may vary with hydrographic regimes and particulate matter loadings.

Considering the changing fire regimes in the Arctic (Kelly et al., 2015), the intrinsic tie of Py-DOC with discharge in the region (Myers-Pigg et al., 2015; Stubbins et al., 2015), and changing hydrological regimes (Wrona et al., 2016), the transport of PyC from Arctic terrestrial to aquatic systems is likely to increase. As the Arctic Ocean continental margins have recently been suggested as an efficient location for PyC burial (Fang et al., 2016), understanding the phase distribution of PyC during transport through rivers and estuaries is relevant for understanding overall PyC fluxes, the potential degradation of PyC during transit, and losses of PyC from the active carbon cycle through burial into sediments.

AUTHOR CONTRIBUTIONS

All authors contributed to experimental design for this study. RT and AM collected and processed the samples. AM and PL interpreted the data and prepared the manuscript. All authors participated in revisions and approved the final manuscript.

FUNDING

This project was funded under the TOMCAR-Permafrost Marie Curie International Reintegration Grant FP7-PEOPLE-2010-RG (project reference: 277059) within the Seventh European Community Framework Programme awarded to RT (http://www.tomcar.fr). Yenisei River daily discharge data was provided by the Arctic Great Rivers Observatory (NSF-1107774). Travel and living expenses were also funded thanks to GDRI Car-Wet-Sib II and INP-Toulouse SMI program.

ACKNOWLEDGMENTS

We thank the Chateaubriand Fellowship Program led by the Office for Science and Technology of the Embassy of France in the United States, which provided funding for AM to spend 6 months at EcoLab in France. We thank Nikita Tananaev for his assistance while in Igarka, including sampling, coordination and use of field facilities. The Melnikov Permafrost Institute is thanked for their hospitality and support of this research. Sample collection and transport could not have been possible without the hard work of countless amazing people, including those in Toulouse at EcoLab, the team at ULISSE, Elena Fedorova, the entire Geocryology Laboratory team in Igarka, and particularly Anatolii Pimov. We thank R. Amon, K. Kaiser, and M. Norwood for helpful comments on earlier versions of this manuscript. Figure S1 was created with assistance from M. Norwood. We also thank two reviewers for their constructive and helpful comments on this manuscript. Open access publication fees were supported in part by the Gordon and Betty Moore Foundation.

SUPPLEMENTARY MATERIAL

The Supplementary Material for this article can be found online at: http://journal.frontiersin.org/article/10.3389/fmars.2017.00038/full#supplementary-material

REFERENCES

Abiven, S., Hengartner, P., Schneider, M. P. W., Singh, N., and Schmidt, M. W. I. (2011). Pyrogenic carbon soluble fraction is larger and more aromatic in aged charcoal than in fresh charcoal. *Soil Biol. Biochem.* 43, 1615–1617. doi: 10.1016/j.soilbio.2011.03.027

Amon, R. M. W., Rinehart, A. J., Duan, S., Louchouarn, P., Prokushkin, A., Guggenberger, G., et al. (2012). Dissolved organic matter sources in large Arctic Rivers. *Geochim. Cosmochim. Acta* 94, 217–237. doi: 10.1016/j.gca.2012.07.015

Ascough, P., Bird, M., Francis, S., Thornton, B., Midwood, A., Scott, A., et al. (2011). Variability in oxidative degradation of charcoal: influence of production conditions and environmental exposure. *Geochim. Cosmochim. Acta* 75, 2361–2378. doi: 10.1016/j.gca.2011.02.002

Bhiry, N., Delwaide, A., Allard, M., Bégin, Y., Filion, L., Lavoie, M., et al. (2011). Environmental change in the great whale river region, Hudson Bay: five decades

of multidisciplinary research by Centre d'études Nordiques (CEN). *Ecoscience* 18, 182–203. doi: 10.2980/18-3-3469

Brandes, J. A., Cody, G. D., Rumble, D., Haberstroh, P., Wirick, S., and Gelinas, Y. (2008). Carbon K-edge XANES spectromicroscopy of natural graphite. *Carbon* 46, 1424–1434. doi: 10.1016/j.carbon.2008.06.020

Canadian Forest Service (2016). *National Fire Database — Agency Fire Data*. Natural Resources Canada, Canadian Forest Service, Northern Forestry Centre, Edmonton, AB. Available online at: http://cwfis.cfs.nrcan.gc.ca/ha/nfdb

Coppola, A. I., Ziolkowski, L. A., Masiello, C. A., and Druffel, E. R. M. (2014). Aged black carbon in marine sediments and sinking particles. *Geophys. Res. Lett.* 41, 2427–2433. doi: 10.1002/2013GL059068

Cotrufo, M. F., Boot, C. M., Kampf, S., Nelson, P. A., Brogan, D. J., Covino, T., et al. (2016). Redistribution of pyrogenic carbon from hillslopes to stream corridors following a large montane wildfire. *Global Biogeochem. Cycles* 30, 1348–1355. doi: 10.1002/2016GB005467

Czimczik, C. I., and Masiello, C. A. (2007). Controls on black carbon storage in soils. *Global Biogeochem. Cycles* 21:GB3005. doi: 10.1029/2006GB002798

Ding, Y., Watanabe, A., and Jaffé, R. (2014). Dissolved black nitrogen (DBN) in freshwater environments. *Org. Geochem.* 68, 1–4. doi: 10.1016/j.orggeochem.2013.12.009

Ding, Y., Yamashita, Y., Dodds, W. K., and Jaffé, R. (2013). Dissolved black carbon in grassland streams: is there an effect of recent fire history? *Chemosphere* 90, 2557–2562. doi: 10.1016/j.chemosphere.2012.10.098

Dittmar, T., de Rezende, C. E., Manecki, M., Niggemann, J., Ovalle, A. R. C., Stubbins, A., et al. (2012). Continuous flux of dissolved black carbon from a vanished tropical forest biome. *Nat. Geosci.* 5, 618–622. doi: 10.1038/ngeo1541

Elias, V. O., Simoneit, B. R. T., Cordeiro, R. C., and Turcq, B. (2001). Evaluating levoglucosan as an indicator of biomass burning in Carajas, Amazonia: a comparison to the charcoal record. *Geochim. Cosmochim. Acta* 65, 267–272. doi: 10.1016/S0016-7037(00)00522-6

Elmquist, M., Semiletov, I., Guo, L., and Gustafsson, Ö. (2008). Pan-Arctic patterns in black carbon sources and fluvial discharges deduced from radiocarbon and PAH source apportionment markers in estuarine surface sediments. *Global Biogeochem. Cycles* 22:GB2018. doi: 10.1029/2007GB002994

Fang, Z., Yang, W., Chen, M., Zheng, M., and Hu, W. (2016). Abundance and sinking of particulate black carbon in the western Arctic and Subarctic Oceans. *Sci. Rep.* 6:29959. doi: 10.1038/srep29959

Gao, X., Norwood, M., Frederick, C., McKee, A., Masiello, C. A., and Louchouarn, P. (2016). Organic geochemical approaches to identifying formation processes for middens and charcoal-rich features. *Org. Geochem.* 94, 1–11. doi: 10.1016/j.orggeochem.2016.01.007

Goñi, M. A., Yunker, M. B., Macdonald, R. W., and Eglinton, T. I. (2005). The supply and preservation of ancient and modern components of organic carbon in the Canadian Beaufort Shelf of the Arctic Ocean. *Mar. Chem.* 93, 53–73. doi: 10.1016/j.marchem.2004.08.001

Güereña, D. T., Lehmann, J., Walter, T., Enders, A., Neufeldt, H., Odiwour, H., et al. (2015). Terrestrial pyrogenic carbon export to fluvial ecosystems: lessons learned from the white Nile watershed of East Africa. *Global Biogeochem. Cycles* 29, 1911–1928. doi: 10.1002/2015GB005095

Guggenberger, G., Rodionov, A., Shibistova, O., Grabe, M., Kasansky, O. A., Fuchs, H., et al. (2008). Storage and mobility of black carbon in permafrost soils of the forest tundra ecotone in Northern Siberia. *Glob. Chang. Biol.* 14, 1367–1381. doi: 10.1111/j.1365-2486.2008.01568.x

Hammes, K., Schmidt, M. W. I., Smernik, R. J., Currie, L. A., Ball, W. P., Nguyen, T. H., et al. (2007). Comparison of quantification methods to measure fire-derived (black/elemental) carbon in soils and sediments using reference materials from soil, water, sediment and the atmosphere. *Global Biogeochem. Cycles* 21:GB3016. doi: 10.1029/2006GB002914

Hammes, K., Torn, M. S., Lapenas, A. G., and Schmidt, M. W. I. (2008). Centennial black carbon turnover observed in a Russian steppe soil. *Biogeosciences* 5, 1339–1350. doi: 10.5194/bg-5-1339-2008

Hansen, M. C., Potapov, P. V., Moore, R., Hancher, M., Turubanova, S. A., Tyukavina, A., et al. (2013). High-resolution global maps of 21st-century forest cover change. *Science* 342, 850–853. doi: 10.1126/science.1244693

Harvey, O. R., Kuo, L. J., Zimmerman, A. R., Louchouarn, P., Amonette, J. E., and Herbert, B. E. (2012). An index-based approach to assessing recalcitrance and soil carbon sequestration potential of engineered black carbons (biochars). *Environ. Sci. Technol.* 46, 1415–1421. doi: 10.1021/es2040398

Hedges, J. I., Keil, R. G., and Benner, R. (1997). What happens to terrestrial organic matter in the ocean? *Org. Geochem.* 25, 195–212. doi: 10.1016/S0146-6380(97)00066-1

Hockaday, W. C., Grannas, A. M., Kim, S., and Hatcher, P. G. (2007). The transformation and mobility of charcoal in a fire-impacted watershed. *Geochim. Cosmochim. Acta* 71, 3432–3445. doi: 10.1016/j.gca.2007.02.023

Holmes, R. M., McClelland, J. W., Peterson, B. J., Tank, S. E., Bulygina, E., Eglinton, T. I., et al. (2012). Seasonal and annual fluxes of nutrients and organic matter from large rivers to the Arctic ocean and surrounding seas. *Estuaries Coasts* 35, 369–382. doi: 10.1007/s12237-011-9386-6

Hudon, C., Morin, R., Bunch, J., and Harland, R. (1996). Carbon and nutrient output from the great Whale river (Hudson Bay) and a comparison with other rivers around Quebec. *Can. J. Fish. Aquat. Sci.* 53, 1513–1525. doi: 10.1139/f96-080

Hunsinger, G. B., Mitra, S., Warrick, J. A., and Alexander, C. R. (2008). Oceanic loading of wildfire-derived organic compounds from a small mountainous river. *J. Geophys. Res. Biogeosci.* 113:G02007. doi: 10.1029/2007JG000476

Jaffe, R., Ding, Y., Niggemann, J., Vahatalo, A. V., Stubbins, A., Spencer, R. G., et al. (2013). Global charcoal mobilization from soils via dissolution and riverine transport to the oceans. *Science* 340, 345–347. doi: 10.1126/science.1231476

Kaiser, K., and Guggenberger, G. (2000). The role of DOM sorption to mineral surfaces in the preservation of organic matter in soils. *Org. Geochem.* 31, 711–725. doi: 10.1016/S0146-6380(00)00046-2

Kasischke, E. S., Christensen, N. L., and Stocks, B. J. (1995). Fire, global warming and the carbon balance of boreal forests. *Ecol. Appl.* 5, 437–451. doi: 10.2307/1942034

Kawahigashi, M., Kaiser, K., Kalbitz, K., Rodionov, A., and Guggenberger, G. (2004). Dissolved organic matter in small streams along a gradient from discontinuous to continuous permafrost. *Glob. Chang. Biol.* 10, 1576–1586. doi: 10.1111/j.1365-2486.2004.00827.x

Kawahigashi, M., Kaiser, K., Rodionov, A., and Guggenberger, G. (2006). Sorption of dissolved organic matter by mineral soils of the Siberian forest tundra. *Glob. Chang. Biol.* 12, 1868–1877. doi: 10.1111/j.1365-2486.2006.01203.x

Keiluweit, M., Nico, P. S., Johnson, M. G., and Kleber, M. (2010). Dynamic molecular structure of plant biomass-derived black carbon (biochar). *Environ. Sci. Technol.* 44, 1247–1253. doi: 10.1021/es9031419

Kelly, R., Genet, H., McGuire, A. D., and Hu, F. S. (2015). Palaeodata-informed modelling of large carbon losses from recent burning of boreal forests. *Nat. Clim. Chang.* 6, 79–82. doi: 10.1038/nclimate2832

Kirchgeorg, T., Schupbach, S., Kehrwald, N., McWethy, D. B., and Barbante, C. (2014). Method for the determination of specific molecular markers of biomass burning in lake sediments. *Org. Geochem.* 71, 1–6. doi: 10.1016/j.orggeochem.2014.02.014

Knicker, H. (2011). Pyrogenic organic matter in soil: its origin and occurrence, its chemistry and survival in soil environments. *Quaternary Int.* 243, 251–263. doi: 10.1016/j.quaint.2011.02.037

Kuo, L.-J., Herbert, B. E., and Louchouarn, P. (2008a). Can levoglucosan be used to characterize and quantify char/charcoal black carbon in environmental media? *Org. Geochem.* 39, 1466–1478. doi: 10.1016/j.orggeochem.2008.04.026

Kuo, L.-J., Louchouarn, P., and Herbert, B. E. (2008b). Fate of CuO-derived lignin oxidation products during plant combustion: application to the evaluation of char input to soil organic matter. *Org. Geochem.* 39, 1522–1536. doi: 10.1016/j.orggeochem.2008.07.011

Kuo, L.-J., Louchouarn, P., and Herbert, B. E. (2011a). Influence of combustion conditions on yields of solvent-extractable anhydrosugars and lignin phenols in chars: implications for characterizations of biomass combustion residues. *Chemosphere* 85, 797–805. doi: 10.1016/j.chemosphere.2011.06.074

Kuo, L.-J., Louchouarn, P., Herbert, B. E., Brandenberger, J. M., Wade, T. L., and Crecelius, E. (2011b). Combustion-derived substances in deep basins of Puget Sound: historical inputs from fossil fuel and biomass combustion. *Environ. Pollut.* 159, 983–990. doi: 10.1016/j.envpol.2010.12.012

Lakshmanan, C. M., Gal-Or, B., and Hoelsche, H. E. (1970). Production of levoglucosan by pyrolysis of carbohydrates. *Die Stärke* 22, 221–227. doi: 10.1002/star.19700220703

Louchouarn, P., Kuo, L.-J., Wade, T. L., and Schantz, M. (2009). Determination of levoglucosan and its isomers in size fractions of aerosol standard reference materials. *Atmos. Environ.* 43, 5630–5636. doi: 10.1016/j.atmosenv.2009.07.040

Masiello, C. A. (2004). New directions in black carbon organic geochemistry. *Mar. Chem.* 92, 201–213. doi: 10.1016/j.marchem.2004.06.043

Masiello, C. A., and Louchouarn, P. (2013). Ecology. fire in the ocean. *Science* 340, 287–288. doi: 10.1126/science.1237688

McClelland, J. W., Holmes, R. M., Peterson, B. J., Raymond, P. A., Striegl, R. G., Zhulidov, A. V., et al. (2016). Particulate organic carbon and nitrogen export from major Arctic Rivers. *Global Biogeochem. Cycles* 30, 629–643. doi: 10.1002/2015GB005351

Miesel, J. R., Hockaday, W. C., Kolka, R. K., and Townsend, P. A. (2015). Soil organic matter composition and quality across fire severity gradients in coniferous and deciduous forests of the southern boreal region. *J. Geophys. Res. Biogeosci*. 120, 1124–1141. doi: 10.1002/2015JG002959

Moody, J. A., Shakesby, R. A., Robichaud, P. R., Cannon, S. H., and Martin, D. A. (2013). Current research issues related to post-wildfire runoff and erosion processes. *Earth Sci. Rev*. 122, 10–37. doi: 10.1016/j.earscirev.2013.03.004

Myers-Pigg, A. N., Louchouarn, P., Amon, R. M. W., Prokushkin, A., Pierce, K., and Rubtsov, A. (2015). Labile pyrogenic dissolved organic carbon in major Siberian Arctic Rivers: implications for wildfire-stream metabolic linkages. *Geophys. Res. Lett*. 42, 377–385. doi: 10.1002/2014GL062762

Naisse, C., Girardin, C., Lefevre, R., Pozzi, A., Maas, R., Stark, A., et al. (2015). Effect of physical weathering on the carbon sequestration potential of biochars and hydrochars in soil. *GCB Bioenergy* 7, 488–496. doi: 10.1111/gcbb.12158

Nguyen, B. T., Lehmann, J., Hockaday, W. C., Joseph, S., and Masiello, C. A. (2010). Temperature sensitivity of black carbon decomposition and oxidation. *Environ. Sci. Technol.* 44, 3324–3331. doi: 10.1021/es903016y

Norwood, M. J., Louchouarn, P., Kuo, L. J., and Harvey, O. R. (2013). Characterization and biodegradation of water-soluble biomakers and organic carbon extracted from low temperature chars. *Org. Geochem.* 56, 111–119. doi: 10.1016/j.orggeochem.2012.12.008

Ponomarev, E., Kharuk, V., and Ranson, K. (2016). Wildfires dynamics in Siberian Larch forests. *Forests* 7:125. doi: 10.3390/f7060125

Preston, C. M., and Schmidt, H. W. H. (2006). Black (pyrogenic) carbon: a synthesis of current knowledge and uncertainties with special considerations of boreal regions. *Biogeosciences* 3, 397–420. doi: 10.5194/bg-3-397-2006

Rodionov, A., Amelung, W., Haumaier, L., Urusevskaja, I., and Zech, W. (2006). Black carbon in the zonal steppe soils of Russia. *J. Plant Nutr. Soil Sci.* 169, 363–369. doi: 10.1002/jpln.200521813

Running, S. W. (2006). Is global warming causing more, larger wildfires. *Science* 313, 927–928. doi: 10.1126/science.1130370

Ryan, S. E., Dwire, K. A., and Dixon, M. K. (2011). Impacts of wildfire on runoff and sediment loads at little Granite Creek, western Wyoming. *Geomorphology* 129, 113–130. doi: 10.1016/j.geomorph.2011.01.017

Sang, X. F., Gensch, I., Kammer, B., Khan, A., Kleist, E., Laumer, W., et al. (2016). Chemical stability of levoglucosan: an isotopic perspective. *Geophys. Res. Lett.* 43, 5419–5424. doi: 10.1002/2016GL069179

Santín, C., Doerr, S. H., Kane, E. S., Masiello, C. A., Ohlson, M., de la Rosa, J. M., et al. (2016). Towards a global assessment of pyrogenic carbon from vegetation fires. *Glob. Chang. Biol.* 22, 76–91. doi: 10.1111/gcb.12985

Santín, C., Doerr, S. H., Preston, C. M., and Gonzalez-Rodriguez, G. (2015). Pyrogenic organic matter production from wildfires: a missing sink in the global carbon cycle. *Glob. Chang. Biol.* 21, 1621–1633. doi: 10.1111/gcb.12800

Schmidt, M. W. I., and Noack, A. G. (2000). Black carbon in soils and sediments: analysis, distribution, implications, and current challenges. *Global Biogeochem. Cycles* 14, 777–793. doi: 10.1029/1999GB001208

Schneider, M. P. W., Hilf, M., Vogt, U. F., and Schmidt, M. W. I. (2010). The benzene polycarboxylic acid (BPCA) pattern of wood pyrolyzed between 200°C and 1000°C. *Org. Geochem.* 41, 1082–1088. doi: 10.1016/j.orggeochem.2010.07.001

Schneider, M. P. W., Smittenberg, R. H., Dittmar, T., and Schmidt, M. W. I. (2011). Comparison of gas with liquid chromatography for the determination of benzenepolycarboxylic acids as molecular tracers of black carbon. *Org. Geochem.* 42, 275–282. doi: 10.1016/j.orggeochem.2011.01.003

Serkiz, S. M., and Perdue, E. M. (1990). Isolation of dissolved organic matter from the Suwannee River using reverse osmosis. *Water Res.* 24, 911–916. doi: 10.1016/0043-1354(90)90142-S

Shakesby, R. A., and Doerr, S. H. (2006). Wildfire as a hydrological and geomorphological agent. *Earth Sci. Rev.* 74, 269–307. doi: 10.1016/j.earscirev.2005.10.006

Shakya, K. M., Louchouarn, P., and Griffin, R. J. (2011). Lignin-derived phenols in Houston Aerosols: implications for natural background sources. *Environ. Sci. Technol.* 45, 8268–8275. doi: 10.1021/es201668y

Soja, A. J., Tchebakova, N. M., French, N. H. F., Flannigan, M. D., Shugart, H. H., Stocks, B. J., et al. (2007). Climate-induced boreal forest change: predictions versus current observations. *Glob. Planet. Change* 56, 274–296. doi: 10.1016/j.gloplacha.2006.07.028

Stubbins, A., Niggemann, J., and Dittmar, T. (2012). Photo-lability of deep ocean dissolved black carbon. *Biogeosciences* 9, 1661–1670. doi: 10.5194/bg-9-1661-2012

Stubbins, A., Spencer, R. G. M., Mann, P. J., Holmes, R. M., McClelland, J. W., Niggemann, J., et al. (2015). Utilizing colored dissolved organic matter to derive dissolved black carbon export by Arctic Rivers. *Front. Earth Sci.* 3:63. doi: 10.3389/feart.2015.00063

Vonk, J. E., van Dongen, B. E., and Gustafsson, Ö. (2010). Selective preservation of old organic carbon fluvially released from sub-Arctic soils. *Geophys. Res. Lett.* 37:L11605. doi: 10.1029/2010GL042909

Wagner, S., Cawley, K. M., Rosario-Ortiz, F. L., and Jaffé, R. (2015). In-stream sources and links between particulate and dissolved black carbon following a wildfire. *Biogeochemistry* 124, 145–161. doi: 10.1007/s10533-015-0088-1

Wang, X., Xu, C., Druffel, E. M., Xue, Y., and Qi, Y. (2016). Two black carbon pools transported by the Changjiang and Huanghe Rivers in China. *Global Biogeochem. Cycles* 30, 1778–1790. doi: 10.1002/2016GB005509

Ward, C. P., Sleighter, R. L., Hatcher, P. G., and Cory, R. M. (2014). Insights into the complete and partial photooxidation of black carbon in surface waters. *Environ. Sci. Process. Impacts* 16, 721–731. doi: 10.1039/C3EM00597F

Wrona, F. J., Johansson, M., Culp, J. M., Jenkins, A., Mård, J., Myers-Smith, I. H., et al. (2016). Transitions in Arctic ecosystems: ecological implications of a changing hydrological regime. *J. Geophys. Res. Biogeosci.* 121, 650–674. doi: 10.1002/2015jg003133

Yunker, M. B., Backus, S. M., Graf Pannatier, E., Jeffries, D. S., and Macdonald, R. W. (2002). Sources and significance of Alkane and PAH hydrocarbons in Canadian Arctic Rivers. *Estuar. Coast. Shelf Sci.* 55, 1–31. doi: 10.1006/ecss.2001.0880

Yunker, M., Macdonald, R. W., and Whitehouse, B. G. (1994). Phase associations and lipid distributions in the seasonally ice-covered Arctic estuary of the Mackenzie Shelf. *Org. Geochem.* 22, 651–669. doi: 10.1016/0146-6380(94)90131-7

Ziolkowski, L. A., and Druffel, E. R. M. (2010). Aged black carbon identified in marine dissolved organic carbon. *Geophys. Res. Lett.* 37:L16601. doi: 10.1029/2010GL043963

Conflict of Interest Statement: The authors declare that the research was conducted in the absence of any commercial or financial relationships that could be construed as a potential conflict of interest.

frontiers in Marine Science

ORIGINAL RESEARCH
published: 09 January 2017
doi: 10.3389/fmars.2016.00280

Impact of Wetland Decline on Decreasing Dissolved Organic Carbon Concentrations along the Mississippi River Continuum

Shuiwang Duan[1], Yuxiang He[2], Sujay S. Kaushal[2], Thomas S. Bianchi[3], Nicholas D. Ward[3,4] and Laodong Guo[5]*

[1] Department of Geology and Earth System Science Interdisciplinary Center, University of Maryland, College Park, MD, USA, [2] National Water Center, National Weather Service, National Oceanic and Atmospheric Administration, Silver Spring, MD, USA, [3] Department of Geological Sciences, University of Florida, Gainesville, FL, USA, [4] Whitney Laboratory for Marine Bioscience, University of Florida, St. Augustine, FL, USA, [5] School of Freshwater Sciences, University of Wisconsin-Milwaukee, Milwaukee, WI, USA

OPEN ACCESS

Edited by:
Javier Arístegui, University of Las Palmas de Gran Canaria, Spain

Reviewed by:
X. Antón Álvarez-Salgado, Spanish National Research Council, Spain
Jie Xu, South China Sea Institute of Oceanology (CAS), China

***Correspondence:**
Shuiwang Duan
sduan@umd.edu

Specialty section:
This article was submitted to Marine Biogeochemistry, a section of the journal Frontiers in Marine Science

Received: *26 September 2016*
Accepted: *13 December 2016*
Published: *09 January 2017*

Citation:
Duan S, He Y, Kaushal SS, Bianchi TS, Ward ND and Guo L (2017) Impact of Wetland Decline on Decreasing Dissolved Organic Carbon Concentrations along the Mississippi River Continuum. Front. Mar. Sci. 3:280. doi: 10.3389/fmars.2016.00280

Prior to discharging to the ocean, large rivers constantly receive inputs of dissolved organic carbon (DOC) from tributaries or fringing floodplains and lose DOC via continuous *in situ* processing along distances that span thousands of kilometers. Current concepts predicting longitudinal changes in DOC mainly focus on *in situ* processing or exchange with fringing floodplain wetlands, while effects of heterogeneous watershed characteristics are generally ignored. We analyzed results from a 17-year time-series of DOC measurements made at seven sites and three expeditions along the entire Mississippi River main channel with DOC measurements made every 17 km. The results show a clear downstream decrease in DOC concentrations that was consistent throughout the entire study period. Downstream DOC decreases were primarily (~63–71%) a result of constant dilutions by low-DOC tributary water controlled by watershed wetland distribution, while *in situ* processing played a secondary role. We estimate that from 1780 to 1980 wetland loss due to land-use alterations caused a ca. 58% decrease in in DOC concentrations in the tributaries of the Mississippi River. DOC reductions caused by watershed wetland loss likely impacted the capacity for the river to effectively remove nitrogen via denitrification, which can further exacerbate coastal hypoxia. These findings highlight the importance of watershed wetlands in regulating DOC longitudinally along the headland to ocean continuum of major rivers.

Keywords: dissolved organic carbon, wetlands, Mississippi River Basin, river continuum, in-stream processes, land use-land cover

INTRODUCTION

Draining an area of ~28% of the Earth's surface, the 25 largest rivers in terms of discharge are responsible for over 40% of the global flux of DOC from rivers to the oceans (McKee, 2003). Within major river systems, DOC also plays an important role in driving microbially-mediated denitrification (Philip and Townsend, 2010) and greenhouse gas emissions (Raymond et al., 2013), and affecting the transport and toxicity of metals and trace organic contaminants

(Aiken et al., 2011). A limited understanding of the fundamental processes controlling spatiotemporal variability of river DOC at the basin-scale restricts our ability to accurately predict the influence of future scenarios (e.g., land use-land cover and climate change) on fluvial DOC levels. Current concepts predicting mechanisms for DOC variations from the headwaters to the mouth of major rivers primarily focus on *in situ* processing (Vannote et al., 1980) and hydrologic exchange with fringing floodplain wetlands (Sedell et al., 1989). *In situ* processing causes DOC loss as a result of microbial degradation coupled with photochemical oxidation (Amon and Benner, 1997; Ward et al., 2013) and sorption onto minerals (Aufdenkampe et al., 2001), whereas autochthonous inputs to riverine DOC are generally more labile and thus largely recycled (Stanley et al., 2012). Fringing floodplains can considerably augment river DOC levels (Tockner et al., 1999; Hedges et al., 2000) owing to high levels of both algal and aquatic plant production. Relatively speaking, the effects of heterogeneous watershed characteristics have been generally ignored in river continuum approaches characterizing riverine DOC dynamics (Vannote et al., 1980; Sedell et al., 1989). This is particularly surprising when considering it is well known that DOC concentrations vary with climate zone (Schlesinger and Melack, 1981) and land use -land cover (LULC) (Butman et al., 2015). Wetland coverage is often the best predictor of DOC concentrations in rivers and streams (Gergel et al., 1999; D'Amore et al., 2016). However, LULC (e.g., wetland distribution) is seldom used to interpret DOC changes in large river systems. Models and theoretical concepts (e.g., SPARROW Shih et al., 2010 and the urban watershed continuum Kaushal and Belt, 2012) have been developed to link river water quality to watershed characteristics, but relative contributions of *in situ* vs. watershed controls on riverine DOC are rarely quantified.

Controls on river DOC may change in watersheds that are highly impacted by complex human alterations, such as North America's largest river, the Mississippi River (MR; **Figure 1**). For example, Butman et al. (2015) determined that 8% of the DOC present in rivers today is radiocarbon-depleted (i.e., millennial aged) organic carbon that has been mobilized as a result of human disturbances. The MR has been greatly altered during the last few centuries by: (1) large-scale conversion of watershed wetlands to farmlands (Dahl and Johnson, 1991), (2) construction of high and low dams in primary tributaries, and (3) an extensive network of flood-control levees (Wiener et al., 1996). Dam constructions generally increase the *in situ* processing time of riverine DOC, while artificial levees and large-scale conversion of watershed land use may affect DOC inputs from wetlands in floodplain and watershed. Prior studies in the Mississippi River have reported a downstream trend of decreasing DOC concentrations during three seasons from 1991 to 1992 (Leenheer et al., 1995). Based on the sparse temporal variability in the above study, it is unclear whether this trend is a consistent phenomenon in the MR (Duan et al., 2007, 2014). Such observations of a downstream decrease is different from other large river systems, where DOC concentrations increase or there are no apparent changes along the downstream gradient (Lara et al., 1998; Hedges et al., 2000; Wu et al., 2007). Reasons for these differences among the rivers (e.g., differential watershed characteristics vs. fundamental differences in *in situ* processing mechanisms) remain unclear.

In this study, DOC data from three intensive samplings along the Mississippi River were reanalyzed along with a 17 year time-series of DOC measurements starting in 1997 in an effort to unravel the processes regulating longitudinal changes in DOC concentrations in the MR. Further, we compare our results to longitudinal DOC changes in the world's major rivers to determine the importance of unique watershed characteristics. A combined mass balance and regression approach was used to estimate the relative contributions from *in situ* processing vs. tributary inputs, which are most likely controlled by watershed land use and climate. We hypothesize that watershed wetland distribution controls DOC levels of tributaries and DOC longitudinal changes along the Mississippi River. Decreases in DOC as a result of wetland loss may have large implications on the role that wetlands play in controlling DOC abundance, denitrification, and nitrogen fluxes from major rivers to coastal waters, such as the Gulf of Mexico (Schramm et al., 2009).

MATERIALS AND METHODS

Water Quality Data

Past measurements of DOC and temperature made during three intensive samplings along the MR main channel from 1991 to 1992, which were used here for comparison and reanalysis, were collected from U.S. Geological Survey Open-File Report 94-4191 (Leenheer et al., 1995) and Open-File Report 94-523 (Moody, 1995), respectively. These expeditions were conducted in summer 1991 (June 23 to July 1), fall 1991 (September 25 to October 4), and spring 1992 (March 25 to April 4). Samples were taken near the center of the river approximately every 17 km from downriver to upriver between New Orleans and Minneapolis. DOC concentrations were also measured in the 17 primary tributaries up to six times (twice for the 3 seasons). Water samples were collected from just below water surface and DOC was analyzed using a high-temperature catalytic oxidation method (Leenheer et al., 1995).

Long-term water quality data were collected from the U.S. Geological Survey (USGS) National Stream Quality Accounting Network (NASQAN) webpage (http://water.usgs.gov/nasqan/). The data were obtained for all available sites on the Mississippi River main stem (Clinton, Grafton, Thebes, Vicksburg, St. Francisville, Baton Rouge, and Belle Chasse; **Figure 1**) and its primary tributaries (Iowa River at Wapello, Des Moines River at Keosauqua, Illinois River at Valley City, the Missouri River at Hermann, the Ohio River at Dam 53 near Grand Chain, the Arkansas River at David D Terry Lock and Dam below Little Rock, and the Yazoo River below Steele Bayou near Long Lake). Data at most sites covered the whole period of water years of 1997 to 2013 except the Des Moines River (2009–2013), and the LMR at Vicksburg (2008–2013), Baton Rouge (2008–2013), and Belle Chasse (2007–2013). Water sampling frequency varied but generally ranged from 6 up to 24 times per year; the most frequent collections occurred during spring high flow period. Methods for sample collections and measurements of

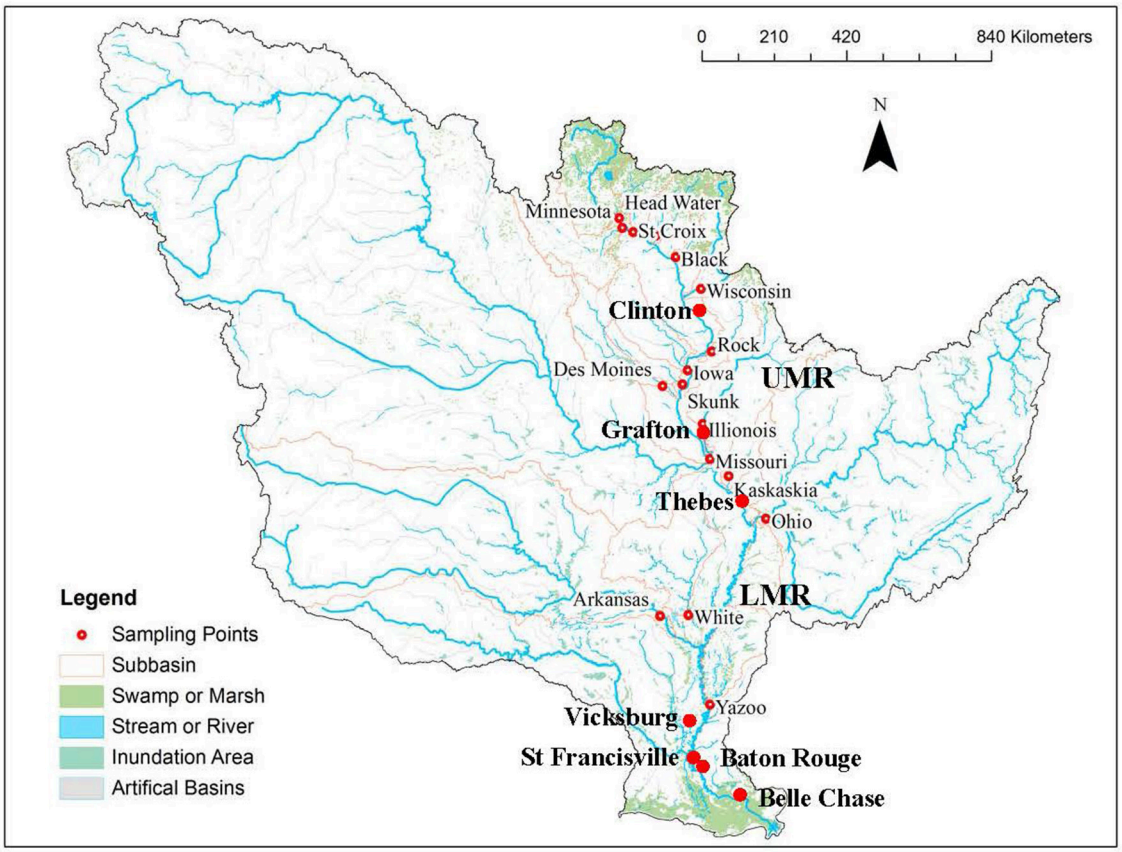

FIGURE 1 | Map for U.S. Geological Survey monitoring stations on the Mississippi River main stem (large dots) and the primary tributaries (small dots), and distribution of wetland (in green) in the Mississippi River watershed. Thebes was the dividing point of the upper and lower Mississippi River (UMR and LMR).

water temperatures and DOC are available at Wilde (2006) and Brenton and Arnett (1993)—the same as those used in Leenheer et al. (1995).

Estimating Contributions of Tributaries Inputs vs. *In situ* Processing

Long-term USGS DOC concentration data (with water discharges) were used to separate contributions of tributary inputs from that of *in situ* processing to the longitudinal DOC decreases in the Upper Mississippi River (UMR, from Clinton to Thebes) and the Lower Mississippi River (LMR, from Thebes to St. Francisville) based on DOC mass balances. Mean daily water discharge data were assembled from the records of the U.S. Army Corps of Engineers (USACE; http://www.usace.army.mil/) or the USGS (http://waterdata.usgs.gov/usa/nwis/). In each river section (UMR or LMR), we used conservative mixing of tributaries with main stem water to estimate DOC concentrations at the downriver station; fractions explained and unexplained by conservative mixing were tributary inputs and in-situ transformation, respectively. That is, contributions from tributary inputs were the difference between *in situ* DOC measurements at the upstream station and DOC estimates for the downriver station. Meanwhile, contributions of *in situ* transformation were the difference between the DOC estimates and measurements at the downstream station. Positive values of the contributions from tributary inputs and *in situ* processing suggest dilutions by tributaries and *in situ* loss, while negative values imply increases in concentrations by tributary inputs and *in situ* production/floodplain inputs.

In order to estimate DOC concentrations of the UMR and LMR at the downstream stations, daily DOC fluxes of each input station (upstream main stem or tributaries) and output station were initially estimated from discrete DOC concentration measurements and continuous average daily flow using the USGS LOADEST method (http://water.usgs.gov/software/loadest/). LOADEST estimates constituent loads in streams and rivers by developing a regression model, given a time series of streamflow, constituent concentrations, and additional data inputs. The model is well documented in the published literature and is accepted as a valid means of calculating annual solute loads from a limited number of water quality measurements. We used measurements of DOC concentrations and streamflow during the same dates for model calibrations. The models, which contained up to seven parameters, captured the dependence of concentrations on discharge and season and any long-term

trends. Daily discharge data for the study period were prepared for LOADEST models so that daily fluxes of DOC were estimated for the whole study period, once the model had been calibrated. From the returning files, results from the adjusted maximum likelihood estimates (AMLE) were used to modify loading equations to correct for transformation bias. Additionally, a period-weighted approach[28] was used to verify above LOADEST method. In this approach, a measured DOC concentration was assumed to represent a period around which the sample was collected; this allowed for connecting measured concentrations through time by a piecewise linear function.

The estimated DOC daily loads were used for DOC mass balances for the UMR and LMR before a mean travel time from each input station to the output station was known. The travel time was obtained by finding the best correlations between daily discharge data at an input and an output station (Duan et al., 2010). More specifically, daily water discharges of the two stations were used for correlation analysis, with data of the input station moved forward a few days until the highest significance level of the correlation was achieved. The number of days that data needed to be adjusted was taken as the mean residence time between the two stations. This approach for travel time was verified by comparing water discharge inputs and output of each river section shown as in Duan et al. (2010). Once residence time from each input site was known, the daily water discharges and DOC loads of the input stations were re-assembled by moving them forward by the number of days that represented their mean travel times to the output station.

Mass balances of water discharges were initially conducted, and the unbalanced discharges were assumed to come from ungauged small tributaries. These discharges were then multiplied by mean daily DOC concentrations of ungauged tributaries (assumed to be averages of the selected tributaries) to estimate daily DOC inputs from these tributaries. Finally, total inputs of daily water discharges and DOC loads (gauged and ungauged) were then summarized, and daily DOC concentrations at the downriver stations were obtained by dividing total daily DOC inputs by total daily water inputs.

Watershed Land Use Land Cover and Climate Data

To identify controls of watershed characteristics on DOC concentrations of the primary tributaries, correlation analyses were conducted between mean DOC concentrations of the tributaries and their watershed LULC and climatic parameters (air temperature, precipitation and runoff ratio). Relationships were tested using Pearson's correlations ($p < 0.05$, Pearson's correlation). DOC data collected during the three expeditions of 1991–1992 were used, because more tributaries (17 in total) were sampled during these expeditions than the USGS sites with long-term DOC data (only seven) (**Figure 1**). For most tributaries, the data were representative because DOC was measured up to six times a year across seasons. National Land Cover Dataset 1992 (NLCD 1992; http://www.epa.gov/mrlc/nlcd.html) was used for land use data collection in order to match the time when DOC concentrations were measured. NLCD 1992 data were a 21-class land cover classification scheme applied consistently over the United States.

Mean air temperature and precipitation during a close period (1990–1995) were obtained from the NCEP North American Regional Reanalysis (NARR) dataset and the forcing data for the North Land Assimilation System (NLDAS). The near-surface mean air temperature was adjusted vertically to account for terrain height difference between NARR and NLDAS. Precipitation was a product of temporal disaggregation applied directly on the NLDAS grid based on gauge-only CPC daily precipitation analysis, and orographically-adjusted according to the widely used PRISM climatology.

Sub-watersheds of the 17 primary tributaries were divided from the Mississippi River basin. Boundary polygons of each watershed were generated based on USGS 8-digit hydrologic unit code (HUC). The LULC, annual mean air temperature and precipitation of each sub-watershed were extracted from data of the whole Mississippi watershed according to its boundary polygon using the ArcGIS spatial analyst tools. Annual runoff of each sub-watershed was calculated by dividing annual water discharge with watershed drainage area, and the annual runoff was then divided by annual precipitation to estimate runoff ratio (runoff / precipitation × 100%); data of water discharge and drainage area were from http://waterdata.usgs.gov/usa/nwis/.

RESULTS

Longitudinal Changes in DOC Concentrations along the MR

Results showed that the downstream decrease in DOC concentrations along the main stem was consistent throughout the study period. High-resolution spatial data of 1991–1992 (**Figures 2A–C**) demonstrated that DOC concentrations decreased gradually, except for two rapid drops shortly after the confluence of major tributaries (Missouri and Ohio Rivers). DOC concentrations of major tributaries also displayed a longitudinal decreasing trend (**Figures 2A–C**; r^2 ranging from 0.52 to 0.74, $p < 0.05$). To be consistent with data of 1991–1992, long-term USGS DOC data (1997–2013) were presented seasonally. These new records showed that DOC concentrations in the main stem consistently decreased downstream of MR headwaters across seasons throughout the study period (**Figures 2D–G**; r^2 ranging from 0.87 to 0.96, depending on seasons, $p < 0.05$). The coefficients of variation were minor (C.V. = 0.4–10%) showing strong confidence.

Interestingly, the decreases in DOC concentrations were generally accompanied by downstream increases in water temperatures across seasons (one exception in **Figure 2A**) (**Figures 2B–G**; r^2 ranging from 0.81 to 0.98, $p < 0.05$). As a result, DOC concentrations and water temperatures were negatively correlated (r^2 ranging from 0.80 to 0.94, $p < 0.05$; one except of June-July 1991), but the slope changed with seasons suggesting complex temperature effects (**Figure 3**).

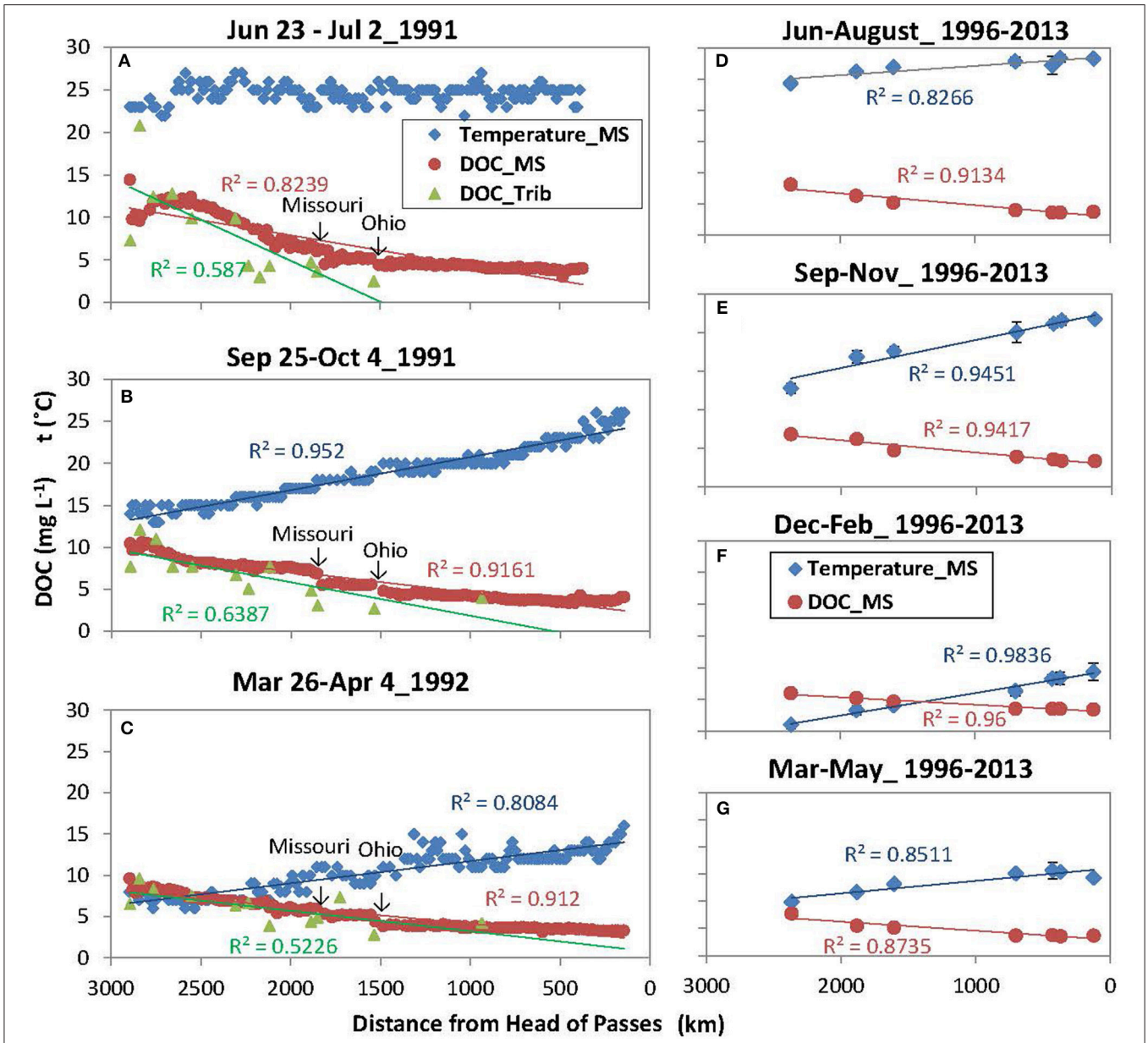

FIGURE 2 | Downstream changes in dissolved organic carbon (DOC) concentrations and water temperatures in the Mississippi River (MS) and its tributaries (Trib) during three expeditions from 1991–1992 (A–C, left) and 1997–2013 (**D–G**, right). Regression lines are shown for statistically significant trends ($p < 0.05$). 1991–1992 measurements were obtained from the U.S. Geological Survey Open-File Report 94–4191 and Open-File Report 94–523.

Contributions of Tributary Inputs and *In situ* Processing to DOC Reductions

The contributions of tributary inputs and *in situ* processing to downstream DOC decreases were positive across all months (**Figure 4**), indicating that the downstream reductions of DOC concentrations were a combined effect of tributary dilution (by low-DOC water) and *in situ* loss. The contributions from tributary dilutions were positively correlated with water discharge in the LMR (**Figure 4B**; $r^2 = 0.81$, $p < 0.01$), as well as in the UMR but the correlation was less significant (**Figure 4A**; two outliers of March and June; $r^2 = 0.63$, $p < 0.05$). The contributions of *in situ* processing also exhibited pronounced seasonal variations. In the LMR section, this seasonal pattern strictly followed that of water temperatures (**Figure 4D**; $r^2 = 0.88$, $p < 0.05$), but it was positively correlated with both water temperature and water discharge in the UMR (**Figure 4C**; $r^2 = 0.36$ and 0.55, $p < 0.05$).

Summing for the entire study period, we found that the effects of tributary dilution accounted for 71 and 63% of the DOC deceases in the UMR and

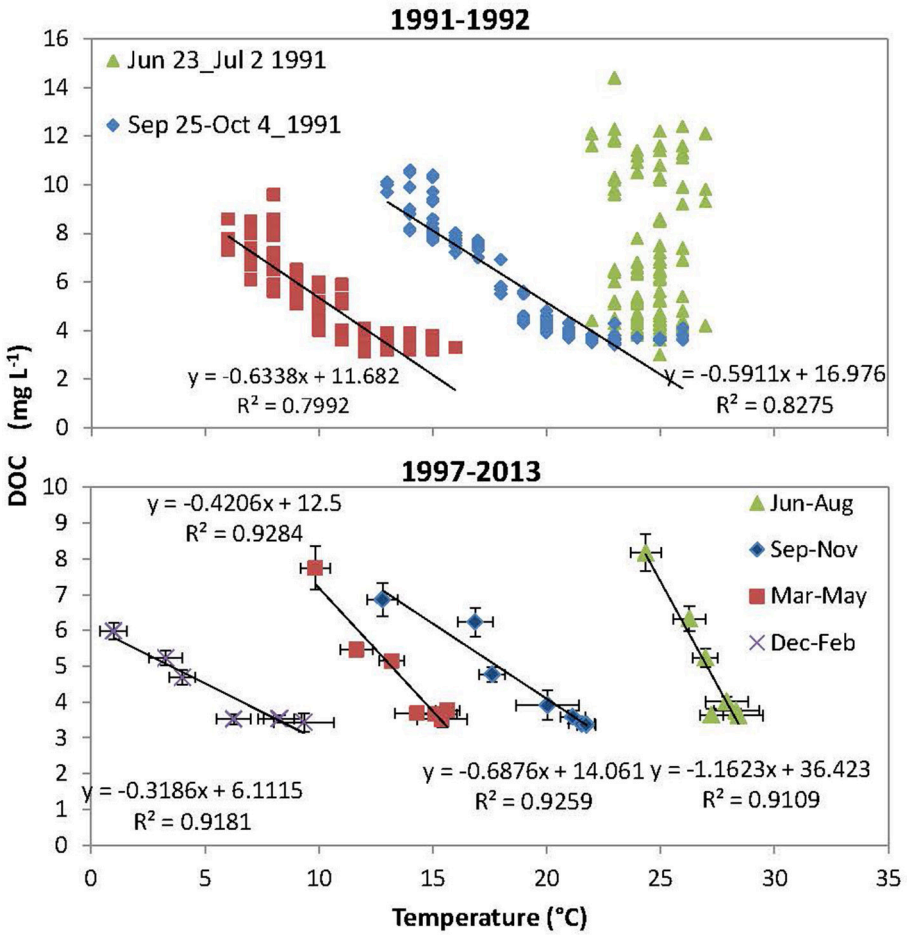

FIGURE 3 | Correlations between DOC concentration and water temperature at the Mississippi River main stem during the three longitudinal sampling expeditions of 1991–1992 (upper) and during four seasons of 1997–2013 **(bottom)**. Bars showed standard errors for every season.

LMR, respectively. The effects of tributary dilution were 2.4 times and 1.7 times that of *in situ* processing losses.

Control of Watershed Wetland Distribution on DOC Decreases

Patterns of DOC spatial variability across the Mississippi tributaries tightly followed that of watershed wetland coverage, with both parameters showing a downstream decrease from north-to- south (**Figure 5A**). In particular, DOC concentrations of the 17 primary tributaries were positively correlated with watershed wetland coverage (**Figure 5D**; $r^2 = 0.88$, $p < 0.05$), whereas no significant correlation was found with any other type of land-use regime. Although tributary DOC concentrations also varied inversely with temperature, precipitation and runoff ratio (**Figures 5B,C**), the correlation coefficients were much lower ($r^2 = 0.57$, 0.23, and 0.03, respectively). Moreover, we found watershed wetland coverage (wetland %) can be regressed negatively with mean air temperature (Temp) and runoff ratio (runoff%), but positively with annual precipitation (Pptn) with an r^2 of 0.80 (Equation 1 and **Figure 5E**):

$$\textit{wetland}\,\% = \mathbf{17.03} - \mathbf{2.10}\,\textit{Temp}\,(^{\circ}\textit{C}) + \mathbf{0.031}\textit{Pptn}\,(\textit{mm}) - \mathbf{0.506}\textit{Runoff}\,\% \quad (1)$$

Where the standard errors of the estimates of the intercept and the three coefficients of the equation were 2.67, 0.32, 0.007, and 0.111, respectively.

DISCUSSION

Consistent Longitudinal Pattern of DOC Concentrations along the Mississippi River

Our data suggest that the longitudinal decreases in DOC concentrations along the Mississippi River showed a consistent pattern. The downstream decreases were not only observed in the three high-resolution spatial data of 1991–1992 (**Figures 2A–C**), but also the long-term USGS DOC data (1997–2013) with intensive measurements (biweekly to monthly) (**Figures 2D–G**). Reviews on all available longitudinal DOC data of major rivers of the world (**Table 1**) found that the consistent downstream

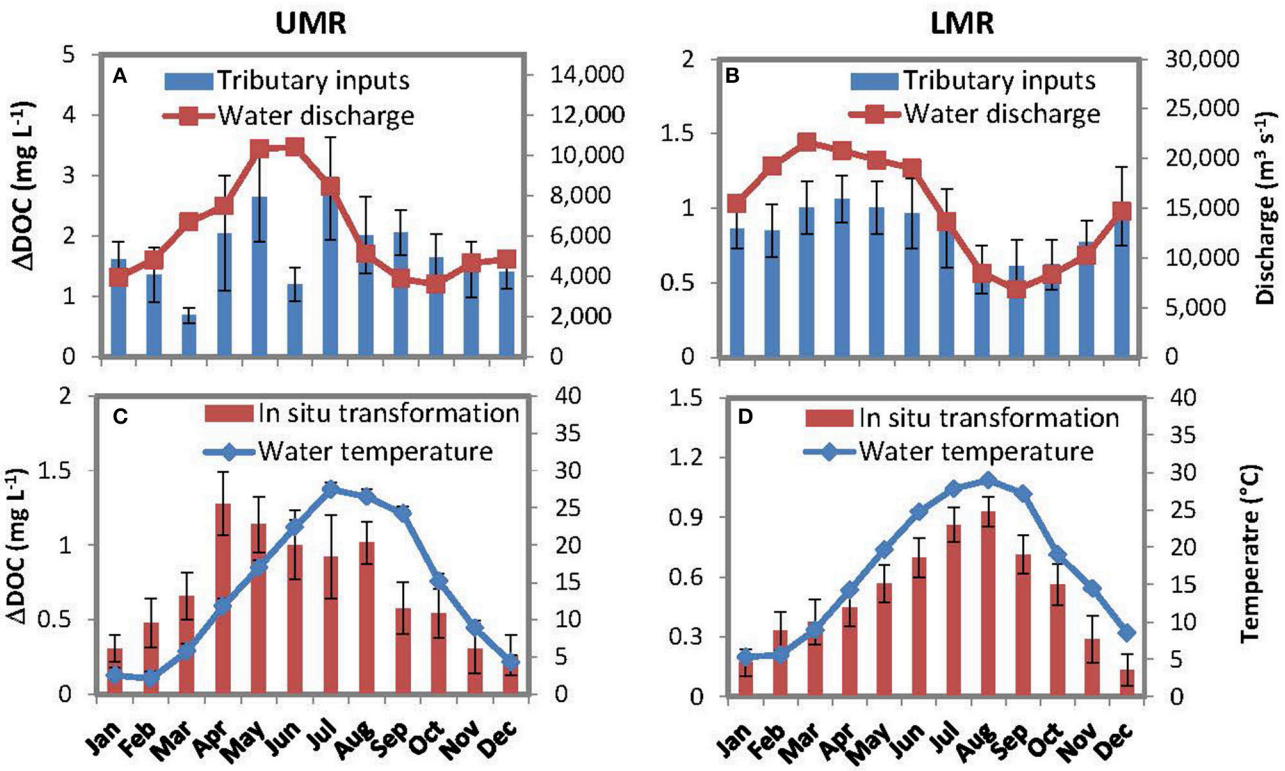

FIGURE 4 | Monthly-averaged river discharge and contributions of tributary inputs to the downstream DOC decreases in the UMR and LMR from January 1997–September 2013 (A,B), and monthly-averaged water temperature and contributions of *in situ* transformation to the downstream DOC decreases (C,D). All values are presented in averages with standard errors.

decreases in DOC concentrations along the MR were globally unique. Most rivers showed no obvious gradients or features (e.g., Lena; Lara et al., 1998, Columbia; Prahl et al., 1998, Paraná; Depetris and Kempe, 1993, and Yellow; Zhang et al., 2013), while other rivers displayed an increase or decrease only in a river section (e.g., Yangtze; Wu et al., 2007; Zhang et al., 2014 and Colorado; Miller, 2012). Consistent downstream increases occurred in the Amazon River (Hedges et al., 2000) and the St. Lawrence below the Great Lakes (Massicotte and Frenette, 2011). The unique longitudinal DOC pattern along the MR suggests that either fundamental *in situ* process are differentially expressed in the MR, or that watershed characteristics are the primary control on longitudinal DOC changes.

The UMR is one of the three primary tributaries of the Mississippi River (the other are the Missouri, and the Ohio Rivers), and it represents neither the longest tributary nor the tributary carrying the most discharge. It seems that choosing either of the other tributaries as the origin of the LMR would change this story, since both are well known to have lower DOC concentrations than the upper MR. However, the UMR was chosen as the source, like a few other rivers (e.g., the Potomac River, USA), because it flows in the same direction as the main stem and thus crosses more climate zones and/or land-cover regimes. Therefore, the consistent downstream changes in DOC concentrations along the MR could be attributed to changes in climate zones and land-cover regimes reflecting DOC concentrations of tributaries.

Tributary Inputs as a Dominant Control on the DOC Longitudinal Changes

This study used a mass balance approach for isolating physical (e.g., dilution) and biogeochemical (e.g., bio/photodegradation) controls on DOC concentrations along the MR. To complete the mass balance it was necessary to assume that DOC concentrations of unsampled small tributaries (including inputs from floodplains) were equivalent to the average concentration observed in primary tributaries of the same region. This assumption was partially satisfied. First, despite large uncertainty, there was a regional pattern of DOC concentrations, i.e., higher in UMR watershed and lower in LMR watershed (**Figure 5A**). Moreover, although DOC inputs from floodplains can be substantial in natural lowland rivers (Mulholland and Kuenzler, 1979), the impact of floodplains should be much less because the Mississippi River (especially the LMR) was leveed and >90% of the floodplain was isolated from the river (Wiener et al., 1996). Our mass balance approach was also verified with seasonal data (**Figure 4**). For example, we found that contributions of *in situ* transformation were positively correlated with water temperature (**Figures 4C,D**). This relationship corresponds with the observed temperature dependence of both bacterial decomposition and

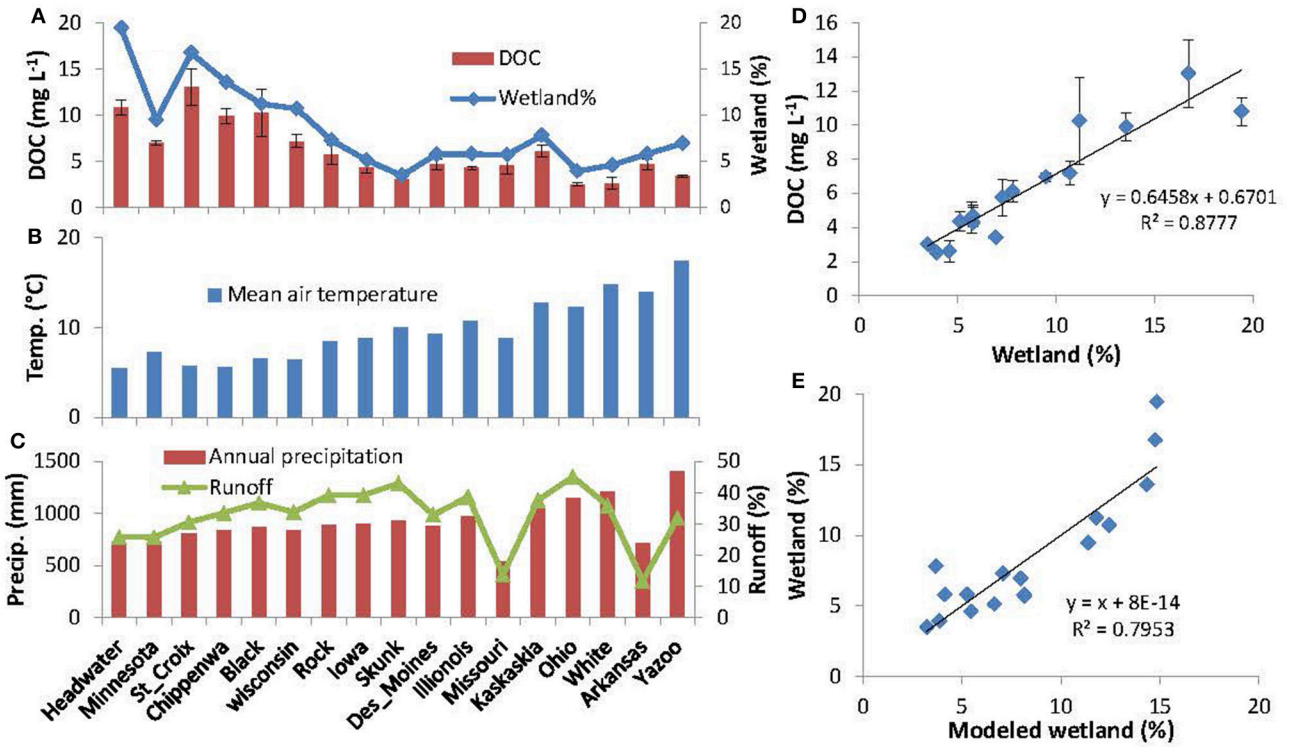

FIGURE 5 | Downstream changes in DOC concentration in tributaries, watershed wetland coverage (wetland %), mean air temperature, annual precipitation, and runoff ratio (A–C); correlations between tributary DOC concentrations and watershed wetland area coverage (D); and comparison between watershed wetland % and modeled wetland % with Equation 1 (E). DOC concentrations of the tributaries were obtained from U.S. Geological Survey Open-File Report 94-4191. DOC concentrations were measured up to six times at different times for a year and presented as averages with standard errors.

TABLE 1 | Comparison for longitudinal changes in DOC concentrations along major rivers of the world.

Name	Trend	Distance (km)	References
Mississippi	Gradual downstream decreases	2900	Leenheer et al., 1995; Duan et al., 2007
Amazon	Downstream increases	3000	Hedges et al., 2000; Ward et al., 2015
Yangtze	Increase 1500-km upper section	4000	Wu et al., 2007; Zhang et al., 2014
Lower St. Lawrence	Downstream increases	400	Massicotte and Frenette, 2011
Lena	No obvious gradients or features	1800	Lara et al., 1998
Parana/Uruguay	No obvious gradients or features	1300	Depetris and Kempe, 1993
Lower Columbia	Little/no downstream gradient	350	Prahl et al., 1998
Yellow	Highest in the middle reach	4500	Zhang et al., 2013
Colorado River	Decrease in lower section	2300	Miller, 2012

photochemical oxidation (Davidson and Janssens, 2006; Porcal et al., 2015)—the two major pathways for *in situ* DOC loss in aquatic systems (Cole et al., 2007). The lower coefficient of correlation between DOC concentration and temperature in the UMR (4c) was probably due to additional DOC loss pathways, such as sorption onto particles (Aufdenkampe et al., 2001), DOC flocculation (Benedetti et al., 2003) and exchanges with floodplains (Tockner et al., 1999). Meanwhile, we also found that contributions from tributary dilutions on DOC decreases were all positively correlated with water discharge in both river sections (**Figures 4A,B**). This relationship matched well with the fact that DOC concentrations and water discharge are generally positively correlated in most tributaries of the Mississippi watershed (Irena et al., 2015).

Using the above mass balance approach, our results showed that tributary inputs are the primary control on riverine DOC longitudinal changes, while *in situ* processing play a secondary role. It was estimated that the effects of tributary dilution accounted for 71and 63% of the DOC deceases in the UMR and LMR, respectively, which is 2.4 times and 1.7

times that of *in situ* transformation losses, respectively. It is possible that tributaries dilute DOC concentrations in the MR because of the same longitudinal reduction phenomenon present within the tributaries themselves on a smaller scale, e.g., DOC concentrations decrease as the tributary flows toward the main channel (**Figures 2A,C**). On the other hand, although DOC concentrations and water temperature were negatively correlated downstream the river (**Figure 3**), this relationship did not support that the downriver decreases in DOC concentration was due to increasing *in situ* processing—that could be enhanced with higher temperatures at the downriver sites. This negative relationship did occur all the time (e.g., June-July 1991), and temperatures and DOC were not correlated if all-year data were included (**Figure 3**). In fact, when mean DOC *in situ* loss rates were estimated from data shown in **Figure 4** (normalized to river length), we found that the *in situ* loss rates decreased from 0.93 $\mu g\ L^{-1}km^{-1}$ in the colder UMR to 0.43 $\mu g\ L^{-1}km^{-1}$ in the warmer LMR, in contrast to the temperature gradient. Thus, we hypothesize that temperature-dependent *in situ* processing were not the primary control on the downstream distribution of DOC in the Mississippi River.

Recent studies highlight the importance of *in situ* processing of DOC and CO_2 emissions from many major river systems (Richey et al., 2002; Raymond et al., 2013). For example, it is reported that CO_2 emissions from the Amazon River are an order of magnitude higher than fluvial DOC flux (Raymond et al., 2013). This finding, however, does not conflict with the results of this study. That is, although DOC *in situ* processing can be substantial, it may only modify the magnitude of DOC spatial variability but does not alter DOC longitudinal patterns along a river network, *per se*. Otherwise, one would expect that DOC concentrations would longitudinally decrease for most large rivers worldwide, which is not observed. Therefore, longitudinal DOC variability in major river systems are likely highly dependent on the structure of tributary networks and the LULC regime of the surrounding watershed.

Wetland Distribution Effects on River DOC Longitudinal Patterns

Data from this study showed that tributary DOC concentrations were tightly correlated with watershed wetland coverages, both of which decreased from headwater watersheds to the watersheds of the LMR (**Figure 5A**). Tributary DOC concentrations also varied inversely with temperature, precipitation and runoff ratio with less significance (**Figures 5B,C**), but it was more likely that these variables were controls for the formation of wetlands (Equation 1). That is, the occurrences of large areas of wetlands in the headwater sub-basins probably attributed to topographical depressions, cool climates, and abundant moisture in this region. Moreover, the negative relationship between wetland extent and air temperature also explains the complex relationship between DOC concentrations and water temperature, which varied seasonally (**Figure 3**). Therefore, wetland distribution (occurring mainly in headwaters) is likely the primary control on tributary DOC concentrations and downstream DOC decreases along the main stem of the MR. The tight coupling of tributary DOC concentrations with watershed wetland coverage observed here was also consistent with prior reviews showing occurrence of maximal DOC concentrations in wetlands (Schlesinger and Melack, 1981; Spitzy and Leenheer, 1991). This is also consistent with findings showing that wetland coverage was the best predictor of DOC concentration in rivers and streams (Mulholland and Kuenzler, 1979; Massicotte and Frenette, 2011).

With this relationship determined, wetland distribution can be used to interpret longitudinal patterns of DOC concentrations along major world rivers. For example, in more naturally flowing systems that have higher connectivity to floodplain wetlands, like the Amazon River, DOC increases downstream concurrent with high rates of *in situ* processing as a result of floodplain wetland inputs to the river (Hedges et al., 2000; Ward et al., 2015). Wetlands also play an important role in driving CO_2 production in large rivers (Abril et al., 2014; Borges et al., 2015) due to aquatic plant respiration and enhanced *in situ* processing due to both breakdown of wetland-derived OC and processes, such as priming effects, which can stimulate the breakdown of terrestrially-derived OC in the presence of fresh autochthonous OC (Guenet et al., 2014; Bianchi et al., 2015; Ward et al., 2016). In contrast, in rivers where wetlands are primarily located in headwater sub-watersheds and floodplain wetland extent is limited (as a result of human development; Wiener et al., 1996), such as the MR (**Figure 1**), DOC concentrations decrease gradually from headwaters to the river mouth due to tributary dilution. Therefore, the effects of wetland distribution should be highlighted when we examine the controls on longitudinal changes in DOC concentrations along large rivers with respect to global and regional carbon budgets.

Historical Wetland Loss and Effect on Mississippi Watershed C and N

A significant fraction of wetland extent in the UMR has been lost during the last few centuries (1780–1980) due to large-scale conversion of wetlands to farmlands in the Ohio/MR Valleys and dam constructions in the UMR for navigation (Shih et al., 2010). In the LMR, a large fraction of floodplain wetlands have also been replaced with arable land, and human-made levees have resulted in a reduction of about 90% of the local inputs from the remaining floodplain wetlands in the region (Wiener et al., 1996). Based on EPA estimates of U.S. wetland extent in 1780 and 1980 for each state (Dahl, 1990), we calculated wetland losses for each tributary using ARC GIS. In total, wetland coverage of the MR watershed decreased from 8.8 to 3.1%, showing a wetland loss as high as 65% during this period. As previously discussed, such a drastic alteration to wetland extent likely played a key role in shaping the amount and composition of DOC that was exported from the watershed over the last several centuries, and helped form the downstream trends in DOC variability observed here in the present day. For example, based on the regression of tributary DOC concentrations with watershed wetland coverage (**Figure 5D**), we estimate that mean DOC concentrations of the MR tributaries decreased from 6.35 mg L^{-1} in 1780 to 2.66 mg L^{-1} in 1980 on average, having decreased by 58% or up to 3.69 mg L^{-1}. Of course, there are many other factors in the basin

that also affect carbon dynamics in the MR, including agricultural and urban development and channel modifications (e.g., dam constructions) throughout the UMR (Wiener et al., 1996). However, our data show agricultural or urban land cover was not correlated with river DOC concentrations. Dam construction may increase residence time for DOC *in situ* processing, but the effect of damming of riverine DOC is generally complicated (Wehr et al., 1997; Nadon et al., 2015) and thus less effective relative to watershed wetland loss.

Historical wetland loss and the associated DOC reductions may have further implications for the regional cycles of nutrients (nitrogen, phosphorus and silicon; Struyf and Conley, 2009). Reductions in wetlands would have local effects (e.g., nutrient sinks) as well as downstream effects from DOC export. For local effects, nitrogen, phosphorus and dissolved silicon can be retained via biological uptake or sedimentation, and high DOC exerts an important control on the occurrence of denitrification (the major process for nitrogen removal) by providing an energy source and anaerobic conditions (Philip and Townsend, 2010). Large amounts of DOC exported from wetland may cause anaerobic conditions in downstream rivers and nitrogen removal *via* denitrification. Thus, historical wetland loss in the UMR watershed and the LMR floodplain may have greatly reduced the capacity of this river system to retain nitrogen and other nutrients. Consequently, high nutrient yields from the croplands of MR watershed due to increased fertilizer application could be further enhanced by the wetland loss to some extent (Mitsch et al., 2005; Schramm et al., 2009). This finding has major implications for the implementation of restoration strategies to reduce nutrient fluxes from the MR to the Gulf of Mexico, which unfortunately continues to be ignored (Rabotyagov et al., 2014). In some cases these inundated wetland environments act as important sinks for river nitrogen, and their loss through land-use change can exacerbate hypoxia in coastal waters.

FUTURE PERSPECTIVES

Consistent long-term monitoring of aquatic systems, along with mechanistic modeling is necessary for constraining how earth systems will react to changing conditions in the future (e.g., climate, land use land cover, and population density). While detailed mechanisms can be difficult to disentangle in large river systems, the basin-integrated signal present in the main channel of a large river allows the use of simple models, such as those presented here to elucidate large scale, broadly defined processes (e.g., *in situ* processing vs. tributary inputs) across large spatial scales (e.g., continental). Constraining the mechanisms that drive biogeochemical fluxes from the land to the sea on a conceptual and quantitative basis is essential to understanding how natural systems interact, the influence that human activities have on these processes, and how these processes have/will change in the future.

AUTHOR CONTRIBUTIONS

SD, YH, and SK conceived of the modeling approach. SD compiled the DOC data from the literature and performed the model analyses. SD, TB, NW, and LG performed comparisons of the Mississippi River to other large rivers worldwide. All authors contributed to the writing and critical evaluation of the manuscript.

FUNDING

This research was supported by NASA grant NASA NNX11AM28G, NSF Awards EAR 1521224, DBI 0640300, CBET 1058502, and EAR-1426844. The Jon and Beverly Thompson Endowed Chair of Geological Science at the University of Florida.

ACKNOWLEDGMENTS

Stuart Findlay provided helpful comments on an earlier version of the manuscript. We thank the USGS for the historic data evaluated here. Open access publication fees were supported in part by the Gordon and Betty Moore Foundation.

REFERENCES

Abril, G., Martinez, J. M., Artigas, L. F., Moreira-Turcq, P., Benedetti, M. F., Vidal, L., et al. (2014). Amazon River carbon dioxide outgassing fuelled by wetlands. *Nature* 505, 395–398. doi: 10.1038/nature12797

Aiken, G. R., Gilmourb, C. C., Krabbenhoftc, D. P., and Oremd, W. (2011). Dissolved organic matter in the florida everglades: implications for ecosystem restoration. *Crit. Rev. Env. Sci. Technol.* 41, 217–248. doi: 10.1080/10643389.2010.530934

Amon, R., and Benner, R. (1997). Photochemical and microbial consumption of dissolved organic carbon and dissolved oxygen in the Amazon River system. *Geochim. Cosmochim. Acta* 60, 1783–1792. doi: 10.1016/0016-7037(96)00055-5

Aufdenkampe, A. K., Hedges, J. I., and Richey, J. E. (2001). Sorptive fractionation of dissolved organic nitrogen and amino acids onto fine sediments within the Amazon Basin. *Limnol. Oceanogr.* 46, 1921–1935. doi: 10.4319/lo.2001.46.8.1921

Benedetti, M. F., Mounier, S., Filizola, N., Benaim, J., and Seyler, P. (2003). Carbon and metal concentrations, size distributions and fluxes in major rivers of the Amazon Basin. *Hydrol. Process.* 17, 1363–1377. doi: 10.1002/hyp.1289

Bianchi, T. S., Thornton, D., Yvon-Lewis, S., King, G., Eglinton, T., Shields, M. R., et al. (2015). Positive priming of terrestrially-derived dissolved organic matter in a freshwater microcosm system. *Geophys. Res. Lett.* 42, 5460–5467. doi: 10.1002/2015gl064765

Borges, A. V., Abril, G., Darchambeau, F., Teodoru, C. R., Deborde, J., Vidal, L. O., et al. (2015). Divergent biophysical controls of aquatic CO_2 and CH_4 in the World's two largest rivers. *Sci. Rep.* 5:15614. doi: 10.1038/srep15614

Brenton, R. W., and Arnett, T. L. (1993). *Methods of Analysis by the U.S. Geological Survey National Water Quality Laboratory - Determination of Dissolved Organic Carbon by UV-Promoted Persulfate Oxidation and Infrared Spectrometry*, Open-File Report 92–480; U. S. Geological Survey.

Butman, D. E., Wilson, H. F., Barnes, R. T., Xenopoulos, M. A., and Raymond, P. A. (2015). Increased mobilization of aged carbon to rivers by human disturbance. *Nat. Geosci.* 8, 112–116. doi: 10.1038/ngeo2322

Cole, J. J., Prairie, Y. T., Caraco, N. F., McDowell, W. H., Tranvik, L. J., Striegl, R. G., et al. (2007). Plumbing the global carbon cycle: integrating inland waters into the terrestrial carbon budget. *Ecosystems* 10, 172–185. doi: 10.1007/s10021-006-9013-8

Dahl, T. E. (1990). *Wetland Losses in the United States 1780's to 1980's; U.S.* Washington, DC: Department of the Interior, Fish and Wildlife Service.

Dahl, T. E., and Johnson, C. E. (1991). *Wetlands-Status and Trends in the Conterminous United States, Mid-1970's to Mid-1980's; U.S.* Washington, DC: Fish and Wildlife Service.

D'Amore, D. V., Edwards, R. T., and Biles, F. E. (2016). Biophysical controls on dissolved organic carbon concentrations of Alaskan coastal temperate rainforest streams. *Aquat. Sci.* 78:381. doi: 10.1007/s00027-015-0441-4

Davidson, E. A., and Janssens, I. A. (2006). Temperature sensitivity of soil carbon decomposition and feedbacks to climate change. *Nature* 440, 165–173. doi: 10.1038/nature04514

Depetris, P. J., and Kempe, S. (1993). Carbon dynamics and sources in the Paraná River. *Limnol. Oceanogr.* 38, 382–395. doi: 10.4319/lo.1993.38.2.0382

Duan, S. W., Allison, M. A., Bianchi, T. S., McKee, B. A., Shiller, A. M., Guo, L., et al. (2014). "Sediment, organic carbon, nutrients, and trace elements: sources, transport, and biogeochemical cycles in the lowermost Mississippi River," in *Biogeochemical Dynamics at Major River-Coastal Interfaces: Linkages with Global Climate Change*, Vol. 16, eds T. S. Bianchi, M. A. Allison, and W. J. Cai (Cambridge: Cambridge University Press), 397–420.

Duan, S. W., Bianchi, T. S., Santschi, P. H., and Amon, R. M. W. (2010). Effects of tributary inputs and in-channel processes on nutrient export from the Mississippi and Atchafalaya Rivers. *Mar. Freshwater Res.* 61, 1029–1038. doi: 10.1071/MF09235

Duan, S. W., Bianchi, T. S., Shiller, A. M., and Dria, K. (2007). Variability in the bulk composition and abundance of dissolved organic matter in the lower Mississippi and Pearl rivers. *J. Geophys. Res. Biogeosci.* 112:G02024. doi: 10.1029/2006jg000206

Gergel, S. E., Turner, M. G., and Kratz, T. K. (1999). Dissolved organic carbon as an indicator of the scale of watershed influence on lakes and rivers. *Ecol. Appl.* 91, 1377–1390. doi: 10.1890/1051-0761(1999)009[1377:DOCAAI]2.0.CO;2

Guenet, B., Danger, M., Harrault, L., Allard, B., Jauset-Alcala, M., Bardoux, G., et al. (2014). Fast mineralization of land-born C in inland waters: first experimental evidences of aquatic priming effect. *Hydrobiologia* 721, 35–44. doi: 10.1007/s10750-013-1635-1

Hedges, J. I., Mayorga, E., Tsamakis, E., McClain, M. E., Aufdenkampe, A., Quay, P., et al. (2000). Organic matter in Bolivian tributaries of the Amazon River: a comparison to the lower mainstream. *Limnol. Oceanogr.* 45, 1449–1466. doi: 10.4319/lo.2000.45.7.1449

Irena, F., McKnight, D. M., Pellerin, B., Green, M. B., Bergamaschi, B., Aiken, G. R., et al. (2015). The river as a chemostat: fresh perspectives on dissolved organic matter flowing down the river continuum. *Can. J. Fish. Aquat. Sci.* 72, 1272–1285. doi: 10.1139/cjfas-2014-0400

Kaushal, S. S., and Belt, K. T. (2012). The urban watershed continuum: evolving spatial and temporal dimensions. *Urban Ecosyst.* 15, 409–435. doi: 10.1007/s11252-012-0226-7

Lara, R. J., Rachold, V., Kattner, G., Hubberten, H. W., Guggenberger, G., Skoog, A., et al. (1998). Dissolved organic matter and nutrients in the Lena River, Siberian Arctic: characteristics and distribution. *Mar. Chem.* 59, 301–309. doi: 10.1016/S0304-4203(97)00076-5

Leenheer, J. A., Barber, L. B. II, Rostad, C. E., and Noyes, T. I. (1995). *Data on Natural Organic Substances in Dissolved, Colloidal, Suspended-Silt, and -Clay and Bed-Sediment Phases in the Mississippi River and Some of its Tributaries, 1991–1992*. Report 94–4191, US Geological Survey Water Resources Investigations, Denver, CO.

Massicotte, P., and Frenette, J. J. (2011). Spatial connectivity in a large river system: Resolving the sources and fate of dissolved organic matter. *Ecol. Appl.* 21, 2600–2617. doi: 10.1890/10-1475.1

McKee, B. (2003). *RiOMar: The Transport, Transformation and Fate of Carbon in River-Dominated Ocean Margins*. Report of the RiOMarWorkshop, 1–3 November 2001. Tulane University, New Orleans.

Miller, M. P. (2012). The influence of reservoirs, climate, land use and hydrologic conditions on loads and chemical quality of dissolved organic carbon in the Colorado River. *Water Resour. Res.* 48:W00M02. doi: 10.1029/2012WR012312

Mitsch, W. J., Day, J. W., Zhang, L., and Lane, R. R. (2005). Nitrate-nitrogen retention in wetlands in the Mississippi River Basin. *Ecol. Eng.* 24, 267–278. doi: 10.1016/j.ecoleng.2005.02.005

Moody, J. A. (1995). *Chemical Data for Water Samples Collected during Four Upriver Cruises on the Mississippi River between New Orleans, Louisiana, and Minneapolis, Minnesota, May 1990–April 1992: U.S.* Report 94–523, Geological Survey Open-File.

Mulholland, P. J., and Kuenzler, E. J. (1979). Organic carbon export from upland and forested wetland watersheds. *Limnol. Oceanogr.* 24, 960–966. doi: 10.4319/lo.1979.24.5.0960

Nadon, M. J., Metcalfe, R. A., Williams, C. J., Somers, K. M., and Xenopoulos, M. A. (2015). Assessing the effects of dams and waterpower facilities on riverine dissolved organic matter composition. *Hydrobiologia* 744, 145–164. doi: 10.1007/s10750-014-2069-0

Philip, G. T., and Townsend, A. R. (2010). Stoichiometric control of organic carbon–nitrate relationships from soils to the sea. *Nature* 464, 1178–1181. doi: 10.1038/nature08985

Porcal, P., Dillon, P. J., and Molot, L. A. (2015). Temperature dependence of photodegradation of dissolved organic matter to dissolved inorganic carbon and particulate organic carbon. *PLoS ONE* 10:e0128884. doi: 10.1371/journal.pone.0128884

Prahl, F. G., Small, L. F., Sullivan, B. A., Cordell, J., Simenstad, C. A., Crump, B. C., et al. (1998). Biogeochemical gradients in the lower Columbia River. *Hydrobiologia*, 361, 37–52. doi: 10.1023/A:1003129124747

Rabotyagov, S. S., Campbell, T. D., White, M., Arnold, J. G., Atwood, J., Norfleet, M. L., et al. (2014). Cost-effective targeting of conservation investments to reduce the northern Gulf of Mexico hypoxic zone. *Proc. Natl. Acad. Sci. U.S.A.* 111, 18530–18535. doi: 10.1073/pnas.1405837111

Raymond, P. A., Hartmann, J., Lauerwald, R., Sobek, S., McDonald, C., Hoover, M., et al. (2013). Global carbon dioxide emissions from inland waters. *Nature* 503, 355–359. doi: 10.1038/nature12760

Richey, J. E., Melack, J. M., Aufdenkampe, A. K., Ballester, V. M., and Hess, L. L. (2002). Outgassing from Amazonian rivers and wetlands as a large tropical source of atmospheric CO_2. *Nature* 416, 617–620. doi: 10.1038/416617a

Schlesinger, W. H., and Melack, J. M. (1981). Transport of organic carbon in the world's rivers. *Tellus* 33, 172–187. doi: 10.1111/j.2153-3490.1981.tb01742.x

Schramm, H. L., Cox, M. S., Tietjen, T. E., and Ezell, A. W. (2009). Nutrient dynamics in the lower Mississippi River floodplain: comparing present and historic hydrologic conditions. *Wetlands* 29, 476–487. doi: 10.1672/08-62.1

Sedell, J. R., Richey, J. E., and Swanson, F. J. (1989). "The river continuum concept: A basis for the expected ecosystem behavior of very large rivers?" in *Proceedings of the International Large River Symposium*, ed D. P. Dodge (Ottawa, ON: Canada Department of Fisheries and Oceans), 49–55.

Shih, J.-S., Alexander, R. B., Smith, R. A., Boyer, E. W., Schwarz, G. E., and Chung, S. (2010). *An Initial SPARROW Model of Land Use and In-Stream Controls on Total Organic Carbon in Streams of the Conterminous United States,* Open-File Report 2010–1276; U. S. Geological Survey.

Spitzy, A., and Leenheer, J. (1991). "Dissolved Organic Carbon in Rivers," in *Biogeochemistry of Major World Rivers*, *Scope 43*, eds E. T. Degens, S. Kempe, and J. E. Richey (Chichester: J. Wiley & Sons), 213–232.

Stanley, E. H., Powers, S. M., Lottig, N. R., Buffam, I., and Crawford, J. T. (2012). Contemporary changes in dissolved organic carbon of human dominated rivers: is there a role for DOC management? *Freshwater Biol.* 57, 26–42. doi: 10.1111/j.1365-2427.2011.02613.x

Struyf, E., and Conley, D. J. (2009). Silica: an essential nutrient in wetland biogeochemistry. *Front. Ecol. Environ.* 7, 88–94. doi: 10.1890/070126

Tockner, K., Pennetzdorfer, D., Reiner, N., Schiemer, F., and Ward, J. V. (1999). Hydrological connectivity, and the exchange of organic matter and nutrients in a dynamic river-floodplain system (Danube, Austria). *Freshwater Biol.* 41, 521–535. doi: 10.1046/j.1365-2427.1999.00399.x

Vannote, R. L., Minshall, G. W., Cummins, K. W., Sedell, J. R., and Cushing, C. E. (1980). The River continuum concept. *Can. J. Fish. Aquat. Sci.* 37, 130–137. doi: 10.1139/f80-017

Ward, N. D., Bianchi, T. S., Sawakuchi, H. O., Gagne-Maynard, W., Cunha, A. C., Brito, D. C., et al. (2016). The reactivity of plant-derived organic matter and the potential importance of priming effects in the lower Amazon River. *J. Geophys. Res. Biogeosci.* 121, 1522–1539. doi: 10.1002/2016jg003342

Ward, N. D., Keil, R. G., Medeiros, P. M., Brito, D. C., Cunha, A. C., Dittmar, T., et al. (2013). Degradation of terrestrially derived macromolecules in the Amazon River. *Nat. Geosci.* 6, 530–533. doi: 10.1038/ngeo1817

Ward, N. D., Krusche, A. V., Sawakuchi, H. O., Brito, D. C., Cunha, A. C., Moura, J. M. S., et al. (2015). The compositional evolution of dissolved and particulate organic matter along the lower Amazon River-Óbidos to the ocean. *Mar. Chem.* 177, 244–256. doi: 10.1016/j.marchem.2015.06.013

Wehr, J. D., Lonergan, S. P., and Thorp, J. H. (1997). Concentrations and controls of dissolved organic matter in a constricted-channel region of the Ohio River. *Biogeochemistry* 38, 41–65. doi: 10.1023/A:1005708326368

Wiener, J. G., Fremling, C. R., Korschgen, C. E., Kenow, K. P., Kirsch, E. M., Rogers, S. J., et al. (1996). "Mississippi River," in *Status and Trends of the Nation's Biological Resources*, eds M. J. Mac, P. A. Opler, C. E. P. Haecker, and P. D. Doran (Washington, DC: National Weather Research Center U.S. Geological Survey), 351–384.

Wilde, F. D. (2006). *Temperature (ver. 3.0): U.S. Geological Survey Techniques of Water-Resources Investigations, Book 9, Chap. A6., Sec. 6.1*. Available online at: http://pubs.water.usgs.gov/twri9A6/

Wu, Y., Zhang, J., Liu, S. M., Zhang, Z. F., Yao, Q. Z., Hong, G. H., et al. (2007). Sources and distribution of carbon within the Yangtze River system. *Estuar. Coast. Shelf Sci.* 71, 13–25. doi: 10.1016/j.ecss.2006.08.016

Zhang, L., Xue, M., Wang, M., Cai, W.-J., Wang, L., and Yu, Z.-G. (2014). The spatiotemporal distribution of dissolved inorganic and organic carbon in the main stem of the Changjiang (Yangtze) River and the effect of the Three Gorges Reservoir. *J. Geophys. Res. Biogeosci.* 119, 741–757. doi: 10.1002/2012jg002230

Zhang, L. J., Wang, L., Cai, W.-J., Liu, D. M., and Yu, Z. G. (2013). Impact of human activities on organic carbon transport in the Yellow River. *Biogeosciences* 10, 2513–2524. doi: 10.5194/bg-10-2513-2013

Conflict of Interest Statement: The authors declare that the research was conducted in the absence of any commercial or financial relationships that could be construed as a potential conflict of interest.

frontiers in Marine Science

ORIGINAL RESEARCH
published: 14 March 2017
doi: 10.3389/fmars.2017.00069

Microbially-Mediated Transformations of Estuarine Dissolved Organic Matter

Patricia M. Medeiros[1], Michael Seidel[1,2], Scott M. Gifford[3], Ford Ballantyne[4], Thorsten Dittmar[2], William B. Whitman[5] and Mary Ann Moran[1]*

[1] Department of Marine Sciences, University of Georgia, Athens, GA, USA, [2] Research Group for Marine Geochemistry (ICBM-MPI Bridging Group), Institute for Chemistry and Biology of the Marine Environment, Carl von Ossietzky University of Oldenburg, Oldenburg, Germany, [3] Department of Marine Sciences, University of North Carolina, Chapel Hill, NC, USA, [4] Odum School of Ecology, University of Georgia, Athens, GA, USA, [5] Department of Microbiology, University of Georgia, Athens, GA, USA

Microbially-mediated transformations of dissolved organic matter (DOM) in a marsh-dominated estuarine system were investigated at the molecular level using ultrahigh resolution mass spectrometry. In addition to observing spatial and temporal variability in DOM sources in the estuary, multiple incubations with endogenous microorganisms identified the influence of DOM composition on biodegradation. A clear microbial preference for degradation of compounds associated with marine DOM relative to those of terrestrial origin was observed, resulting in an overall shift of the remaining DOM toward a stronger terrigenous signature. During short, 1-day long incubations of samples rich in marine DOM, the molecular formulae that were enriched had slightly smaller mass (20–30 Da) and number of carbon atoms compared to the molecular formulae that were depleted. Over longer time scales (70 days), the mean differences in molecular mass between formulae that were depleted and enriched were substantially larger (~270 Da). The differences in elemental composition over daily time scales were consistent with transformations in functional groups; over longer time scales, the differences in elemental composition may be related to progressive transformations of functional groups of intermediate products and/or other reactions. Our results infused new data toward the understanding of DOM processing by bacterioplankton in estuarine systems.

Keywords: dissolved organic matter, biodegradation, estuarine processes, DOM composition, FT-ICR MS

OPEN ACCESS

Edited by:
Toshi Nagata, University of Tokyo, Japan

Reviewed by:
Dave Kirchman, University of Delaware, USA
Hiroshi Ogawa, University of Tokyo, Japan

****Correspondence:***
Patricia M. Medeiros
medeiros@uga.edu

Specialty section:
This article was submitted to Marine Biogeochemistry, a section of the journal Frontiers in Marine Science

Received: *12 December 2016*
Accepted: *27 February 2017*
Published: *14 March 2017*

Citation:
Medeiros PM, Seidel M, Gifford SM, Ballantyne F, Dittmar T, Whitman WB and Moran MA (2017) Microbially-Mediated Transformations of Estuarine Dissolved Organic Matter. Front. Mar. Sci. 4:69. doi: 10.3389/fmars.2017.00069

INTRODUCTION

Bacterioplankton control the flux of dissolved organic matter (DOM) into the coastal microbial food web and influence the release of inorganic carbon to atmospheric and offshore reservoirs. Thousands of compounds make up the estuarine DOM pool, each with different biological turnover rates (Poretsky et al., 2010). This complex DOM pool is processed by a diverse community of heterotrophic bacteria composed of hundreds of taxa (Giovannoni and Stingl, 2005) with varying ecological strategies for the uptake and metabolism of carbon using largely uncharacterized biochemical pathways (Cottrell and Kirchman, 2000; Mou et al., 2007). While measures of changes in chemical characteristics and bulk metabolic rates have provided considerable insights into DOC turnover (Kirchman et al., 2001; Repeta et al., 2002; Benner and Kaiser, 2003; Hertkorn et al., 2006), alone they are insufficient to fully understand the transformation of this complex mixture.

Riverine input can be a large source of DOM of terrigenous origin to estuaries and coastal areas (Hedges et al., 1997; Fichot and Benner, 2014; Medeiros et al., 2016). As riverine DOM is transported toward the ocean, its quantity and composition is often altered (Cole et al., 2007) by a variety of chemical, biological and physical processes (Tzortziou et al., 2008), making estuaries hot spots of DOM cycling. Significant gradients exist in the composition of DOM in estuaries (Sleighter and Hatcher, 2008; Medeiros et al., 2015c; Seidel et al., 2015). In general, DOC concentrations and the DOM aromaticity decrease toward the ocean (Abdulla et al., 2013) at the same time that DOM lability increases (D'Andrilli et al., 2015). Despite intense cycling, a large portion of compounds persist during estuarine passage (Osterholz et al., 2016).

Understanding transformations of the DOM pool in estuaries is important to constraint the characteristics of the DOM introduced to the coastal zone (Bauer and Bianchi, 2011) that may ultimately reach the deep sea (Opsahl and Benner, 1997). Characterizing DOM degradation remains challenging, however, due to the complex nature of DOM, the variety of microbial metabolic pathways, and the various environmental conditions that regulate bacterial metabolism (Eichinger et al., 2011). Despite these challenges, much has been learned by tracking changes in DOC concentration and DOM composition during incubation experiments, including the variation in biomineralization rates as a function of DOM source (e.g., Moran and Zepp, 1997; Obernosterer and Benner, 2004), the relationship of microbial activity to the production of labile (e.g., Kawasaki and Benner, 2006) and refractory (e.g., Ogawa et al., 2001; Jiao et al., 2010; Lechtenfeld et al., 2015) DOM, and how bacterial-derived refractory material compares structurally to refractory DOM in the ocean (e.g., Osterholz et al., 2015). Studies using ultrahigh resolution mass spectrometry have revealed additional molecular-level transformations in DOM as a result of microorganism activity (Kujawinski et al., 2004), including a significant decrease in the molecular diversity of terrigenous DOM (Seidel et al., 2015) and a preferential degradation of oxygen-rich molecules on a time scale of several days (Kim et al., 2006; Medeiros et al., 2015c; Seidel et al., 2015).

Here, we use incubation experiments lasting from 24 h to 70 days to identify microbially-mediated transformations in DOM composition based on ultrahigh resolution mass spectrometry analysis. The incubations were pursued using water from three sites along a marsh-dominated estuary characterized by strong spatial and temporal variability in DOM sources, including terrigenous, marine, and salt marsh inputs (Medeiros et al., 2015a). The estuarine system is characterized by large interannual variability, and some of the incubations captured a record drought during fall 2012, when river discharge was the lowest recorded since measurements began in 1931 (Medeiros et al., 2015a). The two main goals of this study were to (1) identify how DOM from different sources influence the patterns of DOM transformation at the molecular level due to biodegradation, and to (2) identify the dominant changes in DOM composition resulting from microbially-mediated transformations over time scales from hours to months.

METHODS

Sample Collection and Microbial Incubations

DOM was collected in the Altamaha-Doboy-Sapelo Estuary off the southeastern U.S. coast in November 2012 and May 2013. Samples were collected in triplicate at three locations: the Altamaha River (salinity S = 0 to 11; strong terrigenous inputs), the mouth of Doboy Sound (S = 22.9 to 34.6; large marine influence) and near the head of Sapelo Sound (S = 9.1 to 31.5; mixture of terrigenous, marine and salt marsh inputs; Medeiros et al., 2015a) (Figure S1). All samples were collected during high tide. Immediately after collection, triplicate water samples from each site were filtered sequentially through Whatman GF/D filters (pre-combusted at 450°C for 5 h; nominal 2.7 μm pore size) and 0.2 μm Pall Supor membrane filters into pre-combusted amber glass bottles. Fifty milliliters aliquots of the filtrate from each sampling site were set aside in separated beakers for the preparation of microbial inocula. For that, the 0.2 μm filters from all locations were aseptically cut into pieces and equal areas of the filters were pooled into 50 mL aliquots of 0.2 μm filtrate from each of the three sites and stirred for 30 min. The resulting filtrates, now containing microbes from all sites, were added back to the appropriate set of bottles. This ensured that functional capabilities of the microbes were similar during all incubations and changes in DOM composition could therefore be attributed predominantly to the different initial composition of the DOM pools. We note that fine particles that passed through the GF/D filter but were retained in the 0.2 μm membrane were likely also introduced to the bottles. After the addition of inorganic nutrients (20 μM Na_2PO_4 and 50 μM NH_4Cl), a triplicate set from each sampling site was immediately filtered (0.2 μm) in order to characterize the initial condition for each experiment. Aliquots were stored frozen for DOC analysis, and the remaining filtrates were acidified to pH 2 (using HCl) and DOM was extracted using solid phase extraction (SPE) cartridges (Agilent Bond Elut PPL) as in Dittmar et al. (2008). We refer to those samples as T0.

The remaining triplicate sets were incubated in the dark at the temperature measured at the time of collection for up to 70 days. At days 35 and 70, samples were filtered, acidified, and DOM was extracted using PPL cartridges as described previously. These samples are referred to as T35 and T70. Shorter-term incubations lasting 24 h were also conducted with water collected at the mouth of Doboy Sound in February and in December of 2011 (referred to as T1). Aliquots for DOC analysis were collected for all incubations as described above (i.e., prior to acidification, stored frozen).

Chemical Analyses

In all cases, DOC concentration in water samples and extracts (i.e., dried and redissolved in ultrapure water) was measured with a Shimadzu TOC-V_{CPH} analyzer. Analytical accuracy and precision were tested against the Consensus Reference Material (Hansell, 2005) and were better than 5%. SPE extraction efficiency across all samples was 75 ± 5% of the DOC. Bulk $\delta^{13}C$ of extracted DOC (SPE-DOC) was

measured with a Finnigan MAT 251 isotope ratio mass spectrometer after complete drying. Procedural blanks did not yield detectable amounts of carbon isotope contamination. The molecular composition of DOM extracts (15 mg C L^{-1} in 1:1 methanol/water) was analyzed using a 15T Fourier transform ion cyclotron resonance mass spectrometer (FT-ICR MS; Bruker Daltonics) with electrospray ionization (negative mode) as in Seidel et al. (2014). Spectra were internally calibrated with >100 known $C_xH_yO_z$ molecular formulae over the mass range in the samples. With this calibration procedure, a mass error of <0.1 ppm was achieved. Before each sample set, blank checks with methanol and ultrapure water were measured. Molecular formulae were calculated in the mass range between 150 and 850 Da by applying the following restrictions: $^{12}C_{1-130}{}^{1}H_{1-200}O_{1-150}{}^{14}N_{0-4}S_{0-2}P_{0-2}$. Assignment of molecular formulae was done considering a maximum mass error of 0.5 ppm and using the criteria described by Rossel et al. (2013). Only compounds with a signal-to-noise ratio of 4 or higher were used in the analysis to eliminate inter-sample variability based on peaks that were close to the limit of detection. Additional details of molecular formulae assignment are given in Seidel et al. (2014). A sample from the North Equatorial Pacific Intermediate Water collected at station NELHA off Big Island in Hawaii at 674 m water depth (Osterholz et al., 2015; Riedel et al., 2016) was also analyzed repeatedly (41 times) in order to characterize differences in DOM composition as identified by FT-ICR MS that arise solely due to instrument variability.

Patterns of variability in FT-ICR MS-derived DOM composition were distinguished by principal component (PC) analysis using all replicates simultaneously as in Medeiros et al. (2015a,b,c). All PCs shown here are significantly different (95% confidence level) from results of PC analysis of spatially and temporally uncorrelated random processes (Overland and Preisendorfer, 1982). The Wilcoxon rank-sum test was used for comparisons between groups of compounds, as in Osterholz et al. (2016).

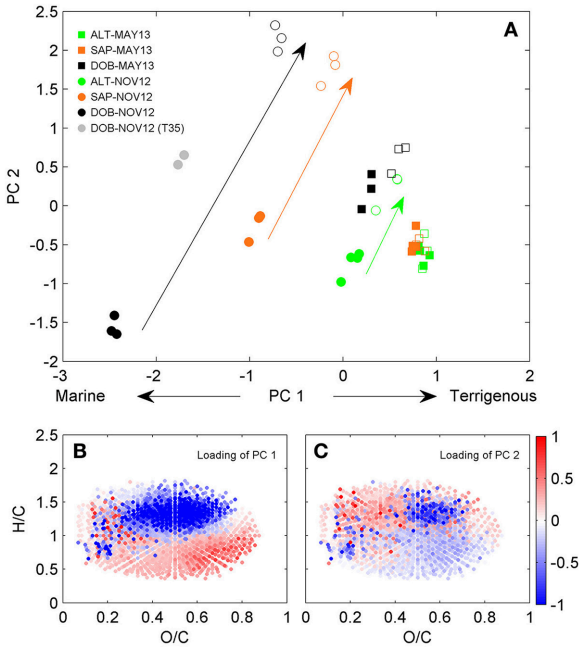

FIGURE 1 | Principal component analysis of DOM composition. (A) Scores of the first two principal components are shown color coded. Solid and open symbols represent T0 and T70, respectively. Small gray circles are T35 for incubation of Doboy Sound water in November 2012. Color coded arrows are shown for illustrative purposes, emphasizing the extent of transformation in DOM composition between pre- and post-incubated samples in November 2012 based on the first two principal components (i.e., samples close together in principal component space are more similar to each other, while samples that are far apart are more different to each other in terms of DOM composition). Van Krevelen diagrams color coded with loadings of **(B)** PC1 and **(C)** PC2 are also shown. For a given sample, if the score of a PC (shown in panel **A**) is negative, then DOM is relatively enriched with compounds associated with molecular formulae whose loadings for that PC (shown in **B** or **C**) are negative, and depleted with those whose loadings are positive. The opposite is true if the score of a given PC is positive.

RESULTS

Spatial and Temporal Variations in DOM Composition

A detailed characterization of spatial and temporal differences in DOM composition in this system has been presented in Medeiros et al. (2015a). We briefly summarize results here for comparison with microbially-mediated transformations described in the next section. DOC concentrations were substantially lower near the ocean at Doboy Sound than at the other sites (Table S1) and increased at all locations in May 2013 when river discharge was high. The pre-incubation samples (T0; solid symbols) were spread along the first PC (PC1) axis (**Figure 1A**), which separated samples with high salinity (e.g., Doboy in November 2012) from those with low salinity (e.g., Altamaha in May 2013) (Table S1) (see caption of **Figure 1** for example of interpretation of the analysis). The correlation coefficient between PC1 and salinity for the pre-incubation samples was −0.87 ($p < 0.01$). The loading of PC1 (**Figure 1B**) shows a pattern typical of river-to-ocean transects (Medeiros et al., 2015c), with high salinity samples enriched with compounds with high H/C ratios compared to low-salinity samples, which is consistent with the higher abundance of aliphatic structures in marine DOM (Sleighter and Hatcher, 2008; Osterholz et al., 2016). This is also consistent with the strong gradient in DOM sources in the system associated with terrigenous vs. oceanic inputs (Medeiros et al., 2015a).

For any given location, samples from May 2013 had higher DOC concentrations and DOM with a more terrigenous character than samples from November 2012 (e.g., samples from Altamaha River in May 2013 had higher PC1 scores than samples from Altamaha River in November 2012; the same is true for samples from Sapelo to Doboy Sounds; **Figure 1A**), a pattern consistent with their lighter $\delta^{13}C$ values (Table S1). This difference probably resulted from a severe drought in fall 2012, when the Altamaha River discharge was anomalously low (Medeiros et al., 2015a). During that time, salinity at all sampling sites was higher than in May 2013 (Table S1), which is consistent with the more marine character of the DOM observed in November 2012.

Microbially-Mediated Transformations in DOM Composition

In addition to capturing the gradient in DOM composition in the estuary (section Spatial and Temporal Variations in DOM Composition), the PC analysis shown in **Figure 1** also captured microbially-mediated transformations of the DOM. The largest transformations in DOM as captured by the first 2 principal components [i.e., the largest distances in PC space between T0 (solid symbols) and T70 (open symbols) for a given incubation in **Figure 1A**] occurred in samples with a more marine character (i.e., Doboy Sound in November 2012, black circles), decreasing progressively in samples with a more terrigenous signature. Incubations of Altamaha River water in May 2013 (green squares), when discharge was near the seasonal maximum (Medeiros et al., 2015a), yielded no significant changes in DOM composition as detected by the first 2 PCs (a different pattern of DOM transformation was observed in that case; see Figure S2).

It is interesting to note that microbially-mediated transformations resulted in changes on both the first and second PCs. The PC1 scores at the end of the incubations (T70) were generally higher than those at the start of the incubations (T0). Since large PC1 scores are associated with terrigenous DOM (see section Spatial and Temporal Variations in DOM Composition), this indicates that microbial degradation resulted in DOM with a more terrigenous character. This presumably resulted from preferential degradation of marine DOM, which is indeed thought to be more labile than freshwater DOM (D'Andrilli et al., 2015). As marine DOM (i.e., molecular formulae shown in blue in **Figure 1B**) was degraded during the experiment, terrigenous DOM (i.e., molecular formulae shown in red in **Figure 1B**) became relatively more important compared to the initial state. The shift toward a terrigenous signature (i.e., a shift toward high values along the PC1 axis) was stronger in the samples that had a stronger marine signature initially (**Figure 1A**). For the incubations of Doboy Sound water in November 2012, in particular, PC1 changed substantially during the incubation, representing 53% of the distance along the PC1 axis between marine (solid black circle, PC1 $= -2.45 \pm 0.03$) and terrigenous (solid green square, PC1 $= +0.86 \pm 0.05$) DOM. In other words, PC1 (**Figures 1A,B**) captured the fraction of the DOM that is statistically different between the sites and is related to the gradient in DOM composition due to terrigenous vs. marine inputs (as shown in section Spatial and Temporal Variations in DOM Composition). Biodegradation during the incubation of Doboy Sound water from November 2012 resulted in large enough changes in that fraction captured by PC1 that the DOM composition as identified by FT-ICR MS at the end of the experiment (open black circles in **Figure 1A**) was nearly as similar to riverine DOM (solid green squares) as it was to the original pre-incubated marine DOM (solid black circles). We note that photo-degradation generally produces the opposite effect, with riverine DOM resembling marine DOM in its broad molecular composition after extensive photo-degradation mainly due to removal of aromatics (Riedel et al., 2016).

Pre- and post-incubation samples were also characterized by different PC2 scores (**Figure 1A**). Microbially-mediated transformations therefore also resulted in a shift in DOM composition that did not fall along the terrigenous-marine gradient captured by PC1. The loading of PC2 reveals that molecules characterized by low O/C and high H/C ratios (molecules in red in **Figure 1C**) were relatively enriched at the end of the incubations. A detailed investigation of those changes is presented in the next section.

DOM Transformations at Doboy Sound

These analyses show that microbial degradation resulted in shifts in DOM composition so that the pool as a whole lost some of its marine characteristics and became more similar to terrigenous DOM. However, the analyses included samples from different locations and times. To examine the specific chemical formula changes occurring during biodegradation, the PC analysis was repeated considering only incubations of DOM from Doboy Sound in November 2012. This removed effects of spatial and temporal variability in DOM composition from the analysis, so that transformations could be primarily attributed to biodegradation.

DOC concentrations decreased progressively during the course of the incubation (Table S1), indicating remineralization of a fraction of the DOM pool. The score of the first principal component (referred to as $PC1_{DOB-long}$) increased with time (**Figure 2A**), and compounds associated with molecular formulae shown in blue in **Figure 2B** (negative loading) decreased in relative abundance during microbial processing while those associated with formulae shown in red (positive loading) increased with processing. As such, compounds that decreased or increased in relative abundance had distinct chemical characteristics. There was a relative enrichment of molecules that occupy the upper left corner of the van Krevelen diagram after the incubation (**Figure 2B**), i.e., a shift toward low O/C and high H/C ratios, which is consistent with molecular transformations observed in dark incubations of DOM from the Amazon River mouth (Medeiros et al., 2015c; Seidel et al., 2015). Additionally, while formulae whose relative abundances strongly decreased after the incubation (i.e., more negative loadings of $PC1_{DOB-long}$ in **Figure 2B**) were characterized by high masses (553.5 $\pm$ 78.7 Da), formulae whose relative abundances were enriched after the incubation (i.e., more positive $PC1_{DOB-long}$ loading in **Figure 2B**) were characterized by significantly lower masses (286.0 $\pm$ 93.9 Da) (**Figure 3A** and **Table 1**; Wilcoxon rank-sum test, $p < 0.01$). Molecular formulae associated with compounds that were preferentially depleted during the incubation were also characterized by a significantly higher numbers of carbon, hydrogen and oxygen atoms compared to compounds whose relative abundance enriched due to microbially-mediated transformations in DOM composition (**Figures 3B–D**; Wilcoxon rank-sum test, $p < 0.01$). They were also characterized by lower aromaticity indices (AI*; a measure of the aromaticity of the molecules; Koch and Dittmar, 2006, 2016; **Figure 3H**), although the differences are small (but still significant; Wilcoxon rank-sum test, $p < 0.01$). Lastly, the transformations in DOM composition resulting from biodegradation (**Figure 2B**) were compared with the DOM composition variability associated with differences in terrigenous

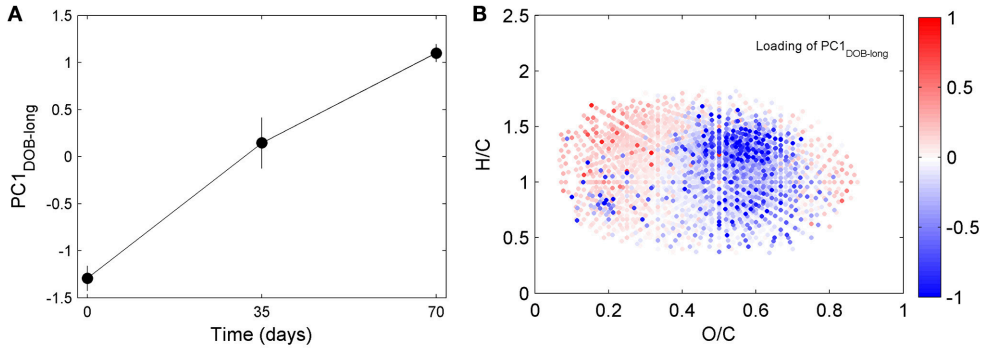

FIGURE 2 | Principal component analysis of DOM composition for long incubation of Doboy Sound water in November 2012. Samples collected at T0, T35, and T70 are separated along $PC1_{DOB\text{-}long}$ axis. **(A)** Time series of scores of $PC1_{DOB-long}$ during incubation. **(B)** Van Krevelen diagram color coded with loading of $PC1_{DOB-long}$. Molecular formulae shown in red were relatively enriched at the end of the incubation.

and marine inputs (**Figure 1B**) on a molecular basis. Molecular formulae associated with compounds whose relative abundances decreased after the microbial transformation (blue dots in **Figure 2B**) were generally also associated with compounds enriched in marine DOM (blue dots in **Figure 1B**), although there is substantial scatter around the bin averages (**Figure 3E**). Molecular formulae associated with compounds whose relative abundances increased after the incubation, on the other hand, were associated with compounds enriched in terrigenous DOM, with much smaller scatter around the bin averages. Thus, the marine DOM appeared to be preferentially transformed during the incubations, leaving behind relatively more terrigenous DOM, which is consistent with results shown in **Figure 1**. The large scatter around the formulae associated with the compounds depleted during the incubation (**Figure 3E**) indicated that, although there is a preference for biotransformation of marine DOM, a fraction of the compounds enriched in terrigenous DOM were also transformed during the incubation.

Repeating the PC analysis using only samples from days 0 to 35 (T0 and T35), T0 and T70, or T35 and T70 led to results similar to those obtained using all time points together. This indicates that the dominant pattern of DOM compositional change associated with biodegradation remained similar during the course of the incubation, at least at the monthly time scale captured by the sampling. Moreover, when the T0, T35 and T70 samples from Doboy Sound were analyzed together, approximately 60% of the total change in $PC1_{DOB-long}$ occurred in the first 35 days (i.e., from -1.29 ± 0.13 to 0.15 ± 0.27 along $PC1_{DOB-long}$ axis; **Figure 2A**), with the remaining 40% of the change (i.e., from 0.15 ± 0.27 to 1.10 ± 0.09; **Figure 2A**) occurring in the second half of the incubation. This indicates that active DOM transformations occurred throughout the experiment.

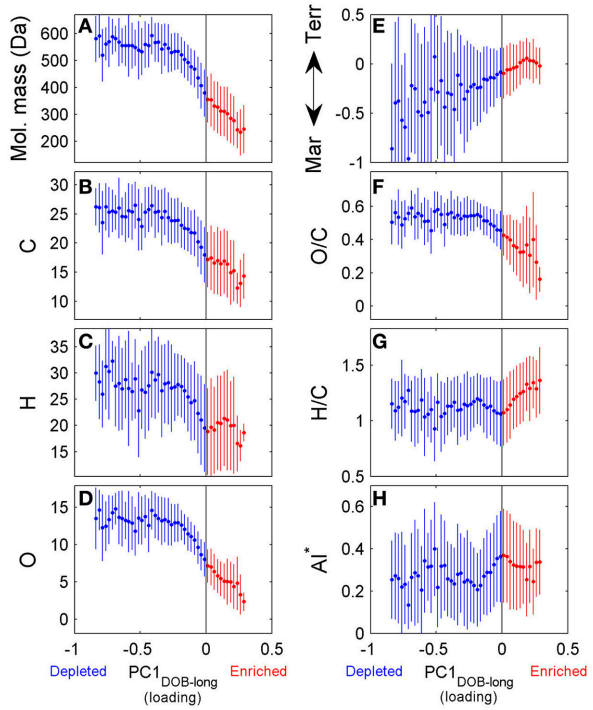

FIGURE 3 | Chemical characteristics of molecular formulae whose relative abundances were depleted (blue) or enriched (red) during incubation of Doboy Sound water in November 2012. Loading of $PC1_{DOB-long}$ shown on x-axis in all panels are values from **Figure 2B**. Fifty uniformly spaced bins were selected spanning the range of the values of the loading of $PC1_{DOB-long}$. Then, for each bin, the average ± 1 standard deviation of each chemical characteristic [molecular mass **(A)**, number of carbon **(B)**, hydrogen **(C)**, and oxygen **(D)** atoms, oxygen/carbon **(F)** and hydrogen/carbon **(G)** ratios] were computed. Y-axis on panel **(E)** distinguishing marine and terrigenous DOM are values from **Figure 1B**. AI*: modified aromaticity index **(H)** (Koch and Dittmar, 2006, 2016).

Changes in DOM Composition Over Short Time Scales

We have also investigated changes in DOM composition during the 24-h long incubations (T0-T1; **Table 1**). At those short time scales, the overall change in DOC concentrations were quite small (Table S1). Molecular formulae which were enriched after the 1-day experiments had chemical characteristics that were

TABLE 1 | Chemical characteristics of formulae whose relative abundances were enriched vs. depleted during incubations of Doboy Sound samples.

Chemical	Short term incubations						Long term incubation		
	February 2011 (T0-T1)			December 2011 (T0-T1)			November 2012 (T0-T35-T70)		
Characteristics	Depleted	Enriched	Difference	Depleted	Enriched	Difference	Depleted	Enriched	Difference
Mass (Da)	500.0 ± 111.1	474.4 ± 130.8	−25.6	486.1 ± 103.0	458.6 ± 108.4	−27.6	553.5 ± 78.7	286.0 ± 93.9	−267.4
C	23.2 ± 5.9	22.3 ± 6.6	−0.9	23.2 ± 5.5	20.3 ± 5.8	−2.8	24.9 ± 4.2	15.1 ± 4.6	−9.8
H	27.9 ± 9.0	23.0 ± 9.5	−4.9	28.4 ± 8.1	21.7 ± 8.5	−6.7	28.2 ± 7.5	19.6 ± 7.2	−8.6
O	10.6 ± 3.6	10.3 ± 4.3	−0.3	10.0 ± 3.4	10.7 ± 3.5	0.7	13.2 ± 3.0	4.5 ± 3.1	−8.8

Values given are average ±1 standard deviation. Differences between chemical characteristic of enriched and depleted formulae are also shown.

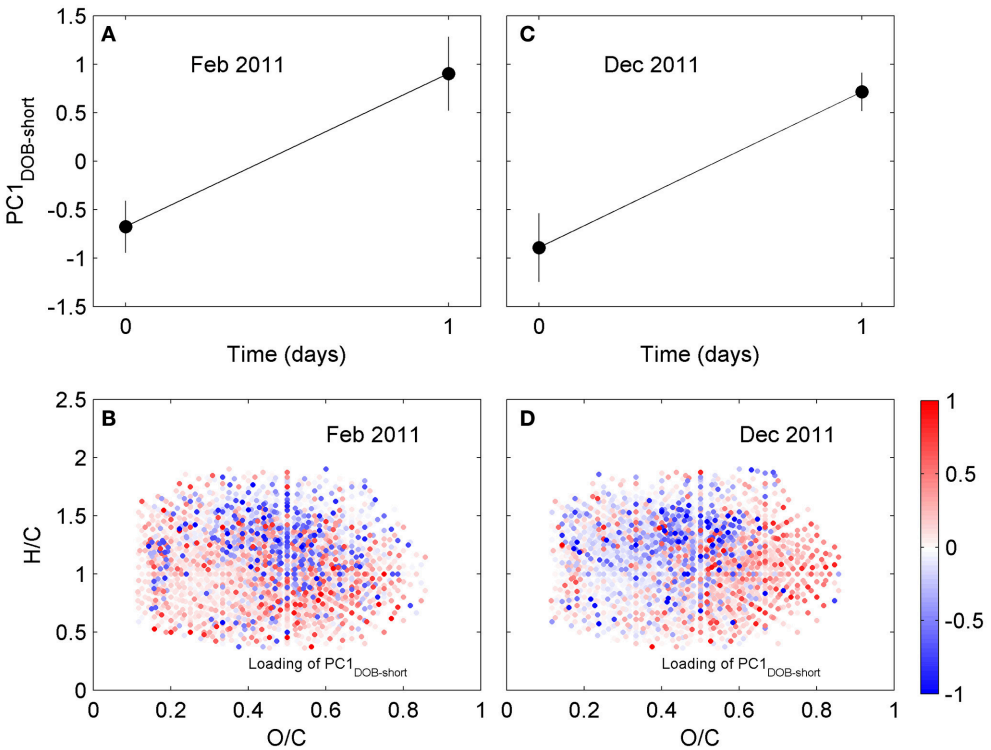

FIGURE 4 | Principal component analysis of DOM composition for short incubation of Doboy Sound water in (A,B) February and **(C,D)** December 2011. **(A,C)** Time series of scores of $PC1_{DOB-short}$ during incubation. **(B,D)** Van Krevelen diagram with loading of $PC1_{DOB-short}$. Molecular formulae shown in red were relatively enriched at the end of the incubations.

similar to those whose relative abundances decreased, occupying similar regions in van Krevelen space (**Figure 4**). For example, molecular formulae that were preferentially depleted after the 1-day incubations had masses of 485–500 Da, while formulae that were preferentially enriched had masses of 460–475 Da (**Table 1**; those differences were statistically significant; Wilcoxon rank-sum test, $p < 0.01$). Thus, the difference in the average mass of molecular formulae whose relative abundance decreased vs. increased during the short incubations ($\sim\Delta$ mass = 25–30 Da) was substantially smaller than the difference observed in the incubation lasting 70 days ($\sim\Delta$ mass = 270 Da; **Table 1**). Likewise, the differences in the number of carbon and oxygen atoms between compounds whose relative abundances decreased vs. increased in the 1-day incubations were also small (23 vs. 20–22 carbon atoms, respectively; unaltered for oxygen atoms; **Table 1**).

Changes in DOM Composition at Sapelo Sound and the Altamaha River

We also pursued a separate PC analysis for the other sets of replicates from each long incubation (e.g., from Sapelo Sound in May 2013, from Altamaha River in November 2012), similarly to the analysis presented in **Figures 2**, **3**. The analysis revealed a progressive shift in the attributes of transformed DOM (**Figure 5**). In the 70-day incubation of DOM from the Altamaha River in May 2013 (i.e., water rich in terrigenous material; **Figure 1**), the compounds whose relative abundance enriched and decreased during the incubation had similar molecular

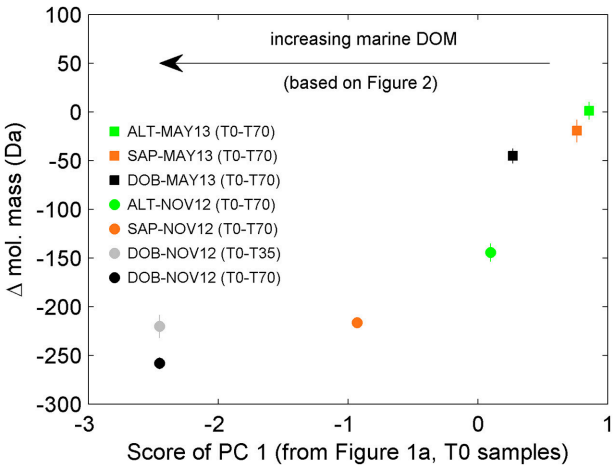

FIGURE 5 | Difference in average mass of molecular formulae whose relative abundances were enriched vs. depleted during the incubations. Negative values indicate that molecular formulae whose relative abundance were significantly enriched have smaller mass than those significantly depleted. The marine signature of the DOM pool as detected by PC analysis (see **Figure 1**) increases from right to left (e.g., more terrigenous signature for Altamaha River water in May 2013, ALT-MAY13; more marine signature for Doboy Sound water in November 2012, DOB-NOV12). Error bars are standard error of the mean. In some cases, error bars are smaller than the size of the symbols.

masses (**Figure 5**). In that regard, results were qualitatively similar to the 1-day incubation (T0-T1) of the more marine-influenced Doboy Sound DOM (**Table 1**). As the marine character of the sample increased (as identified in **Figure 1A**), the mass difference between decreasing vs. increasing compounds also increased (**Figure 5**). For the incubation of Doboy Sound water from November 2012, increasing the duration of the experiment from 35 to 70 days led to a slight (but statistically significant) increase in the mass difference between compounds depleted vs. enriched.

DISCUSSION

Temporal Changes in DOM Transformation

Since the average mass difference between compounds whose relative abundance significantly increased vs. decreased in the short incubation of Doboy Sound water is small (average of 20–30 Da; **Table 1**) and they often occupy similar regions in van Krevelen space (**Figure 4**), it is possible that those differences are reflecting transformations of functional groups. Side chain oxidation (e.g., Filley et al., 2002), demethylation, or hydroxylation (e.g., Crawford and Crawford, 1980) of compounds present in the initial DOM pool (i.e., at T0) would lead to a reduction in the abundance of those compounds at the end of the incubation and to an increase in the abundance of compounds with slightly lower molecular masses. For example, vanillic acid (∼168 Da) can be converted via demethylation to protocatechuic acid (∼154 Da) (Merkens et al., 2005). In this case, the difference in the mass of the compounds that were consumed and produced is small at 14.0157 Da (-CH_2). If multiple progressive transformations occur, however, then the difference in the mass of the compounds consumed and produced will be larger (Bugg et al., 2011). As an example, the lignin model biphenyl compound 5,5′-dehydrodivanillate (∼332 Da) can be transformed by bacterial degradation via an O-demethylation followed by a subsequent ring cleavage (Masai et al., 2007). If the resulting product is further hydrolyzed, decarboxylated, and then demethylated, protocatechuic acid is generated. In this case, the change in the mass between compounds consumed and produced progressively increases with each transformation (i.e., O-demethylation, ring cleavage, etc), reaching ∼178 Da for the end result (i.e., comparing 5,5′-dehydrodivanillate and protocatechuic acid). Although, those examples come from investigations of microbial degradation of terrigenous material in soils, they provide illustrations of how biodegradation of DOM may result in small shifts in masses initially, and to large shifts in masses later on associated with additional, progressive transformations of the intermediate products. This scenario is consistent with the progression observed for microbially-mediated transformations in DOM composition in the incubations shown here. For Doboy Sound water, for example, the short term incubations yielded small differences in the average mass of the compounds whose relative abundances significantly decreased vs. increased (**Table 1**), which could be associated with the removal of a functional group (e.g., demethylation). If those resulting products are further transformed progressively via modification of additional functional groups (e.g., demethylation followed by hydroxylation and decarboxylation), then a large difference in the average mass of the compounds whose relative abundances significantly decreased vs. increased would be expected, which is consistent with results from the long-term incubations (**Table 1**). Alternatively, the large difference in masses between consumed and produced compounds in the long-term incubation could also be a result of different reactions. It will be interesting to see if emerging tools in analytical chemistry, microbiology and informatics (Moran et al., 2016) will allow for future studies to identify the specific pathways that occur in the transformation of DOM.

Microbially-Mediated DOM Compositional Changes at the Molecular Level

In the previous section, we hypothesized that progressive modifications of functional groups could explain why the differences in the masses of compounds whose relative abundance decreased vs. increased was small in short-term incubations, and comparatively larger in long-term experiments. Here, we compare the elemental composition of the compounds that changed significantly during the incubations to identify if those changes are consistent with that hypothesis.

The molecular formulae associated with the compounds whose relative abundance changed during the 1-day incubations have masses that are similar to each other. This does not necessarily mean, however, that they can be related to each other via transformations of side functional groups. Compounds with similar masses can have very different elemental compositions,

and FT-ICR MS analysis does not give direct information about structure (e.g., Longnecker et al., 2015). We therefore investigated the possibility of transformations of functional groups using a strictly probabilistic approach. The analysis began by first selecting all molecular formulae associated with compounds whose relative abundance significantly increased after a given incubation. For the 1-day incubation (triplicate) from February 2011, for example, there were 496 such molecular formulae. For each of these, we computed the difference between its elemental composition and the elemental composition of all molecular formulae associated with compounds whose relative abundance decreased during the incubation (there were 408 such formulae in the February 2011 incubation). Therefore, the February 2011 calculation yielded a total of 202,368 (496 × 408) possible composition differences of potential substrates and products. Lastly, we sorted those composition differences to identify how often a potential change in elemental composition appeared (see Figure S3 for an example of the calculation). The rationale behind this calculation is that, if the microbial community is transforming the DOM via modification of a specific functional group, then it is more likely that a difference in elemental composition between compounds whose relative abundance decreased vs. increased equivalent to that modification will appear more often in the difference matrix. For example, if the microbial community is actively demethylating (i.e., targeting $-CH_3$), then it is more likely that a difference in elemental composition of a CH_2 (e.g., replacement of a CH_3 group by an H) between compounds whose relative abundance changed will be common. If, on the other hand, the differences in molecular formulae between relatively depleted and enriched compounds appear random, then it seems less likely that the microbial community is biasing their activity toward specific molecular modifications. If the most frequent composition differences in the 1-day incubations involve additions and removals of large numbers of carbon and heteroatoms, then the similarity in masses (**Table 1**) is likely simply coincidental and unlikely to have resulted from direct transformation of side functional groups. For example, although $C_{16}H_6O_9$ and $C_{13}H_{13}O_7NS$ have a small mass difference of 14.9599 Da, the former cannot be converted into the latter via simple transformations of side functional groups given the large difference in their elemental composition.

The calculations revealed that, for the 1-day incubations, the most common differences in elemental composition were those involving a small number of C, H, and/or O atoms (e.g., removal or addition of a CH_2; removal of an O) (Table S2) and a small mass (Figure S4). This indicates that compounds whose relative abundances were significantly decreased vs. increased in the short incubations not only had similar masses (**Table 1**) and occupied similar regions in van Krevelen space (**Figure 4**), but many of them also had similar elemental compositions (i.e., small differences in the number of atoms in Table S2). Of the 200 most frequently observed composition differences shown in Table S2, 82 appeared in both the February and the December 2011 short incubations. If the analysis is expanded to include the 800 most frequently observed composition differences, then 268 appear in both incubations. Some of the most common composition differences that appeared in both the February and the December 2011 short incubations are listed in **Table 2**. For the 70-day incubation, on the other hand, the most frequent composition differences involve a net removal of a much larger number of C, H, and O (e.g., net removal of $C_{16}H_8O_{15}$, Table S2) and a larger mass (Figure S4). These could be related to changes in functional groups occurring sequentially (e.g., demethylation followed by hydroxylation and decarboxylation, whose cumulative result would be a large change in elemental composition) and/or other reactions. There is no overlap between the composition differences appearing in the short and long incubations. It is likely that similar changes do occur in the long incubations, but because of their cumulative effect (i.e., changes occurring on intermediate products) the net change in elemental composition is different than in the short incubations. These results are consistent with our previous hypothesis that changes in DOM composition in the 1-day incubations may be related to transformations in side functional groups (with a small change in elemental composition and mass), while changes in the long incubations may be related to progressive transformations (and thus with a larger change in elemental composition and mass). We note that previous incubations of coastal water lasting for up to 9 days have not revealed a significant impact of incubation time on DOM composition (Kujawinski et al., 2016). Our analysis of short- (1 day) and long-term (35 or 70 days) incubations indicate that significant differences can occur over these longer time scales.

TABLE 2 | Most common potential transformations in elemental compositions that would have resulted in a decrease in molecular mass after short-term incubations.

Average[a] Rel. Freq.	Combination of atoms possibly removed	Mass
0.84	CH_2	−14.0157
0.83	CH_2O	−30.0106
0.81	CH_4	−16.0313
0.78	O	−15.9949
0.76	H_2	−2.0157
0.72	C	−12.0000
0.68	CO	−27.9949
0.67	C_2H_4	−28.0313
0.64	CH_6	−18.0470
0.64	C_2H_4O	−44.0262
0.62	C_2H_6O	−46.0419
0.60	C_3H_8O	−60.0575
0.59	C_2H_2O	−42.0106
0.59	H_2O	−18.0106
0.58	CH_4O	−32.0262
0.57	$C_3H_{10}O$	−62.0732
0.56	C_2H_8	−32.0626
0.55	C_3H_4	−40.0313
0.55	H_4	−4.0313
0.54	C_3H_6O	−58.0419

[a]*Average of short-term incubations of Doboy Sound water (February and December 2011).*

The patterns just described for short- and long-term incubations are not due to instrument variability or noise. First, the principal component analysis separated the pre-incubation samples from those collected at the end of the experiments in both cases (**Figures 2A**, **4A,C**). If the transformation in DOM composition shown in the van Krevelen diagrams (**Figures 2B**, **4B,D**) were simply due to instrument noise, there would be no reason to expect separation between pre- and post-incubation samples in the principal component analysis. Second, we repeated the analysis using all 41 injections of the sample from the North Equatorial Pacific Intermediate Water collected at station NELHA off Hawaii. The differences in elemental composition between those samples (which in this case were entirely due to instrument variability) were mostly random, with small and large changes in molecular mass occurring frequently.

It is important to note some of the limitations of the analysis. The calculation provides a check for consistency only, since it is possible that even when the difference in elemental composition is small (small number of C, H, and/or O atoms), the structure of the compounds that underlies the predicted formula may not allow for that particular transformation. In addition, the analytical methods used here are focused on the investigation of compounds with molecular mass larger than about 150–160 Da. As reviewed by Kujawinski (2011), previous studies have shown that small molecules that are ubiquitous in cellular biomass can be easily assimilated into cells through dedicated transport systems. Since those compounds fall outside our analytical window, however, the transformations in DOM composition reported here are only representative of the fraction in the 150–850 Da range that can be detected by FT-ICR MS analysis. The analyses are also only representative of the fraction of the DOM that is retained in the solid phase extraction resin. Saccharides, for example, are known to be consumed by microorganisms (e.g., Rich et al., 1996), but are generally not well captured by the resin used here. As such, some of the DOC decrease observed in the incubations is likely related to a fraction of the DOM that is not captured by the FT-ICR MS analysis. The statistically significant transformations in composition reported in the short-term incubations reveal, however, that at least a portion of the labile DOM was captured by the solid phase extraction. Lastly, we note that we have focused here on transformations of estuarine DOM due to microbial degradation. *In situ* transformations are influenced by additional processes, including photochemistry and flocculation.

In summary, our analyses of microbial-mediated changes in DOM composition in an estuarine system characterized by strong terrigenous and marine inputs identified significant transformations. Analyses at the molecular level revealed a general preference for degradation of compounds that are enriched in marine DOM, which resulted in the remaining DOM becoming relatively more terrigenous. Transformations observed during short-term incubations resulted in a small difference in the average mass of compounds whose relative abundance decreased vs. increased, and a novel probabilistic approach revealed that changes in elemental composition were consistent with modifications of functional groups. Over longer time scales, the differences in mass were significantly larger, possibly a result of additional changes in function groups of intermediate products. Despite limitations, and given the challenges of actually identifying transformations in the complex DOM mixture, the analysis presented here serves as a step toward shedding light into these elusive processes. Future studies combining this probabilistic approach, NMR analysis and other techniques that provide direct information about structure, and biological gene expression at a highly-resolved scale will be particularly useful to tackle the biological complexity of carbon turnover.

AUTHOR CONTRIBUTIONS

PM conceived and designed the research; PM, MS, and TD generated and processed FT-ICR MS data. SG, FB, WW, and MM contributed materials/analysis tools. PM analyzed the data. PM wrote the paper; all authors commented on the manuscript.

ACKNOWLEDGMENTS

We thank D. Kirchman and H. Ogawa for their constructive comments and suggestions, which led to a much improved manuscript. This research was supported by the National Science Foundation through the Sapelo Island Microbial Carbon Observatory (SIMCO, OCE-1356010). Additional support was provided by the NSF—Georgia Coastal Ecosystems Long Term Ecological Research program (GCE-LTER, OCE-1237140). We thank the University of Georgia Marine Institute at Sapelo Island for logistical support. This is University of Georgia Marine Institute contribution number 1058.

SUPPLEMENTARY MATERIAL

The Supplementary Material for this article can be found online at: http://journal.frontiersin.org/article/10.3389/fmars.2017.00069/full#supplementary-material

REFERENCES

Abdulla, H., Minor, E., Dias, R., and Hatcher, P. (2013). Transformations of the chemical compositions of high molecular weight DOM along a salinity transect: using two dimensional correlation spectroscopy and principal component analysis approaches. *Geochim. Cosmochim. Acta* 118, 231–246. doi: 10.1016/j.gca.2013.03.036

Bauer, J., and Bianchi, T. (2011). "Dissolved organic carbon cycling and transformation," in *Treatise on Estuarine and Coastal Science. Vol. 5*, eds E. Wolanski and D. McLusky (Waltham, MA: Academic Press), 7–67.

Benner, R., and Kaiser, K. (2003). Abundance of amino sugars and peptidoglycan in marine particulate and dissolved organic matter. *Limnol. Oceanogr.* 48, 118–128. doi: 10.4319/lo.2003.48.1.0118

Bugg, T., Ahmad, M., Hardiman, E., and Singh, R. (2011). The emerging role for bacteria in lignin degradation and bio-product formation. *Curr. Opin. Biotechol.* 22, 394–400. doi: 10.1016/j.copbio.2010.10.009

Cole, J., Prairie, Y., Caraco, N., McDowell, W., Transvik, L., Striegl, R., et al. (2007). Plumbing the global carbon cycle: integrating inland waters into the terrestrial carbon budget. *Ecosystems* 10, 171–184. doi: 10.1007/s10021-006-9013-8

Cottrell, M. T., and Kirchman, D. L. (2000). Natural assemblages of marine proteobacteria and members of the *Cytophaga-Flavobacter* cluster consuming low- and high-molecular weight dissolved organic matter. *Appl. Environ. Microbiol.* 66, 1692–1697. doi: 10.1128/AEM.66.4.1692-1697.2000

Crawford, D., and Crawford, R. (1980). Microbial degradation of lignin, enzyme. *Microb. Technol.* 2, 11–22. doi: 10.1016/0141-0229(80)90003-4

D'Andrilli, J., Cooper, W., Foreman, C., and Marshall, A. (2015). An ultrahigh-resolution mass spectrometry index to estimate natural organic matter lablity. *Rapid Commun. Mass Spectrom.* 29, 2385–2401. doi: 10.1002/rcm.7400

Dittmar, T., Koch, B., Hertkorn, N., and Kattner, G. (2008). A simple and efficient method for the solid-phase extraction of dissolved organic matter (SPE-DOM) from seawater. *Limnol. Oceanogr. Methods* 6, 230–235. doi: 10.4319/lom.2008.6.230

Eichinger, M., Poggiale, J. C., and Sempéré, R. (2011). "Toward a mechanistic approach to modeling bacterial DOC pathways: a review," in *Microbial Carbon Pump in the Ocean*, eds N. Jiao, F. Azam, and S. Sanders (Washington, DC: Science/AAAS), 66–68.

Fichot, C. G., and Benner, R. (2014). The fate of terrigenous dissolved organic carbon in a river-influenced ocean margin. *Glob. Biogeochem. Cycles* 28, 300–318. doi: 10.1002/2013GB004670

Filley, T., Cody, G., Goodell, B., Jellison, J., Noser, C., and Ostrofsky, A. (2002). Lignin demethylation and polysaccharide decomposition in spruce sapwood degraded by brown rot fungi. *Org. Geochem.* 33, 111–124. doi: 10.1016/S0146-6380(01)00144-9

Giovannoni, S. J., and Stingl, U. (2005). Molecular diversity and ecology of microbial plankton. *Nature* 437, 343–348. doi: 10.1038/nature04158

Hansell, D. A. (2005). Dissolved organic carbon reference material program. *Eos Trans. Am. Geophys. Union* 86, 318. doi: 10.1029/2005EO350003

Hedges, J., Keil, R., and Benner, R. (1997). What happens to terrestrial organic matter in the ocean? *Org. Geochem.* 27, 195–212. doi: 10.1016/S0146-6380(97)00066-1

Hertkorn, N., Benner, R., Frommberger, M., Schmitt-Kopplin, P., Witt, M., et al. (2006). Characterization of a major refractory component of marine dissolved organic matter. *Geochim. Cosmochim. Acta* 70, 2990–3010. doi: 10.1016/j.gca.2006.03.021

Jiao, N., Herndl, G., Hansell, D., Benner, R., Kattner, G., Wilhelm, S., et al. (2010). Microbial production of recalcitrant dissolved organic matter: long-term carbon storage in the global ocean. *Nat. Rev. Microbiol.* 8, 593–599. doi: 10.1038/nrmicro2386

Kawasaki, N., and Benner, R. (2006). Bacterial release of dissolved organic matter during cell growth and decline: molecular origin and composition. *Limnol. Oceanogr.* 51, 2170–2180. doi: 10.4319/lo.2006.51.5.2170

Kim, S., Kaplan, L., and Hatcher, P. (2006). Biodegradable dissolved organic matter in a temperate and a tropical stream determined from ultrahigh resolution mass spectrometry. *Limnol. Oceanogr.* 51, 1054–1063. doi: 10.4319/lo.2006.51.2.1054

Kirchman, D. L., Meon, B., Ducklow, H. W., Carlson, C. A., Hansell, D. A., and Steward, G. F. (2001). Glucose fluxes and concentrations of dissolved combined neutral sugars (polysaccharides) in the Ross Sea and Polar Front Zone, Antarctica. *Deep-sea Res. II, Top. Stud. Oceanogr.* 48, 4179–4197. doi: 10.1016/S0967-0645(01)00085-6

Koch, B. P., and Dittmar, T. (2006). From mass to structure: an aromaticity index for high-resolution mass data of natural organic matter. *Rapid Commun. Mass Spectrom.* 20, 926–932. doi: 10.1002/rcm.2386

Koch, B. P., and Dittmar, T. (2016). Erratum: from mass to structure: an aromaticity index for high-resolution mass data of natural organic matter. *Rapid Commun. Mass Spectrom.* 30:250. doi: 10.1002/rcm.7433

Kujawinski, E. B. (2011). The impact of microbial metabolism on marine dissolved organic matter. *Ann. Rev. Mar. Sci.* 3, 567–599. doi: 10.1146/annurev-marine-120308-081003

Kujawinski, E. B., Del Vecchio, R., Blough, N., Klein, G., and Marshall, A. (2004). Probing molecular-level transformations of dissolved organic matter: insights on photochemical degradation and protozoan modification of DOM from electrospray ionization Fourier transform ion cyclotron resonance mass spectrometry. *Mar. Chem.* 92, 23–37. doi: 10.1016/j.marchem.2004.06.038

Kujawinski, E. B., Longnecker, K., Barrot, K., Weber, R., and Soule, M. (2016). Microbial community structure affects marine dissolved organic matter composition. *Front. Mar. Sci.* 3:45. doi: 10.3389/fmars.2016.00045

Lechtenfeld, O., Hertkorn, N., Shen, Y., Witt, M., and Benner, R. (2015). Marine sequestration of carbon in bacterial metabolites. *Nat. Comm.* 6:6711. doi: 10.1038/ncomms7711

Longnecker, K., Futrelle, J., Coburn, E., Soule, M., and Kujawinski, E. (2015). Environmental metabolomics: databases and tools for data analysis. *Mar. Chem.* 177, 366–373. doi: 10.1016/j.marchem.2015.06.012

Masai, E., Katayama, Y., and Fukuda, M. (2007). Genetic and biochemical investigations on bacterial catabolic pathways for lignin-derived aromatic compounds. *Biosci. Biotechnol. Biochem.* 71, 1–15. doi: 10.1271/bbb.60437

Medeiros, P. M., Seidel, M., Dittmar, T., Whitman, W. B., and Moran, M. A. (2015a). Drought-induced variability in dissolved organic matter composition in a marsh-dominated estuary. *Geophys. Res. Lett.* 42, 6446–6453. doi: 10.1002/2015GL064653

Medeiros, P. M., Seidel, M., Niggemann, J., Spencer, R. G. M., Hernes, P. J., Yager, P. L., et al. (2016). A novel molecular approach for tracing terrigenous dissolved organic matter into the deep ocean, *Glob. Biogeochem. Cycles* 30, 689–699. doi: 10.1002/2015GB005320

Medeiros, P. M., Seidel, M., Powers, L. C., Dittmar, T., Hansell, D. A., and Miller, W. L. (2015b). Dissolved organic matter composition and photochemical transformations in the northern North Pacific Ocean. *Geophys. Res. Lett.* 42, 863–870. doi: 10.1002/2014GL062663

Medeiros, P. M., Seidel, M., Ward, N. D., Carpenter, E. J., Gomes, H. R., Niggemann, J., et al. (2015c). Fate of the Amazon River dissolved organic matter in the tropical Atlantic Ocean. *Glob. Biogeochem. Cycles* 29, 677–690. doi: 10.1002/2015GB005115

Merkens, H., Beckers, G., Wirtz, A., and Burkovski, A. (2005). Vanillate metabolism in *Corynebacterium glutamicum*. *Curr. Microb.* 51, 59–65. doi: 10.1007/s00284-005-4531-8

Moran, M. A., Kujawinski, E. B., Stubbins, A., Fatland, R., Aluwihare, L., Buchan, A., et al. (2016). Deciphering ocean carbon in a changing world. *Proc. Natl. Acad. Sci. U.S.A.* 113, 3143–3151. doi: 10.1073/pnas.1514645113

Moran, M. A., and Zepp, R. (1997). Role of photoreactions in the formation of biologically labile compounds from dissolved organic matter. *Limnol. Oceanogr.* 42, 1307–1316. doi: 10.4319/lo.1997.42.6.1307

Mou, X., Hodson, R., and Moran, M., A. (2007). Bacterioplankton assemblages transforming dissolved organic compounds in coastal seawater. *Environ. Microbiol.* 9, 2025–2037. doi: 10.1111/j.1462-2920.2007.01318.x

Obernosterer, I., and Benner, R. (2004). Competition between biological and photochemical processes in the mineralization of dissolved organic carbon. *Limnol. Oceanogr.* 49, 117–124. doi: 10.4319/lo.2004.49.1.0117

Ogawa, H., Amagai, Y., Koike, I., Kaiser, K., and Benner, R. (2001). Production of refractory dissolved organic matter by bacteria. *Science* 292, 917–920. doi: 10.1126/science.1057627

Opsahl, S., and Benner, R. (1997). Distribution and cycling of terrigenous dissolved organic matter in the ocean. *Nature* 386, 480–482. doi: 10.1038/386480a0

Osterholz, H., Kirchman, D., Niggemann, J., and Dittmar, T. (2016). Environmental drivers of dissolved organic matter molecular composition in the Delaware estuary. *Front. Earth Sci.* 4:95. doi: 10.3389/feart.2016.00095

Osterholz, H., Niggemann, J., Giebel, H., Simon, M., and Dittmar, T. (2015). Inefficient microbial production of refractory dissolved organic matter in the ocean. *Nat. Commun.* 6:7422. doi: 10.1038/ncomms8422

Overland, J., and Preisendorfer, R. (1982). A significance test for principal components applied to a cyclone climatology. *Mon. Weather Rev.* 110, 1–4.

Poretsky, R. S., Sun, S., Mou, X., and Moran, M., A. (2010). Transporter genes expressed by coastal bacterioplankton in response to dissolved organic carbon. *Environ. Microbiol.* 12, 616–627. doi: 10.1111/j.1462-2920.2009.02102.x

Repeta, D. J., Quan, T., Aluwihare, L. I., and Chen, R. F. (2002). Chemical characterization of high molecular weight dissolved organic matter in fresh and marine waters. *Geochim. Cosmochim. Acta* 66, 955–962. doi: 10.1016/S0016-7037(01)00830-4

Rich, J. II., Ducklow, H. W., and Kirchman, D. L. (1996). Concentrations and uptake of neutral monosaccharides along 140°W in the equatorial Pacific: contribution of glucose to heterotrophic bacterial activity and the DOM flux. *Limnol. Oceanogr.* 41, 595–604. doi: 10.4319/lo.1996.41.4.0595

Riedel, T., Zark, M., Vähätalo, A., Niggemann, J., Spencer, R., Hernes, P., et al. (2016). Molecular signatures of biogeochemical transformations in dissolved organic matter from ten

world rivers. *Front. Earth. Sci.* 4:85. doi: 10.3389/feart.2016.00085

Rossel, P. E., Vähätalo, A. V., Witt, M., and Dittmar, T. (2013). Molecular composition of dissolved organic matter from a wetland plant (*Juncus effusus*) after photochemical and microbial decomposition (1.25 yr): common features with deep sea dissolved organic matter. *Org. Geochem.* 60, 62–71. doi: 10.1016/j.orggeochem.2013.04.013

Seidel, M., Beck, M., Riedel, T., Waska, H., Suryaputra, I., Schnetger, B., et al. (2014). Biogeochemistry of dissolved organic matter in an anoxic intertidal creek bank. *Geochim. Cosmochim. Acta* 140, 418–434. doi: 10.1016/j.gca.2014.05.038

Seidel, M., Yager, P., Ward, N., Carpenter, E., Gomes, H., Krusche, A., et al. (2015). Molecular-level changes of dissolved organic matter along the Amazon River-to-ocean continuum. *Mar. Chem.* 177, 218–231. doi: 10.1016/j.marchem.2015.06.019

Sleighter, R., and Hatcher, P. (2008). Molecular characterization of dissolved organic matter (DOM) along a river to ocean transect of the lower Chesapeake Bay by ultrahigh resolution electrospray ionization Fourier transform ion cyclotron resonance mass spectrometry. *Mar. Chem.* 110, 140–152. doi: 10.1016/j.marchem.2008.04.008

Tzortziou, M., Neale, P., Osburn, C., Megonigal, J., Maie, N., and Jaffé, R. (2008). Tidal marshes as a source of optically and chemically distinctive colored dissolved organic matter in the Chesapeake Bay. *Limnol. Oceanogr.* 53, 148–159. doi: 10.4319/lo.2008.53.1.0148

Conflict of Interest Statement: The authors declare that the research was conducted in the absence of any commercial or financial relationships that could be construed as a potential conflict of interest.

frontiers in Earth Science

ORIGINAL RESEARCH
published: 02 May 2017
doi: 10.3389/feart.2017.00031

Composition and Transformation of Dissolved Organic Matter in the Baltic Sea

Michael Seidel[1], Marcus Manecki[1,2], Daniel P. R. Herlemann[2], Barbara Deutsch[3†], Detlef Schulz-Bull[2], Klaus Jürgens[2] and Thorsten Dittmar[1]*

[1] Research Group for Marine Geochemistry (ICBM-MPI Bridging Group), Institute for Chemistry and Biology of the Marine Environment (ICBM), Carl von Ossietzky University of Oldenburg, Oldenburg, Germany, [2] Leibniz Institute for Baltic Sea Research, Warnemünde (IOW), Germany, [3] Baltic Sea Centre, Stockholm University, Stockholm, Sweden

OPEN ACCESS

Edited by:
Toshi Nagata, University of Tokyo, Japan

Reviewed by:
Clare Elizabeth Davis, University of Liverpool, UK
Youhei Yamashita, Hokkaido University, Japan

***Correspondence:**
Michael Seidel
m.seidel@uni-oldenburg.de

†Present Address:
Barbara Deutsch, Biota—Institut für Ökologische Forschung und Planung GmbH, Bützow, Germany

Specialty section:
This article was submitted to Marine Biogeochemistry, a section of the journal Frontiers in Earth Science

Received: *07 November 2016*
Accepted: *06 April 2017*
Published: *02 May 2017*

Citation:
Seidel M, Manecki M, Herlemann DPR, Deutsch B, Schulz-Bull D, Jürgens K and Dittmar T (2017) Composition and Transformation of Dissolved Organic Matter in the Baltic Sea. Front. Earth Sci. 5:31. doi: 10.3389/feart.2017.00031

The processing of terrestrial dissolved organic matter (DOM) in coastal shelf seas is an important part of the global carbon cycle, yet, it is still not well understood. One of the largest brackish shelf seas, the Baltic Sea in northern Europe, is characterized by high freshwater input from sub-arctic rivers and limited water exchange with the Atlantic Ocean *via* the North Sea. We studied the molecular and isotopic composition and turnover of solid-phase extractable (SPE) DOM and its transformation along the salinity and redox continuum of the Baltic Sea during spring and autumn. We applied ultrahigh-resolution mass spectrometry and other geochemical and biological approaches. Our data demonstrate a large influx of terrestrial riverine DOM, especially into the northern part of the Baltic Sea. The DOM composition in the central Baltic Sea changed seasonally and was mainly related to autochthonous production by phytoplankton in spring. Especially in the northern, river-dominated basins, a major fraction of riverine DOM was removed, likely by bio- and photo-degradation. We estimate that the removal rate of terrestrial DOM in the Baltic Sea (Bothnian Bay to the Danish Straits/Kattegat area) is 1.6–1.9 Tg C per year which is 43–51% of the total riverine input. The export of terrestrial DOM from the Danish Straits/Kattegat area toward the North Sea is 1.8–2.1 Tg C per year. Due to the long residence time of terrestrial DOM in the Baltic Sea (total of ca. 12 years), seasonal variations caused by bio- and photo-transformations and riverine discharge are dampened, resulting in a relatively invariant DOM molecular and isotopic signature exported to the North Sea. In the deep stagnant basins of the Baltic Sea, the DOM composition and dissolved organic nitrogen concentrations changed seasonally, likely because of vertical particle transport and subsequent degradation releasing DOM. DOM in the deep anoxic basins was also enriched in sulfur-containing organic molecules, pointing to abiotic sulfurization of DOM under sulfidic conditions.

Keywords: Baltic Sea, sub-arctic rivers, discharge, dissolved organic matter, ultrahigh-resolution mass spectrometry, seasonal variation

INTRODUCTION

Shelf seas are often strongly influenced by riverine inputs of nutrients and organic matter. Although they represent only a small part of the total ocean, about 20% of the marine organic matter production and 80% of organic matter deposition to ocean sediments occurs there (Borges, 2005). Yet, the carbon cycling in coastal waters is still not well understood, partly because the different carbon sources and sinks are highly complex (Gattuso et al., 1998; Ward et al., 2017).

In coastal shelf seas and estuaries, dissolved organic matter (DOM) is derived from land plants, riverine and autochthonous (marine) primary production (Stedmon et al., 2010; Bauer and Bianchi, 2011; Osburn and Stedmon, 2011; Deutsch et al., 2012). Removal and transformation of terrestrial DOM occurs through processes such as flocculation (Sholkovitz et al., 1978), microbial and photo-degradation (Hernes and Benner, 2003; Obernosterer and Benner, 2004; Gonsior et al., 2009; Spencer et al., 2009; Stubbins et al., 2010). Complete remineralization releases inorganic chemical species that then serve as nutrients for aquatic microbes and phytoplankton (Vähätalo and Zepp, 2005). High concentrations of chromophoric DOM in many estuaries limit primary production due the lower light penetration in the water column (Urtizberea et al., 2013). Studying and untangling these features still poses a major challenge because these processes often occur simultaneously, and because of the dynamic nature of estuarine systems (Bauer and Bianchi, 2011).

The Baltic Sea is a shelf sea with high inputs of nutrients from surrounding rivers that stimulate large phytoplankton blooms from spring to autumn, which effectively take up CO_2. At the same time, high primary production of organic matter (OM) stimulates heterotrophic activity, which is further enhanced by the input of terrestrial DOM from rivers. The net uptake or release of atmospheric CO_2 differs for the different subbasins of the Baltic Sea (Thomas et al., 2010; Kuliński and Pempkowiak, 2011; Gustafsson et al., 2014; Ylöstalo et al., 2016): the central Baltic Sea is a CO_2 sink, while the northern Bothnian Bay is a weak source of CO_2 to the atmosphere (Löffler et al., 2012; Schneider et al., 2014).

It is likely that increasing temperature and precipitation will lead to a higher riverine export of terrestrial DOM (Voss et al., 2011; Räike et al., 2016). Understanding the fate of this enhanced input of terrestrial carbon in sub-arctic shelf seas along marine-terrestrial and redox-gradients is therefore important. The Baltic Sea is an ideal system to study the biogeochemical cycling of DOM in terrestrial-to-marine and in oxic-to-anoxic gradients in detail, because of its estuarine character in combination with long water residence times ranging from months to years (Savchuk, 2005). The Baltic Sea in northern Europe is a semi-enclosed, brackish marginal sea. It is characterized by limited water exchange with the Atlantic Ocean *via* the North Sea and high freshwater input from rivers. The shallowness and infrequent inflow of saline and dense North Sea water causes a permanent stratification in the central Baltic Proper at water depths >60 m (Kuliński and Pempkowiak, 2012). The northern drainage basin is dominated by sub-arctic boreal forests while the southern basin is dominated by agriculture and high population density. Consequently, parts of the southern Baltic Sea are threatened by eutrophication and extension of bottom water anoxia (Thomas et al., 2010). Hypoxic conditions are reached when oxygen concentrations fall below 2 mL L^{-1} and alternative terminal electron acceptors, such as nitrate and sulfate, are used during heterotrophic degradation of organic matter by microbes (Conley et al., 2009). Microbial sulfate reduction causes sulfidic conditions in the deep anoxic basins of the central Baltic Sea (Savchuk, 2005; Voss et al., 2011).

Previous studies have used molecular biomarkers, isotopes, and optical properties to differentiate marine and terrestrial sources of DOM in the Baltic Sea (Højerslev et al., 1996; Bianchi et al., 1997; Stedmon et al., 2000, 2010; Alling et al., 2008; Osburn and Stedmon, 2011; Deutsch et al., 2012). For example, the concentration of suspended lignin phenols (unique biomarkers for vascular plants, e.g., Hernes and Benner, 2003) decreased from north to the south due to high freshwater inflow into the northern Baltic Sea (Bianchi et al., 1997). Stable carbon isotope ratios of high-molecular weight (HMW) DOM revealed a non-conservative behavior and removal of terrestrial HMW DOM in the Baltic Sea (Alling et al., 2008; Deutsch et al., 2012). Residence times for terrestrial HMW DOM ranged from 2.8 years in the northern to 4.5 years in the southern Baltic Sea, and more than 50% of it was proposed to be removed in the coastal Baltic Sea (Deutsch et al., 2012). Osburn and Stedmon (2011) used optical and chemical DOM properties and estimated that 0.8 Tg yr^{-1} terrestrial dissolved organic carbon (DOC) was exported from the Baltic to the North Sea. The molecular composition, the transformation and the export of low molecular weight terrestrial DOM, however, remains unexplored.

Ultrahigh-resolution Fourier-transform ion cyclotron resonance mass spectrometry (FT-ICR-MS) is a powerful tool to deepen our understanding of DOM processing in estuarine settings, because it resolves thousands of molecular formulae in the very complex DOM mixtures. Consequently, this technique was used to study the transformation of DOM in a wide range of aquatic systems, including terrestrial-to-marine and oxic-to-anoxic transition zones (Koch et al., 2005; Kim et al., 2006; Sleighter and Hatcher, 2008; Schmidt et al., 2009; Longnecker and Kujawinski, 2011; Lechtenfeld et al., 2013). For example, in the Delaware Estuary (USA), compositional differences at the molecular level were not reflected in changes of DOC concentrations (Osterholz et al., 2016). Several other studies have shown that the transformation of terrestrial and the new production of autochthonous (marine) DOM compounds leave characteristic molecular imprints (Sleighter and Hatcher, 2008; Kujawinski et al., 2009; Medeiros et al., 2015a,b; Seidel et al., 2015b). Aromatic terrestrial DOM compounds generally decrease along salinity gradients while the DOM heteroatom content increases due to autochthonous production (Sleighter and Hatcher, 2008; Osterholz et al., 2016). Likewise, the alteration of DOM under different redox-regimes can leave identifiable molecular imprints such as the relative enrichment of sulfur-containing compounds (Schmidt et al., 2009; Seidel et al., 2014, 2015a; Sleighter et al., 2014; Gomez-Saez et al., 2016).

Here we used ultrahigh-resolution mass spectrometry to determine the DOM molecular composition in the Baltic Sea

from the sub-arctic north to the boreal south during spring and autumn sampling and relate it to geochemical and biological tracers. We aimed to answer the following research questions: What is the composition and the fate of DOM from marine and terrestrial sources in the Baltic Sea? How do the anoxic conditions influence the DOM composition and transformations? How do DOM and carbon fluxes to the North Sea vary seasonally?

MATERIALS AND METHODS

Study Site

The Baltic Sea consists of five major basins, the Bothnian Bay, the Bothnian Sea, the Baltic Proper, the Gulf of Riga, and the Gulf of Finland (**Figure 1**). The freshwater inflow to the Baltic Sea is ∼480 km^3 yr^{-1}, of which 200 and 100 km^3 yr^{-1} are received by the Bothnian Bay (e.g., inflow of the Kalix River) and the Gulf of Finland (Neva River), respectively (Voss et al., 2011). Surface salinity ranges from two in the northernmost Bothnian Bay to >20 in the Kattegat and >30 in the Skagerrak. Deep-water salinity is 3–7 in the Bothnian Sea >50 m depth and 10–13 in the central Baltic Sea >60 m depth (Kullenberg and Jacobsen, 1981; Voss et al., 2011). Due to the shallow connection, water exchange between the Baltic Sea and the North Sea is limited. Following a typical estuarine circulation pattern, North Sea water enters through the Skagerrak and Kattegat at the bottom while brackish Baltic Sea water builds an outflow of water on top. The halocline in the central Baltic Sea at about 60 m limits vertical water mixing, and bottom water exchange between the deep basins of the Baltic Sea is further limited by sills. This causes the development of bottom water anoxia in the deep basins such as the Gotland and Landsort Deeps.

Sampling, Chemical, and Biological Analyses

Samples were collected during two cruises with *R/V Meteor*, in November/December 2011 (leg M86/1, autumn), and in May/June 2012 (leg M87/3, spring; **Figure 1**). Sampling in 2012 covered the spring flood of sub-arctic rivers draining large permafrost areas in the Northern Baltic region.

Conductivity, temperature, chlorophyll *a* fluorescence and dissolved oxygen concentrations of the water samples were measured *in situ* using a conductivity-temperature-depth sensor (Sea-Bird 911 CTD), a fluorometer (Wetlabs ECO FLNTU), and a dissolved oxygen sensor (Sea-Bird SBE43) connected to the sampling rosette.

Dissolved inorganic phosphate, nitrite, nitrate, ammonium, and silicate concentrations were measured in filtered samples following standard photometric methods (Grasshoff et al., 1999), using a continuous-flow analyzer (FLOWSYS, Alliance Instruments). The samples were filtered through pre-combusted Whatman GF/F filters and stored at −20°C until analysis. Ammonium was determined directly after sampling using a UV mini 1,240 photometer (Shimadzu). Precision was <10%, and detection limits were: nitrite 0.05 μM, nitrate 0.125 μM, ammonium 0.5 μM, phosphate 0.125 μM, silicate 0.5 μM. Dissolved organic nitrogen concentrations (DON) were calculated as difference between total dissolved nitrogen (TDN) and nitrate + nitrite + ammonium concentrations.

DOC and TDN were measured in the filtered and acidified (pH 2, HCl, p.a.) water samples by high temperature catalytic oxidation on a Shimadzu TOC-VCPH instrument. Analytical accuracy and precision were tested against the deep-sea reference sample (D. Hansell, University of Miami, USA) and were better than 5%.

DOM was extracted from 250 mL of filtered and acidified (HCl, pH 2, p.a.) water as described by Dittmar et al. (2008) using solid phase extraction (SPE) with cartridges filled with a styrene divinyl benzene polymer (Agilent Bond Elut PPL, 1 g). The methanol extracts were stored frozen in the dark until further analysis. The extraction efficiencies were determined as SPE-DOC divided by bulk DOC concentrations. SPE-DOC was determined by drying an aliquot of the SPE-DOM extract (at 40°C) and re-dissolving it in ultrapure water.

The stable carbon isotope composition was determined on SPE-DOM. Extracts containing ca. 20 μg of DOC were pipetted into Sn caps (IVA, Germany) and subsequently dried at 40°C in an oven. The isotopic composition was analyzed in duplicates on an isotope-ratio-monitoring mass spectrometer (Finnigan MAT 252, Bremen, Germany) *via* a Conflo II split interface. The stable carbon isotope ratios are reported in δ notation relative to the Vienna Pee Dee Belemnite. Precision and accuracy was <0.5‰ and procedural blanks did not yield detectable amounts of carbon isotope contamination.

For bacterial enumeration, 4 mL samples were fixed for 1 h with 400 μL of 1% (final concentration) paraformaldehyde and 0.5% (final concentration) glutaraldehyde, shock frozen in liquid nitrogen, and stored at −80°C until processed by flow cytometry. Samples were measured on a FacsCalibur bench cytometer (Becton Dickinson) using a modification of the method of Gasol et al. (1999). Briefly, 0.2-μm-filtered SYBR Green solution (2.4 M potassium citrate, 0.2 M dimethyl sulfoxide and 5 μL SYBR Green) was mixed with 300 μL of the sample. The mixture was incubated for 30 min in the dark and measured for 3 min in a flow cytometer at a medium, previously determined flow rate. The diluted bead solution was microscopically evaluated against the measurements received by the flow cytometry. The flow diagrams were evaluated using the software CellQuestPro. Cells with chlorophyll autofluorescence (including cells of Synechococcus, picoeukaryotes, and nanoeukaryotes) were measured without SYBR Green staining based on autofluorescence in the FL2 (phycoerythrin) and FL3 (chlorophyll *a*) detectors of the FacsCalibur bench cytometer as described by Gasol et al. (1999).

FT-ICR-MS Analysis

The methanol extracts were diluted with ultrapure water and methanol (MS grade) to yield a DOC concentration of 10 mg L^{-1} in 1:1 methanol:water (*v/v*) for the analysis with FT-ICR-MS (15 Tesla solariX, Bruker Daltonik). We used electrospray ionization (ESI) in negative mode. Instrument settings and molecular formulae assignments are described in detail in Seidel et al. (2014). The capillary voltage was 4 kV in negative mode. Ions were accumulated in the hexapole for 0.3 s and data were acquired in broadband mode using 4 megaword data sets and

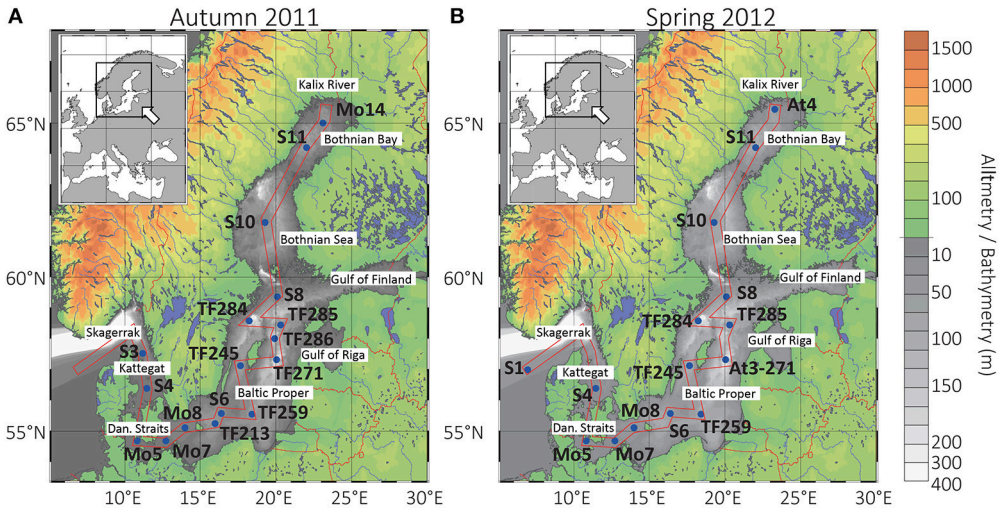

FIGURE 1 | Map of the Baltic Sea with sampling stations. Sampling transects in autumn 2011 **(A)** and in spring 2012 **(B)**. The Gotland and Landsort Deeps are located at stations TF271 (autumn), At3-271 (spring), and TF284 (autumn and spring), respectively. Dan. Straits, Danish Straits.

a scanning range of 150–2,000 Da with 500 scans accumulated per mass spectrum. Mass spectra were calibrated internally with a list of known compounds in the targeted mass range (achieved mass accuracy <0.1 ppm). Molecular formulae were assigned to peaks with a signal-to-noise ratio >4 applying the criteria described by Koch et al. (2007) with a mass tolerance of <0.5 ppm. The signal intensities of peaks with assigned molecular formulae were normalized to the sum of all peak intensities with identified molecular formulae in each sample, and normalized peak intensities were multiplied by a factor of 10,000. The aromaticity and the degree of unsaturation of compounds were assessed using the modified aromaticity index (AI_{mod}; Koch and Dittmar, 2006, 2016). This parameter was developed to identify aromatic and condensed aromatic structures in DOM molecular formulae data acquired by ultrahigh-resolution MS. AI_{mod} values >0.5 are indicative for aromatic compounds, AI_{mod} values ≥0.67 are unambiguous indicators for condensed aromatic compounds. Intensity-weighted averages of AI_{mod}, number of atoms per molecular formula (carbon, C, hydrogen, H, oxygen, O, nitrogen, N, sulfur, S, and phosphorus, P), and molar ratios (hydrogen-to-carbon, H/C and oxygen-to-carbon, O/C) were calculated for each sample by considering the peak intensity of each assigned molecular formula as described in Seidel et al. (2014).

Molecular compound groups were assigned to molecular formulae as described in Seidel et al. (2014): group (1), polycyclic aromatics (PCAs, AI_{mod} >0.66), including condensed combustion-derived dissolved black carbon if C > 15 (Dittmar and Koch, 2006), (2) highly aromatic compounds with aliphatic side chains (HACs, Koch and Dittmar, 2006) ($0.66 \geq AI_{mod} \geq 0.50$), (3) highly unsaturated compounds (HUCs, $AI_{mod} < 0.50$ and H/C < 1.5), including lignin degradation products (Stenson et al., 2003) and carboxyl-rich alicyclic molecules (CRAM, Hertkorn et al., 2006), (4) unsaturated aliphatic compounds ($2.0 \geq H/C > 1.5$, N = 0), (5) saturated compounds, including lipids (H/C > 2.0 and O/C < 0.9), (6) saturated compounds (H/C > 2.0) with O/C > 0.9, including carbohydrate molecular formulae, and (7) unsaturated aliphatic compounds containing N, including peptide molecular formulae ($2.0 > H/C \geq 1.5$, N > 0). Further, we separated the molecular formulae according to their heteroatom content, i.e., (8) molecular formulae that contain N, (9) molecular formulae that contain S, (10) molecular formulae that contain P, and (11) molecular formulae that contain N and S. The molecular categorizing using ultrahigh-resolution MS provides information about likely structures behind the identified molecular formulae. The molecular structure assignment for molecular formulae is ambiguous because several different isomers may exist for a single molecular formula. However, the assignment of compound groups based on molecular level information obtained by FT-ICR-MS has been successfully used to identify biogeochemical processing of DOM (e.g., Kim et al., 2003; Schmidt et al., 2009). The proportion of each compound group is reported as the percentage of molecular formulae of a given compound group relative to the total number of molecular formulae detected in the sample.

Statistical Analyses and Terrestrial DOC Flux Calculations

Principal coordinate analysis (PCoA) was performed on a Bray-Curtis dissimilarity matrix of the normalized peak intensities of all detected DOM molecular formulae. DOM molecular endmembers were identified using Ward's hierarchical clustering based on a Bray-Curtis dissimilarity matrix and PCoA. The DOM compound groups and environmental data (including DOC concentrations, stable carbon isotope composition of SPE-DOM, chlorophyll concentrations, concentrations of dissolved nitrogen species, silicate, phosphate, oxygen, salinity, and water temperature) were fitted *post-hoc* to the PCoA scores using the envfit function of the vegan package (Oksanen et al., 2015) within the R statistical platform (R core team, 2015). The correlation of environmental parameters to the DOM molecular composition

(PCoA) was tested with 10,000 permutations and was considered significant if $p < 0.1$. Pearson correlations were used to assess the linear relationship between DOM compound groups and environmental parameters (α level 0.05). All contour plots and maps were produced using the Ocean Data View software (Schlitzer, 2016).

We determined how the concentrations of the measured nutrients, DOC, the ^{13}C isotopic composition of SPE-DOM and the relative abundance of DOM compound groups deviated from simple linear mixing of marine and terrestrial endmembers by using the correlation and regression analyses described previously by Seidel et al. (2015a). For the present study, we modified this approach by scaling the relative abundances of the molecular compound groups to the DOC concentrations (i.e., by multiplying the relative abundance of each compound group to the DOC concentration of each sample) before normalizing the data to values between 0 (minimum) and 1 (maximum). In short, this analysis gives a relative measure Δ_{mix} indicating the percentage that a measured parameter deviates from values expected from simple linear mixing of two endmembers (if significantly correlated to salinity, $p \leq 0.05$) or averaged measured values (if endmembers had similar values). High Δ_{mix} values (>10%) describe a relatively high variability of the parameter in comparison to values expected from a linear mixing model or in relation to the average measured value along the salinity gradient. It is very important to note that this approach is not intended to describe the Baltic Sea as a simple two-endmember mixing model, i.e., a system where the terrestrial DOM from the northern basin rivers (e.g., Kalix or Neva Rivers) mixes with the marine DOM from the North Sea in the south. As mentioned before, almost two-thirds of the Baltic Sea riverine freshwater inflow occurs in the northern basins but additional terrestrial DOM is supplied to the southern Baltic Sea by rivers such as the Oder, Nemunas, and Vistula Rivers. Our mixing analysis was therefore intended as a first-order approach to assess the dynamics of the DOM composition along the estuarine gradient when considering the two most extreme endmembers (sub-arctic terrestrial *vs.* marine DOM) of the Baltic Sea. In this analysis, deviations from the mixing of these endmembers can thus be due to removal or production of DOM compounds but also due to enrichment or depletion of the DOM compounds caused by to the input of freshwater with different DOC concentrations compared to the northern rivers along the salinity gradient.

The relative proportion of terrestrial SPE-DOM was calculated using $\delta^{13}C$ SPE-DOM under consideration of terrestrial ($\delta^{13}C_{terr}$) and marine/autochthonous ($\delta^{13}C_{marine}$) endmembers:

$$\text{terrestrial SPE-DOM (\%)} = \frac{\delta^{13}C_{sample} - \delta^{13}C_{marine}}{\delta^{13}C_{terr} - \delta^{13}C_{marine}} \times 100$$

The terrestrial and marine endmembers were determined by extrapolating the range of $\delta^{13}C$ SPE-DOM values and DOC concentrations along the salinity gradient to salinities 0 and 35, respectively. Accordingly, the endmembers used for calculating the relative proportion of terrestrial SPE-DOM were salinity 0, $\delta^{13}C$ SPE-DOM −28‰, DOC 400 μM and salinity 35, $\delta^{13}C$ SPE-DOM −22‰, DOC 100 μM, respectively.

To extend our simplified mixing analysis, we also calculated the terrestrial DOC fluxes between the basins using a box model approach where we considered the in- and outflow for the basins of the Bothnian Bay, Bothnian Sea, Baltic Proper (including Gulf of Finland and Gulf of Riga), Danish Straits, and Kattegat area. The terrestrial DOC fluxes were calculated using the DOC concentrations (without PPL extraction), the relative proportions of terrestrial SPE-DOC from this study (with PPL extraction), and water flows between basins reported previously by Savchuk (2005). The net terrestrial DOC balance per basin (loss rate) was calculated as the difference of influx and outflux, i.e., the terrestrial DOC input by rivers (Gustafsson et al., 2014) and adjacent basins minus the outflow to adjacent basins. The residence times of terrestrial DOC were calculated for each basin by dividing the total stock of terrestrial DOC in each basin by all inputs of terrestrial DOC into the basin (sum of the inputs from adjacent basins and rivers). The reported values are basin averaged means ± standard deviations (of all concentration and isotope data determined in each basin). We note that for calculating fluxes and residence times of terrestrial DOC, we used the terrestrial SPE-DOC values (calculated percentage of terrestrial DOC using ^{13}C isotopic composition of DOC after PPL extraction) and the overall DOC pool (without PPL extraction). Although, PPL extraction has a poor recovery for very low molecular weight ionic compounds (Raeke et al., 2016), it provides a major fraction of the overall DOM (Green et al., 2014). As in previous studies (Seidel et al., 2015a,b; Osterholz et al., 2016), our extraction efficiencies were not correlated to salinity. We therefore assume that representative fractions of the marine and terrestrial DOM pools were extracted along the salinity gradient and that the terrestrial SPE-DOC values can be applied to infer the contribution of terrestrial DOC to the overall DOC pool.

RESULTS

General Water Characteristics

Temperatures were highest in the seawater entering from the North Sea through the Skagerrak and Kattegat. A steeper temperature gradient developed in spring compared with the temperature gradient in autumn (**Figures 2A,B**). Surface salinity increased from 2.7 to 26 (autumn) and 35 (spring) from the Kalix River outflow stations (Bothnian Bay) toward the marine water inflow at the Skagerrak and Kattegat. In the Bothnian Bay and Sea, salinity was <6 throughout the water column while in the Gotland Deep and Landsort Deep the water was more saline with salinities between 10 and 12 (**Figures 2C,D**). Dissolved oxygen concentrations were highest in the surface layers from the Bothnian Bay to the Skagerrak (6–10 mL L^{-1}). Oxygen concentrations were lower in the deep central Baltic Sea with hypoxic conditions (<1.4 mL L^{-1}) >100 m water depth (Gotland and Landsort Deeps). Anoxic conditions prevailed in >120 m (Gotland Deep) and >140 m depth (Landsort Deep), respectively (**Figures 2E,F**).

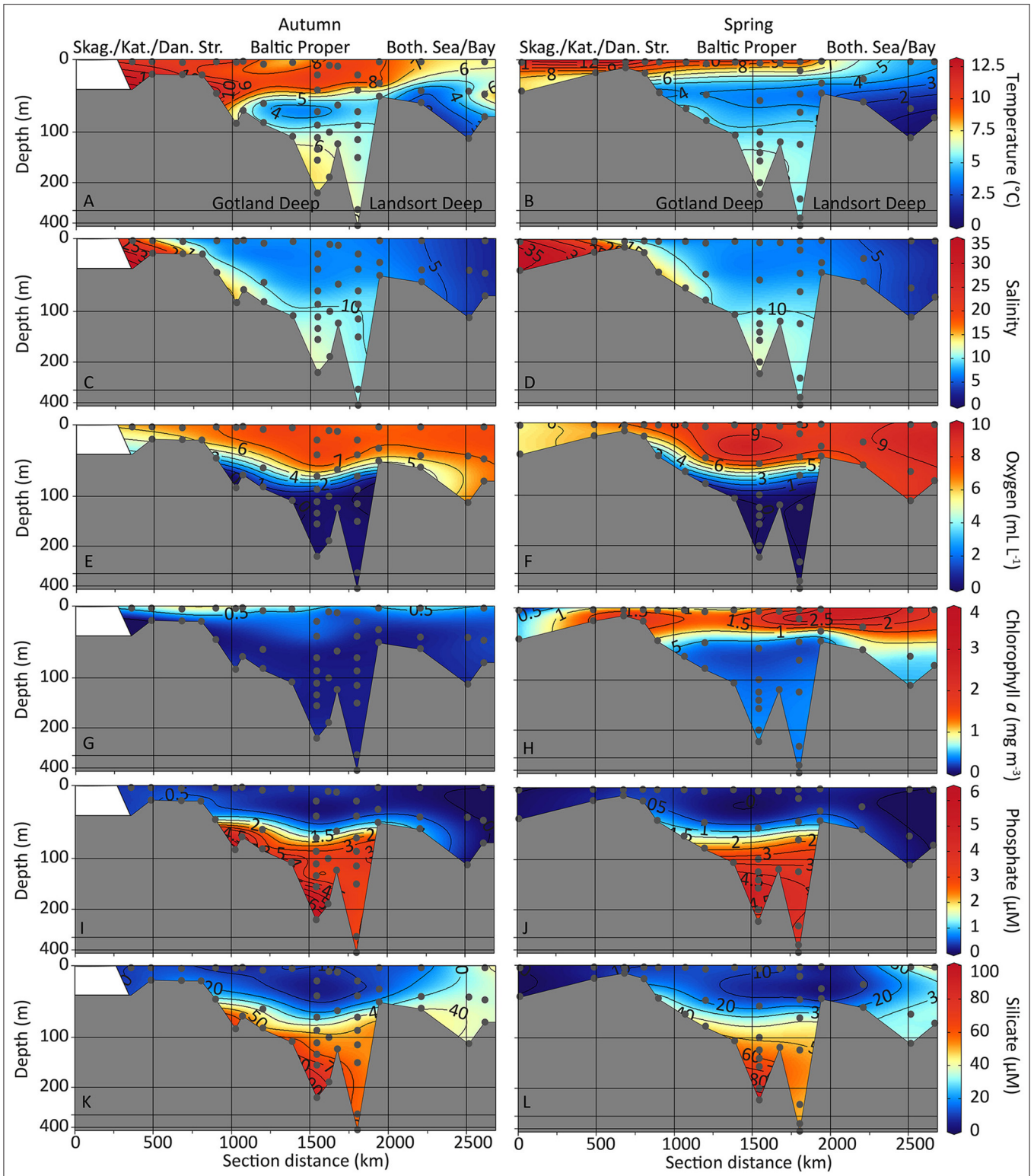

FIGURE 2 | Contour depth plots of the sampling transects. Water temperature **(A,B)**, salinity **(C,D)**, dissolved oxygen concentrations **(E,F)**, concentrations of chlorophyll *a* **(G,H)**, phosphate **(I,J)**, and silicate **(K,L)** are shown for autumn (left) and spring (right) sampling. Non-linear depth scale. Skag., Skagerrak; Kat., Kattegat; Dan. Str., Danish Straits; Both. Sea/Bay, Bothnian Sea and Bothnian Bay.

Inorganic Nutrients and Cell Numbers

Chlorophyll *a* concentrations were highest in the surface water of the Kattegat area and the southern Baltic Proper (stations S4 to TF245, **Figure 1**) with values between 0.6 and 1 mg m^{-3} in autumn (**Figure 2G**). In spring, chlorophyll *a* concentrations were high in the surface waters of the Bothnian Sea (1.8 mg m^{-3} at station At4) and the southern Baltic Proper (1.3 mg m^{-3} at station Mo5) and increased to values of up to 3.5 mg m^{-3} at the Landsort Deep (station TF284, **Figure 1**) at 14 m depth (**Figure 2H**). For the autumn sampling campaign, the number of primary producers was also assessed by enumeration of cells with chlorophyll autofluorescence (including cells of Synechococcus, picoeukaryotes, and nanoeukaryotes, Supplementary Figure 1A). These data matched closely the chlorophyll data that were assessed using the fluorescence detector connected to the sampling rosette, i.e., highest concentrations of primary producers were found in the southern Baltic Proper (Supplementary Figure 1A). In addition, the concentration of prokaryotes was assessed by flow cytometry. Prokaryotic cell numbers were highest in the surface waters of the southern Baltic Proper, in the Bothnian Bay and in the hypoxic/anoxic water masses of the Gotland Deep and Landsort Deep (Supplementary Figure 1B).

Phosphate and silicate concentrations were highest in the anoxic Gotland and Landsort Deeps (**Figures 2I–L**). Phosphate concentrations in the Landsort Deep were up to 5.1 μM (spring) and 6.5 μM (autumn) and in the Gotland Deep up to 3.9 μM (spring) and 3.5 μM (autumn). Silicate concentrations in the Gotland Deep were up to 97 μM (spring) and 93 μM (autumn) and in the Landsort Deep up to 53 μM (spring) and 60 μM (autumn). Phosphate concentrations were ≤0.5 μM (below detection limit) in autumn and spring in the surface samples throughout the Baltic Sea (**Figures 2I,J**). Silicate concentrations were elevated in the surface waters of the Bothnian Bay (37–40 μM and 35–43 μM in autumn and spring, respectively) but depleted in the surface samples of the Baltic Proper (4.2–13 μM and 0–15 μM in autumn and spring, respectively, **Figures 2K,L**).

TDN concentrations in autumn were high at the surface in the Bothnian Bay (station Mo14 with 30 μM TDN) while in the Baltic Proper, surface TDN concentrations were lower with 14–18 μM (autumn, Supplementary Figure 2A) and 12–18 μM (spring, Supplementary Figure 2B). TDN concentrations were highest in the bottom water of the Gotland Deep with 55 and 60 μM in spring and autumn, respectively (Supplementary Figures 2A,B). In the bottom water of the Landsort Deep, TDN concentrations were 21 μM (spring) and 22 μM (autumn, Supplementary Figures 2A,B), respectively. Nitrate concentrations were highest in the Bothnian Bay with values of up to 8.2 μM at station S11 in autumn (**Figure 3A**) and 6.4 μM in spring (**Figure 3B**). In the Baltic Proper, nitrate concentrations decreased to levels below the detection limit (0.125 μM) in the surface samples (**Figure 3B**). Nitrite concentrations were generally low (<0.5 μM) with the highest values during autumn (Supplementary Figures 2C,D). Ammonium concentrations were highest in the anoxic waters of the Gotland and Landsort Deeps (**Figures 3C,D**). The ammonium concentrations positively correlated with silicate and phosphate concentrations in autumn (Supplementary Figure 3) and spring (Supplementary Figure 4). Ammonium concentrations were lower in spring compared to autumn (Landsort Deep 6.4 μM compared to 11 μM, and Gotland Deep 11 μM compared to 31 μM in **Figures 3C,D**). DON concentrations were high in the Baltic Proper (surface concentrations 15–17 μM and 9.2–17 μM in autumn and spring, respectively, **Figures 3E,F**). High DON concentrations were also found in the bottom water of the anoxic Gotland (29 μM in autumn and 28 μM in spring) and Landsort Deeps (11 μM in autumn and 15 μM in spring, **Figures 3E,F**). The TDN concentrations positively correlated to DON concentrations in autumn (Supplementary Figure 3) and spring (Supplementary Figure 4) while DON also positively correlated with ammonium concentrations in spring (Supplementary Figure 4).

DOC Concentrations and Isotopic Composition

DOC concentrations were highest in the Bothnian Bay and Bothnian Sea close to the Kalix River outflow with 379 μM during the spring flood (Bothnian Bay station At4, surface, **Figure 1**). During autumn, highest DOC concentrations occurred in the Baltic Proper and the Bothnian Sea (301–341 μM from station Mo7 to S10, surface to 70 m depth) while in the Bothnian Bay, DOC concentrations were 304–308 μM (stations S11 and Mo14, 11–41 m depth, **Figures 1**, **4A**). Toward the Kattegat (station S4), DOC concentrations decreased to 187 μM in autumn (**Figure 4A**). In spring, DOC concentrations decreased to 118 μM in the Skagerrak (station S1, **Figures 1**, **4B**).

For both sampling campaigns, samples from the Bothnian Bay were characterized by depleted $\delta^{13}C$ SPE-DOM signatures (between −27.9 and −27.1‰ in autumn at stations Mo14 and S11, and between −27.4 and −26.7‰ in spring at stations At4 and S11). Samples from the North Sea and Kattegat were more enriched (−25.2‰ in autumn at station S3, and −23.2‰ in spring at station S1, **Figures 1**, **4C,D**). The isotopic composition of samples from the central Baltic Proper were between −27.0 and −25.2‰ (autumn) and −27.3 and −25.3‰ (spring, **Figures 4C,D**). The relative abundance of terrestrial SPE-DOC ranged from almost 100% close to the Kalix River outflow in the Bothnian Bay and decreased to ca. 75% in the Bothnian Sea (**Figures 4E,F**). Within the Baltic Proper basin, terrestrial SPE-DOC was uniformly distributed with values between 70 and 75%. A decrease to 53% was found in the Kattegat bottom water (inflowing North Sea water) while the surface water (outflowing Baltic Sea water) contained 69% (autumn) and 78% (spring) terrestrial SPE-DOC, respectively. The most marine station at Skagerrak in the North Sea (station S1 in **Figure 1**, salinity 34.9 in spring) contained 5.5% terrestrial SPE-DOC in the bottom and 24% terrestrial SPE-DOC in the surface water (**Figure 4F**).

Distribution of DOM Molecular Compound Groups

SPE-DOM extraction efficiencies were 77 ± 10% (n = 51, whereby few samples with extraction efficiencies above 90 and below 40% were not considered because they were likely

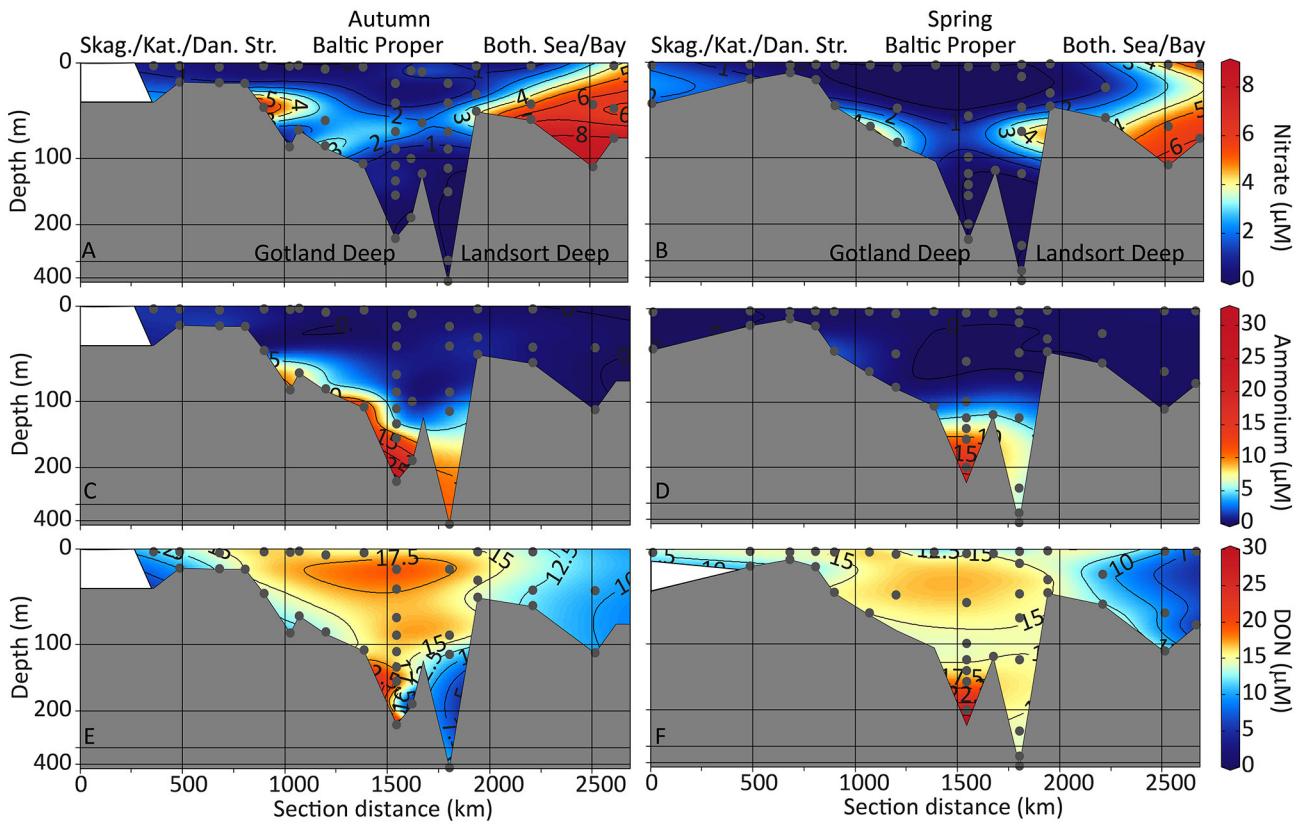

FIGURE 3 | Contour depth plots of the sampling transects. Nitrate **(A,B)**, ammonium **(C,D)**, and dissolved organic nitrogen (DON; **E,F**) concentrations are shown for autumn (left) and spring (right) sampling. Non-linear depth scale. Skag., Skagerrak; Kat., Kattegat; Dan. Str., Danish Straits; Both. Sea/Bay, Bothnian Sea and Bothnian Bay.

erroneous). Extraction efficiencies were not correlated to salinity ($p > 0.05$, $r = -0.27$, $n = 51$). This supports our assumption that there was no preferential extraction of terrestrial over marine compounds from the DOM that is extracted with the PPL method. In total, ca. 6,000 molecular formulae were identified in the SPE-DOM. From the Kalix River outflow toward the Bothnian Sea, most molecular formulae were highly aromatic and highly unsaturated molecular formulae (groups 1–3 were up to 90% of all molecular formulae, Supplementary Figures 5A–F). Condensed and highly aromatic compounds (groups 1 and 2) were most abundant in the Bothnian Bay and Bothnian Sea, decreasing from 7.2% (group 1) and 16% (group 2) to 4.5% (group 1) and 14% (group 2) in the Baltic Proper. In this area, also the highest percentage of aromatic compounds, an indicator for terrestrial DOM, was found (weighted-average AI_{mod} in **Figures 5A,B**). Accordingly, salinity and $\delta^{13}C$ SPE-DOM values were negatively correlated to condensed aromatics (group 1, in autumn and spring) or highly aromatic compounds (group 2, in spring only) (Supplementary Figures 3, 4). The relative abundances of highly unsaturated compounds (group 3, Supplementary Figures 5E,F) and unsaturated aliphatics (group 4, Supplementary Figures 5G,H) were highest in the marine inflow area of the Kattegat with values of up to 72% (group 3) and 15% (group 4), respectively. The relative abundance of saturated compounds (group 5, Supplementary Figures 5I,J) was highest in autumn in the marine inflow waters at the Kattegat (up to 1.4%), while in spring, values were low throughout the Baltic Sea (<0.6%). Saturated compounds with high O/C ratios (group 6) were close to zero and were therefore excluded from further analyses. Unsaturated compounds containing N (group 7, including peptide molecular formulae, Supplementary Figures 5K,L) contributed up to 1.2% throughout the Baltic Sea in autumn and were <1% in spring. In our regression analyses, all compound groups (scaled to DOC concentrations), apart from saturated compounds (group 5), were negatively correlated to salinity in autumn ($p < 0.05$, Supplementary Figure 6). In spring, compound groups 1–4 negatively correlated with salinity whereas groups 5–11 did not (Supplementary Figure 6). Group 7 compounds positively correlated with DON concentrations in spring (Supplementary Figure 4), when DON concentrations were highest in the anoxic Landsort and Gotland Deeps (**Figure 3F**).

N-containing compounds (group 8) were most abundant in the marine inflow water at the Kattegat (up to 26% of all molecular formulae; **Figures 5C,D**). S-containing formulae (group 9, **Figures 5E,F**) were abundant in the marine inflow water (up to 22% of all molecular formulae) and in the anoxic

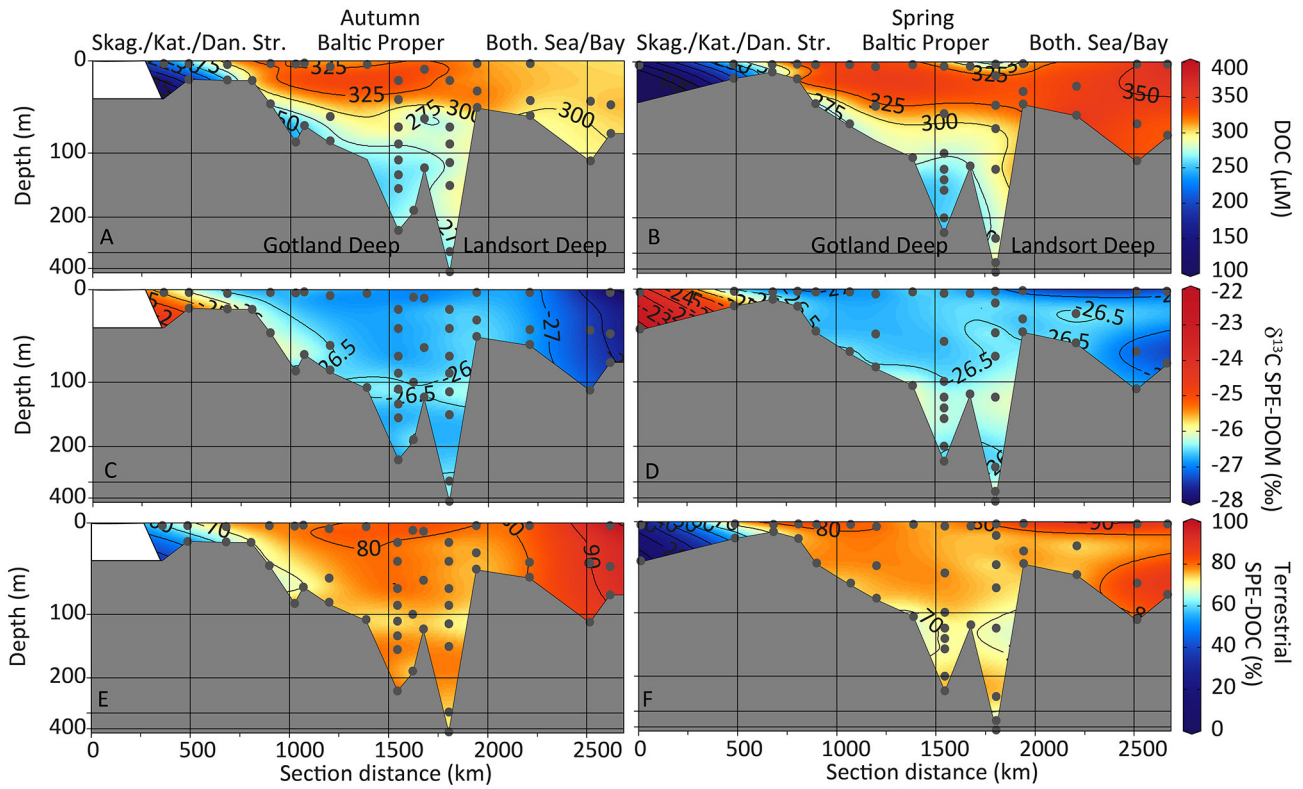

FIGURE 4 | Contour depth plots of the sampling transects. Bulk DOC concentrations **(A,B)**, ^{13}C isotopic SPE-DOM composition **(C,D)**, and the relative abundance of terrestrial SPE-DOC (based on δ^{13}C SPE-DOM; **E,F**) are shown for autumn (left) and spring (right) sampling. Non-linear depth scale. Skag., Skagerrak; Kat., Kattegat; Dan. Str., Danish Straits; Both. Sea/Bay, Bothnian Sea and Bothnian Bay.

bottom water of the Gotland Deep and Landsort Deep (18–22% of all molecular formulae). P-containing formulae (group 10) were most abundant in the marine inflow water in autumn (up to 6% of all molecular formulae; **Figures 5G,H**).

Total DOC concentrations negatively correlated with salinity ($p < 0.01$) in spring ($r = -0.70$, $n = 41$) and autumn ($r = -0.75$, $n = 36$; **Figure 6A**). Likewise, terrestrial DOC concentrations (based on δ^{13}C SPE-DOM) negatively correlated with salinity in both seasons ($p < 0.01$; Supplementary Figure 6). The DOC-concentration-scaled relative abundances of highly aromatic compounds (group 2, **Figure 6B**) and unsaturated aliphatic compounds (group 4, **Figure 6C**) were also negatively correlated to salinity ($p < 0.01$). In spring, the DOC-concentration-scaled relative abundances of unsaturated aliphatics (compound group 4) deviated more from linear mixing compared to autumn (**Figure 6C**).

Statistical Analyses

In PCoA analysis, the samples were correlated to eight (autumn, **Figure 7A**) and nine (spring, **Figure 7B**) environmental parameters ($p < 0.1$). In the ordination plots, the first two axes explained between 68 and 74% of the DOM molecular variability (spring and autumn, respectively). PCoA and cluster analyses revealed three DOM molecular clusters that generally followed the salinity and oxygen gradients, i.e., (1) terrestrial-oxic, (2) brackish-to-marine oxic, and (3) brackish suboxic-to-anoxic (**Figure 7**). In PCoA, the projections of sampling points onto the vectors depict correlations with the corresponding environmental parameters. In autumn and spring, the identified clusters correlated with salinity, δ^{13}C SPE-DOM, water temperature (brackish-to-marine oxic cluster, blue circles in **Figure 7**), DOC, nitrate and dissolved oxygen concentrations (terrestrial-oxic cluster, green circles in **Figure 7**), as well as depth and phosphate concentrations (suboxic-to-anoxic cluster, red circles in **Figure 7**). In spring, samples from the brackish-to-marine samples also correlated with DON concentrations (**Figure 7B**).

In autumn, marine-influenced samples correlated with the percentage of DOM groups 4, 5, 8, 9, and 10 (unsaturated aliphatics, saturated, N-, S-, and P-containing compounds, **Figure 7A**). Terrestrially influenced samples correlated with groups 1, 2, 3, 7, and 11 (polycyclic aromatic, highly aromatic, highly unsaturated, unsaturated aliphatic with N, and NS-containing compounds, **Figure 7A**). In spring, marine-influenced samples correlated with DOM compound groups 3, 4, 7, 8, 9, 10, and 11 (highly unsaturated, unsaturated aliphatic with/without N, saturated, N-, S-, P-, and NS-containing compounds, **Figure 7B**). More terrestrial influenced samples

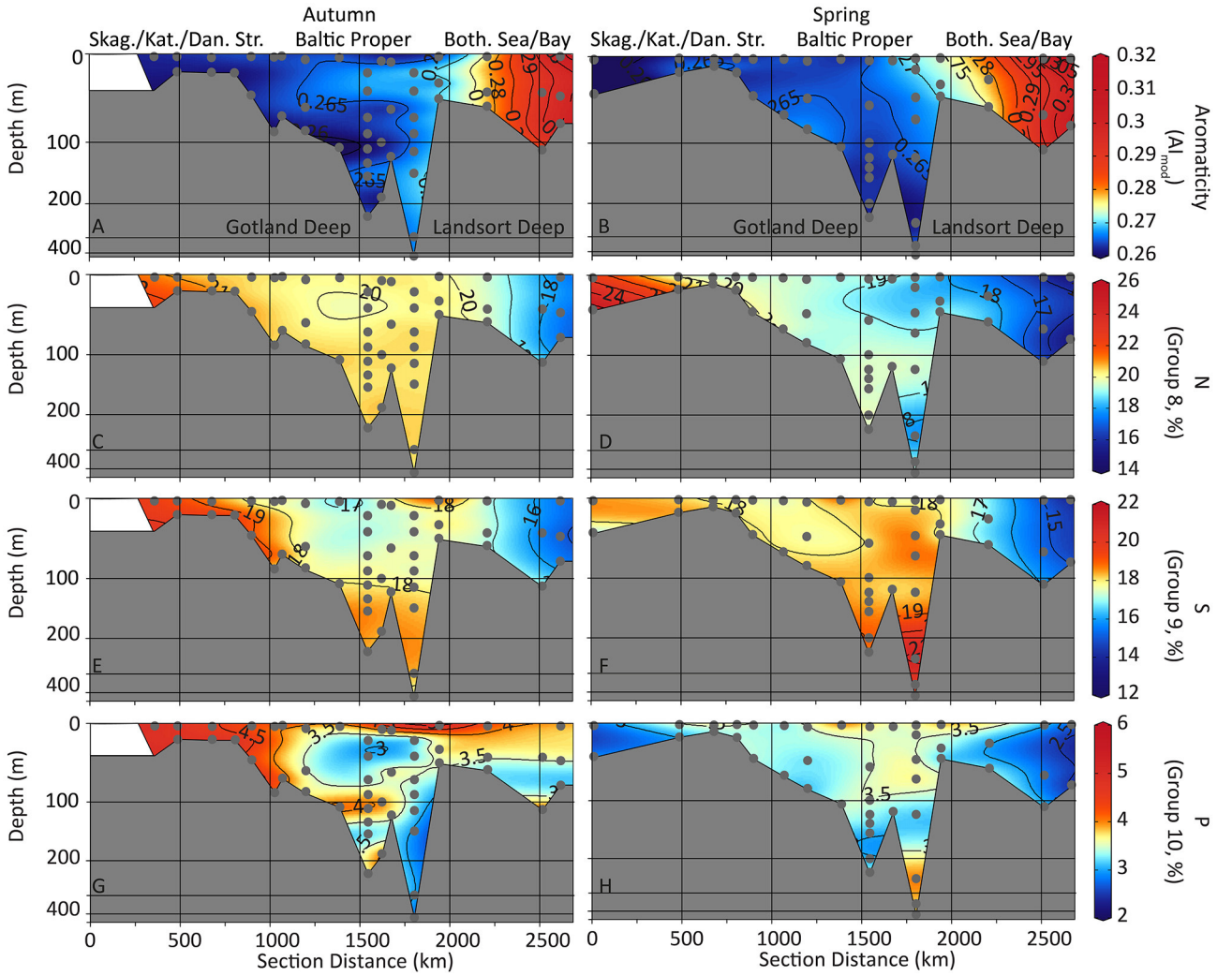

FIGURE 5 | Contour depth plots of the sampling transects. Weighted averages of DOM aromaticity (Al_{mod}; **A,B**) and compound groups of DOM containing nitrogen **(C,D)**, sulfur **(E,F)**, or phosphorus **(G,H)** (DOM groups 8, 9, and 10) are shown for autumn (left) and spring (right) sampling. Averages are weighted by FT-ICR-MS signal intensity. Non-linear depth scale. Skag., Skagerrak; Kat., Kattegat; Dan. Str., Danish Straits; Both. Sea/Bay, Bothnian Sea and Bothnian Bay.

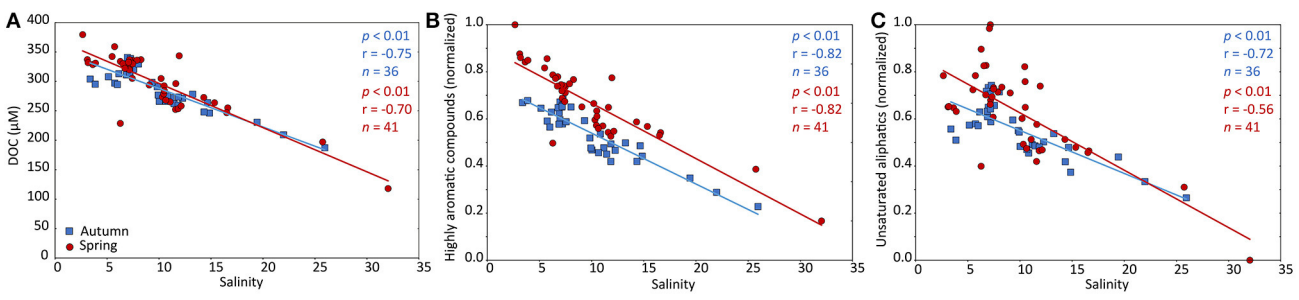

FIGURE 6 | DOC concentrations and the distribution of DOM molecular compound groups along the salinity gradient. Relationship of bulk DOC concentrations **(A)**, the relative abundance of highly aromatic compounds **(B)** and unsaturated aliphatic compounds (**C**; molecular formulae of groups 2 and 4, respectively) and salinity for autumn (blue squares) and spring (red circles) samples. The solid lines represent linear regressions. The relative abundance of the compound groups was scaled to the DOC concentrations and normalized to their minimum and maximum values. Bulk DOC concentrations and the highly aromatic compounds strongly correlated with salinity indicative for mixing of riverine and marine DOM. Unsaturated aliphatic compounds were more variable compared to linear mixing suggesting complex processing along the salinity gradient.

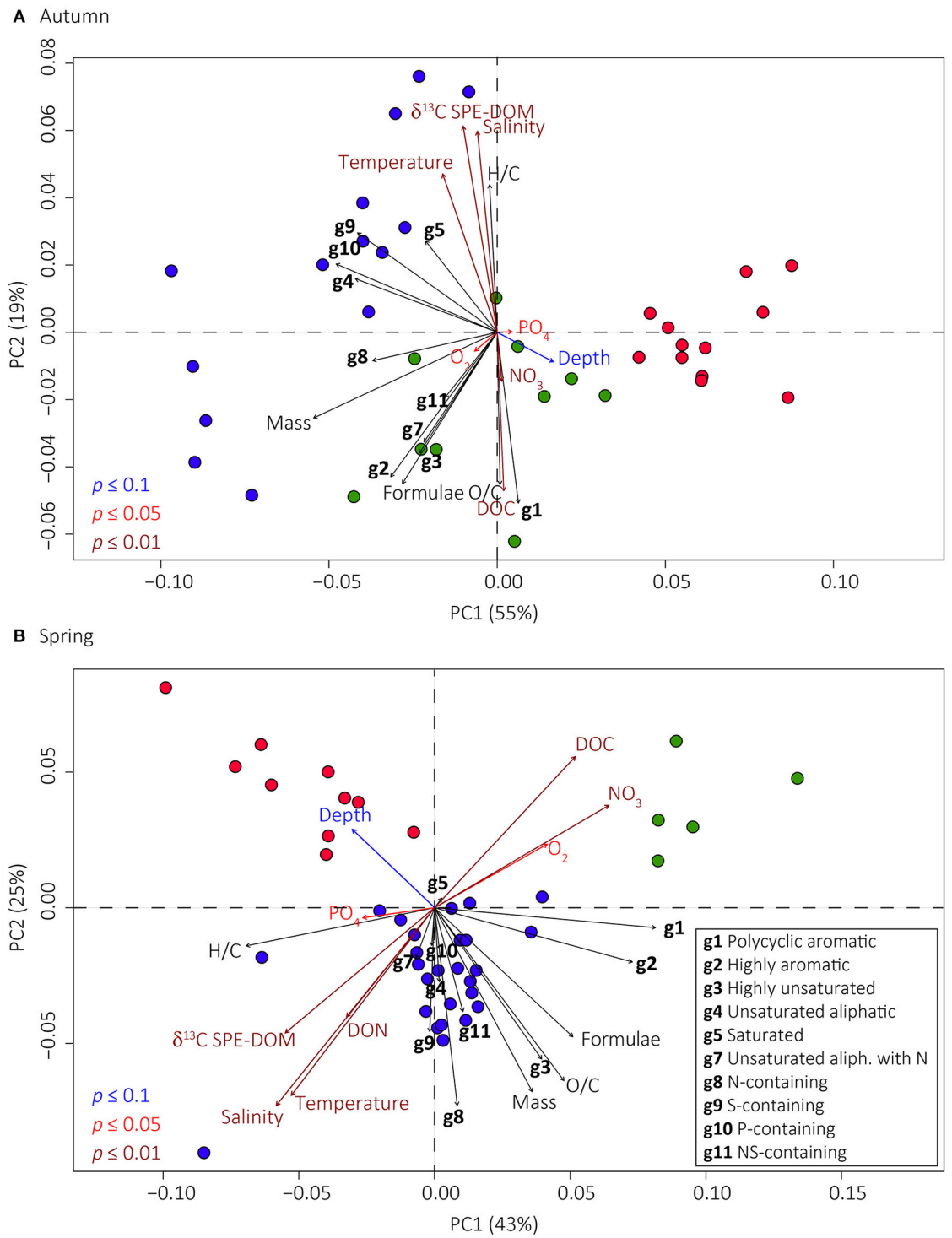

FIGURE 7 | Principal coordinate analyses (PCoA) based on Bray-Curtis dissimilarities of the relative abundance of DOM molecular formulae. Shown are the PCoA for autumn **(A)** and spring **(B)** samples, respectively. The percentages give the DOM molecular variability as explained by the axes. Colored circles identify the three main DOM clusters that were found in terrestrial-oxic (green circles), marine-to-brackish oxic (blue circles), and brackish suboxic-to-anoxic conditions (red circles). Environmental parameters (significantly correlated with $p \leq 0.1$, $p \leq 0.05$, and $p \leq 0.01$ blue, red, and dark red arrows, respectively), DOM compound groups (groups g1–g10 specified in legend shown in **B**; black arrows) and intensity weighted averages of O/C or H/C ratios and masses ("O/C," "H/C," "Mass") and average number of molecular formulae per sample ("Formulae") were fitted onto the ordination. Correlations with compound group 6 (saturated compounds with high O/C ratios) were not significant and are therefore not shown. The projections of sampling points onto the vector arrows show maximum correlations with the corresponding molecular compound groups, environmental, and molecular parameters.

correlated with DOM groups 1 and 2 (polycyclic aromatic and highly aromatic compounds, **Figure 7B**).

Comparison of DOM Molecular Endmembers

The characteristic DOM molecular signatures of the terrestrial, marine, oxic, and anoxic water masses were described by calculating the molar averages of the enriched molecular formulae of the endmembers that were identified in PCoA and cluster analyses. These were the samples from stations Mo14 and At-4 (Bothnian Bay surface close to the Kalix River outflow; terrestrial endmembers), S4 (19 m depth at Kattegat), and S1 (surface close to Skagerrak; marine endmembers) and TF284 (Landsort Deep at 430 m depth; anoxic endmembers) for the autumn and spring cruises, respectively (see **Figure 1** for sampling positions). Molecular formulae enriched in terrestrial DOM had higher masses, more carbon and more oxygen atoms, higher O/C and lower H/C ratios than DOM from marine or from anoxic water masses (**Table 1**). Enriched marine and DOM from anoxic water masses contained 7- to 33-fold more nitrogen, sulfur, and phosphorus (N-, S-, and P-) atoms compared to terrestrial DOM (**Table 1**). In spring, N-atoms in marine compounds were 2-fold higher compared to autumn (**Table 1**). Marine water masses in autumn were almost twice as much enriched in S-atoms compared to anoxic DOM compounds. In spring however, S-atoms were more enriched in anoxic DOM compared to marine DOM (**Table 1**). The S-content of marine DOM varied between the seasons with higher values in autumn compared to spring. Molecular formulae relatively enriched in the terrestrial endmember water in the Bothnian Bay were mainly polycyclic aromatics, highly aromatic, and highly unsaturated compounds (groups 1–3 were 97% of the enriched compounds, Supplementary Table 1). Unsaturated aliphatic compounds, with or without nitrogen and saturated compounds (groups 4–7), contributed comparatively more to the molecular formulae enriched in the marine and anoxic DOM samples (15–32% in spring and 13–22% in autumn, Supplementary Table 1).

We characterized molecular formulae that were relatively enriched in the seawater bottom inflow in 17–19 m depth at station S4 (i.e., marine compounds that are transported from the North Sea to the Baltic Sea) and brackish surface outflow at station S4 (i.e., terrestrial compounds that are exported from the Baltic Sea to the North Sea; **Table 2**) through the Kattegat and Skagerrak (station S4 in **Figure 1**). The outflowing water had a higher number of molecular formulae than North Sea water entering the Baltic Sea ("formulae" in **Table 2**). The outflowing water was relatively enriched with molecular formulae with higher masses and more carbon atoms while the inflowing water was enriched with molecular formulae containing nitrogen, sulfur and phosphorus heteroatoms. These trends were more pronounced in spring compared to autumn.

Terrestrial DOC Fluxes

The relative proportion of terrestrial DOC decreased from 90 ± 3% and 86 ± 5% in the Bothnian Bay to 60 ± 8% and 66 ± 17% in the western Baltic Sea at the Skagerrak/Kattegat area (stations S1, S3, and S4 in **Figure 1**) in autumn and spring, respectively (**Table 3**). Using our box model approach, we estimated a loss of terrestrial DOC in the Baltic Sea (sum of values from Bothnian Bay to Danish Straits) of 1.6–1.9 Tg C yr^{-1} (43–51% of total riverine input). The Baltic Proper (including terrestrial DOC inputs from the Gulf of Riga and Gulf of Finland) was the biggest sink for terrestrial DOC with 1.8 ± 0.8 Tg C yr^{-1} (autumn) and 2.5 ± 0.9 Tg C yr^{-1} (spring) net removal. Removal of

TABLE 1 | Characteristics of DOM molecular formulae (means of molecular parameters ± SD) that were relatively enriched in the terrestrial (riverine sources), marine (autochthonous sources), and anoxic (deep basins) end members in autumn and spring as identified by principal coordinate and cluster analyses.

	Autumn			Spring		
	Terrestrial[b]	Marine	Anoxic	Terrestrial	Marine	Anoxic
Formulae[a]	508	197	85	788	163	113
Mass (Da)	582.5 ± 126.8	446.1 ± 88.8	416.0 ± 109.3	530.9 ± 132.8	482.7 ± 90.8	441.2 ± 101.9
C	27.5 ± 5.6	20.9 ± 5.0	20.3 ± 6.8	24.8 ± 5.9	22.2 ± 4.4	20.8 ± 5.6
H	23.4 ± 9.1	26.4 ± 6.3	22.5 ± 6.8	20.1 ± 8.9	28.3 ± 6.8	27.0 ± 11.1
O	14.1 ± 4.6	7.6 ± 3.8	7.5 ± 4.8	13.2 ± 4.7	9.7 ± 3.7	7.8 ± 3.7
N	0.06 ± 0.36	0.64 ± 1.03	0.65 ± 1.03	0.04 ± 0.28	1.32 ± 1.15	0.54 ± 0.93
S	0.06 ± 0.30	1.00 ± 0.75	0.55 ± 0.62	0.06 ± 0.32	0.39 ± 0.56	0.72 ± 0.7
P	0.03 ± 0.16	0.22 ± 0.42	0.11 ± 0.32	0.01 ± 0.09	0.10 ± 0.30	0.30 ± 0.46
O/C	0.52 ± 0.15	0.38 ± 0.20	0.42 ± 0.27	0.54 ± 0.17	0.44 ± 0.16	0.39 ± 0.18
H/C	0.85 ± 0.31	1.34 ± 0.43	1.19 ± 0.42	0.79 ± 0.26	1.30 ± 0.30	1.31 ± 0.37
AI_{mod}	0.49 ± 0.19	0.23 ± 0.22	0.30 ± 0.25	0.51 ± 0.19	0.19 ± 0.19	0.22 ± 0.21

[a] *Number of enriched molecular formulae ("Formulae"), intensity-weighted means of molecular masses of enriched molecular formulae ("Mass," in Dalton), intensity-weighted means of the number of atoms per molecular formula (C, H, O, N, S, P), molar ratios (O/C, H/C), and of aromaticity index (AI_{mod}).*

[b] *Stations Mo14 and At-4 (surface of Bothnian Bay close to Kalix River outflow; terrestrial DOM endmembers), S4 (19 m depth in Kattegat) and S1 (surface close to Skagerrak; marine DOM endmembers) and TF284 (Landsort Deep in 430 m depth; anoxic DOM endmembers) were used for the autumn and spring samples, respectively. See* ***Figure 1*** *for sampling positions and* ***Figure 7*** *for distribution of clusters in PCoA.*

terrestrial DOC in the Bothnian Bay was 0.3 ± 0.1 Tg C yr^{-1} (autumn) and 0.3 ± 0.3 Tg C yr^{-1} in spring (**Table 3**). The terrestrial DOC balances in the Bothnian Sea and the Danish Straits were slightly negative or close to zero (**Table 3**). The export of terrestrial DOC from the Danish Straits into the Kattegat area was between 1.8 and 2.1 Tg C yr^{-1} in autumn and spring, respectively. The fluxes were slightly higher in spring compared to autumn. The residence times of terrestrial DOC were 3.7–3.8 years in the Bothnian Bay, 3.2–3.4 years in the Bothnian Sea, and 4.5–4.9 years in the Baltic Proper (**Table 3**). The residence time of terrestrial DOC in the Danish Straits and Kattegat area was 0.3–0.4 years (**Table 3**).

TABLE 2 | Characteristics of DOM molecular formulae (mean of molecular parameters ± SD) that were enriched in inflowing bottom water from the North Sea (into the Baltic Sea) and outflowing surface water from the Baltic Sea (into the North Sea) through the Kattegat area.

	Autumn		Spring	
	Inflow[b]	Outflow	Inflow	Outflow
Formulae[a]	117	506	84	864
Mass (Da)	440.9 ± 140.0	505.9 ± 128.1	419.5 ± 144.8	511.9 ± 120.1
C	20.7 ± 6.9	23.6 ± 6.3	20.7 ± 7.2	24.0 ± 6.1
H	24.0 ± 9.7	25.5 ± 9.6	21.1 ± 8.4	26.3 ± 9.8
O	8.5 ± 4.8	11.1 ± 4.9	8.0 ± 4.5	11.5 ± 4.6
N	0.54 ± 0.96	0.35 ± 0.82	0.63 ± 1.04	0.30 ± 0.79
S	0.69 ± 0.79	0.40 ± 0.67	0.35 ± 0.56	0.27 ± 0.54
P	0.12 ± 0.33	0.09 ± 0.29	0.11 ± 0.32	0.07 ± 0.25
O/C	0.42 ± 0.20	0.47 ± 0.20	0.4.0 ± 0.19	0.49 ± 0.19
H/C	1.21 ± 0.43	1.10 ± 0.36	1.06 ± 0.34	1.1 ± 0.33
AI_{mod}	0.29 ± 0.25	0.33 ± 0.21	0.38 ± 0.23	0.32 ± 0.21

[a] *Number of enriched molecular formulae ("Formulae"), intensity-weighted mean of molecular masses of enriched molecular formulae ("Mass," in Dalton), intensity-weighted means of the number of atoms per molecular formula (C, H, O, N, S, P), molar ratios (O/C, H/C), and of aromaticity index (AI_{mod}).*

[b] *Inflowing North Sea bottom water (17–19 m depth) and outflowing Baltic Sea surface water at station S4 (Kattegat, see **Figure 1** for sampling positions).*

DISCUSSION

Bulk Geochemical and Biological Parameters

The distribution of the chemical constituents in the Baltic Sea water was largely driven by mixing of marine and riverine water masses and by the vertical redox zonation of the water column. The thermal stratification was weaker in autumn compared to spring (water temperature in **Figures 2A,B**), indicating enhanced convective overturning in the surface mixed layer. Reduced stratification was probably due to a combination of stronger wind-induced mixing, surface cooling as well as reduced inflow of riverine freshwater in autumn (Nausch et al., 2012). In winter, the water column of the Baltic Sea is vertically mixed down to the halocline, whereas in spring, a seasonal thermocline generally forms at about 20 m depth (Eilola and Stigebrandt, 1998). Water masses below the halocline in the deep stagnant basins is only replaced during major inflow events, which have not occurred between 2004 and 2014 (Mohrholz et al., 2015), i.e.,

TABLE 3 | Concentrations of DOC and relative abundance of terrestrial DOC (%) in comparison to the riverine DOC input and removal rates of terrestrial DOC (in Tg C per year) for the basins of the Baltic Sea in autumn and spring (means ± SD).

			Terrestrial	Riverine DOC[a]	Balance terr.[b]	Residence time[c]
Basin	Season	DOC mg L^{-1}	DOC (%)	Input (Tg yr^{-1})	DOC (Tg yr^{-1})	Terr. DOC (yrs)
Bothnian Bay	Autumn	3.6 ± 0.1	90 ± 3	0.7	0.3 ± 0.1	3.7
	Spring	4.1 ± 0.3	86 ± 5		0.3 ± 0.3	3.8
Bothnian Sea	Autumn	3.7 ± 0.2	78 ± 3	0.5	0 ± 0.4	3.2
	Spring	4.0 ± 0.2	79 ± 7		−0.3 ± 0.5	3.4
Baltic Proper	Autumn	3.5 ± 0.4	77 ± 5	2.4	1.8 ± 0.8	4.9
	Spring	3.5 ± 0.4	74 ± 6		2.5 ± 0.9	4.5
Danish Straits	Autumn	3.4 ± 0.6	69 ± 8	0.1	−0.1 ± 1.1	
	Spring	3.7 ± 0.5	75 ± 5		−0.8 ± 1.1	
Kattegat	Autumn	2.6 ± 0.5	60 ± 8	0.2	NA	0.3*
	Spring	2.7 ± 0.5	66 ± 17		NA	0.4
Average[d]	Autumn	3.6 ± 0.7	79 ± 10	–	–	3.9
	Spring	3.8 ± 0.7	79 ± 11	–	–	3.9
Sum	Autumn	–	–	3.7	1.9 ± 1.5	11.8
	Spring	–	–	3.7	1.6 ± 1.5	11.8

[a] *Riverine DOC input per basin from Gustafsson et al. (2014); Baltic Proper includes Gulf of Finland and Gulf of Riga.*

[b] *Terrestrial DOC balance per basin; positive (negative) numbers indicate removal (input) of terrestrial DOC compared to the terrestrial DOC input from adjacent rivers and basins; NA, not available.*

[c] *Average residence time (in years, yrs) of terrestrial DOC (terr. DOC) for each basin.*

[d] *Average or sum of values from Bothnian Bay to Danish Straits.*

[*] *Residence times for the combined Danish Straits and Kattegat area.*

during and around the time our samples were taken (2011 and 2012).

Nitrogen is provided to the Baltic Sea by riverine and atmospheric inputs, nitrogen fixation and nutrient recycling within the water column (Thomas et al., 2010). During the autumn months, stronger wind-induced mixing provides the surface and subsurface mixed layers with recycled nutrients from below the thermocline. At the same time in late autumn, the overall phytoplankton biomass (as indicated by chlorophyll *a* concentrations, **Figures 2G,H**) was lower. Consequently, higher depth-integrated nitrate concentrations were found in the Bothnian Bay in autumn compared to spring (**Figures 3A,B**).

Nitrate (**Figures 3A,B**) and silicate concentrations (**Figures 2K,L**) were higher in the surface layers of the Bothnian Sea compared to the central Baltic Sea, where these nutrients were depleted in the photic zone, probably due to phytoplankton growth. Silicate and nitrate were still detectable in the areas with high freshwater input such as the Bothnian Bay, where rivers are important nutrient sources (Savchuk, 2005). Dissolved silica and dissolved phosphate are mainly derived from riverine inputs and they are removed as biogenic particles by growth of phytoplankton such as diatoms (Rahm and Danielsson, 2007; Conley et al., 2008). Sinking particles export silica, nitrogen and phosphorus into the deeper water layers where the particles settle and partly dissolve (Struck et al., 2004; Savchuk, 2005). Below the halocline in the stagnant anoxic Gotland and Landsort Deeps, dissolved silicate (**Figures 2K,L**), phosphate (**Figures 2I,J**), and ammonium (**Figures 3C,D**) can accumulate (Nausch and Nehring, 1996; Nausch et al., 2012).

The DOC concentrations of the terrestrial endmembers in the Bothnian Bay were slightly elevated in spring (**Figures 4A,B**). This was likely due to the flushing of soils and fast response to precipitation events and snow melt. In general, boreal and sub-arctic river systems are characterized by a pronounced seasonality of their hydrograph, because of elevated spring peak flow due to snowmelt (Smedberg et al., 2006). But considering the long residence time of terrestrial DOC in the various basins of the Baltic (see Discussion below), the effect of seasonal runoff is dampened on a basin scale. DOC concentrations strongly correlated with salinity during both seasons but with noticeable deviations from two-endmember mixing (**Figure 6A**). Positive deviations of DOC concentrations indicate release of DOM during the spring phytoplankton bloom whereas negative deviations suggest degradation of terrestrial DOC. Similar to bulk DOC, the concentration of terrestrial DOC was largely driven by dilution with seawater along the salinity gradient, but noticeable deviations from simple mixing indicate processing of terrestrial DOM along the salinity gradient (Supplementary Figure 6). It is important to keep in mind that in our simplified linear mixing model, we assumed that all terrestrial and marine sources in the Baltic Sea have the same endmember characteristics in terms of stable carbon isotopes and DOC concentrations. This may not be the case, because the various rivers draining into the Baltic Sea differ, especially in their DOC concentrations (e.g., Deutsch et al., 2012). This adds uncertainty to our two-endmember mixing model.

Nonetheless, our considerations are consistent with previous findings. On average, 20–60 μM particulate organic carbon is seasonally produced by phytoplankton in the Baltic Proper during the spring and summer blooms (Nausch et al., 2012), a part of which is likely released in dissolved form. Removal of terrestrial DOM was previously observed in the Baltic Sea (Alling et al., 2010; Deutsch et al., 2012). The bioavailability of terrestrial DOM depends strongly on the catchment area (Asmala et al., 2013; Riedel et al., 2016). However, a more significant sink for terrestrial DOM in the Baltic Sea, and coastal oceans in general, is probably photo-mineralization and bacterial uptake of the photo-produced labile DOM (Miller and Zepp, 1995; Aarnos et al., 2012). In fact, Aarnos et al. (2012) calculated that the total annual photochemical mineralization exceeds the annual input of photo-reactive riverine DOM, suggesting that also autochthonous DOM is photo-transformed in the Baltic Sea. The biodegradation of terrestrial DOC is likely to be significant on time scales of weeks to months due to the semi-labile to refractory character of terrestrial DOC that is exported to the Baltic Sea (Herlemann et al., 2014; Kuliński et al., 2016). The net heterotrophy that was observed in parts of the Baltic Sea suggests that a part of the terrestrial DOC pool is important for supporting bacterial mineralization (Algesten et al., 2006).

DOM Composition in Relation to Marine and Terrestrial Sources

In the riverine-influenced samples, we found a stable carbon isotopic composition of SPE-DOM that is typical for C3 land plants, i.e., between −28 to −25‰, whereas the marine-influenced samples were in the range for marine phytoplankton OM, i.e., around −22‰ (Benner et al., 1997; Guo et al., 2003). C3 plants, such as woody gymnosperms, are a main source for the terrigenous DOM that is discharged into the northern Baltic Sea (Bianchi et al., 1997; Deutsch et al., 2012). This is supported by our finding that most of the riverine DOM consisted of highly aromatic and highly unsaturated molecular formulae, which include lignin degradation products (Stenson et al., 2003), polyphenols (Koch and Dittmar, 2006), but also combustion-derived compounds (Dittmar and Koch, 2006). Molecular formulae with a comparatively low hydrogen content (low H/C ratios) are a general feature of terrestrial DOM due to the high content of aromatic compounds such as degraded lignins and tannins (Sleighter and Hatcher, 2008; Schmidt et al., 2009) and mobilized black carbon from soils (Dittmar et al., 2012; Jaffé et al., 2013).

The non-targeted DOM molecular analyses using ultrahigh-resolution MS allows to distinguish different DOM sources and complex transformations in estuaries and river plumes (Medeiros et al., 2015a,b; Seidel et al., 2015b; Osterholz et al., 2016). Using the PCoA multivariate statistical approach, we identified the molecular composition of the endmembers of the autochthonous marine and allochthonous terrestrial sources, as well as oxic-to-anoxic transformations in the Baltic Sea. The terrestrial endmembers had a higher number of molecular formulae (508–788 enriched terrestrial compounds compared to 163 and 197 enriched compounds in the

marine endmembers, **Table 1**) and contributed more aromatic compounds as indicated by the higher aromaticity (higher AI_{mod}, **Figures 5A,B**) compared to the marine DOM endmembers. The marine endmembers were enriched with saturated compounds (lower AI_{mod} values) compared to the terrestrial endmembers (**Table 1**). The saturation of DOM compounds increased also along other river-to-ocean transects (Sleighter and Hatcher, 2008; Medeiros et al., 2015b; Seidel et al., 2015b). This is because marine DOM is enriched in aliphatic structures compared to freshwater samples that are enriched in aromatic compounds. Our data are consistent with these previously observed trends.

The molecular formulae that were enriched in the marine endmembers were characterized by higher contents of N-, S-, and P-atoms compared to the enriched terrestrial molecular formulae (**Table 1**). A higher proportion of DOM from phytoplankton and microbial biomass that is enriched in N, P and S-heteroatoms, such as peptides, nucleotides, and lipid degradation products, have also been previously observed in marine DOM (Kujawinski et al., 2004; Sleighter and Hatcher, 2008; Schmidt et al., 2011; Gonsior et al., 2011a; Seidel et al., 2015a). For example, in the Amazon plume and Delaware estuary, the increase of aliphatic compounds was related to addition of DOM from phytoplankton and the biotransformation of terrestrial DOM (Medeiros et al., 2015b; Osterholz et al., 2016). In line with these previous findings, our data demonstrate that the autochthonous production of DOM in the Baltic Sea and possibly also biotransformation of terrestrial compounds are a source for aliphatic N-, S-, and P-heteroatom containing compounds to the estuarine DOM pool.

The seasonal changes between the enriched compounds of the terrestrial endmembers were comparatively small (**Table 1**). The terrestrial DOM endmembers were from stations close to the Kalix River outflow in the Bothnian Bay (**Figure 1**). This suggests that at this location the seasonal DOM molecular changes were relatively minor and that the input of mobilized land-plant derived material was the main source of riverine DOM that was transported to the Bothnian Bay. In contrast, the changes between the marine endmembers and the anoxic endmembers were more pronounced. For example, during the spring phytoplankton bloom, the average N-content was 2-fold higher in the marine DOM compared to autumn (**Table 1**). As mentioned previously, the higher N- content in the molecular formulae can be attributed to DOM from autochthonous (marine) sources (e.g., Sleighter and Hatcher, 2008), particularly in spring, with higher phytoplankton biomass.

A previous study has shown that (chromophoric) DOM is transported from the North Sea (German Bight) into the Baltic Sea *via* the Jutland Coastal current through the Kattegat area (Stedmon et al., 2010). The sulfidic porewater in the tidal flats of the North Sea is strongly enriched with sulfurized DOM and the porewater discharge is a DOM source to the water column (Seidel et al., 2014). The Skagerrak/Kattegat area (**Figures 5E,F**), the marine endmember samples (**Table 1**), and the DOM from seawater flowing into the Baltic Sea (**Table 2**) were relatively enriched with S-containing DOM (particularly during autumn, when the phytoplankton biomass was lower compared to spring). This may indicate that the S-rich DOM from the North Sea tidal flats is transported into the Skagerrak/Kattegat area. Another possible source for the S-containing compounds is the discharge from the more anthropogenically influenced rivers of the southwestern Baltic Sea. Compared to the less populated sub-arctic north, more dissolved organic sulfur compounds may be introduced by wastewater (Gonsior et al., 2011b; Wagner et al., 2015) in the densely populated southwestern basins.

The distribution of the molecular DOM compound groups along the salinity gradient was strongly influenced by mixing (**Figure 6**; Supplementary Figure 6). However, similar to bulk and terrestrial DOC concentrations, there was considerable scatter around the mixing lines, which indicates active processing of DOM in the Baltic Sea. Especially DOM compound groups that were identified as typical marine (compounds groups 5–11) showed largest deviations from conservative mixing in spring, which can be associated to autochthonous production in the spring blooms. The high abundance of aromatic compounds makes terrestrial DOM highly susceptible to photochemical degradation (Hernes and Benner, 2003; Gonsior et al., 2009; Stubbins et al., 2010) which would explain the observed depletion of the aromatic compound groups (groups 1 and 2) at mid salinity in both seasons.

During its transit through the Baltic Sea, DOM became more enriched in autochthonous (phytoplankton-produced) compounds, which was more pronounced in spring compared to autumn (**Table 1**). A net accumulation of more aliphatic compounds (**Figure 6C**) and marine DOC (**Figure 4F**) was observed in spring, which is likely due to new addition of OM compounds during the phytoplankton bloom. In combination with the quantitative DOC data and the analysis of the ^{13}C isotopic composition of SPE-DOM, we found indications for processing of terrestrial DOC in the Baltic Sea. A general trend for the Baltic Sea may be inferred: marine DOC accumulates due to the high phytoplankton primary production in spring whereas net (terrestrial) DOC removal occurs in autumn (without a noticeable accumulation of marine DOC). Thus, our data suggest that the carbon budget (here as DOC depletion/accumulation) can shift between net CO_2 uptake (conversion to OM) and net release (remineralization of OM to CO_2) which varies between the basins but also seasonally (Thomas et al., 2010; Kuliński and Pempkowiak, 2011; Gustafsson et al., 2014; Ylöstalo et al., 2016). In line with that, Algesten et al. (2006) previously suggested net heterotrophy in the Gulf of Bothnia because of terrestrial DOC processing.

DOM Transport from the Baltic Sea to the North Sea

The riverine inflow from the northern Bothnian Bay (e.g., Kalix River) and Bothnian Sea provide ca. 1.2 Tg terrestrial DOC per year (Gustafsson et al., 2014). For that area, our box model calculations resulted in terrestrial DOC removal rates of up to 0.3 Tg C per year (**Table 3**). Rivers draining into the Baltic Proper, the Gulf of Finland (Neva River) and the Gulf of Riga contribute ca. 2.4 Tg terrestrial DOC per year (Gustafsson et al., 2014). In that area, terrestrial DOC removal rates were between 1.8 and 2.5 Tg C per year. Overall, we estimated that 43–51% of the total riverine input of the 3.7 Tg terrestrial DOC is removed between the

Bothnian Sea and the Danish Straits/Kattegat area. The fact that we estimated zero and even negative net balances for some of the lower basins highlights that their carbon budget may be in close balance, but it also emphasizes that the terrestrial DOC budgets (such as the DOC input terms) are still not well-constrained.

Our calculated export of 1.8–2.1 Tg terrestrial DOC per year to the Danish Straits (for autumn and spring, respectively) is comparable to the previously reported net flux of ca. 3 Tg total organic carbon per year by Gustafsson et al. (2014). It is, however, higher than the 0.8 Tg C per year which was based on optical measurements of chromophoric DOM (Osburn and Stedmon, 2011). In a previous study, Deutsch et al. (2012) found that the relative proportion of terrestrial HMW DOM decreased to 43% which is in line with our data. We calculated residence times for terrestrial DOC (i.e., the time that terrestrial DOC spends on average in each basin) of 3.7–4.9 years (**Table 3**) which also agrees well with previously reported values (Alling et al., 2008; Deutsch et al., 2012; Gustafsson et al., 2014). The water residence times (5.1, 3.2, and 4.4 years for Bothnian Bay, Bothnian Sea, and Baltic Proper, respectively; Savchuk, 2005) are higher or in the same range, indicating removal of terrestrial DOC on the time scales of water transport through the Baltic Sea. Yet, a significant fraction of the terrestrial DOC was resistant to removal in the Baltic Sea and was transported to the North Sea and presumably to the Atlantic Ocean. The residence time of terrestrial DOC in the Danish Straits and Kattegat area is relatively short (0.3–0.4 years, **Table 3**), probably because this area is relatively shallow and more mixed compared to the deeper basins of the Baltic Sea. However, the similar fluxes of terrestrial DOC to the North Sea in spring and autumn suggest that seasonal changes of OM production and riverine discharge are dampened. We propose that this is due to the long residence time of terrestrial DOC in the Baltic Sea.

After passage through the Baltic Sea, the outflowing DOM was more enriched in autochthonous (marine) compounds than the terrestrial endmember (but still contained a more terrestrial signature than the North Sea inflow). There was a substantial increase in N (6- to 8-fold increase), S (5- to 7-fold increase), and P (3- to 7-fold increase) heteroatoms in the molecular formulae after transit through the Baltic Sea compared to the riverine inflow at the northern Bothnian Bay (comparing the terrestrial endmember in **Table 1** to the outflow in **Table 2** in spring and autumn, respectively), suggesting that primary production and biotransformation in the Baltic Sea act as sources of these compounds. At the same time, aromatic terrestrial compounds were depleted in the outflow (AI_{mod} decreased from 0.49 and 0.51 to 0.33 and 0.32 in spring and autumn, respectively, compared to the terrestrial endmember; **Tables 1, 2**).

The identified processes appear to be applicable to other regions and to larger scales, although their relative extent will certainly depend on seasonal and spatial variabilities such as redox zonation, river discharge, circulation patterns, and DOM residence times. Arctic shelf seas, for example, show similar river runoff schemes as the Baltic Sea, with pronounced spring flood events. Furthermore, more than 50% of terrestrial DOC is removed on the Eurasian shelf before reaching the Arctic Ocean. Yet, this removal occurs on shorter time scales (2–5 years; Alling et al., 2010; Letscher et al., 2011) compared to the Baltic Sea (11.8 years, **Table 3**; and Alling et al., 2008; Stedmon et al., 2010; Deutsch et al., 2012). It remains to be resolved how these fluxes and rates change interannually, or if they are susceptible to changes in land use and an increase of (labile) terrestrial DOC export from sub-arctic rivers.

DOM Alterations in the Hypoxic Basins of the Baltic Sea

We observed an enrichment of DON in the central Baltic Sea (**Figures 3E,F**). This area is influenced by the discharge of rivers draining watersheds with high agricultural land use which could be important DON sources (Stålnacke et al., 1999; Voss et al., 2011). We also observed high chlorophyll concentrations in the regions with high DON concentrations (**Figures 2G,H**) and high abundances of phytoplankton (data for autumn only, Supplementary Figure 1). Thus, DON release from autochthonous sources such as cyanobacteria (Voss et al., 2005, 2011) is another likely explanation for the observed DON patterns. The DON concentrations positively correlated with unsaturated aliphatic N-containing compounds in spring (group 7, Supplementary Figure 4) which include peptide molecular formulae (Kujawinski et al., 2004; Sleighter and Hatcher, 2008) being consistent with an autochthonous production of DON.

The DON concentrations below the halocline were in the same range as in the photic zone in spring (**Figure 3F**). The similar DON concentrations in surface and bottom waters may reflect a recalcitrant background of DON. It also indicates DON transport below the halocline into the anoxic basins, probably by sinking particles and subsequent release of DON due to degradation processes. The anoxic endmember contained also more marine SPE-DOC in spring (33%) compared to autumn (27%; **Figures 4E,F**). Associated with this trend was a higher abundance of typical marine DOM compounds groups in spring compared to fall in the anoxic basins (compound groups 4, 5, and 7 with/without N were 32% in spring but only 13% in autumn, Supplementary Table 1). Such seasonal changes in the stagnant anoxic basins are remarkable and indicate active processing and seasonal inputs into these basins. The particle export to the deep anoxic basins is likely coupled with the seasonal changes of organic matter composition in the overlaying water column, for example, the higher autochthonous production in spring compared to autumn. In turn, this could mean that if the export of terrestrial organic matter from rivers should change (Voss et al., 2011; Räike et al., 2016), it may also affect the DOM composition in the deep anoxic basins of the Baltic Sea.

Our data also highlight additional modification of the DOM in the anoxic basins. The DOM compounds of the deep anoxic basins were more enriched with sulfur-containing compounds compared to the terrestrial endmember (**Table 1**). Abiotic sulfurization reactions between sulfide species and DOM have been proposed previously to be responsible for the observed elevated dissolved organic sulfur compounds in sulfidic environments (Schmidt et al., 2009; Seidel et al., 2014; Gomez-Saez et al., 2016). Potential abiotic sulfurization reactions include the exchange of an oxygen by a sulfur atom or exchanging H_2O,

H_2, and/or O_2 by addition of H_2S per DOM molecular formulae (Schmidt et al., 2009; Gomez-Saez et al., 2016). It has further been hypothesized that abiotic sulfurization reactions may increase the recalcitrant character of DOM, which may explain why these compounds accumulate under anoxic conditions (Seidel et al., 2014).

CONCLUSIONS

We identified the molecular imprints of the sources and transformations of DOM in the Baltic Sea. Our box model calculations demonstrated that in both, spring and autumn, the Baltic Sea was a net sink for terrestrial DOM, including condensed and highly aromatic DOM compounds. We also found a net accumulation of autochthonous DOM in the Baltic Proper in spring, likely resulting from OM production during the phytoplankton bloom. Phytoplankton production and possibly also the bio- and photo-transformation of terrestrial compounds are sources for aliphatic, nitrogen-, sulfur-, and phosphorous-rich compounds to the Baltic Sea. Seasonal changes of the DOM composition and dissolved organic nitrogen concentrations were found in the deep, stagnant, and anoxic basins, indicating vertical transport of organic particles and organic matter processing in the basins. DOM in the anoxic basins was enriched with sulfur compounds. Abiotic sulfurization reactions in the sulfidic basins are proposed as a likely reason. The inflow of sulfur-rich DOM from North Sea tidal flats and the discharge from the more anthropogenically influenced rivers are likely contributing additional sulfur-containing DOM to the southwestern Baltic Sea and the Kattegat area. Using a box model approach, we estimated that between 43 and 51% of the total terrestrial DOC that is supplied by rivers is removed in the Baltic Sea, while 1.8–2.1 Tg terrestrial DOC is exported per year to the North Sea. These fluxes were comparable for spring and autumn. This suggests that, due to the long residence times of terrestrial DOC in the Baltic Sea (3.7 years in the Bothnian Bay to 6.9 years in the Baltic Proper), seasonal changes of biotransformation and riverine discharge of terrestrial DOM become largely undetectable. More research is needed to reliably predict how the outflow of terrestrial DOM will change over longer time spans if the riverine export of terrestrial DOM from the sub-arctic north should increase in the future.

AUTHOR CONTRIBUTIONS

MS, MM, and TD conceived the study; MS and MM performed chemical analyses; KJ and DH provided microbiological data; MS, TD, and BD performed flux calculations; DH and DS provided nutrient data; MS wrote the manuscript with significant contributions from all authors.

FUNDING

This work was supported by the ATKiM Project from the Leibniz Society (SAW-2011-IOW-3) to DH, KJ, and MM as well as by the German Science Foundation (DFG, JU 367/15-1) to KJ, and by the Leibniz Institute for Baltic Sea Research Warnemünde.

ACKNOWLEDGMENTS

We thank the captains and crews of *R/V Meteor* for their help during the sampling campaigns (legs M86 and M87). We are also thankful to Matthias Friebe, Katrin Klaproth, and Ina Ulber (University of Oldenburg, Germany) for technical assistance. We further acknowledge the reviewers and the editor for their thoughtful and valuable comments that led to an improved manuscript.

SUPPLEMENTARY MATERIAL

The Supplementary Material for this article can be found online at: http://journal.frontiersin.org/article/10.3389/feart.2017.00031/full#supplementary-material

REFERENCES

Aarnos, H., Ylöstalo, P., and Vähätalo, A. V. (2012). Seasonal phototransformation of dissolved organic matter to ammonium, dissolved inorganic carbon, and labile substrates supporting bacterial biomass across the Baltic Sea. *J. Geophys. Res.* 117, G01004. doi: 10.1029/2010jg001633

Algesten, G., Brydsten, L., Jonsson, P., Kortelainen, P., Löfgren, S., Rahm, L., et al. (2006). Organic carbon budget for the Gulf of Bothnia. *J. Mar. Syst.* 63, 155–161. doi: 10.1016/j.jmarsys.2006.06.004

Alling, V., Humborg, C., Mörth, C.-M., Rahm, L., and Pollehne, F. (2008). Tracing terrestrial organic matter by $\delta^{34}S$ and $\delta^{13}C$ signatures in a subarctic estuary. *Limnol. Oceanogr.* 53, 2594–2602. doi: 10.4319/lo.2008.53.6.2594

Alling, V., Sanchez-Garcia, L., Porcelli, D., Pugach, S., Vonk, J. E., van Dongen, B., et al. (2010). Nonconservative behavior of dissolved organic carbon across the Laptev and East Siberian seas. *Glob. Biogeochem. Cycles* 24:GB4033. doi: 10.1029/2010GB003834

Asmala, E., Autio, R., Kaartokallio, H., Pitkänen, L., Stedmon, C., and Thomas, D. (2013). Bioavailability of riverine dissolved organic matter in three Baltic Sea estuaries and the effect of catchment land use. *Biogeosciences* 10, 6969–6986. doi: 10.5194/bg-10-6969-2013

Bauer, J., and Bianchi, T. (2011). Dissolved organic carbon cycling and transformation. *Treat. Estuar. Coast. Sci.* 5, 7–67. doi: 10.1016/B978-0-12-374711-2.00502-7

Benner, R., Biddanda, B., Black, B., and McCarthy, M. (1997). Abundance, size distribution, and stable carbon and nitrogen isotopic compositions of marine organic matter isolated by tangential-flow ultrafiltration. *Mar. Chem.* 57, 243–263. doi: 10.1016/S0304-4203(97)00013-3

Bianchi, T. S., Rolff, C., and Lambert, C. D. (1997). Sources and composition of particulate organic carbon in the Baltic Sea: the use of plant pigments and lignin-phenols as biomarkers. *Mar. Ecol. Prog. Ser.* 156, 25–31. doi: 10.3354/meps156025

Borges, A. V. (2005). Do we have enough pieces of the jigsaw to integrate CO_2 fluxes in the coastal ocean? *Estuaries* 28, 3–27. doi: 10.1007/BF02732750

Conley, D. J., Björck, S., Bonsdorff, E., Carstensen, J., Destouni, G., Gustafsson, B. G., et al. (2009). Hypoxia-related processes in the Baltic Sea. *Environ. Sci. Technol.* 43, 3412–3420. doi: 10.1021/es802762a

Conley, D. J., Humborg, C., Smedberg, E., Rahm, L., Papush, L., Danielsson, Å., et al. (2008). Past, present and future state of the biogeochemical Si cycle in the Baltic Sea. *J. Mar. Syst.* 73, 338–346. doi: 10.1016/j.jmarsys.2007.10.016

Deutsch, B., Alling, V., Humborg, C., Korth, F., and Mörth, C. M. (2012). Tracing inputs of terrestrial high molecular weight dissolved organic matter within the Baltic Sea ecosystem. *Biogeosciences* 9, 4465–4475. doi: 10.5194/bg-9-4465-2012

Dittmar, T., de Rezende, C. E., Manecki, M., Niggemann, J., Coelho Ovalle, A. R., Stubbins, A., et al. (2012). Continuous flux of dissolved black carbon from a vanished tropical forest biome. *Nat. Geosci.* 5, 618–622. doi: 10.1038/ngeo1541

Dittmar, T., Koch, B., Hertkorn, N., and Kattner, G. (2008). A simple and efficient method for the solid-phase extraction of dissolved organic matter (SPE-DOM) from seawater. *Limnol. Oceanogr. Methods* 6, 230–235. doi: 10.4319/lom.2008.6.230

Dittmar, T., and Koch, B. P. (2006). Thermogenic organic matter dissolved in the abyssal ocean. *Mar. Chem.* 102, 208–217. doi: 10.1016/j.marchem.2006.04.003

Eilola, K., and Stigebrandt, A. (1998). Spreading of juvenile freshwater in the Baltic proper. *J. Geophys. Res.* 103, 27795–27807. doi: 10.1029/98JC02369

Gasol, J. M., Zweifel, U. L., Peters, F., Fuhrman, J. A., and Hagström, A. (1999). Significance of size and nucleic acid content heterogeneity as measured by flow cytometry in natural planktonic bacteria. *Appl. Environ. Microbiol.* 65, 4475–4483.

Gattuso, J.-P., Frankignoulle, M., and Wollast, R. (1998). Carbon and carbonate metabolism in coastal aquatic ecosystems. *Annu. Rev. Ecol. Syst.* 29, 405–434. doi: 10.1146/annurev.ecolsys.29.1.405

Gomez-Saez, G. V., Niggemann, J., Dittmar, T., Pohlabeln, A. M., Lang, S. Q., Noowong, A., et al. (2016). Molecular evidence for abiotic sulfurization of dissolved organic matter in marine shallow hydrothermal systems. *Geochim. Cosmochim. Acta* 190, 35–52. doi: 10.1016/j.gca.2016.06.027

Gonsior, M., Peake, B. M., Cooper, W. T., Podgorski, D., D'Andrilli, J., and Cooper, W. J. (2009). Photochemically induced changes in dissolved organic matter identified by ultrahigh resolution Fourier transform ion cyclotron resonance mass spectrometry. *Environ. Sci. Technol.* 43, 698–703. doi: 10.1021/es8022804

Gonsior, M., Peake, B. M., Cooper, W. T., Podgorski, D. C., D'Andrilli, J., Dittmar, T., et al. (2011a). Characterization of dissolved organic matter across the Subtropical Convergence off the South Island, New Zealand. *Mar. Chem.* 123, 99–110. doi: 10.1016/j.marchem.2010.10.004

Gonsior, M., Zwartjes, M., Cooper, W. J., Song, W., Ishida, K. P., Tseng, L. Y., et al. (2011b). Molecular characterization of effluent organic matter identified by ultrahigh resolution mass spectrometry. *Water Res.* 45, 2943–2953. doi: 10.1016/j.watres.2011.03.016

Grasshoff, K., Kremling, K., and Ehrhardt, M. (1999). *Methods of Seawater Analysis*. Weinheim: Wiley-VCH.

Green, N. W., Perdue, E. M., Aiken, G. R., Butler, K. D., Chen, H., Dittmar, T., et al. (2014). An intercomparison of three methods for the large-scale isolation of oceanic dissolved organic matter. *Mar. Chem.* 161, 14–19. doi: 10.1016/j.marchem.2014.01.012

Guo, L., Tanaka, N., Schell, D. M., and Santschi, P. H. (2003). Nitrogen and carbon isotopic composition of high-molecular-weight dissolved organic matter in marine environments. *Mar. Ecol. Prog. Ser.* 252, 51–60. doi: 10.3354/meps252051

Gustafsson, E., Deutsch, B., Gustafsson, B. G., Humborg, C., and Mörth, C. M. (2014). Carbon cycling in the Baltic Sea — the fate of allochthonous organic carbon and its impact on air–sea CO_2 exchange. *J. Mar. Syst.* 129, 289–302. doi: 10.1016/j.jmarsys.2013.07.005

Herlemann, D. P. R., Manecki, M., Meeske, C., Pollehne, F., Labrenz, M., Schulz-Bull, D., et al. (2014). Uncoupling of bacterial and terrigenous dissolved organic matter dynamics in decomposition experiments. *PLoS ONE* 9:e93945. doi: 10.1371/journal.pone.0093945

Hernes, P. J., and Benner, R. (2003). Photochemical and microbial degradation of dissolved lignin phenols: implications for the fate of terrigenous dissolved organic matter in marine environments. *J. Geophys. Res.* 108, 3291. doi: 10.1029/2002JC001421

Hertkorn, N., Benner, R., Frommberger, M., Schmitt-Kopplin, P., Witt, M., Kaiser, K., et al. (2006). Characterization of a major refractory component of marine dissolved organic matter. *Geochim. Cosmochim. Acta* 70, 2990–3010. doi: 10.1016/j.gca.2006.03.021

Højerslev, N. K., Holt, N., and Aarup, T. (1996). Optical measurements in the North Sea-Baltic Sea transition zone. I. On the origin of the deep water in the Kattegat. *Cont. Shelf Res.* 16, 1329–1342. doi: 10.1016/0278-4343(95)00075-5

Jaffé, R., Ding, Y., Niggemann, J., Vähätalo, A. V., Stubbins, A., Spencer, R. G. M., et al. (2013). Global charcoal mobilization from soils via dissolution and riverine transport to the oceans. *Science* 340, 345–347. doi: 10.1126/science.1231476

Kim, S., Kaplan, L. A., and Hatcher, P. G. (2006). Biodegradable dissolved organic matter in a temperate and a tropical stream determined from ultra-high resolution mass spectrometry. *Limnol. Oceanogr.* 51, 1054–1063. doi: 10.4319/lo.2006.51.2.1054

Kim, S., Kramer, R. W., and Hatcher, P. G. (2003). Graphical method for analysis of ultrahigh-resolution broadband mass spectra of natural organic matter, the Van Krevelen Diagram. *Anal. Chem.* 75, 5336–5344. doi: 10.1021/ac034415p

Koch, B. P., and Dittmar, T. (2006). From mass to structure: an aromaticity index for high-resolution mass data of natural organic matter. *Rapid Commun. Mass Spectrom.* 20, 926–932. doi: 10.1002/rcm.2386

Koch, B. P., and Dittmar, T. (2016). From mass to structure: an aromaticity index for high-resolution mass data of natural organic matter. *Rapid Commun. Mass Spectrom.* 30, 250–250. doi: 10.1002/rcm.7433

Koch, B. P., Dittmar, T., Witt, M., and Kattner, G. (2007). Fundamentals of molecular formula assignment to ultrahigh resolution mass data of natural organic matter. *Anal. Chem.* 79, 1758–1763. doi: 10.1021/ac061949s

Koch, B. P., Witt, M. R., Engbrodt, R., Dittmar, T., and Kattner, G. (2005). Molecular formulae of marine and terrigenous dissolved organic matter detected by electrospray ionization Fourier transform ion cyclotron resonance mass spectrometry. *Geochim. Cosmochim. Acta* 69, 3299–3308. doi: 10.1016/j.gca.2005.02.027

Kujawinski, E. B., Del Vecchio, R., Blough, N. V., Klein, G. C., and Marshall, A. G. (2004). Probing molecular-level transformations of dissolved organic matter: insights on photochemical degradation and protozoan modification of DOM from electrospray ionization Fourier transform ion cyclotron resonance mass spectrometry. *Mar. Chem.* 92, 23–37. doi: 10.1016/j.marchem.2004.06.038

Kujawinski, E. B., Longnecker, K., Blough, N. V., Vecchio, R. D., Finlay, L., Kitner, J. B., et al. (2009). Identification of possible source markers in marine dissolved organic matter using ultrahigh resolution mass spectrometry. *Geochim. Cosmochim. Acta* 73, 4384–4399. doi: 10.1016/j.gca.2009.04.033

Kuliński, K., Hammer, K., Schneider, B., and Schulz-Bull, D. (2016). Remineralization of terrestrial dissolved organic carbon in the Baltic Sea. *Mar. Chem.* 181, 10–17. doi: 10.1016/j.marchem.2016.03.002

Kuliński, K., and Pempkowiak, J. (2011). The carbon budget of the Baltic Sea. *Biogeosciences* 8, 3219–3230. doi: 10.5194/bg-8-3219-2011

Kuliński, K., and Pempkowiak, J. (2012). *Carbon Cycling in the Baltic Sea*. Springer: Springer Science & Business Media.

Kullenberg, G., and Jacobsen, T. S. (1981). The Baltic Sea: an outline of its physical oceanography. *Mar. Pollut. Bull.* 12, 183–186. doi: 10.1016/0025-326X(81)90168-5

Lechtenfeld, O. J., Koch, B. P., Gašparović, B., Frka, S., Witt, M., and Kattner, G. (2013). The influence of salinity on the molecular and optical properties of surface microlayers in a karstic estuary. *Mar. Chem.* 150, 25–38. doi: 10.1016/j.marchem.2013.01.006

Letscher, R. T., Hansell, D. A., and Kadko, D. (2011). Rapid removal of terrigenous dissolved organic carbon over the Eurasian shelves of the Arctic Ocean. *Mar. Chem.* 123, 78–87. doi: 10.1016/j.marchem.2010.10.002

Löffler, A., Schneider, B., Perttilä, M., and Rehder, G. (2012). Air–sea CO_2 exchange in the Gulf of Bothnia, Baltic Sea. *Cont. Shelf Res.* 37, 46–56. doi: 10.1016/j.csr.2012.02.002

Longnecker, K., and Kujawinski, E. B. (2011). Composition of dissolved organic matter in groundwater. *Geochim. Cosmochim. Acta* 75, 2752–2761. doi: 10.1016/j.gca.2011.02.020

Medeiros, P. M., Seidel, M., Dittmar, T., Whitman, W. B., and Moran, M. A. (2015a). Drought-induced variability in dissolved organic matter composition in a marsh-dominated estuary. *Geophys. Res. Lett.* 42, 6446–6453. doi: 10.1002/2015GL064653

Medeiros, P. M., Seidel, M., Ward, N. D., Carpenter, E. J., Gomes, H. R., Niggemann, J., et al. (2015b). Fate of the Amazon River dissolved organic matter in the tropical Atlantic Ocean. *Glob. Biogeochem. Cycles* 29, 677–690. doi: 10.1002/2015GB005115

Miller, W. L., and Zepp, R. G. (1995). Photochemical production of dissolved inorganic carbon from terrestrial organic matter: significance to the oceanic

organic carbon cycle. *Geophys. Res. Lett.* 22, 417–420. doi: 10.1029/94GL03344

Mohrholz, V., Naumann, M., Nausch, G., Krüger, S., and Gräwe, U. (2015). Fresh oxygen for the Baltic Sea – an exceptional saline inflow after a decade of stagnation. *J. Mar. Syst.* 148, 152–166. doi: 10.1016/j.jmarsys.2015.03.005

Nausch, G., Feistel, R., Umlauf, L., Mohrholz, V., Nagel, K., and Siegel, H. (2012). *Hydrographisch-Hydrochemische Zustandseinschätzung der Ostsee 2011*. Meereswissenschaftliche Berichte, 86, Leibniz-Institut für Ostseeforschung Warnemünde.

Nausch, G., and Nehring, D. (1996). "Third periodic assessment of the state of the marine environment of the Baltic Sea, 1989-93," in *Baltic Proper: Hydrochemistry, Baltic Sea Environment Proceedings 64B* (Helsinki: Helsinki Commission - Baltic Marine Environment Protection Commission), 80–84.

Obernosterer, I., and Benner, R. (2004). Competition between biological and photochemical processes in the mineralization of dissolved organic carbon. *Limnol. Oceanogr.* 49, 117–124. doi: 10.4319/lo.2004.49.1.0117

Oksanen, J., Blanchet, F. G., Kindt, R., Legendre, P., Minchin, P. R., O'Hara, R. B., et al. (2015). *Vegan: Community Ecology Package*. R package version 2.3-0. Available online at: http://CRAN.R-project.org/package=vegan

Osburn, C. L., and Stedmon, C. A. (2011). Linking the chemical and optical properties of dissolved organic matter in the Baltic–North Sea transition zone to differentiate three allochthonous inputs. *Mar. Chem.* 126, 281–294. doi: 10.1016/j.marchem.2011.06.007

Osterholz, H., Kirchman, D. L., Niggemann, J., and Dittmar, T. (2016). Environmental drivers of dissolved organic matter molecular composition in the Delaware Estuary. *Front. Earth Sci.* 4:95. doi: 10.3389/feart.2016.00095

Raeke, J., Lechtenfeld, O. J., Wagner, M., Herzsprung, P., and Reemtsma, T. (2016). Selectivity of solid phase extraction of freshwater dissolved organic matter and its effect on ultrahigh resolution mass spectra. *Environ. Sci.* 18, 918–927. doi: 10.1039/c6em00200e

Rahm, L., and Danielsson, Å. (2007). Spatial heterogeneity of nutrients in the Baltic Proper, Baltic Sea. *Estuar. Coast. Shelf Sci.* 73, 268–278. doi: 10.1016/j.ecss.2007.01.009

Räike, A., Kortelainen, P., Mattsson, T., and Thomas, D. N. (2016). Long-term trends (1975–2014) in the concentrations and export of carbon from Finnish rivers to the Baltic Sea: organic and inorganic components compared. *Aquat. Sci.* 78, 505–523. doi: 10.1007/s00027-015-0451-2

Riedel, T., Zark, M., Vähätalo, A., Niggemann, J., Spencer, R., Hernes, P., et al. (2016). Molecular signatures of biogeochemical transformations in dissolved organic matter from ten World Rivers. *Front. Earth Sci.* 4:95. doi: 10.3389/feart.2016.00085

R core team (2015). *R: A Language and Environment for Statistical Computing*. Vienna: R Foundation for Statistical Computing. Available online at: http://www.R-project.org/

Savchuk, O. P. (2005). Resolving the Baltic Sea into seven subbasins: N and P budgets for 1991–1999. *J. Mar. Syst.* 56, 1–15. doi: 10.1016/j.jmarsys.2004.08.005

Schlitzer, R. (2016). *Ocean Data View*. Available online at: http://odv.awi.de

Schmidt, F., Elvert, M., Koch, B. P., Witt, M., and Hinrichs, K.-U. (2009). Molecular characterization of dissolved organic matter in pore water of continental shelf sediments. *Geochim. Cosmochim. Acta* 73, 3337–3358. doi: 10.1016/j.gca.2009.03.008

Schmidt, F., Koch, B. P., Elvert, M., Schmidt, G., Witt, M., and Hinrichs, K.-U. (2011). Diagenetic transformation of dissolved organic nitrogen compounds under contrasting sedimentary redox conditions in the Black Sea. *Environ. Sci. Technol.* 45, 5223–5229. doi: 10.1021/es2003414

Schneider, B., Gülzow, W., Sadkowiak, B., and Rehder, G. (2014). Detecting sinks and sources of CO_2 and CH_4 by ferrybox-based measurements in the Baltic Sea: three case studies. *J. Mar. Syst.* 140(Pt A), 13–25. doi: 10.1016/j.jmarsys.2014.03.014

Seidel, M., Beck, M., Riedel, T., Waska, H., Suryaputra, I. G. N. A., Schnetger, B., et al. (2014). Biogeochemistry of dissolved organic matter in an anoxic intertidal creek bank. *Geochim. Cosmochim. Acta* 140, 418–434. doi: 10.1016/j.gca.2014.05.038

Seidel, M., Beck, M., Riedel, T., Waska, H., Suryaputra, I. G. N. A., Schnetger, B., et al. (2015a). Benthic-pelagic coupling of nutrients and dissolved organic matter composition in an intertidal sandy beach. *Mar. Chem.* 176, 150–163. doi: 10.1016/j.marchem.2015.08.011

Seidel, M., Yager, P. L., Ward, N. D., Carpenter, E. J., Gomes, H. R., Krusche, A. V., et al. (2015b). Molecular-level changes of dissolved organic matter along the Amazon river-to-ocean continuum. *Mar. Chem.* 177, 218–231. doi: 10.1016/j.marchem.2015.06.019

Sholkovitz, E. R., Boyle, E. A., and Price, N. B. (1978). The removal of dissolved humic acids and iron during estuarine mixing. *Earth Planet. Sci. Lett.* 40, 130–136. doi: 10.1016/0012-821X(78)90082-1

Sleighter, R. L., Chin, Y.-P., Arnold, W. A., Hatcher, P. G., McCabe, A. J., McAdams, B. C., et al. (2014). Evidence of incorporation of abiotic S and N into prairie wetland dissolved organic matter. *Environ. Sci. Technol. Lett.* 1, 345–350. doi: 10.1021/ez500229b

Sleighter, R. L., and Hatcher, P. G. (2008). Molecular characterization of dissolved organic matter (DOM) along a river to ocean transect of the lower Chesapeake Bay by ultrahigh resolution electrospray ionization Fourier transform ion cyclotron resonance mass spectrometry. *Mar. Chem.* 110, 140–152. doi: 10.1016/j.marchem.2008.04.008

Smedberg, E., Mörth, C.-M., Swaney, D. P., and Humborg, C. (2006). Modeling hydrology and silicon-carbon interactions in taiga and tundra biomes from a landscape perspective: implications for global warming feedbacks. *Glob. Biogeochem. Cycles* 20:GB2014. doi: 10.1029/2005GB002567

Spencer, R. G. M., Stubbins, A., Hernes, P. J., Baker, A., Mopper, K., Aufdenkampe, A. K., et al. (2009). Photochemical degradation of dissolved organic matter and dissolved lignin phenols from the Congo River. *J. Geophys. Res.* 114:G03010. doi: 10.1029/2009jg000968

Stålnacke, P., Grimvall, A., Sundblad, K., and Tonderski, A. (1999). Estimation of riverine loads of nitrogen and phosphorus to the Baltic Sea, 1970–1993. *Environ. Monit. Assess.* 58, 173–200. doi: 10.1023/A:1006073015871

Stedmon, C. A., Markager, S., and Kaas, H. (2000). Optical properties and signatures of chromophoric dissolved organic matter (CDOM) in Danish coastal waters. *Estuar. Coast. Shelf Sci.* 51, 267–278. doi: 10.1006/ecss.2000.0645

Stedmon, C. A., Osburn, C. L., and Kragh, T. (2010). Tracing water mass mixing in the Baltic–North Sea transition zone using the optical properties of coloured dissolved organic matter. *Estuar. Coast. Shelf Sci.* 87, 156–162. doi: 10.1016/j.ecss.2009.12.022

Stenson, A. C., Marshall, A. G., and Cooper, W. T. (2003). Exact masses and chemical formulas of individual Suwannee River fulvic acids from ultrahigh resolution electrospray ionization Fourier transform ion cyclotron resonance mass spectra. *Anal. Chem.* 75, 1275–1284. doi: 10.1021/ac026106p

Struck, U., Pollehne, F., Bauerfeind, E., and Bodungen, B. V. (2004). Sources of nitrogen for the vertical particle flux in the Gotland Sea (Baltic Proper)—results from sediment trap studies. *J. Mar. Syst.* 45, 91–101. doi: 10.1016/j.jmarsys.2003.11.012

Stubbins, A., Spencer, R. G. M., Chen, H. M., Hatcher, P. G., Mopper, K., Hernes, P. J., et al. (2010). Illuminated darkness: molecular signatures of Congo River dissolved organic matter and its photochemical alteration as revealed by ultrahigh precision mass spectrometry. *Limnol. Oceanogr.* 55, 1467–1477. doi: 10.4319/lo.2010.55.4.1467

Thomas, H., Pempkowiak, J., Wulff, F., and Nagel, K. (2010). "The Baltic Sea," in *Carbon and Nutrient Fluxes in Continental Margins - A Global Synthesis,* Global Change - the IGBP Series, eds K. K. Liu, L. Atkinson, R. Quinones, and L. Talaue-McManus (Berlin: Springer), 334–345.

Urtizberea, A., Dupont, N., Rosland, R., and Aksnes, D. L. (2013). Sensitivity of euphotic zone properties to CDOM variations in marine ecosystem models. *Ecol. Model.* 256, 16–22. doi: 10.1016/j.ecolmodel.2013.02.010

Vähätalo, A. V., and Zepp, R. G. (2005). Photochemical mineralization of dissolved organic nitrogen to ammonium in the Baltic Sea. *Environ. Sci. Technol.* 39, 6985–6992. doi: 10.1021/es050142z

Voss, M., Dippner, J. W., Humborg, C., Hürdler, J., Korth, F., Neumann, T., et al. (2011). History and scenarios of future development of Baltic Sea eutrophication. *Estuar. Coast. Shelf Sci.* 92, 307–322. doi: 10.1016/j.ecss.2010.12.037

Voss, M., Emeis, K. C., Hille, S., Neumann, T., and Dippner, J. W. (2005). Nitrogen cycle of the Baltic Sea from an isotopic perspective. *Glob. Biogeochem. Cycles* 19, 1–15. doi: 10.1029/2004gb002338

Wagner, S., Riedel, T., Niggemann, J., Vähätalo, A. V., Dittmar, T., and Jaffé, R. (2015). Linking the molecular signature of heteroatomic dissolved organic matter to watershed characteristics in world rivers. *Environ. Sci. Technol.* 49, 13798–13806. doi: 10.1021/acs.est.5b00525

Ward, N., Bianchi, T., Medeiros, P., Seidel, M., Richey, J., Keil, R., et al. (2017). Where carbon goes when water flows: carbon cycling across the aquatic continuum. *Front. Mar. Sci.* 4:7. doi: 10.3389/fmars.2017.00007

Ylöstalo, P., Seppälä, J., Kaitala, S., Maunula, P., and Simis, S. (2016). Loadings of dissolved organic matter and nutrients from the Neva River into the Gulf of Finland – biogeochemical composition and spatial distribution within the salinity gradient. *Mar. Chem.* 186, 58–71. doi: 10.1016/j.marchem.2016.07.004

Conflict of Interest Statement: The authors declare that the research was conducted in the absence of any commercial or financial relationships that could be construed as a potential conflict of interest.

frontiers in Earth Science

ORIGINAL RESEARCH
published: 17 November 2016
doi: 10.3389/feart.2016.00095

Environmental Drivers of Dissolved Organic Matter Molecular Composition in the Delaware Estuary

Helena Osterholz[1], David L. Kirchman[2], Jutta Niggemann[1] and Thorsten Dittmar[1]*

[1] ICBM-MPI Bridging Group for Marine Geochemistry, Institute for Chemistry and Biology of the Marine Environment, Carl von Ossietzky University, Oldenburg, Germany, [2] School of Marine Science and Policy, University of Delaware, Lewes, DE, USA

Estuaries as connectors of freshwater and marine aquatic systems are hotspots of biogeochemical element cycling. In one of the best studied temperate estuaries, the Delaware Estuary (USA), we investigated the variability of dissolved organic matter (DOM) over five sampling cruises along the salinity gradient in August and November of 3 consecutive years. Dissolved organic carbon (DOC) concentrations were more variable in the upper reaches of the estuary (245 ± 49 μmol DOC L^{-1}) than at the mouth of the estuary (129 ± 14 μmol L^{-1}). Bulk DOC decreased conservatively along the transect in November but was non-conservative with increased DOC concentrations mid-estuary in August. Detailed analysis of the solid-phase extractable DOM pool via ultrahigh resolution mass spectrometry (Fourier-transform ion cyclotron resonance mass spectrometry, FT-ICR-MS) revealed compositional differences at the molecular level that were not reflected in changes in concentration. Besides the mixing of terrestrial and marine endmember signatures, river discharge levels and biological activity impacted DOM molecular composition. DOM composition changed less between August and November than along the salinity gradient. Relative contributions of presumed photolabile DOM compounds did not reveal non-conservative behavior indicative of photochemical processing, suggesting that on the timescales of estuarine mixing photochemical removal of molecules plays a minor role in the turbid Delaware Bay. Overall, a large portion of molecular formulae overlapped between sampling campaigns and persisted during estuarine passage. Extending the analysis to the structural level via the fragmentation of molecular masses in the FT-ICR-MS, we found that the relative abundance of isomers along the salinity gradient did not change, indicating a high structural similarity of aquatic DOM independent of the origin. These results point toward a recalcitrant character of the DOM supplied by the Delaware River. We demonstrate that in addition to bulk DOC quantification, detailed information on molecular composition is essential for constraining sources of DOM and to identify the processes that impact estuarine DOM, thereby controlling amount and composition of DOM eventually discharged to the ocean through estuaries.

Keywords: dissolved organic matter, Delaware Estuary, FT-ICR-MS, discharge, conservative mixing, seasonal variation, collision-induced fragmentation

OPEN ACCESS

Edited by:
Nicholas David Ward, University of Florida, USA

Reviewed by:
Yina Liu, Pacific Northwest National Laboratory, USA
Elizabeth Ann Canuel, Virginia Institute of Marine Science, USA

****Correspondence:***
Helena Osterholz
helena.osterholz@uni-oldenburg.de

Specialty section:
This article was submitted to Marine Biogeochemistry, a section of the journal Frontiers in Earth Science

Received: *26 August 2016*
Accepted: *20 October 2016*
Published: *17 November 2016*

Citation:
Osterholz H, Kirchman DL, Niggemann J and Dittmar T (2016) Environmental Drivers of Dissolved Organic Matter Molecular Composition in the Delaware Estuary. Front. Earth Sci. 4:95. doi: 10.3389/feart.2016.00095

INTRODUCTION

Large amounts of terrigenous organic matter are channeled through rivers and estuaries into the oceans—approximately 0.25×10^{15} g are transported in the form of dissolved organic carbon (DOC) annually (Hedges et al., 1997). The true amount of the DOC exported from land is likely higher as some regions (for example northern high-latitude rivers, Holmes et al., 2011), diffuse flows and flood events (Cole et al., 2007; Raymond and Saiers, 2010) are not well constrained to date. During transit, the size and composition of the riverine dissolved organic matter (DOM) pool is transformed through a multitude of biotic and abiotic processes. Despite decades of research on estuarine and coastal DOM cycling, we still lack understanding of the mechanisms and magnitudes of these modifications, thereby possibly resulting in misinterpretation of characteristics of the riverine DOM discharged to the coastal seas and ultimately reaching the deep ocean (Bauer and Bianchi, 2011).

Generally, bulk DOC concentrations decrease along estuaries from the river to the ocean while at the same time, the composition of the DOM pool changes. On molecular level, the aromaticity of the DOM decreases (Abdulla et al., 2013), while molecular weight, carbohydrate content (Abdulla et al., 2010), heteroelement content (Sleighter and Hatcher, 2008) and lability increase (D'Andrilli et al., 2015) with increasing salinity. Positive and negative deviations from a conservative mixing line defined by high-DOC river water and the low-DOC marine endmember are frequently observed (Cadée, 1982; Middelburg and Herman, 2007; Sharp et al., 2009). Estuaries are complex systems where, in addition to mixing of fresh- and marine waters, diffuse sources such as subterranean groundwater discharge (Taniguchi et al., 2002), aeolian and anthropogenic input (Liu et al., 2005; Tzortziou et al., 2015) add to the intricacy of biogeochemical cycling. Abiotic processes shaping the DOM pool along the estuarine gradient of pH, ionic strength and turbidity include the adsorption on and desorption from mineral surfaces (Keil et al., 1994; Mayer, 1994), flocculation (Eisma, 1986), aggregation or precipitation. Loss of organic carbon from the dissolved phase in the estuarine turbidity maximum (e.g., Miller, 1999), where the concentration of particulate organic carbon is usually the highest, is accompanied by a loss in aromaticity and nitrogen-containing compounds, as these compounds are preferentially adsorbed (Aufdenkampe et al., 2001; Riedel et al., 2012). Photodegradation processes, although generally thought to be minor in riverine systems due to the low transmission (Spencer et al., 2009), exhibit the highest impact on aromatic moieties of terrestrial origin (Stubbins et al., 2010). By decreasing the average molecular weight and increasing the contribution of aliphatic compounds, the bioavailability of the DOM can increase through photochemically mediated breakdown of molecules especially in tropical regions (Medeiros et al., 2015b). Biological processes, in temperate regions influenced by seasonality, such as selective uptake and transformation by heterotrophic microbes (Azam et al., 1994; Bourgoin and Tremblay, 2010), as well as addition of compounds via autochthonous production (Pennock and Sharp, 1986) likewise shape the estuarine DOM pool. Medeiros et al. (2015b) for example showed that phytoplankton-derived DOM inputs introduce saturated compounds in the tropical Amazon plume. DOM export by the Yukon River to the Bering Sea was highly stable over seasons, with enhanced DOM photo- and biolability in spring due to higher inputs of carbohydrates and aromatic moieties (Cao et al., 2016). Previous studies have furthermore shown that the DOC concentration in rivers increases with discharge (Schiff et al., 1998; Raymond and Saiers, 2010), superimposing the influence of most other environmental drivers. At high discharge, riverine DOM composition tends to carry a stronger terrigenous signal (Spencer et al., 2008). A similar observation was made by Medeiros et al. (2015a) who found strong seasonal variability in molecular DOM composition in the marsh-dominated Altamaha-Doboy-Sapelo estuary. This variability was driven mainly by river flow, leading to a stronger terrigenous signature at high discharge.

In our study, we investigate estuarine carbon cycling in the tidal Delaware River and Bay, located on the east coast of the USA. The freshwater flow into the estuary is dominated by the Delaware River, which supplies nearly 60% of the freshwater to the bay; the Schuylkill and other smaller rivers supply another 14% (Sutton et al., 1996). In total, these rivers account for >80% of freshwater input into the estuary. The water column of the Delaware Estuary is usually well-mixed, although stratification can build up near the mouth of the bay, particularly during summer (Garvine et al., 1992). The bay has an estimated flushing time of about 80 to 180 days (Ketchum, 1952; Sharp et al., 1982; Cifuentes et al., 1990). In parts heavily urbanized, its waters carry a high nutrient loading from the Philadelphia area and saline waters reach as far as ∼125 km from the mouth (Biggs et al., 1983). The estuary has been extensively monitored over the last 30 years with a focus on carbon and nutrient fluxes (Sharp et al., 2009). Different sources of the DOM and particulate organic matter (POM) have been identified along the estuary: isotope and biomarker studies of ultrafiltered DOM have identified a terrestrial signal in the river and turbid middle estuary transitioning to a more algal and zooplankton-dominated signal in the lower estuary and coastal ocean (Mannino and Harvey, 1999, 2000b). Further compositional changes of the DOM pool have been examined at the level of chemical classes, e.g., total amino acids and polysaccharides (Hoch and Kirchman, 1995; Mannino and Harvey, 2000a; Kirchman and Borch, 2003), which in addition to mixing of marine and terrestrial signatures reveal a seasonal imprint as well as processing in the estuarine turbidity maximum. Of the rivers draining into the Middle Atlantic Bight, the Delaware River however carries a high proportion of allochthonous DOC and aged carbon (Hossler and Bauer, 2013).

We characterized the main drivers of DOM concentration and composition between August and November over 3 years (five sampling cruises) along the salinity gradient of the Delaware estuary, thereby allowing inferences about the modified terrestrial signal ultimately reaching the Atlantic Ocean. In addition to bulk DOC concentrations, we assessed the compositional variation of solid-phase extractable (SPE) DOM using ultrahigh resolution mass

spectrometry (Fourier-Transform Ion Cyclotron Resonance Mass Spectrometry, FT-ICR-MS), which allowed the assignment of thousands of different molecular formulae to a water sample (Stenson et al., 2003; Koch et al., 2005, 2007). Further, we applied collision-induced fragmentation to reveal possible structural changes within the SPE-DOM pool along the salinity gradient that might be hidden on molecular formula level. The different levels of analytical resolution provided unprecedented insight into the DOM cycling in the Delaware estuary. Overall, we used the new opportunities presented by FT-ICR-MS to build on the previous body of work in the Delaware and other study systems and to gain a more detailed understanding of DOM at the molecular level.

MATERIALS AND METHODS

Site Description and Sample Collection

Sampling was carried out from about 160 km upstream from the mouth of the estuary to a station just outside of the Delaware Bay during five cruises over three years (November 7–10 2011, August 9–13 2012, November 12–16 2012, August 3–7 2013, and November 18–21 2013). Water was obtained by a CTD rosette-mounted Niskin bottle from ∼0.5 m depth. Ammonium, nitrate, phosphate, and silicate concentrations were measured with a SEAL Analytical AA3 Continuous Segmented Flow Analyzer using standard procedures (Sharp et al., 2009). The concentration of total chlorophyll *a* was estimated in acetone extracts by fluorometry. Light attenuation was estimated from the intensity of photosynthetically active radiance over a depth profile measured with a Biospherical PNF-210 radiometer. A microcentrifuge approach was used to estimate leucine incorporation (added concentration of 20 nM) (Kirchman, 2001). Sampling locations and environmental parameters are summarized in Table S1 and Figure S1.

River discharge at Trenton and Schuylkill gage stations was obtained from the USGS Water Information System (waterdata.usgs.gov). We calculated the sum of discharge for 7, 14, 28, 56, and 112 days before the start of each sampling campaign and found the same general trend (Figure S2). The summed discharge of 112 days was chosen for further calculations because it lies well within the residence time of the estuary which is between 80 to 180 days (Ketchum, 1952; Sharp et al., 1982; Cifuentes et al., 1990).

Dissolved Organic Matter Analysis

For quantification and molecular analysis of the DOM, water was filtered through precombusted glass fiber filters (GF/F, Whatman), acidified to pH 2 with 25% HCl (p.a. grade), and stored at 4°C in the dark before being shipped to Germany for analysis. Concentrations of DOC and total dissolved nitrogen (TDN) were measured via high temperature catalytic oxidation on a Shimadzu TOC-VCPH analyzer equipped with a TDN module. Accuracy and precision were monitored with consensus reference material (DSR, D. Hansell, University of Miami) and were better than 5%. DON was estimated by subtracting nitrate and ammonium concentrations from TDN. The DOM was solid-phase extracted according to Dittmar et al. (2008) using 1 g PPL columns (Agilent Bond Elut), and the resulting methanol extracts were stored at −20°C in the dark. The concentration of extractable DOC was determined from the extracts after complete removal of the methanol and dissolution in ultrapure water. Methanol extracts were diluted to a DOC concentration of 20 mg C L^{-1} in a methanol:water mixture of 1:1 (v/v) and submitted to Fourier Transform Ion Cyclotron Resonance Mass Spectrometry on a solariX FT-ICR-MS (Bruker Daltonik GmbH) equipped with an electrospray ionization source (Bruker Apollo II) applied in negative mode. 500 scans in a mass window from 150 to 2000 Da were accumulated and molecular formulae were calculated with the following restrictions: $^{12}C_{1\text{-}130}{}^{1}H_{1\text{-}200}O_{1\text{-}50}{}^{14}N_{0\text{-}4}S_{0\text{-}2}P_{0\text{-}1}$ to masses above the method detection limit after Riedel and Dittmar (2014). Additionally, masses detected in less than three samples were removed prior to further analysis.

Each sample was normalized to the sum of FT-ICR-MS signal intensities and corrected for dilution per sample. The modified aromaticity index (AI_{mod}, Koch and Dittmar, 2006 as corrected and reported in the erratum published in 2016), double bond equivalents (DBE) and weighted molar ratios were calculated for each sample. The molecular formulae were assigned to compound groups according to their O/C and H/C ratios as described in Seidel et al. (2014). Here, the seven main groups with their subcategories include (1) polycyclic aromatics (PCA, $AI_{mod} > 0.66$) subdivided into PCA containing more than 15 C atoms indicative of dissolved black carbon, PCA with less than 15 C atoms, or PCA containing a heteroelement; (2) polyphenols ($0.5 < AI_{mod} \leq 0.66$) with high (O/C $\geq$ 0.5) or low oxygen (O/C $<$ 0.5) content; (3) highly unsaturated aliphatics ($AI_{mod} \leq 0.5$, H/C $<$ 1.5, O/C $<$ 0.9) with high (O/C $\geq$ 0.5) or low (O/C $<$ 0.5) oxygen content; (4) unsaturated aliphatics ($1.5 < H/C \leq 2$, O/C $<$ 0.9, $N = 0$) with high (O/C $\geq$ 0.5) or low (O/C $<$ 0.5) oxygen content; (5) saturated fatty acids (H/C $>$ 2, O/C $<$ 0.9) with or without heteroelements; (6) carbohydrate-like formulae (O/C $>$ 0.9) with or without (N,S,P = 0) heteroelements; and (7) peptide-like molecular formulae ($1.5 < H/C < 2$, O/C $<$ 0.9, $N > 0$). The assignment of a formula to a compound class is not unambiguous since the grouping does not take into account all possible isomers. Calculated and intensity-weighted molecular composition and molecular categories per sample are provided in Table S1.

In order to investigate the structural DOM composition along the salinity gradient, we fragmented six nominal masses of two homologous series (*m/z* 269, 283, 297, 341, 365, and 379 Da) of three samples from the sampling campaign in November 2012 (salinities 0.8, 14.7, and 30.7) via collision-induced fragmentation in the FT-ICR-MS. The nominal masses were chosen to compare to a previous publication using the same approach (Osterholz et al., 2015), to span a broad mass range and to have a high relative signal intensity suitable for fragmentation. The November 2012 cruise was chosen for the fragmentation experiment as the DOC concentrations behaved conservatively, being representative of the conditions in the estuary most of the time except for bloom or very high discharge conditions. For the fragmentation, methanol extracts were diluted to a DOC concentration of 60 mg C L^{-1} in a methanol:water mixture of 1:1 (v/v). The collision voltage was chosen to yield similar signal intensities of the

most intense fragments and varied between 13 V and 18 V. 150 scans were accumulated for each analysis performed in duplicates. Molecular formula assignment to fragmentation mass spectra was done as described above. We identified 423 fragments resulting from the neutral losses of H_2O, CH_4O, $2H_2O$, CO_2, CO_2+H_2O, CO_2+CH_4O, $2CO_2$, $2CO_2+H_2O$, $2CO_2+CH_4O$, $3CO_2$, $3CO_2+H_2O$ or $3CO_2+CH_4O$. Only molecular formulae that were detected in the two replicate analyses were analyzed in further detail. The relative signal intensity of each fragment ion was divided by the sum of the intensities of all major fragment signal intensities plus the precursor ion signal intensity for better comparison between samples. The normalized fragment intensities were then grouped by neutral loss and compared between samples.

Statistical Analysis

Conservative mixing lines (**Figures 1**, **2**) were constructed using the respective mean concentrations/values of the two samples of highest and lowest salinity. The deviation of each sample from the theoretical mixing line was then calculated and averaged over the whole transect. A high value therefore represents a high variability of the parameter in relation to the values expected for a conservative mixing scenario, similar as described in Seidel et al. (2015a).

Multivariate statistical analyses were performed using R (version 3.2.2) and the package vegan (Oksanen et al., 2015). All analyses were run on normalized intensities of signals with molecular formula assignment which were corrected for dilution. Four extraction efficiencies (on carbon basis) above 100 and below 40% were likely erroneous and were replaced by the average value of extraction efficiencies of other samples (67%). Principal coordinate analyses (PCoA) were performed on Bray Curtis distance matrices (Bray and Curtis, 1957). Environmental vectors were fitted to the respective PCoA scores using the envfit function in the vegan package. Spearman rank correlations were calculated between single molecular formulae intensities and environmental parameters. Only correlations between a formula and an environmental parameter with a $p < 0.01$ were considered in further analysis and discussion. The non-parametric Wilcoxon rank-sum test was used for comparisons between groups of samples.

RESULTS

Environmental Characterization of the Delaware Bay

DOC, TDN and nitrate concentrations as well as turbidity generally decreased along the salinity gradient (**Figure 1**, Figure S1). Several biological parameters influenced by water temperature and light availability varied greatly between the two months (August and November) we sampled. These parameters included microbial abundance, chlorophyll *a* concentration and leucine incorporation as well as silicate concentrations (**Figure 2**, Figure S1). Freshwater discharge did not vary consistently between the two seasons.

Most environmental parameters deviated from conservative mixing along the salinity gradient. Nitrate concentrations, for example, were always high in the oligohaline zone, decreasing toward the ocean with a negative deviation from conservative mixing at intermediate salinities. Most of the total dissolved nitrogen in the Delaware estuary is inorganic. DON concentration did not vary consistently along the estuarine salinity gradient or with season.

Silicate concentrations were depleted at the freshwater end of the estuary in August, while in November concentrations were high because the river contributes large amounts of dissolved silicate into the estuary. Chlorophyll *a* concentration (**Figure 2**) and leucine incorporation (Figure S1) differed between the two campaigns that took place in August, yet covaried significantly ($\rho = 0.82$, $p < 0.01$) with highest values observed in the oligo- and polyhaline zones in August 2013 and overall high values during August 2012.

DOC concentrations decreased linearly (conservatively) during estuarine mixing in November (**Figure 1**). In August, however, changes in DOC concentrations were non-conservative; deviations from conservative mixing were significantly higher in August than in November (Wilcoxon rank-sum test, $p < 0.01$). Overall, DOC concentrations were more variable at the freshwater end; the coefficient of variation (CV) at low salinity was 20% (salinity < 1, mean DOC $245 \pm 49\,\mu mol\ L^{-1}$, $n = 14$) while it was 11% in marine waters (salinity > 30, mean DOC $129 \pm 14\,\mu mol\ L^{-1}$, $n = 14$). At salinities of less than 1, DOC concentrations were significantly lower in August than in November by 1.4-fold (Wilcoxon rank-sum test, $p < 0.01$). DOC concentrations in marine waters did not vary substantially between the 2 months. DOC concentrations at the high or low salinity extremes did not correlate significantly with discharge.

A turbidity maximum was apparent at salinities between 0 and 5 during all cruises; turbidity then decreased toward the ocean. Turbidity patterns were neither related to discharge nor revealed an impact on phytoplankton growth or DOC concentration.

Dissolved Organic Matter Molecular Composition

In the whole dataset consisting of 121 solid-phase extracted DOM samples, 12666 unique molecular formulae (MF) within the mass range of 154–885 Da were identified. Of those, 3093 MF (24%) were present in all 121 samples. Further, 78% of all MF were detected at least once during each of the five cruises. Considering each cruise separately, 34–45% of the MF were observed in every sample (November 2011: $n = 22$, August 2012: $n = 26$, November 2012: $n = 25$, August 2013: $n = 26$, November 2013: $n = 22$).

Principal coordinate analysis was performed on a Bray-Curtis dissimilarity matrix (Bray and Curtis, 1957) calculated using relative signal intensities of all samples (**Figure 3**). The two major axes of variation together encompassed almost 80% of the variability of the dataset. Salinity was highly positively correlated to principal coordinate PC1 ($\rho = 0.78$, $p < 0.001$, **Figure 1**), whereas silicate and DOC concentration were negatively correlated with PC1 ($\rho = -0.95$ and -0.57, respectively, $p < 0.001$). Discharge was strongly associated

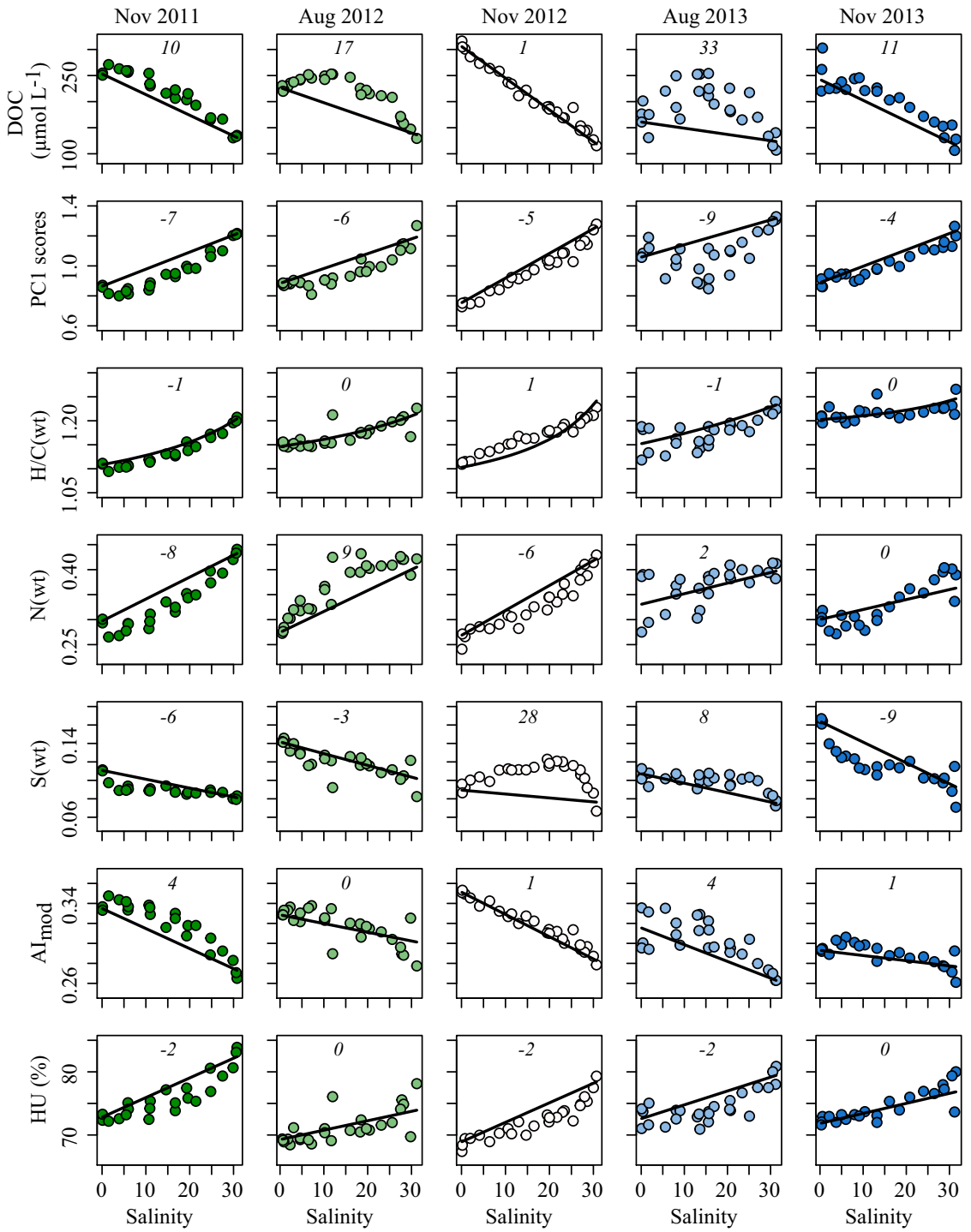

FIGURE 1 | DOC concentration and characteristics of DOM molecular composition (rows) vs. salinity for all five cruises (columns). PC1 scores are from **Figure 3** (1 was added to each score for data representation); H/C ratio, N- and S-content of molecular formulae were weighted by peak intensity; AI_{mod}, modified aromaticity index; HU, percentage of highly unsaturated compounds. Solid lines represent conservative mixing lines calculated using averages of the two samples of lowest and highest salinities, respectively. Numbers in italics denote percentage of deviation between the conservative mixing line and the measured values (see section Materials and Methods).

with PC2 ($\rho = -0.75$, $p < 0.001$, **Figure 4**), the second axis of variation comprising 25% of the variability of the DOM molecular data. Microbial abundance, bacterial production (leucine incorporation) and chlorophyll *a* concentration were correlated with the third and/or fourth PCs, encompassing 6 and 3% of the variation in the data, respectively (Figures S3, S5E,F).

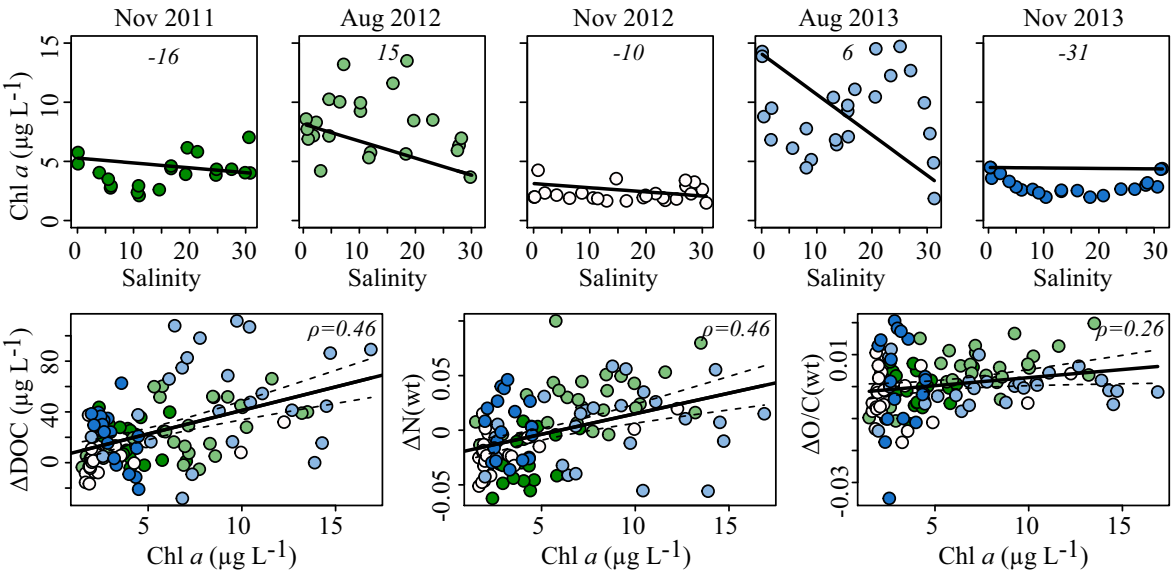

FIGURE 2 | (Top row) Chlorophyll *a* concentration vs. salinity for all five cruises. Solid lines represent conservative mixing lines calculated using averages of the two samples of lowest and highest salinities, respectively. Numbers in italics denote percentage of deviation between the conservative mixing line and the measured values (see Methods). (**Bottom row**) Chlorophyll *a* concentration vs. the deviation from conservative mixing of DOC concentration, weighted N content and weighted O/C ratio noted as Δ. The color of the symbols in the bottom row indicates the cruise as defined in the top row. Solid lines represent linear regression, and dashed lines denote standard error. Spearman rank correlations for each parameter vs. chlorophyll *a* concentration are given. Significance of correlations is $p < 0.01$.

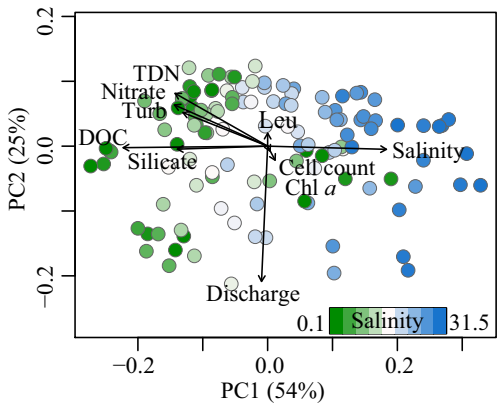

FIGURE 3 | Principal coordinate analysis based on Bray-Curtis dissimilarities of relative peak intensities, color-coded by salinity of each sample. Shown are the first two principal coordinates, accounting for 54 and 25% of the total variability in the dataset. Environmental parameters (black) are fitted to the ordination. Leu, Leucine incorporation; Turb, Turbidity.

Three environmental parameters (salinity, discharge, chlorophyll *a* concentration) were chosen for a more detailed investigation of changes in molecular DOM composition. These three parameters each represent one group of co-correlating environmental variables identified via hierarchical clustering (Figure S4).

Almost half of all identified molecular formulae, capturing 85 ± 5% of the total signal intensity of each sample, decreased in intensity with increasing salinity. The overall aromaticity of the SPE-DOM, assessed via the modified aromaticity index AI_{mod}, strongly decreased (**Figure 1**, **Table 1**). A molecular formulae based measure for terrigenous input, I_{terr} proposed by Medeiros et al. (2016), decreased from ∼0.5 at the freshwater end to ∼0.2 in the most marine waters and was highly negatively correlated with salinity ($\rho = -0.79$, $p < 0.001$). The relative contribution of sulfur to DOM molecular composition exhibited a weak relationship with salinity, overall decreasing toward the ocean. SPE-DOM N-containing molecular formulae, average molecular mass and H/C ratio all increased with increasing salinity (**Figure 1**, Figures S5A,B, Table S1). The relative abundance of highly unsaturated compounds, representing the largest compound class, likewise increased. The index for labile compounds above the molecular lability boundary (MLB) of H/C > 1.5, the MLB_{wL} proposed by D'Andrilli et al. (2015), slightly increased toward the ocean for all cruises except in November 2012 ($\rho = 0.23$, $p < 0.05$).

At high discharge in the Delaware Bay, we found high values for O/C ratio, molecular mass and highly unsaturated compounds (**Figure 4**). The subgroup of oxygen-rich highly unsaturated compounds emphasizes this trend (**Figure 4**, **Table 1**, Figures S5C,D). We observed only a slight increase in aromaticity, while the I_{terr} did not correlate significantly with discharge ($p > 0.05$). The MLB_{wL} was highly negatively linked with discharge ($\rho = -0.80$, $p < 0.001$). About 2000 molecular formulae were positively affected by discharge and another 3000 were negatively affected, in total accounting for ∼60% of total signal intensity (**Table 1**).

Chlorophyll *a* concentration and microbial activity were highly correlated; therefore only chlorophyll *a* was chosen for

TABLE 1 | Characteristics of molecular formulae correlating positively (POS) or negatively (NEG) with salinity, discharge and chlorophyll *a* concentration as well as of those molecules exhibiting no correlation to either one of the three environmental parameters.

	Salinity		Discharge		Chlorophyll *a*		No correlation
	NEG	POS	NEG	POS	NEG	POS	
MF	5690 ± 848	353 ± 96	2171 ± 180	2981 ± 999	162 ± 12	604 ± 258	471 ± 126
MW	371 ± 19	399 ± 10	302 ± 8	481 ± 13	334 ± 10	430 ± 27	414 ± 12
C	17.79 ± 0.81	17.69 ± 0.37	15.16 ± 0.44	21.56 ± 0.65	17.51 ± 0.47	18.04 ± 1.37	18.86 ± 0.68
H	20.40 ± 0.91	22.72 ± 0.55	20.18 ± 0.66	23.53 ± 1.30	22.45 ± 0.69	20.47 ± 2.32	25.33 ± 1.17
O	8.24 ± 0.62	8.54 ± 0.29	5.73 ± 0.21	12.04 ± 0.31	6.08 ± 0.26	10.66 ± 0.64	9.07 ± 0.26
N	0.21 ± 0.02	1.87 ± 0.04	0.33 ± 0.06	0.33 ± 0.05	0.22 ± 0.05	1.23 ± 0.08	0.82 ± 0.06
S	0.104 ± 0.021	0.065 ± 0.027	0.149 ± 0.037	0.059 ± 0.011	0.053 ± 0.023	0.201 ± 0.049	0.150 ± 0.031
P	0.001 ± 0.001	0.004 ± 0.004	0.004 ± 0.002	0.004 ± 0.002	0.007 ± 0.005	0.008 ± 0.006	0.057 ± 0.029
O/C	0.47 ± 0.02	0.48 ± 0.01	0.39 ± 0.01	0.57 ± 0.01	0.35 ± 0.01	0.60 ± 0.02	0.50 ± 0.01
H/C	1.15 ± 0.04	1.29 ± 0.01	1.32 ± 0.01	1.08 ± 0.05	1.27 ± 0.02	1.13 ± 0.08	1.34 ± 0.02
AI_{mod}	0.32 ± 0.02	0.18 ± 0.01	0.25 ± 0.01	0.30 ± 0.03	0.30 ± 0.01	0.26 ± 0.06	0.16 ± 0.02
DBE	8.7 ± 0.6	8.3 ± 0.1	6.2 ± 0.1	11.0 ± 0.6	7.4 ± 0.2	9.4 ± 0.8	7.6 ± 0.2
Compound classes (% of total)							
PCA	2.7 ± 0.8	0 ± 0	0.4 ± 0.2	2.9 ± 1.2	1.6 ± 0.7	0.9 ± 0.7	0.3 ± 0.2
PCA < C15	1.2 ± 0.4	0 ± 0	0.4 ± 0.2	0.6 ± 0.3	1.6 ± 0.7	0.0 ± 0.1	0 ± 0
PCA ≥ C15	1.4 ± 0.6	0 ± 0	0 ± 0	2.3 ± 1.0	0 ± 0	0.8 ± 0.6	0.3 ± 0.2
PCA-X	2.7 ± 0.7	0.1 ± 0.1	1.9 ± 0.4	1.2 ± 0.6	0.2 ± 0.2	11.5 ± 5.8	2.6 ± 1.5
PP	14.0 ± 2.4	1.0 ± 0.7	8.1 ± 0.9	11.7 ± 3.9	5.4 ± 1.6	8.2 ± 3.5	3.5 ± 1.2
PP O-rich	43 ± 1.4	0 ± 0	0.3 ± 0.1	8.0 ± 2.9	0.3 ± 0.1	5.9 ± 3.2	0.3 ± 0.2
PP O-poor	9.7 ± 1.4	1.0 ± 0.7	7.9 ± 0.9	3.7 ± 1.1	5.1 ± 1.6	2.2 ± 0.7	3.2 ± 1.2
HU	72.1 ± 3.3	95.0 ± 2.0	69.5 ± 2.0	83.1 ± 5.3	88.4 ± 3.3	69.2 ± 7.8	70.2 ± 3.3
HU O-rich	28.3 ± 3.8	35.0 ± 3.0	9.9 ± 1.3	59.9 ± 3.4	1.4 ± 0.4	61.7 ± 7.4	31.2 ± 3.0
HU O-poor	43.8 ± 4.0	59.9 ± 2.9	59.6 ± 2.5	23.2 ± 4.0	87.0 ± 3.7	7.5 ± 3.3	39.0 ± 2.6
UA	8.3 ± 1.9	1.2 ± 0.6	18.0 ± 1.5	0.7 ± 0.3	1.8 ± 0.7	3.9 ± 2.1	17.5 ± 2.6
UA O-rich	1.7 ± 0.4	1.0 ± 0.5	3.9 ± 0.5	0.4 ± 0.1	0 ± 0	2.2 ± 0.9	8.2 ± 1.0
UA O-poor	6.6 ± 1.6	0.2 ± 0.2	14.2 ± 1.4	0.3 ± 0.2	1.8 ± 0.7	1.7 ± 1.7	9.3 ± 2.1
FA-X	0.1 ± 0.0	0.0 ± 00.1	0.4 ± 0.3	0.1 ± 0.1	2.1 ± 1.4	0.7 ± 1.0	0.3 ± 0.4
Sugars	0.1 ± 0.0	0 ± 0	0 ± 0	0 ± 0	0 ± 0	0.1 ± 0.1	0.1 ± 0.1
Sugars-X	0 ± 0	0.3 ± 0.2	0 ± 0	0.1 ± 0.1	0.1 ± 0.2	0.5 ± 0.4	0.8 ± 0.3
Peptides	0.1 ± 0.0	2.4 ± 0.9	1.5 ± 0.4	0.1 ± .0.1	0.3 ± 0.1	5.1 ± 2.4	4.6 ± 1.3

Values represent formulae counts (MF), intensity-weighted molecular mass in Dalton (MW), element contribution (C, H, O, N, S, P), molar ratios (O/C, H/C), molecular indices (AI_{mod}, DBE) and relative contribution to compound classes (PCA, polycyclic aromatics; PCA<15 or ≥15, PCA with less than or more/equal to 15 C atoms; -X, containing heteroelements (N, S, P); PP, polyphenols; HU, highly unsaturated compounds; UA, unsaturated aliphatics; FA, fatty acids).

further investigation. Overall, chlorophyll *a* concentration was variable along the salinity gradient, but consistently displayed positive deviations from conservative mixing in August and negative deviations in November (**Figure 2**). Only a few molecules varied consistently with chlorophyll *a* concentration and accounted for ∼6% of the total signal intensity (Figure S5E, **Table 1**). The molecular variation associated with the chlorophyll *a* gradient was, however, markedly different from random correlations as tested with a dataset of normally distributed, random variables (Figure S5H). During periods of high phytoplankton biomass and microbial production, DOM was enriched in N, S, O, unsaturated aliphatics, polyphenolic compounds as well as sugar- and peptide-like molecular formulae (**Table 1**). To explore the correlations in more detail, the deviations from conservative mixing of DOC concentrations and molecular parameters were calculated (ΔDOC, ΔN, ΔO/C); significant increases are shown in **Figure 2**. The MLB_{wL} and I_{terr} did not correlate significantly with chlorophyll *a* concentrations ($p > 0.05$).

The 471 ± 126 molecular formulae that correlated with one of the three factors ($p > 0.01$) accounted for ∼3% of the total signal intensity and were widely distributed over the van Krevelen space occupied by a typical DOM sample, but were less prevalent in the low-H/C and high-O/C region (Figure S5G).

Dissolved Organic Matter Structural Analysis

Fragmentation of six nominal masses from three samples along the salinity gradient in Nov 2012 was used to detect potential preferential removal or addition of DOM structural features along the salinity gradient of the Delaware Estuary. A total of

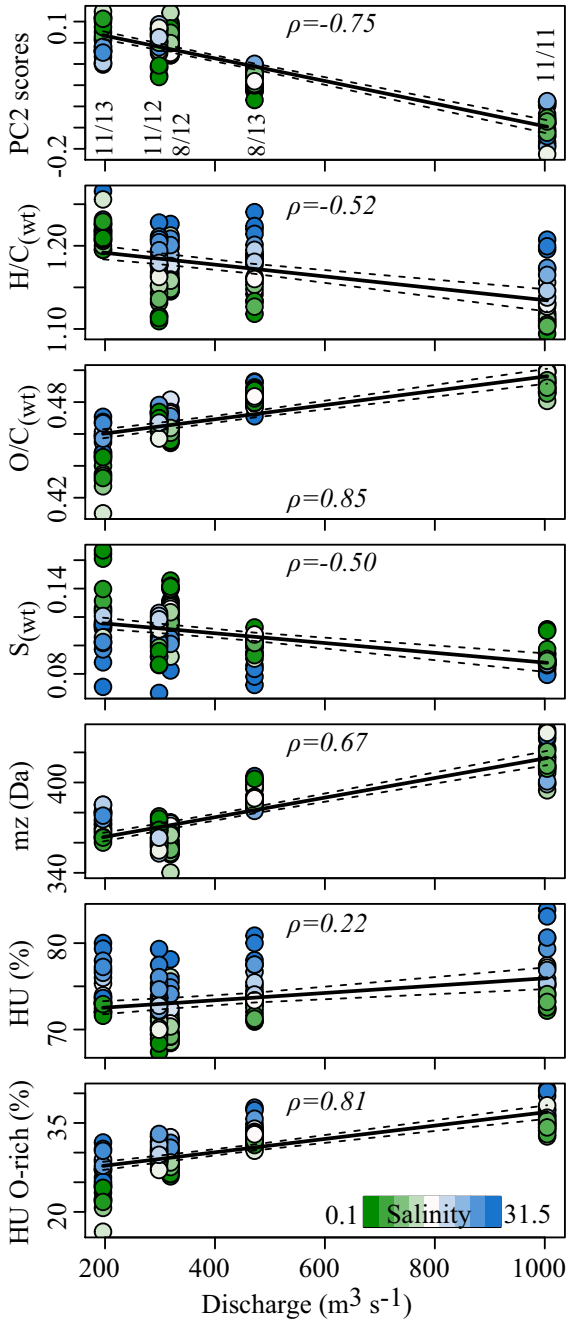

FIGURE 4 | Characteristics of DOM molecular formulae vs. discharge. All samples per cruise are plotted and colored according to salinity. Cruise is marked in the top panel as MM/YY. Solid lines represent linear regression, dashed lines denote standard error. Spearman rank correlations for each parameter vs. discharge are given (ρ). Significance of correlations is $p < 0.001$, except for HU where $p < 0.05$. HU, highly unsaturated compounds; PC2 scores are taken from **Figure 3**.

423 detected fragments were normalized and grouped by neutral loss (H_2O, CO_2, CH_4O as well as combinations and multiples thereof). We did not detect any of the OCH_2 functionalities described by Liu et al. (2011). These neutral losses represent a component of lignin biopolymers generated from wood extract and C18-extracted black waters and were thus presumed to occur in the terrigenous DOM. In pairwise comparisons of the relative signal intensities per neutral loss, a ratio of 1 indicates that no differences in neutral losses were observed between samples. This in turn suggests that a formula with the same molecular mass has a similar structure, regardless of its sampling location within the salinity gradient of the estuary. Although there were some deviations from the ratio of 1 among samples taken at different salinities, the fragmentation patterns did not differ significantly (Wilcoxon rank-sum test, $p > 0.05$, **Figure 5**).

DISCUSSION

In order to investigate the environmental drivers of DOM quantity and quality in a temperate estuarine system, we combined quantitative analysis of DOC concentrations with ultrahigh resolution mass spectrometric analysis of solid-phase extractable (SPE) DOM from samples from the entire salinity gradient of the Delaware estuary over 3 years. The analytical window provided by the combination of PPL-SPE and FT-ICR-MS allowed us to examine a large, otherwise inaccessible portion of the DOM pool; in this study on average 67 ± 6% of the DOC was captured with our solid-phase extraction method. The PPL columns used here poorly recover very small and polar compounds (Raeke et al., 2016), but absorb a wide range of compounds of varying polarity and are thought to provide a major fraction of the natural DOM (Green et al., 2014; Li et al., 2016). The extraction efficiency did not significantly change along the salinity gradient of the estuary, indicating that our method captured a reproducible fraction of the estuarine DOM pool. FT-ICR-MS analysis of our SPE-DOM samples allowed us to gain valuable information on molecular composition and explore variation with biogeochemical properties. Additional insights into DOM structural features were revealed with in-cell fragmentation.

Mixing of Terrigenous and Marine DOM along the Salinity Gradient

On its way from soils to the ocean margins, DOM can undergo transformations in molecular composition that are not reflected in the DOC concentrations along the salinity gradient. Besides a slight decrease in molecular formulae richness ($\rho = -0.29$, $p < 0.01$) and the Shannon diversity index ($\rho = -0.44$, $p < 0.001$) along the salinity gradient, condensed aromatic compounds, AI_{mod}, and polyphenols indicating DOM of terrigenous origin were higher in the low salinity region. Proportions of highly unsaturated compounds and molecular mass increased with increasing salinity, as did the contributions of nitrogen-containing molecular formulae and sugar- and peptide-like compounds that are thought to be products of more recent primary production (Amon et al., 2001). Our results are overall in line with previous studies applying ultrahigh resolution mass spectrometry to molecularly characterize DOM. These have shown that DOM tends to become more aliphatic, has a higher heteroelement content (N, S, P), and contains

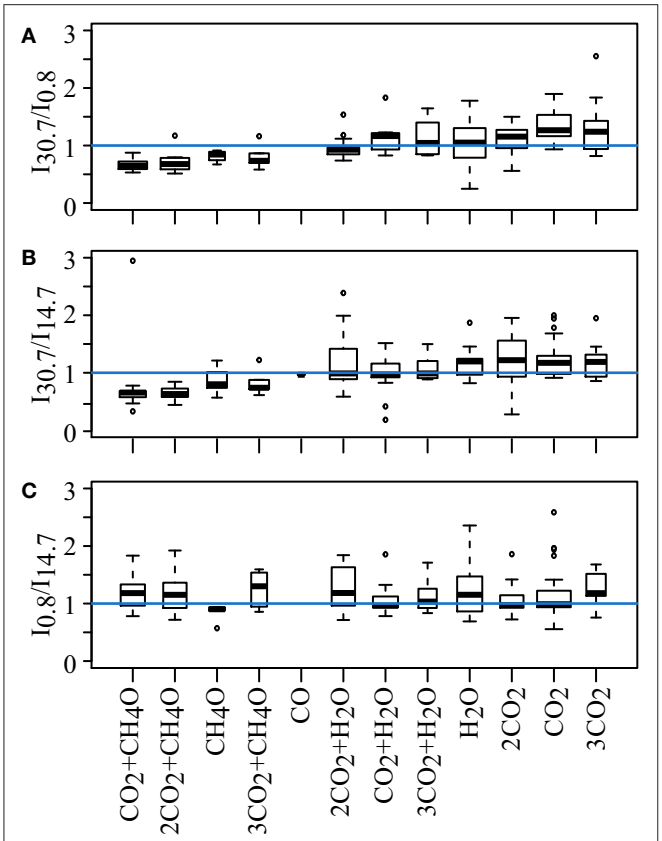

FIGURE 5 | Fragmentation of 18 nominal masses at different salinities (0.8, 14.7, 30.7, Nov 2012), resulting in 423 identified fragments. Boxplots show normalized intensities of fragments grouped by neutral loss; pairwise comparisons are **(A)** salinity 30.7 to 0.8, **(B)** salinity 30.7 to 14.7, and **(C)** salinity 0.8 to 14.7. Blue line denotes ratio of 1 in pairwise comparisons of samples. Relative intensities of averaged neutral losses did not differ significantly between samples (Wilcoxon rank-sum test, $p < 0.01$). Box widths are proportional to the number of observations in the groups.

lower abundances of oxygen-rich molecules along gradients of increasing salinity in temperate (Sleighter and Hatcher, 2008) and tropical estuaries (Medeiros et al., 2015b; Seidel et al., 2015b). Highly unsaturated compounds, however, are thought to mainly comprise soil-derived "humics" and other highly unsaturated compounds according to Šantl-Temkiv et al. (2013). It has to be kept in mind that FT-ICR-MS detects relative signal intensities and grouping into molecular classes is reported in proportions, i.e., if one compound class such as the polyphenols strongly decreases in a sample, another compound class or classes must increase. The less oxygenated polyphenols decrease more strongly with increasing salinity than the oxygen-rich subgroup (**Table 1**) which includes many phenolic acids. This finding illustrates that the classification into broad compound groups does not unambiguously identify the origin and fate of the molecules. Further, although unsaturated aliphatic compounds have previously been shown to be abundant in the ocean supposedly due to the DOM from marine organisms (Sleighter and Hatcher, 2008; Seidel et al., 2015a), they exhibited no relationship with salinity in our study.

Data on DON concentration and the molecular composition data give a different picture about sources of DOM in the estuary. DON concentrations were similar along the whole transect whereas increased DON concentrations have been observed previously in freshwater parts of estuaries (Badr et al., 2008). However, there was a strong positive correlation between relative intensities of N-containing molecular masses and salinity ($\rho = 0.77$, $p < 0.001$). This is consistent with the hypothesis that marine DOM is mainly derived from autochthonous production and contains more heteroelements than DOM from terrestrial sources (Sleighter and Hatcher, 2008). In addition to a higher N content of the SPE-DOM molecular formulae, we also observed a slightly positive correlation between the relative abundance of P in the assigned molecular formulae and salinity ($\rho = 0.18$, $p < 0.05$).

We propose that variation in the endmembers (river and ocean) is preserved more clearly in the DOM molecular composition than in DOC concentration. The coefficient of variation (CV) of DOC concentrations was 20% ($245 \pm 49\,\mu mol\ L^{-1}$) in waters with salinities <1 and 11% ($129 \pm 14\,\mu mol\ L^{-1}$) in waters with salinity > 30. In contrast, the CV of the Bray-Curtis dissimilarity of the SPE-DOM samples was similar for the low and high salinity samples (35 and 31%, respectively). Put differently, DOC concentrations decreased along the salinity gradient and reached similarly low levels in the marine waters while DOM molecular composition remained diverse among the five cruises. This discordance in trends of concentration and composition could be caused by the removal of DOM fractions not captured with our SPE-method. A more likely explanation is the consistent removal or dilution or both of SPE-DOM over the whole captured mass range, supported by the strong correlation of DOM molecular composition with salinity (e.g., **Figures 1**, **3**).

The fact that few molecules increase in relative intensity toward the ocean indicates that dilution and/or degradation processes are by far more important than new production of DOM compounds in shaping DOM composition in this system. Many compounds present at the freshwater source were detected along the whole salinity gradient (34–45%, calculated separately for each cruise). Together with the high percentage of compounds that were detected repeatedly during each cruise (78%), these data indicate a common source of DOM from land that is preserved due to the recalcitrant nature of these compounds. Hossler and Bauer (2013) indeed report a high degree of allochthonous (40–96%) and aged DOC (1–23%) in the Delaware River and Bay. A second possibility is that some compounds are actually removed while others with different structures but the same molecular formulae are produced during the transit through the estuary, thus masking a lower-level DOM variability in the system (Sleighter and Hatcher, 2008). Since structure can be deduced from molecular formula only in extreme cases, i.e., for molecules with very low H/C ratios (Koch and Dittmar, 2006), we conducted fragmentation experiments applying FT-ICR-MS/MS to three samples along the salinity gradient at low, mid and high salinity of the November 2012 cruise. Collision-induced fragmentation has been shown to distinguish samples with similar molecular formulae fingerprints, but different structural

composition (Osterholz et al., 2015). The neutral losses of H_2O, CO_2, and CH_4O as well as combinations and multiples thereof are markedly different in relative intensity and exhibit ratios up to 4 when comparing relative fragment intensities of fresh, biologically produced and aged oceanic DOM. The same neutral losses were detected in the fragmentation experiments with Delaware Estuary DOM (**Figure 5**). However, none of the fragment intensities differed significantly between samples. This finding indicates that structures in aquatic DOM were highly similar, irrespective of their origin from marine or terrestrial sources. For our study, we infer that during estuarine mixing, there were no changes in DOM composition at the structural level that were overlooked at molecular formula level.

The Influence of Discharge Levels

During our five sampling campaigns we did not observe correlations between discharge regimes and DOC concentrations. This remained true even if only the low-salinity samples (salinity < 1, $n = 14$) were taken into account, which would be most directly affected by discharge. For forested streams in the eastern United States as well as the Amazon, high DOC concentrations at the onset of high discharge events and low DOC concentrations at low discharge have been reported (Raymond and Saiers, 2010; Ward et al., 2013). Other studies using a similar analysis approach to the one used here have detected positive correlations between DOC concentration and discharge (Raymond and Bauer, 2001; Medeiros et al., 2015b). The Delaware Estuary in general shows a weak axial salinity response to freshwater input, probably due to vertical shear flow dispersion and the action of lateral shear coupled to a strong lateral salinity gradient (Garvine et al., 1992). DOC, mostly exhibiting conservative behavior, accordingly showed no strong influence of discharge.

Although discharge did not affect DOC concentrations it affected DOM molecular composition. According to correlation analysis of the principal coordinates, discharge was identified as the second most important driver of DOM molecular composition responsible for about a quarter of the total variability. We observed a pronounced shift in DOM composition between low/normal discharge situations where the discharge was around or below the yearly mean flow of $\sim 400\,m^3\ s^{-1}$ provided by the Delaware and Schuylkill River (Polis and Kupferman, 1973) and high discharge regimes ($> 400\,m^3\ s^{-1}$, **Figure 4**). DOM associated with high river discharge was enriched in condensed aromatics, oxygen-rich polyphenols, oxygen-rich highly unsaturated compounds and a higher AI_{mod}, all indicative of higher terrigenous DOM input (Meyers-Schulte and Hedges, 1986; Koch et al., 2005). The specific positive correlation with oxygen-rich aromatic compounds presumably relates to the input of lignin- and tannin-like compounds with high O/C ratio (**Table 1**, **Figure 4**). Lignins are complex aromatic biopolymers that make up a major component of vascular plant biomass (Sarkanen and Ludwig, 1971). They are an important component of riverine DOM (Ertel et al., 1986). Tannins are produced by some algae but primarily are constituents of higher plant tissue (Hedges and Weliky, 1989). They are thought to be quickly removed from aquatic environments via decomposition, precipitation, and sorption to sediments (Maie et al., 2008). Litterfall and plant debris are degraded in forest soils, from which rainfall events can mobilize tannins and lignin, leading to high concentrations in the Delaware River when discharge is high. The average mass of the compounds associated with discharge rates was higher than of those compounds negatively correlating with discharge. This is opposite of the expected trend as terrigenous SPE-DOM tends to have a lower molecular weight when compared to marine DOM analyzed via FT-ICR-MS (Koch et al., 2005; Medeiros et al., 2015b). Tannins, in molecular weight from 500 to 3000 Da (Bate-Smith, 1968), and lignin polymers of similar or higher molecular weight increased in abundance at high discharge and therefore could contribute to this increase in average molecular mass of the entire DOM pool. Forest and wetland coverage of the watershed decreases from the upper basin toward the bay but nevertheless accounts for the major land use of the Delaware basin (49 and 8%, respectively, Partnership for the Delaware Estuary, 2012). Forests and wetlands are possible sources for this terrigenous DOM. Another much debated source of DOC to the Delaware Estuary are the *Spartina alterniflora*-dominated wetlands surrounding especially the lower estuary. Hossler and Bauer (2012) reported a contribution of carbon originating from plants with a C_4-photosynthetic mechanism to DOC of up to 51% in the Delaware River. Since the production of maize, a C_4 plant, is low in the Delaware watershed, the salt marshes might be a large source of this C_4-organic matter. According to Benner et al. (1987) and Cifuentes (1991) and references therein, the marshes do not seem to export large quantities of organic matter to the estuarine water column. These sources, however, cannot be deciphered through the methods applied in our study.

Further, the river tended to carry more S-containing DOM to the freshwater end of the estuary at low to intermediate discharge scenarios ($\rho = -0.54$, $p < 0.001$, **Figure 4**, **Table 1**). The anthropogenically influenced portion of the Delaware River (land cover: 26% agriculture, 15% developed land, Partnership for the Delaware Estuary, 2012) especially in the central and lower watershed, may introduce dissolved organic sulfur (DOS) compounds originating from e.g., wastewater input and agriculture (Gonsior et al., 2011; Wagner et al., 2015), which would be less diluted at low river discharge. In the same manner, DOS compounds formed during early diagenesis in sediments could be released into the water column (Seidel et al., 2014) or be exported from the salt marshes surrounding the Delaware Bay (Luther et al., 1986). The Delaware Bay nevertheless carried SPE-DOS in ranges comparable to less anthropogenically influenced rivers such as Lena, Amazon and Congo (Wagner et al., 2015).

Seasonal DOM Imprint Due to Biological Processes

The impact of biological processes on DOM concentration and composition was assessed through chlorophyll *a* concentration as a proxy for phytoplankton biomass and bacterial activity measured via leucine incorporation. Due to their high co-correlation, these two factors cannot be distinguished in our correlative approach ($\rho = 0.82$, $p < 0.001$). There were

no significant correlations between DOC and chlorophyll *a* concentrations or with leucine incorporation rates.

Only a small portion of molecular formulae comprising about 6% of the total signal intensity correlated positively or negatively with chlorophyll *a* (**Table 1**). This number is similar to the percentage of molecular formulae attributed to phytoplankton and/or biodegradation-related processes in the Amazon (Medeiros et al., 2015b). The authors report selective removal of compounds with high O/C ratios via biodegradation (Sun et al., 1997; Kim et al., 2006) and input of phytoplankton-derived material of low O/C ratio (Landa et al., 2014). This was not observed for the Delaware system, where we found that oxygen-rich polyphenols and highly unsaturated compounds increased with chlorophyll *a* concentration. The higher heteroelement content and occurrence of saturated compounds are consistent with phytoplankton-derived DOM (Sleighter and Hatcher, 2008). Phytoplankton classes differed significantly not only between August and November sampling, but also between the different years (Kirchman et al., in press), possibly producing different DOM compounds and thereby hampering the detection of a uniform "biological signature."

Abiotic Factors Influencing DOM Composition

At increasing ionic strength, abiotic processes such as flocculation and absorption to particles may influence DOM composition (Hernes and Benner, 2003). Selective removal of terrestrially derived compounds such as humic acids (Fox, 1983; Ertel et al., 1986) has been reported during estuarine mixing, as well as sorption of amino acids and dissolved polysaccharides to particles in the turbidity maximum zone of the Delaware Estuary (Mannino and Harvey, 2000a). Flocculation with metal salts, for example, has been shown to selectively remove more aromatic compounds (Riedel et al., 2012). Cifuentes (1991) proposed the release of lignin phenols from resuspended sediments in the turbid regions of the Delaware Estuary. We were not able to attribute changes in DOC concentration or molecular DOM composition to adsorption processes in this zone through our correlative approach, i.e., correlating relative FT-ICR-MS signal intensities or bulk DOC concentrations with an environmental factor (here: turbidity). Likely, extensive DOM processing before it reaches the river and estuary (Goñi and Gardner, 2003), the small relative contribution of those compound classes to the total DOC pool, the low spatial resolution of the sampling points in and around the turbidity maximum and the strong superimposing signal of the mixing of fresh- and saltwater in combination all hinder the recognition of a turbidity maximum signal. In a recent publication, Hermes and Sikes (2016) showed that POC concentrations are highest in the bottom waters of the estuarine turbidity maximum and sampling at that depth might have revealed a stronger imprint of DOM-POM interaction that are not evident at the 0.5 m sampling depth chosen for our study.

Additionally, photochemical processes are known to shape the DOM pool by removing (condensed) aromatic structures, especially in rivers with watersheds dominated by forests and grassland (Hernes and Benner, 2003; Stubbins et al., 2010; Riedel et al., 2016). This process would yield a negative concave relationship of, for example, condensed aromatics and polyphenols, vs. salinity as both sunlight exposure potential and time increase while the more colored freshwater is diluted along the estuary. As these compound classes decreased linearly along the salinity gradient, there was no evidence of a significant contribution of photochemical alteration to estuarine DOM processing in the Delaware Estuary. Further, we analyzed the relative contribution of molecular formulae identified as photo-labile, photo-resistant and photo-produced by Stubbins et al. (2010) for the Congo River, but no pattern indicative of photochemical alteration emerged (data not shown).

In line with our findings, no large in situ sources or sinks of chromophoric DOM in the Delaware Estuary were reported by Del Vecchio and Blough (2004). These and other authors found photochemical processing to be more important in clearer waters offshore with higher light penetration depths for the Delaware, Amazon, and Mississippi river plumes (Hernes and Benner, 2003; Medeiros et al., 2015b; Seidel et al., 2015b). Indeed, an extensive photochemical DOM sink during August months was described also for the Delaware Estuary plume by Vodacek et al. (1997). The authors further assume oceanic and terrestrial DOM pools mixing in the estuary and on the shelf to originate from constant or very similar sources, which is consistent with a high overlap of detected molecular formulae described in this study.

CONCLUSION

In our study, we revealed DOM molecular-level variations that are masked by looking at DOC concentrations alone. Mixing of fresh- and marine waters, hydrological conditions, and also biological processes alter the composition of the DOM discharged through the Delaware Estuary into the Atlantic Ocean. For the first time, we applied collision-induced fragmentation to nominal masses along a salinity gradient, demonstrating that the chemical structures behind DOM molecular formulae exhibit a high similarity independent of their origin from marine or terrestrial environments.

Understanding the numerous processes occurring during land-to-ocean carbon transport is of utmost significance to the global carbon cycle as riverine discharge of DOC alone is sufficient to support the turnover of DOC throughout the entire marine environment (Williams and Druffel, 1987). Future increase in discharge due to increased precipitation and storm events projected by climate change scenarios and land use change reducing forest cover will most probably alter the signature of the DOM reaching the ocean, corroborating the need for further monitoring especially of such well-understood land-to-ocean connectors as the Delaware Estuary.

RESOURCE IDENTIFICATION INITIATIVE

CRAN: RRID:SCR_003005, vegan: RRID:SCR_011950.

AUTHOR CONTRIBUTIONS

DK, TD, and JN conceived the study. HO analyzed the samples and wrote the manuscript with considerable input of all coauthors.

FUNDING

This work was supported by NSF grants OCE-1030306 and OCE-1261359 to DK. HO, JN, and TD were funded by the University of Oldenburg, Germany.

ACKNOWLEDGMENTS

The field work was only possible with the help of Matt Cottrell, Monica Stegman, Thomas Lankiewicz, Katie Kalis, Raphaël Lami, and Dave Kieber while Liying Yu was essential in the laboratory analyses. We are grateful to Matthias Friebe and Ina Ulber for DOC/TDN analysis and to Katrin Klaproth for FT-ICR-MS analysis.

SUPPLEMENTARY MATERIAL

The Supplementary Material for this article can be found online at: http://journal.frontiersin.org/article/10.3389/feart.2016.00095/full#supplementary-material

REFERENCES

Abdulla, H. A. N., Minor, E. C., Dias, R. F., and Hatcher, P. G. (2013). Transformations of the chemical compositions of high molecular weight DOM along a salinity transect: using two dimensional correlation spectroscopy and principal component analysis approaches. *Geochim. Cosmochim. Acta* 118, 231–246. doi: 10.1016/j.gca.2013.03.036

Abdulla, H. A. N., Minor, E. C., Dias, R. F., and Hatcher, P.G. (2010). Changes in the compound classes of dissolved organic matter along an estuarine transect: a study using FTIR and C-13 NMR. *Geochim. Cosmochim. Acta* 74, 3815–3838. doi: 10.1016/j.gca.2010.04.006

Amon, R. M. W., Fitznar, H. P., and Benner, R. (2001). Linkages among the bioreactivity, chemical composition, and diagenetic state of marine dissolved organic matter. *Limnol. Oceanogr.* 46, 287–297. doi: 10.4319/lo.2001.46.2.0287

Aufdenkampe, A. K., Hedges, J. I., Richey, J. E., Krusche, A. V., and Llerena, C. A. (2001). Sorptive fractionation of dissolved organic nitrogen and amino acids onto fine sediments within the Amazon Basin. *Limnol. Oceanogr.* 46, 1921–1935. doi: 10.4319/lo.2001.46.8.1921

Azam, F., Smith, D. C., Steward, G. F., and Hagström, Å. (1994). Bacteria-organic matter coupling and its significance for oceanic carbon cycling. *Microb. Ecol.* 28, 167–179. doi: 10.1007/BF00166806

Badr, E.-S. A., Tappin, A. D., and Achterberg, E. P. (2008). Distributions and seasonal variability of dissolved organic nitrogen in two estuaries in SW England. *Mar. Chem.* 110, 153–164. doi: 10.1016/j.marchem.2008.04.007

Bate-Smith, E. C. (1968). The phenolic constituents of plants and their taxonomic significance. *J. Linn. Soc. Lond. Bot.* 60, 325–356. doi: 10.1111/j.1095-8339.1968.tb00094.x

Bauer, J. E., and Bianchi, T. S. (2011). "Dissolved organic carbon cycling and transformation," in *Treatise on Estuarine and Coastal Science*, Vol. 5, eds E. Wolanski and D. S. McLusky (Waltham, MA: Academic Press), 7–67.

Benner, R., Fogel, M. L., Sprague, E. K., and Hodson, R. E. (1987). Depletion of 13C in lignin and its implications for stable carbon isotope studies. *Nature* 329, 708–710. doi: 10.1038/329708a0

Biggs, R. B., Sharp, J. H., Church, T. M., and Tramontano, J. M. (1983). Optical properties, suspended sediments, and chemistry associated with the turbidity maxima of the Delaware Estuary. *Can. J. Fish. Aquat. Sci.* 40, 172–179. doi: 10.1139/f83-279

Bourgoin, L.-H., and Tremblay, L. (2010). Bacterial reworking of terrigenous and marine organic matter in estuarine water columns and sediments. *Geochim. Cosmochim. Acta* 74, 5593–5609. doi: 10.1016/j.gca.2010.06.037

Bray, J. R., and Curtis, J. T. (1957). An ordination of the upland forest communities of southern Wisconsin. *Ecol. Monogr.* 27, 326–349. doi: 10.2307/1942268

Cadée, G. C. (1982). Tidal and seasonal variation in particulate and dissolved organic carbon in the western dutch Wadden Sea and Marsdiep tidal inlet. *Neth. J. Sea Res.* 15, 228–249. doi: 10.1016/0077-7579(82)90006-0

Cao, X., Aiken, G. R., Spencer, R. G. M., Butler, K., Mao, J., and Schmidt-Rohr, K. (2016). Novel insights from NMR spectroscopy into seasonal changes in the composition of dissolved organic matter exported to the Bering Sea by the Yukon River. *Geochim. Cosmochim. Acta* 181, 72–88. doi: 10.1016/j.gca.2016.02.029

Cifuentes, L. A. (1991). Spatial and temporal variations in terrestrially-derived organic-matter from sediments of the Delaware Estuary. *Estuaries* 14, 414–429. doi: 10.2307/1352266

Cifuentes, L. A., Schemel, L. E., and Sharp, J. H. (1990). Qualitative and numerical analyses of the effects of river inflow variations on mixing diagrams in estuaries. *Estuar. Coast. Shelf Sci.* 30, 411–427. doi: 10.1016/0272-7714(90)90006-D

Cole, J. J., Prairie, Y. T., Caraco, N. F., Mcdowell, W. H., Tranvik, L. J., Striegl, R. G., et al. (2007). Plumbing the global carbon cycle: integrating inland waters into the terrestrial carbon budget. *Ecosystems* 10, 172–185. doi: 10.1007/s10021-006-9013-8

D'Andrilli, J., Cooper, W. T., Foreman, C. M., and Marshall, A. G. (2015). An ultrahigh-resolution mass spectrometry index to estimate natural organic matter lability. *Rapid Commun. Mass Spectrom.* 29, 2385–2401. doi: 10.1002/rcm.7400

Del Vecchio, R., and Blough, N. V. (2004). Spatial and seasonal distribution of chromophoric dissolved organic matter and dissolved organic carbon in the Middle Atlantic Bight. *Mar. Chem.* 89, 169–187. doi: 10.1016/j.marchem.2004.02.027

Dittmar, T., Koch, B., Hertkorn, N., and Kattner, G. (2008). A simple and efficient method for the solid-phase extraction of dissolved organic matter (SPE-DOM) from seawater. *Limnol. Oceanogr. Methods* 6, 230–235. doi: 10.4319/lom.2008.6.230

Eisma, D. (1986). Flocculation and de-flocculation of suspended matter in estuaries. *Neth. J. Sea Res.* 20, 183–199. doi: 10.1016/0077-7579(86)90041-4

Ertel, J. R., Hedges, J. I., Devol, A. H., Richey, J. E., and Ribeiro, M. D. N. G. (1986). Dissolved humic substances of the Amazon River system. *Limnol. Oceanogr.* 31, 739–754. doi: 10.4319/lo.1986.31.4.0739

Fox, L. E. (1983). The removal of dissolved humic acid during estuarine mixing. *Estuar. Coast. Shelf Sci.* 16, 431–440. doi: 10.1016/0272-7714(83)90104-X

Garvine, R. W., Mccarthy, R. K., and Wong, K.-C. (1992). The axial salinity distribution in the Delaware Estuary and its weak response to river discharge. *Estuar. Coast. Shelf Sci.* 35, 157–165. doi: 10.1016/S0272-7714(05)80110-6

Goñi, M. A., and Gardner, I. R. (2003). Seasonal dynamics in dissolved organic carbon concentrations in a Coastal Water-table aquifer at the forest-marsh interface. *Aquat. Geochem.* 9, 209–232. doi: 10.1023/B:AQUA.0000022955.82700.ed

Gonsior, M., Zwartjes, M., Cooper, W. J., Song, W., Ishida, K. P., Tseng, L. Y., et al. (2011). Molecular characterization of effluent organic matter identified by ultrahigh resolution mass spectrometry. *Water Res.* 45, 2943–2953. doi: 10.1016/j.watres.2011.03.016

Green, N. W., Perdue, E. M., Aiken, G. R., Butler, K. D., Chen, H., Dittmar, T., et al. (2014). An intercomparison of three methods for the large-scale isolation of oceanic dissolved organic matter. *Mar. Chem.* 161, 14–19. doi: 10.1016/j.marchem.2014.01.012

Hedges, J. I., Keil, R. G., and Benner, R. (1997). What happens to terrestrial organic matter in the ocean? *Org. Geochem.* 27, 195–212.

Hedges, J. I., and Weliky, K. (1989). Diagenesis of conifer needles in a coastal marine environment. *Geochim. Cosmochim. Acta* 53, 2659–2673. doi: 10.1016/0016-7037(89)90137-3

Hermes, A. L., and Sikes, E. L. (2016). Particulate organic matter higher concentrations, terrestrial sources and losses in bottom waters of the turbidity maximum, Delaware Estuary, U.S.A. *Estuar. Coast. Shelf Sci.* 180, 179–189. doi: 10.1016/j.ecss.2016.07.005

Hernes, P. J., and Benner, R. (2003). Photochemical and microbial degradation of dissolved lignin phenols: implications for the fate of terrigenous dissolved

organic matter in marine environments. *J. Geophys. Res. Oceans* 108:3291. doi: 10.1029/2002JC001421

Hoch, M. P., and Kirchman, D. L. (1995). Ammonium uptake by heterotrophic bacteria in the Delaware Estuary and adjacent coastal waters. *Limnol. Oceanogr.* 40, 886–897. doi: 10.4319/lo.1995.40.5.0886

Holmes, R. M., Mcclelland, J. W., Peterson, B. J., Tank, S. E., Bulygina, E., Eglinton, T. I., et al. (2011). Seasonal and annual fluxes of nutrients and organic matter from large Rivers to the Arctic Ocean and surrounding Seas. *Estuar. Coasts* 35, 369–382. doi: 10.1007/s12237-011-9386-6

Hossler, K., and Bauer, J. E. (2012). Estimation of riverine carbon and organic matter source contributions using time-based isotope mixing models. *J. Geophys. Res. Biogeosci.* 117, G03035. doi: 10.1029/2012jg001988

Hossler, K., and Bauer, J. E. (2013). Amounts, isotopic character, and ages of organic and inorganic carbon exported from rivers to ocean margins: 1. Estimates of terrestrial losses and inputs to the Middle Atlantic Bight. *Global Biogeochem. Cycles* 27, 331–346. doi: 10.1002/gbc.20033

Keil, R. G., Montlucon, D. B., Prahl, F. G., and Hedges, J. I. (1994). Sorptive preservation of labile organic matter in Marine Sediments. *Nature* 370, 549–552. doi: 10.1038/370549a0

Ketchum, B. H. (1952). The distribution of salinity in the estuary of the Delaware River. *Woods Hole Oceanogra. Instit. Rep.* 52–103. doi: 10.1575/1912/5339

Kim, S., Kaplan, L. A., and Hatcher, P. G. (2006). Biodegradable dissolved organic matter in a temperate and a tropical stream determined from ultra-high resolution mass spectrometry. *Limnol. Oceanogr.* 51, 1054–1063. doi: 10.4319/lo.2006.51.2.1054

Kirchman, D. L. (2001). "Measuring bacterial biomass production and growth rates from leucine incorporation in natural aquatic environments," in *Methods in Microbiology*, ed J. H. Paul (St. Petersburg, FL: Academic Press), 227–237.

Kirchman, D. L., and Borch, N. H. (2003). Fluxes of dissolved combined neutral sugars (polysaccharides) in the Delaware Estuary. *Estuaries* 26, 894–904. doi: 10.1007/BF02803348

Koch, B. P., and Dittmar, T. (2006). From mass to structure: an aromaticity index for high-resolution mass data of natural organic matter. *Rapid Commun. Mass Spectrom.* 20, 926–932. doi: 10.1002/rcm.2386

Koch, B. P., Dittmar, T., Witt, M., and Kattner, G. (2007). Fundamentals of molecular formula assignment to ultrahigh resolution mass data of natural organic matter. *Anal. Chem.* 79, 1758–1763. doi: 10.1021/ac061949s

Koch, B. P., Witt, M. R., Engbrodt, R., Dittmar, T., and Kattner, G. (2005). Molecular formulae of marine and terrigenous dissolved organic matter detected by electrospray ionization Fourier transform ion cyclotron resonance mass spectrometry. *Geochim. Cosmochim. Acta* 69, 3299–3308. doi: 10.1016/j.gca.2005.02.027

Landa, M., Cottrell, M. T., Kirchman, D. L., Kaiser, K., Medeiros, P. M., Tremblay, L., et al. (2014). Phylogenetic and structural response of heterotrophic bacteria to dissolved organic matter of different chemical composition in a continuous culture study. *Environ. Microbiol.* 16, 1668–1681. doi: 10.1111/1462-2920.12242

Li, Y., Harir, M., Lucio, M., Kanawati, B., Smirnov, K., Flerus, R., et al. (2016). Proposed guidelines for solid phase extraction of suwannee River dissolved organic matter. *Anal. Chem.* 88, 6680–6688. doi: 10.1021/acs.analchem.5b04501

Liu, W., Wang, Y., Russell, A., and Edgerton, E. S. (2005). Atmospheric aerosol over two urban–rural pairs in the southeastern United States: chemical composition and possible sources. *Atmos. Environ.* 39, 4453–4470. doi: 10.1016/j.atmosenv.2005.03.048

Liu, Z., Sleighter, R. L., Zhong, J., and Hatcher, P. G. (2011). The chemical changes of DOM from black waters to coastal marine waters by HPLC combined with ultrahigh resolution mass spectrometry. *Estuar. Coast. Shelf Sci.* 92, 205–216. doi: 10.1016/j.ecss.2010.12.030

Luther, G. W. III, Church, T. M., Scudlark, J. R., and Cosman, M. (1986). Inorganic and organic sulfur cycling in salt-marsh pore waters. *Science* 232, 746–749. doi: 10.1126/science.232.4751.746

Maie, N., Pisani, O., and Jaffé, R. (2008). Mangrove tannins in aquatic ecosystems: their fate and possible influence on dissolved organic carbon and nitrogen cycling. *Limnol. Oceanogr.* 53, 160–171. doi: 10.4319/lo.2008.53.1.0160

Mannino, A., and Harvey, H. R. (1999). Lipid composition in particulate and dissolved organic matter in the Delaware Estuary: sources and diagenetic patterns. *Geochim. Cosmochim. Acta* 63, 2219–2235. doi: 10.1016/S0016-7037(99)00128-3

Mannino, A., and Harvey, H. R. (2000a). Biochemical composition of particles and dissolved organic matter along an estuarine gradient: Sources and implications for DOM reactivity. *Limnol. Oceanogr.* 45, 775–788. doi: 10.4319/lo.2000.45.4.0775

Mannino, A., and Harvey, H. R. (2000b). Terrigenous dissolved organic matter along an estuarine gradient and its flux to the coastal ocean. *Org. Geochem.* 31, 1611–1625. doi: 10.1016/S0146-6380(00)00099-1

Mayer, L. M. (1994). Relationships between mineral surfaces and organic carbon concentrations in soils and sediments. *Chem. Geol.* 114, 347–363. doi: 10.1016/0009-2541(94)90063-9

Medeiros, P. M., Seidel, M., Dittmar, T., Whitman, W. B., and Moran, M. A. (2015a). Drought-induced variability in dissolved organic matter composition in a marsh-dominated estuary. *Geophys. Res. Lett.* 42, 6446–6453. doi: 10.1002/2015GL064653

Medeiros, P. M., Seidel, M., Niggemann, J., Spencer, R. G. M., Hernes, P. J., Yager, P. L., et al. (2016). A novel molecular approach for tracing terrigenous dissolved organic matter into the deep ocean. *Global Biogeochem. Cycles* 30, 689–699. doi: 10.1002/2015GB005320

Medeiros, P. M., Seidel, M., Ward, N. D., Carpenter, E. J., Gomes, H. R., Niggemann, J., et al. (2015b). Fate of the Amazon River dissolved organic matter in the tropical Atlantic Ocean. *Global Biogeochem. Cycles* 29, 677–690. doi: 10.1002/2015GB005115

Meyers-Schulte, K. J., and Hedges, J. I. (1986). Molecular evidence for a terrestrial component of organic matter dissolved in ocean water. *Nature* 321, 61–63. doi: 10.1038/321061a0

Middelburg, J. J., and Herman, P. M. J. (2007). Organic matter processing in tidal estuaries. *Mar. Chem.* 106, 127–147. doi: 10.1016/j.marchem.2006.02.007

Miller, A. E. J. (1999). Seasonal investigations of dissolved organic carbon dynamics in the Tamar Estuary, U.K. *Estuar. Coast. Shelf Sci.* 49, 891–908. doi: 10.1006/ecss.1999.0552

Oksanen, J., Blanchet, F. G., Kindt, R., Legendre, P., Minchin, P. R., O'Hara, R. B., et al. (2015). *Vegan: Community Ecology Package, R Package Version 2.3-1*. Available online at: http://CRAN.R-project.org/package=vegan

Osterholz, H., Niggemann, J., Giebel, H. A., Simon, M., and Dittmar, T. (2015). Inefficient microbial production of refractory dissolved organic matter in the ocean. *Nat. Commun.* 6, 7422. doi: 10.1038/ncomms8422

Partnership for the Delaware Estuary (2012). *Technical Report for the Delaware Estuary and Basin*. A complete section author list is available at the end of the report.

Pennock, J. R., and Sharp, J. H. (1986). Phytoplankton production in the Delaware Estuary - Temporal and spatial variability. *Mar. Ecol. Prog. Ser.* 34, 143–155. doi: 10.3354/meps034143

Polis, D., and Kupferman, S. L. (1973). *Physical Oceanography*. Newark, NJ: College of Marine Studies, University of Delaware.

Raeke, J., Lechtenfeld, O. J., Wagner, M., Herzsprung, P., and Reemtsma, T. (2016). Selectivity of solid phase extraction of freshwater dissolved organic matter and its effect on ultrahigh resolution mass spectra. *Environ. Sci. Process. Impacts* 18, 918–927. doi: 10.1039/c6em00200e

Raymond, P. A., and Bauer, J. E. (2001). DOC cycling in a temperate estuary: a mass balance approach using natural 14C and 13C isotopes. *Limnol. Oceanogr.* 46, 655–667. doi: 10.4319/lo.2001.46.3.0655

Raymond, P. A., and Saiers, J. E. (2010). Event controlled DOC export from forested watersheds. *Biogeochemistry* 100, 197–209. doi: 10.1007/s10533-010-9416-7

Riedel, T., Biester, H., and Dittmar, T. (2012). Molecular fractionation of dissolved organic matter with metal salts. *Environ. Sci. Technol.* 46, 4419–4426. doi: 10.1021/es203901u

Riedel, T., and Dittmar, T. (2014). A Method detection limit for the analysis of natural organic matter via fourier transform ion cyclotron resonance mass spectrometry. *Anal. Chem.* 86, 8376–8382. doi: 10.1021/ac501946m

Riedel, T., Zark, M., Vähätalo, A. V., Niggemann, J., Spencer, R. G. M., Hernes, P. J., et al. (2016). Molecular signatures of biogeochemical transformations in dissolved organic matter from ten World Rivers. *Front. Earth Sci.* 4:85. doi: 10.3389/feart.2016.00085

Sarkanen, K., and Ludwig, C. (1971). *Lignins: Occurrence, Formation, Structure, and Reactions*. New York, NY: John Wiley and Sons, Inc.

Schiff, S., Aravena, R., Mewhinney, E., Elgood, R., Warner, B., Dillon, P., et al. (1998). Precambrian shield Wetlands: hydrologic control of the sources and export of dissolved organic matter. *Clim. Change* 40, 167–188. doi:10.1023/A:1005496331593

Seidel, M., Beck, M., Greskowiak, J., Riedel, T., Waska, H., Suryaputra, I. G. N. A., et al. (2015a). Benthic-pelagic coupling of nutrients and dissolved organic matter composition in an intertidal sandy beach. *Mar. Chem.* 176, 150–163. doi: 10.1016/j.marchem.2015.08.011

Seidel, M., Beck, M., Riedel, T., Waska, H., Suryaputra, I. G. N. A., Schnetger, B., et al. (2014). Biogeochemistry of dissolved organic matter in an anoxic intertidal creek bank. *Geochim. Cosmochim. Acta* 140, 418–434. doi: 10.1016/j.gca.2014.05.038

Seidel, M., Yager, P. L., Ward, N. D., Carpenter, E. J., Gomes, H. R., Krusche, A. V., et al. (2015b). Molecular-level changes of dissolved organic matter along the Amazon River-to-ocean continuum. *Mar. Chem.* 177, 218–231. doi: 10.1016/j.marchem.2015.06.019

Sharp, J. H., Culberson, C. H., and Church, T. M. (1982). The chemistry of the Delaware Estuary - General considerations. *Limnol. Oceanogr.* 27, 1015–1028. doi: 10.4319/lo.1982.27.6.1015

Sharp, J. H., Yoshiyama, K., Parker, A. E., Schwartz, M. C., Curless, S. E., Beauregard, A. Y., et al. (2009). A biogeochemical view of Estuarine Eutrophication: seasonal and spatial trends and correlations in the Delaware Estuary. *Estuar. Coasts* 32, 1023–1043. doi: 10.1007/s12237-009-9210-8

Sleighter, R. L., and Hatcher, P. G. (2008). Molecular characterization of dissolved organic matter (DOM) along a river to ocean transect of the lower Chesapeake Bay by ultrahigh resolution electrospray ionization Fourier transform ion cyclotron resonance mass spectrometry. *Mar. Chem.* 110, 140–152. doi: 10.1016/j.marchem.2008.04.008

Spencer, R. G. M., Aiken, G. R., Wickland, K. P., Striegl, R. G., and Hernes, P. J. (2008). Seasonal and spatial variability in dissolved organic matter quantity and composition from the Yukon River basin, Alaska. *Global Biogeochem. Cycles* 22, GB4002. doi: 10.1029/2008GB003231

Spencer, R. G. M., Stubbins, A., Hernes, P. J., Baker, A., Mopper, K., Aufdenkampe, A. K., et al. (2009). Photochemical degradation of dissolved organic matter and dissolved lignin phenols from the Congo River. *J. Geophys. Res. Biogeosci.* 114, G03010. doi: 10.1029/2009JG000968

Stenson, A. C., Marshall, A. G., and Cooper, W. T. (2003). Exact masses and chemical formulas of individual Suwannee River fulvic acids from ultrahigh resolution electrospray ionization fourier transform ion cyclotron resonance mass spectra. *Anal. Chem.* 75, 1275–1284. doi: 10.1021/ac026106p

Stubbins, A., Spencer, R. G. M., Chen, H., Hatcher, P. G., Mopper, K., Hernes, P. J., et al. (2010). Illuminated darkness: molecular signatures of Congo River dissolved organic matter and its photochemical alteration as revealed by ultrahigh precision mass spectrometry. *Limnol. Oceanogr.* 55, 1467–1477. doi: 10.4319/lo.2010.55.4.1467

Sun, L., Perdue, E. M., Meyer, J. L., and Weis, J. (1997). Use of elemental composition to predict bioavailability of dissolved organic matter in a Georgia River. *Limnol. Oceanogr.* 42, 714–721. doi: 10.4319/lo.1997.42.4.0714

Sutton, C., O'Herron, J., and Zappalorti, R. (1996). *The Scientific Characterization of the Delaware Estuary. Technical Report (DRBC Project No. 321; HA File No. 93.21)*. Delaware Estuary Program, U.S. Environmental Protection Agency, New York.

Taniguchi, M., Burnett, W. C., Cable, J. E., and Turner, J. V. (2002). Investigation of submarine groundwater discharge. *Hydrol. Process.* 16, 2115–2129. doi: 10.1002/hyp.1145

Šantl-Temkiv, T., Finster, K., Dittmar, T., Hansen, B. M., Thyrhaug, R., Nielsen, N. W., et al. (2013). Hailstones: a window into the microbial and chemical inventory of a storm cloud. *PLoS ONE* 8:e53550. doi: 10.1371/journal.pone.0053550

Tzortziou, M., Zeri, C., Dimitriou, E., Ding, Y., Jaffé, R., Anagnostou, E., et al. (2015). Colored dissolved organic matter dynamics and anthropogenic influences in a major transboundary river and its coastal wetland. *Limnol. Oceanogr.* 60, 1222–1240. doi: 10.1002/lno.10092

Vodacek, A., Blough, N. V., Degrandpre, M. D., Degrandpre, M. D., and Nelson, R. K. (1997). Seasonal variation of CDOM and DOC in the Middle Atlantic Bight: terrestrial inputs and photooxidation. *Limnol. Oceanogr.* 42, 674–686. doi: 10.4319/lo.1997.42.4.0674

Wagner, S., Riedel, T., Niggemann, J., Vähätalo, A. V., Dittmar, T., and Jaffé, R. (2015). Linking the molecular signature of heteroatomic dissolved organic matter to watershed characteristics in world rivers. *Environ. Sci. Technol.* 49, 13798–13806. doi: 10.1021/acs.est.5b00525

Ward, N. D., Keil, R. G., Medeiros, P. M., Brito, D. C., Cunha, A. C., Dittmar, T., et al. (2013). Degradation of terrestrially derived macromolecules in the Amazon River. *Nat. Geosci.* 6, 530–533. doi: 10.1038/ngeo1817

Williams, P. M., and Druffel, E. R. M. (1987). Radiocarbon in dissolved organic matter in the central North Pacific Ocean. *Nature* 330, 246–248. doi: 10.1038/330246a0

Conflict of Interest Statement: The other authors declare that the research was conducted in the absence of any commercial or financial relationships that could be construed as a potential conflict of interest.

The handling Editor declared a past co-authorship with the author TD and states that the process nevertheless met the standards of a fair and objective review.

frontiers in Marine Science

ORIGINAL RESEARCH
published: 24 February 2017
doi: 10.3389/fmars.2017.00043

Influence of Major Storm Events on the Quantity and Composition of Particulate Organic Matter and the Phytoplankton Community in a Subtropical Estuary, Texas

*Nicolas E. Reyna, Amber K. Hardison * and Zhanfei Liu **

Marine Science Institute, University of Texas at Austin, Port Aransas, TX, USA

OPEN ACCESS

Edited by:
Nicholas David Ward, Pacific Northwest National Laboratory (DOE), USA

Reviewed by:
Gupta G.V.M., Ministry of Earth Sciences, India
Ana Rosa Arellano, University of Florida, USA
Allison Myers-Pigg, Texas A&M University, USA

***Correspondence:**
Amber K. Hardison
amber.hardison@utexas.edu
Zhanfei Liu
zhanfei.liu@utexas.edu

Specialty section:
This article was submitted to Marine Biogeochemistry, a section of the journal Frontiers in Marine Science

Received: *08 November 2016*
Accepted: *07 February 2017*
Published: *24 February 2017*

Citation:
Reyna NE, Hardison AK and Liu Z (2017) Influence of Major Storm Events on the Quantity and Composition of Particulate Organic Matter and the Phytoplankton Community in a Subtropical Estuary, Texas. Front. Mar. Sci. 4:43. doi: 10.3389/fmars.2017.00043

Variations in the freshwater inflow regimes of estuaries due to perturbations, such as storm events, alter the source, and composition of particulate organic matter (POM) and the phytoplankton community which are key links in estuarine carbon and nitrogen cycling. To evaluate the impact of varying freshwater discharge on POM quantity and composition and the phytoplankton community, monthly samples of surface water were collected at four long-term monitoring stations from 2012–2015 in a subtropical estuarine system, the Mission-Aransas Estuary, Texas (USA). This system is characterized by a semiarid climate, drought, and sporadic precipitation events. We analyzed organic carbon and nitrogen content, carbon and nitrogen stable isotopes, and chlorophyll *a* and accessory pigments of the POM samples. Following a prolonged dry spell (2012–2015), consecutive major storm events in spring 2015 led to a dramatic freshening of the entire estuary. Large increases in particulate organic carbon (POC) concentrations and decreases in $\delta^{13}C$ values of POC over several weeks following the storms suggest an increase in *in-situ* production at lower salinities as a result of increased freshwater inflow. These changes in bulk POM coincided with an increase in chlorophyll *a* concentration, further indicating a significant contribution by phytoplankton to the elevated POM. Concurrently, pigment biomarkers revealed a significant (10-fold) increase in the cyanobacterial pigment, zeaxanthin, and further 16S rRNA analysis showed that *Cyanobium* spp. was responsible for the observed bloom. The combination of environment conditions, including freshening, high temperature, and high nutrients, likely contributed to the cyanobacteria bloom. These results show that episodic rain events can substantially affect estuarine phytoplankton community composition, which impacts the available energy resources for secondary production and thus may have ecosystem-wide implications on productivity.

Keywords: mission aransas estuary, storms, particulate organic matter, carbon and nitrogen isotopes, accessory pigments, cyanobacteria, phytoplankton pigments, phytoplankton

INTRODUCTION

Estuaries provide a valuable link between terrestrial and oceanic environments through the transport, regeneration, and production of particulate organic matter (POM). POM includes both living and non-living organic matter and is the base of the food web in estuarine systems. Although concentrations of POM in estuaries are typically higher than those in the open ocean, POM in both environments consists of both labile and refractory compounds (Canuel et al., 1995; Harvey and Mannino, 2001). Autochthonous POM sources, such as estuarine phytoplankton, contain a higher relative fraction of labile POM than allochthonous sources, making them a preferable food source for primary consumers (Monbet, 1992; Canuel, 2001; Volkman et al., 2008). This fraction of the POM pool is more readily assimilated by consumers and therefore has a greater impact on the metabolism of the system than the typically more refractory terrestrially-derived organic matter (Day et al., 1989; Canuel et al., 1995; Volkman et al., 2008), although in some cases terrestrial organic matter can be biologically or photochemically labile in estuaries (Hernes and Benner, 2003; Ward et al., 2012, 2013). Estuaries are characterized by strong gradients in physical, chemical, and biological forces such as salinity and nutrient cycling which produce spatiotemporally heterogeneous conditions for phytoplankton growth and affect the availability of this nutritious, labile source of POM (Harding, 1994).

Due to their fast growth rates and importance to aquatic food webs, phytoplankton communities can rapidly respond to a range of environmental perturbations such as storm events, making them a sensitive and crucial indicator for detecting ecological change in estuaries (Peierls et al., 2003; Cloern and Dufford, 2005; Paerl et al., 2010). This has led to extensive characterization of phytoplankton communities in temperate estuaries such as San Francisco and Chesapeake Bays (e.g., Cloern and Dufford, 2005; Adolf et al., 2006; Harding et al., 2015). These systems typically experience high freshwater discharge in the spring as a result of snowmelt and rainfall. Riverine export of nutrients and warming temperatures often lead to a seasonal spring diatom bloom (Cloern and Dufford, 2005; Adolf et al., 2006; Harding et al., 2015). Phytoplankton community composition has been studied extensively in temperate estuaries with high freshwater inflows, but estuaries with low inflow and salinities that vary broadly over time have been less studied (Murrell et al., 2007). Phytoplankton community composition in temperate estuaries is commonly regulated by nutrients, flushing time, temperature, and light availability, whereas environmental controls in estuaries with episodic flooding events can vary drastically from year to year (Bianchi et al., 1997; Pinckney et al., 1998; Paerl et al., 2010; Dorado et al., 2015). Increases in terrestrially derived inorganic nutrients transported by freshwater inflows often cause a shift toward larger-celled phytoplankton, such as diatoms, which have relatively faster growth rates and reduced consumption by grazers (Cloern and Dufford, 2005; Reynolds, 2006). However, this is not always the case, as high levels of nutrients and high temperatures can lead to blooms of small-celled phytoplankton, such as cyanobacteria (Juhl and Murrell, 2005; Ren et al., 2009; Riekenberg et al., 2015).

As intensity and frequency of episodic events are projected to increase (Huntington, 2006), it is important to understand how storms impact biogeochemical processes in estuaries. As an ideal model for subtropical regions, the microtidal Mission-Aransas Estuary (MAE) is located on the western edge of the Gulf of Mexico in south Texas, with a strong episodic nature of precipitation and resulting freshwater inflow events (Mooney and McClelland, 2012; Bruesewitz et al., 2013; Lebreton et al., 2016). Compared to more "traditional" estuarine models, the MAE is often nutrient limited due to the lack of inorganic nutrient influx related to low runoff and river discharge (Mooney and McClelland, 2012; Bruesewitz et al., 2013). Episodic high freshwater inflows to the MAE significantly impact POM source and concentration (Mooney and McClelland, 2012; Lebreton et al., 2016), yet it remains unclear how storm events affect phytoplankton communities in the MAE. Phytoplankton communities in the MAE have not been systematically characterized, but in this region, chromophytes, haptophytes, pelagophytes, and dinoflagellates generally are the dominant species (Qian et al., 1996).

The objective of this study was to elucidate the impact of storm events on temporal and spatial patterns of POM and phytoplankton communities in the MAE. Previous work in the MAE determined that large storm events lead to elevated POM concentrations and depleted $\delta^{13}C$ values of particulate organic carbon (POC) (Mooney and McClelland, 2012). Specifically, we hypothesized that high salinity drought conditions would have low POM concentrations, relatively enriched $\delta^{13}C$-POC, and smaller-celled phytoplankton (e.g., cyanobacteria). Inversely, low salinity post-flood conditions would have elevated POM concentrations, relatively depleted $\delta^{13}C$-POC, and larger-celled phytoplankton (e.g., diatoms). Phytoplankton community structure was determined using established algorithms of accessory pigments, including fucoxanthin, which is mainly produced by diatoms, and zeaxanthin, which represents cyanobacteria (Qian et al., 2003).

MATERIALS AND METHODS

Site Description

The MAE is a shallow, bar-built estuary spanning approximately 200,000 acres with an average depth of 2 m (Diener, 1975; Armstrong, 1982). The system receives low base freshwater inflow and sporadic pulses from the Mission and Aransas rivers which discharge into Copano Bay (**Figure 1**). These two rivers have similar drainage areas (2,000–2,700 km^2), but the Aransas River is impacted by cultivated crops and wastewater treatment plants while the Mission River is relatively pristine (Mooney and McClelland, 2012).

Compounded with limited exchange with the Gulf of Mexico via the tidal inlet at the Port Aransas Shipping Channel, calculated water replacement times within the estuary are as long as 3 years (Armstrong, 1982; Solis and Powell, 1999). Lateral exchange with San Antonio Bay to the north and Corpus Christi Bay to the south can also have an impact on estuarine water quality. For example, during large flood events, the San Antonio

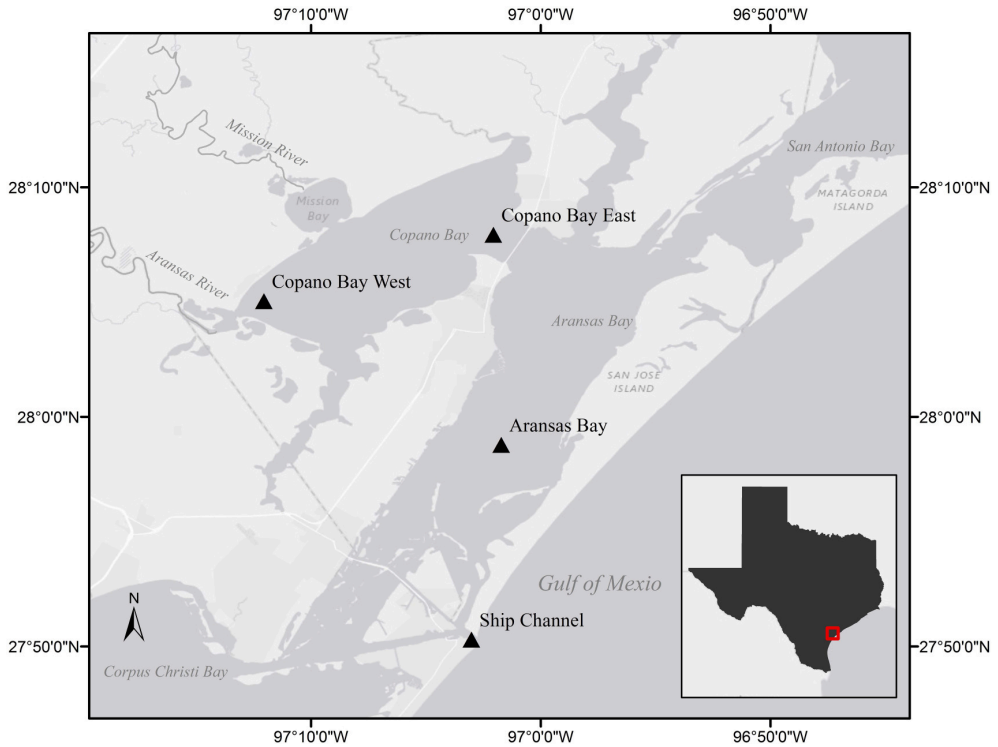

FIGURE 1 | Stations sampled in the Mission-Aransas Estuary (MAE) identified by station name and triangle. Light gray shading indicates land while dark gray indicates water. The inset shows the study area (in red) in relation to the Texas Gulf coast.

and Guadalupe rivers discharge freshwater into San Antonio Bay which can make its way into the estuary via Mesquite Bay and the Intracoastal Waterway (**Figure 1**; Armstrong, 1982; Longley, 1994).

The Mission-Aransas National Estuarine Research Reserve (MANERR) runs a system-wide monitoring program (SWMP) that continuously records water quality data and collects monthly nutrient samples at four stations along the inshore to offshore transect of our sampling region (**Figure 1**). Two of these stations are located in Copano Bay, a secondary bay more heavily influenced by freshwater inflow due to discharge via the adjacent Mission and Aransas rivers. The Copano Bay West station, located at the mouth of the Aransas River, represents the riverine endmember station in this system while the Copano Bay East station exchanges more openly with the adjacent Aransas Bay. The Aransas Bay station reflects the influence of freshwater inflows on the estuary with increased distance from the river endmember. The station located at the Port Aransas Shipping Channel (Ship Channel station hereafter), which is as the major tidal inlet with the Gulf of Mexico, represents the marine endmember in the MAE.

Sample Collection, Water Quality, and Nutrient Analysis

From 2012 to 2015, surface water samples (0–0.5 m) were collected twice a month from March through October, and once a month from November through February at each of the four SWMP stations. Briefly, 2–4 L of surface water were collected from each station using acid-cleaned high density polyethylene bottles, kept on ice, and transported back to the University of Texas Marine Science Institute for filtration on the day of collection. Particles were obtained by filtering 85 to 1000 mL of the water onto a pre-combusted (450°C, 5 h) glass fiber filter (0.7 μm Whatman GF/F, 47 mm diameter) using low vacuum pressure, and triplicate filters were stored at −80°C until elemental, pigment, and DNA analyses.

At each station, salinity and temperature (°C) were measured continuously every 15 min by YSI 6600 V2 sondes (Yellow Springs Instruments) mounted on sampling platforms 0.5 m above the benthos. The MANERR also collects and analyzes monthly surface water nutrient samples at each station. After collection, samples are immediately stored in the dark on ice. Inorganic nutrient (NO_3^-, NO_2^-, NH_4^+, and PO_4^{3-}) concentrations are determined with a QuAAtro nutrient autoanalyzer (Seal Analytical) using standard colorimetric methods (precision is ± two standard deviations for each parameter). NO_3^-, NO_2^-, and NH_4^+ were summed together and presented as dissolved inorganic nitrogen (DIN). All National Estuarine Research Reserve (NERR) water quality data is available for download at the Centralized Data Management Office (CDMO, http://cdmo.baruch.sc.edu).

POC and PN Concentrations and Source Characterization

Half of one 47 mm filter was used per time point for carbon and nitrogen determination. The filters were acidified in a fumigation chamber with concentrated (12 N) hydrochloric (HCl) acid for

24 h to remove inorganic carbon (Hedges and Stern, 1984). Following acid fumigation, the filters were allowed to vent off excess acid for 4–6 h and then dried at 60°C for at least 24 h. POC and particulate nitrogen (PN) concentrations (μM) and stable isotope ratios (‰) were determined using an Elementar Micro Cube elemental analyzer (Elementar Analysensysteme GmbH, Hanau, Germany) interfaced to an Isoprime VisION isotope ratio mass spectrometer (Isoprime Ltd., Stockport, UK) at the UC-Davis Stable Isotope Facility (UCD-SIF). Stable isotope values were expressed in δ notation relative to carbon in Vienna PeeDee Belemnite and nitrogen in air. Precision at the UCD-SIF for C/N content is within 5%, for $\delta^{13}C$ is ± 0.2‰, and for $\delta^{15}N$ is ± 0.3‰. It should be noted that HCl fumigation of previously frozen filters has been shown to lead to artificially lower $\delta^{15}N$-PN values (0.1 ‰), but this added uncertainty was acceptable given the natural variability in environmental POM samples (Lorrain et al., 2003).

Pigment Analysis and Phytoplankton Community Composition

The second (whole, untreated) 47 mm GFF filter per time point was used for pigment analysis. Pigment extraction followed the protocol of Sun et al. (1991, 1994). Briefly, pigments on filters were extracted twice with 3 mL of 100% acetone by sonication in chilled water for 15 min in the dark. The extracts were combined and analyzed using high performance liquid chromatography (HPLC) coupled with a UV-vis detector. The pigment analysis followed the protocol of McTigue et al. (2015). Briefly, a binary gradient of 28 mM tetrabutylammonium acetate (TBA) in methanol (30%:70%, v:v; eluent A) and methanol (eluent B) was used. Eluent B was ramped from 5 to 95% in 22 min, and held for 7 min before decreasing to 5% within 2 min. A C_8 HPLC column (Agilent Eclipse XDB, 3.5 μm, 4.6-mm diameter × 150-mm length) was used, and the eluted pigments were detected by visible absorbance (wavelength = 450 nm). Concentrations were determined by comparing pigment peaks of equal retention time to those of certified commercial standards (DHI, VWR, and Sigma-Aldrich). Analyzed pigments included chlorophyll *a,* and the accessory pigments fucoxanthin, peridinin, zeaxanthin, prasinoxanthin, 19-hex-fucoxanthin, 19-but-fucoxanthin, alloxanthin, and chlorophyll *b*.

Chlorophyll *a* is targeted as a proxy for fresh algal POM. Specific microalgal groups can be detected using the accessory pigments: Chlorophyll *b* for chlorophytes; fucoxanthin in diatoms; peridinin in dinoflagellates; prasinoxanthin in prasinophytes; 19-hex-fucoxanthin in haptophytes; and zeaxanthin in cyanobacteria, which includes prochlorophytes (Wright et al., 1996; Morata and Renaud, 2008; Szymczak-Zyla et al., 2008). The relative chlorophyll *a* contributions of different algal groups to total phytoplankton biomass were calculated using the pigment algorithms summarized by Qian et al. (2003) (**Table 1**), which were based on previous studies and the analysis of phytoplankton cultures (Letelier et al., 1993; Andersen et al., 1996; Mackey et al., 1996; Wright and van den Enden, 2000). Negative algal group contributions were removed and reported as zero. The sum of the calculated major phytoplankton groups in the total chlorophyll *a* was normalized to 100% in order to compare compositional changes of phytoplankton spatially and temporally.

TABLE 1 | Pigment equations used for separating chlorophyll *a* biomass between the major phytoplankton taxa in the MAE (Qian et al., 2003).

Algal Groups	Equations
Cyanobacteria	$[Chl\ a]_{cyano} = [Zeaxanthin] + 0.5[Chl\ b]$
Prymnesiophytes	$[Chi\ a]_{prymn} =$ 1.3[19-hex-fucoxanthin]–0.1[19-but-fucoxanthin + Fucoxanthin]
Pelagophytes	$[Chl\ a]_{pela} =$ 0.9[19-but-fucoxanthin]–0.02[19-hex-fucoxanthin]
Dinoflagellates	$[Chi\ a]_{dino} = 1.5[Peridinin]$
Diatoms	$[Chl\ a]_{diat} = 0.8\{[Fucoxanthin]–(0.02[19\text{-}hex\text{-}fucoxanthin] +$ 0.14[19-but-fucoxanthin])}
Cryptophytes	$[Chl\ a]_{cryp} = 4[Alloxanthin]$
Prasinophytes	$[Chi\ a]_{pras} = 2.1[Prasinoxanthin]$

Chl a, chlorophyll a; Chl b, chlorophyll b; cyano, cyanobacteria; prymn, prymnesiophytes; pela, pelagophytes; dino, dinoflagellates; diat, diatoms; cryp, cryptophytes; pras, prasinophytes. Note that cyanobacteria include prochlorophytes.

DNA Sequencing

To identify specific cyanobacterial species of the phytoplankton community, DNA was extracted from the GF/F filters (untreated half filter) using the PowerMag Soil DNA isolation kit (MO BIO) according to the manufacturer's instructions. The sequencing (Illumina Miseq) was performed using 28F and 519R to amplify the 500 bp region of 16S rRNA gene by the Research and Testing Laboratory (RTL) (Lubbock, Texas). The sequence data were analyzed according to the bioinformatics pipeline of RTL. Operational taxonomic unit (OTU) clustering was performed at 97% using USEARCH before classification against a 16S database derived from GenBank.

Statistics

Using R version 3.3.1 (http://www.r-project.org; R Core Team, 2013), a pairwise Pearson correlation test was performed between the POM characteristics, algal group biomass, water quality parameters, and nutrient concentrations at each station throughout the study period, with a significance cutoff of $p < 0.05$. Principal component analysis (PCA) was performed on data from Copano Bay West, including phytoplankton composition (%), DIN, PO_4^{3-}, salinity, and temperature using MATLAB (Xue et al., 2011).

RESULTS

River Discharge, Salinity, and Surface Water Temperature

Freshwater is delivered to Copano Bay from the Mission and Aransas rivers, so daily mean discharge data from both rivers were combined for the study period, October 30, 2012 to October 29, 2015 (**Figure 2A**). From October 2012 to early March 2015 (28 months) there was only one combined discharge event above 100 $m^3\ s^{-1}$, representing a prolonged "dry period." In contrast, from March 2015 to the end of October 2015 (4 months) there

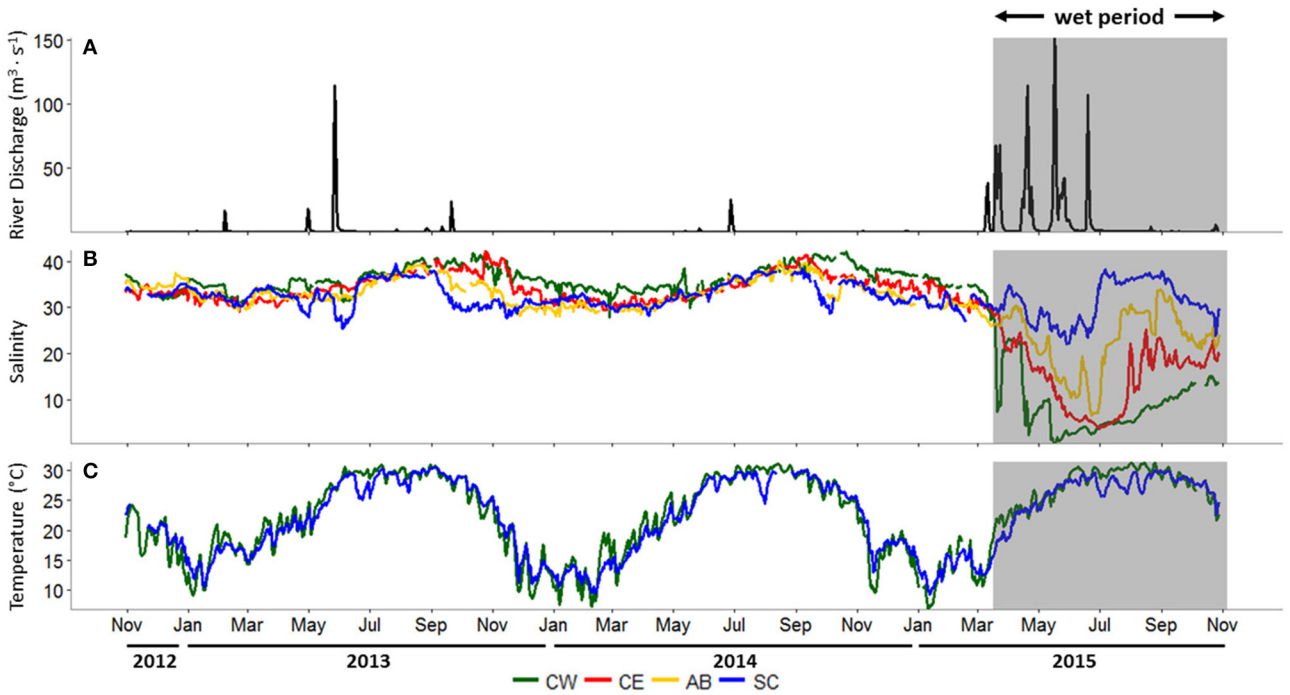

FIGURE 2 | (A) Combined river discharge (m^3 s^{-1}) from USGS (U.S. Geological Survey) gages on the Mission and Aransas rivers, **(B)** salinity at all stations, **(C)** surface water temperature (°C) at the Copano Bay East and Ship Channel stations, October 30, 2012 to October 29, 2015. In all panels, the wet period is indicated by a shaded box. CW, Copano Bay West; CE, Copano Bay East; AB, Aransas Bay; SC, Ship Channel.

were three such events, indicating a "wet period" (gray box in **Figure 2A**). The average daily discharge during this wet period was 8.7 m^3 s^{-1}, more than 10 times higher than during the dry period (0.8 m^3 s^{-1}).

During the dry period, average daily salinity at all stations ranged from 26 to 42 (**Figure 2B**). Copano Bay West salinity decreased from 35 to 7 during late March 2015 due to a major storm event (**Figure 2B**). Over the next month, salinity at this station rose to 23 before falling to 2 in late April following a second major storm event. Over the next month, salinity at Copano Bay West rose to 10 before falling to 0 in mid-May as a consequence of a third major storm event. The recurrence of these major storm events over a period of approximately 2 months kept salinity at this station low (<10) until early September 2015. Copano Bay East salinity followed a similar pattern as Copano Bay West in response to the spring 2015 storm events, albeit with a slower, steadier decline (**Figure 2B**), presumably due to its more open location at the mouth of Copano Bay. From March to July 2015 salinity decreased from 32 to 4 and remained below 10 until late July 2015. Similarly, Aransas Bay salinity decreased from 31 to 7 over this 4-month period, but by late July 2015 had reached values of 30 due to its closer proximity to and flushing with the inlet with the Gulf of Mexico (Port Aransas Shipping Channel) (**Figure 2B**). The Ship Channel station was the least impacted by the spring 2015 storm events. However, salinity at this station did respond to these events by falling from 35 to 22 from April to late May 2015 (**Figure 2B**).

Average daily surface water temperatures at Copano Bay West and the Ship Channel displayed consistent annual patterns throughout the study period (**Figure 2C**). This is representative of surface water temperature patterns across the MAE (unpublished data, MANERR). During June temperatures typically reach ∼30°C and are sustained until September, when they begin to fall until reaching annual lows of ∼10°C between December and February (**Figure 2C**).

Spatial and Temporal Patterns of Inorganic Nutrients and Chlorophyll *a*

During the dry period, concentrations of DIN, dominated by NH_4^+ (∼60% of DIN, data not shown), were generally low, punctuated by episodic peaks throughout the year, ranging from 0 to 5.9 μmol-N L^{-1} at all stations (**Figure 3A**). During fall 2013, Aransas Bay and Ship Channel DIN concentrations peaked at 3.3 and 5.9 μmol-N L^{-1}, respectively. A similar seasonal pattern was seen at both stations in 2014, along with elevated summer and fall concentrations at Copano Bay East. The major storm events during spring 2015 significantly increased DIN concentrations, most notably in Copano Bay (**Figure 3A**). At Copano Bay West, DIN increased from 0.2 to 23.3 μmol-N L^{-1} between April 10 and May 20, 2015. Concurrently, at Copano Bay East, DIN increased from 4.5 to 14.1 μmol-N L^{-1}. These elevated concentrations were dominated by NO_3^-, making up 99 and 67% of DIN at Copano Bay West and East, respectively (data not shown). Values at both Copano Bay stations dropped to dry

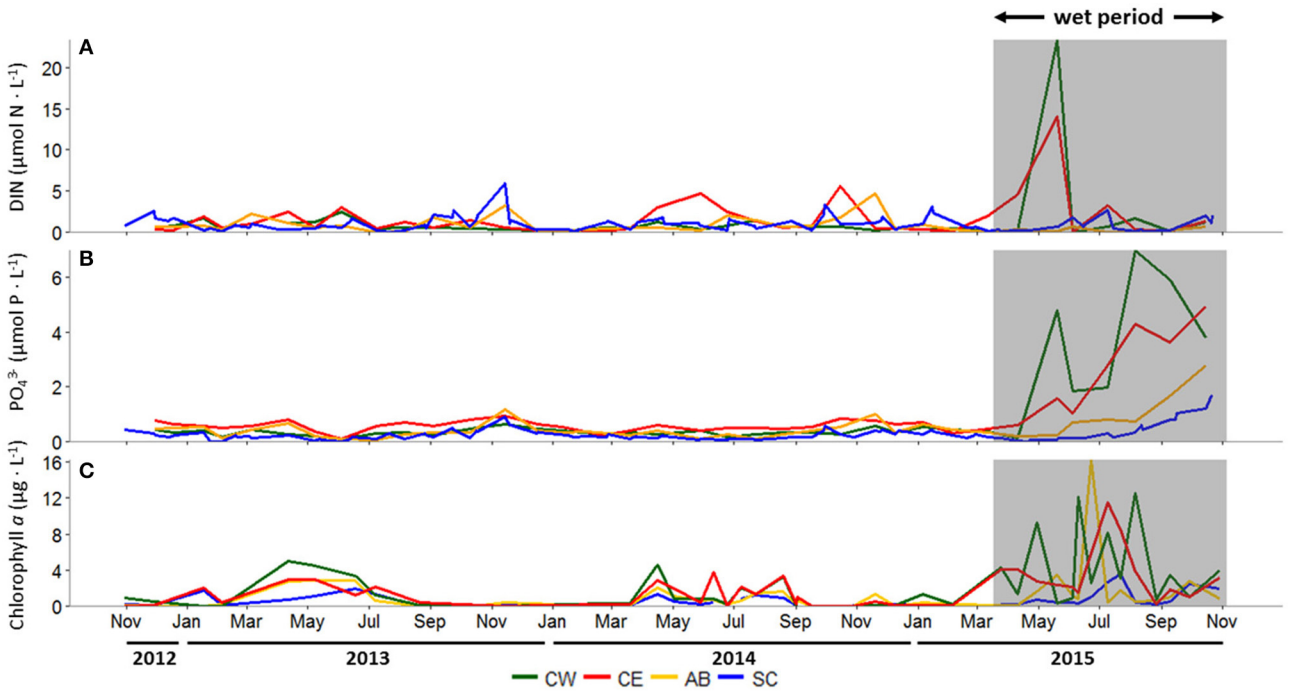

FIGURE 3 | (A) Dissolved inorganic nitrogen (DIN; µmol N L^{-1}), **(B)** phosphate (PO_4^{3-}; µmol P L^{-1}), and **(C)** chlorophyll *a* (µg L^{-1}) concentrations at all stations, October 30, 2012 to October 29, 2015. In all panels, the wet period is indicated by a shaded box. CW, Copano Bay West; CE, Copano Bay East; AB, Aransas Bay; SC, Ship Channel.

period levels by early June 2015 and remained low throughout the study period (**Figure 3A**).

PO_4^{3-} concentrations ranged from 0 to 1.2 µmol-P L^{-1} at all stations throughout the dry period, remaining relatively low over time (**Figure 3B**). Copano Bay PO_4^{3-} concentrations began to increase concurrently with DIN in late May 2015, however in contrast to DIN, which peaked briefly in May-June, PO_4^{3-} concentrations continued to rise throughout the wet period. Copano Bay West PO_4^{3-} peaked at 7.0 µmol-P L^{-1} in early August 2015 (**Figure 3B**). In contrast, at Copano Bay East, Aransas Bay, and the Ship Channel, maximum values were lower (4.9, 2.8, and 1.7 µmol-P L^{-1}, respectively), and did not occur until late October 2015 (**Figure 3B**).

Chlorophyll *a* concentrations across the estuary remained < 5 µg L^{-1} during the dry period, but showing a seasonal pattern of elevated concentrations during spring-summer (**Figure 3C**). Following the major storm events of spring 2015, however, chlorophyll *a* concentrations increased from 1 to 12 µg L^{-1} between June 4 and 10, 2015 at Copano Bay West (**Figure 3C**). Values at this station fluctuated from 3 to 13 µg L^{-1} for 2 months until dropping to 1 µg L^{-1} in late August 2015. At Copano Bay East, chlorophyll *a* increased from 2 to 12 µg L^{-1} between June 10 and July 9, 2015, showing a lag (∼1 month) in response to the storm events compared to Copano Bay West (**Figure 3C**). Values at Copano Bay East remained > 9 µg L^{-1} for 2 weeks. Similarly, in Aransas Bay, chlorophyll *a* increased from 1 to 16 µg L^{-1} between June 10 and 23, 2015. Although this station had the highest overall value during the study period, chlorophyll *a* concentrations there remained < 2 µg L^{-1} throughout the rest of the summer (∼2 months), showing a shorter bloom than seen in Copano Bay. At the Ship Channel, chlorophyll *a* remained < 2 µg L^{-1} throughout the study period, with the exception of July 2015 when it peaked at 4 µg L^{-1}, concurrent with the summer peaks at the other stations (**Figure 3C**).

Spatial and Temporal Patterns in POM Concentration and Isotopic Values

During the dry period, POC concentrations at Aransas Bay, and Copano Bay West and East were elevated in spring (**Figure 4A**). However, during the wet period, POC concentrations in Copano Bay were the highest of the study period. From 2012 to 2015, POC concentrations ranged from 23 to 653 µmol-C L^{-1} at Copano Bay West, 14 to 329 µmol-C L^{-1} at Copano Bay East, 22 to 187 µmol-C L^{-1} at Aransas Bay, and 10 to 89 µmol-C L^{-1} at the Ship Channel station. The highest concentrations at Copano Bay West, Aransas Bay, and the Ship Channel during the dry period were 342, 187, and 89 µmol-C L^{-1}, respectively, and peaked in March 2013. POC concentration at Copano Bay East during the dry period peaked at 152 µmol-C L^{-1} in early April 2014. During the wet period, POC concentrations were higher at the two Copano Bay stations (∼3-fold) than the Aransas Bay and Ship Channel stations. Copano Bay West POC concentrations began to increase in late March 2015 and peaked at 653 µmol-C L^{-1} in early August 2015, but did not exceed 300 µmol-C L^{-1} until early July 2015. At Copano Bay East, POC concentrations

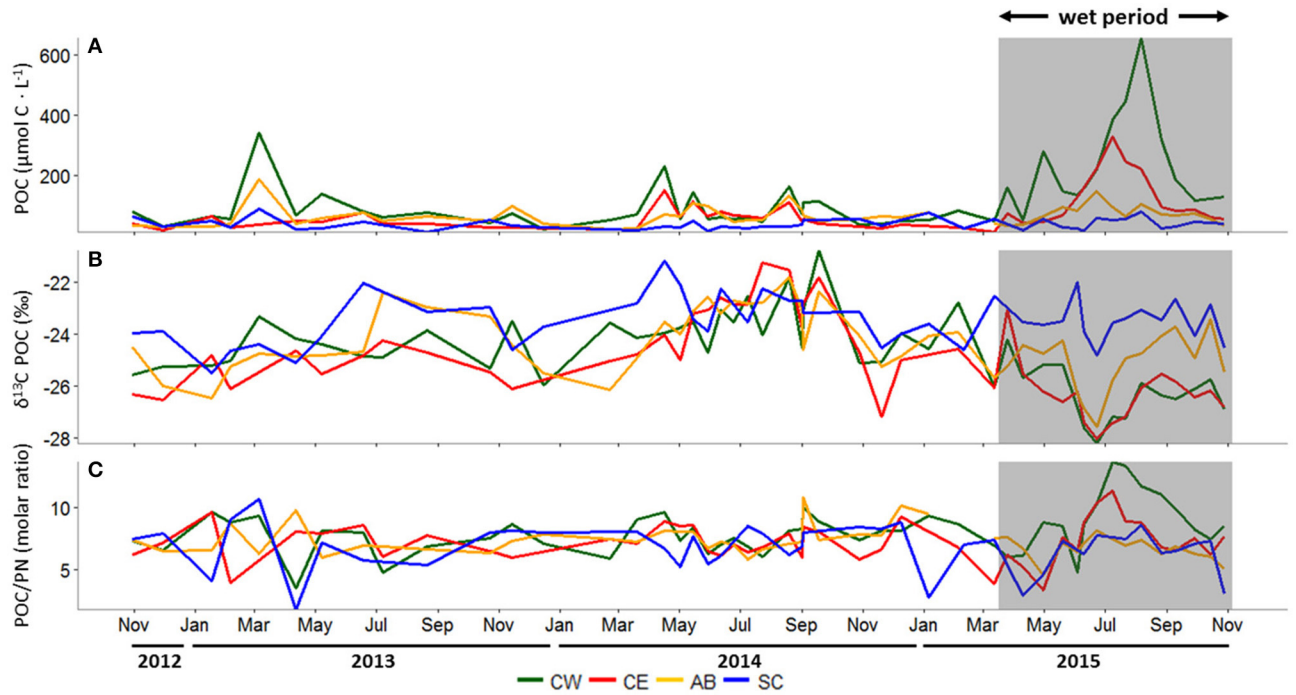

FIGURE 4 | (A) Particulate organic carbon (POC) concentration (µmol C L^{-1}), **(B)** δ^{13}C-POC (‰), and **(C)** the molar ratio of POC to particulate nitrogen (PN) at all stations, October 30, 2012 to October 29, 2015. In all panels, the wet period is indicated by a shaded box. CW, Copano Bay West; CE, Copano Bay East; AB, Aransas Bay; SC, Ship Channel.

began to increase in early June 2015 and peaked at 329 µmol-C L^{-1} in early July 2015.

δ^{13}C-POC in the MAE showed similar patterns at all three bay stations (Copano Bay East, Copano Bay West, Aransas Bay) during the study period; values ranged from −28.2 to −20.8‰, with a shift from relatively enriched to depleted values in June 2015 (**Figure 4B**). Copano Bay West displayed the greatest variation in δ^{13}C-POC, accounting for the minimum and maximum values seen across the estuary throughout the study period. This may be due to the station's close proximity to the Aransas River mouth, making it more heavily influenced by freshwater inputs. The most enriched values at all three bay stations (excluding the Ship Channel) were recorded from July to September 2014. The more enriched δ^{13}C-POC values correlated with higher salinities in Copano Bay ($R^2 = 0.70$; $p < 0.001$) and Aransas Bay ($R^2 = 0.66$; $p < 0.001$) throughout the entire study period, although no increase in δ^{13}C was observed during summer 2013, when salinities and temperatures were nearly identical to those during summer 2014. The most depleted δ^{13}C values at the three bay stations over the study period occurred in June 2015, showing a response to the storm-driven influx of freshwater and leading to more depleted average δ^{13}C-POC values at Copano Bay West during the wet period (−26.3 ± 1.1‰) relative to the dry period (−24.1 ± 1.2‰).

PN and POC concentration patterns were similar ($R^2 = 0.59$; $p < 0.007$), with highest concentrations detected during summer 2015, but PN was more variable than POC (**Supplementary Figure 1**). PN concentrations ranged from 4 to 65 µmol-N L^{-1}at Copano Bay West, 3 to 34 µmol-N L^{-1} at Copano Bay East, 3 to 35 µmol-N L^{-1} at Aransas Bay, and 3 to 33 µmol-N L^{-1} at the Ship Channel station. δ^{15}N-PN in the MAE, ranging from 3.6 to 12.7‰, showed less noticeable patterns over time than δ^{13}C-POC (**Supplementary Figure 1**).

Molar C/N ratios of POM ranged from 1.7 to 13.7 across the MAE and stayed relatively constant during the dry period (**Figure 4C**). During the wet period, there was a shift toward higher ratios (C/N > 10) from the end of June to September 2015 at Copano Bay East and West. This C/N ratio increase occurred as POC concentrations increased, concurrent with a depletion in POC δ^{13}C (**Figure 4**).

Spatial and Temporal Patterns in Phytoplankton Community Composition

The average percentage of total chlorophyll *a* accounted for by individual phytoplankton taxa showed that cyanobacteria and diatoms were the dominant taxa in the MAE during both the dry and the wet periods, but the community composition shifted after the major storm events of spring 2015 (**Figure 5**; **Table 2**). At Copano Bay West, both taxa displayed distinct shifts in average biomass between the dry and wet periods (**Figure 5A**). During the dry period, the average biomass of cyanobacteria and diatoms were 29 ± 3 and 43 ± 4%, respectively (**Table 2**). In contrast, during the wet period these averages were 59 ± 9 and 17± 5% for cyanobacteria and diatoms, respectively, showing a shift toward a cyanobacteria-dominated

system. A similar trend was observed at the Copano Bay East and Aransas Bay stations, albeit with a more muted response in Aransas Bay (**Table 2**; **Supplementary Figure 2**). Further DNA sequencing of the Copano Bay West samples showed that the cyanobacterial community in the dry period were dominated by *Prochlorococcus* spp. (56–61%), followed by *Cyanobium* spp. (19–24%) and *Synechococcus* spp. (16–19%); during the wet period, *Cyanobium* spp. became the dominant species (75–78%) from June to August, but decreased to 35% in October 2015 (**Supplementary Figure 3**).

Unlike the three bay stations, phytoplankton community composition at the Ship Channel was similar during the dry and wet periods (**Figure 5B**; **Table 2**). The average biomass of cyanobacteria and diatoms during both periods were 22 ± 4 and 52 ± 5%, respectively. Average dinoflagellate biomass increased from 7 ± 1 to 12 ± 4% during the wet period, with an accompanying decrease in average pelagophyte biomass. DNA sequencing results showed that *Synechococcus* spp. dominated the Ship Channel cyanobacteria community (92%) in 2013, but the community became more diverse during the wet period with contributions from *Synechococcus* spp. (42%), *Prochlorococcus* spp. (31%), and *Cyanobium* spp. (25%) (**Supplementary Figure 3**).

DISCUSSION

POM Source Following Storm Events

Freshwater discharge into the MAE has been variable over the past decade; multi-year droughts with very low baseflows are interspersed with large storm events occurring at high frequency for many months at a time, as seen during the study period (**Figure 2A**) and in previous studies (Mooney and McClelland, 2012; Bruesewitz et al., 2013; Lebreton et al., 2016). These sporadic freshwater inflows significantly influence system-wide salinity, with a decreasing degree of influence along the inshore to offshore transect (**Figure 2B**). During summer 2015, there was a substantial peak in POC concentration in Copano Bay, surpassing any values observed during the dry period, when salinities were more stable across the estuary (**Figures 2B**, **4A**). These results fit the pattern described previously in this system by Mooney and McClelland (2012): during 2007 (a wet year), POC concentrations in Copano Bay remained elevated for many months following major storm events in July before showing a sharp decline as salinities began to rise in spring 2008 (a dry year). The observed increase in POC during the present study can therefore be attributed to the freshening of the estuary as a result of the exponential increase in river discharge.

Sources of POC in estuaries can be inferred from the δ^{13}C-POC values. δ^{13}C-POC across the MAE are typically ∼ −24‰ under drought conditions, but following major storm events decrease to as low as −28‰ (**Figure 4B**; Mooney and McClelland, 2012). The depletion in δ^{13}C-POC is consistent with an expected depletion in dissolved inorganic carbon δ^{13}C-DIC concurrent with decreasing salinity associated with the mixing of riverine (δ^{13}C-DIC ∼ −11‰, Fogel et al., 1992) and marine (δ^{13}C-DIC ∼ 0‰, Fogel et al., 1992) water masses, with a muted effect at the Ship Channel as a result of flushing with nearshore Gulf waters (**Figure 4B**; Mooney and McClelland, 2012). Riverine δ^{13}C-DIC can drive down the estuarine δ^{13}C-POC through uptake and fixation by estuarine phytoplankton (**Figure 4B**; Fogel et al., 1992). Delivery of freshwater phytoplankton from the rivers to the bay may also have contributed to the lower δ^{13}C signal that we observed ($\delta^{13}C = -31.4$‰, Lebreton et al., 2016). While depleted δ^{13}C values in river water are often attributed to C3 plant contributions from the surrounding terrestrial landscape, this is not a viable explanation in this system because POM in the Mission and Aransas rivers becomes enriched in δ^{13}C-POC during storm flow conditions ($\delta^{13}C = -22$ to −20‰, Mooney and McClelland, 2012). In any case, the fact that POC concentrations and stable isotope values in the bay changed gradually over several weeks following the storms (**Figures 4A,B**) points to a buildup of in-situ production rather than organic matter delivered to Copano Bay via the Mission and Aransas rivers. *In-situ* production likely played a key role in POM dynamics throughout the wet period, as the result of initial inoculation by river-borne phytoplankton followed by increased growth of phytoplankton within the bay under relatively fresh conditions.

Following major storm events during the summer of 2015, phytoplankton biomass (chlorophyll *a*) at all bay stations increased, confirming enhanced *in-situ* production (**Figure 3C**). Both chlorophyll *a* and POC peaked first in May (**Figures 3C**, **4A**). Then, POC reached exceptionally high levels in August, which occurred as a slow buildup of the standing stock through the summer. Chlorophyll *a* showed sustained high levels during the summer. These dynamics indicate two distinct peaks of phytoplankton production during the wet period. DIN concentrations also peaked in May, reflecting riverine input, then dropped precipitously, and remained low, likely supporting the initial increase in phytoplankton production (**Figure 3A**). Concurrent with the increased production in late summer, the C/N of Copano Bay POM increased (>10), most notably at Copano Bay West (**Figure 4C**). After the May phytoplankton community used the available river-derived DIN, the established phytoplankton community likely became nitrogen-limited, indicating that the rising C/N may be attributed to gradual nitrogen limitation of phytoplankton in Copano Bay (**Figures 3A,C**, **4C**; Goldman, 1980).

Phytoplankton Community Shifts after Storm Events

Disturbances to water column hydrology, specifically drops in salinity related to hurricanes and other major storm events, have been well documented to have significant impacts on estuarine phytoplankton community composition (Qian et al., 1996; Peierls et al., 2003; Paerl et al., 2014b). For example, following the landfall of Hurricane Floyd in the fall of 1999, phytoplankton community composition in the Pamlico Sound, North Carolina, underwent numerous shifts: dinoflagellates, which typically have a strong spring bloom in the system, were rare outside of a moderate bloom the following spring, along with significant cyanobacterial blooms (exceeding pre-hurricane levels) during the subsequent two summers (Peierls et al., 2003).

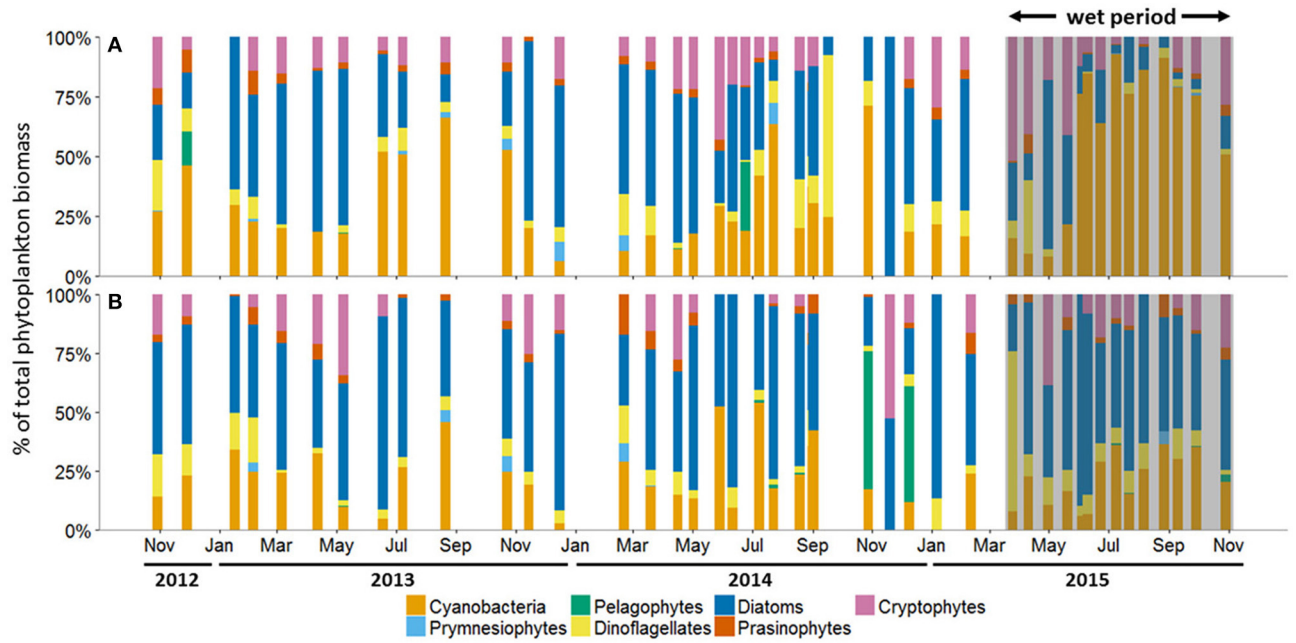

FIGURE 5 | Phytoplankton community composition as percent (%) of total biomass at the (A) Copano Bay West and **(B)** Ship Channel stations, October 30, 2012 to October 29, 2015. In all panels, the wet period is indicated by a shaded box. CW, Copano Bay West; CE, Copano Bay East; AB, Aransas Bay; SC, Ship Channel.

TABLE 2 | Average biomass percentages (%) of each phytoplankton taxa at all stations in the MAE during both the dry and wet periods (all values are presented as average ± standard error).

Station	Period	Cyanobacteria	Prymnesiophytes	Pelagophytes	Dinoflagellates	Diatoms	Prasinophytes	Cryptophytes
CW	Dry	29 (±3)	1 (±0)	1 (±0)	10 (±2)	43 (±4)	3 (±0)	13 (±2)
	Wet	59 (± 9)	0 (±0)	0 (±0)	4 (±2)	17 (±5)	1 (±1)	18 (±4)
CE	Dry	24 (±3)	1 (±1)	3 (±2)	12 (±3)	38 (±5)	4 (±1)	19 (±3)
	Wet	59 (±7)	0 (±0)	0 (±0)	6 (±2)	14 (±4)	2 (±0)	19 (±4)
AB	Dry	21 (±2)	1 (±1)	11 (±4)	4 (±1)	42 (±4)	2 (±0)	19 (±3)
	Wet	42 (±7)	1 (±0)	0 (±0)	4 (±1)	34 (±7)	2 (±1)	17 (±4)
SC	Dry	22 (±3)	1 (±0)	4 (±3)	7 (±1)	51 (±3)	4 (±1)	11 (±2)
	Wet	21 (±3)	0 (±0)	0 (±0)	12 (±4)	53(±5)	3 (±1)	10 (±3)

CW, Copano Bay West; CE, Copano Bay East; AB, Aransas Bay; SC, Ship Channel.

In our study, phytoplankton community structure shifted dramatically after the 2015 spring storms with the estuarine-wide drop in salinity, particularly at Copano Bay West (**Figure 5A**). From April 30 to June 4, high percentages of diatom biomass corresponded with the initial peaks in chlorophyll *a*, POC, and DIN (**Figures 3A,C**, **4A**, **5A**), suggesting that the initial DIN pulse may have led to the rapid growth of diatoms. However, the continued increase in freshwater inflow associated with subsequent major storm events during the summer led to an increase and dominance by small-celled cyanobacteria, in contrast to an increase in large cell phytoplankton, as was hypothesized (**Figure 5**). The largest POC peak and sustained high levels of chlorophyll *a* during the summer reflected cyanobacterial production. Similarly, there was an increase in zeaxanthin (a cyanobacterial indicator) concentration in Aransas Bay during the summer of 1992 when salinities were depressed (<5) as the result of a large freshwater influx into the system (Qian et al., 1996). Prior to June 2015, the spring estuarine phytoplankton community was dominated by diatoms, followed by cryptophytes, dinoflagellates, and prasinophytes. However, during the wet period cyanobacteria became the dominant phytoplankton. For example, cyanobacteria accounted for 59% of total phytoplankton biomass at Copano Bay West during the wet period (**Table 2**; **Figure 5A**). Although slight increases in cyanobacterial biomass were noted during the two previous summers, this class of phytoplankton typically accounted for less than 29% (±3%) of the phytoplankton community prior to the wet period. Furthermore, cyanobacterial dominance of the phytoplankton community in Copano Bay continued until late September, when salinities rose to 13 and 18 at

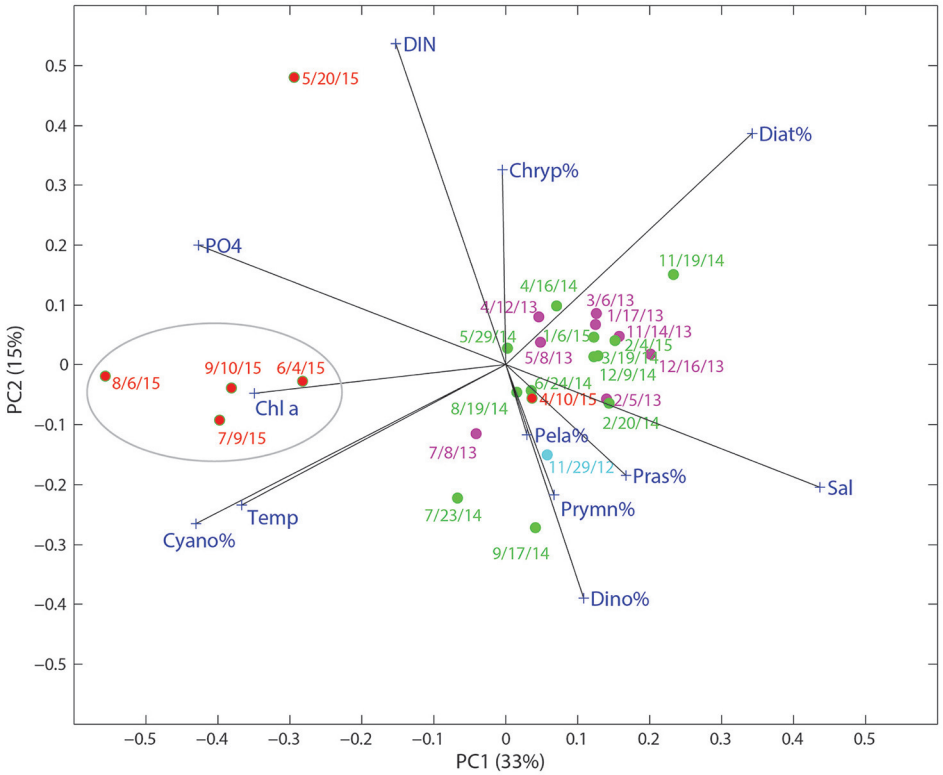

FIGURE 6 | Score and loading results for principal component (PC) 1 and PC2 from principal component analysis (PCA) on a data matrix including phytoplankton community composition (%), nutrients (DIN and PO_4^{3-}), temperature, and salinity at the Copano Bay West station. Dates in red text correspond to the "wet period" of 2015. Circled area refers to samples taken during the period of highest phytoplankton biomass.

Copano Bay West and East, respectively (**Table 2**; **Figure 5A**; **Supplementary Figure 2A**). As with POM, a muted response in phytoplankton community composition occurred at Aransas Bay (**Table 2**; **Supplementary Figure 2B**). This variation in phytoplankton community response between the two bays can be explained by the flushing gradient within the system and its exchange with the Gulf of Mexico, which is further illustrated by the more rapid increase in salinity at Aransas Bay following the flood event (**Figure 2B**). Also, although not characterized in this study, lateral water exchange with Mesquite Bay to the north and Corpus Christi Bay to the south is expected to have had an impact on flushing in Aransas Bay (Armstrong, 1982; Longley, 1994). Estuarine and nearshore water masses are exchanged more readily in Aransas Bay due to its close proximity to the Port Aransas Shipping Channel, where community composition and salinity showed a relatively small and brief response to the storm events (**Figures 2B**, **5B**). Most notably, this dominance of cyanobacteria (59% of phytoplankton biomass at Copano Bay West) was not seen in either of the previous two summers, when salinities were higher, and is therefore attributed to the formation of a niche for either a riverine species or an existing estuarine species with a tolerance for low salinities. Note that there is uncertainty in our calculated phytoplankton composition, since cellular content of pigments in phytoplankton cells can change with physiological state, such as nutrients and light (Qian et al., 2003). However, this should not significantly affect our results, as we analyzed more than 3 years of time-series data with the same cycling of light levels and similar nitrogen-limited conditions.

Environmental conditions may have played an important role in enhancing the growth of cyanobacteria in this system. The large pulses of freshwater, together with high surface temperatures (~30°C) from June to September, may have contributed to the cyanobacteria bloom. In the PCA biplot of relative phytoplankton biomass and various environmental parameters for Copano Bay West, cyanobacteria were particularly enriched in the samples from the wet period, well separated from the rest of the samples along PC 1 (**Figure 6**). From the PCA, the development of cyanobacteria appears to be related to temperature, PO_4^{3-}, and water freshening (opposite of salinity). Although cyanobacteria tend to have slow growth rates compared to other phytoplankton taxa, they have been shown to respond more strongly to temperature in field and laboratory studies (Juhl and Murrell, 2005; Reynolds, 2006; Paerl et al., 2014a). Three of the major phytoplankton taxa in the MAE, diatoms, dinoflagellates, and cyanobacteria, have growth optima ranges of 15–18°, 20–23°, and 25–30°C, respectively (Paerl et al., 2014a; Dorado et al., 2015). In addition, zeaxanthin shows stronger temperature dependence than other accessory pigments in the New River Estuary, North Carolina (Hall et al., 2013). Therefore, higher temperature, together with lower salinity

and high PO_4^{3-} concentrations, appear to be the major factors supporting the cyanobacterial bloom after the storms events.

In addition to lowered salinity and increased temperature, DIN and PO_4^{3-} concentrations were higher during the wet period and can therefore be attributed to riverine export of inorganic nutrients (**Figures 3A,B**, **6**). Copano Bay DIN peaked in May 2015, but was drawn down quickly, as discussed previously; this DIN peak corresponded to the higher percentages of diatoms, suggesting their role in DIN uptake. The rapid disappearance of DIN may have also been due to processes such as denitrification and anammox likely occurring in sediments of this shallow water system (Bruesewitz et al., 2013). The subsequent shift toward a cyanobacteria-dominated system even though DIN concentrations remained low from June to September, suggested that cyanobacteria thrived under nitrogen-limited conditions (**Figures 3C**, **5A**, **6**). Copano Bay PO_4^{3-} concentrations increased more gradually, and began reaching peak concentrations across the estuary as chlorophyll *a* concentrations began to drop, suggesting that PO_4^{3-} was rapidly recycled following the cyanobacterial bloom; this pattern was consistent with a previous study in the system (**Figures 3B,C**; Mooney and McClelland, 2012). Relative to the rapid removal of DIN, concentrations of PO_4^{3-} remain high throughout the wet period, indicating inefficient removal of phosphorus by the system (e.g., via microbial uptake and/or particle adorption). Cyanobacterial species that were observed in a recent study of the Breton Sound Estuary, Louisiana generally had low salinity tolerances, and it was determined that temperature, salinity, and DIN concentrations best explained annual patterns in phytoplankton community composition (Riekenberg et al., 2015). Additionally, cyanobacteria tend to be buoyant and become established in stable water columns, such as those experienced in most marine systems during the summer when the water column is stratified (Riekenberg et al., 2015). Low salinities and high temperatures created an ideal situation for the shift to a cyanobacteria-dominated phytoplankton community in the MAE during summer 2015. Additionally, it is possible that decreased filter feeding pressure contributed to the sustained increase in cyanobacterial biomass. A study on the impact of flood events on oyster populations in Copano Bay found that depressed salinities during the summer of 2007 led to reductions in oyster abundance and filtration rates (Pollack et al., 2011), which could lead to the persistence of ungrazed phytoplankton biomass in this shallow (<2 m) water column.

DNA sequencing data showed that in addition to the phytoplankton community shifting to become more cyanobacteria-dominated, the cyanobacterial community itself shifted from being dominated by *Prochlorococcus* spp. to *Cyanobium* spp. after the storm events (**Table 2**; **Supplementary Figure 3A**). *Cyanobium* spp. is a unicellular autotrophic coccoid picocyanobacteria (0.6–4.5 μm cell length × 0.3–1.7 μm cell width) (Komárek and Cepak, 1998; Komarek et al., 1999). Given their small size, some cells may have passed through the combusted glass fiber filter (0.7 μm pore size), leading to a potentially low estimate of *Cyanobium* spp. abundance. If we were actually underestimating the abundance of cyanobacteria, then this further strengthens our conclusions of cyanobacterial dominance. In a study of cyanobacterial communities in Chesapeake Bay, temperature was the most dominant environmental factor controlling picocyanobacterial populations; *Cyanobium* spp. occurrence was associated with lower salinities (Cai et al., 2010). In a study of cyanobacterial communities in the upper mixed layer (0–10 m) of the Baltic Sea, temperature and salinity were the potential drivers in structuring summer cyanobacterial communities (Bertos-Fortis et al., 2016). Picocyanobacteria were present in this layer year-round, and *Cyanobium* spp., in particular, have the ability to thrive in dynamic environments (such as the MAE) which is the reason for their year-round presence despite seasonal changes (Bertos-Fortis et al., 2016). Additionally, opportunistic picocyanobacteria occurrence was mainly explained by changes in temperature and salinity which matches the pattern seen in the present study; *Cyanobium spp.* dominated during the low salinity summer 2015 wet period, and *Prochlorococcus* spp. dominating during the high salinity summers of 2013 and 2014 (**Figures 2B**, **4A**; **Supplementary Figure 3A**; Bertos-Fortis et al., 2016).

Although *Cyanobium* spp. are not known nitrogen fixing bacteria, DIN assimilation can be the primary fate of DIN in the MAE during drought conditions even when measured DIN concentrations are low (**Figure 3A**; Stal, 2009; Hou et al., 2012; Bruesewitz et al., 2015). This indicates that high DIN regeneration coupled with high uptake, along with a high surface to volume ratio due to their small size, may have allowed *Cyanobium spp.* to continue flourishing for several months after DIN concentrations had dropped (**Figure 3A**; **Supplementary Figure 3A**). Overall, picocyanobacteria dominated the summer cyanobacterial community in the MAE throughout the study period, but lower salinities related to consecutive major storm events led to *Cyanobium* spp. dominating the picocyanobacterial community during the summer of 2015.

CONCLUSIONS AND IMPLICATIONS

POM source and concentration can indicate changes in the source of estuarine production, but this may be too coarse to elucidate fine changes in the source of production in the MAE. Using photosynthetic pigments, we determined that periods of drought favor a more diverse assemblage of phytoplankton, with relatively high diatom and dinoflagellate biomass. Major flood events led to a picocyanobacteria-dominated phytoplankton community, specifically *Cyanobium* spp., which was present in summer picocyanobacterial communities throughout the study period. The timing of the consecutive storm events in spring 2015 had a profound impact on the ability of this species to dominate, as rising temperatures and depressed salinities opened up a niche for this species to flourish. Changes in phytoplankton community composition can drastically affect the transfer of energy to higher trophic levels, thus having major implications for ecosystem-wide productivity (Cloern and Dufford, 2005), and is a topic for further study in this system. This study also suggests that this system is very efficient

at removing the riverine-derived DIN after the storm events, but the flux of PO_4^{3-} to the coastal ocean through the ship channel may be significant (Bhavya et al., 2016; Krishna et al., 2016).

In a region where recreational and commercial fishing are important to the local economy, impacts on ecosystem productivity should be carefully monitored. Given the importance of cultivated crops in the Mission-Aransas watershed, understanding the impact of freshwater inflows on the phytoplankton community in this estuary is key to the management of these vital sporadic freshwater inflows. Furthermore, cyanobacteria show extreme plasticity toward changes in environmental conditions and aquatic systems across the world, and cyanobacterial bloom frequency and duration are projected to increase in response to climate change (Paerl et al., 2014a; Bertos-Fortis et al., 2016).

AUTHOR CONTRIBUTIONS

NR, AH, and ZL conceived, designed, and wrote the paper.

ACKNOWLEDGMENTS

We thank J. Liu, S. Liu, K. Jackson, J. Xue, and C. Bonsell for help with pigment analyses and lab support. Thanks also to the MANERR staff: J. Tunnell, C. Hyatt, C. Croulet, and H. Samberson for help with sample collection and logistical support. We are grateful for substantive comments on previous drafts of this paper from E. Buskey, J. McClelland, and three reviewers. N. Reyna was partially supported by the University of Texas Graduate School Diversity Mentoring Fellowship. This research was partially funded by National Oceanic and Atmospheric Administration (NA15NOS4780185) and by operations grants to the Mission-Aransas National Estuarine Research Reserve from the Office of Coastal Management, National Oceanic and Atmospheric Administration. System-Wide Monitoring Program data was collected by the research staff of the Mission-Aransas NERR and hosted by the Central Data Management Office of the National Estuarine Research Reserve System. Publication supported in part by an Institutional Grant (NA14OAR4170102) to the Texas Sea Grant College Program from the National Sea Grant Office, National Oceanic and Atmospheric Administration, U.S. Department of Commerce.

SUPPLEMENTARY MATERIAL

The Supplementary Material for this article can be found online at: http://journal.frontiersin.org/article/10.3389/fmars.2017.00043/full#supplementary-material

Supplementary Figure 1 | (A) Particulate nitrogen (PN) concentration and **(B)** δ^{15}N-PN (‰) at all stations, October 30, 2012 to October 29, 2015. In all panels, the wet period is indicated by a shaded box. CW, Copano Bay West; CE, Copano Bay East; AB, Aransas Bay; SC, Ship Channel.

Supplementary Figure 2 | Phytoplankton community composition as percent (%) of total biomass at the (A) Copano Bay East and **(B)** Aransas Bay stations, October 30, 2012 to October 29, 2015. In all panels, the wet period is indicated by a shaded box.

Supplementary Figure 3 | Cyanobacterial community composition as displayed by cyanobacterial operational taxonomic units (OTUs) at the (A) Copano Bay West and **(B)** Ship Channel stations.

REFERENCES

Adolf, J. E., Yeager, C. L., Miller, W. D., Mallonee, M. E., and Harding, L. W. Jr. (2006). Environmental forcing of phytoplankton floral composition, biomass, and primary productivity in Chesapeake Bay, USA. *Estuar. Coast. Shelf Sci.* 67, 108–122. doi: 10.1016/j.ecss.2005.11.030

Andersen, R. A., Bidigare, R. R., Keller, M. D., and Latasa, M. (1996). A comparison of HPLC pigment signatures and electron microscopic observations for oligotrophic waters of the North Atlantic and Pacific Oceans. *Deep Sea Res. II* 43, 517–537.

Armstrong, N. E. (1982). "Responses of Texas estuaries to freshwater inflows," in *Estuarine Comparisons*, ed V. S. Kennedy (New York, NY: Academic Press), 103–120.

Bertos-Fortis, M., Farnelid, H. M., Lindh, M. V., Casini, M., Andersson, A., Pinhassi, J., et al. (2016). Unscrambling cyanobacteria community dynamics related to environmental factors. *Front. Microbiol.* 7:625. doi: 10.3389/fmicb.2016.00625

Bhavya, P. S., Kumar, S., Gupta, G. V. M., Sudheesh, V., Sudharma, K. V., Varrier, D. S., et al. (2016). Nitrogen uptake dynamics in a tropical eutrophic estuary (Cochin, India) and adjacent coastal waters. *Estuar. Coasts* 39, 54–67. doi: 10.1007/s12237-015-9982-y

Bianchi, T. S., Baskaran, M., DeLord, J., and Ravichandran, M. (1997). Carbon cycling in a shallow turbid estuary of southeast Texas: the use of plant pigment biomarkers and water quality parameters. *Estuaries* 20, 404–415.

Bruesewitz, D. A., Gardner, W. S., Mooney, R. F., and Buskey, E. J. (2015). Seasonal water column NH4 + cycling along a semi-arid sub-tropical river–estuary continuum: responses to episodic events and drought conditions. *Ecosystems* 18, 792–812. doi: 10.1007/s10021-015-9863-z

Bruesewitz, D. A., Gardner, W. S., Mooney, R. F., Pollard, L., and Buskey, E. J. (2013). Estuarine ecosystem function response to flood and drought in a shallow, semiarid estuary: nitrogen cycling and ecosystem metabolism. *Limnol. Oceanogr.* 58, 2293–2309. doi: 10.4319/lo.2013.58.6.2293

Cai, H., Wang, K., Huang, S., Jiao, N., and Chen, F. (2010). Distinct patterns of picocyanobacterial communities in winter and summer in the Chesapeake Bay. *Appl. Environ. Microbiol.* 76, 2955–2960. doi: 10.1128/AEM.02868-09

Canuel, E. A. (2001). Relations between river flow, primary production and fatty acid composition of particulate organic matter in San Francisco and Chesapeake Bays: a multivariate approach. *Org. Geochem.* 32, 563–583. doi: 10.1016/S0146-6380(00)00195-9

Canuel, E. A., Cloern, J. E., Ringelberg, D. B., Guckert, J. B., and Rau, G. H. (1995). Molecular and isotopic tracers used to examine sources of organic matter and its incorporation into the food webs of San Francisco Bay. *Limnol. Oceanogr.* 40, 67–81.

Cloern, J. E., and Dufford, R. (2005). Phytoplankton community ecology: principles applied in San Francisco Bay. *Mar. Ecol. Prog. Ser.* 285, 11–28. doi: 10.3354/meps285011

Day, J. W. Jr., Hall, C. A. S., Kemp, W. M., Yanez-Arancibia, A., and Christian, R. R. (eds.). (1989). "Microbial ecology and organic detritus in estuaries," in *Estuarine Ecology* (New York, NY: John Wiley & Sons), 257–308.

Diener, R. A. (1975). *Cooperative Gulf of Mexico Estuarine Inventory and Study - Texas: Area Description, NOAA Technical Report NMFS CIRC-393.* U.S. Dept. of Commerce, National Oceanic and Atmospheric Administration, Seattle, WA.

Dorado, S., Booe, T., Steichen, J., McInnes, A. S., Windham, R., Shepard, A., et al. (2015). Towards an understanding of the interactions between freshwater

inflows and phytoplankton communities in a subtropical estuary in the Gulf of Mexico. *PLoS ONE* 10:e0130931. doi: 10.1371/journal.pone.0130931

Fogel, M. L., Cifuentes, L. A., Velinsky, D. J., and Sharp, J. H. (1992). Relationship of carbon availability in estuarine phytoplankton to isotopic composition. *Mar. Ecol. Prog. Ser.* 82, 291–300.

Goldman, J. C. (1980). "Physiological processes, nutrient availability, and the concept of relative growth rate in marine phytoplankton ecology," in *Primary Productivity in the Sea*, ed P. G. Falkowski (New York, NY: Plenum Press), 179–194.

Hall, N. S., Paerl, H. W., Peierls, B. L., Whipple, A. C., and Rossignol, K. L. (2013). Effects of climatic variability on phytoplankton community structure and bloom development in the eutrophic, microtidal, New River Estuary, North Carolina, USA. *Estuar. Coast. Shelf Sci.* 117, 70–82. doi: 10.1016/j.ecss.2012.10.004

Harding, L. W. Jr. (1994). Long-term trends in the distribution of phytoplankton in Chesapeake Bay: roles of light, nutrients and streamflow. *Mar. Ecol. Prog. Ser.* 104, 267–291.

Harding, L. W. Jr., Adolf, J. E., Mallonee, M. E., Miller, W. D., Gallegos, C. L., Perry, E. S., et al. (2015). Climate effects on phytoplankton floral composition in Chesapeake Bay. *Estuar. Coast. Shelf Sci.* 162, 53–68. doi: 10.1016/j.ecss.2014.12.030

Harvey, H. R., and Mannino, A. (2001). The chemical composition and cycling of particulate and macromolecular dissolved organic matter in temperate estuaries as revealed by molecular organic tracers. *Org. Geochem.* 32, 527–542. doi: 10.1016/S0146-6380(00)00193-5

Hedges, J. I., and Stern, J. H. (1984). Carbon and nitrogen determinations of carbonate-containing solids. *Limnol. Oceanogr.* 29, 657–663.

Hernes, P. J., and Benner, R. (2003). Photochemical and microbial degradation of dissolved lignin phenols: implications for the fate of terrigenous dissolved organic matter in marine environments. *J. Geophys. Res.* 108, 3291. doi: 10.1029/2002JC001421

Hou, L., Liu, M., Carini, S. A., and Gardner, W. S. (2012). Transformation and fate of nitrate near the sediment–water interface of Copano Bay. *Cont. Shelf Res.* 35, 86–94. doi: 10.1016/j.csr.2012.01.004

Huntington, T. G. (2006). Evidence for intensification of the global water cycle: review and synthesis. *J. Hydrol.* 319, 83–95. doi: 10.1016/j.jhydrol.2005.07.003

Juhl, A. R., and Murrell, M. C. (2005). Interactions between nutrients, phytoplankton growth, and microzooplankton grazing in a Gulf of Mexico estuary. *Aquat. Microb. Ecol.* 38, 147–156. doi: 10.3354/ame038147

Komárek, J., and Cepak, V. (1998). Cytomorphological characters supporting the taxonomic validity of Cyanothece (Cyanoprokaryota). *Plant Syst. Evol.* 210, 25–39.

Komarek, J., Kopecky, J., and Cepak, V. (1999). Generic characters of the simplest cyanoprokaryotes Cyanobium, Cyanobacterium, and Synechococcus. *Cryptogam. Algol.* 20, 209–222. doi: 10.1016/S0181-1568(99)80015-4

Krishna, M. S., Prasad, M. H. K., Rao, D. B., Viswanadham, R., Sarma, V. V. S. S., and Reddy, N. P. C. (2016). Export of dissolved inorganic nutrients to the northern Indian Ocean from the Indian monsoonal rivers during discharge period. *Geochim. Cosmochim. Acta* 172, 430–443. doi: 10.1016/j.gca.2015.10.013

Lebreton, B., Pollack, J. B., Blomberg, B., Palmer, T. A., Adams, L., Guillou, G., et al. (2016). Origin, composition and quality of suspended particulate organic matter in relation to freshwater inflow in a south Texas estuary. *Estuar. Coast. Shelf Sci.* 170, 70–82. doi: 10.1016/j.ecss.2015.12.024

Letelier, R. M., Bidigare, R. R., Hebel, D. V., Ondrusek, M., Winn, C. D., and Karl, D. M. (1993). Temporal variability of phytoplankton community structure based on pigment analysis. *Limnol. Oceanogr.* 38, 1420–1437.

Longley, W. L. (1994). *Freshwater Inflows to Texas Bays and Estuaries: Ecological Relationships and Methods for Determination of Needs*. Austin: Texas Water Development Board and Texas Parks and Wildlife Department.

Lorrain, A., Savoye, N., Chauvaud, L., Paulet, Y., and Naulet, N. (2003). Decarbonation and preservation method for the analysis of organic C and N contents and stable isotope ratios of low-carbonated suspended particulate material. *Anal. Chim. Acta* 491, 125–133. doi: 10.1016/S0003-2670(03)00815-8

Mackey, M. D., Mackey, D. J., Higgins, H. W., and Wright, S. W. (1996). Chemtax—a program for estimating class abundances from chemical markers: application to HPLC measurements of phytoplankton. *Mar. Ecol. Prog. Ser.* 144, 265–283.

McTigue, N. D., Bucolo, P., Liu, Z., and Dunton, K. H. (2015). Pelagic-benthic coupling, food webs, and organic matter degradation in the Chukchi Sea: insights from sedimentary pigments and stable carbon isotopes. *Limnol. Oceanogr.* 60, 429–445. doi: 10.1002/lno.10038

Monbet, Y. (1992). Control of phytoplankton biomass in estuaries: a comparative analysis of microtidal and macrotidal estuaries. *Estuaries* 15, 563–571.

Mooney, R. F., and McClelland, J. W. (2012). Watershed export events and ecosystem responses in the Mission-Aransas National Estuarine Research Reserve, south Texas. *Estuar. Coasts.* 35, 1468–1485. doi: 10.1007/s12237-012-9537-4

Morata, N., and Renaud, P. E. (2008). Sedimentary pigments in the western Barents Sea: a reflection of pelagic-benthic coupling? *Deep Sea Res. II Top. Stud. Oceanogr.* 55, 2381–2389. doi: 10.1016/j.dsr2.2008.05.004

Murrell, M. C., Hagy, J. D. III, Lores, E. M., and Greene, R. M. (2007). Phytoplankton production and nutrient distributions in a subtropical estuary: importance of freshwater flow. *Estuar. Coasts* 30. 390–402. doi: 10.1007/BF02819386

Paerl, H. W., Hall, N. S., Peierls, B. L., and Rossignol, K. L. (2014a). Evolving paradigms and challenges in estuarine and coastal eutrophication dynamics in a culturally and climatically stressed world. *Estuar. Coasts* 37, 243–258. doi: 10.1007/BF02819386

Paerl, H. W., Hall, N. S., Peierls, B. L., Rossignol, K. L., and Joyner, A. R. (2014b). Hydrologic variability and its control of phytoplankton community structure and function in two shallow, coastal, lagoonal ecosystems: the Neuse and New River Estuaries, North Carolina, USA. *Estuar. Coasts.* 37(Suppl. 1), S31–S45. doi: 10.1007/s12237-013-9686-0

Paerl, H. W., Rossignol, K. L., Hall, S. N., Peierls, B. L., and Wetz, M. S. (2010). Phytoplankton community indicators of short- and long-term ecological change in the anthropogenically and climatically impacted Neuse River Estuary, North Carolina, USA. *Estuar. Coasts* 33, 485–497. doi: 10.1007/s12237-009-9137-0

Peierls, B. L., Christian, R. R., and Paerl, H. W. (2003). Water quality and phytoplankton as indicators of hurricane impacts on a large estuarine ecosystem. *Estuaries* 26, 1329–1343. doi: 10.1007/BF02803635

Pinckney, J. L., Paerl, H. W., Harrington, M. B., and Howe, K. E. (1998). Annual cycles of phytoplankton community-structure and bloom dynamics in the Neuse River Estuary, North Carolina. *Mar. Biol.* 131, 371–381.

Pollack, J. B., Kim, H., Morgan, E. K., and Montagna, P. A. (2011). Role of flood disturbance in natural oyster (Crassostrea virginica) population maintenance in an estuary in south Texas, USA. *Estuar. Coasts* 34, 187–197. doi: 10.1007/s12237-010-9338-6

Qian, Y., Jochens, A. E., Kennicutt, M. C., and Biggs, D. C. (2003). Spatial and temporal variability of phytoplankton biomass and community structure over the continental margin of the northeast Gulf of Mexico based on pigment analysis. *Cont. Shelf Res.* 23, 1–17. doi: 10.1016/S0278-4343(02)00173-5

Qian, Y., Kennicutt, M. C., Svalberg, J., Macko, S. A., Bidigare, R. R., and Walker, J. (1996). Suspended particulate organic matter (SPOM) in Gulf of Mexico estuaries: compound-specific isotope analysis and plant pigment compositions. *Org. Geochem.* 24, 875–888.

R Core Team (2013). *R: A Language and Environment for Statistical Computing*. Vienna: R Foundation for Statistical Computing. Available online at: http://www.R-project.org/

Ren, L., Rabalais, N. N., Turner, R. E., Morrison, W., and Mendenhall, W. (2009). Nutrient limitation on phytoplankton growth in the Upper Barataria Basin, Louisiana: microcosm bioassays. *Estuar. Coasts* 32, 958–974. doi: 10.1007/s12237-009-9174-8

Reynolds, C. S. (2006). *The Ecology of Phytoplankton*. Cambridge: Cambridge University Press.

Riekenberg, J., Bargu, S., and Twilley, R. (2015). Phytoplankton community shifts and harmful algae presence in a diversion influenced estuary. *Estuar. Coasts* 38, 2213–2226. doi: 10.1007/s12237-014-9925-z

Solis, R. S., and Powell, G. L. (1999). "Hydrography, mixing characteristics, and residence times of Gulf of Mexico estuaries," in *Biogeochemistry of Gulf of Mexico Estuaries*, ed T. S. Bianchi (New York, NY: John Wiley & Sons), 29–61.

Stal, L. J. (2009). Is the distribution of nitrogen-fixing cyanobacteria in the oceans related to temperature? *Environ. Microbiol.* 11, 1632–1645. doi: 10.1111/j.1758-2229.2009.00016.x

Sun, M., Aller, R. C., and Lee, C. (1991). Early diagenesis of chlorophyll-a in Long Island Sound sediments: a measure of carbon flux and particle reworking. *J. Mar. Res.* 49, 379–401.

Sun, M., Aller, R. C., and Lee, C. (1994). Spatial and temporal distributions of sedimentary chloropigments as indicators of benthic processes in Long Island Sound. *J. Mar. Res.* 52, 149–176.

Szymczak-Zyla, M., Kowalewska, G., and Louda, J. W. (2008). The influence of microorganisms on chlorophyll a degradation in the marine environment. *Limnol. Oceanogr.* 53, 851–862. doi: 10.4319/lo.2008.53.2.0851

Volkman, J. K., Revill, A. T., Holdsworth, D. G., and Fredericks, D. (2008). Organic matter sources in an enclosed coastal inlet assessed using lipid biomarkers and stable isotopes. *Org. Geochem.* 39, 689–710. doi: 10.1016/j.orggeochem.2008.02.014

Ward, N. D., Keil, R. G., Medeiros, P. M., Brito, D. C., Cunha, A. C., Dittmar, T. D., et al. (2013). Degradation of terrestrially derived macromolecules in the Amazon River. *Nat. Geosci.* 6, 530–533. doi: 10.1038/NGEO1817

Ward, N. D., Ricky, J. E., and Keil, R. G. (2012). Temporal variation in river nutrient and dissolved lignin phenol concentrations and the impact of storm events on nutrient loading to Hood Canal, Washington, USA. *Biogeochemistry* 111, 629–645. doi: 10.1007/s10533-012-9700-9

Wright, S. W., Thomas, D. P., Marchant, H. J., Higgins, H. W., Mackey, M. D., and Mackey, D. J. (1996). Analysis of phytoplankton of the Australian sector of the Southern Ocean: comparisons of microscopy and size frequency data with interpretations of pigment HPLC data using the "CHEMTAX" matrix factorisation program. *Mar. Ecol. Prog. Ser.* 144, 285–298.

Wright, S. W., and van den Enden, R. L. (2000). Phytoplankton community structure and stocks in the East Antarctic marginal ice zone (BROKE survey, January–March 1996) determined by CHEMTAX analysis of HPLC pigment signatures. *Deep Sea Res. II* 47, 2363–2400. doi: 10.1016/S0967-0645(00)00029-1

Xue, J., Lee, C., Wakeham, S. G., and Armstrong, R. A. (2011). Organic Geochemistry Using principal components analysis (PCA) with cluster analysis to study the organic geochemistry of sinking particles in the ocean. *Org. Geochem.* 42, 356–367. doi: 10.1016/j.orggeochem.2011.01.012

Conflict of Interest Statement: The authors declare that the research was conducted in the absence of any commercial or financial relationships that could be construed as a potential conflict of interest.

frontiers in Marine Science

ORIGINAL RESEARCH
published: 02 December 2016
doi: 10.3389/fmars.2016.00250

Short-Term Dissolved Organic Carbon Dynamics Reflect Tidal, Water Management, and Precipitation Patterns in a Subtropical Estuary

Peter Regier[1,2] *and Rudolf Jaffé*[1,2]*

[1] Department of Chemistry and Biochemistry, Florida International University, Miami, FL, USA, [2] Southeast Environmental Research Center, Florida International University, Miami, FL, USA

Estuaries significantly impact the global carbon cycle by regulating the exchange of organic matter, primarily in the form of dissolved organic carbon (DOC), between terrestrial and marine carbon pools. Estuarine DOC dynamics are complex as tides and other hydrological and climatic drivers can affect carbon fluxes on short and long time scales. While estuarine and coastal DOC dynamics have been well-studied, variations on short time scales are less well-constrained. Recent advancements in sonde technology enable autonomous *in situ* collection of high frequency DOC data using fluorescent dissolved organic matter (FDOM) as a proxy, dramatically improving our capacity to characterize rapid changes in DOC, even in remote ecosystems. This study utilizes high-frequency FDOM measurements to untangle rapid and complex hydrologic drivers of DOC in the Shark River estuary, the main drainage of Everglades National Park, Florida. Non-conservative mixing of FDOM along the salinity gradient suggested mangrove inputs accounted for 6% of the total DOC pool. Average changes in FDOM concentrations through individual tidal cycles ranged from less than 10% to greater than 50% and multi-day trends >100% change in FDOM concentration were observed. Salinity and water level both inversely correlated to FDOM at sub-hourly and daily resolutions, while freshwater controls via precipitation and water management were observed at diel to monthly time-scales. In particular, the role of water management in rapidly shifting estuarine salinity gradients and DOC export regimes at sub-weekly time-scales was evident. Additionally, sub-hourly spikes in ebb tide FDOM indicated rapid exchange of DOC between mangrove sediments and the river channel. DOC fluxes calculated from high-resolution FDOM measurements were compared to monthly DOC measurements with high-resolution fluxes considerably improving accuracy of fluxes (thereby constraining carbon budgets). This study provides a better understanding of short-term DOC dynamics and associated hydrological drivers and indicates the importance of high-frequency measurements to accurately constrain coastal carbon processes and budgets, particularly in coastal systems increasingly altered by hydrologic restoration and climate change.

Keywords: dissolved organic carbon (DOC), mangrove estuary, fluorescence sensor, water management, carbon fluxes

OPEN ACCESS

Edited by:
Patricia M. Medeiros, University of Georgia, USA

Reviewed by:
Piotr Kowalczuk, Institute of Oceanology Polish Academy of Sciences, Poland
Heather Erin Reader, Technical University of Denmark, Denmark

***Correspondence:**
Rudolf Jaffé
Jaffer@fiu.edu

Specialty section:
This article was submitted to Marine Biogeochemistry, a section of the journal Frontiers in Marine Science

Received: *23 September 2016*
Accepted: *17 November 2016*
Published: *02 December 2016*

Citation:
Regier P and Jaffé R (2016) Short-Term Dissolved Organic Carbon Dynamics Reflect Tidal, Water Management, and Precipitation Patterns in a Subtropical Estuary. Front. Mar. Sci. 3:250. doi: 10.3389/fmars.2016.00250

INTRODUCTION

Estuaries are the continental-oceanic interface of the global aquatic carbon (C) cycle. Terrestrially derived organic C is transported to coastal margins through these systems, primarily as dissolved organic carbon (DOC; Hedges et al., 1997). Tidal wetlands and estuaries, which occupy a small portion of world coastlines, account for an estimated third of all organic C buried in coastal sediments (Bauer et al., 2013), serving as a globally relevant C sink (Chmura et al., 2003; Bridgham et al., 2006). DOC also influences biogeochemical cycling within estuaries, including regulating the transport of nutrients and metals (Boyer et al., 1997; Qualls and Richardson, 2003; Yamashita and Jaffé, 2008) and impacts microbial communities (Tranvik, 1998; Fellman et al., 2010). Components of the DOC pool which absorb UV light, known as chromophoric dissolved organic matter (CDOM), control benthic productivity through light attenuation in the water column (Osburn et al., 2009; Ganju et al., 2014).

DOC dynamics vary dramatically across temporal scales (Spencer et al., 2007; Jollymore et al., 2012), from sub-hourly changes in tidal systems (e.g., Bergamaschi et al., 2012) to inter-annual trends (e.g., Evans et al., 2005). Characterizing the patterns and drivers of DOC variability to understand ecological impacts and constrain coastal C budgets thus requires information spanning a wide range of temporal resolutions. Although long-term investigations of coastal DOC dynamics are relatively common (e.g., Chen et al., 2013; Regier et al., 2016), equivalent studies at high temporal resolution are lacking due to the complex logistics and laboratory costs associated with DOC sampling in remote estuarine environments. However, high-resolution measurements are critical for temporally dynamic systems like estuaries, where rapid water quality changes observable in high-frequency measurements may not be accurately represented by weekly or monthly sampling intervals (Kirchner et al., 2004; Jollymore et al., 2012; Sobczak and Raymond, 2015).

The solution to this dearth of high-frequency DOC information lies in recent technological advances in multi-parameter sondes coupled with sensors measuring fluorescent dissolved organic matter (FDOM), a proxy for DOC (Downing et al., 2009). Sondes combine sensors, data-logging and internal power sources into a single water-proof instrument to achieve high-frequency sampling intervals *in situ*, eliminating the need for laboratory analysis except to calibrate proxy relationships. These sensors have been applied in a range of environments, including lakes (Watras et al., 2015), streams and rivers (Pellerin et al., 2012; Wilson et al., 2013), wetlands (Ryder et al., 2014), and coastal systems (Downing et al., 2009; Bergamaschi et al., 2012). High-frequency FDOM data provide the resolution necessary to fill in knowledge gaps beyond the scope of conventional monthly sampling frequencies. For instance, high-frequency FDOM measurements have facilitated the development of ecosystem-specific proxies for mercury (Bergamaschi et al., 2012), nutrients (Wilson et al., 2013; Etheridge et al., 2014), and DOC lability (Wilson et al., 2013). Likewise, high-resolution characterization of DOC proxies have provided new insight into processes controlling diel carbon cycles (Watras et al., 2015), rapid changes in hydrologic export of DOC (Bergamaschi et al., 2012; Wilson et al., 2013) and the role of DOC in light attenuation within optically complex waters (Ganju et al., 2014). As such, the application of instruments capable of high-frequency DOC data collection holds great potential for advancing our understanding of temporally dynamic aquatic ecosystems.

In the present study, high-resolution measurements were collected to examine patterns and trends in DOC at sub-hourly time-scales in the coastal estuaries of Everglades National Park (ENP). Landscape-scale restoration efforts underway to re-establish hydrologic connectivity along the Everglades flow-path are expected to alter seasonal timing, quantity and quality of freshwater inflows to ENP (Sklar et al., 2005), but the potential effects on ecosystem function remain uncertain (Estenoz and Bush, 2015). Since hydrology controls DOC dynamics in this system, it is expected that changes in the balance between freshwater (due to changes in management and rainfall) and saltwater intrusion (due to sea-level rise) will alter DOC cycling and export patterns (Orem et al., 2015; Regier et al., 2016). To this end, significant efforts have been placed into understanding the spatial and temporal patterns of DOC quality and quantity across the Everglades landscape (Maie et al., 2006a; Yamashita et al., 2010; Chen et al., 2013). In addition, DOC export patterns and drivers have been investigated at low and high temporal resolutions (Bergamaschi et al., 2012; Cawley et al., 2014; Regier et al., 2016). However, the relationship between rapidly changing and complex estuarine hydrology and high-resolution DOC dynamics for this system remains mostly undetermined. This study applies high-frequency measurements of FDOM to this knowledge gap, to better understand the hydrologic drivers of short-term DOC patterns in the Shark River, located in the mangrove forests of the coastal Everglades. In addition, this study builds on previous characterization of long-term DOC flux drivers (Regier et al., 2016) by linking short-term (daily) to long-term (monthly) DOC export regimes.

METHODS

Site Description

Data for this study was collected in the Shark River estuary, located in the coastal ecotone of southwest ENP (**Figure 1**). The Shark River connects vast upstream freshwater wetlands to coastal margins and is situated within the largest contiguous mangrove forest in the United States. Data was collected at SRS-5 (**Figure 1**), a monitoring site maintained by the Florida Coastal Everglades Long Term Ecological Research (FCE-LTER) project. The site is subject to semi-diurnal tides and experiences distinct wet and dry seasons, where the wet season delivers the majority of annual freshwater inflows to the estuary via rainfall and inputs through water management structures (Duever et al., 1994; Saha et al., 2012).

Instrument Calibration and Setup

High-frequency data were collected *in situ* (measured directly in the water column) using an EXO-2 water quality sonde (Yellow Springs Instrument Company (YSI), Ohio). The sensor measuring FDOM had excitation and emission wavelength

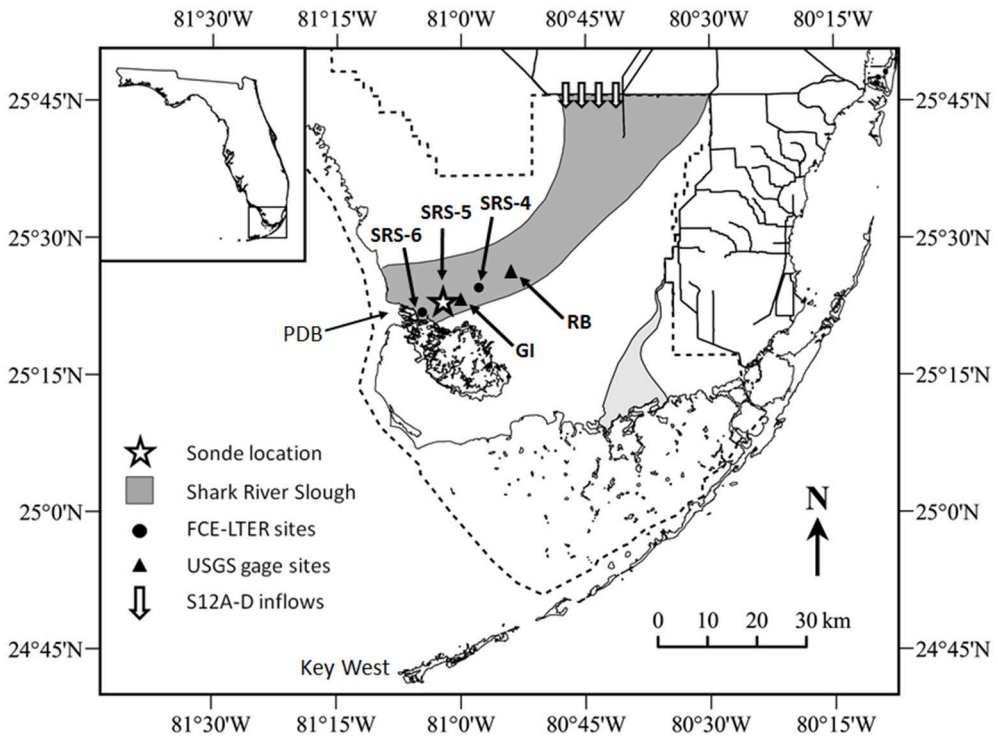

FIGURE 1 | Map of the study area, including long-term monitoring station and USGS gage station locations, where GI stands for Gunboat Island (#252230081021300) and RB stands for Rookery Branch (#022908295). S12A-D water management structures are marked on the northern border of Everglades National Park. PDB, Ponce de Leon Bay, the marine endmember for Shark River transects.

ranges of 365 ± 5 and 480 ± 40 nm, respectively, with a range of 0–300 ppb quinine sulfate equivalents (QSE) and resolution of 0.01 ppb QSE reported by the manufacturer. The sonde was calibrated prior to deployment according to manufacturer protocols and again immediately after instrument retrieval. Calibration solutions for FDOM fluorescence were made from quinine sulfate dihydrate diluted with 0.05 M H_2SO_4, with calibration errors lower than 5% for all deployments. Fluorescence of FDOM is reported in quinine sulfate units (QSU). Prior to deployment, sensors were wrapped in copper tape and surrounded by an anti-fouling sensor guard to minimize impacts of biofouling. Additionally, a wiper was programmed to clean sensor heads every 3 h. In spite of these precautions, sensor drift was detected in two time-series, which were not included in this study. For the data presented here, no drift was detected based on pre and post-calibration. Evidence of erratic turbidity spikes during preliminary deployments indicated interference due to crab activity, known to alter particulate and nutrient dynamics in mangrove sediments (Kristensen and Alongi, 2006). In order to protect against this, mesh was installed over openings in the sensor guard so that water flowed through uninhibited but crabs were unable to interfere with data collection.

Data Collection

A total of five time-series were collected between November 2014 and November 2015 averaging 27 days in duration (**Table 1**). Two time-series were collected during the wet-dry seasonal transition (T1 and T2), two during the dry season (D1 and D2) and one during the wet season (W1). The sonde was equipped with six external sensors (temperature/conductivity, pH, dissolved oxygen (DO), turbidity, FDOM, and chlorophyll) and one internal pressure sensor for measuring depth. The sonde was secured to the boardwalk at SRS-5 and situated adjacent to the riverbank with sensor heads located ∼0.5 meters below the lowest low tide mark. Ancillary hydrologic data was retrieved from the USGS gage at Gunboat Island (#252230081021300), located <1 km upstream from SRS-5 (**Figure 1**). As the sonde was not deployed relative to a standard vertical datum, stage values collected by the sonde were not directly comparable between time-series. Therefore, stage data from the USGS gage at Gunboat Island was matched to sonde stage using time-lagged correlations. After matching, sonde stage and USGS stage showed strong linear relationships ($r > 0.93$, $p < 0.0001$ for all time-series).

Data collected at 15 minute intervals from sonde and USGS sources are denoted as 15-min. Tidally filtered discharge was reported at hourly resolution after applying the PL33 low-pass filter for removal of tidal fluctuations (Flagg et al., 1976). Daily averages of high temporal resolution measurements were also reported, with the first and last day of each time-series excluded since these dates did not capture 24 h of continuous data. Long-term daily salinity data for calculations of δ-salinity was retrieved from the Gulf of Mexico Coastal Ocean Observing System (GCOOS) station GBIF1 (http://data.gcoos.org/index.php) as hourly data and binned to daily averages, where days with <12

TABLE 1 | Average values of selected hydrologic variables for each time-series.

Time-series	Start Date	End Date	GI Stage (m)*	Discharge (m^3/s)*	Filtered discharge (m^3/s)*	Rainfall (mm)	S12A-D inflows (m^3/s)	Stage at Key West (mm)
T1	11/4/2014	11/20/2014	−0.22	6.20	4.64	1.78	8.18	−0.72
D1	1/8/2015	2/9/2015	−0.17	−6.11	−5.07	0.51	1.70	−2.23
D2	3/16/2015	4/6/2015	−0.13	−4.46	−4.43	0.76	0.00	−2.99
W1	6/2/2015	7/1/2015	−0.20	−4.13	−4.89	4.32	0.00	−2.43
T2	10/1/2015	11/1/2015	0.07	−0.17	0.84	2.03	10.17	0.72

**Stage and discharge calculated from 15-min data, filtered discharge calculated from hourly data, all other variables calculated from daily data (first and last day of each time-series are clipped).*

measurements were excluded. Rainfall data was collected at the Shark River station of the Everglades Depth Estimation Network (EDEN, http://sofia.usgs.gov/eden/). Water management inflows were calculated as the sum of daily average discharge for S12A-D structures (USGS gages, http://waterdata.usgs.gov/).

Fluorescence Interference and Corrections

Corrections for thermal quenching of fluorescence were conducted following methods of Watras et al. (2011). Briefly, temperature and FDOM fluorescence were measured simultaneously for water samples collected at SRS-4, SRS-5, and SRS-6 (**Figure 1**) over a broad temperature range (5–30°C) exceeding the expected seasonal temperature range for SRS-5. Based on linear regression, a correction factor ($\rho = -0.0064 \pm 0.0004$) was established. A reference temperature (T_r) of 25°C was used instead of 20°C to reflect sub-tropical temperature regimes.

Interference from dissolved and suspended materials that absorb or scatter light can alter *in situ* fluorescence measurements, and impact instruments differently based on geometry of the sensor optics (Downing et al., 2012). For dissolved materials, absorbance of UV radiation by CDOM can be presented as absorbance at 254 nm (A_{254}, unitless) or absorption coefficients (a_{254}) (Hu et al., 2002; Kowalczuk et al., 2010). As a quantitative measurement, a_{254} is preferred to A_{254} as a_{254} values are comparable between studies regardless of path length. However, A_{254} values are also reported here to facilitate comparison with values presented by Downing et al. (2012) and Cawley et al. (2014). Conversion of A_{254} to a_{254} was performed using Equation 2 in Kowalczuk et al. (2010) where path length was 1 cm for both Downing et al. (2012) and Cawley et al. (2014).

The Shark River is characterized by relatively high CDOM absorbance (A_{254}) ranging from 0.1 to 0.6 (a_{254}: 23–138 m^{-1}) based on Cawley et al. (2014). Figure 1 in Downing et al. (2012) indicates this range of absorbance values equates to FDOM attenuation up to ∼15%. Monthly absorbance data collected upstream (SRS-4) and downstream (SRS-6) of the study site (**Figure 1**) spanning 11/2014–05/2015 were used to estimate SRS-5 absorbance as the average of SRS-4 and SRS-6 (Figure S1). Estimated A_{254} values for SRS-5 (average A_{254}: 0.44, average a_{254}: 101 m^{-1}) indicated that, at least for the portion of the study period represented in **Figure 1**, attenuation due to dissolved materials accounted of <10% of the FDOM signal based on a closed path sensor with optics at 90° (Downing et al., 2012).

To assess fluorescence interference due to suspended solids (measured as turbidity), a turbid solution containing 15 g of mangrove sediment collected at SRS-5 (dried, ground, and sieved through a 30-mesh screen) and ∼4 L of filtered low-absorbance (A_{254}: 0.09, a_{254}: 21 m^{-1}) mangrove creek water was mixed (water was filtered using combusted 0.7 μm GF/F filters). The solution was equilibrated for 48 h to negate potential FDOM inputs leached from the sediments (Downing et al., 2012; Lee et al., 2015). The solution was then placed in a constantly stirred vessel connected to a YSI flow-cell containing the FDOM and turbidity sensors with previously acid-washed tubing and a peristaltic pump. Sequential removal of turbidity was achieved by siphoning 250 mL aliquots from the stirred vessel, filtering and then returning the filtrate to solution (Figure S2). As previously observed, highly turbid waters attenuated FDOM fluorescence considerably (Downing et al., 2012; Lee et al., 2015). Less turbid conditions (values < 100 FNU) showed a strong linear relationship ($r = 0.99$, $p < 0.0001$, $n = 216$) to FDOM (Figure S2, values <100 FNU). For this study, turbidity values were generally low with 0.5% of turbidity values exceeding 100 FNU and 1.9% exceeding 25 FNU. Based on linear regression of turbidity values lower than 100 FNU in Figure S2, it is estimated that 25 FNU attenuated <5% of the total FDOM fluorescence signal. Furthermore, spikes in turbidity did not appear to elicit anomalous FDOM signals (e.g., Figure S3). This suggests that, while attenuation of fluorescence by suspended solids likely influences FDOM signals, a simple correction for the effects of turbidity on FDOM signals may not be appropriate (Lee et al., 2015). As such, turbidity corrections were not applied to FDOM measurements (See Section Statistics and FDOM Errors for estimates of error).

Establishing the FDOM-DOC Relationship

The relationship between FDOM and DOC was calibrated by collecting grab samples concurrent with *in situ* FDOM measurements. Due to high seasonal and spatial variability of DOC optical properties in the Shark River (Cawley et al., 2014), the FDOM:DOC relationship was established both with spatial transects and temporal sampling. Four seven-point spatial transects were collected from the marine end member (Ponce De Leon Bay) to the freshwater end member at SRS-4 (**Figure 1**). Transects were collected during wet and dry seasons and seasonal transitions and temporal data were collected through portions of two consecutive tidal cycles. DOC samples were filtered through 0.7 μm GF/F filters and quantified on a Shimadzu TOC analyzer

after acidification and purging to remove inorganic C. A total of 53 paired measurements of DOC and FDOM collected from 02/2015 to 04/2016 exhibited strong linear correlation ($r = 0.96$, $p < 0.0001$, Figure S4) yielding a conversion equation of FDOM (QSU) $= 0.11 * \text{DOC}$ (μM) $+ 19.06$. The root mean square error (RMSE) for this regression was $\pm$9.8 QSU or $\pm$7.5% of the average FDOM value (See Section Statistics and FDOM Errors). Due to the error component associated with converting FDOM fluorescence to DOC concentrations, FDOM measurements were primarily reported in QSU throughout the manuscript while DOC concentrations were reported in μM or ppm for comparison with literature values and to facilitate calculating DOC fluxes. DOC fluxes were calculated as the product of DOC concentration and discharge.

Statistics and FDOM Errors

All statistical analyses were performed using the JMP® Version 12 statistical package (SAS Institute Inc., Cary, NC, 1989–2007). Results of linear regressions are reported as correlations (r). Changes in FDOM presented as percent were calculated using the average FDOM value for the study (130.8 QSU) for consistency. Non-conservative mixing lines were calculated for regression plots of FDOM vs. salinity (e.g., **Figure 3**), based on previously published methods (Cawley et al., 2014).

Mangrove inputs during FDOM spikes were quantified for three consecutive tidal cycles in T2 with clear ebb tide spikes (**Figure 5**). For each tidal cycle, consecutive data points were connected with lines. Next, a baseline was drawn by connecting the lowest FDOM value at the start of the tidal cycle to the lowest value at the end of the tidal cycle. The baseline was then set to zero, so integrations only included the change in FDOM during the tidal cycle rather than the entire FDOM signature. Next, spikes were removed by connecting the points immediately preceding and following the spike. Finally, each tidal cycle was integrated with and without FDOM spikes using the "AUC" package in R (Ballings and Van den Poel, 2013). The integration process is represented graphically in Figure S5. FDOM contributions from the three tidal cycles ranged from 5.7 to 14.8% and were estimated to account for up to 24% in other tidal cycles.

Error terms associated with each of the three potential interferences to *in situ* FDOM measurements are identified in Section Fluorescence Interference and Corrections. The correction factor for temperature was based on linear regression of $r > 0.99$ ($p < 0.0001$) with and RMSE <1 QSU. For dissolved materials, attenuation was estimated at <10% based on A_{254} values for the site. For suspended solids, attenuation/scattering effects on FDOM were estimated at less than 5% for >98% of the data-set. Assuming attenuation of dissolved and suspended solids is additive, FDOM measurements may be ∼15% lower than actual FDOM values. These conditions represent the upper limits of FDOM attenuation based on high levels of dissolved matter (A_{254}: 0.44, a_{254}: 101 m^{-1}) and high turbidity (25.0 FNU). As attenuation from dissolved and suspended solids is not corrected for in FDOM values reported in this study, it is important to remember these potential sources of under-linearity when interpreting QSU values.

RESULTS

Environmental Conditions

This study covers a period of limited freshwater delivery to the Shark River estuary due to below-average rainfall and consequent reductions in water management inputs across the northern border of ENP into Shark River Slough (**Table 1**). This limited rainfall led to moderate to severe drought for the region stretching from the early dry season through the early wet season (droughtmonitor.unl.edu). The combination of these factors resulted in lower than normal discharge rates from the Shark River, with net negative flows (marine inflows to the estuary) from 12/2014 to 09/2015, the longest period of negative discharge for the 2002–2015 data record (USGS gage #252230081021300, tidally filtered discharge). As such, time-series D1, D2, and W1 (early dry, late dry and early wet seasons, respectively) all received minimal freshwater inputs from water management (although W1 received increased rainfall). In contrast, T1 and T2 time-periods exhibited high discharge rates for the estuary linked to high inflows from the S12A-D structures (**Figure 1**). Sea level acted as an additional hydrologic control and increased from D2 through T2, with the highest daily mean sea level value recorded at Key West between 1913 and 2013 occurring on 10/01/2015, the start-date for T2 (CO-OPS[1]). Basic statistics for *in situ* water quality data collected for this study are displayed in **Table 2** by time-series. Salinity and freshwater hydrology were inversely related, with lowest salinity during periods of high freshwater discharge and low sea-level (T1). Salinity increased through D1 and peaked during D2 due to minimal freshwater inputs. Salinity values decreased throughout W1 due to increased rainfall and during T2 due to increased water management inflows (**Table 1**). Dissolved oxygen (DO) inversely co-varied with

TABLE 2 | Averages and standard deviations for water quality variables by time-series.

Time-series	# of data	Temperature (°C)	Salinity	pH
T1	1517	22.75 (1.03)	14.69 (6.06)	7.46 (0.04)
D1	3054	21.18 (1.34)	17.91 (6.28)	7.47 (0.06)
D2	1998	26.13 (1.08)	27.02 (4.27)	7.51 (0.05)
W1	2767	29.7 (1.21)	22.81 (5.21)	7.5 (0.06)
T2	2933	27.25 (1.03)	21.6 (6.92)	7.42 (0.1)

Time-series	DO (mg/L)	FDOM (QSU)	Turbidity (FNU)	Chlorophyll (μg/L)
T1	4.27 (0.43)	132.89 (22.27)	6.43 (5.02)	2.93 (0.44)
D1	4.22 (0.59)	146.67 (32.5)	9.61 (26.47)	5.53 (5.85)
D2	3.03 (0.48)	116.68 (30.27)	7.25 (7)	6.07 (3.32)
W1	1.99 (0.41)	139.55 (24.3)	6.33 (23.82)	5.53 (1.21)
T2	2.74 (0.72)	114.52 (22.42)	9.96 (19.08)	7.68 (18.5)

[1]Center for Operational Oceanographic Products and Services (CO-OPS) (2016-07-14): NOAA Monthly Mean Sea Level Summary Data for the Key West, Florida, Water Level Station (FCE) (NOAA/NOS Co-OPS ID 8724580) from 01-Jan-1913 to Present. Center for Operational Oceanographic Products and Services (CO-OPS); Long Term Ecological Research Network. doi: 10.6073/pasta/4fca540ab6a8146f26b97c4eb1186a80.

seasonal patterns in temperature and on diel time-scales, with higher values during the day. In general, turbidity increased with channel velocity (both positive and negative), suggesting control by tidal or wind-induced erosion rather than allochthonous delivery to the estuary, matching previously reported decoupling of particulate and dissolved carbon pools for this system (He et al., 2014).

Values for FDOM ranged from 55.2 to 208.6 QSU, matching previously reported QSU values for maximum fluorescence intensity in coastal mangrove rivers of the Everglades (Jaffé et al., 2004). High tidal variability was clearly evident for the high resolution data, with variation of the FDOM signal in excess of 100% between consecutive low and high tides (e.g., 1/26/15 and 3/27/15, **Figure 2**). Highest FDOM values occurred during the beginning of the dry season, similar to previously observed longer-term seasonal trends upstream of SRS-5, which have been attributed to a combination of evaporation-mediated concentration and water management inputs (Chen et al., 2013). In contrast, FDOM values were considerably lower during the late dry season (D2) when DOC concentrations are historically higher in the upstream freshwater marshes (Chen et al., 2013).

Relationships between FDOM, Water Quality, and Hydrology

To quantitatively assess the relationships between water quality, hydrology and FDOM, linear regression of FDOM vs. parameters in **Table 2** is presented in **Table 3** as correlations, both for 15-min data and daily averages. Of these parameters, salinity had the strongest relationship to FDOM at both temporal scales. The relationship between FDOM and stage had the second highest *r*-values, with a higher correlation for daily data. At daily resolution, filtered discharge exhibited the third strongest correlation (though weak: $r = 0.28$). Temperature, pH, and filtered discharge showed weak correlations to FDOM for the high-resolution data ($r = -0.20$, -0.24, and 0.24, respectively) as did temperature, discharge and turbidity for daily resolution ($r = -0.22$, 0.17, and -0.22, respectively). Based on the above (see **Table 3**), salinity, stage, and tidally filtered discharge (at daily resolution) were investigated as potential drivers of high-frequency FDOM dynamics.

Salinity and FDOM

Measurements of FDOM at 15-min intervals showed distinct semi-diurnal patterns related to tidal influence and inversely tracked salinity patterns where highest FDOM values corresponded to lowest salinity for each tidal cycle (**Figure 2**), as observed in other mangrove systems (Dittmar and Lara, 2001). Correlations to FDOM were higher for 15-min than daily measurements (**Table 3**), indicating tidal control. The relationship between salinity and FDOM was examined using the ratio of the two variables (FDOM:salinity) shown in **Figure 3A**. A clear divide in the data-set was observed through this relationship, where T1 and T2 had lower FDOM:salinity

TABLE 3 | Correlations (*r*) of FDOM to water quality and hydrology variables.

Parameter	15-min	Daily
Temperature (°C)	−0.20	−0.22
Salinity	−0.83	−0.78
pH	−0.24	−0.14
DO (mg/L)	0.00	0.00
Turbidity (FNU)	0.00	−0.22
Chlorophyll (μg/L)	0.00	0.10
Stage (m)	−0.60	−0.73
Discharge (m3/s)	0.00	0.17
Filtered Discharge (m3/s)	0.24	0.28

15-min data measured at 15 minute increments except filtered discharge (hourly); daily data averages of 15-min data.

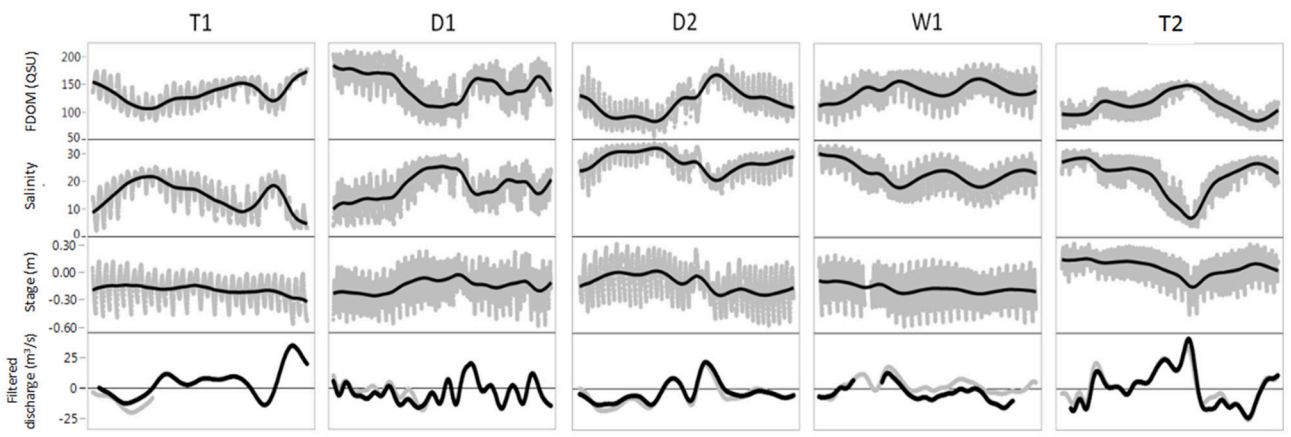

FIGURE 2 | FDOM, salinity, stage and tidally filtered discharge for the 5 time-series: T1, D1, D2, W1, and T2 (see Table 1 for dates). Gray dots are 15-min interval measurements for FDOM, salinity and stage. Black lines for FDOM, salinity and stage are smoothing lines to highlight multi-day trends. For filtered discharge, black lines is hourly tidally filtered discharge measured at Gunboat Island. Gray filtered discharge lines represent data from the adjacent Harney River drainage to serve as reference for gaps in the Gunboat discharge record.

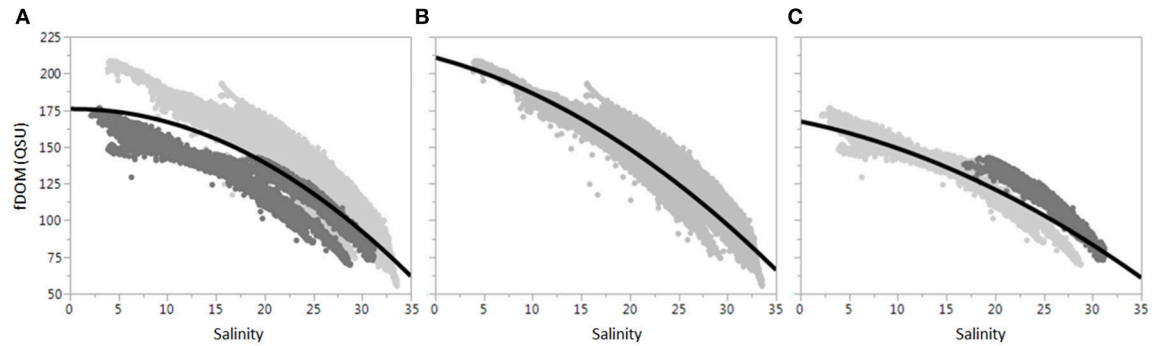

FIGURE 3 | The FDOM:salinity relationship. (A) Shows all data together, while **(B,C)** divide the data-set into D&W and T sub-groups, respectively. The dark gray dots for **(A)** are T time-series. The dark gray dots for **(C)** are discussed in Section Water Management and Rainfall Control Daily FDOM Patterns.

ratios compared to the remaining three time-series. This divide matched closely with management-driven inflows as well as tidally filtered discharge (both considerably higher for T1 and T2, see **Table 1**). A similar divide in the DOC:salinity ratio observed by (Cawley et al., 2014) indicated that T1 and T2 most closely resembled wet season characteristics while the remaining time-series matched the dry season. As outlined in Section Environmental Conditions, the study period experienced abnormal hydrology, and the divide in FDOM:salinity confirmed that conventional seasonal wet/dry timing did not fit this data-set. Rather, seasonal transition time-series (T1 and T2) resembled classic wet season hydrology and salinity gradients while the remaining three time-series resembled dry season conditions due to reduced rainfall and consequent drought. Based on this observation, the data-set was divided into two sub-groups: the first for time-series during periods of low freshwater inflow (D1, D2, and W1, **Figure 3B**), the second for time-series during periods of high freshwater inflow (T1 and T2, **Figure 3C**). Dividing the data-set in this manner dramatically improved linear regression fits ($r = 0.94$ for D&W, $r = 0.93$ for T) in comparison to the full data-set ($r = 0.83$). An additional split in **Figure 3C** during T2 was observed, where FDOM:salinity ratios transitioned from high salinity and low freshwater inputs to dramatically increased freshwater inflows and low salinity. To examine this, T2 was sub-divided into two sections: before and during the start of high outflows (positive discharge from the estuary, **Figure 2**) and during and after high outflows. The first sub-group clustered more with D&W time-series due to enhanced saltwater presence, higher stage and low or negative filtered discharge (**Figure 3C**, dark gray points). The second sub-grouping fell in the same FDOM:salinity region as T1: characteristic of high water management inflows in spite of high sea levels.

The data presented in **Figure 3** suggest a non-conservative relationship between FDOM and salinity, where FDOM values were higher at the mid-estuary than would be expected for conservative (linear) mixing behavior of freshwater and marine endmembers. A similar relationship was previously reported for this location by Cawley et al. (2014), who determined that non-conservative inputs were primarily due to DOC contributions from the riparian mangrove forests. Following this hypothesis, FDOM:salinity plots were fitted with quadratic regression lines which improved fits over linear regression (full data-set: $r = 0.85$, D&W: $r = 0.94$, T: $r = 0.94$). Non-conservative inputs were calculated for individual neap and spring tides for each time-series ($n = 20$) as the difference between integrations of quadratic and linear fits (Cawley et al., 2014). An average non-conservative input percentage of $6 \pm 2\%$ was estimated with a maximum of 9% (neap tide, D2) and a minimum of 3% for the consecutive spring tide.

FDOM and Tidal Dynamics

Tidal FDOM patterns were inversely related to stage with a temporal lag component, where highest tidal values for FDOM lagged lowest stage (low tide) by 1–2 h. Stage correlations to FDOM (FDOM:stage) were considerably higher for daily data (**Table 3**), likely due to the temporal lag observed at tidal time-scales. When tidal FDOM patterns were time-matched to stage (lowest FDOM values time-lagged to coincide with peak stage), a much stronger regression was achieved ($r = -0.77$), similar to FDOM:salinity. As with salinity, the FDOM:stage data was divided into T and D&W groupings, with a better fit for D&W ($r = -0.79$) than T ($r = -0.72$), indicating stronger tidal control of FDOM:stage dynamics during periods of low freshwater inflows. Values of FDOM were consistently higher for neap tides (average 136.4 QSU) compared to spring tides (average 124.6 QSU). Neap tides also exhibited lower salinity, lower stage and higher tidally filtered discharge, indicating reduced tidal influence. The difference in FDOM between neap and spring tides was considerably larger for T time-series (+17.1 QSU, average of spring and neap: 119.8 QSU) compared to D&W time-series (+10.2 QSU, average of spring and neap: 136.5 QSU). In general, decreasing FDOM trends were observed during spring tides, while increasing trends accompanied neap tides. Differences in neap/spring FDOM patterns provided evidence that greater freshwater influence during neap tides led to higher allochthonous DOC inputs to the estuary. In addition, this suggested a temporal decoupling between weekly (spring/neap tides) and monthly (time-series) resolutions for the relationship between freshwater discharge and FDOM where neap tides

increased both filtered discharge rates and FDOM signals while **Figure 3** indicated dilution of FDOM (lower signal) during periods of increased freshwater delivery.

Rapid changes in FDOM during ebb tides were consistently observed near the tidal FDOM minimum which did not fit the semi-diurnal sinusoidal tidal signature. Examples of these FDOM patterns along with additional parameters are shown in **Figure 4**, with the unexpected spikes highlighted in black. These FDOM spikes consistently coincided with a knee observed in ebb tide stage patterns which could not be fully explained by tidal flow asymmetry typically observed in mangrove channels (Mazda et al., 1995). The knee denoted a deceleration of falling water levels attributed to geomorphological control of tidal hydrodynamics by riparian mangrove forests. Specifically, it was hypothesized that these patterns correspond to tidally regulated porewater exchange between mangrove sediments and the river channel. The location where the sonde was deployed is immediately adjacent to mangrove sediments perforated with crab burrows, a feature shown to enhance hydraulic connectivity of mangrove sediments to the water column [up to 20% in some systems, Stieglitz et al. (2013)]. Reduced dissolved oxygen (DO) levels, often associated with porewater hypoxia in mangrove ecosystems (Bouillon et al., 2007), were generally present during FDOM spikes supporting the hypothesis of porewater contributions. However, these patterns were somewhat variable, with examples in **Figure 4** showing consistently depleted DO concurrent with FDOM spikes during T2 but not T1.

Daily FDOM Dynamics

Multi-day patterns in FDOM (see smoothing lines in **Figure 2**) corresponded to freshwater input patterns observed as tidally filtered discharge. Correlation of daily FDOM values to filtered discharge was relatively weak for the whole data set ($r = 0.30$, $n = 145$, $p = 0.0009$) and for D&W ($r = 0.29$, $n = 77$, $p = 0.0083$) but stronger for T ($r = 0.60$, $n = 45$, $p < 0.0001$), likely due to substantial water management inputs during T1 and T2. To quantify the impact of filtered discharge on changes in FDOM, the difference in FDOM between consecutive days was calculated as $\delta\text{-FDOM} = \text{FDOM}_{(x+1)} - \text{FDOM}_{(x)}$ where x is the date. Based on δ-FDOM calculations for time-series, daily changes in FDOM of +40.0 QSU to −28.6 QSU indicate equivalent shifts of +377.4 μM (+31%) to −274.7 μM (−22%) for DOC concentrations. The regression of δ-FDOM:filtered discharge ($r = 0.65$, $n = 115$, $p < 0.0001$) showed a much stronger relationship than FDOM:filtered discharge ($r = 0.30$, $n = 120$, $p = 0.0009$). Interestingly, correlations between filtered discharge and δ-FDOM were stronger for D&W ($r = 0.74$, $n = 72$, $p < 0.0001$) than T ($r = 0.71$, $n = 43$, $p < 0.0001$), which was unexpected since T time-series were more strongly linked to filtered discharge patterns. Regression slopes for T and D&W (0.01 and 0.03, respectively) indicated that equivalent changes in filtered discharge yielded a change in the FDOM signal three times greater for dry season time-series compared to wet season. This was attributed to lower stage during D&W time-series (**Table 1**), leading to smaller volume in the Shark River. The corresponding evapo-concentration of the Shark River DOC pool would be more sensitive to dilution from changes in freshwater flow.

DOC Fluxes

Previously, long-term DOC fluxes were calculated for this site based on monthly DOC concentrations and tidally filtered discharge (Regier et al., 2016), with modeling of monthly flux

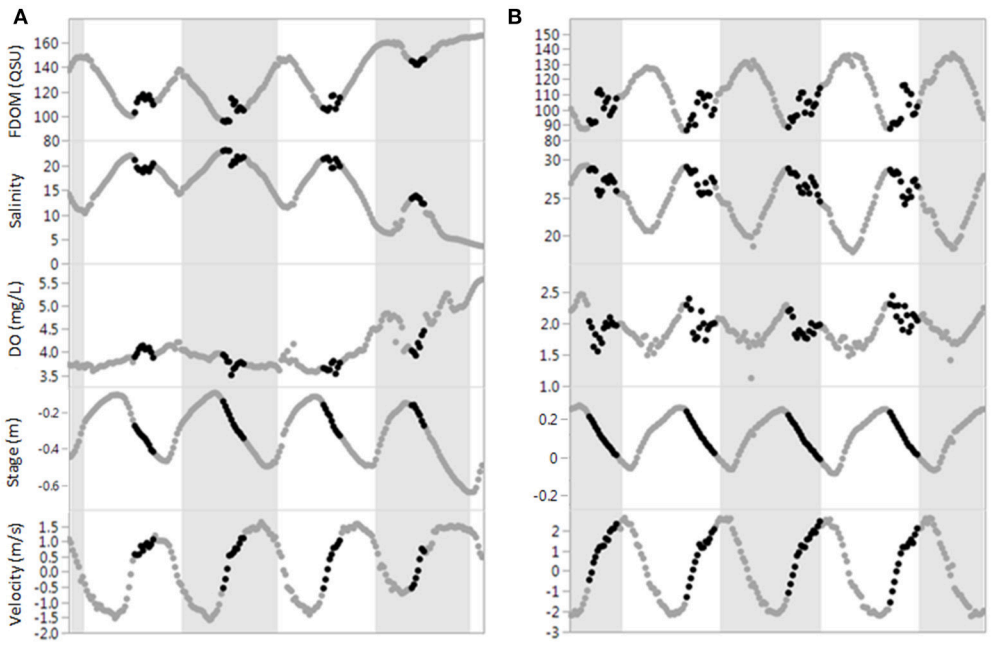

FIGURE 4 | Time-series comparing mangrove inputs during T1 (**A**, left) and T2 (**B**, right). Black points highlight FDOM spikes during ebb tide. Note that lower salinities during T1 show no FDOM spike. In contrast, T2 has very pronounced spikes.

values predicted by salinity, rainfall, water management inflows, and the Atlantic Multidecadal Oscillation (AMO), a long-term climatic index. Short-term fluxes based on DOC (using FDOM as a proxy) and hourly tidally filtered discharge were calculated for this study to compare and contrast patterns and drivers of DOC fluxes in the Shark River across temporal scales. Both T time-series exhibited net positive flux values (DOC exported from the estuary), averaging $3.4 * 10^9$ mg C d^{-1}. In contrast, all D&W time-series had negative flux values averaging $-4.5 * 10^9$ mg C d^{-1}, indicating considerably longer DOC residence times between periods of positive filtered discharge (average movement calculated from velocities of 2432 m d^{-1} for D&W in comparison to 8843 m d^{-1} for T time-series in relation to ∼9500 m from the study site to the river mouth). For hourly flux values, no correlations for water quality or hydrology variables (except discharge) were observed, including salinity and stage, which both correlated to long-term fluxes (Regier et al., 2016). As discharge was higher during neap tides, DOC fluxes were also considerably higher, with averages of $2.8 * 10^9$ mg C d^{-1} and $-5.9 * 10^9$ mg C d^{-1} for neap and spring, respectively. This pattern held true when fluxes were sub-divided into D&W and T groupings with neap tide fluxes $6.2 * 10^9$ mg C d^{-1} and $1.2 * 10^{10}$ mg C d^{-1} higher than spring tide fluxes for D&W and T subsets, respectively.

To validate the extrapolation of high-frequency FDOM measurements to DOC values and improve the accuracy of DOC flux determinations, flux values were calculated from daily DOC data (based on FDOM as a proxy) and monthly grab samples where the DOC value at the beginning of each time-series was extrapolated to all days in the time-series (Gaiser and Childers, 2016). As the two sets of fluxes were determined for the same days using the same filtered discharge data, the only difference was the application of low-resolution vs. high-resolution DOC concentrations in the estimates. The resulting flux calculations were compared using linear regression (**Figure 6**), with stronger correlations for D&W time-series ($r = 0.95$, $n = 73$, $p < 0.0001$) in comparison to T time-series ($r = 0.93$, $n = 43$, $p < 0.0001$). To interpret if fluxes based on monthly grab samples were over-estimated or under-estimated in comparison to high-frequency flux calculations, a 1:1 line was included. In general, linear regression for D&W fell slightly below the 1:1 line (slope = 0.80), indicating monthly fluxes were under-estimated (**Figure 6A**) while T time-series were on or above the line (slope = 1.25), particularly for high fluxes during T2 (**Figure 6B**).

DISCUSSION

High-resolution measurements of FDOM showed highly dynamic DOC behavior controlled at tidal and daily time-scales by a mixture of tidal influence, freshwater inputs, and exchange with mangrove forests. Whereas tidal control was consistent for all time-series, freshwater control of FDOM was more sporadic and varied seasonally. The study period was unique as the two major sources of freshwater to the Shark River (rainfall and water management inflows), which are usually coupled (though time-lagged, Saha et al., 2012) were separated, allowing for a comparison of the influence of each freshwater source on high-resolution FDOM dynamics. In addition, previously unobserved spikes during ebb tide were identified as likely originating from porewater exchange with the mangrove forests. While tidal control is evident at hourly resolution and freshwater influence is well-characterized at daily resolution, the abovementioned mangrove-derived spikes would not be observable, even at hourly resolution.

Tidal-Scale FDOM Dynamics

The observed semi-diurnal variability in FDOM patterns in contrast to those of salinity and stage suggest strong tidal control of DOC leading to significant inverse relationships for all time-series with the former and weaker correlations with the latter. These relationships have been well-established in this region (Bergamaschi et al., 2012; Cawley et al., 2014) with salinity identified as a significant predictor of long-term DOC fluxes (Regier et al., 2016). However, untangling the influences of salinity and stage on estuarine DOC dynamics remains difficult (requiring controlled experimental conditions, e.g., Chambers et al., 2014) as these factors tightly co-vary. Data presented here shows that FDOM is temporally coupled to salinity and lags stage, suggesting that high-frequency DOC dynamics are primarily controlled by tidal drivers rather than simply by physical hydrology (stage).

A recent mesocosm study of C response to salinity and inundation in mangrove peat soils from the region found that higher salinity decreased porewater DOC by 2.8 ± 3.3 ppm (23 ± 27% of average DOC for this study), while increased inundation enhanced DOC concentrations by 3.6 ± 4.5 ppm [30 ± 37%; based on a 8 cm increase in stage; (Chambers et al., 2014)]. Findings from the current study of an inverse relationship between DOC and salinity at tidal time-scales match findings from the mesocosm study (Chambers et al., 2014). However, increased salinity conditions equivalent to those reported by Chambers et al. (2014) yielded a much larger decrease in DOC (−7.5 ppm or −62% for D&W time-series in **Figure 3B**, −5.0 ppm or −41% for T time-series in **Figure 3C**).

In contrast, the inverse relationship between tidal stage and DOC (attributed to dilution) does not match with higher DOC in inundated mesocosm experiments (Chambers et al., 2014). In the latter, an equivalent increase in stage of 8 cm yields decreased DOC of considerably smaller magnitudes (−0.7 ppm or −6% for D&W time-series, −0.5 ppm or −4% for T time-series).

Decoupled response of DOC to inundation between mesocosm and *in situ* measurements may stem from the estimated small contributions of mangrove-derived DOC at this location (∼6% of the DOC pool), whereas the mesocosm results present changes in DOC exclusively from mangrove peats. Based on Chambers et al. (2014), increased inundation is expected to decrease the concentration of the overall DOC pool through dilution while simultaneously enhancing mangrove inputs. As sea level rise drives higher saltwater intrusion and increased inundation in this region, higher C loss from the mangrove forest (See also Section Mangrove Contributions to the DOC Pool) is expected to account for a larger portion of the

Shark River DOC pool and increase outwelling of mangrove-derived DOC (Dittmar and Lara, 2001). Such processes are expected to increase light attenuation in the water column (Ganju et al., 2014) of adjacent light-sensitive seagrass and coral reef communities (Shank et al., 2010; McPherson et al., 2011) through long-range DOC transport (Maie et al., 2012; Yamashita et al., 2013. However, DOC export from this region in general is predicted to decrease in the future due to shifting hydrology due to climate change (Regier et al., 2016). Thus, the potential balance between enhanced mangrove forest inundation and predictions based on long-term DOC datasets remains to be determined. Better understanding of the potentially complex relationship between inundation and DOC export is therefore crucial for low-relief coastal systems like mangrove forests, where ecosystem sustainability is based on accretion keeping pace with sea-level rise (McKee, 2011). Mangrove accretion is primarily dependent on primary productivity (Cahoon and Lynch, 1997) and correlates to organic C burial rates, which are below global averages for the Shark River (Breithaupt et al., 2014). Thus, potential DOC losses from mangrove peats due to the combined effects of increased salinity and inundation could increase the vulnerability of the coastal mangrove fringe to submergence.

Mangrove Contributions to the DOC Pool

The DOC pool in the Shark River is strongly influenced by upper watershed freshwater wetland sources, combined with mangrove inputs (Yamashita et al., 2010; Bergamaschi et al., 2012; Cawley et al., 2014). However, it is not clear from previous studies if this mangrove contribution is related to porewater inputs, litter leachates, or combinations of these. As such, these contributions could respond differently to inundation patterns, tidal action, changes in primary productivity, and associated litter-fall. Bouillon et al. (2007) reported considerable porewater contributions of DOC (estimated at 30% of the total DOC pool) draining a mangrove forest in Tanzania during ebb tide, with porewaters exhibiting considerably higher salinity than the creek water column. In contrast, the notably lower percentage of DOC attributed to mangrove inputs in the Shark River indicates that porewater DOC may not account for a considerable component of the DOC pool. However, this is likely due to the large allochthonous DOC inputs received from upstream freshwater marshes in the Everglades, whereas the Tanzania creek system received minimal freshwater inputs (Bouillon et al., 2007).

However, the abovementioned spikes in FDOM during ebb tide provide new information on the role of mangrove inputs to this system. Although non-conservative mixing calculations indicate that mangrove DOC comprises a relatively minor component of the total DOC pool, FDOM spikes indicate seasonally variable contributions exceeding the 6% mangrove input estimation. For three consecutive tidal cycles, FDOM signals were compared by including or excluding the FDOM spikes (**Figure 5**). Based on this comparison, between 5.7 and 14.8% of the total change in FDOM during these tidal cycles was attributed to mangrove porewater inputs. The percent contribution of FDOM spikes varied with season, with higher and more consistent mangrove DOC contributions observed during the T time-series compared to D&W time-series. This supports previous research reporting higher CDOM production during wet periods compared to dry periods (Shank et al., 2010). However, the magnitude of these FDOM spikes infer that the majority of mangrove DOC export into the river during ebb tide (estimated at 65% for SRS-6, Romigh et al., 2006) occurs at rapid time-scales (1–2 h). Thus, accurately characterizing this highly dynamic exchange process to constrain aquatic C fluxes in mangrove forests requires high-frequency measurements.

Seasonal variation in FDOM spikes also gives insight into the potential role of mangrove porewaters and primary production in DOC exchange between mangrove forests and the river channel. If primary production preferentially dictated mangrove DOC inputs over hydrology, it would be expected that the highest inputs (largest spikes) would coincide with peak primary productivity during the wet-season (Castañeda-Moya et al., 2013). However, spikes are smaller and less consistent during W1 than T1 or T2, suggesting that the extent and duration of tidal

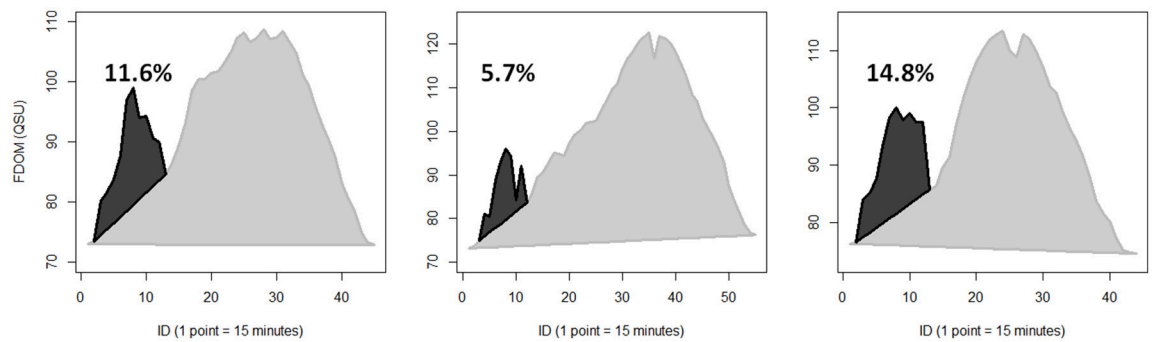

FIGURE 5 | Quantification of rapid spikes in FDOM during ebb tide attributed to mangrove porewater inputs were calculated for three consecutive tidal cycles during T2. Dark gray areas outlined in black represent FDOM spikes associated with ebb tide mangrove porewater inputs. Light gray areas outlined in gray represent the rest of the change in FDOM during each tidal cycle, where change is defined as FDOM above a baseline running from the lowest FDOM value at the start of the tidal cycle to the lowest FDOM value at the end of the tidal cycle. Percentages indicate the percent of FDOM change attributed to ebb tide mangrove porewater inputs.

inundation rather than patterns in primary productivity controls the magnitude of DOC porewater exchange. Furthermore, this may indicate that DOC spikes are more strongly associated with leaching from mangrove sediments and porewater exchange, rather than direct leaching from mangrove leaves and stems (Maie et al., 2006b; Romigh et al., 2006).

Water Management and Rainfall Control Daily FDOM Patterns

Daily and multi-day patterns in FDOM showed clear links to freshwater inputs (**Figure 2**, Section Daily FDOM Dynamics), indicating the essential role of upstream hydrology in regulating DOC concentrations in the Shark River. In particular, inflows from water management structures drive a division in FDOM:salinity ratios between time-series (**Figure 3**). Of the hydrologic parameters influencing the estuarine salinity gradient, water management structures are the only means of directly regulating freshwater inflows to this system, with natural delivery of freshwater from rainfall and potential groundwater inputs and seepage through barriers to flow (Saha et al., 2012). A comparison of T1 and T2 time-series demonstrates the control of FDOM temporal dynamics exerted by managed freshwater inputs. Both T1 and T2 exhibit similar FDOM:salinity ratios (**Figure 3**), suggesting similar DOC source and mixing dynamics. However, neither the salinity gradient (dramatically different sea levels, **Table 1**, and salinity, **Table 2**, between the two time-series) nor rainfall (similar for all time-series except W1) can explain the similar FDOM:salinity distributions for T1 and T2 in contrast to the other three time-series. Instead, freshwater control by water management inflows appears to link these time-series (high for T1 and T2, low or absent for the other time-series). This is evident in the shift of FDOM:salinity observed for T2 (**Figure 3C** and Section Salinity and FDOM) from ratios characteristic of the dry-season to wet-season which occurred in less than a day. Based on this rapid change along with the divide in **Figure 2**, it is clear that water management inflows (either directly or indirectly) control Shark River hydrology and DOC dynamics and export at short time-scales.

Both rainfall and water management inputs were identified as significant freshwater drivers of long-term DOC fluxes in this system, with rainfall contributing almost double the modeling power as managed inflows (Regier et al., 2016). For the high-frequency data collected during this study, the influence of rainfall is less obvious than water management, likely due to unsusually low precipitation rates for all time-series except for W1 (**Table 1**). The clearest evidence of rainfall driving changes in DOC occurred with onset of the rainy season (between D2 and W1). Low FDOM values for D2 (relative to D1) were attributed to enhanced saltwater intrusion into upstream freshwater marshes observed through semi-diurnal tidal signatures in stage data at the Rookery Branch gage 20 km upstream of SRS-5 (#022908295, http://waterdata.usgs.gov/). Subsequently increased FDOM during W1 was attributed to the enhanced hydrologic connectivity of the estuary to upstream marsh regions as a result of increased rainfall. Decreased DOC concentration and exports due to drought conditions (e.g., D2) have been reported for other coastal wetland systems (e.g., Ardón et al., 2016). Likewise, rainfall events have been linked to increased DOC concentrations in both marsh and mangrove systems (Bergamaschi et al., 2012; Ryder et al., 2014), although shifts in other drivers between D2 and W1 like soil temperature may be partially responsible for the changes in DOC concentration (Davidson and Janssens, 2006; Ryder et al., 2014).

During the study period, the influences of water management and rainfall on daily FDOM dynamics were evident. However, whereas water management inflows dramatically shifted estuarine hydrology from negative to positive discharge, rainfall did not. The importance of water management to maintain seasonal freshwater delivery has been well-established for this region (Sklar et al., 2005; Obeysekera et al., 2014). High-frequency measurements presented here indicate that, particularly during periods of below-average freshwater flow (e.g., drought), water management inputs are capable of rapidly altering salinity and associated water quality gradients in the coastal Everglades. Based on this, corrective actions by water management (e.g., emergency water releases to slow saltwater intrusion during periods of high drought) guided by high-frequency monitoring provides managers with new tools to rapidly respond to observed or predicted environmental problems. Likewise, as this region is clearly sensitive to managed inflows, high-frequency measurements are increasingly critical in the monitoring of estuarine response to changes in freshwater inputs.

Linking Short-Term and Long-Term Fluxes

Hydrology is the primary driver of DOC fluxes, and the strong linear fits in **Figure 6** confirm this. However, differences in fluxes based on monitoring frequency of DOC concentrations are evident through the deviations of fluxes from the 1:1 line. In general, D&W time-series cluster together close to 1:1 (**Figure 6A**), suggesting that during periods of lower freshwater inflows and therefore less variable filtered discharge (**Figure 2**), interpolating daily DOC fluxes from monthly DOC values is relatively accurate. In contrast, T time-series show more variability (**Figure 6B**), where T1 flux calculations closely follow the 1:1 line but T2 does not. In particular, high flux values during T2 are dramatically over-estimated (up to 180%) by interpolation of monthly DOC to daily resolution. This is likely due to large and rapid fluctuations in discharge (**Figure 2**) driving rapid changes in DOC concentrations. As such, interpolation of daily fluxes from monthly DOC sampling frequencies may be applicable during periods of relatively static discharge, but is not sufficiently accurate to constrain DOC export rates during periods of variable freshwater flows. This supports previous findings that weekly grab sampling was temporally inadequate to characterize DOC fluxes during rapid shifts in hydrology (Jollymore et al., 2012; Pellerin et al., 2012). Thus, current long-term monitoring projects seeking to better constrain C budgets in dynamic aquatic systems like estuaries could greatly benefit from the simultaneous application of high-frequency measurements.

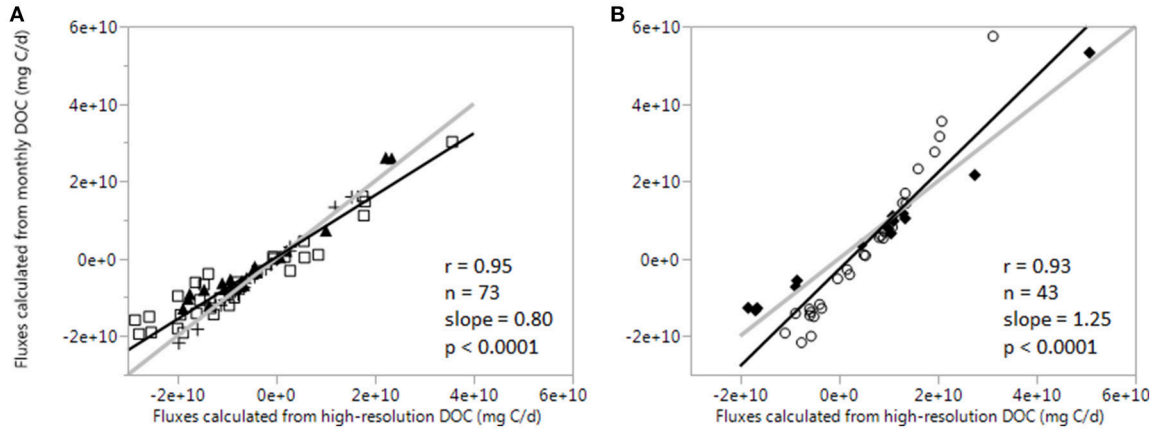

FIGURE 6 | Comparison of DOC fluxes calculated using the same discharge data but different data sources of DOC (different sampling resolutions). Fluxes calculated from monthly grab samples are on the y-axis, fluxes calculated from daily averges of high-resolution FDOM measurements are on the x-axis. **(A)** Plots D&W time-series (D1: open squares, D2: solid triangles, W1: crosses). **(B)** Plots T time-series (T1: solid diamonds, T2: open circles). Solid gray lines are best fit linear regressions and dashed black lines represent a 1:1 line.

CONCLUSIONS

A suite of environmental drivers, including salinity, stage and tidally filtered discharge, were identified as regulators of high-frequency FDOM patterns in the Shark River estuary. Values for FDOM were dynamic at tidal time-scales, changing in excess of 100% between consecutive low and high tides during periods of high freshwater discharge. The drivers of FDOM manifested in multiple distinct patterns, with salinity and stage varying semi-diurnally with tides, and knees in ebb tide stage corresponding to spikes in FDOM potentially attributed to mangrove porewater inputs accounting for up to 24% the tidal FDOM signal, particularly during periods of higher inundation. Freshwater discharge also controlled daily and multi-day changes in FDOM (up to ±25%), indicating hydrologically driven shifts in DOC concentration, and potentially source. The influence of water management on DOC dynamics in the mangrove estuary demonstrated the capability of managed inflows to restore the salinity gradient and accompanying estuarine C dynamics following pronounced drought and elevated sea levels. Rainfall was observed to alter DOC concentrations but had less influence over salinity and FDOM than water management (potentially related to drought conditions during much of this study). In general, managed inflows most strongly affected FDOM dynamics during seasonal transitions while precipitation preferentially and expectedly, controlled FDOM during the onset of the wet season. While management strategies currently focus on longer term hydrologic response (e.g., seasonal to inter-annual) in the context of Everglades restoration, rapid response of the coastal zone to freshwater inflows suggests the ability of water management to control hydrology in the mangrove ecotone at much shorter time-scales. Since response of DOC mixing and source dynamics to environmental drivers changes across temporal scales, integration of high-frequency data into current long-term monitoring programs is essential to understand temporally complex relationships between water quality and hydrology.

Hydrology, climate and management have all been identified as drivers of long-term DOC export in the Shark River (Regier et al., 2016), and findings here generally support that these drivers apply to short-term (hours to days) variations in DOC (based on FDOM as a proxy). Adaptive restoration management relies on constantly improving our understanding of ecosystem function and response to climatic and management factors. Further investigating key ecological indicators like biogeochemistry and nutrient transport spanning spatial and temporal scales will advance modeling capabilities and inform management decision-making. High-resolution measurements of FDOM provide new insights into organic matter cycling in coastal systems and indicate the potential value of high-frequency data to complement and expand existing long-term monitoring programs through a temporally integrated understanding of biogeochemical processes and nutrient budgets in dynamic coastal ecosystems.

AUTHOR CONTRIBUTIONS

PR performed field work, data analysis, interpretations, and contributed to writing the manuscript. RJ obtained the funding to support this study, designed the study, assisted in data analyses and interpretation and writing the manuscript.

ACKNOWLEDGMENTS

This work was primarily supported through the George Barley Endowment and is associated with the NSF-funded Florida Coastal Everglades LTER (DBI-0620409) and the SFWSC programs. The authors thank John Kominoski for helpful comments on the original manuscript, Mike Rugge for assistance

with **Figure 1** and Rafael Travieso for help in the field. The authors also thank Piotr Kowalczuk and Heather Erin Reader for comments that greatly improved this manuscript. This is contribution number 816 from the Southeast Environmental Research Center.

SUPPLEMENTARY MATERIAL

The Supplementary Material for this article can be found online at: http://journal.frontiersin.org/article/10.3389/fmars.2016.00250/full#supplementary-material

REFERENCES

Ardón, M., Helton, A. M., and Bernhardt, E. S. (2016). Drought and saltwater incursion synergistically reduce dissolved organic carbon export from coastal freshwater wetlands. *Biogeochemistry* 127, 411–426. doi: 10.1007/s10533-016-0189-5

Ballings, M., and Van den Poel, D. (2013). *AUC: Threshold Independent Performance Measures for Probabilistic Classifiers*. R package version 0.3.0. Available online at: https://CRAN.R-project.org/package=AUC

Bauer, J. E., Cai, W.-J., Raymond, P. A., Bianchi, T. S., Hopkinson, C. S., and Regnier, P. A. G. (2013). The changing carbon cycle of the coastal ocean. *Nature* 504, 61–70. doi: 10.1038/nature12857

Bergamaschi, B. A., Krabbenhoft, D. P., Aiken, G. R., Patino, E., Rumbold, D. G., and Orem, W. H. (2012). Tidally driven export of dissolved organic carbon, total mercury, and methylmercury from a mangrove-dominated estuary. *Environ. Sci. Technol.* 46, 1371–1378. doi: 10.1021/es2029137

Bouillon, S., Middelburg, J. J., Dehairs, F., Borges, A. V., Abril, G., Flindt, M. R., et al. (2007). Importance of intertidal sediment processes and porewater exchange on the water column biogeochemistry in a pristine mangrove creek (Ras Dege, Tanzania). *Biogeosciences* 4, 311–322. doi: 10.5194/bg-4-311-2007

Boyer, J. N., Fourqurean, J. W., and Jones, R. D. (1997). Spatial characterization of water quality in Florida Bay and Whitewater Bay by multivariate analyses: zones of similar influence. *Estuaries* 20, 743–758. doi: 10.2307/1352248

Breithaupt, J. L., Smoak, J. M., Smith, T. J., and Sanders, C. J. (2014). Temporal variability of carbon and nutrient burial, sediment accretion, and mass accumulation over the past century in a carbonate platform mangrove forest of the Florida Everglades. *J. Geophys. Res. Biogeosci.* 119, 2032–2048. doi: 10.1002/2014jg002715

Bridgham, S. D., Megonigal, J. P., Keller, J. K., Bliss, N. B., and Trettin, C. (2006). The carbon balance of North American wetlands. *Wetlands* 26, 889–916. doi: 10.1672/0277-5212(2006)26[889:TCBONA]2.0.CO;2

Cahoon, D. R., and Lynch, J. C. (1997). Vertical accretion and shallow subsidence in a mangrove forest of southwestern Florida, USA. *Mangroves Salt Marshes* 1, 173–186. doi: 10.1023/A:1009904816246

Castañeda-Moya, E., Twilley, R. R., and Rivera-Monroy, V. H. (2013). Allocation of biomass and net primary productivity of mangrove forests along environmental gradients in the Florida Coastal Everglades, USA. *For. Ecol. Manage.* 307, 226–241. doi: 10.1016/j.foreco.2013.07.011

Cawley, K. M., Yamashita, Y., Maie, N., and Jaffé, R. (2014). Using optical properties to quantify fringe mangrove inputs to the dissolved organic matter (DOM) pool in a subtropical estuary. *Estuaries Coasts* 37, 399–410. doi: 10.1007/s12237-013-9681-5

Chambers, L. G., Davis, S. E., Troxler, T., Boyer, J. N., Downey-Wall, A., and Scinto, L. J. (2014). Biogeochemical effects of simulated sea level rise on carbon loss in an Everglades mangrove peat soil. *Hydrobiologia* 726, 195–211. doi: 10.1007/s10750-013-1764-6

Chen, M., Maie, N., Parish, K., and Jaffé, R. (2013). Spatial and temporal variability of dissolved organic matter quantity and composition in an oligotrophic subtropical coastal wetland. *Biogeochemistry* 115, 167–183. doi: 10.1007/s10533-013-9826-4

Chmura, G. L., Anisfeld, S. C., Cahoon, D. R., and Lynch, J. C. (2003). Global carbon sequestration in tidal, saline wetland soils. *Global Biogeochem. Cycles* 17, 1111. doi: 10.1029/2002GB001917

Davidson, E. A., and Janssens, I. A. (2006). Temperature sensitivity of soil carbon decomposition and feedbacks to climate change. *Nature* 440, 165–173. doi: 10.1038/nature04514

Dittmar, T., and Lara, R. J. (2001). Driving forces behind nutrient and organic matter dynamics in a mangrove tidal creek in North Brazil. *Estuar. Coast. Shelf Sci.* 52, 249–259. doi: 10.1006/ecss.2000.0743

Downing, B. D., Boss, E., Bergamaschi, B. A., Fleck, J. A., Lionberger, M. A., Ganju, N. K., et al. (2009). Quantifying fluxes and characterizing compositional changes of dissolved organic matter in aquatic systems *in situ* using combined acoustic and optical measurements. *Limnol. Oceanogr. Methods* 7, 119–131. doi: 10.4319/lom.2009.7.119

Downing, B. D., Pellerin, B. A., Bergamaschi, B. A., Saraceno, J. F., and Kraus, T. E. C. (2012). Seeing the light: the effects of particles, dissolved materials, and temperature on *in situ* measurements of DOM fluorescence in rivers and streams. *Limnol. Oceanogr. Methods* 10, 9. doi: 10.4319/lom.2012.10.767

Duever, M. J., Meeder, J. F., Meeder, L. C., and McCollom, J. M. (1994). "The climate of South Florida and its role in shaping the Everglades ecosystem," in *Everglades: the Ecosystem and Its Restoration*, eds S. M. Davis and J. C. Ogden (Boco Raton, FL: St. Lucie Press), 225–248.

Estenoz, S., and Bush, E. (2015). Everglades restoration science and decision-making in the face of climate change: a management perspective. *Environ. Manage.* 55, 876–883. doi: 10.1007/s00267-015-0452-x

Etheridge, J. R., Birgand, F., Osborne, J. A., Osburn, C. L., Burchell, M. R., and Irving, J. (2014). Using *in situ* ultraviolet-visual spectroscopy to measure nitrogen, carbon, phosphorus, and suspended solids concentrations at a high frequency in a brackish tidal marsh. *Limnol. Oceanogr. Meth.* 12, 10–22. doi: 10.4319/lom.2014.12.10

Evans, C. D., Monteith, D. T., and Cooper, D. M. (2005). Long-term increases in surface water dissolved organic carbon: observations, possible causes and environmental impacts. *Environ. Pollut.* 137, 55–71. doi: 10.1016/j.envpol.2004.12.031

Fellman, J. B., Spencer, R. G. M., Hernes, P. J., Edwards, R. T., D'Amore, D. V., and Hood, E. (2010). The impact of glacier runoff on the biodegradability and biochemical composition of terrigenous dissolved organic matter in near-shore marine ecosystems. *Mar. Chem.* 121, 112–122. doi: 10.1016/j.marchem.2010.03.009

Flagg, C. N., Vermersch, J. A., and Beardsley, R. C. (1976). *New England Shelf dynamics experiment (March, 1974) Data Report Part II: The Moored Array*. MIT Report, 76–1.

Gaiser, E., and Childers, D. (2016). *Water Quality Data (Grab Samples) from the Shark River Slough, Everglades National Park (FCE), from May 2001 to Present. Long Term Ecological Research Network*. doi: 10.6073/pasta/bb732e1e254c2a797afee65e6c21d535

Ganju, N. K., Miselis, J. L., and Aretxabaleta, A. L. (2014). Physical and biogeochemical controls on light attenuation in a eutrophic, back-barrier estuary. *Biogeosciences* 11, 7193–7205. doi: 10.5194/bg-11-7193-2014

He, D., Mead, R. N., Belicka, L., Pisani, O., and Jaffé, R. (2014). Assessing source contributions to particulate organic matter in a subtropical estuary: a biomarker approach. *Org. Geochem.* 75, 129–139. doi: 10.1016/j.orggeochem.2014.06.012

Hedges, J. I., Keil, R. G., and Benner, R. (1997). What happens to terrestrial organic matter in the ocean? *Org. Geochem.* 27, 195–212. doi: 10.1016/S0146-6380(97)00066-1

Hu, C., Muller-Karger, F. E., and Zepp, R. G. (2002). Absorbance, absorption coefficient, and apparent quantum yield: a comment on common ambiguity in the use of these optical concepts. *Limnol. Oceanogr.* 47, 1261–1267. doi: 10.4319/lo.2002.47.4.1261

Jaffé, R., Boyer, J. N., Lu, X., Maie, N., Yang, C., Scully, N. M., et al. (2004). Source characterization of dissolved organic matter in a subtropical mangrove-dominated estuary by fluorescence analysis. *Mar. Chem.* 84, 195–210. doi: 10.1016/j.marchem.2003.08.001

Jollymore, A., Johnson, M. S., and Hawthorne, I. (2012). Submersible UV-Vis spectroscopy for quantifying streamwater organic carbon dynamics: implementation and challenges before and after forest harvest in a headwater stream. *Sensors (Basel)* 12, 3798–3813. doi: 10.3390/s120403798

Kirchner, J. W., Feng, X. H., Neal, C., and Robson, A. J. (2004). The fine structure of water-quality dynamics: the (high-frequency) wave of the future. *Hydrol. Process.* 18, 1353–1359. doi: 10.1002/hyp.5537

Kowalczuk, P., Zablocka, M., Sagan, S., and Kulinski, K. (2010). Fluorescence measured *in situ* as a proxy of CDOM absorption and DOC concentration in the Baltic Sea. *Oceanologia* 52, 431–471. doi: 10.5697/oc.52-3.431

Kristensen, E., and Alongi, D. M. (2006). Control by fiddler crabs (*Uca vocans*) and plant roots (*Avicennia marina*) on carbon, iron, and sulfur biogeochemistry in mangrove sediment. *Limnol. Oceanogr.* 51, 1557–1571. doi: 10.4319/lo.2006.51.4.1557

Lee, E.-J., Yoo, G.-Y., Jeong, Y., Kim, K.-U., Park, J.-H., and Oh, N.-H. (2015). Comparison of UV–VIS and FDOM sensors for *in situ* monitoring of stream DOC concentrations. *Biogeosciences* 12, 3109–3118. doi: 10.5194/bg-12-3109-2015

Maie, N., Boyer, J. N., Yang, C., and Jaffé, R. (2006a). Spatial, geomorphological, and seasonal variability of CDOM in estuaries of the Florida Coastal Everglades. *Hydrobiologia* 569, 135–150. doi: 10.1007/s10750-006-0128-x

Maie, N., Jaffé, R., Miyoshi, T., and Childers, D. L. (2006b). Quantitative and qualitative aspects of dissolved organic carbon leached from senescent plants in an oligotrophic wetland. *Biogeochemistry* 78, 285–314. doi: 10.1007/s10533-005-4329-6

Maie, N., Yamashita, Y., Cory, R. M., Boyer, J. N., and Jaffé, R. (2012). Application of excitation emission matrix fluorescence monitoring in the assessment of spatial and seasonal drivers of dissolved organic matter composition: sources and physical disturbance controls. *Appl. Geochem.* 27, 917–929. doi: 10.1016/j.apgeochem.2011.12.021

Mazda, Y., Kanazawa, N., and Wolanski, E. (1995). Tidal asymmetry in mangrove creeks. *Hydrobiologia* 295, 51–58. doi: 10.1007/BF00029110

McKee, K. L. (2011). Biophysical controls on accretion and elevation change in Caribbean mangrove ecosystems. *Estuar. Coast. Shelf Sci.* 91, 475–483. doi: 10.1016/j.ecss.2010.05.001

McPherson, M. L., Hill, V. J., Zimmerman, R. C., and Dierssen, H. M. (2011). The optical properties of greater Florida bay: implications for seagrass abundance. *Estuar. Coast. Shelf Sci.* 34, 1150. doi: 10.1007/s12237-011-9411-9

Obeysekera, J., Barnes, J., and Nungesser, M. (2014). Climate sensitivity runs and regional hydrologic modeling for predicting the response of the greater Florida Everglades ecosystem to climate change. *Environ. Manage.* 55, 749–762. doi: 10.1007/s00267-014-0315-x

Orem, W., Newman, S., Osborne, T. Z., and Reddy, K. R. (2015). Projecting changes in Everglades soil biogeochemistry for carbon and other key elements, to possible 2060 climate and hydrologic scenarios. *Environ. Manage.* 55, 776–798. doi: 10.1007/s00267-014-0381-0

Osburn, C. L., Retamal, L., and Vincent, W. F. (2009). Photoreactivity of chromophoric dissolved organic matter transported by the Mackenzie River to the Beaufort Sea. *Mar. Chem.* 115, 10–20. doi: 10.1016/j.marchem.2009.05.003

Pellerin, B. A., Saraceno, J. F., Shanley, J. B., Sebestyen, S. D., Aiken, G. R., Wollheim, W. M., et al. (2012). Taking the pulse of snowmelt: *in situ* sensors reveal seasonal, event and diurnal patterns of nitrate and dissolved organic matter variability in an upland forest stream. *Biogeochemistry* 108, 183–198. doi: 10.1007/s10533-011-9589-8

Qualls, R. G., and Richardson, C. J. (2003). Factors controlling concentration, export, and decomposition of dissolved organic nutrients in the Everglades of Florida. *Biogeochemistry* 62, 197–229. doi: 10.1023/A:1021150503664

Regier, P., Brice-o, H. O., and Jaffé, R. (2016). Long-term environmental drivers of DOC fluxes: linkages between management, hydrology and climate in a subtropical coastal estuary. *Estuar. Coast. Shelf Sci.* 182, 112–122. doi: 10.1016/j.ecss.2016.09.017

Romigh, M. M., Davis, S. E., Rivera-Monroy, V. H., and Twilley, R. R. (2006). Flux of organic carbon in a riverine mangrove wetland in the Florida Coastal Everglades. *Hydrobiologia* 569, 505–516. doi: 10.1007/s10750-006-0152-x

Ryder, E., de Eyto, E., Dillane, M., Poole, R., and Jennings, E. (2014). Identifying the role of environmental drivers in organic carbon export from a forested peat catchment. *Sci. Total Environ.* 490, 28–36. doi: 10.1016/j.scitotenv.2014.04.091

Saha, A. K., Moses, C. S., Price, R. M., Engel, V., Smith, T. J. III, and Anderson, G. (2012). A hydrological budget (2002–2008) for a large subtropical wetland ecosystem indicates marine groundwater discharge accompanies diminished freshwater flow. *Estuaries Coasts* 35, 459–474. doi: 10.1007/s12237-011-9454-y

Shank, G. C., Lee, R., Vahatalo, A., Zepp, R. G., and Bartels, E. (2010). Production of chromophoric dissolved organic matter from mangrove leaf litter and floating Sargassum colonies. *Mar. Chem.* 119, 172–181. doi: 10.1016/j.marchem.2010.02.002

Sklar, F. H., Chimney, M. J., Newman, S., McCormick, P., Gawlik, D., Miao, S., et al. (2005). The ecological–societal underpinnings of Everglades restoration. *Front. Ecol. Environ.* 3, 161–169. doi: 10.1890/1540-9295(2005)003[0161:TEUOER]2.0.CO;2

Sobczak, W. V., and Raymond, P. A. (2015). Watershed hydrology and dissolved organic matter export across time scales: minute to millennium. *Freshw. Sci.* 34, 392–398. doi: 10.1086/679747

Spencer, R. G. M., Pellerin, B. A., Bergamaschi, B. A., Downing, B. D., Kraus, T. E. C., Smart, D. R., et al. (2007). Diurnal variability in riverine dissolved organic matter composition determined by *in situ* optical measurement in the San Joaquin River (California, USA). *Hydrol. Process.* 21, 3181–3189. doi: 10.1002/hyp.6887

Stieglitz, T. C., Clark, J. F., and Hancock, G. J. (2013). The mangrove pump: the tidal flushing of animal burrows in a tropical mangrove forest determined from radionuclide budgets. *Geochim. Cosmochim. Acta* 102, 12–22. doi: 10.1016/j.gca.2012.10.033

Tranvik, L. J. (1998). "Degradation of dissolved organic matter in humic waters by bacteria," in *Aquatic Humic Substances Ecological Studies*, eds D. O. Hessen and L. J. Tranvik (Berlin, Heidelberg: Springer), 259–283.

Watras, C. J., Hanson, P. C., Stacy, T. L., Morrison, K. M., Mather, J., Hu, Y.-H., et al. (2011). A temperature compensation method for CDOM fluorescence sensors in freshwater. *Limnol. Oceanogr. Methods* 9, 296–301. doi: 10.4319/lom.2011.9.296

Watras, C. J., Morrison, K. A., Crawford, J. T., McDonald, C. P., Oliver, S. K., and Hanson, P. C. (2015). Diel cycles in the fluorescence of dissolved organic matter in dystrophic Wisconsin seepage lakes: implications for carbon turnover. *Limnol. Oceanogr.* 60:482–496. doi: 10.1002/lno.10026

Wilson, H. F., Saiers, J. E., Raymond, P. A., and Sobczak, W. V. (2013). Hydrologic drivers and seasonality of dissolved organic carbon concentration, nitrogen content, bioavailability, and export in a Forested New England Stream. *Ecosystems* 16, 604–616. doi: 10.1007/s10021-013-9635-6

Yamashita, Y., Boyer, J. N., and Jaffé, R. (2013). Evaluating the distribution of terrestrial dissolved organic matter in a complex coastal ecosystem using fluorescence spectroscopy. *Cont. Shelf Res.* 66, 136–144. doi: 10.1016/j.csr.2013.06.010

Yamashita, Y., and Jaffé, R. (2008). Characterizing the Interactions between Trace Metals and Dissolved Organic Matter Using Excitation–Emission Matrix and Parallel Factor Analysis. *Environ. Sci. Technol.* 42, 7374–7379. doi: 10.1021/es801357h

Yamashita, Y., Scinto, L. J., Maie, N., and Jaffé, R. (2010). Dissolved organic matter characteristics across a subtropical wetland's landscape: application of optical properties in the assessment of environmental dynamics. *Ecosystems* 13, 1006–1019. doi: 10.1007/s10021-010-9370-1

Conflict of Interest Statement: The authors declare that the research was conducted in the absence of any commercial or financial relationships that could be construed as a potential conflict of interest.

frontiers in Marine Science

ORIGINAL RESEARCH
published: 28 February 2017
doi: 10.3389/fmars.2017.00021

Surface Gradients in Dissolved Organic Matter Absorption and Fluorescence Properties along the New Zealand Sector of the Southern Ocean

Eurico J. D'Sa[1]* *and Hyun-cheol Kim*[2]

[1] Department of Oceanography and Coastal Sciences, Louisiana State University, Baton Rouge, LA, USA, [2] Korea Polar Research Institute, Incheon, South Korea

The Southern Ocean plays a critical role in the global carbon cycle; dissolved organic matter (DOM), a component in the carbon cycling, can be characterized optically. Sea surface chromophoric dissolved organic matter (CDOM) absorption and fluorescence properties were examined in the New Zealand sector of the Southern Ocean (NZSSO) along a transect encompassing various hydrographic fronts associated with the Antarctic Circumpolar Current (ACC) during summer. Phytoplankton chlorophyll, dissolved organic carbon (DOC) and CDOM absorption were observed to be most elevated off the New Zealand shore and then decreased to low values [chlorophyll: 0.21 ± 0.06 mg m^{-3}; DOC: 54.19 ± 4.02 μM, and CDOM absorption coefficient at 325 nm (a_g325): 0.097 ± 0.061 m^{-1}] between the Subtropical (STF) and Antarctic Polar (APF) Fronts. Increases in phytoplankton biomass and DOC concentrations between the fronts were associated with meanders or eddies observed in satellite sea surface salinity and chlorophyll imagery. Overall, CDOM absorption was the dominant contributor to total absorption at 443 nm with implications for ocean color. Beyond the APF in the Antarctic Zone, an elevated chlorophyll band likely associated with upwelled waters transitioned to low chlorophyll in the summer ice edge zone that influenced DOM optical properties. A latitudinal increase in a_g325 and corresponding decrease in spectral slope S (μm^{-1}) poleward from the STF could be due to a combination of factors including, decreasing CDOM photooxidation, upwelling of high-CDOM waters or bacterial CDOM production in the Antarctic Zone. Parallel factor analysis (PARAFAC) of fluorescence spectra identified two protein-like (C1 and C2) and two humic-like (C3 and C4) components common in the global ocean. a_g325 and the humic-like C4 fluorescent component were positively correlated to chlorophyll, indicating biological control. Surface distribution of the protein-like C1 and C2 and the marine humic-like C3 components showed patterns that appeared to be influenced by both physical and biological processes. This study provides insights into surface CDOM optical properties and its transformation along a complex topographically influenced sector of the Southern Ocean that could be used to trace changes linked to the meridional overturning circulation.

Keywords: CDOM, DOC, EEMs, PARAFAC, chlorophyll, absorption, Southern Ocean

OPEN ACCESS

Edited by:
Michael Seidel,
University of Oldenburg, Germany

Reviewed by:
X. Antón Álvarez-Salgado,
Spanish National Research Council, Spain
Isabel Reche,
University of Granada, Spain
Leanne C. Powers,
University of Maryland Center for Environmental Science, USA

***Correspondence:**
Eurico J. D'Sa
ejdsa@lsu.edu

Specialty section:
This article was submitted to Marine Biogeochemistry, a section of the journal Frontiers in Marine Science

Received: *07 November 2016*
Accepted: *17 January 2017*
Published: *28 February 2017*

Citation:
D'Sa EJ and Kim H-c (2017) Surface Gradients in Dissolved Organic Matter Absorption and Fluorescence Properties along the New Zealand Sector of the Southern Ocean. Front. Mar. Sci. 4:21. doi: 10.3389/fmars.2017.00021

INTRODUCTION

The Southern Ocean, comprising a region from the Subtropical Front (STF) to the Antarctic continent connects the three main oceanic basins through the easterly flowing Antarctic Circumpolar Current (ACC) that plays a significant role in the global biogeochemical processes and carbon cycling (Sarmiento and LeQuere, 1996). Driven by the strong westerly winds, the ACC consists of several narrow and persistent fronts that contribute to the ocean overturning circulation and the upwelling of carbon and nutrients to the surface ocean that supports much of the ocean's productivity (Orsi et al., 1995; Belkin and Gordon, 1996; Daly et al., 2001; Budillon and Rintoul, 2003; Marshall and Speer, 2012). While the Southern Ocean is considered a high-nutrient low-chlorophyll (HNLC) region due mainly to iron limitation (Boyd et al., 1999), many productive regions especially during the spring-summer months contribute significantly to the global primary production, carbon cycling, and biogeochemical processes (Arrigo et al., 1998; Daly et al., 2001; Hiscock et al., 2003; Honjo, 2004; McNeil and Tilbrook, 2009). The chromophoric dissolved organic matter (CDOM) is the fraction of the dissolved organic matter (DOM) pool that absorbs light in the UV and visible region of the spectrum. It influences ocean color and light propagation in oceanic waters, and provides useful information on DOM sources and sinks (Blough and Del Vecchio, 2002; Nelson and Siegel, 2002, 2013; Swan et al., 2009).

Photosynthetic plankton in the surface ocean is the main source of oceanic DOM and is principally exported to deeper waters through mixing and downwelling of water parcels (Hansell and Carlson, 2001; Jiao et al., 2010; Hansell, 2013). Components of this DOM pool in the form of humic, fulvic, and amino acids impart characteristic absorption and fluorescence properties that can be used to characterize CDOM composition and the diagenetic state (Mopper and Schultz, 1993; Coble, 1996; Stedmon and Markager, 2005). CDOM can be produced *in situ* by biological production (authochthonous), primarily through microbial remineralization of organic matter or transported from terrestrial sources (Blough and Del Vecchio, 2002; D'Sa, 2008; D'Sa and DiMarco, 2009; Romera-Castillo et al., 2010). It is removed by photochemical degradation and microbial consumption and is influenced by physical processes such as circulation, upwelling, or mixing (Blough and Del Vecchio, 2002; Nelson et al., 2010). The spectral absorption property of CDOM especially over the narrow 275–295 nm wavelength interval (S or $S_{275-295}$) has been used to gain insights into source, molecular size and reactivity with elevated slope values linked to photo-oxidative degradation (Helms et al., 2008; D'Sa et al., 2014). While CDOM optical properties have been studied in various oceanic regions (Nelson and Siegel, 2002, 2013; Kitidis et al., 2006; Swan et al., 2009), only limited studies have been reported for the Southern Ocean (Kieber et al., 2009; Ortega-Retuerta et al., 2009; Del Castillo and Miller, 2011; Nelson et al., 2010; Nelson and Gauglitz, 2016).

A subfraction of CDOM that fluoresces when excited with UV light (fluorescent DOM or FDOM) is used in the characterization of CDOM using excitation-emission matrix spectroscopy (EEMs) wherein a three-dimensional fluorescence intensity landscape is obtained across a range of excitation (e.g., 250–450 nm) and emission (e.g., 290–550 nm) wavelengths (Coble, 1996). EEM spectra of different fractions of FDOM such as humic-like and protein-like fluorophores display characteristic signatures in the EEM spectra. For example, humic-like material with greater aromaticity ("A" and "C" type compounds typically of terrestrial origin) generally display broad fluorescence peaks with emission typically at longer wavelengths in comparison to marine humics or "M" type compounds attributed to biological activity. In contrast, protein-like fluorescent material display narrower peaks typically in the UV spectral region with characteristics similar to tryptophan and tyrosine-like amino acids likely derived from marine planktonic organisms or bacterial activity (Coble, 1996; Yamashita and Tanoue, 2003; Stedmon and Markager, 2005). Due to the overlapping contribution of the various fluorophores in the EEMs, statistical approaches such as parallel factor analysis (PARAFAC) are commonly used to decompose CDOM EEMs data into their individual fluorescent components that have provided a more quantitative and qualitative assessment of its composition (Stedmon et al., 2003; Stedmon and Bro, 2008) in various oceanic regions (Murphy et al., 2008; Jorgensen et al., 2011; Catalá et al., 2015, 2016; D'Sa et al., 2016), including the Southern Ocean (Wedborg et al., 2007; Nelson and Gauglitz, 2016).

A characteristic feature of the Southern Ocean is the presence of fronts (STF, SAF, APF, and SACCF) that transition the Southern Ocean from the warm subtropical waters into cold polar waters thus separating zones of uniform water properties in a series of step-like changes in temperature, salinity, and biogeochemical processes (Belkin and Gordon, 1996; Budillon and Rintoul, 2003; Honjo, 2004). In the New Zealand sector of the Southern Ocean (NZSSO), however, the location of these fronts are strongly influenced by prominent topographic features that include the Campbell Plateau, the Pacific Australian Ridge (PAR) and the highly productive Ross Sea to the south (Gordon, 1975). Surface CDOM absorption properties have previously been reported for the NZSSO during early spring (Kieber et al., 2009) while DOM fluorescence at a single wavelength has been reported for a transect on the western Pacific Ocean east of New Zealand (Yamashita et al., 2007). Knowledge on CDOM absorption contribution to the total absorption has been useful in improving satellite estimates of chlorophyll and primary production in the Southern Ocean (Reynolds et al., 2001; Siegel et al., 2002; Lee et al., 2011).

In this study, CDOM absorption and fluorescence properties were examined from surface measurements conducted during a transect of the Korean Research vessel *Araon* along the ~172°E meridian between New Zealand and Terra Nova Bay (TNB) in the Ross Sea. Additionally, surface absorption budgets were obtained to assess CDOM contribution to the total absorption field while satellite-derived salinity and chlorophyll estimates were used to assess synoptic large-scale features (e.g., meanders and eddies) to aid the interpretation of CDOM optical measurements in the NZSSO.

METHODS

Sampling and Study Area

Seawater samples (27) were collected from a flow-through system obtained from a depth of ~2 m as the Korean ice breaker and research vessel *Araon* transected from Christchurch, NZ to TNB in the western Ross Sea from 30 January to 6 February 2014 (**Figure 1**). Sub-samples were then filtered through GF/F filters and the filtrate stored in acid cleaned pre-combusted amber bottles with teflon-lined caps at 4°C in a refrigerator for later laboratory processing for CDOM absorption and fluorescence. Filtered GF/F samples were also preserved in a freezer for measurements of chlorophyll concentrations and particulate absorption. Sampling from the flow-through system was however discontinued between 68 and 74°S due to the presence of summer sea-ice. Seawater temperature was measured at the outflow of the flow-through system; however, differences in temperature between the inlet and outlet of the flow-through likely existed and the data has been mainly used to examine broad temperature trends along the transect. The main topographic features such as the Chatham Rise (CR), Campbell Plateau (CP), and the PAR system are shown (**Figure 1**), along with the locations of fronts such as the Subtropical (STF), Subantarctic (SAF) and its northern (NSAF) and southern (SSAF) branches, Antarctic Polar (APF), and the Southern Antarctic Circumpolar Current (SACCF) Fronts in the NZSSO (**Figure 1**).

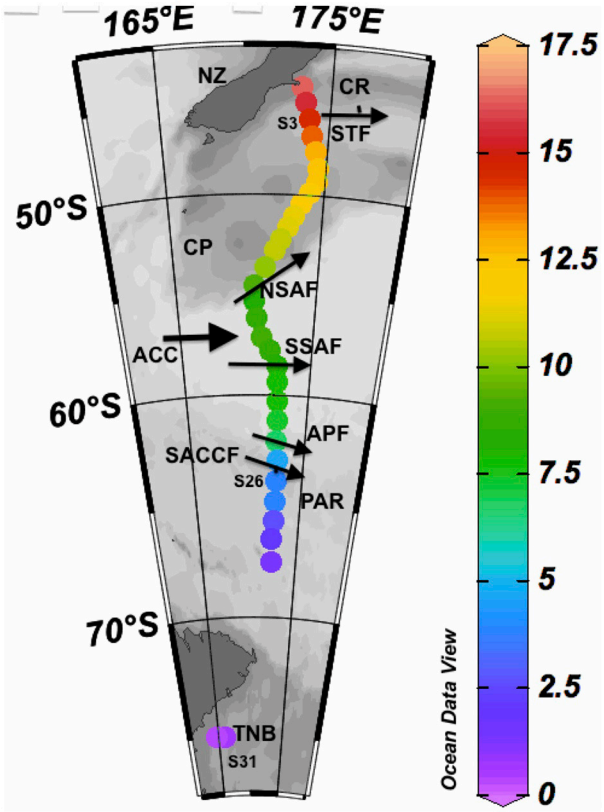

FIGURE 1 | Study site. Sea surface temperature (SST) shown at sampling stations obtained between 30 Jan and 6 Feb, 2014 along a transect between Christchurch, New Zealand (NZ) and Terra Nova Bay (TNB) in the western Ross Sea. Thick arrow indicates the direction of the Antarctic Circumpolar Current (ACC) and the thinner arrows indicate the approximate locations of the Subtropical Front (STF), the Subantarctic Front (SAF) and its northern (NSAF) and southern (SSAF) branches, the Antarctic Polar Front (APF), and the Southern Antarctic Circumpolar Current Front (SACCF). CR and PAR indicate the locations of the Chatham Rise and the Pacific Australian Ridge, respectively. Also shown are the locations of three sampling stations (S3, S26, S31) discussed in the text.

Chlorophyll Concentrations

Seawater samples (500 ml) were filtered through Whatman GF/F filters (25 mm diameter) for the fluorometric determination of chlorophyll (Holm-Hansen et al., 1965) using a Turner Designs Model 10AU fluorometer calibrated with pure chlorophyll a (Sigma Chemical Company).

DOC Measurements

Samples for dissolved organic carbon (DOC) were filtered through pre-rinsed Whatman GF/F filters and stored in acid cleaned, pre-combusted amber bottles with Teflon-lined caps in a freezer. Laboratory measurements of DOC were made on a Shimadzu TOC 5000A (with ASI-5000A autosampler) using a high temperature combustion method to convert carbon compounds to carbon dioxide, including using the Consensus Reference Material (CRM) for QA/QC (Benner and Strom, 1993; Hansell and Carlson, 2001).

CDOM and Particulate Absorption Measurements

Water samples collected from the flow-through system were filtered immediately through pre-rinsed Whatman GF/F filters under low vacuum and stored in acid cleaned, pre-combusted amber bottles at 4°C in the dark before laboratory analysis. After the filtered samples were allowed to reach ambient room temperature, absorbance measurements of CDOM (A(λ)) were obtained on a WPI Ultrapath™ system from 190 to 722 nm on either 0.5 m or 2.0 waveguide cells. To minimize differences in refractive index between sample and reference which cause offsets in absorbance measurements (D'Sa et al., 1999; D'Sa and DiMarco, 2009), a reference salt solution was prepared using granular NaCl (Mallinckrodt) and Milli-Q water to closely match the seawater samples. Absorbance data were corrected by subtracting the mean value over a 10 nm interval (695–705 nm) of the measured absorbance at 700 nm from each wavelength and the $a_g(\lambda)$ (m^{-1}) was calculated using the equation:

$$ag(\lambda) = 2.303 \times \frac{A(\lambda)}{l} \quad (1)$$

Absorption coefficient at 325 nm (a_g325) was used as a quantitative parameter of CDOM. The spectral slopes for the intervals of 275–295 nm (S or $S_{275-295}$, μm^{-1}) were calculated according to Helms et al. (2008). Due to very low CDOM absorption in the visible, absorption especially at 443 nm was below the detection limit of the instrument for some samples.

Particulate absorption measurements were obtained using the quantitative filter technique (QFT) procedure (Mitchell

et al., 2003). To measure the particulate absorption, 500 ml of surface seawater samples were filtered onto 25 mm GF/F filters under low vacuum and preserved at −80°F before laboratory analysis. Optical density of particles on the filter paper were measured in the transmission mode on a Perkin-Elmer Lambda 850 with an integrating sphere and also on a fiber-optic based spectrophotometer (Naik and D'Sa, 2012) as it provided better sensitivity in comparison to the Lambda 850. Details on the laboratory analysis of particulate absorption on the two systems have been previously described (Naik and D'Sa, 2012; Naik et al., 2013). As both CDOM and particulate absorption were very low, measurements on both the spectrophotometer and waveguide were sensitive to instrument noise and baseline variability resulting in uncertainties for some samples in the visible band of the spectrum. Thus, due to the very low absorption values, the relative absorption budget is reported only at 443 nm, a commonly used wavelength.

EEMs Measurements and PARAFAC Analysis

Filtered seawater samples used for CDOM absorption measurements were also used to record EEMs using a FluoroMax-4 (Jobin Yvon Horiba) fluorometer by scanning the emission spectra from 290 to 550 nm at 5 nm intervals over excitation wavelengths between 250 and 450 nm at 5 nm increments. The EEMs spectra were obtained after correction of the fluorescence spectra for instrument bias, and the water Raman normalization of the fluorescence intensity (Singh et al., 2010; D'Sa et al., 2014). Due to low absorbance of the samples, there was no requirement for inner filter correction of the fluorescence data. The resulting EEM fluorescence observations were evaluated by PARAFAC analysis using the DOM-Fluor toolbox (Stedmon and Bro, 2008), with the model constrained by non-negativity, and run with three to seven components. Model validation was carried out using split-half analysis, residual analysis and random starts (Stedmon and Bro, 2008; D'Sa et al., 2016).

Satellite Data

MODIS Aqua chlorophyll imagery at 4 km were obtained from NASA Ocean Color Giovanni website (giovanni.gsfc.nasa.gov). Due to extensive cloud cover over the study area, imagery averaged between 26 Jan and 10 Feb, 2014 were used that included the sampling period (30 Jan–6 Feb, 2014). Sea surface salinity data (7-day average) from the Aquarius microwave instrument onboard the Aquarius/SAC-D satellite was obtained from NASA Jet Propulsion Laboratory corresponding to the sampling period. A comparison study of the 1° gridded Aquarius sea surface salinity with Argo array salinity product showed standard deviation in salinity values ranging between 0.15 and 0.6 for high-latitude oceans (Lee, 2016).

RESULTS

Surface Physical Properties

Sea surface temperature (∼2 m depth) measured on board the *Araon* during its 8-day transect from New Zealand to Terra Nova Bay (TNB) show gradients and a decreasing meridional trend in temperature (**Figure 1**). Poleward decrease and gradients in sea surface salinity are also observed in the Aquarius satellite salinity imagery (**Figure 2A**) and at matching station locations extracted from the satellite data (**Figure 3**). While frontal positions are best identified from hydrographic data across the ACC, in this study we use underway data and satellite imagery combined with historical observations (Budillon and Rintoul, 2003) to infer latitudinal locations of the fronts during the study period (**Figure 3**).

The STF, which separates the warmer and saltier subtropical surface water from the cooler and fresher subantarctic surface water, marks the northernmost extent of the ACC and remains close to the coast south and east of NZ and then moves offshore. Large gradients in salinity and temperature observed in the convergence zone (**Figures 1**, **2**) have been associated with considerable eddy activity southeast of NZ (Williams, 2004; Fernandez et al., 2014). South of NZ, the Sub Antarctic Front (SAF), a major front of the ACC system bifurcates into northern (NSAF) and southern (SSAF) branches with the NSAF (∼53°S) closely following the steep southeastern flank of the Campbell Plateau (CP) and the SSAF (∼58°S) found over the abyssal plain of the south-west Pacific Basin (Budillon and Rintoul, 2003; Fernandez et al., 2014). Large variability in sea surface salinity south of NZ (**Figure 2A**) indicates eddies and meanders associated with these fronts in the subantarctic zone lying between the STF and SAF (Budillon and Rintoul, 2003). The APF located at ∼62°S and generally found between 60.2 and 62.8°S, is characterized by large gradients in temperature and salinity (**Figure 3**) and delineates the cold Antarctic Surface Water (ASW) to the south (Antarctic Zone) from the warmer subantarctic surface waters to the north. The Antarctic Zone contains the Antarctic divergence (Daly et al., 2001) and the southern boundary of the ACC (SACCF) which in this region follows closely the Pacific-Antarctic Ridge and is located at ∼63.8°S (Budillon and Rintoul, 2003). The seasonal ice zone, generally located south of the SACCF, was ice-covered south of 68°S during the transect. In the western Ross Sea, the Terra Nova Bay polynia is an ice-free coastal region with cold ASW (**Figures 1**, **3**; temperature up to +2°C, $S < 34.5$; Rivaro et al., 2011).

Surface Chlorophyll Distribution

Surface chlorophyll estimates from MODIS reveal elevated concentrations southeast of NZ and Chatham Rise and the STF region (**Figure 2B**). Along the rest of the transect from STF to APF, chlorophyll values were low with few elevated bands that appear related to eddies and meanders associated with the interaction of the STF and the SAF (**Figures 2A,B**). An elevated chlorophyll band south of the APF is observed in the Antarctic Zone while high chlorophyll values were observed further south in the TNB region of the western Ross Sea. A similar pattern was observed in surface chlorophyll from field observations along the transect (**Figure 3**) with low chlorophyll values in the core of the ACC between STF and APF (0.21 ± 0.06 mg m^{-3}) that varied in the range 0.12–0.38 mg

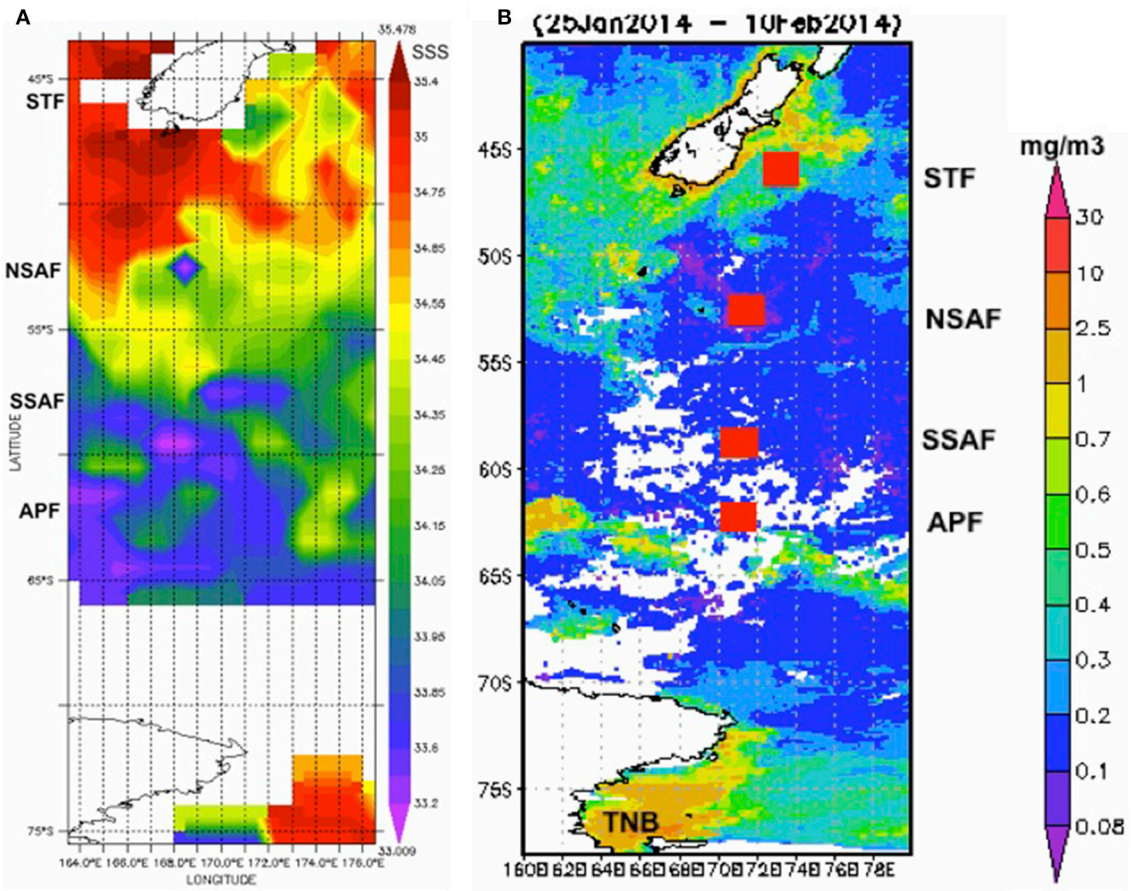

FIGURE 2 | Satellite imagery. (A) Aquarius satellite-derived sea surface salinity for the period 29 Jan–6 Feb, 2014 along the New Zealand sector of the Southern Ocean, and **(B)** MODIS-derived chlorophyll (25 Jan–10 Feb, 2014) with approximate locations of the Southern Ocean fronts (red squares).

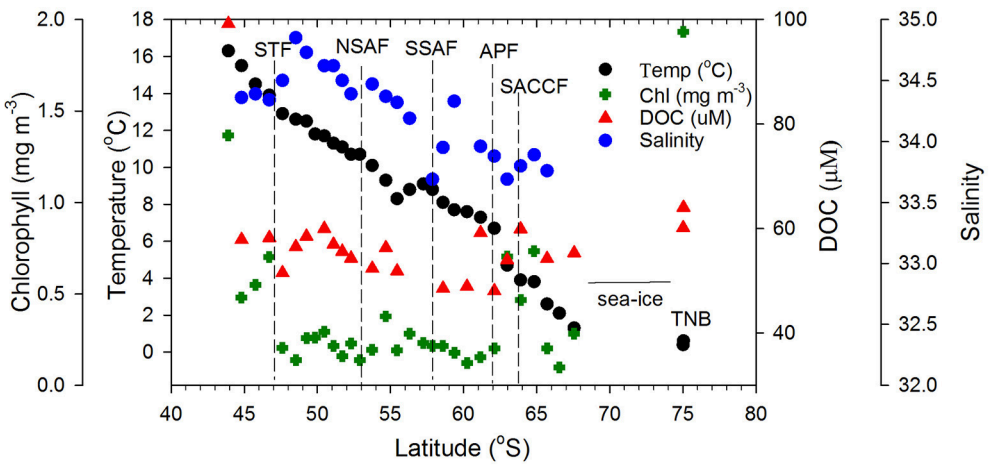

FIGURE 3 | Surface biophysical properties. Sea surface temperature, satellite-derived salinity, chlorophyll, and DOC concentrations along the transect. Dashed vertical lines represent the locations of the Southern Ocean fronts.

m^{-3}, and the more elevated values associated with peaks observed due to meanders and eddies (**Figure 2A**). Higher chlorophyll values were however observed off NZ shore and STF region (0.66 ± 0.43 mg m^{-3}), the elevated band south of the APF (0.64 ± 0.15 mg m^{-3}), with highest values in TNB (2.42 mg m^{-3}).

Surface Dissolved and Particulate Matter Absorption along the Transect

Surface DOC concentrations were high off the NZ shore (66.71±21.88 μM) and TNB (62.11 μM), with slightly elevated values observed coincident with chlorophyll peaks at 50°S, 55°S, and around the APF. In the ACC core (STF to APF) values ranged between 48.07 and 60.01 μM with a mean of 54.19 ± 4.02 μM. a_g325 between the STF and SACCF ranged between 0.024–0.145 m^{-1} (mean of 0.097 ± 0.061 m^{-1}) and showed an increasing trend poleward (**Figure 4**). a_g325 was however elevated in the NZ shelf waters (0.179 ± 0.110 m^{-1}) and in TNB (0.188 m^{-1}). The spectral slope S values (29.45 ± 3.71 μm^{-1}) generally showed an inverse relationship to a_g325 along the transect (**Figure 4**). S was low closest to the NZ shore (station 1) but increased toward STF and generally decreased poleward into the Antarctic Zone (**Figure 4**). a_g325 was positively correlated with chlorophyll (**Figure 5B**; r^2 = 0.48) but was uncorrelated to DOC concentrations (**Figure 5A**).

The relative absorption coefficients in the visible (443 nm) of CDOM, particulate matter (phytoplankton a_{phy} and nonalgal a_{nap}) varied across the transect (**Figure 6**) ranging for a_g443 from 0.0043 to 0.14 m^{-1}, $a_{phy}(443)$ from 0.0043 to 0.14 m^{-1}, and $a_{nap}(443)$ from detection limit to 0.0033 m^{-1}, respectively. Although $a_{nap}(443)$ contributed the least to the total absorption (<10%), its relative contribution increased closer to the NZ coast and south of the APF, coinciding with the band of elevated chlorophyll (**Figure 6A**). Variability in phytoplankton absorption $a_{phy}(443)$ was similar to chlorophyll along the transect with elevated values off the NZ shore and south of APF (**Figures 3**, **6A**). However, its contribution relative to CDOM at 443 nm was variable across the transect being generally greater in regions of high chlorophyll while CDOM dominated at other locations as also indicated by the ternary plot (**Figure 6B**).

Surface FDOM Properties

Typical EEMs spectra obtained from surface samples in the STF, APF, and TNB reveal the presence of prominent peaks in the spectra (**Figure 7A**). These peaks have traditionally been used to characterize CDOM composition using terminology such as A, C, M, B, and T peaks (Coble, 1996). The presence of the marine humic-like M peak (ex/em, ~300/380–420 nm) is clearly observed, while the fluorescence peaks associated with the protein-like material, namely, the tyrosine-like and tryptophan-like aromatic amino acids (in the UV spectral range) appear combined visually. In contrast, the typical humic-like A and C peaks though not visually observable, were present at low background levels. PARAFAC analysis identified four major fluorescent components in the surface waters between NZ and TNB (**Figure 7B**; **Table 1**). The excitation and emission loadings of each of the four components (**Figure 7B**, bottom right; **Table 1**) identified components 1 (C1) and C2 with excitation/emission (ex/em) wavelengths of 260/300 nm and 270/330 nm associated with tyrosine- and tryptophan-like material that is microbially produced (Yamashita and Tanoue, 2003; Murphy et al., 2008). Component 3 with ex/em wavelength of 295/400 nm has been previously identified as the marine or "M" humic-like component of microbial origin (Coble, 1996; Yamashita and Tanoue, 2003; Stedmon and Markager, 2005). The broad fluorescence peak of component 4 (C4) with primary (and secondary) ex/em wavelength peaks at <260(360)/460 nm is similar to previously identified terrestrial humic-like A and C like material and generally ubiquitous in the marine environment (Coble, 1996; Murphy et al., 2008, **Table 1**).

The distribution pattern of the four FDOM components differed along the transect (**Figure 8**). The humic-like C4 component was elevated off NZ shore and TNB and uniformly low between the STF and APF (**Figure 8A**) and was positively correlated to chlorophyll (**Figure 9A**). The C3 marine M-like humic component was found to be elevated off NZ and in regions

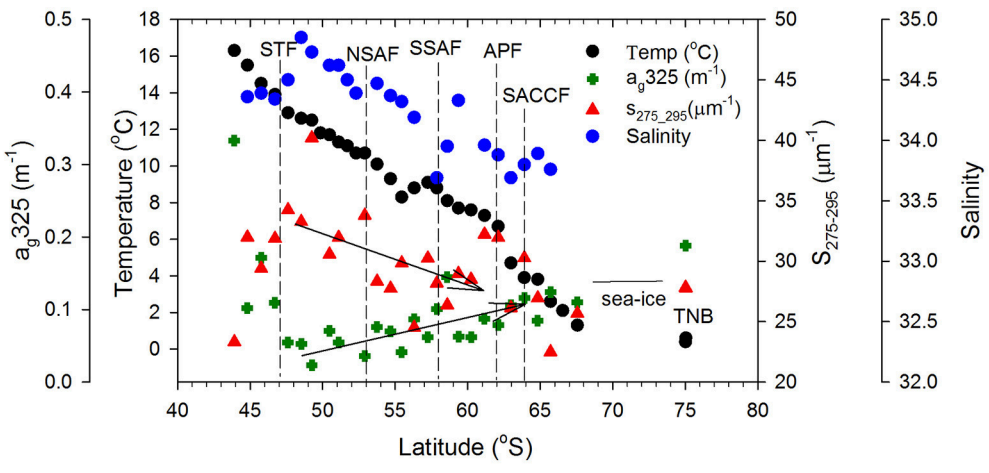

FIGURE 4 | CDOM optical properties. Sea surface temperature, Aquarius satellite-derived salinity, surface CDOM absorption at 325 nm, a_g325 (m^{-1}) and spectral slope $S_{275-295}$ (μm^{-1}) along the ship transect from NZ to TNB. Dashed vertical lines represent the location of the Southern Ocean fronts and the two arrows indicate trends in CDOM absorption and slope between the STF and APF.

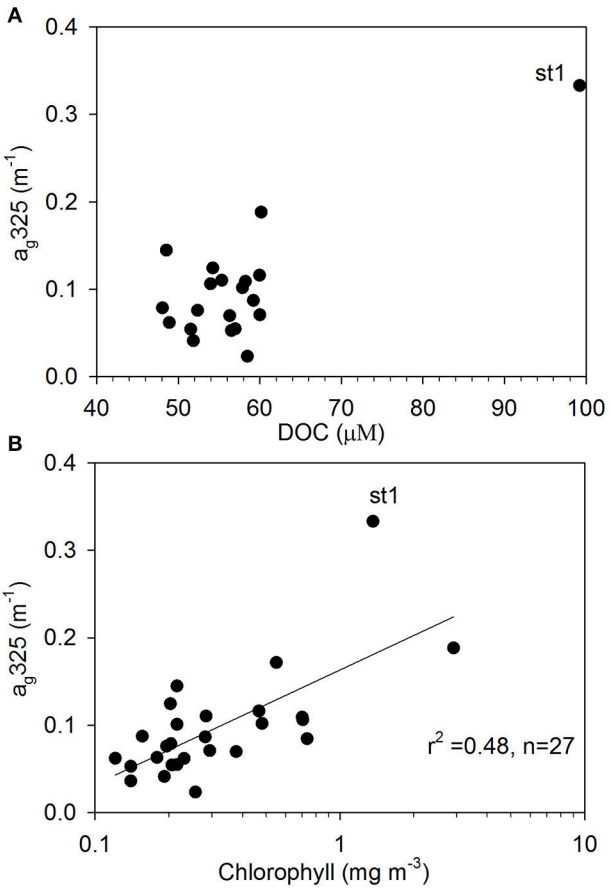

FIGURE 5 | CDOM absorption properties. Relationships between **(A)** DOC and a_g325 (m^{-1}), and **(B)** chlorophyll and a_g325 (m^{-1}) (st1 denotes station 1 closest to the New Zealand shore).

with elevated phytoplankton chlorophyll (**Figure 8A**) but showed no clear trends with chlorophyll (not shown). The two protein-like components C1 and C2 were elevated off NZ and TNB, as well as at/near the fronts (**Figure 8B**), with C1 showing a weak negative correlation to salinity (**Figure 9B**).

DISCUSSION

Biophysical Environment

The STF located south and east off NZ forms the boundary between the warmer/salty, nutrient-poor subtropical waters and the colder/fresher, nutrient rich subantarctic waters. Off the NZ shore, the subtropical surface water, generally located 15–40 km offshore, is modified by mixing with freshwater runoff from land and with the subantarctic water further offshore (Sander et al., 2015; **Figure 2A**). The MODIS imagery (**Figure 2B**) shows a broad band of elevated chlorophyll in the subtropical frontal region around NZ that are thought to be related to the mixing of warm, macronutrient-poor, relatively micronutrient-rich (especially iron) subtropical water with cold, macronutrient-rich and micronutrient-poor subantarctic water (Orsi et al., 1995; Belkin and Gordon, 1996; Boyd et al., 1999). Similar patterns of chlorophyll distribution were previously described with elevated chlorophyll occurring in the STF to the west and east of NZ throughout the year (Murphy et al., 2001) and along a narrow band c. 43°S on the south side of the Chatham Rise and extending eastwards to the Chatham Islands (**Figure 2B**). South of New Zealand, the complex marine topography associated with the Macquarie Ridge and the Campbell Plateau strongly influences the circulation pattern with the ACC undergoing intense wave-like migrations and energetic eddies (Gordon, 1975; Bryden and Heath, 1985). Surface expression of such circulation patterns and associated meanders and eddies observed in the satellite sea surface salinity imagery south of New Zealand (**Figure 2A**) also appear associated with more elevated chlorophyll concentrations observed in the MODIS imagery and field measurements along the transect (∼50 and 55°S; **Figures 2B**, **3**). Similar trends were previously observed linking meanders and eddies to the interaction of the two SAF branches and the complex topography (Campanelli et al., 2011). Nonetheless, chlorophyll concentrations were low in the subantarctic waters (0.2–0.3 mg m^{-3}) and comparable to levels reported in other subantarctic regions (Boyd et al., 1999; Han and Takahashi, 2001; Murphy et al., 2001; Hunt and Hosie, 2006). South of the APF, an elevated chlorophyll band (0.64 ± 0.15 mg m^{-3}; **Figures 2B**, **3**) showed similarity to earlier observations that appear persistent in the region (Moore and Abbott, 2000; Campanelli et al., 2011). This significant increase in phytoplankton biomass has been attributed to iron replenishment in the mixed layer of the Antarctic zone by the Upper Circumpolar Deep Water (UCDW; Hiscock et al., 2003) or to the wind-induced increase of the mixed layer depth (Carranza and Gille, 2015). As in previous observations (Daly et al., 2001; Han and Takahashi, 2001), elevated surface chlorophyll were not observed at fronts, but near fronts or in eddies and meanders (**Figures 2**, **3**). Further south in the summer ice edge zone, relatively low chlorophyll values (**Figure 3**) were similar to values reported in the Australian sector of the Southern Ocean in early austral summer that were attributed to the short time for phytoplankton growth following ice melt or to reduced water column stability due to strong prevailing winds (Han and Takahashi, 2001). In the TNB region of the western Ross Sea, chlorophyll biomass was relatively high (**Figures 2**, **3**) and likely associated with a late summer bloom with values in the range previously reported for surface waters in the area (Rivaro et al., 2011). Overall, surface summer chlorophyll distribution along the NZ transect supported the Southern Ocean as a HNLC region with productive sites linked to meanders and eddies and other local processes.

CDOM Distribution and Absorption Budgets

Surface DOC concentrations in the NZSSO between the STF and SACCF (54.19 ± 4.02 μM) were comparable to those reported in the Australian sector of the Southern Ocean (45–55 μM; Ogawa et al., 1999) and summer surface concentrations in the Ross Sea (55 ± 5μM; Carlson et al., 2000). In comparison to the refractory DOC pool (∼42 μM) observed in deeper waters of the Ross Sea,

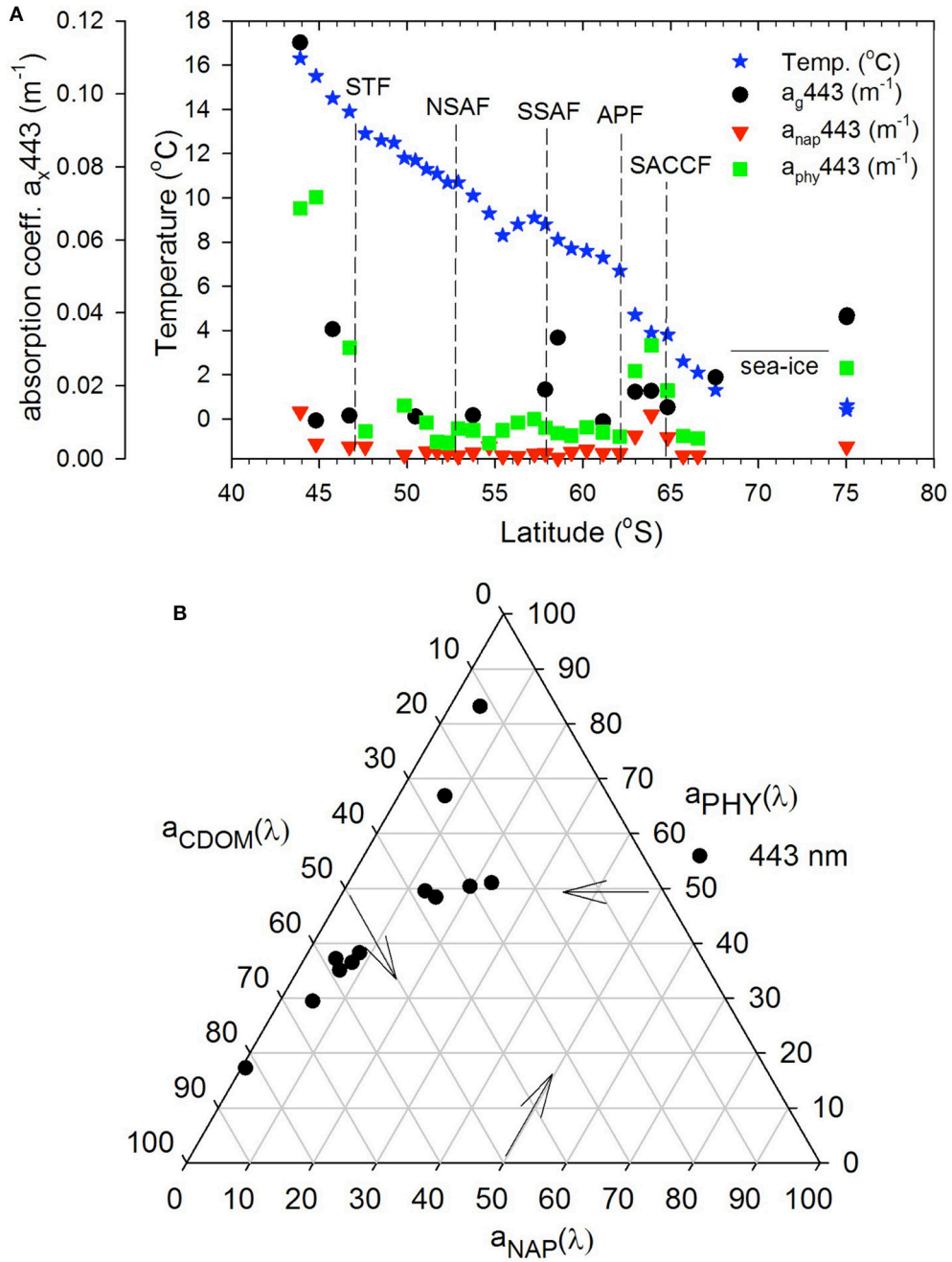

FIGURE 6 | Absorption budgets (a_g, a_{phy}, and a_{nap}) at 443 nm. (A) Absorption coefficients at 443 nm of CDOM, phytoplankton and nonalgal particles along the transect. **(B)** ternary plot of absorption coefficient at 443 nm.

and the Southern Ocean (Ogawa et al., 1999; Carlson et al., 2000), surface DOC in excess of that in deep water is likely associated with a labile or semi-labile fraction of DOM with turnover on varying time scales (hours, days, months to years) that supports heterotrophic microbial production and is potentially important for export (Carlson, 2002; Hansell, 2013).

a_g325 was highest in the NZ shore station and decreased to its lowest values near the STF indicating terrestrial influences on CDOM in the northern sector of the transect. Surface patterns and range of a_g325 distribution in the ACC were generally consistent with earlier reported values in the Pacific region of the Southern Ocean (Nelson et al., 2010). A general poleward increase in a_g325 (0.024–0.145 m^{-1}) and a corresponding decreasing trend in spectral slope S between the STF and APF were likely due to a combination of factors such as (i) decreasing rates of CDOM loss poleward due to solar photodegradation,

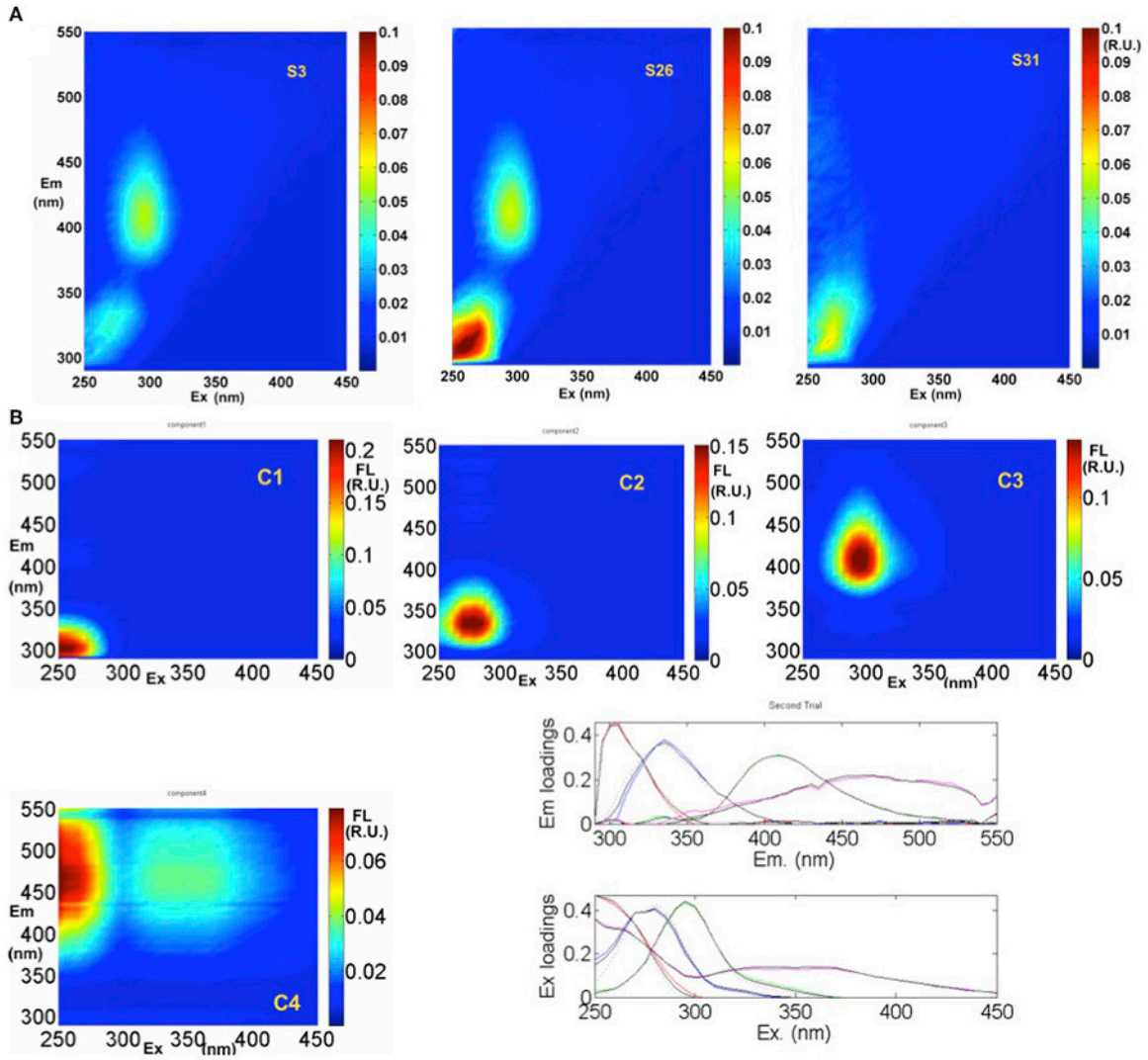

FIGURE 7 | EEMs fluorescence spectra and PARAFAC analysis. (A) Example EEMs at three locations (S3, S26, and S31) along the transect. **(B)** Spectral properties of four fluorescent components (C1, C2, C3, and C4) identified by PARAFAC in Raman Units (R.U.) of intensity. Excitation and emission loadings derived from the four-component PARAFAC model using split-half validation technique (bottom right). Positions of their maxima are given in **Table 1**.

TABLE 1 | Description of the four components identified by PARAFAC analysis of EEMs fluorescence data and their comparisons with previously identified components.

Comp.	Excitation maxima(nm)	Emission Maxima(nm)	Description, probable source	References
C1	260	300	Tyrosine-like, protein-like	B[a], C2[c], C1[d], C1[c], C4[e]
C2	270	330	Tryptophan-like, protein-like	T[a], C1[c], C6[d], C3[e]
C3	295	400	Marine humic-like, microbial	M[a], C3[b], C2[e]
C4	260(360)	460	Humic-like (A and C-like)	A & C[a], C3[c], C3[d], C1[e]

[a]*Coble (1996)*, [b]*Stedmon and Markager (2005)*, [c]*Wedborg et al. (2007)*, [d]*Murphy et al. (2008)*, [e]*Catalá et al. (2015)*.

(ii) upwelling of the CDOM-rich subsurface waters in the Antarctic Zone and its convective transport associated with the wind-driven overturning circulation (Nelson et al., 2010; Marshall and Speer, 2012) or, (iii) to biogeneration of CDOM by bacteria (Ortega-Retuerta et al., 2009). Elevated values of the spectral slope S observed at a meander south of the STF and at fronts (e.g., NSAF, APF, SACCF; **Figures 2**, **4**) suggest that this CDOM optical property could potentially be used to identify such features in the Southern Ocean. CDOM was uncorrelated with DOC (**Figure 5A**) but positively correlated to chlorophyll (**Figure 5B**) suggesting strong biological control on CDOM in the surface waters of the study region.

The light absorption properties of CDOM and particulate matter in the visible (e.g., 443 nm) influences the light field

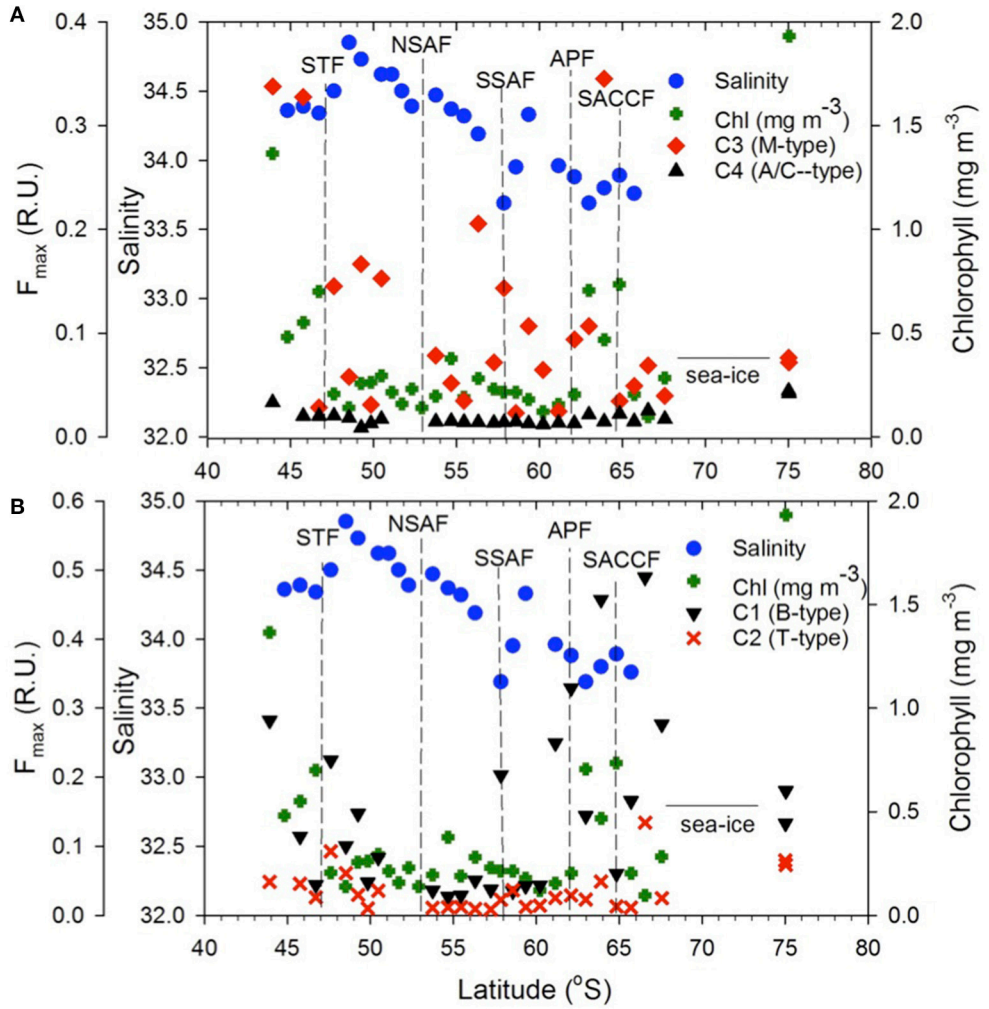

FIGURE 8 | FDOM components. Meridional distribution of the **(A)** C3 and C4, **(B)** C1 and C2 FDOM components, sea surface salinity and chlorophyll along the transect. Dashed vertical lines show locations of the Southern Ocean fronts.

and ocean color. $a_g(443)$ was similar to those reported in other regions of the Southern Ocean (Clementson et al., 2001; Kieber et al., 2009; Del Castillo and Miller, 2011). $a_{phy}(443)$ and $a_{nap}(443)$ between the STF and APF were comparable to those reported in the same latitudinal bands in the Australia sector of the Southern Ocean (Clementson et al., 2001), and other oceanic waters (Bricaud et al., 1998; Naik et al., 2013). $a_{nap}(443)$ was generally <10% of the total absorption but its contribution increased in the elevated chlorophyll band south of the APF (**Figures 6A,B**) likely due to the persistence of this band and the multiple pathways for decay and regeneration of the phytoplankton biomass. Overall, CDOM contribution was greater (50–60%) than phytoplankton absorption (30–40%). However, in the high chlorophyll band south of the APF and in the northern stations off NZ, phytoplankton absorption was dominant. Terrestrial influences off NZ (station 1) and at TNB stations likely contributed to the dominant CDOM contribution (~70 and 80%, respectively; **Figure 6B**). Thus, while the general surface characteristics of the absorption field within the ACC region appear consistent with other regions of the Southern Ocean, effects of deviations in regions such as off NZ on ocean color should be considered in its interpretation.

FDOM Distribution along the Transect

The four PARAFAC fluorescent components identified in the surface waters of the NZSSO have also been reported in other oceanic regions (Murphy et al., 2008; Jorgensen et al., 2011; D'Sa et al., 2014; Catalá et al., 2015, 2016) including the Southern Ocean (Wedborg et al., 2007; Nelson and Gauglitz, 2016). The relative concentrations and latitudinal distribution patterns of the four components however, appeared to be influenced by physical and biological processes along the NZSSO. A positive correlation of the humic-like C4 component to chlorophyll (**Figure 9A**) suggests a strong biological control consistent with previous results documented for the global epipelagic ocean (Catalá et al., 2016). A decreasing trend of the C4 component

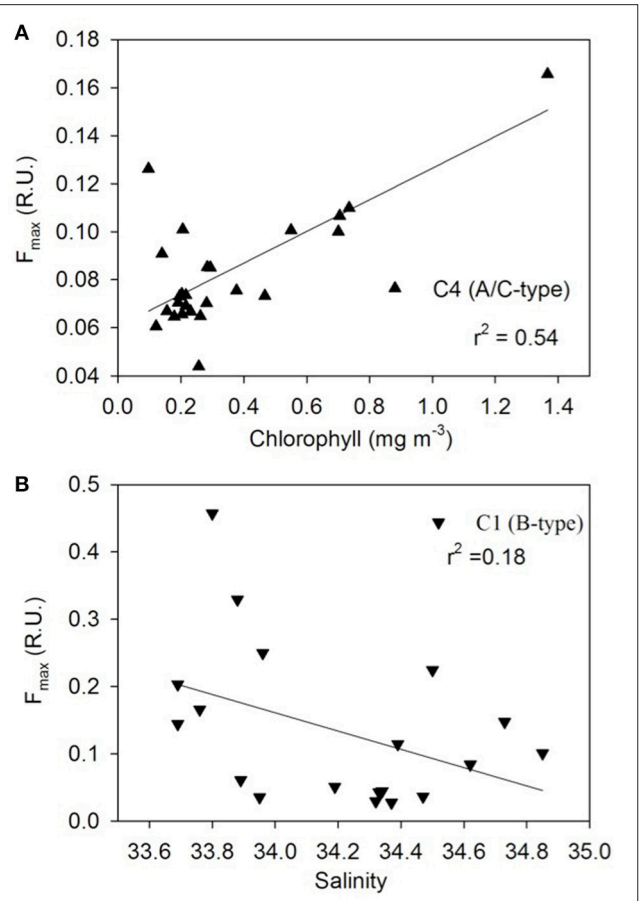

FIGURE 9 | FDOM component properties. Relationships between **(A)** chlorophyll and humic-like C4, and **(B)** satellite-derived sea surface salinity and protein-like C1 components.

with increasing distance from the NZ shore as well as its high intensity in TNB suggest a strong terrestrial influence on this component in these two regions (**Figure 8A**). However, in the isolated region of the Antarctic Zone, elevated C4 values (**Figure 8A**) suggest likely contribution by upwelling associated with the UCDW and is consistent with higher intensity of this humic-like component in deeper waters of the ocean (Catalá et al., 2016; Nelson and Gauglitz, 2016). Furthermore, uniformly elevated C4 intensity in contrast to highly variable chlorophyll distribution in the Antarctic Zone suggests no direct linkage of this component to local productivity. A decreasing trend of C4 to uniformly low background values north of the APF likely due to photobleaching (Catalá et al., 2016) suggests a transformation of this humic-like material in surface waters as it flows equatorward associated with the Southern Ocean's meridional overturning circulation. The transformation of this DOM fluorescent material as the upwelled waters of the UCDW continue equatorward to form the Antarctic Intermediate Water (AAIW) and the Subantarctic Mode Water (SAMW) (Abernathey et al., 2016; Armour et al., 2016) has potential to influence DOM fluorescent composition in the global ocean (Marshall and Speer, 2012). The marine humic-like C3 component in contrast, revealed large variability across the surface waters of the NZSSO. Although a previous study indicated biological control on the distribution of this component in the global epipelagic waters (Catalá et al., 2016), such direct linkage was not observed in this study; rather, trends of elevated C3 in the productive region offshore of NZ and the STF, and the productive band in the Antarctic Zone south of the APF were observed (**Figure 8A**). This component was, however, low in the highly productive surface waters of the TNB, the summer ice edge region, and between the fronts. This pattern likely suggests elevated production of this fraction associated with microbial activity at more productive sites or at sites such as the STF with predominance of regenerated production (Kopcsynska et al., 2001). In contrast, although the TNB site was highly productive (**Figure 3**), the short-term cycling of the cold and high saline waters associated with the TNB polynia may not provide the conditions for the microbial production of this fluorescent fraction of CDOM.

The tyrosine- and tryptophan-like components C1 and C2 revealed broadly similar patterns of distribution with C1 having greater intensity and variability across the transect (**Figure 8B**). Off NZ, C1 showed a steep decline in intensity up to the STF suggesting strong terrestrial influence. It then increased significantly at the STF and thereafter declined toward the APF in concert with decreasing salinity (**Figure 8B**) suggesting some physical control (Catalá et al., 2016) as indicated by a weak negative relationship to coarse estimates of satellite-derived sea surface salinity (**Figure 9B**). However, anomalous increase of this component at or near hydrographic fronts (e.g., STF, SSAF, APF ad SACCF) were observed (**Figure 8B**) and are similar to those reported in the South Africa sector of the Southern Ocean, wherein, pronounced concentrations of the protein-like fluorescent fractions were detected even at great depths (Wedborg et al., 2007), likely indicating linkage to more resistant DOM fractions in the deeper ocean waters (Catalá et al., 2015). Both C1 and C2 showed increases at fronts and low values between the fronts (e.g., NSAF and APF) suggesting some photooxidative loss of these components. Large variability in these two protein-like components in the Antarctic Zone could be due to both physical and biological processes associated with upwelling, elevated phytoplankton biomass and seasonal sea ice effects.

In summary, surface field data combined with satellite (salinity and chlorophyll) and historical hydrographic observations were used to understand the physical regime (specifically, the locations of fronts) and the presence of meanders along the NZSSO, a topographically complex region of the Southern Ocean. CDOM absorption and fluorescence variability along the NZSSO were then examined in relation to frontal positions and biochemical properties (chlorophyll and DOC concentrations) in addition to assessing CDOM absorption contribution to total absorption in the visible band that influences ocean color. In the STF region south of NZ, the interaction of the subtropical and subantarctic waters generally resulted in decreasing levels of chlorophyll and DOC concentrations, and CDOM optical properties that suggested terrestrial influences. However, in the core of the

ACC, between the STF and the APF, surface chlorophyll and DOC concentrations and CDOM absorption were low and consistent with other studies. Fluorescence fractions identified using PARAFAC analysis were consistent with those in other oceanic regions, but revealed patterns influenced by fronts and water properties typical of the NZSSO. In the Antarctic Zone, upwelling of CDOM-rich waters likely associated with the Southern Ocean's overturning circulation and its equatorward transport and transformation could contribute to modified CDOM and FDOM properties that could serve as a tracer of changes in biochemistry associated with the overturning circulation.

AUTHOR CONTRIBUTIONS

ED and HK designed the study and contributed to the manuscript.

FUNDING

Funding for this work was provided by a Korea Polar Research Institute (KOPRI) grant PE16040 (Satellite remote sensing on west Antarctic ocean research: STAR) and partly supported by PE17120.

ACKNOWLEDGMENTS

The authors would like to thank the crew of the KOPRI ice-breaker and research vessel *Araon* and the technicians and students who participated in the Southern Ocean cruise and helped in the laboratory. The authors would like to thank NASA GSFC and JPL for making available the satellite data. The use of the Ocean Data Viewer (http://odv.awi.de) is also gratefully acknowledged. The authors would also like to thank the three reviewers for helpful comments on the manuscript.

REFERENCES

Abernathey, R. P., Cerovecki, I., Holland, P. R., Newsom, E., Mazloff, M., and Talley, L. D. (2016). Water-mass transformation by sea ice in the upper branch of the Southern Ocean overturning. *Nat. Geosci.* 9, 596–601. doi: 10.1038/ngeo2749

Armour, K. C., Marsahll, J., Scott, J. R., Donohue, A., and Newsom, E. R. (2016). Southern Ocean warming delayed by circumpolar upwelling and equatorward transport. *Nat. Geosci.* 9, 549–555. doi: 10.1038/ngeo2731

Arrigo, K., Worthen, D., Schnell, A., and Lizotte, M. P. (1998). Primary production in Southern Ocean waters. *J. Geophys. Res.* 103, 15587–15600. doi: 10.1029/98jc00930

Belkin, I. M., and Gordon, A. L. (1996). Southern Ocean fronts from Greenwich meridian to Tasmania. *J. Geophys. Res.* 101, 3675–3696. doi: 10.1029/95JC02750

Benner, R., and Strom, M. (1993). A critical evaluation of the analytical blank associated with DOC measurements by high temperature catalytic oxidation. *Mar. Chem.* 41, 153–160. doi: 10.1016/0304-4203(93)90113-3

Blough, N. V., and Del Vecchio, R. (2002). "Chromophoric DOM in the coastal environment," in *Biogeochemistry of Marine Dissolved Organic Matter*, eds D. A. Hansell and C. A. Carlson (San Diego, CA: Academic Press), 509–546

Boyd, P., LaRoche, J., Gall, M., Frew, R., and McKay, R. M. L. (1999). The role of iron, light and silicate in controlling algal biomass in sub-Antarctic water SE of New Zealand. *J. Geophys. Res.* 104, 13395–13408. doi: 10.1029/1999JC900009

Bricaud, A., Morel, A., Babin, M., Allali, K., and Claustre, H. (1998). Variations of light absorption by suspended particles with chlorophyll a concentration in oceanic (case 1) waters: analysis and implications for bio-optical models. *J. Geophys. Res.* 103, 31033–31044. doi: 10.1029/98JC02712

Bryden, H. L., and Heath, R. A. (1985). Energetic eddies at the northen edge of the antarctic circumpolar current in the southwest pacific. *Prog. Oceanogr.* 14, 65–85. doi: 10.1016/0079-6611(85)90006-0

Budillon, G., and Rintoul, S. R. (2003). Fronts and upper ocean thermal variability south of New Zealand. *Antarct. Sci.* 15, 141–152. doi: 10.1017/S0954102003001135

Campanelli, A., Massolo, S., Grilli, F., Paschi, E., Rivaro, P., Artegiani, A., et al. (2011). Variability of nutrient and thermal structure in surface waters between New Zealand and Antarctica, October 2004-January 2005. *Polar Res.* 30:7064. doi: 10.3402/polar.v30i0.7064

Carlson, C. A. (2002). "Production and removal processes," in *Biogeochemistry of Marine Dissolved Organic Matter*, eds D. A. Hansell and C. A. Carlson (San Diego, CA: Academic Press), 91–151.

Carlson, C. A., Hansell, D. A., Peltzer, E. T., and Smith, W. O. Jr. (2000). Stocks and dynamics of dissolved and particulate organic matter in the southern Ross Sea, Antarctica. *Deep Sea Res. II* 47, 3201–3225. doi: 10.1016/S0967-0645(00)00065-5

Carranza, M. M., and Gille, S. T. (2015). Southern Ocean wind-driven entrainment enhances satellite chlorophyll-a through the summer. *J. Geophys. Res.* 120, 304–323. doi: 10.1002/2014jc010203

Catalá, T. S., Reche I., Fuentes-Lema A., Romera-Castillo C., Nieto-Cid M., Ortega-Retuerta E., et al. (2015). Turnover time of fluorescent dissolved organic matter in the dark global ocean. *Nat. Commun.* 6:5986. doi: 10.1038/ncomms6986

Catalá, T. S., Alvarez-Salgado, X. A., Otero, J., Iuculano, F., Companys, B., Horstkotte, B., et al. (2016). Drivers of fluorescent dissolved organic matter in the global epipelagic ocean. *Limnol. Oceanogr.* 61, 1101–1119. doi: 10.1002/lno.10281

Clementson, L. A., Parslow, J. S., Turnbull, A. R., McKenzie, D. C., and Rathbone, C. E. (2001). Optical properties of waters in the Australasian sector of the Southern Ocean. *J. Geophys. Res.* 106, 31611–31625. doi: 10.1029/2000jc000359

Coble, P. G. (1996). Characterization of marine and terrestrial DOM in seawater using excitation-emission matrix spectroscopy, *Mar. Chem.* 51, 325–346. doi: 10.1016/0304-4203(95)00062-3

Daly, K. L., Smith, W. O. Jr., Johnson, G. C., DiTullio, G. R., Jones, D. R., Mordy, C. W., et al. (2001). Hydrography, nutrients, and carbon pools in the Pacific sector of the Southern Ocean: implications for carbon flux. *J. Geophys. Res.* 106, 7107–7124. doi: 10.1029/1999JC000090

Del Castillo, C. E., and Miller, R. L. (2011). Horizontal and vertical distributions of colored dissolved organic matter during the Southern Ocean Gas Exchange Experiment. *J. Geophys. Res.* 116, C00F07. doi: 10.1029/2010JC006781

D'Sa, E. J. (2008). Colored dissolved organic matter in coastal waters influenced by the Atchafalaya River, USA: effects of an algal bloom, *J. Appl. Remote Sens.* 2, 023502. doi: 10.1117/1.2838253

D'Sa, E. J., and DiMarco, S. (2009). Seasonal variability and controls on chromophoric dissolved organic matter in a large river- dominated coastal margin, *Limnol. Oceanogr.* 54, 2233–2242. doi: 10.4319/lo.2009.54.6.2233

D'Sa, E. J., Goes, J. I., Gomes, H., and Mouw, C. (2014). Absorption and fluorescence properties of chromophoric dissolved organic matter of the eastern Bering Sea in the summer with special reference to the influence of a cold pool. *Biogeosciences* 11, 3225–3244. doi: 10.5194/bg-11-3225-2014

D'Sa, E. J., Overton, E. B., Lohrenz, S. E., Maiti, K., Turner, R. E., and Freeman, A. (2016). Changing dynamics of dissolved organic matter fluorescence in the northern Gulf of Mexico following the Deepwater Horizon oil spill. *Environ. Sci. Technol.* 50, 4940–4950. doi: 10.1021/acs.est.5b04924

D'Sa, E. J., Steward, R. G., Vodacek, A., Blough, N. V., and Phinney, D. (1999). Determining optical absorption of colored dissolved organic matter in seawater with a liquid capillary waveguide. *Limnol. Oceanogr.* 44, 1142–1148.

Fernandez, D., Bowen, M., and Carter, L. (2014). Intensification and variability of the confluence of subtropical and subantarctic boundary currents east of New Zealand. *J. Geophys. Res. Oceans* 119, 1146–1160. doi: 10.1002/2013JC009153

Gordon, A. L. (1975). An Antarctic oceanographic section along 170°E. *Deep Sea Res.* 22, 357–377.

Han, D.-H., and Takahashi, M. M. (2001). Chlorophyll a biomass of netplankton in surface waters in the Pacific sector of the Southern Ocean in austral summer. *J. Oceanogr.* 57, 581–592. doi: 10.1023/A:1021207719976

Hansell, D. A. (2013). Recalcitrant dissolved organic carbon fractions. *Annu. Rev. Mar. Sci.* 5, 421–445. doi: 10.1146/annurev-marine-120710-100757

Hansell, D. A., and Carlson, C. A. (2001). Marine dissolved organic matter and the carbon cycle. *Oceanography* 14, 41–49. doi: 10.5670/oceanog.2001.05

Helms, J. R., Stubbins, A., Ritchie, J. D., Minor, E. C., Kieber, D. J., and Mopper, K. (2008). Absorption spectral slopes and slope ratios as indicators of molecular weight, source and photobleaching of chromophoric dissolved organic matter. *Limnol. Oceanogr.* 53, 955–969. doi: 10.4319/lo.2008.53.3.0955

Hiscock, M. R., Marra, J., Smith, W. O. Jr., Goericke, R., Measures, C., Vink, S., et al. (2003). Primary productivity and its regulation in the Pacific sector of the Southern Ocean. *Deep Sea Res. II* 50, 533–558. doi: 10.1016/S0967-0645(02)00583-0

Holm-Hansen, O., Lorenzen, C. J., Holmes, R. W., and Strickland, J. D. H. (1965). Fluorometric determination of chlorophyll. *J. Conseil. Conseil Permanent Int. L'explor.* 30, 3–15. doi: 10.1093/icesjms/30.1.3

Honjo, S. (2004). Particle export and the biological pump in the Southern Ocean. *Antarctic Sci.* 16, 501–516. doi: 10.1017/S0954102004002287

Hunt, B. P. V., and Hosie, G. W. (2006). The seasonal succession of zooplankton in the Southern Ocean south of Australia, part II: the sub-antarctic to polar frontal zones. *Deep Sea Res. I* 53, 1203–1223. doi: 10.1016/j.dsr.2006.05.002

Jiao, N., Herndl, G. J., Hansell, D. A., Benner, R., Kattner, G., Wilhelm, S. W., et al. (2010). Microbial production of recalcitrant dissolved organic matter: long-term carbon storage in the global ocean. *Nature Rev. Microbiol.* 8, 593–599. doi: 10.1038/nrmicro2386

Jorgensen, L., Stedmon, C. A., Kragh, T., Markager, S., Middelboe, M., and Sondergaard, M. (2011). Global trends in the fluorescence characteristics and distribution of marine dissolved organic matter. *Mar. Chem.* 126, 139–148. doi: 10.1016/j.marchem.2011.05.002

Kieber, D. J., Toole, D. A., and Kiene, R. P. (2009). "Chromophoric dissolved organic matter cycling during a Ross Sea Phaeocystis Antarctica bloom," in *Smithsonian at the Poles: Contributions to International Polar Year Science*, eds I. Krupnik, M. A. Lang, and S. E. Miller (Washington, DC: Smithsonian Institution Scholarly Press), 309–318.

Kitidis, V., Stubbins, A. P., Uher, G., Goddard, U., Robert, C., Law, C. S., and Woodward, E. M. S. (2006). Variability of chromophoric organic matter in surface waters of the Atlantic Ocean. *Deep Sea Res. II* 53, 1666–1684. doi: 10.1016/j.dsr2.2006.05.009

Kopcsynska, E. E., Dehairs, F., Elskens, M., and Wright, S. (2001). Phytoplankton and microzooplankton variability between the Subtropical and Polar Fronts south of Australia: thriving under regenerative and new production in late summer. *J. Geophys. Res.* 106, 31597–31609. doi: 10.1029/2000JC000278

Lee, T. (2016). Consistency of Aquarius sea surface salinity with Argo products on various spatial and temporal scales. *Geophys. Res. Lett.* 43, 3857–3864. doi: 10.1002/2016GL068822

Lee, Z., Lance, V. P., Shang, S., Vaillancourt, R., Freeman, S., Lubac, B., et al. (2011). An assessment of optical properties and primary production derived from remote sensing in the Southern Ocean (SO GasEx). *J. Geophys. Res.* 16, C00F03. doi: 10.1029/2010jc006747

Marshall, J., and Speer, K. (2012). Closure of the meridional overturning circulation through Southern Ocean upwelling. *Nat. Geosci.* 5, 171–180. doi: 10.1038/ngeo1391

McNeil, B. J., and Tilbrook, B. (2009). A seasonal carbon budget for the sub-Antarctic Ocean, South of Australia. *Mar. Chem.* 115, 196–2010. doi: 10.1016/j.marchem.2009.08.006

Mitchell, B. G., Kahru, M., Wieland, J., and Stramska, M. (2003). *Determination of Spectral Absorption Coefficients of Particles, Dissolved Materials and Phytoplankton for Discrete Water Samples. Ocean Optics Protocols For Satellite Ocean Color Sensor Validation, Revision 4, Vol. 4, Inherent Optical Properties: Instruments, Characterization, Field Measurements and Data Analysis Protocols*. Greenbelt, Maryland: NASA Technical Report.

Moore, J. K., and Abbott, M. R. (2000). Phytoplankton chlorophyll distributions and primary production in the Southern Ocean. *J. Geophys. Res.* 105, 28709–28722. doi: 10.1029/1999JC000043

Mopper, K., and Schultz, C. A. (1993). Fluorescence as a possible tool for studying the nature and water column distribution of DOC components. *Mar. Chem.* 41, 229–238. doi: 10.1016/0304-4203(93)90124-7

Murphy, K. R., Stedmon, C. A., Waite, T. D., and Ruiz, G. M. (2008). Distinguishing between terrestrial and autochthonous organic matter sources in marine environments using fluorescence spectroscopy. *Mar. Chem.* 108, 40–58. doi: 10.1016/j.marchem.2007.10.003

Murphy, R. J., Pinkerton, M. H., Richardson, K. M., Bradford-Grieve, J. M., and Boyd, P. W. (2001). Phytoplankton distributions around New Zealand derived from SeaWiFS remotely-sensed ocean colour data. *N. Z. J. Mar. Freshw. Res.* 35, 343–362. doi: 10.1080/00288330.2001.9517005

Naik, P., and D'Sa, E. J. (2012). Phytoplankton light absorption of cultures and naturalsamples: comparisons using two spectrophotometers. *Optics Express* 20, 4871–4886. doi: 10.1364/OE.20.004871

Naik, P., D'Sa, E. J., Gomes, H. R., Goes, J. I., and Mouw, C. B. (2013). Light absorption properties of southeastern Bering Sea waters: analysis, parameterization and implications for remote sensing. *Rem. Sens. Environm.* 134, 120–143. doi: 10.1016/j.rse.2013.03.004

Nelson, N. B., and Gauglitz, J. M. (2016). Optical signatures of dissolved organic matter transformation in the global ocean. *Front. Mar. Sci.* 2:118. doi: 10.3389/fmars.2015.00118

Nelson, N. B., and Siegel, D. A. (2002). "Chromophoric DOM in the Open Ocean," in *Biogeochemistry of Marine Dissolved Organic Matter*, eds D. A. Hansell and C. A. Carlson (San Diego, CA: Academic Press), 547–578.

Nelson, N. B., and Siegel, D. A. (2013). The global distribution and dynamics of chromophoric dissolved organic matter. *Annu. Rev. Mar. Sci.* 5, 447–476. doi: 10.1146/annurev-marine-120710-100751

Nelson, N. B., Siegel, D. A., Carlson, C. A., and Swan, C. M. (2010). Tracing global biogeochemical cycles and meridional overturning circulation using chromophoric dissolved organic matter. *Geophys. Res. Lett.* 37, L03610. doi: 10.1029/2009GL042325

Ogawa, H., Fukuda, R., and Koike, I. (1999). Vertical distributions of dissolved organic carbon and nitrogen in the Southern Ocean. *Deep-Sea Res.* 46, 1809–1826. doi: 10.1016/S0967-0637(99)00027-8

Orsi, A. H., Whitworth, T. III, and Nowlin, W. D. (1995). On the meridional extent and fronts of the Antarctic Circumpolar Current. *Deep-Sea Res.* 42, 641–673. doi: 10.1016/0967-0637(95)00021-W

Ortega-Retuerta, E., Frazer, T. K., Duarte, C. M., Ruiz-Halpern, S., Tovar-Sanchez, A., Arrieta, J. M., et al. (2009). Biogeneration of chromophoric dissolved organic matter by bacteria and krill in the Southern Ocean. *Limnol. Oceanogr.* 54, 1941–1950. doi: 10.4319/lo.2009.54.6.1941

Reynolds, R. A., Stramski, D., and Mitchell, B. G. (2001). A chlorophyll-dependent semianalytical reflectance model derived from field measurements of absorption and backscattering within the Southern Ocean. *J. Geophys. Res.* 106, 7125–7138. doi: 10.1029/1999JC000311

Rivaro, P., Ianni, C., Massolo, S., Abelmoschi, M. L., De Vittor, C., and Frache, R. (2011). Distribution of dissolved labile and particulate iron and copper in Terra Nova Bay polynya (Ross Sea, Antarctica) surface waters in relation to nutrients and phytoplankton growth. *Cont. Shelf Res.* 31, 879–889. doi: 10.1016/j.csr.2011.02.013

Romera-Castillo, C., Sarmento, H., Alvarez-Salgado, X. A., Gasol, J. M., and Marrase, C. (2010). Production of chromophoric dissolved organic matter by marine phytoplankton. *Limnol. Oceanogr.* 55, 446–454. doi: 10.4319/lo.2010.55.1.0446

Sander, S. G., Tian, F., Ibisanmi, E. B., Currie, K. I., Hunter, K. A., and Frew, R. D. (2015). Spatial and seasonal variations of iron speciation in surface waters of the Subantarctic front and the Otago Continental Shelf. *Mar. Chem.* 173, 114–124. doi: 10.1016/j.marchem.2014.09.001

Sarmiento, J. L., and LeQuere, C. (1996). Oceanic carbon dioxide uptake in a model of century-scale global warming. *Science* 274, 1346–1350. doi: 10.1126/science.274.5291.1346

Siegel, D. A., Maritorena, S., Nelson, N. B., Hansell, D. A., and Lorenzi-Kayser, M. (2002). Global distribution and dynamics of colored dissolved and detrital organic materials. *J. Geophys. Res.* 107, 3228. doi: 10.1029/2001JC000965

Singh, S., D'Sa, E. J., and Swenson, E. M. (2010). Chromophoric dissolved organic matter (CDOM) variability in Barataria Basin using excitation-emission matrix (EEM) fluorescence and parallel factor analysis (PARAFAC).

Sci. Total Environ. 408, 3211–3222. doi: 10.1016/j.scitotenv.2010.03.044

Stedmon, C. A., and Bro, R. (2008). Characterizing dissolved organic matter fluorescence with parallel factor analysis: a tutorial. *Limnol. Oceanogr.* 6, 572–579. doi: 10.4319/lom.2008.6.572

Stedmon, C. A., and Markager, S. (2005). Tracing the production and degradation of authochthonous fractions of dissolved organic matter using fluorescence analysis. *Limnol. Oceanagr.* 50, 1415–1426. doi: 10.4319/lo.2005.50.5.1415

Stedmon, C. A., Markager, S., and Bro, R. (2003). Tracing dissolved organic matter in aquatic environments using a new approach to fluorescence spectroscopy. *Mar. Chem.* 82, 239–254. doi: 10.1016/S0304-4203(03)00072-0

Swan, C. M., Siegel, D. A., Nelson, N. B., Carlson, C. A., and Nsair, E. (2009). Biogeochemical and hydrographic controls on chromophoric dissolved organic matter distribution in the Pacific Ocean. *Deep Sea Res. I* 56, 2175–2192. doi: 10.1016/j.dsr.2009.09.002

Wedborg, M., Persson, T., and Larsson, T. (2007). On the distribution of UV-blue fluorescent organic matter in the Southern Ocean. *Deep-Sea Res. I* 54, 1957–1971. doi: 10.1016/j.dsr.2007.07.003

Williams, M. J. M. (2004). Analysis of quasi-synoptic eddy observations in the New Zealand subantarctic. *N. Z. J. Mar. Freshwater Res.* 38, 183–194. doi: 10.1080/00288330.2004.9517227

Yamashita, Y., and Tanoue, E. (2003). Chemical characterization of protein-like fluorophores in DOM in relation to aromatic amino acids. *Mar. Chem.* 82, 255–271. doi: 10.1016/S0304-4203(03)00073-2

Yamashita, Y., Tsukasaki, A., Nishida, T., and Tanoue, E. (2007). Vertical and horizontal distribution of fluorescent dissolved organic matter in the Southern Ocean. *Mar. Chem.* 106, 498–509. doi: 10.1016/j.marchem.2007.05.004

Conflict of Interest Statement: The authors declare that the research was conducted in the absence of any commercial or financial relationships that could be construed as a potential conflict of interest.

Advantages of publishing in Frontiers

OPEN ACCESS
Articles are free to read for greatest visibility and readership

FAST PUBLICATION
Around 90 days from submission to decision

HIGH QUALITY PEER-REVIEW
Rigorous, collaborative, and constructive peer-review

TRANSPARENT PEER-REVIEW
Editors and reviewers acknowledged by name on published articles

Frontiers
Avenue du Tribunal-Fédéral 34
1005 Lausanne | Switzerland

Visit us: www.frontiersin.org
Contact us: info@frontiersin.org | +41 21 510 17 00

REPRODUCIBILITY OF RESEARCH
Support open data and methods to enhance research reproducibility

DIGITAL PUBLISHING
Articles designed for optimal readership across devices

FOLLOW US
@frontiersin

IMPACT METRICS
Advanced article metrics track visibility across digital media

EXTENSIVE PROMOTION
Marketing and promotion of impactful research

LOOP RESEARCH NETWORK
Our network increases your article's readership